Renaissance Banff II

Bridges Banff

Mathematics, Music, Art, Architecture, Culture

2009

The 12th Annual Bridges Conference

Bridges Banff

Mathematics, Music, Art, Architecture, Culture

Banff International Research Station for Mathematical Innovation and Discovery

The Banff Centre
Banff, Alberta, Canada

Proceedings 2009

Craig S. Kaplan and Reza Sarhangi, Chief Editors
Tarquin Books

Bridges Banff

Scientific Organizers

Nassif Ghoussoub
Scientific Director
Banff International Research Station
University of British Columbia, Canada

Mary E. Hofstetter
President and Chief Executive Officer
The Banff Centre
Banff, Alberta, Canada

Craig S. Kaplan
Cheriton School of Computer Science
University of Waterloo
Waterloo, Ontario, Canada

Reza Sarhangi
Department of Mathematics
Towson University
Towson, Maryland, USA

Local Organizers

Kerry Stauffer
Director, Creative Electronic Environment
The Banff Centre
Banff, Alberta, Canada

Brenda Williams
Station Manager
Banff International Research Station
Banff, Alberta, Canada

Bridges Workshops: Creativity and Learning

Mara Alagic
Department of Curriculum and Instruction
Wichita State University
Wichita, Kansas, USA

Paul Gailiunas
Newcastle, UK

Bridges Visual Art Exhibition

Ergun Akleman (Catalog)
Visualization Department
Texas A&M University
College Station, Texas, USA

Anne Burns (Website, Juror)
Department of Mathematics
Long Island University
Brookville, New York, USA

Robert W. Fathauer (Curator)
Tessellations Company
Phoenix, Arizona, USA

Nat Friedman (Juror)
Department of Mathematics and
Statistics, University at Albany
Albany, New York, USA

Arlene Stamp (Juror)
Calgary, Alberta, Canada

Website and Electronic Correspondence

George W. Hart
Department of Computer Science
Stony Brook University
Stony Brook, New York, USA

Craig S. Kaplan
Cheriton School of Computer Science
University of Waterloo
Waterloo, Ontario, Canada

Conference Advisory Board

George W. Hart
Department of Computer Science
Stony Brook University
Stony Brook, New York, USA

Carlo H. Séquin
CS Division, EECS
University of California Berkeley
Berkeley, California, USA

Chief Editors

Craig S. Kaplan
Cheriton School of Computer Science
University of Waterloo
Waterloo, Ontario, Canada

Reza Sarhangi
Department of Mathematics
Towson University
Towson, Maryland, USA

ISBN: 9780966520194
ISSN: 1099-6702

Printed in the UK by InType Libra

Distributed by MATHARTFUN.COM (`http://mathartfun.com`)
and Tarquin Books (`www.tarquinbooks.com`)

Cover: *Limosa* is a work by Brian Evans, an Associate Professor in the Department of Art and Art History, at the University of Alabama. The full image is presented on the 2009 Bridges Art Exhibition website. The artist says: "Here we see a slice, through the time dimension, of an abstract animation (a mathematical visualization). We see how a single scanline changes as the animation unfolds. This 2D slice of a 4D object is then mapped into sound, so the image is actually a graphical music score. I sonify the score to create music that correlates sonically with what we see unfold visually in the animation. We hear the colors. We listen with our eyes." Jeffrey Rutzky, the cover designer, selected a part of the artwork and harmonized the presentation of the words with the movement of the image.

Cover design: Jeffrey Rutzky
CDROM Production: Craig S. Kaplan

Bridges 2009 Program Committee

Contents

Preface . . . . . *xv*

Regular Papers

Mathematics Is Art 1
Erik Demaine and Martin Demaine

Mathematical Methods in Origami Design 11
Robert J. Lang

Kircher's Mechanical Composer: A Software Implementation 21
Jim Bumgardner

Three Conceptions of Musical Distance 29
Dmitri Tymoczko

Using Turtles and Skeletons to Display the Viewable Sphere 39
David Swart

Notation for a Class of Paperfolded Models 47
Goran Konjevod and Ana Maria Kuprešanin

The Art of Iterated Function Systems with Expanding Functions 55
Philip Van Loocke

Harmonious Dances 63
Karl Schaffer

Bridging Art Museums and Middle School Math Classrooms 69
Benjamin Wells and Philip Wagner

Combinatoria Poetica: Counting and Visualizing Rhyme Patterns in Sonnets 79
Hartmut F.W. Höft

Tubular Sculptures 87
Carlo H. Séquin

Comic Books That Teach Mathematics 97
Bruce Kessler

Art and Nonlinear Projection 105
John Brosz, Sheelagh Carpendale, Faramarz Samavati, Hao Wang and Alan Dunning

Aesthetically Pleasing Azulejo Patterns 115
Russell Hendel

Marking a Physical Sphere with a Projected Platonic Solid 123
Carolyn Yackel

Coloring Uniform Honeycombs 131
Glenn Laigo, Ma. Louise Antonette N. De las Peñas and René Felix

Map-Colored Mosaics 139
Robert Bosch and Andrew Pike

The Unique Eleven-Pointed Star Polygon Design of the Topkapı Scroll 147
B. Lynn Bodner

Composite Digital Mosaics using Duotone Tiles 155
Gary Greenfield

The Symmetry of "Circle Limit IV" and Related Patterns 163
Douglas Dunham

Symmetry and Transformations in the Musical Plane 169
Vi Hart

Counterchange Patterns and Polyhedra 177
B.G. Thomas

Non-Flat Tilings with Flat Tiles 183
Rinus Roelofs

Using Polyhedral Stellations for Creation of Organic Geometric Sculptures 193
Vladimir Bulatov

Polyhedra Through the Beauty of Wood 199
Robert Rollings

Growth Forms 207
George Hart

Using Works of Visual Art to Teach Matrix Transformations 215
James Luke Akridge, Rachel Bowman, Peter Hamburger and Bruce Kessler

Regular 3D Polygonal Circuits of Constant Torsion 223
Tom Verhoeff and Koos Verhoeff

A Garden of Statistically Self-Similar Plants 231
Anne Burns

Real Tornado 239
Akio Hizume and Yoshikazu Yamagishi

Concave Hexagons 243
Paul Gailiunas

A New Method for Designing Iterated Knots 251
Robert Fathauer

A Group Portrait on a Surface of Genus Five 259
Jay Zimmerman

Tiling the Musical Canon with Augmentations of the Ashanti Rhythmic Pattern 265
Carl Bracken, Gary Fitzpatrick and Nadya Markin

Spidronised Space-Fillers 271
Walt van Ballegooijen, Paul Gailiunas and Dániel Erdély

Spirograph Patterns and Circular Representations of Rhythm: Exploring Number Theory Concepts Through Visual, Tangible and Audible Representations 279
Susan Gerofsky, Francisco Gomez, David Rappaport and Godfried Toussaint

On Constructing a Virtual Loom 287
Susan McBurney

ShamsehTrees: Providing Hierarchical Context for Nodes of Interest 293
Katayoon Etemad and Sheelagh Carpendale

Short Papers

Talking About Math/Art: The Long Pause 301
Bathsheba Grossman

The Whitney Music Box 303
Jim Bumgardner

Mathematical Experiments with African Sona Designs 305
Darrah Chavey

Honors Seminar: A Creative Interdisciplinary Approach for Student Exploration 309
Gail Kaplan

Realistic Image Making with Mandelbrot Set 313
Mehrdad Garousi and Khalil Taleslami

An Interdisciplinary First Seminar on Symmetry 315
Tamara Lakins

This Equation is Art 317
Peter Smith

ZenArt, graphic geometrical modules 319
André Génard

Amazing Labyrinths, further Amazing Labyrinths, further developments 321
Samuel Verbiese

Finding a New Route to the Moon Using Paintings 323
Edward Belbruno

Text from Truchet Tiles 325
David Reimann

Geometry and Geodesy: Estimating the Earth's Circumference with Prospective Elementary Teachers 327
Sandy Spitzer

A myriad shades of green 329
Liselott Flodén, Anders Holmbom, Marianne Olsson and Jens Persson

Geometric Transformations in Surface Design Generation 331
Fatma Mete

The Quinary–Permuting Meaning with Generative Poetry 333
Brian Evans

Spelunking Adventure II: Combining Cyclons 335
Curtis Palmer

Binary Based Fresco Restoration 337
Wolfgang Baatz, Massimo Fornasier, Peter A. Markowich and Carola-Bibiane Schönlieb

Plane, Space, Cubism and Perpetual Displacement in 3D Design 339
Joel Varland

Mathematical Classroom Quilts 341
Elaine F. Ellison

Mathematical Iconography in Gaudí's Cosmos 343
Stephen Luecking

Chaos – The Movie 345
Susan Happersett

The Frustrated Mathematician 347
Michael Frantz

An Optical Demonstration of Fractal Geometry 349
Billy C. Scannell, Ben Van Dusen and R.P. Taylor

Using Geometer's Sketchpad to Construct Pop-up Polyhedra as a Tool for Classroom Study of Geometry 351
S. Louise Gould

Workshops

Chaos, Complexity, and Creativity 355
Krystyna Laycraft

Stories Count: Narrative Approaches to Quantitative Learning 363
Suzie Garfield

Creating Islamic Patterns from Folded Shapes 367
E.B. Meenan and B.G. Thomas

Workshop: Working With Patterns To Introduce Mathematics Concepts To Young Children 375
Patricia Bentley

Exploring Some of the Mathematical Properties of Chains 379
Eva Knoll and Tara Taylor

Bridges 09 Interactive Workshop: The Geometry of Longsword and Rapper Sword Locks 383
Susan Gerofsky

The Beautiful Triangle 385
Greg Beiles and Daphne Rosenwald

Perspectives on Perspective 389
Duncan Melville and Sarah Melville

Workshop on The Fusion Project: Bridging Art Museums and Middle School Math Teachers 395
Benjamin Wells and Philip Wagner

A Workshop to Build Three Simple Tensegrity Models for K-12 Mathematics Classrooms 403
Robert McDermott

Transferring Patterns: From Twill to Peyote Stitch 409
Eva Knoll

Author Index 413

Preface

2009 marks the 12th year of the annual Bridges Conference. This year we find ourselves returning to The Banff Centre, a wonderful facility nestled in the Canadian Rockies. It's hard to imagine a location better suited to the spirit of Bridges. The region inspires with its natural beauty. The campus itself has a longstanding reputation as a world leader in art, media and culture, and a tradition of interdisciplinary cooperation. Over the past decade, the Banff International Research Station (BIRS) has grown to become a focal point for mathematical interaction within North America and worldwide, and has made The Banff Centre an ideal place to explore ideas that lie in the intersection of art and mathematics. We are honoured and thrilled that BIRS has invited us back to Banff for Bridges 2009. and hope to make the trip again many times in the future.

As always, we make an effort to bring new and exciting experiences to Bridges. This year we will explore sights around the Banff region as well as some of the studios and facilities on campus at The Banff Centre. Three evenings will be dedicated variously to music, theatre, and film.

Like last year, we collected regular paper, short paper, and workshop submissions using EasyChair, a free conference management service hosted by the University of Manchester. Each submission was then assigned to two members of our international Program Committee for review. In some cases one or more additional reviews were provided by other Program Committee members or by external experts. The quality of the reviewing was quite high, with many reviewers providing fine-grained, detailed advice for improving a paper's content or presentation. In several cases authors wrote back to express their gratitude to the reviewers who helped improve their papers significantly.

Once the reviewing process was complete, Craig S. Kaplan, the chair of the Program Committee, worked with the reviewers and the Bridges organizers to arrive at a decision for each paper. Occasionally the decision process called for additional opinions or communication with the authors. Submissions of all kinds were either accepted as-is, accepted with revisions, or rejected. In addition, some regular paper and workshop submissions were recommended for inclusion in the short papers program. In the end, we arrived at a total of 38 regular papers (including four contributed papers from invited speakers), 24 short papers (including one contributed paper), and 11 workshops. These papers represent a wide range of multidisciplinary work in mathematics, art, culture and pedagogy, from an equally diverse group of authors from around the world. We are certain to have another stimulating week of inspiration and dialogue.

The Bridges Visual Art Exhibition is always a highlight of the conference. Robert Fathauer, the curator, collected submissions. He then assembled a Jury that decided on the works to include in the exhibition. This year we will feature the work of 40 artists working in a variety of visual media. One design by Brian Evans was chosen as the cover image for the Proceedings. The cover was expertly designed by Jeff Rutzky.

In organizing and producing a Bridges Conference, the Bridges Organization relies on the concerted volunteer efforts and general goodwill of a large number of people. The members of the board of the non-profit Bridges Organization work on aspects of conference planning and management throughout the year. Robert Fathauer has worked tirelessly to run the Art Exhibition, as well as hosting the registration website. Mara Alagic and Paul Gailiunas oversee the workshops. This year we received dedicated support and participation from Kameko Higa, Mary Hofstetter, Barry Schiffman and Kerry Staufer at The Banff Centre, and Danny Fan, Wynne Fong, Nassif Ghoussoub and Brenda Williams at BIRS. Who else do we want to thank? Anybody in the list above who doesn't need to be included? To these people we offer our sincere gratitude. They have helped make the conference an event that many of us look forward to all year.

Most of all, we would like to thank everyone who has made the trip to Banff to participate in this year's conference. We look forward to talking to you, seeing your work, exchanging ideas with you, and building one more bridge to another source of inspiration.

The Bridges Organization Board of Directors
http://www.BridgesMathArt.org

Mathematics Is Art

Erik D. Demaine Martin L. Demaine
Computer Science and Artificial Intelligence Laboratory
Massachusetts Institute of Technology
32 Vassar St.
Cambridge, MA 02139, USA
E-mail: {edemaine,mdemaine}@mit.edu

Abstract

This paper gives a few personal examples of how our mathematics and art have inspired and interacted with each other. We posit that pursuing both the mathematical and artistic angles of any problem is both more productive and more fun, leading to new interdisciplinary collaborations.

Introduction

We come from two different backgrounds: Marty's first love was visual arts, while Erik's was mathematics. Over the years, we have learned extensively from each other, and worked collaboratively in both fields. Lately we have found the two fields to be converging more and more in our minds. No longer do we have separate art projects and mathematics projects: many of our projects have both artistic and mathematical angles, and we pursue both.

We find this approach to have several advantages. First, the art and mathematics inspire each other: building sculpture inspires new insights into the mathematics, and mathematical understanding inspires new sculpture. Second, it is harder to get stuck: if the mathematics becomes too difficult to solve, we can switch to illustrating the difficulty visually, and if a sculpture becomes too difficult to build, we can switch to developing a basic mathematical understanding of the structure to be built.

This paper gives a few personal examples of our projects that span both mathematics and art, and how we switched back and forth between the two fields. The first main example, pleated origami, has led to strong sculpture as well as interesting mathematics. The second main example, hinged dissections, has led to strong mathematics as well as interesting design. Both stories span a period of around ten years, with many small steps along the way in both art and mathematics.

Pleated Origami

Our first adventure in mathematical sculpture [7] appeared back at the second BRIDGES (1999), in a paper with Anna Lubiw (then our advisor). We were fascinated by a known geometric origami model, the "pleated hyperbolic paraboloid" or *hypar* shown in Figure 1. The folder makes a simple crease pattern—concentric squares and diagonals alternating mountain and valley—and then the model almost folds itself into a striking saddle surface. To turn these basic forms into more intricate structures, we designed an algorithm for generating sculptures composed of several hypars, automatically determined from a given input polyhedron. Figure 2 shows one example, which the algorithm produces when given a cube as input. Thus our study of

pleating began in the artistic context, using mathematics (specifically algorithms) as a tool to design new sculpture.

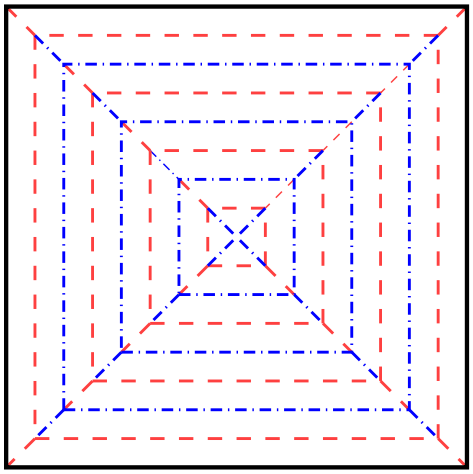

(a) *Hypar crease pattern.*

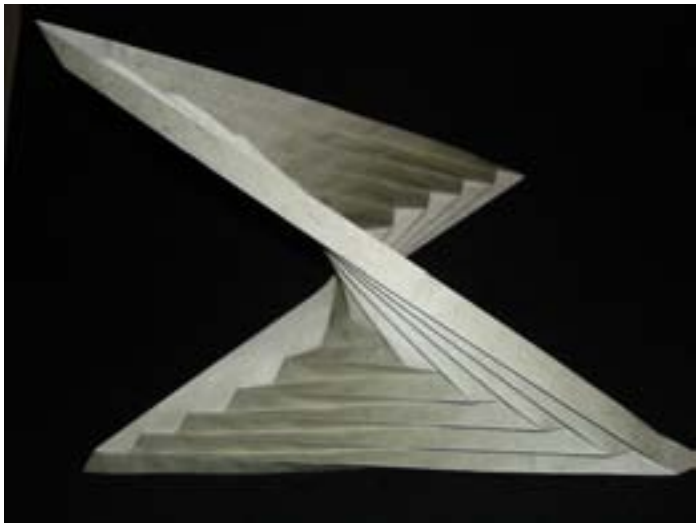

(b) *Folded hypar. [Photo by Jenna Fizel.]*

Figure 1: *Pleated hyperbolic paraboloid (hypar).*

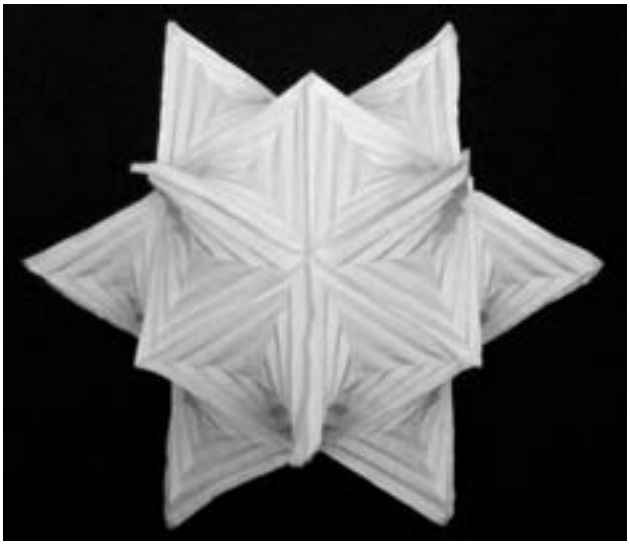

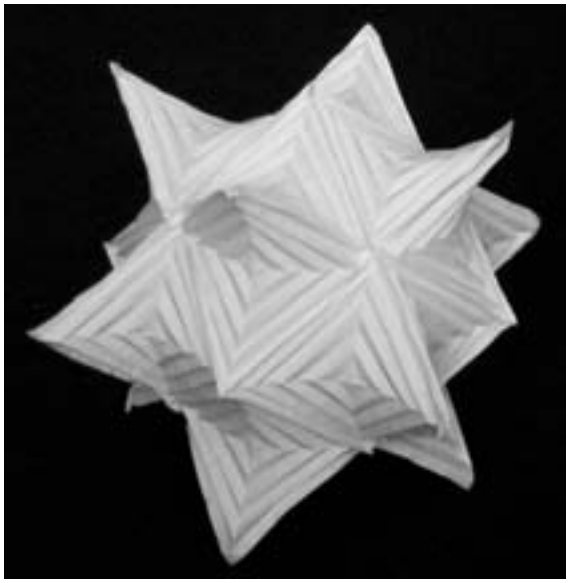

Figure 2: $24 = 6 \cdot 4$ *hypars arranged in the structure of a cube [7].*

Still intrigued by the self-folding nature of the hypar, in 2004–2006 we explored computer simulation of the material properties of paper. With Jenna Fizel (then an architecture student at MIT) and John Ochsendorf (an architecture professor at MIT), we succeeded in reproducing the physical form of hypars using a computer simulation, as shown in Figure 3. This simulation captures just two aspects of paper: the usual mathematical restriction that paper cannot stretch, and a physical property not studied in origami mathematics, the material elasticity of paper. The latter property is that paper tries to reach its memory

state—flat for uncreased paper, and a particular fold angle at creases (depending on how hard the crease was made)—and searches for an equilibrium among these forces. This elasticity is the driving force that makes the hypar naturally take its saddle shape. Our simulation could even capture composite forms such as the 24-hypar representation of the cube, as shown on the right of Figure 3.

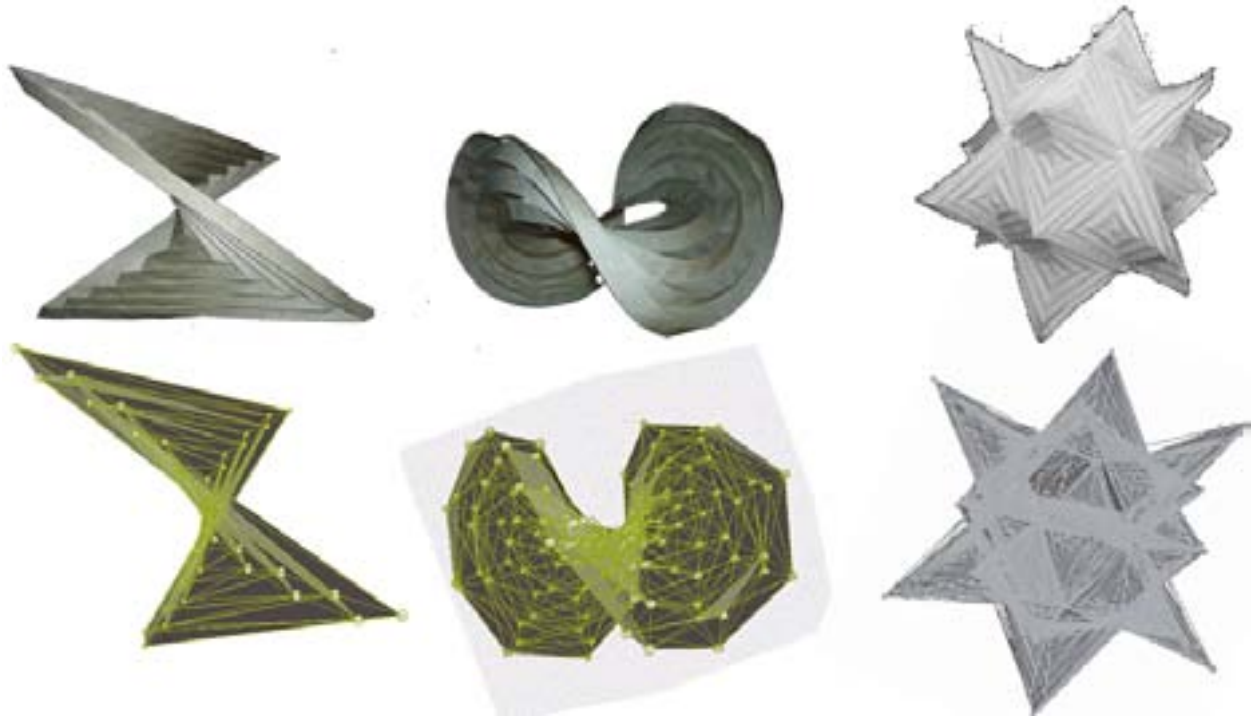

Figure 3: *Simulating self-folding origami. Top: Physical models of paper. Bottom: Analogous simulated models. Left to right: square, circle, and "cube" from Figure 2.*

Thus we turned to mathematics and science to better understand the artistic forms that we were working with. Armed with a computational tool for simulating these forms, we returned to the sculpture side, this time with the goal of illustrating that we can virtually simulate paper folding. Together with Jenna Fizel, we built the sculpture shown in Figure 4, which is a physical realization of a virtual simulation of a physical piece of paper, namely, a hexagon pleated with concentric hexagons and diagonals. This sculpture consists of aluminum rods, representing the creases of the form, and balls that are 3D printed to have holes at the angles found by our simulation. Approximately 1 meter in diameter, we view this construction as a model for a larger, climbable lawn sculpture.

Recently we discovered two surprising facts about the hypar origami model. First, the first appearance of the model is much older than we thought, appearing at the Bauhaus in the late 1920s [2]. Second, together with Vi Hart, Greg Price, and Tomohiro Tachi, we proved that the hypar does not actually exist [5]: it is impossible to fold a piece of paper using exactly the crease pattern of concentric squares plus diagonals (without stretching the paper). This discovery was particularly surprising given our extensive experience actually folding hypars. We had noticed that the paper tends to wrinkle slightly, but we assumed that was from imprecise folding, not a fundamental limitation of mathematical paper. It had also been unresolved mathematically whether a hypar really approximates a hyperbolic paraboloid (as its name suggests). Our result shows one reason why the shape was difficult to analyze for so long: it does not even exist!

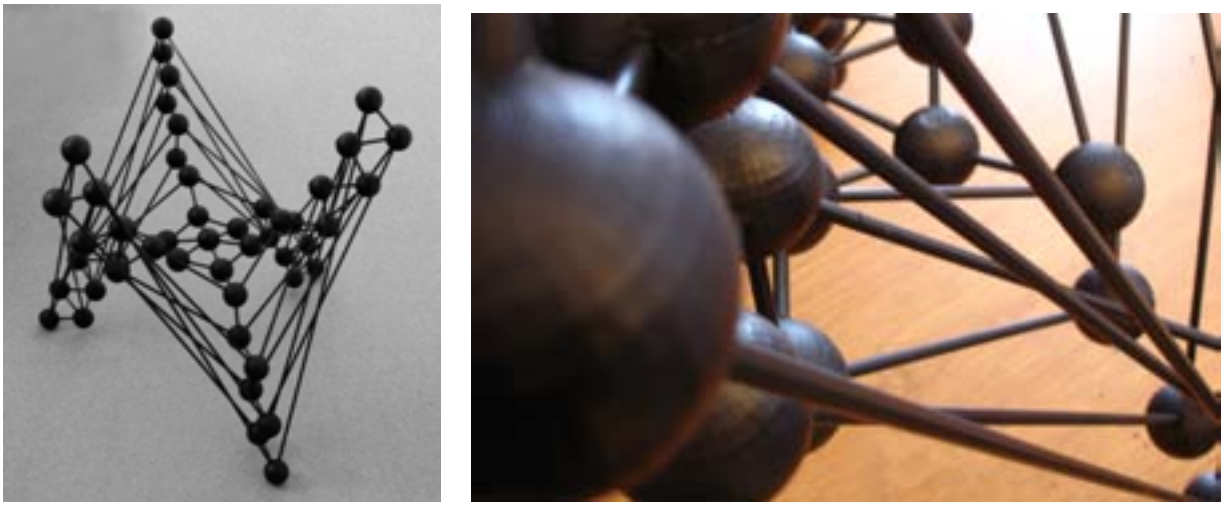

Figure 4: *Physical sculpture built from hexagonal hypar simulation.*

Curved Creases

Our adventure with pleated origami continued in the context of curved creases. Most origami uses straight creases, and in contrast to this origami, relatively little is known about curved creases and how they behave. A simple variation of the hypar, already shown in the middle of Figure 3, folds concentric circles instead of squares, this time with no diagonals but with a circular hole cut out of the center. This model also goes back to the Bauhaus in the late 1920s [2].

We have been experimenting with variations of this circular hypar for several years, as it naturally extends the hypar. On the mathematical side, the curved creases seem to behave quite differently from the straight creases of the hypar, as the resulting origami seems to actually exist [5]. A natural goal is curved-crease origami design: can we harness the power of these self-folding curved-crease forms to fold into desired 3D surfaces? How can we control the equilibrium form, and what (approximate) surfaces are even possible?

This mathematical challenge seems quite difficult, so we have so far focused this chapter of our adventure into the artistic realm. By experimenting with new forms and the effects of small variations, we simultaneously encounter new sculpture and get a better handle on how these forms behave mathematically. We hope one day to have a complete understanding of how to control the equilibrium form through a pleated crease pattern.

Our first main series, shown in Figure 5, is in the permanent collection of the Museum of Modern Art (MoMA) in New York. These pieces make one primary change to the circular hypar: they use a "circle" of total angle more than 360°. Given the hole in the center, the piece of paper is effectively a circular ramp that goes around two or three full circles before attaching to its starting point. Physically, such paper is formed by joining together multiple circles into one big cycle (without a topological Möbius twist). We find that this change to the paper drastically increases the geometric twist caused by the curved creases, and small variations can produce surprisingly different forms.

The MoMA pieces are initially scored with a laser cutter, then folded by hand. In 2009, we designed a new series folded entirely by hand for an exhibit at Art Cézar in Belgium. Figure 6 shows a few examples.

Figure 5: *"Computational Origami" (2008), in the permanent collection and on display at MoMA. Each of the three pieces is roughly 15 inches in diameter.*

Another way to vary the concentric pleating idea uses flat paper but noncircular curves. We started exploring some of these variations in 2003 with abhi shelat (then an MIT PhD student in computer science), including ellipses and partial circles. Most recently, with Duks Koschitz (an MIT PhD student in architecture), we have explored a wide variety of curves with different offset patterns [10]; see Figure 7 for two examples. Our primary mathematical goal is to understand what pleating "works" (produces an interesting 3D form). Along the way, we find interesting sculptural forms.

We are also interested in finding other materials that fold in a way similar to paper, with the motivation of making larger and/or stronger structures. Such materials would be useful for larger sculpture as well as more practical applications like furniture, buildings, and other large-scale constructions. One promising alternative is metal, which is difficult to fold, especially manually, but can produce striking results when successful.

Figure 6: *"Waves" (2009), exhibited at Art Cézar in Belgium. Each of the three pieces is roughly 15 inches in diameter. In reading order: Inner Wave, Splash, and Three Waves Meeting.*

Hinged Dissections

A hinged dissection is a chain of polygonal pieces, hinged together at vertices, that can fold into multiple desired polygons. Perhaps the most famous example, shown in Figure 8, is Dudeney's hinged dissection of an equilateral triangle into a square. Hinged dissections have been thoroughly studied and designed [9], but until recently lacked a general theory. In particular, the major open question that intrigued us was whether hinged dissections exist for any two polygons of the same area.

We started exploring hinged dissections from the mathematical perspective in 1999 [4]. Initially inspired by a web discussion between David Eppstein and Erich Friedman, together we found hinged dissections for "polyforms": shapes made out of n copies of a common shape. The most popular example of polyforms is polyominoes, of Tetris fame, made up of n copies of a unit square joined edge to edge. Our result shows that one hinged dissection can fold into all (exponentially many) polyforms for any desired base shape (squares, equilateral triangles, right isosceles triangles, hexagons, etc.) and any desired value of n. The hinged dissection is also quite simple, dividing each copy of the base shape into a few pieces.

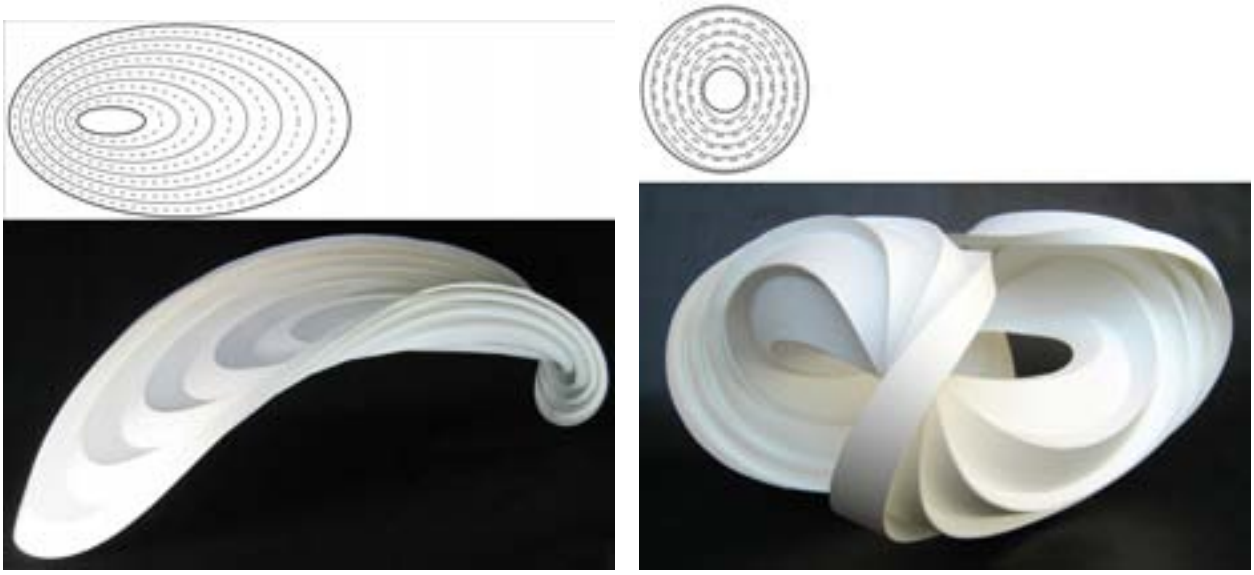

Figure 7: *Two curved-crease models from [10]. Top: Crease patterns. Bottom: Folded models.*

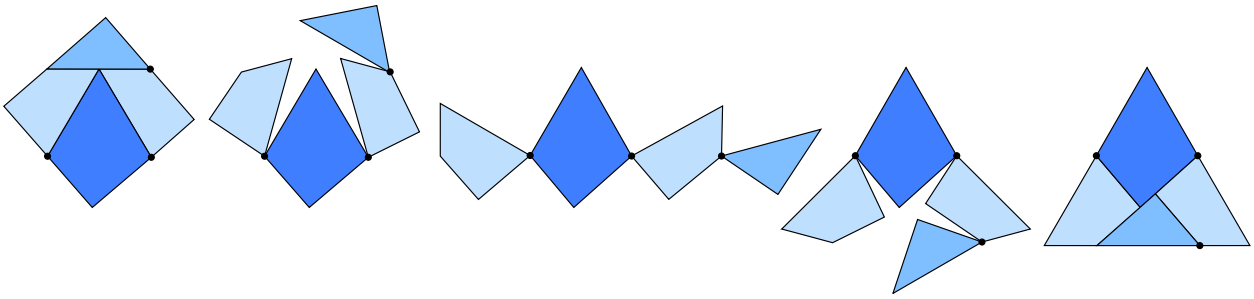

Figure 8: *Dudeney's hinged dissection from 1902.*

Later, Greg Frederickson joined in, and we found that one hinged dissection could fold into polyforms with different base shapes, such as both squares and triangles, by incorporating a hinged dissection similar to Figure 8.

Next we turned to the artistic side, this time in the context of design. On the one hand, we wanted to illustrate the generality of the mathematical result: one hinged dissection could fold into many many shapes. On the other hand, we have always been fascinated by font design. We combined these two desires by designing a font [3], shown in Figure 9, with the property that one hinged dissection can fold into every letter and digit of the font as well as a square. To achieve this property, we needed every letter and digit to have the same area and to be a polyform, in this case with the base shape a right isosceles triangle. The smallest interesting size for the square seemed to be 4×4, resulting in $32 = 4 \cdot 4 \cdot 2$ copies of the base shape and $128 = 32 \cdot 4$ pieces in the hinged dissection.

Returning to mathematics, we found that the hinged-dissection technique of [4] could be applied even more generally. Together with Jeff Lindy and Diane Souvaine, we proved that one hinged dissection could fold into all 3D polyforms, or "polypolyhedra", where the base shape is now a polyhedron such as a cube [6].

While writing down this result, we were contacted by Laurie Palmer, a professor in sculpture from the

(a) *Alphabet designed to have a hinged dissection.*

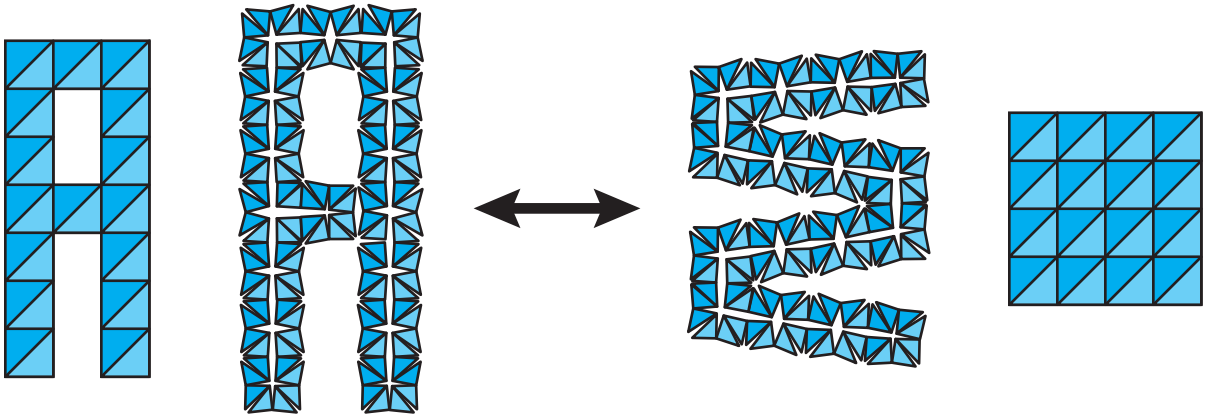

(b) *Shaping the hinged dissection into the letter A and the square.*

Figure 9: *Hinged dissection of the alphabet [3].*

School of the Art Institute of Chicago who was then a Radcliffe Institute Fellow. She wanted to build an interactive sculpture that the viewer could fundamentally change in shape, from a one-dimensional line to a two-dimensional plane to a three-dimensional solid. She already had around 1,000 identical wooden blocks and piano hinges for connecting them together. The striking similarity to the paper we were working on at that moment was a pleasant surprise. We noticed that the hinged dissection for the base shape of a cube generalized to any parallelepiped, in particular her rectangular blocks. We described the (regular) pattern in which she had to hinge the blocks in order to guarantee universal folding, and she built the installation, *The Helium Stockpile*, which exhibited at Radcliffe in April 2004; see Figure 10. Excited about our experience with the collaboration, we wrote a paper together about it [8].

Back to the mathematical realm, last year we finally conquered the general hinged-dissection problem, proving that hinged dissections exist for any desired set of polygons of equal area [1]. The solution required key new insights made by four students: Timothy Abbott (MIT), Zachary Abel (Harvard), David Charlton

Figure 10: *Laurie Palmer's The Helium Stockpile, April 2004 [8].*

(Boston University), and Scott Kominers (Harvard). After nearly ten years of pursuing this problem from artistic and mathematical angles, it is exciting to see the main mathematical problem finally answered. Of course, now the challenge is to design interesting art using the mathematical theory.

Glass

Marty's first artistic endeavor was glass blowing, and returning to those roots, both authors are now active glass blowers at MIT. A recent project with Amy Nichols (MIT glass blower and PhD student in biological engineering) combines our interests in folding and hot glass by attempting to fold glass. A unique property of hot glass is that we cannot touch it (being at around 1400°F), which requires a fundamental shift from the usual approach to folding origami. We chose to embrace the use of gravity as a primary force in glass blowing. To help gravity fold the glass in interesting ways, we fused the initial piece of glass from two chemical mixtures—stiff white glass and soft black glass—and built a simple annealing chamber providing obstacles during the folding process. After this setup, the folding was done entirely by gravity. Figure 11 shows our first sculpture made by this approach, which we hope will lead to many more interesting forms.

References

[1] Timothy G. Abbott, Zachary Abel, David Charlton, Erik D. Demaine, Martin L. Demaine, and Scott D. Kominers. Hinged dissections exist. In *Proceedings of the 24th Annual ACM Symposium on Computational Geometry (SoCG 2008)*, pages 110–119, College Park, Maryland, June 9–11 2008.

[2] Erik Demaine and Martin Demaine. History of curved origami sculpture. http://erikdemaine.org/curved/history/.

[3] Erik D. Demaine and Martin L. Demaine. Hinged dissection of the alphabet. *Journal of Recreational Mathematics*, 31(3):204–207, 2003.

[4] Erik D. Demaine, Martin L. Demaine, David Eppstein, Greg N. Frederickson, and Erich Friedman. Hinged dissection of polyominoes and polyforms. *Computational Geometry: Theory and Applications*, 31(3):237–262, June 2005.

[5] Erik D. Demaine, Martin L. Demaine, Vi Hart, Gregory N. Price, and Tomohiro Tachi. How paper folds between creases. Manuscript, 2009.

Figure 11: *A folded glass sculpture.*

[6] Erik D. Demaine, Martin L. Demaine, Jeffrey F. Lindy, and Diane L. Souvaine. Hinged dissection of polypolyhedra. In *Proceedings of the 9th Workshop on Algorithms and Data Structures*, volume 3608 of *Lecture Notes in Computer Science*, pages 205–217, Waterloo, Canada, August 2005.

[7] Erik D. Demaine, Martin L. Demaine, and Anna Lubiw. Polyhedral sculptures with hyperbolic paraboloids. In *Proceedings of the 2nd Annual Conference of BRIDGES: Mathematical Connections in Art, Music, and Science*, pages 91–100, Winfield, Kansas, 1999.

[8] Erik D. Demaine, Martin L. Demaine, and A. Laurie Palmer. The helium stockpile: A collaboration in mathematical folding sculpture. *Leonardo*, 39(3):233–235, June 2006.

[9] Greg N. Frederickson. *Hinged Dissections: Swinging & Twisting*. Cambridge University Press, August 2002.

[10] Duks Koschitz, Erik D. Demaine, and Martin L. Demaine. Curved crease origami. In *Abstracts from Advances in Architectural Geometry (AAG 2008)*, pages 29–32, Vienna, Austria, September 2008.

Mathematical Methods in Origami Design

Robert J. Lang
Langorigami.com
Alamo, California, USA
robert@langorigami.com
http://www.langorigami.com

Abstract

The marriage of art and mathematics has been widespread and productive, but almost nowhere more productive than in the world of origami. In this paper I will discuss how mathematical ideas led to the development of powerful tools for origami design and will present a step-by-step illustration of the design and realization of a representational origami figure using mathematical design algorithms. Along the way, I will discuss how these mathematical concepts have led to new levels of creative expression within this art.

1 Introduction

The marriage of art and mathematics has been fruitful and productive. Mathematical concepts inspire, enable, and enrich artistic forms, and in many cases, mathematical concepts lead to entirely new expressions, visual, auditory, and conceptual, outside of the traditional milieu of art. It is relatively rare, though, that mathematical ideas have led to a revolution within an existing art—that is, enabling artists to do what they wanted to do within their art, but were previously unable to accomplish. That exact thing is what has happened within the art of *origami*, the Japanese art of paper-folding (usually from an uncut square), over the last twenty years or so. Beginning in the late 1970s and early 1980s, and accelerating more-or-less continuously since then, mathematical design techniques have become essential elements of the origami designers' toolkit, allowing the creation of works only dreamed of in the past, enabling newer, richer, more diverse forms of artistic expression.

Now, while it is tempting to present the world of mathematical origami design as a simple, linear thread of development, in fact there were roots stretching back into the 1950s and 1960s and several different approaches to mathematical design in the 1970s and 1980s investigated by origami artists such as Peter Engel, Jun Maekawa, and Fumiaki Kawahata, among others. But I will talk about the approach I am personally most familiar with, and with which I was closely involved in the development of: circle-river packing. This was, I believe, the first systematic design method that could be used to create and design arbitrarily complicated origami structures.

As often happens in mathematics, when the time is ripe, the same ideas can occur to multiple people, and this was the case with circle-river packing: I (in the US) [1, 3, 4, 6] and Toshiyuki Meguro (in Japan) [10, 9] both developed the concept of circle packing in the late 1980s and then met and compared notes and ideas beginning in 1992, finding surprising overlap between our approaches and sharing ideas in the years that followed. (Shades of Newton and Leibniz, with two differences: Meguro and I got on quite well, and we're only talking about paper-folding, not calculus!) In the years following our meeting, we both traded and refined our concepts and were joined by others who built on and expanded the basic ideas into a regular suite of design algorithms. (I should mention specifically that in recent years I have greatly enjoyed collaborating with Professor Erik Demaine of MIT on the development of improved algorithms and expanding their underlying rigor.)

Fundamental to my own motivation was the goal of developing truly useful techniques for design, and for several years I designed ever more complex origami figures using circles and spacers (the latter were my precursors to "rivers," see below) and nothing more technological than pencil and paper. (My colleague Meguro added compass and straightedge to his crease pattern design arsenal.) However, a paradigm that framed my ideas early on was the idea that it might eventually be possible to use computer programming to solve for complex origami figures, and I began sketching out algorithms for this in the late 1980s. (Early discovery: FORTRAN 77 is a lousy language for computational origami.) Beginning in the 1990s, I began writing what became my program *TreeMaker* (in Object Pascal, then C++), a design program that served both as a repository of algorithms as I developed them and a way to probe their validity and limits [8]. By 1998, *TreeMaker* was up to version 4.0, and had become a useful tool rather than just a toy program; in fact, I realized that it was now capable of solving for origami design patterns that were beyond the ability of an individual armed with only pencil, paper, and compass.

Which is not to say that pencil-and-paper origami designers have not been creating designs as complex as those that *TreeMaker* could create; on the contrary, by recognizing fortuitious geometric alignments and patterns, origami artists could, and still do, design with pencil and paper extremely complex and beautiful works. The most complex origami designs today are usually human-designed, not computer-designed. While its crease pattern may be drawn on computer, advanced origami is designed using a mixture of mathematical ideas and artistic inspiration, with the designer's own imagination the most important tool.

Still, a computerized design serves a useful pedagogical purpose: it provides a vivid illustration of the power of mathematical ideas in achieving a distinctly non-mathematical result. And so, in the bulk of this paper, I would like to walk the reader through the process of concept, design, and folding, for an origami figure: an arthropod. The greatest successes of the circle-river method of design came in the design of insects, spiders, and their ilk, and so I will present here one of my first *TreeMaker* designs: my "Scorpion, opus 379" [5]. Although I have designed more complex figures since then, this remains one of my favorites, both for the geometric structure of its design and its overall appearance.

2 Design

The journey begins with the subject and its abstract description: a tree graph (the "tree" in *TreeMaker*). Or, more prosaically, a "stick figure." The stick figure captures the information that will be produced by the design algorithm, and so its properties—the number, lengths, and connectivities of its edges—are the choice of the designer. The circle-river method of origami design is a step in the creation of a folded figure, but it does not seek to create a specific 3-D form; rather, it produces a shape that has "enough material in the right places." Specifically, it produces a folded shape that has a flap of paper for every appendage of the subject. The algorithm gives relatively little control over the width of those flaps, but it lets one specify the number of flaps, length of each flap, and how they are connected to one another, and for some subjects, that is very useful indeed. That information can be described concisely by a stick figure—which, using the terminology of graph theory, is an "edge-weighted tree graph." Hence, the tree is the starting point for a *TreeMaker* design.

The simplest way to construct the tree is to literally overlay the stick figure on a photograph of the subject, as illustrated in Figure 1. Each stick represents an appendage or body segment of the subject, and will be represented in the origami figure by a flap of paper. The folded shape will be a collection of flaps; we call this collection a "base." Each edge of the tree graph must be assigned a length, which will be the length of the associated flap of paper. By measuring lengths of the various body parts in the photograph, one can choose the desired lengths of the flaps, although it must be noted that one might commonly adjust desired flap lengths from their literal dimensions for artistic reasons.

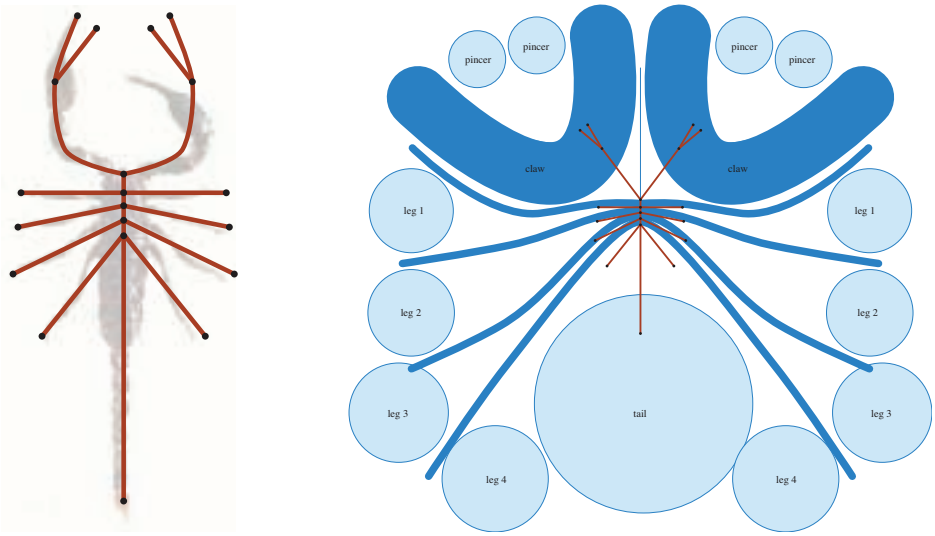

Figure 1 : *Left: the stick figure superimposed over a photograph of the subject. Right: representation of the stick figure by circles and rivers.*

We then transform the stick figure into geometric shapes that represent regions of the paper required by each flap. These shapes are the light and dark regions in the figure. Flaps that are loose at one end, like the legs or pincers, are represented by circles (light), whose radius is equal to the length of the flap. Flaps that are connected to other flaps at both ends, like the body segments or the "arms," are represented by constant-width curves called "rivers" (dark); the width of the river is equal to the length of the corresponding flap. Each geometric shape—circle or river—represents the *minimum* amount of paper required for each of the flaps. It is a remarkable fact that for any valid arrangement of circles and rivers that specify the minimum paper needed, there exists a crease pattern that works for that exact arrangement of circles and rivers.

And so, we must find the most tightly packed arrangement of the circles and rivers within a square. The major rules that apply to this packing are:

- the circles and rivers must be as large as possible but maintain their same relative size to one another;
- they may not overlap;
- the circles do not have to be wholly inside the square, but their centers must be within the square;
- the incidences between the various circles and rivers must match the incidences of their corresponding edges in the tree graph.

The larger the origami base is for a given size square, the more efficient it is; the fewer the layers in each flap; and, generally, the easier it is to fold. And so the first stage of origami design consists of an optimization: finding the most efficient packing of the circles and rivers. This can be done by hand (and it often is), but for this particular design, it is much faster to use *TreeMaker*, which has a nonlinear constrained optimization solver built in. (In the late 1990s, this process took seconds to minutes; with the 1000-fold increase in computing speed, it is now virtually instanteous.) To use *TreeMaker*, we start by drawing the stick figure, as shown in Figure 2 and then typing in the desired lengths of each flap, shown as decimal numbers next to the lines of the stick figure.

The next step is to find the optimum packing of circles and rivers so that all of the circle centers wind up inside the square. *TreeMaker* does this in a fraction of a second, giving the circle arrangement shown in Figure 2. (The rivers are not displayed by *TreeMaker*, but the reader can perhaps imagine them winding

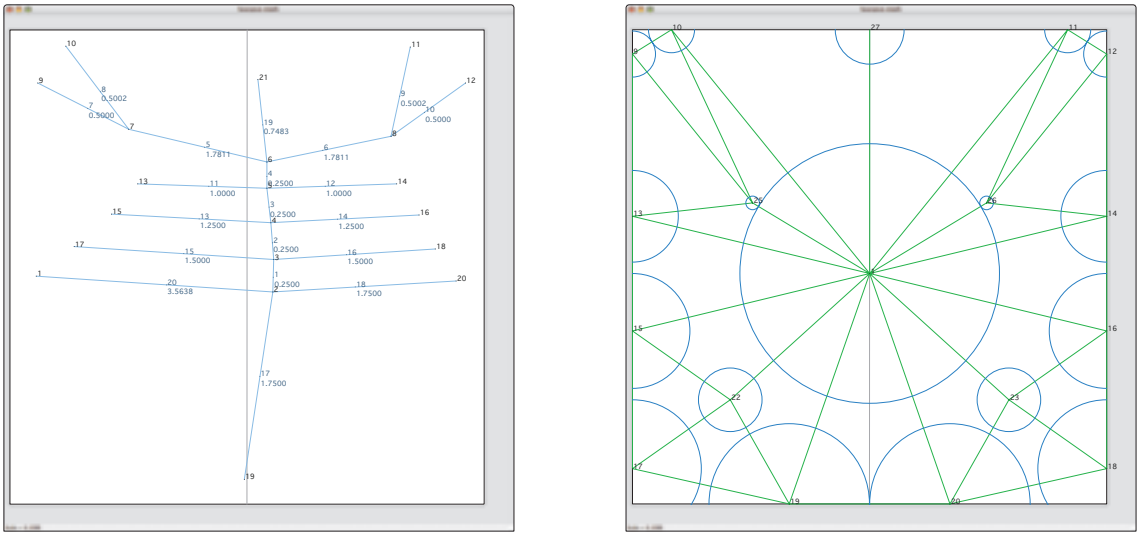

Figure 2: *Left: the stick figure as drawn within* TreeMaker. *Right: Result of the optimization (only circles are shown).*

between the circles.) Whenever two circles and the intervening rivers all touch one another, *TreeMaker* draws a line between the circle centers, shown here in green. These lines are actually some of the creases of the desired folded shape; they form a "skeleton" of the full crease pattern.

Conceptually, one finds the optimum packing by inflating all of the circles and rivers at the same rate with the circle centers trapped within the boundaries of the square and allowing the circles and rivers to move around during the inflation process until they are all wedged into position. This is, effectively, a nonlinear constrained optimization problem, and, stripped of the visual imagery of circles, rivers, and packing, it all boils down to a fairly straightforward algebraic description, which is what is needed for a computer implementation.

We assume that the tree graph can be described by a set of nodes $\{N_i\}$, edges $\{E_j\}$, and edge weights w_j, where the weight w_j gives the desired relative length of the jth flap of the desired base. For every path between two nodes $\{N_i, N_j\}$ we define the *path length* $l_{ij} \equiv \sum_k w_k$ as the (unique) sum of the weights of the edges between nodes N_i and N_j.

With every *leaf node* N_i of the tree graph, we associate a *vertex* $V_i = (x_i, y_i)$, which will be the center of the associated circle (and will also turn out to be the point in the square that maps to the tip of the corresponding flap). We further introduce the *scale factor* m, which sets the size of the folded shape relative to the original tree graph, so that if an edge of the tree graph had desired length w_j, its corresponding flap in the folded form will have actual length mw_j. The non-overlap condition can be expressed as an inequality:

$$|V_i - V_j| \geq m l_{ij}, \tag{1}$$

for every path l_{ij}. The requirement that circle centers lie within the square is similarly expressible as inequalities:

$$0 \leq x_i \leq 1, 0 \leq y_i \leq 1, \tag{2}$$

for every vertex V_i. For ease of foldability, one would like the folded form as large as possible relative to the size of the square; in other words, we should like m to be as large as possible. The solution of the origami optimization problem then becomes a case of maximizing the scale m subject to both sets of inequality constraints. And so, the solution of the arrangement of vertices requires the solution of a nonlinear constrained optimization, with linear and quadratic inequality constraints and a nonconvex feasible region.

A nice feature of this framework is that it is relatively easy to incorporate additional requirements into the basic optimization; for example, one can impose mirror symmetry on the crease pattern by adding additional equality constraints on the coordinates of the affected vertex pairs.

This type of constrained optimization is one that has been studied for decades within computer science. In my first few implementations of *TreeMaker*, I wrote my own constrained optimizer using the Augmented Lagrangian method [11]. On a 68K-based Macintosh (with no floating-point coprocessor), this took several minutes to converge to a solution, and so to make the wait more tolerable, I wrote code that updated the screen after each iteration, so I could watch the circles jostle around and expand, which offered entertainment value, if nothing else. For *TreeMaker 4*, I replaced it with a Feasible Sequential Quadratic Programming (FSQP) algorithm developed by Andre Tits at the University of Maryland [12], which turned out to be about a hundred times faster than my relatively crude code, but it also occasionally sent the evolving solution off into distant corners of feasible solution space—a behavior I was willing to tolerate, given the incredibly improved speed.

But there was another factor at work at the same time; throughout the 1990s, the most effective way to speed up code is often "wait for a faster processor." From the floating-point-in-software 68K Mac to current Intel processors, floating-point processing sped up by a factor of about a thousand, and so for *TreeMaker 5*, I went back to my hand-rolled ALM code, which was slow, but numerically efficient (and could be made open-source). On a modern PC, even this far-from-optimum code still converges almost instantaneously to a high-quality local optimum. Which is not necessarily the global optimum. Artistically, this is a good behavior: it lets the artist find several candidate arrangements by starting from different initial positions, and then choosing the local optimum that best fits other aesthetic criteria.

Whatever algorithm is used, at the end of the optimization, one has the positions of the vertices V_i and the scale factor m. That is sufficient to construct the circle centered on each vertex, as shown in Figure 2 (right). When two circles and all intervening rivers touch, it is an indication that the associated inequality constraint is, in fact, an equality. In the language of constrained optimization, that constraint is said to be *active*, and so we say that the path between the two nodes is *active* as well. It turns out that active paths always correspond to crease lines in the crease pattern associated with a circle packing. These creases turn out to lie along the axis of the folded shape, and so we also call them *axial paths*. They form the framework upon which the rest of the crease pattern is constructed.

3 The Creases

Once we have found the axial paths, it is possible to mathematically construct all of the other folds in the desired shape (which we call a "base")—again, a process that takes a fraction of a second in *TreeMaker*, this time because no optimization is needed; the construction is a straightforward polynomial-time geometric algorithm. *TreeMaker* color-codes the creases according to their structural role: there are axial creases (green), which all wind up along the centerline of the folded model, hinge creases (blue), that run along the junctions between flaps, and ridge creases (red), that define how wide each flap is. These are shown in Figure 3. The creases outline regions of the paper, called facets; the collection of all facets and their intervening creases gives the crease pattern needed to fold the square into the origami base.

The structural information indicated by color tells the designer where in the folded form a given crease lies and provides some hint for how the folded shape goes together, but ultimately, we need to determine whether each crease is a mountain or valley fold. To do this, *TreeMaker* computes the "stacking order" of all of the layers of paper, which is encoded by a graph on the facets that defines how the layers stack. Once we know the stacking order of the layers of paper, we can determine whether each fold is a mountain fold (solid black), valley fold (dashed colored), or is unfolded, or flat (solid gray). The full crease pattern, as computed

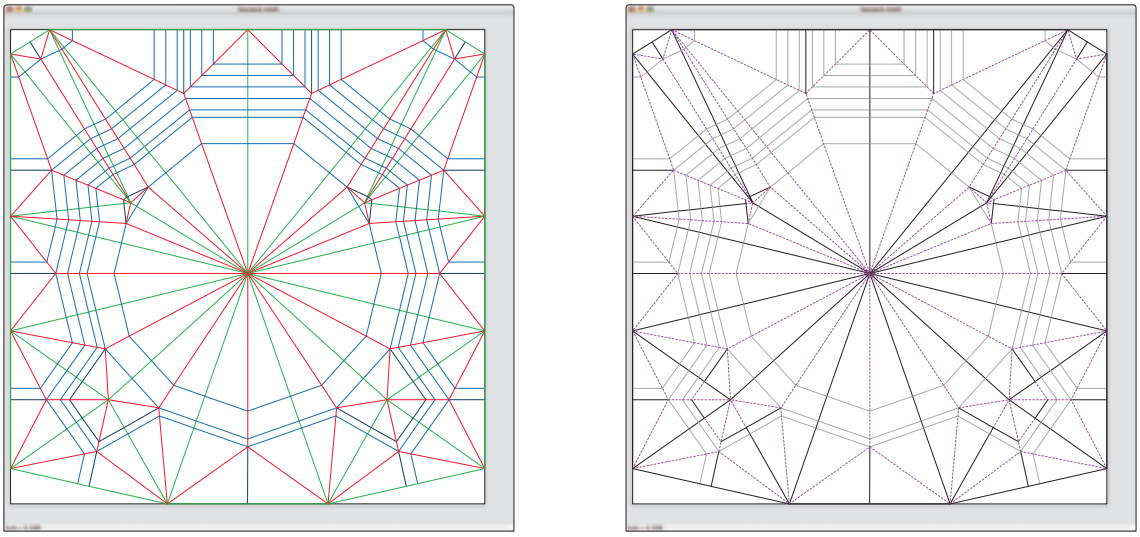

Figure 3 : *Left: The computed crease pattern with structural coloring. Right: Final crease pattern with mountain-valley assignment.*

by *TreeMaker*, is shown in Figure 3. Now, it's time to fold.

4 Folding

The design is only half the battle of creating an origami figure. Actually, it's even less than half. First, we have to fold the crease pattern into the base; then we have to turn the base into the finished form. All we are guaranteed from the algorithm is that the flaps will be of the right number, have the right length, and be connected to each other in the way we originally specified. But there are no guarantees on the flap width, cross section, arrangement of layers, or much of anything else. And at this point in the process, we don't even have a base: we just have the crease pattern for it.

And so, that's what we start with: folding the crease pattern into the base. To accomplish this, we must first transfer the crease pattern from the design to the actual square[1]. This is done by measuring the positions of a few key points, and then forming all of the other creases based on those initial measurements, as shown in Figure 4.

Most complex origami bases have the property that you can't fold them one crease at a time; instead, you must bring all of the creases together at once. That is the case here, so we bring all of the edges of the square together in a single motion. This process is called "the collapse" in origami, because we are "collapsing" the square down to the folded base, as shown in Figures 4–5.

"Collapse"-type folds had appeared in origami occasionally throughout the years, but its ubiquity in complex algorithmic designs came as something of a surprise in the origami world. Published origami designs almost always consisted of a sequence of relatively simple steps, leading smoothly from the initial square to the finished form with no individual step requiring more than three or four creases to happen at once. But complex modern designs are not like that; in fact, it is relatively rare that such a simple folding pattern exists for a complex crease-pattern-based design. Instead, they almost always require all creases to be brought together at once—a process my colleague Brian Chan has dubbed (somewhat mischeviously)

[1]The paper here is a 40 cm square of abaca/hemp paper made by Michael LaFosse, a master papermaker (`http://www.origamido.com`) and origami artist whose handmade papers are prized by origami insect folders around the world.

Figure 4 : *Left: Square with creases transferred to the paper. Right: First stage of the collapse.*

"three easy steps: precrease, collapse, shape." But in each case, the precreasing, the collapsing, and most especially, the shaping, may require several hours for each step.

In this figure, the collapse is relatively simple – only a few tens of creases are involved. (Truly advanced designs may have hundreds of creases participating in the single collapse step.) The result at the end of the collapse step is a flat form: the origami base, shown in Figure 5. It doesn't look like much—certainly, not like a scorpion—but it contains a flap of exactly the right length, connected in exactly the right way, for every leg, arm, pincer, and body segment of the desired subject.

Figure 5 : *Left: The collapse under way. Right: The fully collapsed base.*

The flaps have the right length and connectivity, but not the right width; in fact, most of them are much wider than their corresponding body part. As problems go, that's a pretty good one to have; it's a lot easier to make a fat flap narrower than to make a narrow flap wider, and with arthropods as subject matter, making flaps narrower is the usual requirement. We will need to narrow all parts of this base so that they can better represent the skinny legs, arms, and tail of the scorpion. This is done with a series of what are called "sink

folds," which are, essentially nested sets of inversions of the layers of each flap. Sink folds are tedious to perform (any origami teaching session is guaranteed to elicit a series of groans when a set of sink folds is announced), but they are conceptually straightforward to perform. Figure 6 show the base with some (left) and all (right) of its layers sunken. In the end, the folded paper shape looks not unlike the original tree graph: a collection of long, skinny, connected sticks, each of which will become an appendage of the subject.

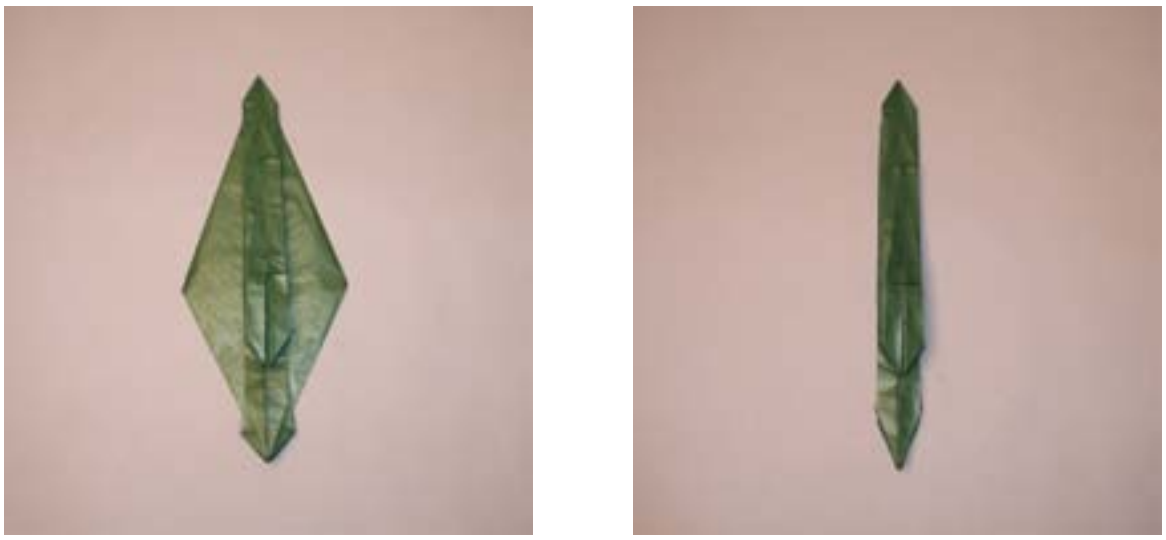

Figure 6 : *Left: The partially narrowed base. Right: The fully narrowed base.*

Last comes the shaping. There is no algorithm for this—and, in fact, this is one part of the process where both craftsmanship and artistry are preeminent in the process. A representional origami figure, no matter how realistic, is, in any absolute sense, still a rather crude approximation of the subject. The artist selects what features to emphasize and what features to minimize in order to convey the essential character of the subject. Craftsmanship is called for, too, to insure that every visible edge, every visible fold falls in the right place to convey the desired impression. A misplaced edge, an unintended wrinkle—these can spoil the visual effect, for the human eye is drawn to lines, ignores smooth surfaces. It is often the case that the shaping takes by far the greatest amount of time when creating a complex origami figure, and this process can last, literally, for days. (For this scorpion, shaping took only a few hours in total.) Figures 7–8 show the final process of shaping, beginning with narrowing of the legs, then proceeding through shaping of the tail and claws, and ending up with the final scorpion form. The narrowing and shaping of the legs is accomplished by selectively dampening flaps as they are folded, a technique called "wet-folding" that was introduced by the great 20th-century origami master Yoshizawa; strips of drafting tape hold the figure in position as it dries.

5 Final Thoughts

The early successes of circle-river packing and its relatives were most vividly seen in the subject matter of origami insects and their kin. In the 1970s, origami insects were considered the ultimate challenge, and at least one origami book flatly declared that an origami grasshopper was "impossible" from a single square. In the 1980s, grasshoppers were not only possible, but folded and then surpassed; and the 1990s saw a golden age of origami insects informally known as the "Bug Wars," in which origami creators vied with one another for the most realistic, leggiest, pointiest, wingiest, horniest creature they could find! (Entomology journals saw a noticeable uptick in their origami subscribers, as origami artists sought out the most challenging possible subjects to take on.) (See [2, 7] for some of my own contributions to this battle.)

Figure 7 : *Left: Narrowing the legs. Right: The curved tail has been folded and shaped.*

Figure 8 : *Left: Final stages of shaping. Right: The finished scorpion, approximately 15 cm long.*

To some degree, the Bug Wars are still going on, but with far more than bugs as their subject matter—complex origami subjects include other animals, plants, human figures, and indeed, purely geometric forms—and the goals of origami artists have moved well beyond "mere realism," to now address the question,"how can I create a visually interesting shape that challenges the mind and perceptions of the viewer?" Design techniques have grown as well; circle-river packing has been expanded to include techniques based on packings of polygons and other shapes, and the ranks of other algorithms for computational origami continues to grow, with contributions now coming from the academic world of computational geometry and other parts of mathematics and computer science. It is a heady time.

And yet, all of these techniques are still no more than tools in the hands of the artist. I am sometimes asked if the development of mathematical design techniques (or, heaven forbid, *computer programs*!) somehow diminishes origami as an artistic activity. To which I answer: these techniques, for all their power, are still just tools, no more than a painter's pigments, or a sculptor's chisels. The quality of the tool does not set the quality of the artwork; what matters most is what you do with those tools. But seeing what origami artists from all over the world have done in recent decades with the tools that computational origamists have given them, and an entirely new generation of conceptual and computational tools coming down the pike, I have no doubt that the future of origami as an art form will be exciting and invigorating for many years to come.

TreeMaker is open-source (GPL), runs on Macintosh OS X, Linux, and Windows computers, and may be downloaded at [8].

References

[1] Robert J. Lang. Mathematical algorithms for origami design. *Symmetry: Culture and Science*, 5(2):115–152, 1994.

[2] Robert J. Lang. *Origami Insects and their Kin*. Dover Publications, 1995.

[3] Robert J. Lang. A computational algorithm for origami design. In *12th ACM Symposium on Computational Geometry*, pages 98–105, 1996.

[4] Robert J. Lang. The tree method of origami design. In Koryo Miura, editor, *Origami Science and Art: Proceedings of the Second International Meeting of Origami Science and Scientific Origami*, pages 73–82, Ohtsu, Japan, 1997.

[5] Robert J. Lang. Scorpion, opus 379, 2002. `http://www.langorigami.com/art/gallery/gallery.php4?name=scorpion_varileg`.

[6] Robert J. Lang. *Origami Design Secrets: Mathematical Methods for an Ancient Art*. A K Peters, 2003.

[7] Robert J. Lang. *Origami Insects II*. Gallery Origami House, 2003.

[8] Robert J. Lang. TreeMaker, 2003. `http://www.langorigami.com/treemaker.htm`.

[9] Toshiyuki Meguro. Jitsuyou origami sekkeihou [practical methods of origami designs]. *Origami Tanteidan Shinbun*, 2(7–14), 1991–1992.

[10] Toshiyuki Meguro. 'Tobu Kuwagatamushi'-to Ryoikienbunshiho ['Flying Stag Beetle' and the circular area molecule method]. In *Oru*, pages 92–95. 1994.

[11] R. T. Rockafellar. Augmented Lagrangian multiplier functions and duality in nonconvex programming. *SIAM Journal on Control*, 12(2):268–285, 1974.

[12] Andre Tits. CFSQP. `http://www.aemdesign.com`.

Kircher's Mechanical Composer: A Software Implementation

Jim Bumgardner
10066 Orcas Ave
Shadow Hills, CA, 91040, USA
E-mail: jbum@jbum.com
Website: krazydad.com

Abstract

A description of a working software implementation of Athanasius Kircher's *Musurgia Mechanics*: The algorithm the Jesuit Polymath invented for non-musicians to set hymns to music, in four-part polyphonic arrangements. This algorithm was used in two related inventions of Kircher's, the *Arca Musarithmica*, and the *Organum Mathematicum*. The author has created a software program that incorporates data from both devices. This software produces files in the open-standard ABC notation, thru which one can produce printed scores and MIDI recordings of 17th century polyphony in great quantity.

Introduction to Kircher

> *The mechanical production of music is nothing other than a certain closely defined method I have invented, by which anyone, even if he has no musical knowledge, may, by the varied application of music-making instruments, compose tunes.*
>
> – Athanasius Kircher [1]

Athanasius Kircher (d. 1680) [figure 1], was a Jesuit Scholar and Polymath who achieved great renown in his lifetime, due to his prodigious output of lavishly illustrated books and his role as curator of one of the first natural history museums at the Collegio Romano. Kircher's books demonstrate his varied expertise in such diverse subjects as Linguistics, Antiquities, Speculative History, Magnetism, Optics, Mechanics, Cryptography, Astrology, Mathematics, Microbiology, Geology and Music. Among the numerous inventions attributed to Kircher are the megaphone, the magic lantern, the aeolean harp and the pantometrum (a "universal measure" for solving geometry problems). Kircher had the advantages of a relentless curiosity and a secure academic position which made him the intellectual center of the Jesuit organization, and put him on the receiving end of voluminous correspondence from distant places. It is no surprise that Kircher was described as "master of a hundred arts."[2]

Figure 1:
Athanasius Kircher

In the years after his death, Kircher began to sink into obscurity. One reason is due to the suppression of the Jesuit order by the Catholic church in the mid-18th century. Another reason is that Kircher's writings inhabit a porous region somewhere between religion and science, and freely combine speculation, intuition with his empiricist experiments in a manner that became outmoded in a society of increasingly humanist thinkers. The Rosetta Stone was another nail in Kircher's coffin, helping to demonstrate that Kircher's once celebrated "translations" of the Egyptian hieroglyphs were only delusions of a fertile but febrile imagination [3].

In recent years, Kircher's star has begun to rise again. The mixture of science, pseudo-science, truth and humbuggery which once tainted his work only serve to make him a more compelling figure in these times when specialization is the rule, and universal knowledge an unattainable dream.

Kircher the musicologist. One of Kircher's most successful and enduring works was *Musurgia Universalis*, published in two large volumes in 1650. In this encyclopedic work, Kircher described nearly everything then known about sound, audio production, sound perception, and western music at the time, borrowing heavily from such previous works as Mersenne's *Harmonie Universelle*. Diarist Samuel Pepys bought a copy in London for 35 shillings in 1668 [4]. The Pepys library at Magdalene College, Cambridge still has a curious (and surprisingly small) box that Pepys built (or commissioned) from plans in Kircher's book: an *Arca Musarithmica*. [Figure 2]

Kicher's *Arca Musarithmica* and *Organum Mathematicum*

Although much of Musurgia Universalis is derivative, Kircher's invention of a music composition algorithm was decidedly modern, anticipating the work of algorithmic music pioneers such as Lejaren Hiller and aleatoric composers like John Cage. Likely influenced by the musical combinatorics of Mersenne [5], and the mechanical inventions of Lull [6], Kircher conceived of a process by which non-musicians could compose music, by converting numbers to pitches, and combining pre-composed phrases into longer pieces.

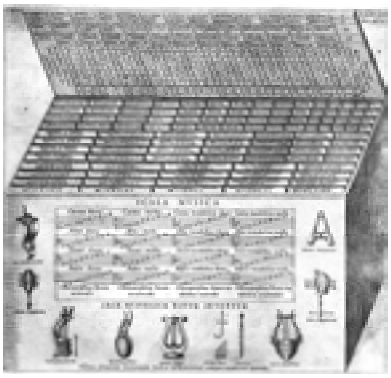

Figure 2:
Arca Musarithmica

Kircher's process was first developed for the *Arca Musarithmica*, described in *Musurgia Universalis*. The Arca was a box containing a series of *columnae* or wooden strips with *tariffa* (tables) affixed to them. The tables contained the information required for Kircher's mechanical method. The composer would pull a set of columns from the box, and string phrases in the columns together to produce a complete piece of music.

Figure 3:
Organum Mathematicum

Kircher later copied these tables and used them in a similar, but more wide-ranging invention, his *Organum Mathematicum* [figure 3], described in the book of the same name by his pupil, Kaspar Schott, and originally constructed in 1661 for the edification of a twelve-year-old archduke, Karl Joseph, son of Habsburg Emporor Leopold I. The Organum, the 17th century equivalent of a laptop computer, was also a box containing wooden strips. The strips were divided into nine sections, which were used to aid in the production of arithmetic, geometry, fortifications, calendars, gnomics, spherics, planetary movements, earthworks and finally, music [7]. The music tables in the Organum were essentially a subset of the tables designed for the Arca (give or take a few transcription errors). Two extant devices can be found in museums in Florence and Munich, respectively. It appears unlikely that any Organum saw much practical use – they were most likely used as expensive gifts and conversation pieces, intended to impress wealthy patrons and cement the Society of Jesu into the intellectual firmament.

Origins of this Project

I first encountered Kircher at the Museum of Jurassic Technology in Los Angeles, around 1999, where I read this misleading (albeit accurate in parts) caption below an illustration of the Arca:

> Arca musarithmica: a primitive mechanical computer that would compose simple random compositions, as well as write messages in cipher, calculate the date of Easter in any year, and design fortifications.

Like Kircher's writings, much of the information at the MJT (which is equal parts art exhibit and museum) can be misleading. Nonetheless, I resolved to find out as much as I could about this apparent precursor to Babbage. I was primarily interested in the musical applications of such a device, having produced my own algorithmic music compositions years ago in college. It sounded like Kircher had invented a clockwork device which composed music. I quickly found that this "primitive mechanical computer" was nothing more than a glorified recipe box. Undaunted, I became determined to produce a software implementation of Kircher's compositional method used in the *Organum*.

At the time, images of the actual tables from Kircher's Organum were hard to come by (complete copies of the relevant works are now readily available online via the Echo archive), and I had a difficult time getting access to the rare book collections at local libraries. I eventually managed to acquire some photocopies of the relevant tables from Schott's book, as well as a German translation of the relevant passages from Dr. Hans-Joaquim Vollrath, a mathematician at Wurzburg university where Kaspar Schott wrote and taught. I am indebted to Dr. Vollrath for his assistance.

The Software Implementation

My software is written in the Perl programming language. It consists of a single script, organum.pl, which makes use of three include ("header") files, which contain the data I transcribed from the writings of Kircher and Schott. Two of the header files contain tables from Kircher's and Schott's books (one contains phrases, and the other contains modes or scales). The third header file contains a set of lyrics, which are to be set to music using Kircher's method.

Data Entry and Representation. The most tedious part of my implementation involved typing in all the tables of numbers and rhythmic values that appear on the *tariffa* (tables) in Schott's book. In some cases, the Perl representation resembles quite closely the original illustrations which appear in *Organum Mathematicum*, as can be seen in a screen snapshot I took while entering the data [Figure 4].

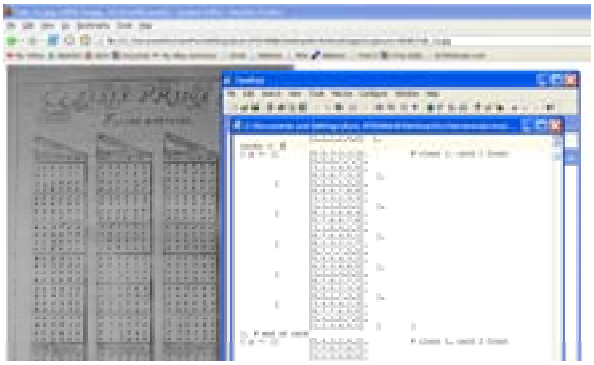

Figure 4: *Data Entry*

Most of the tables I transcribed from Schott's book consist of musical phrases, notated as separate pitch and rhythmic values. The eight rods are divided into two distinct groups: simple and florid.

Four of the rods are used for music in the "simple" style, or first-species counterpoint. In the music produced by these rods, all four voices sing melodies with identical rhythmic values. For each musical phrase, which consists of a set of pitches, a choice of different rhythmic values are provided, in a set of separate tables. In addition, a set of rhythms is provided in the "Tripla" style, which use three per measure, rather than four.

The other four rods contain music in the "florid" style, or fifth-species counterpoint. In these rods, the 4 voices are assigned different rhythmic values, and only one such set of rhythms is provided for each phrase.

The tables are further divided into classes based on the number of syllables per strophe, corresponding to the metrical style of the latin hymns which a church composer would want to set to music. The phrases are arranged in six groups, as follows:

a) Class 1 fronts. "Euripedaean" phrases for setting trochaic trimeter supposedly in the style of Euripedes with six syllables per phrase. An example verse used with this class is "Ave Maris Stella".

b) Class 1 backs. "Anancreonic" phrases for setting trochaic tetrameter with eight syllables per phrase. Kircher's example is "O ter quaterque felix" (O ter QUA ter QUE fe LIX). A modern example would be "We three kings of Orient are."

c) Class 2 fronts. "Archilochan" phrases for setting iambic tetrameter with eight syllables per phrase. Ambrosian hymns, such as "Oh Little Town of Bethlehem," fit this pattern, as does Kircher's example of "Veni Creator Spiritus" (ve NI cre A tor SPI ri TUS).

d) Class 2 backs. "Sapphic" phrases, for setting versus with a syllabic pattern of 11-11-11-5. Examples are "Iste Confessor Domini Sacratus" and "Ut queant axis resonare fibris".

e) Class 3 fronts and backs. "Euripedaean" phrases (trochaic trimeter) in the florid style. The fronts contain the pitches, and the backs contain the corresponding rhythmic values.

f) Class 4 fronts and backs [see figure 5]. "Archilochan" phrases (iambic tetrameter) in the florid style. The fronts contain the pitches, and the backs contain the corresponding rhythmic values.

Figure 5: *Class 4 front and back for the 4th strophe .*

The Class 5 columns contain information used to coerce pitches into the correct register, based on the tonic of the scale in use, and the vocal part (Soprano, Alto, Tenor, Bass). This information appears, in altered form, on the front panel of the Arca.

The Class 6 columns include the *tabellae tonorum* (tone tables), which are employed to convert digits to pitch values, using eight different modes or scales. These same tables appear on the underside of the lid in Kircher's illustration of the Arca. These tables are used to convert the digit values in Kircher's note phrases to specific pitche classes, depending on the mode or scale the composer chooses.

I had some difficulty with these because in music notation of the period, the note B is sometimes implicitly assumed to be flatted, and it is difficult for me to always be certain where Kircher intended it. The tables roughly correspond to the following medieval church modes: Dorian, Hypodorian, Phrygian, Hypophrygian, Lydian, Hypolydian, Mixolydian, Hypomixolydian. The correspondence with these modes is not exact, and I have tried to be true to what Kircher & Schott notated, rather than what is generally documented about these modes.

Input Parameters. My software is a Perl script that is operated from the command line. A typical invocation of the script is shown below.

```
organum.pl -li 5 -csn 6 -mi 6 -rnd -tempo 180 –vl 2
```

These parameters indicate to use lyric-number 5 (from a database of lyrics), card-set 6 (which corresponds to the class 4 "Archilochan" tables), mode 6 (hypolydian), random phrase selection, a MIDI tempo of 180, and to preserve voice leading for step-wise motion of 2 half-steps.

The Algorithm. My algorithm is essentially a nested loop which processes each note of each phrase of each voice (SATB).

A set of phrases are selected from each of four cards, in sequence (the phrases on the last card typically have cadences). If the user has indicated the –rnd parameter, phrases are randomly chosen, otherwise, phrases the user explicitly selects are used. If the cards use simple style counterpoint, then rhythmic phrases are also chosen, in a similar manner. For florid counterpoint, there is only a single choice of rhythmic values for each phrase.

Figuring out the rhythmic value for each note involves nothing more complicated than a table lookup, to retrieve the values specified in the tables.

Figuring out the pitches is a little more complicated. The pitch class of each note (C,C#,D etc.) is obtained by looking up the note number in the list of pitch values for the current mode. Choosing the register (the octave) is a little more complicated. First an appropriate octave is chosen based on the register of the voice and the information from the class 5 data column. In addition, an attempt is made to preserve stepwise motion, allowing the melody to stray slightly outside of the register, if small intervals are being used in the melody.

The three aspects of implementation that have given me the most trouble are a) choosing correct pitch values for Kircher's modes, b) transcribing Kircher's note durations correctly, and c) avoiding awkward leaps in melodic lines, while still honoring the spirit of Kircher's algorithm.

Format of results. My software produces files in the ABC format which contain information for both a MIDI version, and a printed score [figure 6]. In addition, I have produced "sung" versions using Flinger, a text-to-song package written by the late Mike Macon.

The sung versions are produced by producing 4 separate MIDI files (one per melodic line) which contain embedded syllables, from a lyric file which contains phonetic transcriptions of the original latin. The Flinger software converts these to separate audio files, which may then be mixed together and post-processed to add some reverb, using an off-the-shelf audio editor.

Discussion

In implementing this software, and researching Kircher's algorithm, a number of questions occurred to me, which I'll raise here for discussion.

Is it disingenuous to call Kircher's procedure an algorithm? If you define algorithm as "a sequence of well defined instructions," than clearly Kircher's procedure was intended to be an algorithm. However, it was an algorithm intended for humans, and not machines, and as such, it contains a few steps that are difficult to translate into software. For example, Kircher suggests choosing modes based on the character of the selected hymn, and helpfully provided a list of adjectives for each mode such as "heroic," "magnificent," "pius" and so on. To my less delicate and more modern ears, his choice of adjectives seems quite arbitrary, so I have instead chosen modes based on whether they "sound good" or simply by using a random number generator.

Was it the first music algorithm? No. If Kircher's procedure is to be called an algorithm, then so is any well defined musical procedure, such as species counterpoint, which precedes Kircher. Kircher's procedure differs from species counterpoint however, in his use of combining phrases from a fixed set, which appears to be a novel compositional technique of Kircher's, inspired by Lull and Mersenne.

Was it intended for mechanical computation? Although words like "mechanicam" and "artificium" appear repeatedly in Kircher's writing about this process, it seems clear he is talking about human labor. Nonetheless, elsewhere in *Musurgia Universalis*, Kircher wrote about a number of intriguing automatic instruments of the time, such as an elaborate water-powered barrel organ. So it is compelling to ask if Kircher might have put 2 and 2 together and imagined a clockwork machine used for the purposes of composing music. If he had such thoughts, he did not write them down in *Musurgia Universalis*. The closest he came to inventing such a machine is his revolving bell choir (a working reproduction can be seen and heard at the Museum of Jurassic Technology).

Was it an aleatoric algorithm? Some Kircher enthusiasts, such as David Wilson, have described Kircher's algorithm as producing "random compositions", which implies random selection or chance, the hallmarks of an aleatoric algorithm, such as those developed by John Cage. In my opinion, Kircher probably did not intend for chance to play as big a role in his method as it does in my software implementation. Some of the decisions that I make using a random number generator were intended to be made by humans using their best judgement, such as the choice of modes. However, Kircher himself describes the algorithm as being of use for persons "with no musical knowledge". Since such a person would not necessarily be capable of making informed choices for phrase selection, it seems likely that a certain amount of chance would have crept in, regardless of Kircher's intention.

Are any published hymns based on material from the Organum or Arcas? I haven't found any yet, but admittedly, I haven't looked very hard. Since the material produced by Kircher's algorithm is not of particularly high quality, I doubt that any composers of lasting merit would have made much use of it. Interestingly, Kircher himself provides very few complete examples in *Musurgia Universalis* which are derived from his own Arca tables.

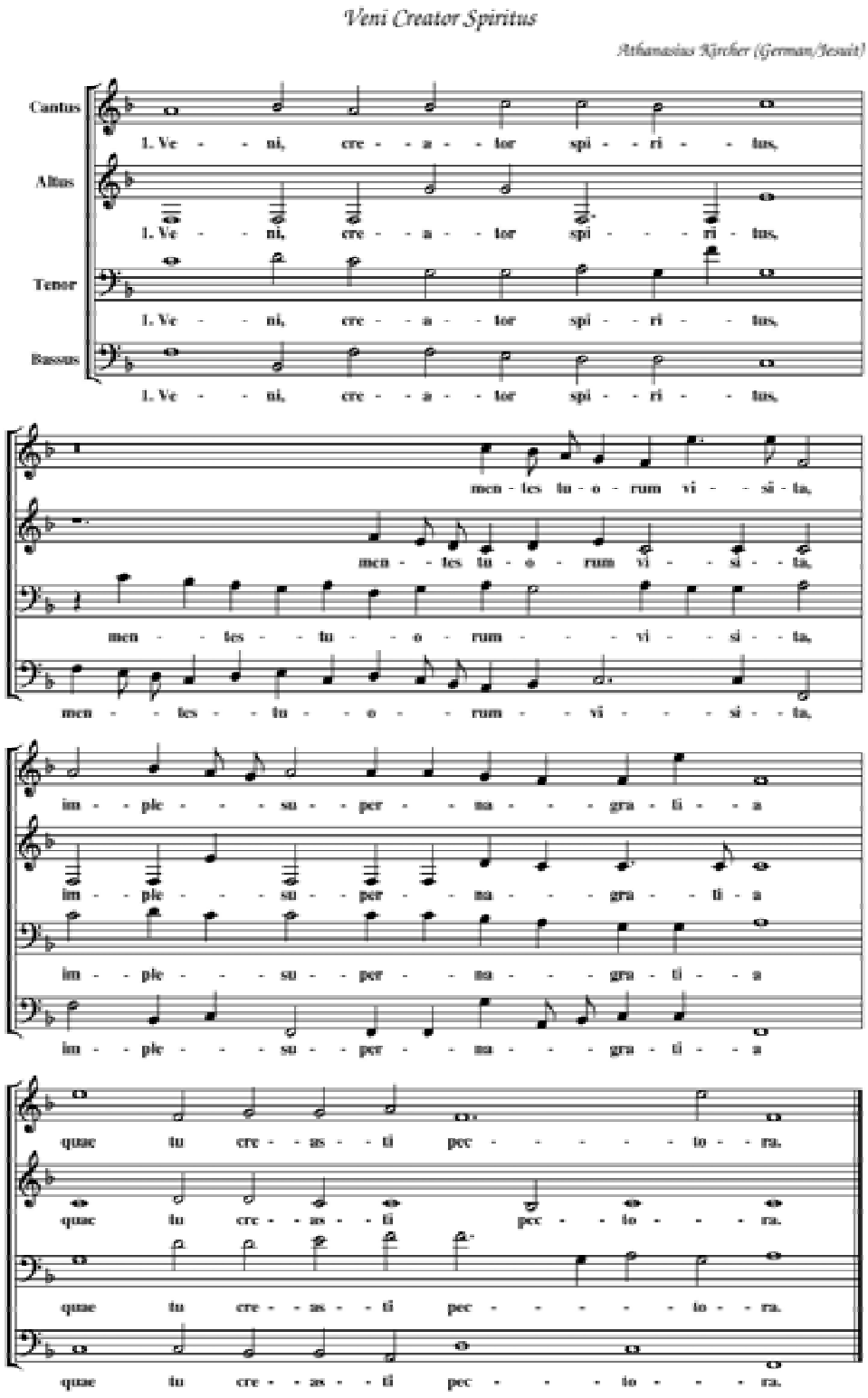

Figure 5 :
Sample Output, using the Class 4 Tables.

Are the phrases in the Arca derived from music in vogue at the time or was the material all written by Kircher? This will be a tough question to answer, since little printed music survives from this period. Also the somewhat uniform and redundant style of the polyphonic snippets used by Kircher may closely resemble other music that wasn't explicitly copied.

Sources

My Perl software program, Organum, can be downloaded at my website:

http://www.krazydad.com/organum.zip

References

[1] Kircher, Athanasius, *Musurgia Universalis*, Vol II, pp. 185., 1650

[2] Reilly, P. Conor, *Athanasius Kircher S. J. : Master of a hundred arts*, Edizioni del Mondo, 1974

[3] Godwin, Joscelyn, *Athanasius Kircher : A Renaissance Man and the Quest for Lost Knowledge*, Thames and Hudson, pp. 56, 1979

[4] Pepys, Samuel, *Diary and Correspondence*, Dodd, Mead and Company, Vol VIII, 1885

[5] Chierotti, Mario, *La musurgia mirifica di Athanasius Kircher: la composizione musicale alla portata di tutti nell'età barocca* Articolo pubblicato su Musica/Realtà, Number 37, April 1992

[6] Murata, Margaret, *Music History in the Musurgia universalis of Athanasius Kicher*, in *The Jesuits: Culture, Sciences, and the Arts, 1540-1773*, J. O'Malley, T. F. Kennedy, S. Harriss, et al., eds (Toronto: University of Toronto Press), pp 206, 1999

[7] Schott, Kaspar, *Organum Mathematicum*, pp 761-857, 1668

Three Conceptions of Musical Distance

Dmitri Tymoczko
310 Woolworth Center, Princeton University, Princeton, NJ 08544.

Abstract

This paper considers three conceptions of musical distance (or inverse "similarity") that produce three different musico-geometrical spaces: the first, based on voice leading, yields a collection of continuous quotient spaces or orbifolds; the second, based on acoustics, gives rise to the Tonnetz and related "tuning lattices"; while the third, based on the total interval content of a group of notes, generates a six-dimensional "quality space" first described by Ian Quinn. I will show that although these three measures are in principle quite distinct, they are in practice surprisingly interrelated. This produces the challenge of determining which model is appropriate to a given music-theoretical circumstance. Since the different models can yield comparable results, unwary theorists could potentially find themselves using one type of structure (such as a tuning lattice) to investigate properties more perspicuously represented by another (for instance, voiceleading relationships).

1 Introduction

We begin with voice-leading spaces that make use of the log-frequency metric [1, 15, 3]. Pitches here are represented by the logarithms of their fundamental frequencies, with distance measured according to the usual metric on $\mathbb{R}$; pitches are therefore "close" if they are near each other on the piano keyboard. A point in $\mathbb{R}^n$ represents an ordered series of pitch classes. Distance in this higher-dimensional space can be interpreted as the aggregate distance moved by a collection of musical "voices" in passing from one chord to another. (We can think of this, roughly, as the aggregate physical distance traveled by the fingers on the piano keyboard.) By disregarding information–such as the octave or order of a group of notes–we "fold" $\mathbb{R}^n$ into a non-Euclidean quotient space or orbifold. (For example, imposing octave equivalence transforms $\mathbb{R}^n$ into the n-torus $\mathbb{T}^n$, while transpositional equivalence transforms $\mathbb{R}^n$ into $\mathbb{R}^{n-1}$, orthogonally projecting points onto the hyperplane whose coordinates sum to zero.) Points in the resulting orbifolds represent equivalence classes of musical objects–such as chords or set classes–while "generalized line segments" represent equivalence classes of voice leadings.[1] For example, Figure 1, from Tymoczko 2006, represents the space of two-note chords, while Figure 2, from Callender, Quinn, and Tymoczko 2008, represents the space of three-note transpositional set classes. In both spaces, the distance between two points represents the size of the smallest voice leading between the objects they represent.

Let's now turn to a very different sort of model, the *Tonnetz* [4, 5, 6] and related structures, which I will describe generically as "tuning lattices." These models are typically discrete, with adjacent points on a particular axis being separated by the same interval. The leftmost lattice in Figure 3 shows the most familiar of these structures, with the two axes representing acoustically pure perfect fifths and major thirds. (One can imagine a third axis, representing either the octave or the acoustical seventh, projecting outward from the paper.) The model asserts that the pitch G4 has an acoustic affinity to both C4 (its "underfifth") and D5 (its "overfifth"), as well as to E♭4 and B4 (its "underthird" and "overthird," respectively). The lattice thus encodes a fundamentally different notion of musical distance than the earlier voice leading models: whereas A3 and A♭3 are very close in log-frequency space, they are four steps apart our tuning lattice. Furthermore,

[1] The adjective "generalized" indicates that these "line segments" may pass through one of the space's singular points, giving rise to mathematical complications.

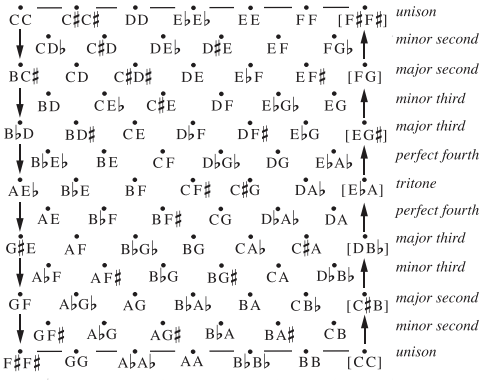

Figure 1: *The Möbius strip representing voice-leading relations among two-note chords.*

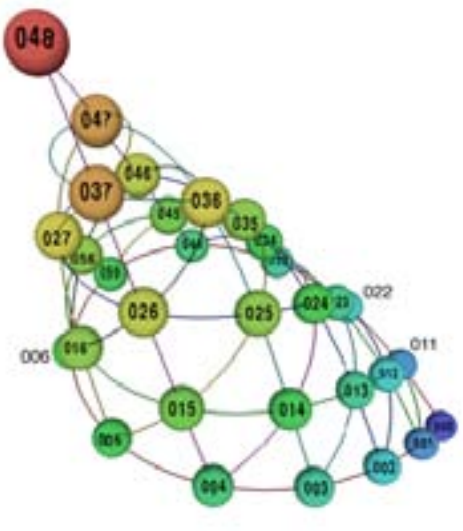

Figure 2: *The cone representing voice-leading relations among three-note transpositional set classes.*

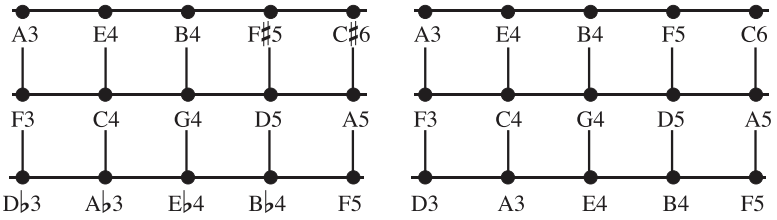

Figure 3: *Two discrete tuning lattices. On the left, the chromatic Tonnetz, where horizontally adjacent notes are linked by acoustically pure fifths, while vertically adjacent notes are linked by acoustically pure major thirds. On the right, a version of the structure that uses diatonic intervals.*

where chords (or more generally "musical objects") are represented by *points* in the voice leadings spaces, they are represented by polytopes in the lattices.

Finally, there are measures of musical distance that rely on chords' shared interval content. From this point of view, the chords C, C♯, E, F♯ and C, D♭, E♭, G resemble one another, since they are "nontrivially homometric" or "Z-related": that is, they share the same collection of pairwise distances between their notes. (For instance, both contain exactly one pair that is one semitone apart, exactly one pair that is two semitones apart, and so on.) However, these chords are *not* particularly close in either of the two models considered previously. It is not intuitively obvious that this notion of "similarity" produces any particular geometrical space. But Ian Quinn has shown that one can use the discrete Fourier transform to generate (in the familiar equal-tempered case) a six-dimensional "quality space" in which chords that share the same interval content are represented by the same point [10, 11, 12, 13, 2]. We will explore the details shortly.

Clearly, these three musical models are very different, and it would be somewhat surprising if there were to be close connections between them. But we will soon see that this is in fact this case.

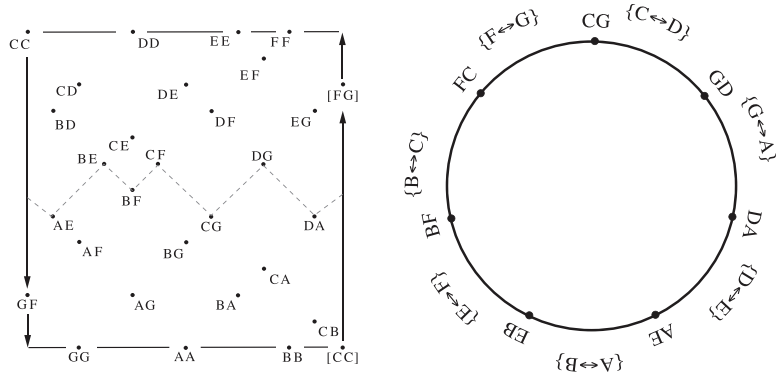

Figure 4: *Left: most efficient voice-leadings between diatonic fifths form a chain that runs through the center of the Möbius strip from Figure 1. Right: these voice leadings form an abstract circle, in which adjacent dyads are related by three-step diatonic transposition, and are linked by single-step voice leading.*

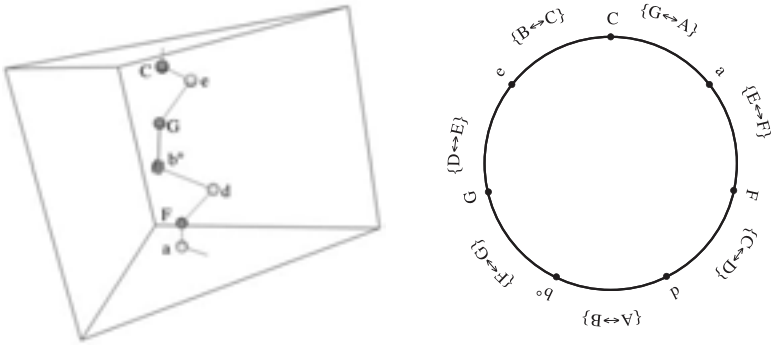

Figure 5: *Left: most efficient voice-leadings between diatonic triads form a chain that runs through the center of the orbifold representing three-note chords. Right: these voice leadings form an abstract circle, in which adjacent triads are linked by single-step voice leading. Note that here, adjacent triads are related by transposition by two diatonic steps.*

2 Voice-leading lattices and acoustic affinity

Voice-leading and acoustics seem to privilege fundamentally different conceptions of pitch distance: from a voice leading perspective, the semitone is smaller than the perfect fifth, whereas from the acoustical perspective the perfect fifth is smaller than the semitone. Intuitively, this would seem to be a fundamental gap that cannot be bridged.

Things become somewhat more complicated, however, when we consider the discrete lattices that represent voice-leading relationships among familiar diatonic or chromatic chords. For example, Figure 4 records the most efficient voice leadings among diatonic fifths–which can be represented using an irregular, one-dimensional zig-zag near the center of the Möbius strip $\mathbb{T}^2/S_2$. (The zig-zag seems to be irregular because the figure is drawn using the chromatic semitone as a unit; were we to use the diatonic step, it would be regular.) Abstractly, these voice leadings form the circle shown on the right of Figure 4. The figure demonstrates that there are purely contrapuntal reasons to associate fifth-related diatonic fifths: from this perspective {C, G} is close to {G, D}, not because of acoustics, but because the first dyad can be transformed into the second by moving the note C up by one diatonic step. One fascinating possibility–which we unfortunately cannot pursue here–is that acoustic affinities actually *derive from* voice-leading facts: it is possible that the ear asso-

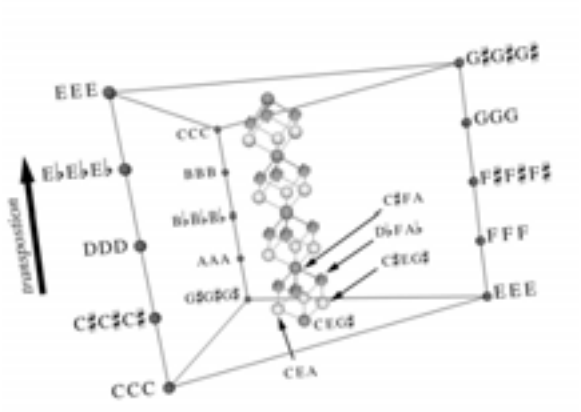

Figure 6 : *Major, minor, and augmented triads as they appear in the orbifold representing three-note chords. Here, triads are particularly close to their major-third transpositions.*

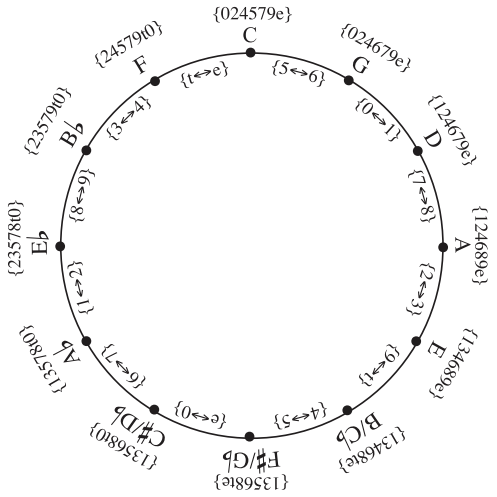

Figure 7 : *Fifth-related diatonic scales form a chain that runs through the center of the seven-dimensional orbifold representing seven-note chords. It is structurally analogous to the circles in Figures 4 and 5.*

ciates the third harmonic of a complex tone with the second harmonic of another tone a fifth above it, and the fourth harmonic of the lower note with the third of the upper, in effect tracking voice-leading relationships among the partials.

Figures 5–7 present three analogous structures: Figure 5 connects triads in the C diatonic scale by efficient voice leading, and depicts third-related triads as being particularly close; Figure 6 shows the position of major, minor, and augmented triads in three-note chromatic chord space, where major-third-related triads are close [7]; Figure 7 shows (symbolically) that fifth-related diatonic scales are close in twelve-note chromatic space. Once again, we see that there are purely contrapuntal reasons to associate fifth-related diatonic scales and third-related triads.

This observation, in turn, raises a number of theoretical questions. For instance: should we attribute the prevalence of modulations between fifth-related keys to the acoustic affinity between fifth-related pitches, or to the voice-leading relationships between fifth-related diatonic scales? One way to study this question would be to compare the frequency of modulations in classical pieces to the voice-leading distances among their associated scales. Preliminary investigations, summarized in Figure 8, suggest that voice-leading distances are in fact very closely correlated to modulation frequencies. Surprising as it may seem, the acoustic affinity of perfect fifth-related notes may be superfluous when it comes to explaining classical modulatory practice. [2]

3 Tuning lattices as approximate models of voice leading

We will now investigate the way tuning lattices like the *Tonnetz* represent voice-leading relationships among familiar sonorities. Here my argumentative strategy will by somewhat different, since it is widely recognized that the *Tonnetz* has something to do with voice leading. (This is largely due to the important work of Richard

[2]Similar points could potentially be made about the prevalence, in functionally tonal music, of root-progressions by perfect fifths. It may be that the diatonic circle of thirds shown in Figure 5 provides a more perspicuous model of functional harmony than do more traditional fifth-based representations.

		Correlation
MAJOR	**Bach**	.96
	Haydn	.93
	Mozart	.91
	Beethoven	.96
MINOR	**Bach**	.95
	Haydn	.91
	Mozart	.91
	Beethoven	.96

Figure 8: *Correlations between modulation frequency and voice-leading distances among scales, in Bach's Well-Tempered Clavier, and the piano sonatas of Haydn, Mozart, and Beethoven. The very high correlations suggest that composers typically modulate between keys whose associated scales can be linked by efficient voice leading.*

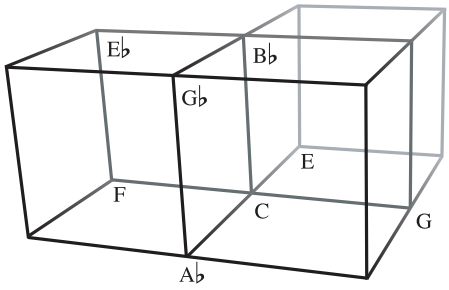

Figure 9: *On this three-dimensional Tonnetz, the C^7 chord is represented by the tetrahedron whose vertices are C, E, G, and B♭. The $C^{ø7}$ chord is represented by the nearby tetrahedron C, E♭, G♭, B♭, which shares the C-B♭ edge.*

Cohn, who has used the *Tonnetz* to study what he calls "parsimonious" voice leading [4].) My goal will therefore be to explain why tuning lattices are only an *approximate* model of contrapuntal relationships, and only for certain chords.

The first point to note is that inversionally related chords on a tuning lattice are near each other when they share common tones.[3] For example, the *Tonnetz* represents perfect fifths by line segments; fifth-related perfect fifths, such as {C, G} and {G, D} are related by inversion around their common note, and are adjacent on the lattice (Figure 3). Similarly, major and minor triads on the *Tonnetz* are represented by triangles; inversionally related triads that share an interval, such as {C, E, G} and {C, E, A}, are joined by a common edge. (On the standard *Tonnetz*, the more common tones, the closer the chords will be: C major and A minor, which share two notes, are closer than C major and F minor, which share only one.) In the three-dimensional *Tonnetz* shown in Figure 9, where the z axis represents the seventh, C^7 is near its inversion $C^{ø7}$. The point is reasonably general, and does not depend on the particular structure of the *Tonnetz* or on the chords involved: on tuning lattices, inversionally related chords are close when they share common tones.[4]

The second point is that acoustically consonant chords often divide the octave relatively evenly; such chords can be linked by efficient voice leading to those inversions with which they share common notes [15, 16].[5] It follows that proximity on a tuning lattice will indicate the potential for efficient voice leading *when the chords in question are nearly even and are related by inversion*. Thus {C, G} and {G, D} can be linked by the stepwise voice leading (C, G)→(D, G), in which C moves up by two semitones. Similarly, the C major and A minor triads can be linked by the single-step voice leading (C, E, G)→(C, E, A), and C^7 can be linked to $C^{ø7}$ by the two semitone voice-leading (C, E, G, B♭)→(C, E♭, G♭, B♭). In each case the chords are

[3] This is not true of the voice leading spaces considered earlier: for example, in three-note chord space {C, D, F} is not particularly close to {F, A♭, B♭}.

[4] In the general case, the notion of "closeness" needs to be spelled out carefully, since chords can contain notes that are very far apart on the lattice. In the applications we are concerned with, chords occupy a small region of the tuning lattice, and the notion of "closeness" is fairly straightforward.

[5] The point is relatively obvious when one thinks geometrically: the two chords divide the pitch-class circle nearly evenly into the same number of pieces; hence, if any two of their notes are close, then each note of one chord is near some note of the other.

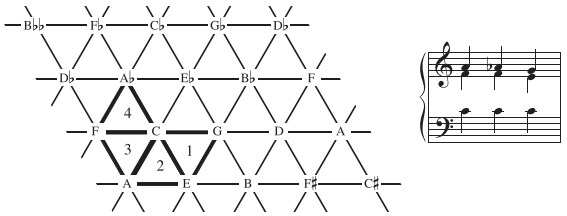

Figure 10: *On the Tonnetz, F major (Triangle 3) is closer to C major (Triangle 1) than F minor (Triangle 4) is. In actual music, however, F minor frequently appears as a passing chord between F major and C major. Note that, unlike in Figure 3, I have here used a Tonnetz in which the axes are not orthogonal; this difference is merely orthographical, however.*

also close on the relevant tuning lattice. (Interestingly, triadic distances on the diatonic *Tonnetz* in Figure 3 exactly reproduce the circle-of-thirds distances from Figure 5.) This will not be true for uneven chords: {C, E} and {E, G♯} are close on the *Tonnetz*, but cannot be linked by particularly efficient voice leading; the same holds for {C, G, A♭} and {G, A♭, D♭}. Tuning lattices are approximate models of voice-leading only when one is concerned with the nearly-even sonorities that are fundamental to Western tonality.

Furthermore, on closer inspection *Tonnetz*-distances diverge from voice-leading distances even for these chords. Some counterexamples are obvious: for instance, {C, G} and {C♯, F♯} can be linked by semitonal voice leading, but are fairly far apart on the *Tonnetz*. Slightly more subtle, but more musically pertinent, is the following example: on the *Tonnetz*, C major is two units away from F major but *three* units from F minor (Figure 10). (Here I measure distance in accordance with "neo-Riemannian" theory, which considers triangles sharing an edge to be one unit apart and which decomposes larger distances into sequences of one-unit moves.) Yet it takes only two semitones of total motion to move from C major to F minor, and three to move from C major to F major. (This is precisely why F minor often appears as a passing chord between F major and C major.) The *Tonnetz* thus depicts F major as being closer to C major than F minor is, even though contrapuntally the opposite is true. This means we cannot use the figure to explain the ubiquitous nineteenth-century IV-iv-I progression, in which the two-semitone motion $\hat{6}\rightarrow\hat{5}$ is broken into a pair of single-semitone steps $\hat{6}\flat\hat{6}\rightarrow\hat{5}$.

One way to put the point is that while adjacencies on the *Tonnetz* reflect voice-leading facts, other relationships do not. As Cohn has emphasized, two major or minor triads share an edge if they can be linked by "parsimonious" voice-leading in which a single voice moves by one or two semitones. If we are interested in this particular kind of voice leading then the *Tonnetz* provides an accurate and useful model. However, there is no analogous characterization of larger distances in the space. In other words, we do not get a recognizable notion of voice-leading distance by "decomposing" voice leadings into sequences of parsimonious moves: as we have seen, (F, A, C)→(E, G, C) can be decomposed into *two* parsimonious moves, while it takes *three* to represent (F, A♭, C)→(E, G, C); yet intuitively the first voice leading is larger than the second. The deep issue here is that it is problematic to assert that "parsimonious" voice leadings are always smaller than nonparsimonious voice-leadings: by asserting that (C, E, A)→(C, E, G) is smaller than (C, F, Af)→(C, E, G), the theorist runs afoul what Tymoczko calls "the distribution constraint," known to mathematicians as the submajorization partial order [15, 8].[6] Tymoczko argues that violations of the distribution constraint invariably produce distance measures that violate intuitions about voice leading; the problem with larger distances on the *Tonnetz* is an illustration of this general point.

Nevertheless, the fact remains that the two kinds of distance are roughly consistent: for major and minor triads, the correlation between *Tonnetz* distance and voice-leading distance is a reasonably high .79.[7]

[6]Metrics that violate the distribution constraint have counterintuitive consequences, such as preferring "crossed" voice leadings to their uncrossed alternatives. Here, the claim that A minor is closer to C major than F minor leads to the F minor/F major problem discussed in Figure 10.

[7]Here I use the L^1 or "taxicab" metric. The correlation between *Tonnetz* distances and the number of shared common tones is an even-higher .9; however, "number of shared common tones" is not interpretable as a voice-leading metric.

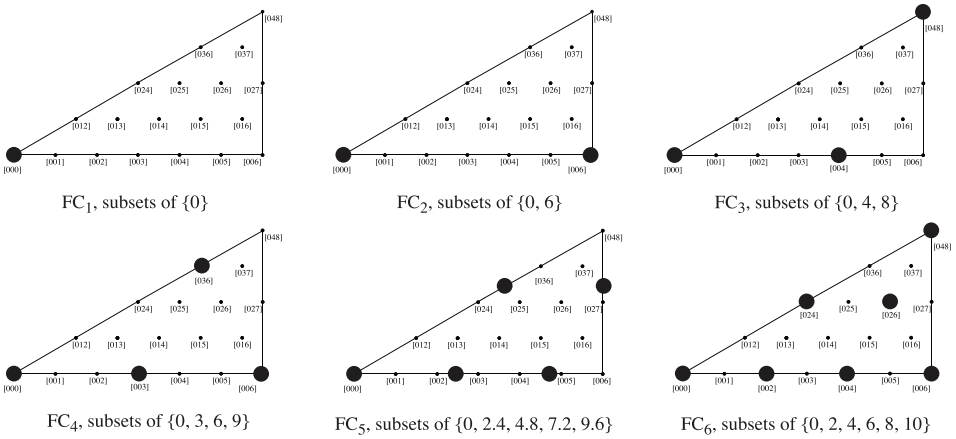

Figure 11 : *The magnitude of a set class's nth Fourier component is approximately linearly related to the size of the minimal voice leading to the nearest subset of the perfectly even n-note chord, shown here as dark spheres.*

Furthermore, since Tymoczko's "distribution constraint" is not intuitively obvious, unwary theorists might well think that they could declare the "parsimonious" voice leading (C, E, G)→(C, E, A) to be smaller than the nonparsimonious (C, E, G)→(C♯, E, G♯). (Indeed, the very meaning of the term "parsimonious" would seem to suggest that some theorists have done so.) Consequently, *Tonnetz*-distances might well appear, at first or even second blush, to reflect some reasonable notion of "voice-leading distance"; and this in turn could lead the theorist to conclude that the *Tonnetz* provides a generally applicable tool for investigating triadic voice-leading. I have argued that we should resist this conclusion: if we use the *Tonnetz* to model chromatic music, than Schubert's major-third juxtapositions will seem very different from his habit of interposing F minor between F major and C major, since the first can be readily explained using the *Tonnetz* whereas the second cannot [6]. The danger, therefore, is that we might find ourselves drawing unnecessary distinctions between these two cases–particularly if we mistakenly assume the *Tonnetz* is a fully faithful model of voice-leading relationships.

4 Voice leading, "quality space," and the Fourier transform

We conclude by investigating the relation between voice leading and the Fourier-based perspective [14, 9, 2]. The mechanics of the Fourier transform are relatively simple: for any number n from 1 to 6, and every pitch-class p in a chord, the transform assigns a two-dimensional vector whose components are

$$V_{p,n} = (\cos(2\pi pn/12), \sin(2\pi pn/12))$$

Adding these vectors together, for one particular n and all the pitch-classes p in the chord, produces a composite vector representing the chord as a whole–its "nth Fourier component." The length (or "magnitude") of this vector, Quinn observes, reveals something about the chord's harmonic character: in particular, chords saturated with $(12/n)$-semitone intervals, or intervals approximately equal to $12/n$, tend to score highly on this index of chord quality.[8] The Fourier transform thus seems to quantify the intuitive sense that chords can be more-or-less diminished-seventh-like, perfect-fifthy, or whole-toneish. Interestingly, "Z-related" chords–or chords with the same interval content–always score identically on this measure

[8]Here I use continuous pitch-class notation where the octave always has size 12, no matter how it is divided. Thus the equal-tempered five-note scale is labeled $\{0, 2.4, 4.8, 7.2, 9.6\}$.

of chord-quality. In this sense, Fourier space (the six-dimensional hypercube whose coordinates are the Fourier magnitudes) seems to model a conception of similarity that emphasizes interval content, rather than voice leading or acoustic consonance.

However, there is again a subtle connection to voice leading: it turns out that the magnitude of a chord's *n*th Fourier component is approximately linearly related to the (Euclidean) size of the minimal voice leading to *the nearest subset* of any perfectly even *n*-note chord.[9] For instance, a chord's first Fourier component (FC_1) is approximately related to the size of the minimal voice leading to any transposition of $\{0\}$; the second Fourier component is approximately related to the size of the minimal voice leading to any transposition of either $\{0\}$ or $\{0, 6\}$; the third component is approximately related to the size of the minimal voice leading to any transposition of either $\{0\}$, $\{0, 4\}$ or $\{0, 4, 8\}$, and so on. Figure 11 shows the location of the subsets of the *n*-note perfectly even chord, as they appear in the orbifold representing three-note set-classes, for values of *n* ranging from 1 to 6 [1, 15, 3]. Associated to each graph is one of the six Fourier components. For any three-note set class, the magnitude of its *n*th Fourier component is a decreasing function of the distance to the nearest of these marked points: for instance, the magnitude of the third Fourier component (FC_3) decreases, the farther one is from the nearest of $\{0\}$, $\{0, 4\}$ and $\{0, 4, 8\}$. Thus, chords in the shaded region of Figure 12 will tend to have a relatively large FC_3, while those in the unshaded region will have a smaller FC_3. Figure 13 shows that this relationship is very-nearly linear for twelve-tone equal-tempered trichords.

Table 1 uses the Pearson correlation coefficient to estimate the relationship between the voice-leading distances and Fourier components, for twelve-tone equal-tempered multisets of various cardinalities. The strong anti-correlations indicate that one variable predicts the other with a very high degree of accuracy. Table 2 calculates the correlation coefficients for three-to-six-note chords in 48-tone equal temperament. These strong anticorrelations, very similar to those in Table 1, show that there continues to be a very close relation between Fourier magnitudes and voice-leading size in very finely quantized pitch-class space. Since 48-tone equal temperament is so finely quantized, these numbers are approximately valid for continuous, unquantized pitch-class space.[10]

Explaining these correlations, though not very difficult, is beyond the scope of this paper. From our perspective, the important question is whether we should measure chord quality using the Fourier transform or voice leading. In particular, the issue is whether the Fourier components model the musical intuitions we want to model: as we have seen, the Fourier transform requires us to measure a chord's "harmonic quality" in terms of its distance from *all* the subsets of the perfectly even *n*-note chord. But we might sometimes wish to employ a different set of harmonic prototypes. For instance, Figure 14 uses a chord's distance from the augmented triad to measure the trichordal set classes' "augmentedness." Unlike Fourier analysis, this purely voice-leading-based method does not consider the triple unison or doubled major third to be particularly "augmented-like"; hence, set classes like $\{0, 1, 4\}$ do not score particularly highly on this index of "augmentedness." This example dramatizes the fact that, when using voice leading, we are free to choose any set of harmonic prototypes, rather than accepting those the Fourier transform imposes on us.

5 Conclusion

The approximate consistency between our three models is in one sense good news: since they are closely related, it may not matter much–at least in practical terms–which we choose. We can perhaps use a tuning lattice such as the *Tonnetz* to represent voice-leading, as long as we are interested in gross contrasts ("near"

[9] Here I measure voice-leading using the Euclidean metric [1, 15, 16].

[10] It would be possible, though beyond the scope of this paper, to calculate this correlation analytically. It is also possible to use statistical methods for higher-cardinality chords. A large collection of randomly generated 24- and 100-tone chords in continuous space produced correlations of .95 and .94, respectively.

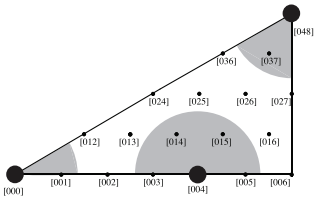

Figure 12: *Chords in the shaded region will have a large FC_3 component, since they are near subsets of $\{0, 4, 8\}$. Those in the unshaded region will have a smaller FC_3 component.*

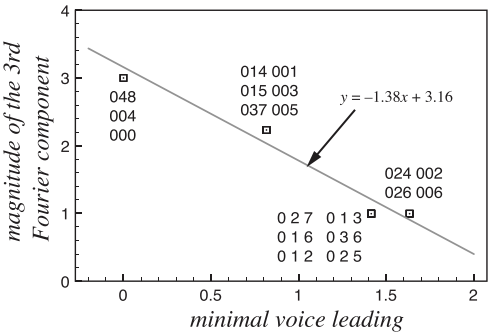

Figure 13: *For trichords, the equation $FC_3 = -1.38VL + 3.16$ relates the third Fourier component to the Euclidean size of the minimal voice leading to the nearest subset of $\{0, 4, 8\}$.*

Table 1: *Correlations between voice-leading distances and Fourier magnitudes.*

	FC_1	FC_2	FC_3	FC_4	FC_5	FC_6
Dyads	-.97	-.96	-.97	-1	-.97	-1*
Trichords	-.98	-.97	-.97	-.98	-.98	-1*
Tetrachords	-.96	-.96	-.95	-.98	-.96	-1*
Pentachords	-.96	-.96	-.95	-.98	-.96	-1*
Hexachords	-.96	-.96	-.95	-.96	-.96	-1*
Septachords	-.96	-.96	-.96	-.97	-.96	-1*
Octachords	-.96	-.96	-.95	-.98	-.96	-1*
Nonachords	-.96	-.96	-.96	-.98	-.96	-1*
Decachords	-.96	-.96	-.96	-.98	-.96	-1*

* Voice leading calculated using L^1 (taxicab) distance rather than L^2 (Euclidean).

Table 2: *Correlations between voice-leading distances and Fourier magnitudes in 48-tone equal temperament.*

	FC_1
Trichords	-.99
Tetrachords	-.97
Pentachords	-.97
Hexachords	-.96

vs. "far") rather than fine quantitative differences ("3 steps away" vs. "2 steps away"). Similarly, we can perhaps use voice-leading spaces to approximate the results of the Fourier analysis, as long as we are interested in modeling generic harmonic intuitions ("very fifthy" vs. "not very fifthy") rather than exploring very fine differences among Fourier magnitudes.

However, if we want to be more principled, then we need to be more careful. The resemblances among our models mean that it is possible to inadvertently use one sort of structure to discuss properties that are more directly modeled by another. And indeed, the recent history of music theory displays some fascinating (and very fruitful) imprecision about this issue. It is striking that Douthett and Steinbach, who first described several of the lattices found in the center of the voice-leading orbifolds–including Figure 6–explicitly presented their work as generalizing the familiar *Tonnetz* [7]. Their lattices, rather than depicting *parsimonious* voice leading among major and minor triads, displayed *single-semitone* voice leadings among a wider range of sonorities; and as a result of this seemingly small difference, they constucted models in which *every distance* can be interpreted as representing voice-leading size. However, this difference only became apparent after it was understood how to embed their discrete structures in the continuous geometrical figures described at the beginning of this paper. Thus one could say that the continuous voice-leading spaces evolved out of the *Tonnetz*, by way of Douthett and Steinbach's discrete lattices, even though the structures now appear to be fundamentally different. Related points could be made about Quinn's "quality space," whose connection to the voice-leading spaces took several years–and the work of several authors–to clarify.

There is, of course, nothing wrong with this: knowledge progresses slowly and fitfully. But our inves-

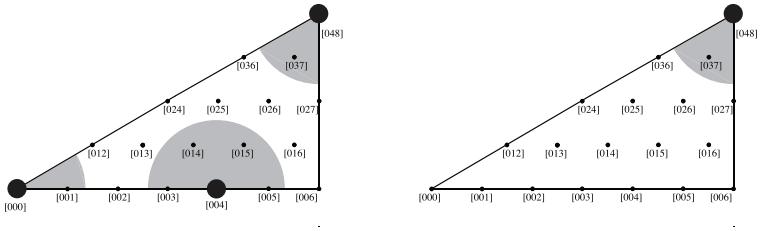

Figure 14: *The mathematics of the Fourier transform requires that we conceive of "chord quality" in terms of the distance to all subsets of the perfectly even n-note chord (left). Purely voice-leading-based conceptions instead allow us to choose our harmonic prototypes freely (right). Thus we can use voice leading to model a chord's "augmentedness" in terms of its distance from the augmented triad, but not the tripled unison* $\{0, 0, 0\}$ *or the doubled major third* $\{0, 0, 4\}$.

tigation suggests that we may want to think carefully about which model is appropriate for which music-theoretical purpose. I have tried to show that the issues here are complicated and subtle: the mere fact that tonal pieces modulate by fifth does not, for example, require us to use a tuning lattice in which fifths are smaller than semitones. (Indeed, the "circle of fifths" C-G-D-... can be interpreted either as a one-dimensional tuning lattice incorporating octave equivalence, or as a diagram of the voice-leading relations among diatonic scales, as in Figure 7.) Likewise, there may be close connections between voice-leading spaces and the Fourier transform, even though the latter associates "Z-related" chords while the former does not. The present paper can be considered a down-payment toward a more extended inquiry, one that attempts to determine the relative strengths and weaknesses of our three different-yet-similar conceptions of musical distance.

References

[1] Clifton Callendar. Continuous transformations. *Music Theory Online*, 10(3), 2004.

[2] Clifton Callendar. Continuous harmonic spaces. Unpublished, 2007.

[3] Clifton Callendar, Ian Quinn, and Dmitri Tymoczko. Generalized voice-leading spaces. *Science*, 320:346–348, 2008.

[4] Richard Cohn. Neo-Riemannian operations, parsimonious trichords, and their 'tonnetz' representations. *Journal of Music Theory*, 41(1):1–66, 1997.

[5] Richard Cohn. Introduction to neo-Riemannian theory: A survey and a historical perspective. *Journal of Music Theory*, 42(2):167–180, 1998.

[6] Richard Cohn. As wonderful as star clusters: Instruments for gazing at tonality in Schubert. *Nineteenth-Century Music*, 22(3):213–232, 1999.

[7] Jack Douthett and Peter Steinbach. Parsiomnious graphs: a study in parsimony, contextual transformations, and modes of limited transposition. *Journal of Music Theory*, 42(2):241–263, 1998.

[8] Rachel Hall and Dmitri Tymoczko. Poverty and polyphony: a connection between music and economics. In R. Sarhangi, editor, *Bridges: Mathematical Conections in Art, Music, and Science*, 2007.

[9] Justin Hoffman. On pitch-class set cartography. Unpublished, 2007.

[10] David Lewin. Re: Intervallic relations between two collections of notes. *Journal of Music Theory*, 3:298–301, 1959.

[11] David Lewin. Special cases of the interval function between pitch-class sets X and Y. *Journal of Music Theory*, 45:1–29, 2001.

[12] Ian Quinn. General equal tempered harmony (introduction and Part I). *Perspectives of New Music*, 44(2):114–158, 2006.

[13] Ian Quinn. General equal tempered harmony (Parts II and III). *Perspectives of New Music*, 45(1):4–63, 2007.

[14] Thomas Robinson. The end of similarity? semitonal offset as similarity measure, 2006. Paper presented at the annual meeting of the Music Theory Society of New York State, Saratoga Springs, NY.

[15] Dmitri Tymoczko. The geometry of musical chords. *Science*, 313:72–74, 2006.

[16] Dmitri Tymoczko. Scale theory, serial theory, and voice leading. *Music Analysis*, 27(1):1–49, 2008.

Using Turtles and Skeletons to Display the Viewable Sphere

David Swart
Waterloo, Ontario, Canada
E-mail: david.swart@sympatico.ca

Abstract

A number of software packages allow us to stitch together photos to capture the entire viewable sphere. To represent the viewable sphere in interesting ways, we introduce a new way to define projections (cartographic mappings from the sphere to the plane) using a turtle language similar to Logo. These projections can be printed, cut out and assembled into photographic equivalents of Termespheres. Further, this new method for defining projections is versatile enough to allow artistic and mathematical explorations and as such, the projections can be interesting in their own right (i.e., without being constructed back into spheres).

1 Motivation

Image stitching software makes it easier for users to create larger, seamless images from photos. Panoramas that capture the entire viewable sphere can be stitched together, but how does one represent, display, and share them? To display these panoramas on a flat computer screen or on paper, we need a mapping from the sphere to the plane. In cartography, these mappings are referred to as *projections* and all projections will introduce some sort of distortion. Despite this, projecting the visible sphere onto the plane has been undertaken by photographers and mathematicians alike, and conformal mappings (mappings with no local distortions) play a big role [5]. But perhaps a more natural medium for representing panoramas would be the photographic equivalent of a *Termesphere* [6]. Dick Termes painted spherical representations of the viewable sphere so that rather than looking outward from the observer's viewpoint, the observer looks inward to the scene on the surface of the sphere. If a spherical representation is chosen, then the photographer's problem would then become one of manufacturability.

A common method for creating globes by gluing thin paper strips called *gores* onto a sphere can result in creases and wrinkles. More gores reduce the amount creases but make the task of assembly more finicky. Another solution is to include features akin to a dressmaker's *darts* where a thin triangle of material is removed and the edges are brought together to shape the sphere. Many commercial globes use this approach. Towards creating complex projections such as gores with darts, this paper describes a versatile approach to designing projections that are suitable for printing and assembling back into spheres.

The problem of covering a sphere with paper will be familiar to those who have seen the work by Demaine *et al.* [4]. Their solution uses the same fundamental mechanism as the one presented here (i.e., the *taut paths* in their terminology are called *skeletons* here). While they discuss metrics for area, perimeter, and tiling the plane, this paper introduces the new concepts of a) a turtle language for the purpose of designing projections more easily b) having a disconnected set of taut line segments c) a focus on mapping the interior imagery and d) an exploration of some different families of projections.

This paper is organized as follows: Section 2 introduces the concept of skeletons and how they map the sphere to a plane while Section 3 describes how we can use a turtle language to define these skeletons. Section 4 walks through an example. Section 5 discusses some tips on implementation. Finally, Section 6 displays some projections created with the new method.

2 Mapping the Sphere to the Plane

In keeping with the idea that we intend to paste the planar projection back onto a sphere, it helps to think of some lines and points on a ball where we glue or tack pieces of paper. And now, imagine pulling the unglued portions of paper taut and down onto the ball. In this scenario, the paper is the plane and the ball is the sphere of course. We call the set of line segments and points that correspond to the glue the *skeleton of the projection.*

The method for mapping the sphere to the plane becomes more apparent when we realize that this skeleton exists as a set of line segments on the sphere and a corresponding set on the plane. We still need to establish how to map the non-skeleton points of the sphere (mimicking pulling the unglued portion of the paper taut). But once we do so, we can define projections by specifying a skeleton as a set of line segments on the sphere, and a corresponding set of line segments with the same lengths on the plane.

Given some line segments on the sphere, some line segments on the plane, and given an arbitrary point on the sphere, the task is to find a point on the plane in the same relative position and distance to the segments on the plane. We define the mapping for both skeleton and non-skeleton points below. In this paper, distance on the sphere refers to great circle-distance (i.e., the distance along the surface).

Definition. Given S, a set of line segments on a sphere, and S' a corresponding set of line segments of the same lengths on the plane, we define a function $\boldsymbol{f_{S,S'}}$ that maps the points on a sphere to the plane. Let p be a point on the sphere. Let segment $ab \in S$ be the segment nearest p, with corresponding segment $a'b' \in S'$. If p lies on ab, then we define $f_{S,S'}(p)$ as the point p' on $a'b'$ such that $|ap|=|a'p'|$. Otherwise, p

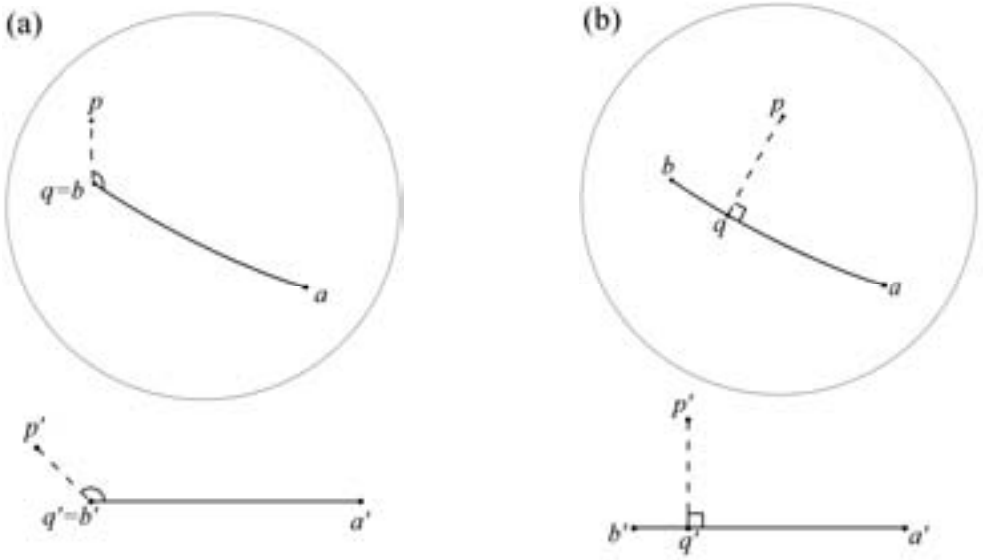

Figure 1: *Mapping a point p on the sphere to a point p′ on the plane based on the nearest segment to p and its corresponding segment on the plane. (a) depicts when p is closest to an endpoint of ab, (b) depicts when it is closest to a non-endpoint*

does not lie on *ab*. So let *q* be the point on *ab* nearest to *p* (without loss of generality, $q \neq a$). Then let q' be the corresponding point on $a'b'$ such that $|aq|=|a'q'|$. We define the function $f_{S,S'}(p)$ as the point p' on the plane, such that $\angle aqp=\angle a'q'p'$ and $|pq|=|p'q'|$.

The above function is not well defined if |ab|=0, i.e., in the degenerate case where the segment is just a point, because the required angle is not defined. However, we can apply $f_{S,S'}$ to skeletons with points if we keep a sense of direction with each skeleton point.

In our intuitive picture of gluing pieces of paper to a ball, we left out the details of what shape the pieces of paper will be. The definition of $f_{S,S'}$ defines the paper shapes when it requires that we must use the nearest segment to map our points. Thus the sphere is divided neatly into *Voronoi regions* (neighborhoods of the closest points) around each line segment. And hence the shapes of the pieces of paper that get glued to the ball are the shapes of these Voronoi regions, mapped around their corresponding skeleton line segments on the plane.

3 Defining a Skeleton with a Turtle Language

The previous section defined a mapping that uses a given skeleton to map the sphere to the plane. To define the skeleton itself, we can make use of the concept of a turtle language. This simplifies the definition of the skeleton line segments and also places the skeleton on the plane in a logical arrangement.

Turtle languages such as Logo are graphic programming languages that use commands to move a "turtle" around on the screen [1]. The turtle has a pen which draws a line along its path. In our situation we have two spaces, the plane and the sphere. It makes sense then to have two turtles, a sphere-turtle and a plane-turtle, which simultaneously obey the same set of instructions.

The list of the primitives that we use is in Table 1. Turtle language commands are usually simple primitives such as "pen up", "move forward 10", and "pen down" however our set of commands use *move-to* and *line-to* commands to accomplish the same thing. The units listed in the table are chosen for practical purposes; a line segment measuring π radians on the sphere corresponds to a line segment of length *n* pixels on the plane.

Table 1 *Commands in our turtle language*.

`R x`	Rotate in place $x \times \pi$ radians counter-clockwise
`M x`	Move $x \times \pi$ radians on the sphere, $x \times n$ pixels on the plane. No segment is created
`L x`	Create a line segment forward $x \times \pi$ radians on the sphere, $x \times n$ pixels on the plane.

Defining the skeleton with a turtle language this way has the benefit of arranging the skeleton on the plane in the right position and at the right distance, such that the mapped Voronoi regions are just touching and the imagery within adjacent regions is aligned.

Since the regions are well aligned by this method, designing a skeleton solely in “sphere-space” usually results in pleasing results on the plane. However, it is still possible to have a mapping where different points on a sphere get mapped to the same position on the plane! (An exercise for the reader is to peel a mandarin orange in one piece such that when flattened, the rind overlaps itself.) In practice, such situations are rare and minor enough to ignore. But if necessary, one could add an “`M 2`” instruction which returns the sphere pointer to its original position, but moves the plane pointer 2*n* pixels away.

4 The Volleyball Projection (A Demonstration)

Let us now illustrate the process of mapping the sphere to the plane based on the design of a volleyball's panels. Instead of a panorama, we use a map of the world for illustration purposes since it is familiar, and it shows up well in this medium. The sphere-turtle starts out in Banff, Alberta, Canada and faces east.

The projection process starts by instructing the sphere-turtle to mark the middles of the leather panels. See Figure 2(a). For instance, the specific turtle instructions for three adjacent panels on a side are:

```
M -1/6; L 1/3; M -1/6; R 1/2; M  1/6; R -1/2;
M -1/6; L 1/3; M -1/6; R 1/2; M -1/3; R -1/2;
M -1/6; L 1/3; M -1/6; R 1/2; M  1/6; R -1/2;
```

The sphere-turtle is moved to the other five sets of three panels and the above sequence is repeated. Simultaneously, the plane-turtle follows along and automatically creates an organized layout. See also Figure 2(a).

The drawn line segments of the turtles' path create the two skeletons used for the mapping, one skeleton on the sphere, and one skeleton on the plane. See Figure 2(b).

The points of the sphere are thus arranged into Voronoi regions around the skeleton's line segments, Figure 2(c). Finally, using $f_{S,S'}$, the points of each Voronoi region are mapped around the corresponding line segments on the plane to create the final volleyball projection. See also Figure 2(c).

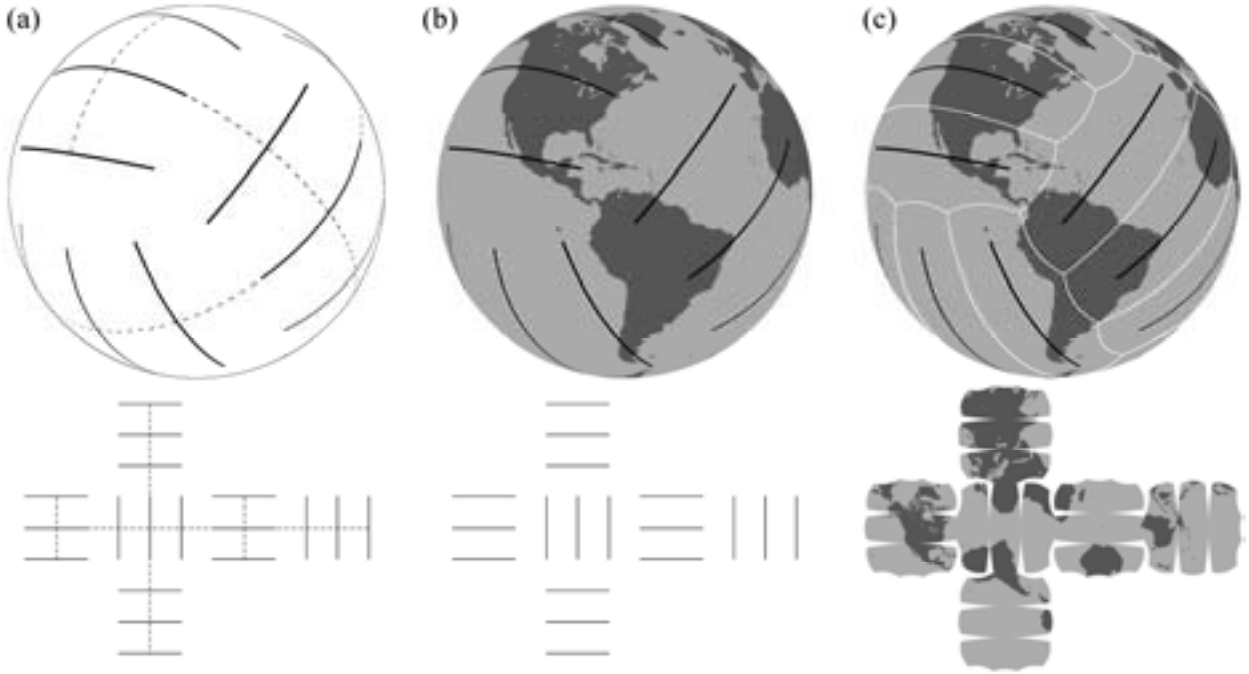

Figure 2: *(a) A single turtle program directs two turtles to draw paths, one on a sphere and one on a plane. (b) Two skeletons (sets of line segments) are thus defined. (c) The points nearest to each line segment on the sphere (Voronoi regions) are mapped to the corresponding segment on the plane.*

5 Implementation

The preceding section demonstrates some important concepts of our skeleton method but does not serve well as a guide to implementing an algorithm. To render an image, we might start with the position of

each pixel p' on the plane and then calculate the point p on the sphere to render. However, the function $f_{S,S'}$ maps points in the opposite direction; we would need to implement its inverse. And yet, $f_{S,S'}$ has *no* inverse in the rare cases when it maps two points on a sphere to the same point on the plane. Our implementation gets around this technicality by blindly ignoring it. (If necessary though, one could use the "`M 2`" work around described at the end of Section 3.)

The pseudocode below may help those wishing to write their own software. We define function $g_{S',S}$ in the same way that $f_{S,S'}$ is defined in Section 2, but with the roles of the sphere and the plane reversed. Thus when $f_{S,S'}(p)=p'$ is single-valued, then yes, $g_{S',S}(p')=p$, but only when p is in the proper Voronoi region on the sphere. The pseudo-code below applies $g_{S',S}$ and then performs this check.

```
The input is a skeleton and a color for each point p on the sphere
for each pixel p' on the plane, do:
    s' ← nearest segment on the plane to p'
    s ← segment on sphere corresponding to s'
    p ← g_{S',S}(p')   (the point on the sphere in the same relative position to s as p' is to s')
    if the nearest segment to p ≠ s then:
        output a blank pixel
    otherwise:
        output the color of p
```

Figure 3: *Pseudocode for one possible implementation*

Our implementation is a Win32 console application written in C, with no graphical user interface. Its running time has not been formally analyzed but experience shows a strong dependency on the number of segments in the skeleton. For instance, it takes about five seconds to render a 2000x2000 image of a two-segment skeleton, but almost 30 minutes for a 600-segment skeleton of the same size.

6 Examples

We finish by looking at some of the projections accomplished with our new method.

6.1 Simple Projections Even very short turtle programs can generate some interesting results. A single point skeleton specified by "`L 0`" creates a projection known as an azimuthal equidistant projection. See Figure 4. A skeleton consisting of a great circle is specified by "`L 2`" and produces a well known and common projection known as an equirectangular projection. See Figure 5.

Figure 4: *An azimuthal equidistant projection centred on Banff.*

Figure 5: *An equirectangular projection, with Banff at the middle of the left edge.*

The previous two projections are notable since they help characterize the interior of any projections produced with our skeleton method. Mathematically, each projection is a piecewise mix of azimuthal equidistant projections and equirectangular projections depending upon the two cases shown in Figure 1.

6.2 Polyhedra. Skeletons consisting of the face centres of polyhedra projected onto the sphere can produce interesting projections. Such projections resemble unfolded and flattened polyhedra, although not exactly (for instance, the edges of the faces are curved). The pentagonal hexecontahedron based projection in Figure 6 is my personal favourite.

6.3 Sport Balls. We have already seen the volleyball. And we have already discussed polyhedra, but the soccerball needs a special mention. In this case, our polyhedron approach mentioned in Section 6.2 does not create regular hexagons: the distance between the face centres of two neighbouring hexagons is greater than between a hexagon and a pentagon, and thus the hexagons' Voronoi regions are not regular. A new feature was added to our turtle language to give a weighting to each skeleton segment. By scaling up the distance to each pentagon centre appropriately, we achieve our soccerball projection in Figure 7.

Figure 6: *A pentagonal hexecontahedron projection*

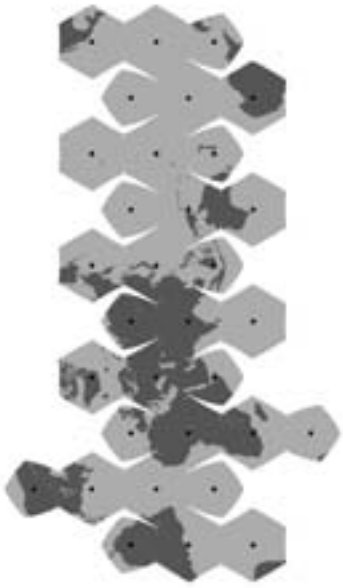

Figure 7: *A soccerball projection*

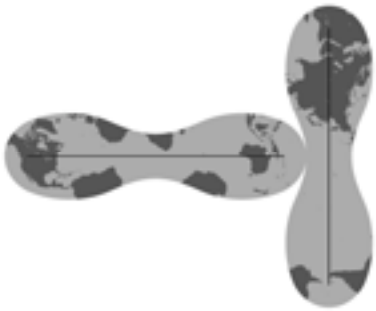

Figure 8: *A baseball projection*

As for baseballs, John Conway once conjectured, "no two definitions of "the correct baseball curve" will give the same answer unless their equivalence is obvious from the start" [3]. The set of turtle instructions "`L 2x; M 1-x; R 1/2; M –x; L 2x;`" with `x`=0.739726 throws another definition into the mix. See Figure 8. The value of `x` was chosen such that the leather flats are $1^{3}/_{16}$ inches wide at the "waist" for a baseball with a circumference of $9^{1}/_{8}$ inches, according to measured values.

6.4 Trail of Small Segments. Lloyd Burchill of Flaming Pear Software created a projection which mimics the peeling of an apple [2]. We can accomplish the same effect by specifying a trail of one hundred or so line segments which spiral from the top to the bottom of the "apple". See Figure 9.

6.5 Gores. The standard layout of gores can be specified with a line segment from pole to pole for each gore. This is well explored in [4]. Dart features are created by adding gaps to the meridians (Figure 10).

Figure 9: *A rind projection, after a projection by Lloyd Burchill*

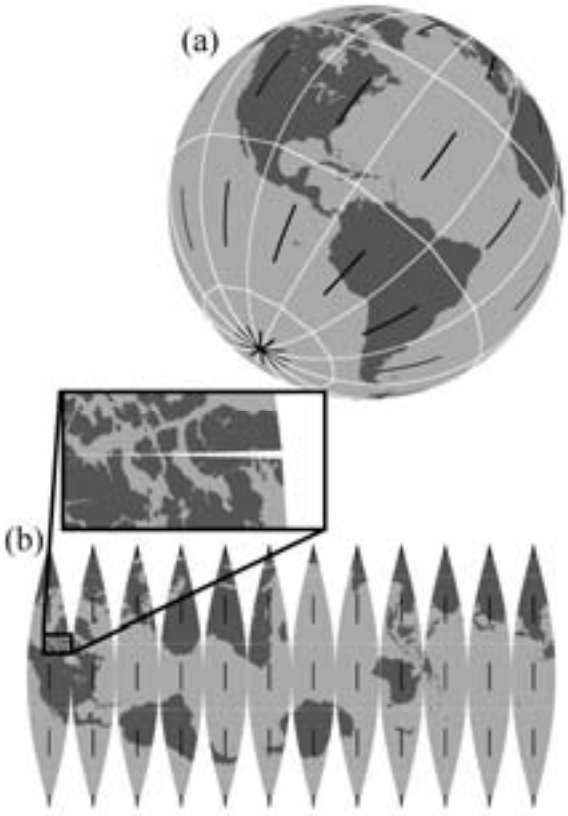

Figure 10: *The skeleton to create gores with darts shown on (a) the sphere and (b) the plane. A dart is shown inset.*

6.6 Photographs. Returning to the original reason for this work, Figure 11 shows a constructed photographic Termesphere using the gore design shown in Figure 10. The paper is cut and glued over a 3" plastic ball and used as a Christmas tree ornament.

We finish by showing how our new projections can be used as a compositional element for panoramas. Figure 12 shows four more projection designs.

Figure 11: *Photographic Termesphere*

7 Acknowledgements

I would like to acknowledge the inspiring work of Lloyd Burchill and Sébastien Pérez-Duarte. I also thank them, Michael Swart, Judy Newell and the anonymous reviewers for their feedback. The source imagery of the earth is courtesy of NASA's Earth Observatory. Figures 11 and 12 are © David Swart. The source imagery for Figure 12(c) is courtesy Sébastien Pérez-Duarte and used with permission.

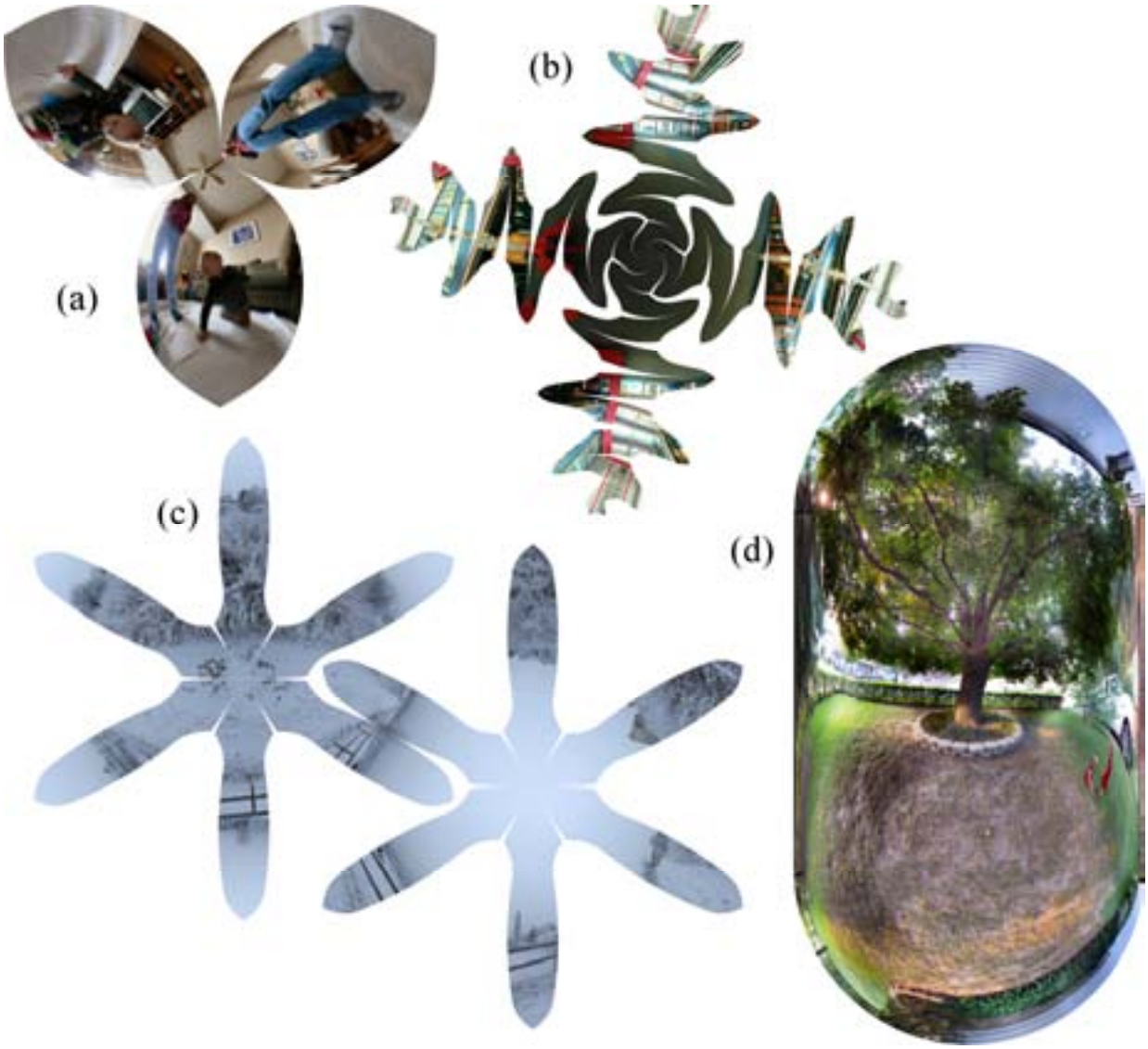

Figure 12: *"Twin's Eye View"(a) uses a three-gore projection as a compositional element. "Meandering Meridians"(b) and "Snowflakes on Snowflakes"(c) explore the potential of the turtle method with less emphasis on their panoramic content. "Under the Maple Tree"(d) is produced by the turtle instruction "*`L 1`*".*

References

[1] Harold Abelson and Andrea diSessa, *Turtle Geometry: The Computer as a Medium for Exploring Mathematics*. MIT Press, Cambridge. 1981.

[2] Lloyd Burchill. English Bay Park. http://www.flickr.com/photos/lloydb/57038900 28 Oct 2005.

[3] John Conway. math-fun. http://www.math.uni-bielefeld.de/~sillke/PUZZLES/baseball 3 Jun 1994.

[4] Erik D. Demaine, Martin L. Demaine, John Iacono, and Stefan Langerman: Wrapping Spheres with Flat Paper, In *Computational Geometry: Theory and Application*, to appear. Special issue of selected papers from the 20th European Workshop on Computational Geometry. 2007.

[5] Daniel M. Germán, Lloyd Burchill, Alexandre Duret-Lutz, Sébastien Pérez-Duarte, Emmanuel Pérez-Duarte, Josh Sommers: Flattening the Viewable Sphere. In *Computational Aesthetics 2007*, pages 23-28. 2007.

[6] Dick Termes. Painting the Total Picture. In *Bridges Leeuwarden: Mathematical Connections in Art, Music and Science Proceedings 2008*, pages 363-368. 2008.

Notation For a Class of Paperfolded Models

Goran Konjevod
Computer Science and Engineering
Arizona State University
Tempe, AZ 85287-5406
Email: goran@asu.edu. *

Ana Maria Kuprešanin
School of Mathematical and Statistical Sciences
Arizona State University
Tempe, AZ 85287-1804
Email: amk@math.asu.edu

Abstract

We propose notation for a class of paperfolded models that uses a simple formula-like string to completely describe the folding process.

1 Introduction

In origami, or paperfolding, there are models that require complex fold steps. In order to describe the folding process in written form, over time an intricate system of diagramming symbols and conventions has been developed. Even so, there have been models that simply defy diagramming and whose authors (designers, or composers) prefer to teach the folding process only in person, or not at all, and instead provide only the *crease pattern* that shows the location (and sometimes sense) of all the folds actually present in the finished model. Of course, a crease pattern alone may not uniquely define the model, but in typical cases it allows for an educated guess at how, for example, the layers of paper should be arranged.

1.1 Pureland origami

So-called *pureland* origami models restrict the folds used in each step to just the basic *mountain* and *valley* folds. In a valley fold, a straight line from one edge of the model to another divides the (normally flat) model into two parts. The fold consists of a single crease along the straight line, and except for the rotation of one of the two parts formed by the crease around the crease, nothing else moves. Pureland origami has been popularized by John Smith through several booklets published by the British Origami Society. Due to the simplicity of individual steps, it is particularly well suited to the teaching of beginners. Since the nature of a simple mountain or valley fold is to rotate one part of the model around the fold crease by 180 degrees, pureland models almost always remain flat.

1.2 Tessellations

As the name suggests, paperfolded *tessellations* are formed by repeating a single pattern, or a small set of patterns, across the whole folded sheet. The folding of tessellations is usually considered to date back to the work of Shuzo Fujimoto [3] and Yoshihide Momotani [7] in the 1960s and 1970s in Japan, although there are known examples of folded tessellations as early as this in the West as well, notably that of Ron Resch. Most folded tessellations require higly complex steps, since the different instances of the pattern to be folded tend to interfere with each other and in fact, the easiest way to fold some tessellations is to carefully coax the precreased or scored sheet into forming all the creases at once. In contrast to such more typical folded tessellations, we study a class that can be folded by iteration of simple mountain and valley folds, that is, a class of *pureland tessellations*.

A *pleat* is formed by a pair of adjacent parallel folds, one a mountain and the other a valley fold.

*This author's work supported in part by NSF grant 0830791.

(a) A tessellation fold by T. Kawasaki

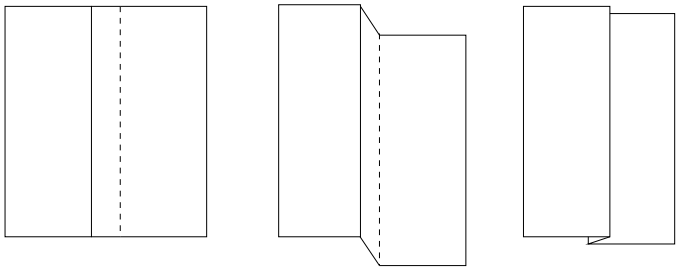

(b) Folding a pleat. Mountain fold (solid line) next to a valley fold (dashed line).

Figure 1: A tessellation that requires complex fold steps or a nonrigid collapse to fold; simple pleat fold.

2 Pleat tessellations

We consider pleat tessellation models formed by folding a sequence of pleats along grid lines parallel to the edges of the initial square, and possibly a few extra valley or mountain folds (the lock). There is no unfolding, so the model belongs to "pureland origami" and in theory lies flat. However, the photographs of models shown in these pages illustrate the difference between the theoretical model and the real life: paper has finite positive thickness and the models shown are obviously not flat. They *can* be forced into lying flat by careful application of force, but as soon as they are released, they spring back into a three-dimensional shape. This behavior is the result of a locking fold applied to (some) edges of the folded sheet. The lock consists of two parallel mountain folds close to the edge, and keeps the pleats folded tightly at the edge. The shape itself is determined by the arrangement of pleats. As in the case of the hyperbolic paraboloid [2], the three-dimensional shape is determined by the tension of the folded sheet, but in this case the thickness of the paper and the elastic properties of its folds play a very significant role. It is an interesting and apparently difficult problem to predict the exact shape formed by a pleat tessellation model. While there has been some work on computer simulations of the physical behavior of folded paper [1, 6, 4], none of it addresses the forces acting between adjacent layers of paper. We are currently studying a mathematical model that allows us to take this issue into consideration. The notation presented here is the (easy) first step in building such a simulation, since it allows a simple input specification to be translated into the folding process and an initial state for the simulation to be computed.

Pleat tessellations appear to have been folded first by Paul Jackson, and a photograph of the basic form, titled "Bulge", appears in his Encyclopedia of Origami & Papercraft Techniques [5]. The basic form has also been used by several origami designers to represent fish scales or snake skin. The more complex pleat tessellations shown here have been folded by the first author, starting in 2006.

3 Pleat tessellation notation

Since all pleats are parallel to the edges of the original square, each pleat is completely specified by four pieces of information: **(a)** *direction* (horizontal or vertical), **(b)** *location* (the coordinate of a point at which the mountain fold of the pleat intersects an edge of the square), **(c)** *sense* (positive or negative—the sign of the difference between the location of the pleat's mountain and valley folds), and **(d)** *width.*

Clearly, each pleat tessellation can be completely described by listing all the pleats to be folded in order. Thus to explain how to fold a pleat tessellation, we need no diagrams!

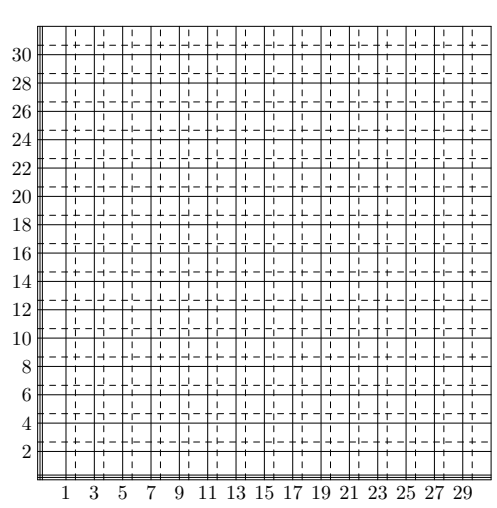

(a) The basic crease pattern with pleat order specified. The mountain folds very close to bottom and left edges are the optional locking folds

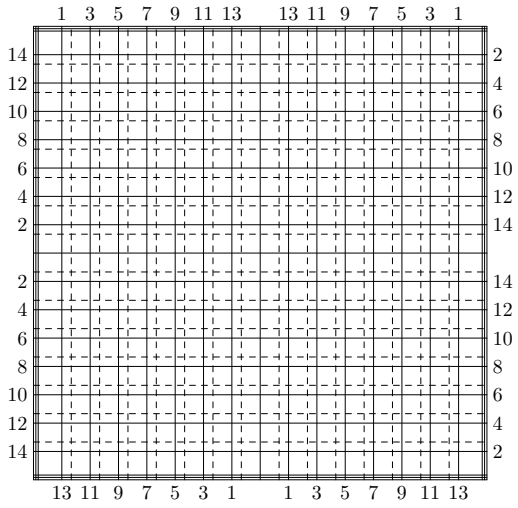

(b) Bottom and left edges: pleat order for flat-bottom bowl or pyramid (locking optional). Top and right edges: pleat order for simple bowl (with lock) or "four peaks" (without lock).

Figure 2: Crease pattern for models in Figures 3(a)–3(d). Each pleat is given a rank in each model. The pleats should be folded in the order specified by these ranks. Pleats assigned equal rank can be folded in any arbitrary order. Each number refers to two creases that form a single pleat. Figure 2(a) shows the pattern for the basic form in Figure 3(a). The bottom and left edges of Figure 2(b) show the sequence of pleats that leads to the pyramid of 3(c), while the top and right edges define the models in Figures 3(b) and 3(d).

We describe two ways to notate a pleat tessellation. The first is very general, and could be generalized to an arbitrary pureland model. There are several precedents for this, most notably the origami instruction language OIL [8]. However, thanks to the restrictions we impose on the creases in pleat tessellations, our task is simpler. In fact, in many cases the notation for a sequence of creases can be compressed, resulting in very short descriptions of some models that appear relatively complex. The second way of notating (typical) pleat tessellations is even more compact, because in addition to individual creases, it uses the fact that typical pleat tessellations are formed by folding one or more regular sequences of pleats, in ways that create symmetric patterns, and that there is only a small number of different ways these sequences are composed and interleaved.

We first describe the general notation for a single pleat, and then, after giving some examples of pleat tessellations defined by listing all their pleats, show some simple ways of compacting the description. Finally, we describe the compact notation.

4 Single pleat

Direction. Each pleat is by definition either horizontal or vertical, and so we use the letters *h* and *v*, respectively, to denote the direction.

Location. It is convenient to express distances and lengths in terms of the size (side length) of the original square—that is, a horizontal fold formed by placing two opposite edges of the square on top of each other and pressing the sheet flat would be at distance $1/2$ from the edge of the square. A pleat that uses this crease as its mountain fold would then be at location $1/2$. On the other hand, if pleats that we fold are all located on a fixed grid, then writing down just the numerators of their locations creates significantly less clutter. In

such a case, though, the numbers are meaningful only if we know the grid size. For example, if we start with a 16×16 grid, the same horizontal crease through the center would have location 8, while in a 32×32 grid its location would be 16. Which of the two units is being used may be indicated, for example, by writing $u = 1/16$. However, since in the first case all the distances are less than 1, and in the other all the distances are at least 1, which unit is used can normally be inferred from the description.

To be consistent in this notation, we set up a coordinate system with origin at the bottom left corner of the square and direct the *x* and *y* axes in the standard way, towards the right and up.

Sense. If we fold a horizontal valley fold, and then some distance above it a horizontal mountain fold, we get a positive pleat. If the mountain fold is below the valley, the difference between the mountain and valley locations is negative, and so the pleat is negative as well.

Width. Again, this is expressed either in terms of the original square size, or in terms of the grid unit distance. In the notation, we will combine the information about the sense and the width of the pleat, by writing the width of a negative pleat as a negative number.

Pleat notation. A pleat formed by a horizontal mountain fold through the center, and a valley fold $1/16$ of the square width below it would be written as $(8/7)h$ (the mountain fold is at distance 8 from the bottom of the square, the pleat is horizontal, and the valley fold is (positive) 1 units below the mountain fold). If the pleat were negative (valley through the center, mountain a unit below), we would write $-(8/7)h$. The simple rule for decoding this notation is: the first number tells us the location of the top crease of the pleat, and the letter the direction. If the pleat is positive, then the mountain fold is above the valley, so the location of the mountain fold is given by the first number. If the pleat is negative, then the first number gives the location of the valley fold.

5 General pleat notation

The basic form. Let's first consider the basic form of Figure 3(a) and take the point of view from which the model bulges upwards. Suppose each pleat is $1/16$ wide and we begin folding from the lower left corner and continue until we run out of paper. Every pleat we fold is negative, because the coordinate of its mountain fold is smaller than that of its valley fold. If we begin with a horizontal pleat, and leave two units before it (for the lock), the notation for this first pleat is $-(3/2)h$. The second pleat will be vertical, and written as $-(3/2)v$. The second horizontal pleat will begin two units above the first. The first of these unit lengths is hidden by the previous pleat, and the second is the portion visible in the final model. Thus the second pair of pleats could be written as $-(6/5)h$ and $-(6/5)v$. Writing out the whole sequence is tedious, so we can simplify the notation by introducing an index. The complete folding sequence for the model is the sequence of pairs of the form

$$\frac{-3i}{3i-1}h\frac{-3i}{3i-1}v,$$

where *i* ranges from 1 to 5 (the largest meaningful coordinate for a 16-unit grid is 16, and 15 is the largest multiple of 3 smaller than this).

Simple bowl. In folding this model, we are effectively interleaving two bulges, one starting from the bottom left and the other from the top right corner. For symmetry, we alternate between folding two horizontal and two vertical pleats. Say we begin with a 32-unit grid. The first horizontal pleat is, as before, $-(3/2)h$. Before folding the corresponding vertical pleat, however, we fold another horizontal pleat at the very top of

the sheet, that is, we fold $(29/30)h$. Note that this pleat is positive, because its mountain fold is above its valley. Thus the bowl is completely described by

$$\frac{-3i}{3i-1}h\frac{32-3i}{32-3i-1}h\frac{-3i}{3i-1}v\frac{32-3i}{32-3i-1}v,$$

for i ranging between 1 and 5.

Drawbacks. The simple bowl from the previous example has two mirror lines. (It "almost" has even more symmetries; only the fact that each pair consisting of a horizontal and a vertical pleat cannot be made at the same time prevents this model from having the symmetry of a square. In a sense, it is globally symmetric, but not locally.) However, this symmetry is not really reflected well in the notation. The problem is that we use the same coordinate system for each pleat. In order to give as much information as possible about a model without need for complicated calculations, we might wish our notation to somehow indicate the inherent symmetries (as well as the "almost symmetries", which ignore the ordering of adjacent layers). In the next section we describe such an approach to the notation of pleat tessellations.

6 Compact notation

In most pleat tessellations, each horizontal pleat is immediately followed by a vertical pleat. In other words, we consistently interlace horizontal and vertical pleats. This leads to models that hold together even when folded from paper that doesn't hold creases too well. The tendency of each crease to unfold is kept in check by its immediate neighbors, which at the same time creates the tension that shapes the final fold without need for wet folding. What this means for notation is that perhaps we've gone too far in trying to describe every single crease: if we know the current pleat, the next one is almost completely determined. This observation leads to the next, more restrictive but much more compact and more visual notation.

Pleat sequences made implicit. The basic form consists of a single sequence of pleat pairs, each horizontal pleat preceded and followed by vertical ones. If we know how many pleat pairs we make, we know exactly what the final result is. We ignore the distinction between a left-handed and a right-handed model (determined by whether the first crease is horizontal or vertical). Thus we may as well describe the bulge by just giving the number of pleat pairs to be folded.

Symmetry. To make the symmetry structure of a pleat tessellation apparent, we specify the degree (the number of symmetric pleat sequences folded), 1 (which may be omitted) or 2. The goal is to give meaning to expressions such as 16 (or equivalently 16^1, the basic bulge model) and 16^2 (the simple bowl).

Unit pleats. The width of paper used by a pleat of width 1 is actually 3 units: to cross the width of an unfolded pleat, we first cross a unit in getting to the mountain fold, then turn the corner around the mountain fold and go back a unit width, and finally turn again, and go another unit to emerge from under the pleat. If we are describing the model just in terms of pleats, and they are all of the same width, it makes sense to use the full width of the strip used up by a pleat as a unit of distance. In other words, in the compact notation writing 16 for a grid size will mean that we can fold 15 pleats from the grid.

Example: bulge. This is the simplest case. If there are k horizontal and k vertical pleats, we write just k.

Example: simple bowl. If the sequence starting from the bottom left is seen as a sequence of positive pleats, then so should be the sequence starting from the top right. This model consists of two basic pairs of pleat sequences, and so we write 15^2.

Example: pyramid. Here, the folding begins in the center and progresses towards the edges of the sheet. These are negative pleats, and therefore we write $(-15)^2$.

Example: Two-fold basket. Here, two pleat sequences begin at the centers of two opposite edges of the sheet. Compared to the basic bulge, one of these is rotated 90 degrees. We write $k \cdot i$ for a length k pleat sequence rotated by $\pi/2$ around an axis normal to the plane of the fold. (Note that this is compatible with the use of -1 for negative pleats.) Thus the two-fold basket may be denoted by $(15i, -15i)$.

Example: wave. Here, we are simultaneously folding a bulge from one and an upside-down ("flipped") bulge from the opposite corner. We denote the flip by the letter f, and so the wave is defined by $(15, 15f)$.

Paper size. We may also specify the paper size (in terms of full pleat width units) before the rest of the expression. Thus, a wave folded beginning with a 32×32 grid could be written as $32 : (15, 15f)^2$.

Example: fancy bowl. In this model the folding sequence for the upside-down pyramid is interlaced with the folding sequence for the bowl, resulting in an inverted pyramid in the middle, and four corners whose shape is exactly the simple bowl shape. We denote this bowl by writing $(7, -7f)^2$.

Example: second-order bowl. A second-order pleat consists of two opposite pleats next to each other. We should group the pairs of simple pleats that form second-order pleats: $32 : (7(1, -1f))^2$

More complicated sequences. The basic rule is: recurse and parenthesize. An expression of the form $(A_1)(A_2)$ instructs us to first fold the sequence specified by A_1, then the one by A_2. The pleats of A_2 will be placed in between those of A_1. See Figure 4(d) for the interleaved bowl, defined by $32 : (8)^2(7)^2$.

7 Final comments

Suggestions for folding. The patterns given in this paper may be sufficient to allow experienced folders to reproduce the models. However, in order to make it easier for others, we briefly describe the process. Most of the pieces described in this paper are based on the square grid. The easiest way to fold a grid is to use a power of 2 as the number of squares along each side, and to always divide an existing unfolded strip of paper in two by aligning an edge of the paper sheet with a previously folded crease. Since many parallel folds will stretch the sheet somewhat, it is best to alternate between dividing in half horizontally and vertically. In order to maintain integrity of the paper sheet, it is best to fold only valley folds (or only mountain folds). Our personal preference is to precrease only one half of each pleat, that is, only the mountain fold, and to create the valley fold "on the fly" once the actual folding begins. The main reason for this is that the multiple layers of paper will cause all but the first few pleats to lie slightly away from their theoretical position. If both the valley and the mountain fold are precreased, this "creep" leads to problems. This approach to folding is another factor that makes the compact notation natural, in that it focuses on individual pleats and assumes a regular grid.

Finally, the lock is achieved by simply folding an edge of the sheet twice: two mountain folds in parallel creating the impression of a rolled edge. If the pleats are held tightly as this is done (not easy, and best attempted slowly and only a few pleats at a time), the two folds will prevent the pleats from opening up and will thus lock the edge.

Acknowledgment. The authors thank the reviewers for a careful reading of the paper and numerous corrections and suggestions for improving the presentation.

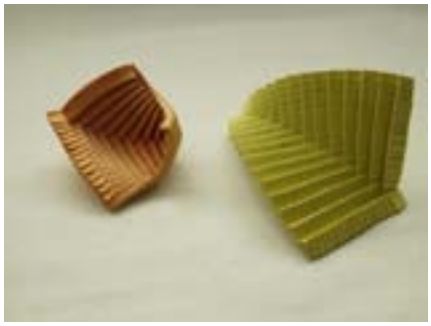

(a) Basic pleat tessellation, locked (the Bulge) and unlocked. 15.

(b) Simple bowl: locked. $(15)^2$.

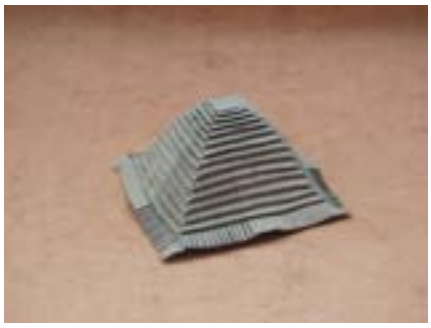

(c) Pyramid. $(-15)^2$.

(d) Simple bowl: unlocked. $(15)^2$.

(e) Wave. $(15, 15f)$.

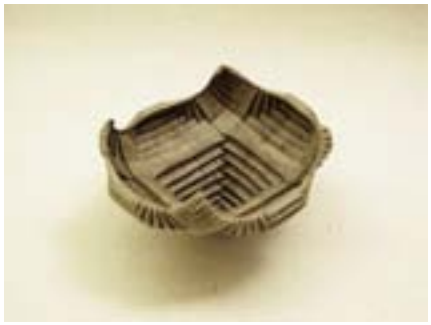

(f) Fancy bowl. $(7, -7f)^2$.

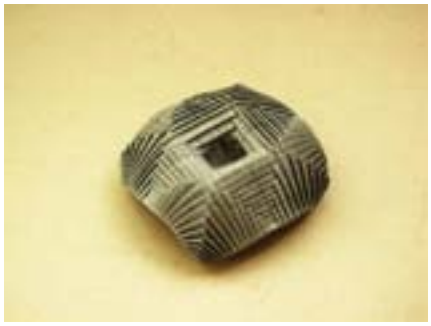

(g) Candy dish. $(10, 5f)^2$.

(h) Two-fold basket. $(15i, -15i)$.

Figure 3: Some pleat tessellations.

References

[1] R. Burgoon, Z. J. Wood, and E. Grinspun. Discrete shells origami. In *Computers and Their Applications*, pages 180–187, 2006.

[2] E. D. Demaine, M. L. Demaine, and A. Lubiw. Polyhedral sculptures with hyperbolic paraboloids. In *Proceedings of the 2nd Annual Conference of BRIDGES: Mathematical Connections in Art, Music, and Science (BRIDGES'99)*, pages 91–100, 1999.

[3] S. Fujimoto. *Twist origami*. 1976. Privately published; reprinted 2007.

[4] Y. Furuta, J. Mitani, and Y. Fukui. Modeling and animation of 3d origami using spring-mass simulation. In *Proceedings of NICOGRAPH International*, 2008.

[5] P. Jackson. *The Encyclopedia of origami & papercraft techniques*. Quarto Publishing, 1991.

[6] D. Koschitz, E. D. Demaine, and M. L. Demaine. Curved crease origami. In *Abstracts from Advances in Architectural Geometry (AAG 2008)*, pages 29–32, 2008.

[7] Y. Momotani. *Origami nyumon*. 1971. Reported by David Lister, `http://www.britishorigami.info/academic/lister/tessel_begin.php`.

[8] J. Smith. *BOS Booklet 4: An Origami Instruction Language*. British Origami Society, 1975.

(a) Second order bowl. $32 : (7(1,-1f))^2$.

(b) Valentine. $32 : (15(1,-1f))$.

(c) Double wave. $44 : (11,11f,11,11f)$.

(d) Interleaved bowl. $32 : (8)^2(7)^2$.

Figure 4: More advanced pleat tessellations.

The Art of Iterated Function Systems With Expanding Functions

Philip Van Loocke
Rectorate
University of Ghent
Sint-Pietersnieuwstraat 25
9000 Gent, Belgium
E-mail:philip.vanloocke@ugent.be

Abstract

Iterated function systems with contracting functions have been widely applied in contexts relating art and science. This paper explores iterated function systems which consist of expanding linear functions. An area in the plane is divided in parts which are defined implicitly by an inverse function technique. With each part, an expanding function is associated. A coloring technique is proposed which yields textures suggestive of sophisticated patterns of depth and light. It is briefly described how a rendering technique for recurrent origami can be obtained as a special case of this method.

Introduction

Iterated function systems defined by contracting functions are a familiar tool among researchers bridging art and science. Such systems yield compact codes for a large variety of images, which can be generated at any desired resolution. This paper describes a fractal image creation technique based on iterated function systems with expanding functions. The method is based on an inverse technique for iterated function systems consisting of two linear holomorphic functions [1]. It is described in this paper in a geometric way. I briefly explain how a rendering technique for recurrent origami can be obtained a special case of this method.

Suppose that an iterated function system $\mathcal{F}$ is defined by n functions f_j (j=1,…,n). In the classical treatment all functions f_j need to be contracting in all directions (see for instance chapter seven in [2] for a formal specification of this constraint). I call a function 'expanding' if its inverse is contracting. Function systems with linear expanding functions have been considered in the context of inverse techniques. In the early nineties Prusinkiewicz formulated such a technique which allows one to color the complement of attractors [3]. I confine myself to an informal description. Suppose that P is a point on the outside of the attractor of $\mathcal{F}$. Let C be a contour which encloses the attractor. Consider compositions of s inverse functions $f_{r_1}^{-1} f_{r_2}^{-1} ... f_{r_s}^{-1}$ with $r_j \in \{1,...,n\}, j = 1,...,s$. Since the inverse functions are expanding, each composition of sufficient length will map P onto a point on the outside of C. Consider the composition for which P travels the longest path inside C before bailing out. The length of this path associates a number with P which can be transformed into one or three color values.

This type of inverse technique has one advantage. The color of a point P is determined by an algorithm that takes this point as argument. In the direct method, one has to wait and see if the chaos game lands on the corresponding pixel until one knows if P is given a colour value (and if so, wait longer until a relative frequency of pixel visitation can be reliably determined). In this sense, an inverse technique acts like the usual method for coloring points of non-linear escape fractals. But there are two drawbacks. First, in contrast with the latter, the inverse technique needs calculation of many trajectories in P. The number of trajectories required increases combinatorially with n, which makes this method in most cases practically

unfeasible if n is larger than 2. Second, it only colors the complement of attractors. There are many situations in which the attractors themselves, and the fractal textures defined on them, are visually interesting objects. In this paper I present a geometric formulation of a different inverse technique, which solves both problems. First I formulate it in a general way. Then I describe two ways in which it can be specified.

Iterated function systems with expanding functions

The basic concepts of the present method are illustrated in Figure 1. Let A be an area in the plane. $S_1,\ldots,$ S_m are disjoint subsets of A. Let B be the set defined by $B = \bigcup_{j=1,\ldots,m} S_j$. Note that $B \subseteq A$. I confine the illustrations to the case in which B is a strict part of A. With each subset S_j, an expanding linear function h_j is associated which maps S_j onto $h_j(S_j)$, which is assumed to be a subset of A as well. Consider the function $g : B \rightarrow A$ which is defined by $g(P)=h_j(P)$ if $P \in S_j$ (j=1,…,m). The algorithm considered in this paper defines for each point $P \in B$ a series of points $P_0,\ldots P_N$. The first point P_0 is initialized by $P_0=P$. Then, P_1 is defined by $P_1=g(P_0)$. If $P_1 \in B$, $P_2=g(P_1)$. Else, if $P_1 \in A \setminus B$, the algorithm terminates. This process is iterated. If $g(P_{k-1}) \in B$, $P_k=g(P_{k-1})$, else the algorithm halts. If the algorithm terminates at step t with $t<N$, a series of N points is constructed by adding $N-t$ times the origin O to $P_0,\ldots P_t$.

In the two last illustrations of next section, the algorithm is made slightly more sophisticated. Suppose that at iteration t a point $P_t \in A \setminus B$ is produced. Then the algorithm continues but P_t is replaced by $h_1^{-1}(P_t)$. For this modification, also points in the complement of B (and hence points in the complement of A) can be processed and lead to a series $P_0,\ldots P_N$. Since h_1^{-1} is contracting, features in the inside of A reappear in magnified version in the complement of A.

The sequence $P_0,\ldots,P_N$ is turned into a color value as follows: q points $Q_1,\ldots,Q_q$ are selected in the plane (these are allowed to be in A but do not have to). For each point P_k in the series $P_0,\ldots P_N$, the distance d_{kj} to all points Q_j is calculated (j=1,…,q). The inverses of the q distances associated with P_k are normalized to one, yielding coefficients c_{kj}. Then, with each point Q_j a quantity ϕ_j is associated in accordance with

$$\phi_j(P) = \sum_{k=1,\ldots N} c_{kj} / k^{\rho}$$

where ρ is a constant which was put to ρ =0.5 in the illustrations which follow. These quantities are linearly combined into $\varphi(P)$:

$$\varphi(P) = \sum_{j=1,\ldots,q} w_j \phi_j(P)$$

where w_j (j=1,…,q) are fixed coefficients. (Exploration of expressions with non-linear combinations, such as combinations of squares of ϕ_j, can be aesthetically rewarding as well). After $\varphi(P)$ has been calculated for each point $P \in B$, it is normalized between zero and one, and next it is turned into three color values by a colormap. In all illustrations in this paper, four points Q_j are used, which are located at the vertices of a square with center at the origin, and which is a scaled version of the unit square. Informally, the points Q_j define neighbourhoods which act as traps. The weight of trap j is a function of the inverse distance

between P_k and the defining point Q_j of the trap (which is expressed by c_{kj}), and different traps contribute in different ways to the quantity onto which the colormap is applied (which is expressed by w_j).

Illustrations for the square

In the first specification of the general concepts, I use an iterated rotation technique to divide B into disjoint subsets S_j. In Figure 1, A is the unit square with center at the origin. B is a smaller square with side $2a$ and four sets S_j are defined by:

$$S_1 = \{(x,y) \mid (x > -b) \,\&\, (x < a) \,\&\, (y > -a) \,\&\, (y < b)\}$$
$$S_2 = \{(x,y) \mid (x > -b) \,\&\, (x < a) \,\&\, (y > b) \,\&\, (y < a)\}$$
$$S_3 = \{(x,y) \mid (x > -a) \,\&\, (x < -b) \,\&\, (y > -b) \,\&\, (y < a)\}$$
$$S_4 = \{(x,y) \mid (x > -a) \,\&\, (x < -b) \,\&\, (y > -a) \,\&\, (y < -b)\}$$

with $b<a$. Similar partitions for the other regular polygons are obtained in a straightforward way (below this is illustrated for the octagon). In case of a square, a scaling is applied onto B with center in the lower right vertex of B, which results in S_1. Then, S_j (j=2,3,4) is the part of B which is not included in $S_1 \bigcup ... \bigcup S_{j-1}$ and which, after rotation around the origin with angle $-(j-1)2\pi/4$, overlaps with S_1. In Figure 4 this procedure is applied to the octagon, but S_j (j=2,…,8) was obtained for rotation of the reduced octagon with different angles. Variation of these rotation angles, and the resulting variation in the definition of S_j, is one way to find aesthetically relevant variations of images.

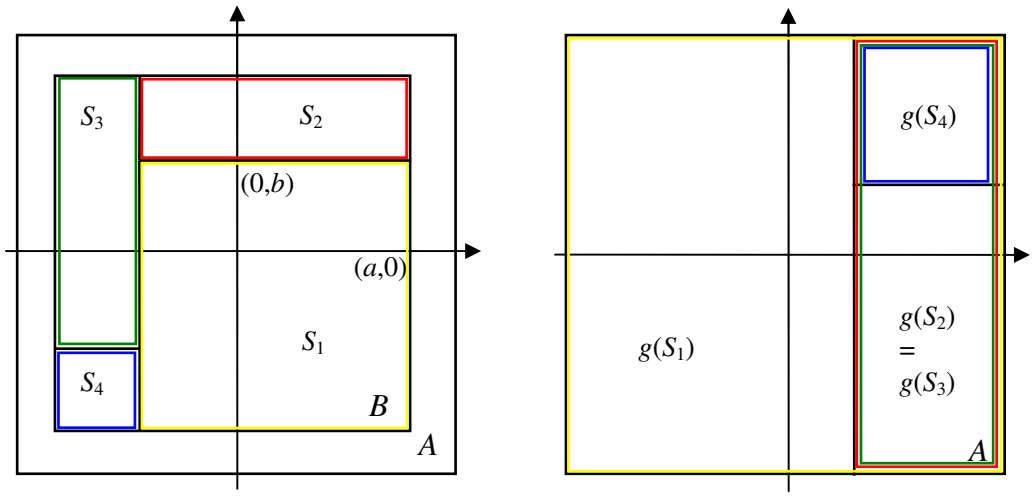

Figure 1: *Left: Partition of subset B of A into four parts S_j. Right: Image of the parts after application of g (the images of S_2 and S_3 are identical and include the image of S_4)*

There are different ways to define the functions h_j, but the most natural strategy is to relate h_j with the way in which the partition of B into the sets S_j was obtained. If these sets are obtained by iterated rotation, the simplest strategy is to dissect the action of h_j into three steps. I specify the procedure for the case of a square set A, but the generalization for other regular polygons is straightforward. Consider a point $P \in S_j$. First P is rotated around the origin with angle $-(j-1)2\pi/4$, so that the resulting point, which is denoted $P_{r,j}$, is in S_1 (points in S_1 are left unmodified by this step). The second step is the same for all h_j. Let C denote the center of S_1. As can be verified on basis of Figure 1, C has coordinates $((a-b)/2,$

$(-a+b)/2$). Let $\gamma=2/(a+b)$. Then, $P_{r,j}$ is translated with the vector which connects C with the origin. Subsequently, the resulting point is subject to a scaling with factor γ and center at the origin (the effect of this scaling on the translation of area S_1 is that the image of the latter coincides with A). These two actions define the second step. Third, the point obtained is rotated around the origin with an angle which is a multiple of $2\pi/4$, and/or subject to a reflection. The reflections and rotations in the third step can be chosen different for different j. (The case of identical rotations and absence of reflection corresponds to the situation considered in [1]).

Turning to complex number notation, the equations involved become very simple. For each point $P \in S_j$, $P_{r,j}$ can be written as $P_{r,j} = P \exp(-i\,(j-1)2\pi/4)$ (where i is the imaginary unit). The point onto which $P_{r,j}$ is mapped after the second step is $\gamma(P_{r,j}-C)$, with $C = (a-b)/2+i(-a+b)/2$. Then, the transformations h_j which lead to Figure 2 simply read $h_j(P) = (\gamma(P_{r,j} - C))^*$, where * denotes the complex conjugate (which corresponds to a reflection; this choice of h_j is illustrated in the right part of Figure 1). The transformations used to obtain Figure 3 are:

$$h_1(P) = \gamma(P_{r,1} - C)\exp(i2\pi/4); \qquad h_2(P) = \gamma(P_{r,2} - C)\exp(i6\pi/4)$$
$$h_3(P) = \gamma(P_{r,3} - C)\exp(i6\pi/4); \qquad h_4(P) = \gamma(P_{r,4} - C)\exp(i2\pi/4)$$

The two other illustrations in this section are based on octagonal sets A and B. The dissection of B in eight subsets is shown in Figure 4. With each set S_j (j=1,…,8) a function h_j is associated in accordance with the recipe specified above. The rotations in the third step of the definition of h_j were put equal to each other. The only difference between the algorithms leading to Figures 5 and 6 is that, in case of Figure 5, the rotations in the third step rotate with an angle $4\pi/8$, whereas in Figure 6, this angle is equal to $2\pi/8$. As was mentioned above, the algorithm used for these figures includes the additional step according to which a point not in $A \setminus B$ is contracted toward the center of S_1 with factor δ (which was put equal to 0.8 in the illustrations).

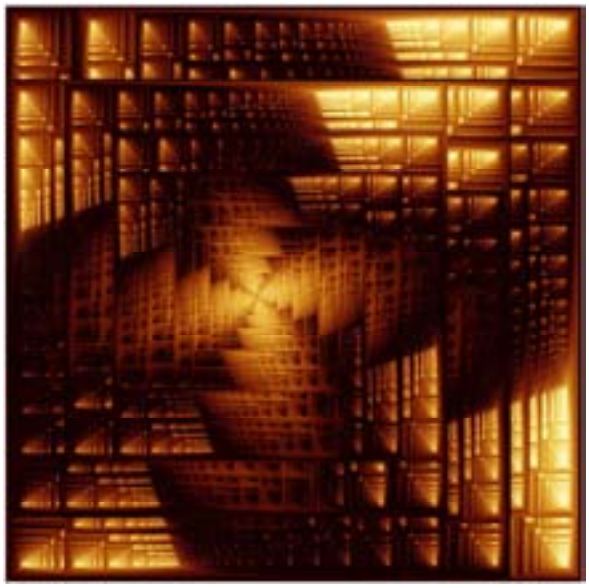

Figure 2: *(left) First illustration for square A, with a=0.9925 and b=0.75 and* **Figure 3***: (right) Second illustration for square A, with same sets S_j and same values of a and b, but for different definition of h_j*

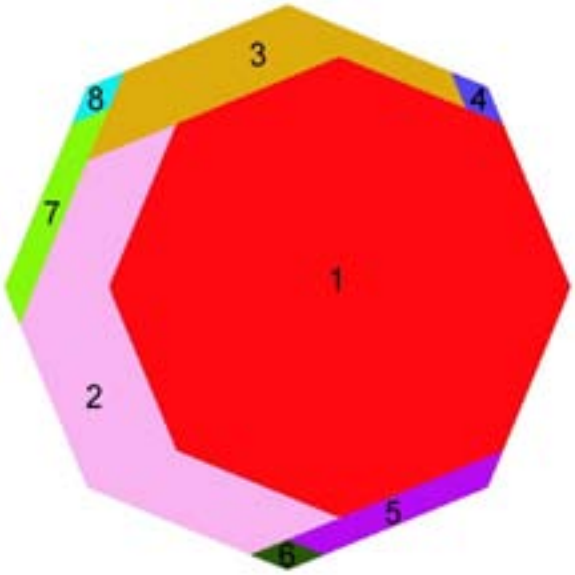

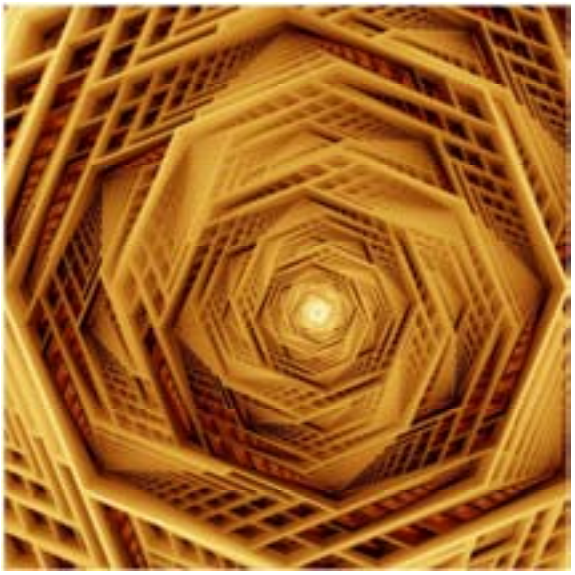

Figure 4:*(left) Partition of octagonal set B into 8 sets S_j and* **Figure 5:** *(right) Octagon-based illustration with rotation angle in third step of h_j equal to $4\pi/8$*

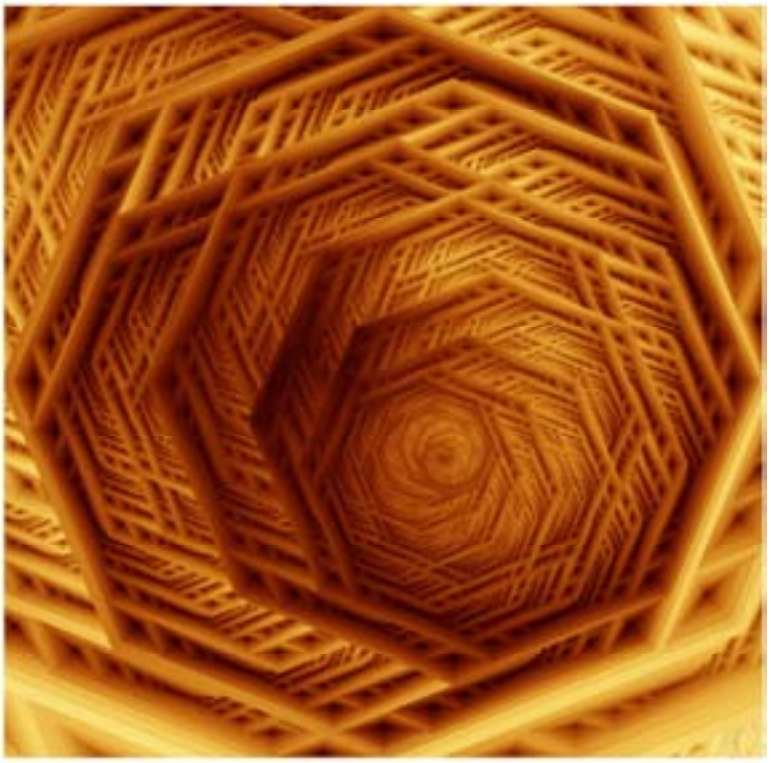

Figure 6*: Octagon-based illustration with rotation angle in third step of h_j equal to $2\pi/8$*

Definition of S_j and h_j by origami

In the second specification of the general concepts, S_j and h_j are defined by an origami process. Suppose that a polygon B is folded so that a smaller version of the same polygon is obtained. After unfolding, the sets S_j are specified by the partition generated by the crease pattern. In order to define h_j, the reduced polygon is magnified (and possibly rotated) so that it coincides with A. For each set S_j, this defines an expanding function which maps S_j onto a subset of A. In combination with the algorithm described above, this is basically all it takes to obtain Figure 8 on basis of the folding described in Figure 7 (Figure 7 for simplicity only shows B. A is a hexadecagon slightly larger than the blue hexadecagon B). Note that the process by which the reduced polygon is magnified has an alternative description. Mathematically, this is equivalent with downscaling the crease pattern to the reduced polygon, after which the folding is iterated. Therefore, the concepts described offer a way to create patterns corresponding to recurrent origami (some possibilities for variation, and a more extended discussion is given in [4]).

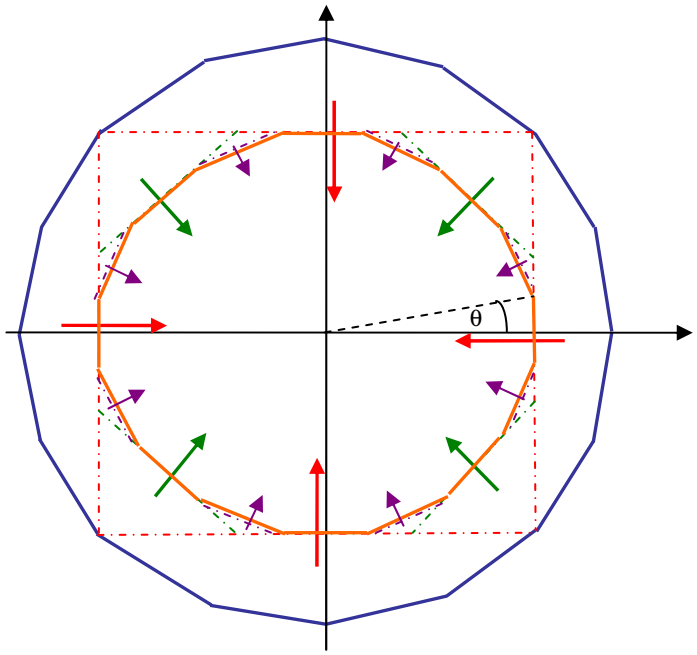

Figure 7: *The blue hexadecagon B is folded inward onto the smaller orange hexadecagon. First the parts between the square and the hexadecagon are folded (see the red arrows). Then the four corners of the square are folded, which results in an octagon (as indicated by the green arrows). Finally eight corners of the octagon are folded (in accordance with the purple arrows), so that the smaller hexadecagon is obtained. In order to define the functions h_j, the latter is rotated first around the origin with angle $\theta=\pi/16$, and next scaled so that it coincides with A.*

Figure 8: *Image obtained by iteration of the origami process in Figure 7*

Discussion

Iterated function systems are classically used with contracting functions. I have illustrated that expanding functions can yield fine results as well. One condition is that the domain on which functions act is divided carefully into parts. I gave two illustrations of how this can be achieved. The first one defines the parts by an iterated rotation method, the second one uses origami. There is little doubt that other partitions can be found which work equally well from an aesthetic point of view. But the latter application has the advantage of relating origami with fractal techniques, which is a domain in which many possibilities remain to be explored.

References

[1] Ph. Van Loocke, *Polygon-based fractals from compressed iterated function systems* (IEEE CG&A, accepted). 2009

[2] M. Field, M. Golubitsky, *Symmetry in chaos. A search for patterns in mathematics, art and nature*, Oxford: Oxford University Press. 1992

[3] P. Prusinkiewicz, M. Hammel, *Escape-time visualization method for language restricted iterated function systems*, Proceedings of Graphics Interface '*92*, Morgan Kaufmann, pp. 213-223. 1992

[4] Ph. Van Loocke, *Combination of basic origami with fractal iteration* (Computers and Graphics, accepted). 2009

Harmonious Dances

Karl Schaffer
Mathematics Department
De Anza College
21250 Stevens Creek Blvd.
Cupertino, CA 95014
E-mail: schafferkarl@deanza.edu

Abstract

Although choreographers may employ mathematical principles when creating dances, overt attention is seldom given to the mathematics by either the audience or the choreographer. We will examine the mathematical elements in several of the author's recently choreographed dances in which mathematical ideas were embedded purposefully and with the intent that the mathematics be at least somewhat visible to the audience. Two of the dances included elements of proofs, and all but one are part of the show "Harmonious Equations," which premiered in 2008.

Introduction

Choreographers often use mathematical principles when creating dances, though usually little overt attention is given to these connections by either the audience or the choreographer. In this paper we will examine the mathematical elements in several of the author's recently choreographed dances. In these dances the mathematical ideas were embedded purposefully and with the intent that the mathematics be visible to the audience. Two of the dances included elements of proofs, and the all but one that we will look at are part of the show "Harmonious Equations," which premiered in 2008.

The Sum of the Internal Angles of a Polygon

In one case the dance utilized a kinesthetic "proof," perhaps better described as an explanation in movement, that the sum of the internal angles of an n-sided polygon is $\pi(n-2)$. The author and sarah-marie belcastro used the proof described below when they performed a short dance composition as part of a 2008 lecture demonstration [1]. The dance uses simple ballet or modern dance steps and turns.

Suppose the internal angles are a_1, a_2, a_3,..., a_n. Most proofs that the author has seen, such as those mentioned in Richeson [2], first sum the external angles $\pi - a_k$. If one "walks" successively along the edges of the polygon, then at the kth vertex one must turn through the external angle $\pi - a_k$, so the overall sum must be 2π, which is the result of walking all the way around the polygon:

$$(\pi - a_1) + (\pi - a_2) + (\pi - a_3) + \ldots + (\pi - a_n) = 2\pi$$

Then the algebraic rearrangement of this expression gives us

$$n\pi - (a_1 + a_2 + a_3 + ... + a_n) = 2\pi$$

or

$$a_1 + a_2 + a_3 + ... + a_n = n\pi - 2\pi = (n-2)\pi$$

Some of the algebraic steps in this proof might be replaced with kinesthetic "steps," as follows. Suppose one walks facing forward along the first side, from vertex v_7 to vertex v_1, turns through the internal angle of the polygon a_1, walks facing backward from v_1 to v_2, and continues in this way for one circuit around the polygon, alternately facing forwards and backwards along sides (Figure 1).

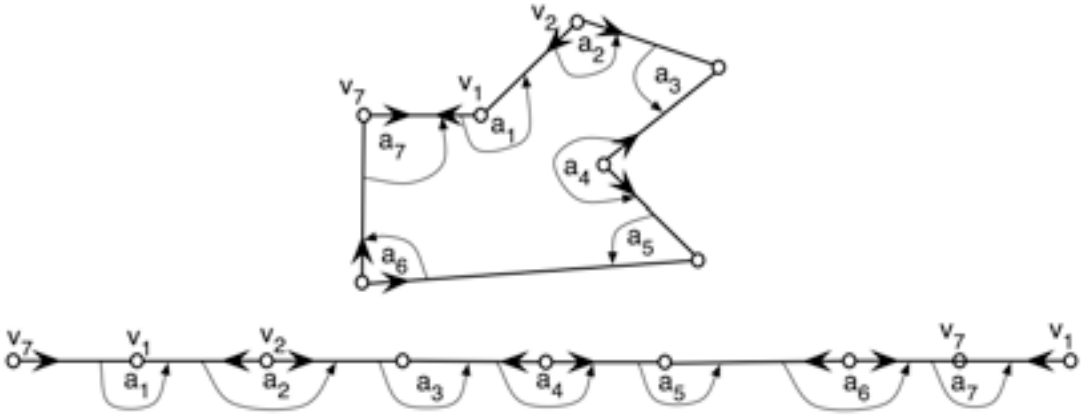

Figure 1: *Kinesthetic proof of the internal angle sum of a polygon.*

If there are an odd number of sides, as in the top diagram in Figure 1, then one ends up facing backwards on the first side after the last internal turn. Note also, in the example shown, the turns through the internal angles are all counterclockwise, while one circuit around the polygon proceeds clockwise. It is easy to see what the total sum will be if we imagine that the sides are all laid out along a straight line, as shown on the bottom of Figure 1. Then the total angle sum will be $n\pi$. However, in bending the path back to the shape of the polygon, so that the final copy of the first edge coincides with its first copy, and in the same direction, we will need to add one total turn in the opposite direction, which must have measurement -2π. Here we assume that the "winding number" in the clockwise direction is one turn, not multiple turns. So the total sum of the internal angles of the polygon must be $n\pi - 2\pi = (n-2)\pi$. This "proof" is easily demonstrated by dancing around the edges, and that is how we used it in the short 2008 composition, in which we proceeded around the edges of a triangle. Of course, here we have implicitly used the fact that the sum of the external angles, each measuring the difference between the straight line of angles and the internal angle that is its supplement, is 2π; but the experience of turning forwards and backwards n times, minus the ultimate 2π rotation, is accomplished physically.

Gauss-Bonnet formula. In that event in 2008, the author also danced a short circular dance phrase verifying that the sum of the angles of a spherical triangle obeys the Gauss-Bonnet formula. In this case the degenerate "triangle" had its vertices on the equater of an imagined unit sphere, so that each of the three turns at vertices measures π. Then the Gauss-Bonnet formula says that

$$\text{(triangle area)(Gaussian curvature)} + \pi = \text{angle sum}$$

Because the area of the sphere is 4π, this particular triangle with its vertices along the equater is really a hemisphere, and has the area of a hemisphere. Also, the curvature of the unit sphere is 1, so

$$(2\pi)(1) + \pi = \text{angle sum} = 3\pi$$

It would be interesting to find a kinesthetic demonstration of the Gauss-Bonnet formula that works for a variety of surfaces, not just a demonstration of one instance.

Harmonious Equations

A series of short mathematical dances were created by the author as part of "Harmonious Equations," directed by Keith Devlin [3], in December of 2008. In this hour-length show Keith gives short verbal explanations of seven important equations, which are then translated into songs composed and sung by the a cappella choral group Zambra. A trio of dancers performs to the musical composition. In the remainder of the paper we will look at the mathematics embedded in these dances.

Pythagoras' Theorem: $a^2 + b^2 = c^2$. In the duet dance accompanying this equation our dancers used the dissection proof of the Pythagorean theorem found by Henry Perigal (1801-1898), shown in Figure 2 (Frederickson [4]). It is based on a dual tiling of the plane, first by the smaller two squares of sides *a* and *b*, then overlaid by a tiling by squares with sides equal to hypotenuse *c*. In the dance we used squares of sides 3, 4, and 5 to connect with Zambra's use of this classic right triangle within their song. This dissection proof is also very similar to that of the Arab mathematician Thabit Ibn Qurra (836-901 AD).

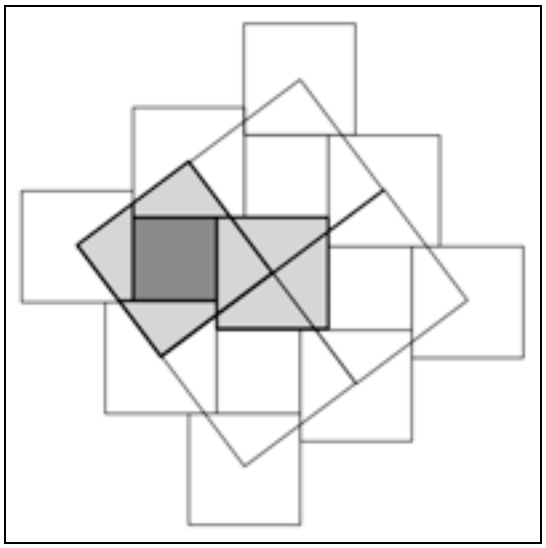

Figure 2: *Perigal's dissection proof of the Pythagorean theorem.*

In this duet, each dancer wields two Styrofoam quadrilaterals, shown light gray in Figure 2; the smaller square with side 3, shown darker here, is mounted on a post, on which it rotates. The dancers make a variety of shapes with the quadrilaterals, finally making the side 4 square, then surrounding the side 3 square to make the side 5 square. In future performances we plan to find a way to make visible to the audience the fact that we are working with the 3, 4, 5 right triangle.

Area of a Circle: Area = πr^2. We can see how much longer the circumference of a circle is than its diameter, by forming our arms into a circle, then spreading them wide. This also gives us an approximate value for π. The joints of the shoulder and arms are such that one may swing the arm in a circle, with the arm functioning as the radius around the central point at the shoulder joint, and it is fun to play with ways the two arms might make such circles in the air at the same time. For this section of Harmonious

Equations we utilized synchronized arm circles, static circles with the arms, and circular floor patterns to create a composition suggesting various danced aspects of circles.

Einstein's equation: $E = mc^2$. We certainly could not use radioactive decay, the phenomenon explored in Einstein's 1905 paper that contained the famous equation, so we chose the next best thing, fluorescence, the understanding of which was greatly furthered by another of Einstein's 1905 papers on the particulate nature of light. In this section we used lines "painted" with white cloth tape on black costumes, and illuminated by black lights, while creating shapes that shimmer and finally "explode," in accompaniment to Zambra's score.

Leibniz's series $\frac{\pi}{4} = 1 - \frac{1}{3} + \frac{1}{5} - \frac{1}{7} + \ldots$. This series is also known as the Madhava- Liebniz series, after the mathematician Madhava Sangamagrama of Kerala, India (1350-1425), whose discovery preceded that by Gottfried Liebniz (1646-1716) by 300 years [5]. We played with the swing time of Zambra's music for this section by using a rhythm game popular among children. In that game, taught to the author by 13 and 14 year old girls when he was dance faculty at a summer ballet workshop, the participants repeatedly play a short rhythm on plastic water bottles, which they pass one person to the right around a circle at the end of each rhythmic phrase. In our dance we used 8 inch "gator foam" (hardened foam core) cubes, showing four sides to the audience. One side is colored yellow, one blue, one black, and the fourth is also black but includes a portion of the Liebniz equation.

We developed a complicated set of switches of the boxes, performed while playing rhythms based on those of the water bottle game. Keeping track of these switches involves symmetry group theory, an area of mathematics concerned with such "transpositions." Though perhaps not directly relevant to this equation, group theory was developed by the mathematician Galois to decide whether certain families of equations are solvable at all.

The boxes are placed in a line on a table facing the audience, and manipulated by three dancers, each of whom grabs a pair of boxes during each of ten short sections of the dance. The dancers slap out rhythms on the boxes while switching their order and also turning one or both 90 degrees. The sequence of ten location switches, for the moment disregarding the turning of the boxes, is shown below using cycle notation. The boxes are numbered 1 through 6 in their original positions, and "*" is used to show composition of permutations, which really means that one permutation immediately follows another. In cycle notation, for example, (135642) indicates that the box in position 1 moves to position 3, 3 moves to 5, and so on, until finally 2 moves to 1. The sequence used in the dance is:

(12)(34)(56) * (12)(34)(56) * (12)(34)(56) * (12)(34)(56)
* (135642) * (identity) * (identity) * (12)(34)(56) * (12)(34)(56) * (12)(34)(56)

Because (12)(34)(56) * (12)(34)(56) = identity, the result of these ten permutations is really just (135642) * (12)(34)(56) = (14)(36) = (14)(36)(2)(5), where (2)(5) is included to indicate that boxes 2 and 5 really end at their starting positions. The final order of the boxes is thus 426153.

The process is further complicated by the fact that on each move each dancer might easily turn one or both boxes 90 degrees clockwise or counterclockwise, producing a variety of colored patterns in the line of boxes. If we let B = black facing, Y = yellow, L = blue, E = equation, the sequence of turns created the following patterns, in order:

LLLLLL,YYYYYY,LYLYLY,LLLLLL,LLLLLL,BLBLBL,

BBBBBB,BEBEBE,BBBBBB,BEBEBE,EEEEEE

The author used this symbolic process to determine the order to place the boxes in at the start of the dance, though the other dancers solved the problem more easily by simply running the dance once and adjusting the starting position according to the locations of the boxes at the end!

Euler's polyhedron formula: V–E+F=2. In this section the dancers use the "hexastar," a hexagon with an extra free edge attached at each vertex, shown in Figure 3, to create a cube, octahedron, two linked tetrahedra, and other shapes (Figure 4). The hexastar is made of 1-inch diameter foam-covered PVC pipe, in 40 inch sections, joined at the vertices by bungee cord (see [6] for further discussion of this prop.) We were looking for one set of twelve PVC pipes that could easily be wielded by 3 dancers. Can the reader visualize how to fold this structure at its vertices in order to do this? (Solutions on last page, Figure 6.)

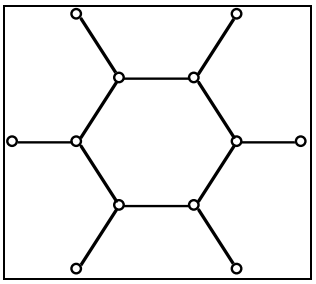

Figure 3: *Hexastar.*

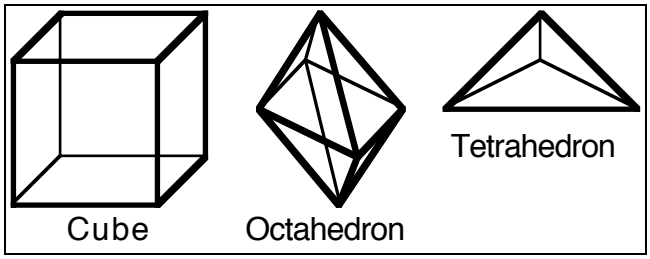

Figure 4: *Platonic solids formed with the hexastar.*

The 6 faces of the cube and 6 vertices of the octahedron are combinatorially related to the 6 edges of the tetrahedron, as suggested in Figure 5. These connections are also used by Zambra in their song,.

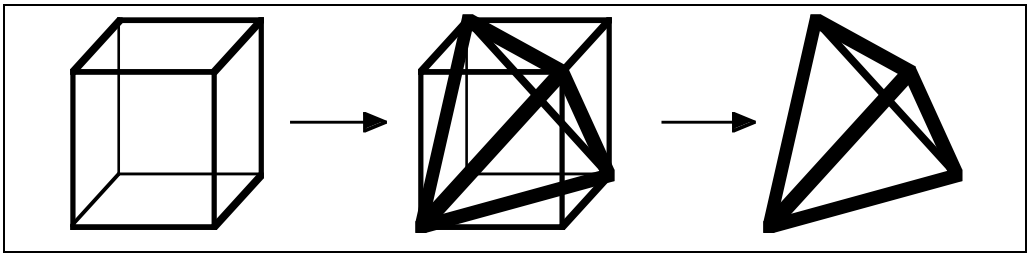

Figure 5: *The cube and the tetrahedron.*

References

[1] sarah-marie belcastro and Karl Schaffer, "Dancing Mathematics and the Mathematics of Dance," AMS/MAA Joint Meetings, San Diego, January, 2008.

[2] Richeson, David. *Euler's Gem: The Polyhedron Formula and the Birth of Topology*. Princeton Univ. Press, 2008.

[3] Keith Devlin, Zambra, and Karl Schaffer, "Harmonious Equations," Dec., 2008, Asilomar, CA.

[4] Greg Frederickson, *Dissections Plane and Fancy.* Cambridge Univ. Press, 1997.

[5] J. J. O'Connor and E F Robertson. "Madhava of Sangamagrama". School of Mathematics and Statistics University of St Andrews, Scotland.
http://www-gap.dcs.st-and.ac.uk/~history/Biographies/Madhava.html. Retrieved on 2009-02-02.

[6] Karl Schaffer, "One-dimensional Origami: Polyhdral Skeletons in Dance," in Origami[4], ed. by Robert Lang, A.K. Peters Press, expected publ. date 2009.

How to fold the hexastar into the cube, octahedron, and tetrahedra. The cube and the octahdron each have 12 edges, as does the hexastar, so no edge duplication is necessary. Also, since the tetrahedron has 6 edges, two tetrahedra will have 12 edges, and no edges are duplicated. It is possible to fold it into one tetrahedron with each edge doubled as shown at the bottom of Figure 6.

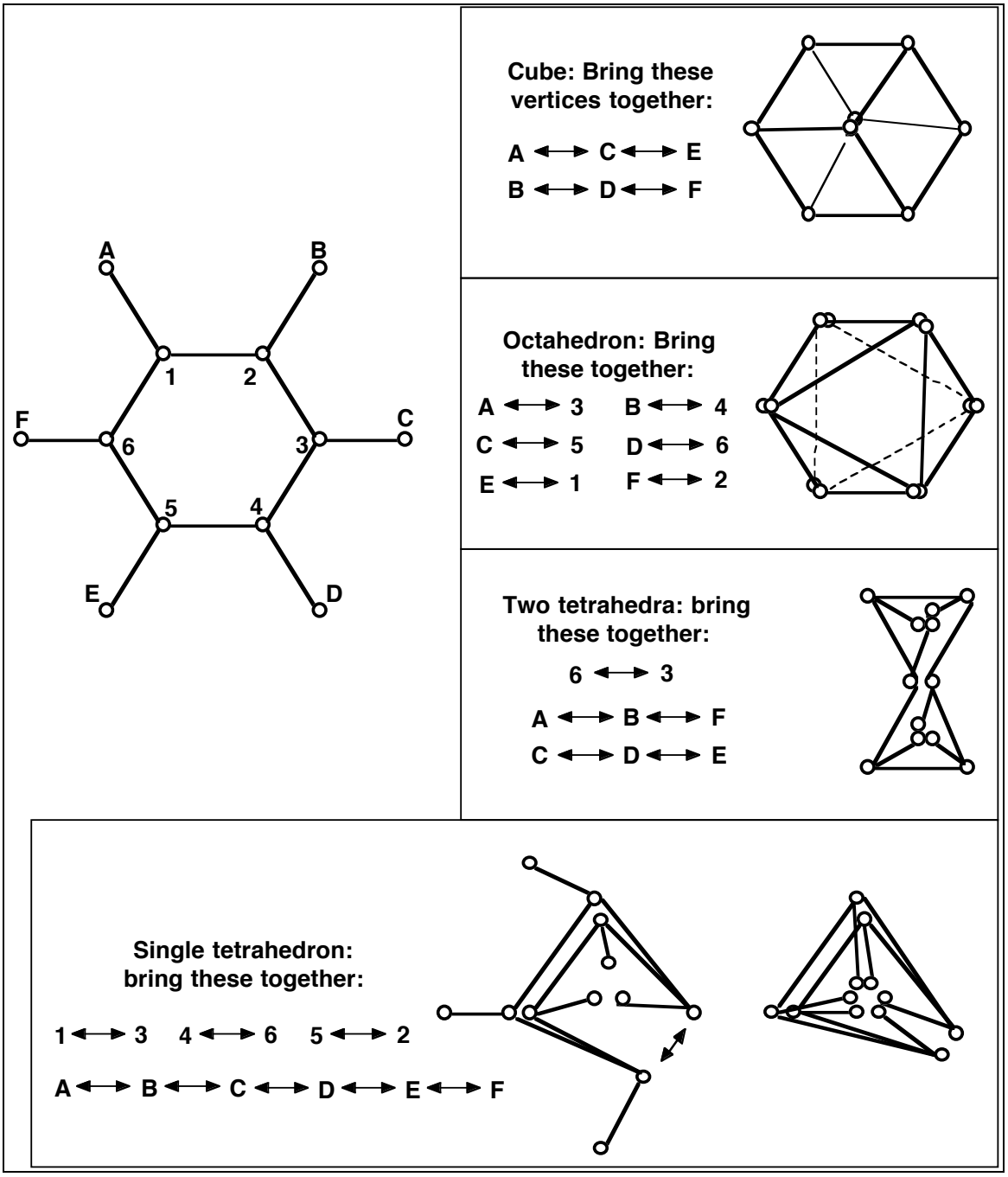

Figure 6: *How to fold the hexastar into cube, octahedron, and tetrahedra.*

Bridging Art Museums and Middle School Math Classrooms

Benjamin Wells *
Departments of Mathematics and Computer Science
University of San Francisco, 2130 Fulton Street, San Francisco CA 94117 USA
E-mail: wells@usfca.edu

Philip Wagner
The Fusion Project, 736 Clipper Street, San Francisco CA 94114 USA

Abstract

The Fusion Project is a research program under development at the University of San Francisco, envisioned by Philip Wagner and directed by Benjamin Wells. With the collaboration of the Fine Arts Museums of San Francisco (and their de Young Museum), it seeks to bring art to the math classroom and math students to the art museum. The goals are to enhance existing curricula in order to improve basic and advanced skills, standards-oriented test scores, and students' interest in mathematics. Therefore, it is a quintessential Bridging project.

1. The Fusion Project: Some Background

Following the US federal program called No Child Left Behind, the performance of US public schools has been judged by standardized test scores in language and mathematics. Time and again, the authors heard that individual teachers' evaluations as well as school funding depend heavily on improvement of student performance on these tests.[1] Despite the pressure and effort, scores remain unacceptably low[2] in California, a state with the seventh largest gross domestic product in the world in 2007.[3] San Francisco schools in particular have been below the program's pass level every year.[4]

Philip Wagner, a retired California businessman, was inspired by his perception of the crisis in math education and his own love for art to create The Fusion Project [1] (FP) as an antidote—or better, a nutritious supplement—to fight this trend in middle school math. The main idea of FP is to engage middle school students in learning some critical math concepts by discovering them displayed in artwork and architectural components of a major art museum. In our view, intervention is required to enhance interest among students who may not recognize the beauty and importance of math in their futures.

If the answer is to use art, where better to find the art than in art museums? In 2006 Phil approached the Fine Arts Museums of San Francisco (FAMSF), whose de Young Museum had recently reopened in an award-winning building in Golden Gate Park. Their Education Department saw the value of FP to students and to their museums and immediately wrote a letter of support, the first step of a unique relationship. We say unique because our queries of art museums in four countries, search on the Internet, and contacts in the Math and Art community report no similar programs.

Leonard Shlain, author of *Art and Physics* [2], referred Phil to Benjamin (Pete) Wells at the University of San Francisco (USF). Pete had hosted the controversial author for four talks in his interdisciplinary courses melding math, science, religion, and art, which he has been teaching over twenty-one years. Moreover, Pete had trained peer teachers to deliver Socratic curricula to entire math classes in 6th–10th grades for eight years under Oakland Public Schools and UC Berkeley sponsorship.

The purposes of FP. The first goal of FP is to demonstrate that some children can improve their interest and understanding in math at a critical grade level. Recognizing the increased significance and political

importance of test results, we also hope to achieve a second goal: improving student scores on the types of problems from the state's standardized math tests that have significant miss rates.

To meet our second goal, we needed to know the math concepts that are most challenging to middle school students. One might think this information would be readily available from the school district or the state, or even be online. Not so. While the State of California releases the total scores for the math test (for example, [3]), it does not identify those math concept areas that are most frequently difficult for students, nor does it summarize test results by individual topics, much less questions. Even teachers are not privy to this apparently classified information. Before we found a solution, we got international help.

FP goes international. In 2006, we learned independently of the workshop "Innovations in Mathematics Education via the Arts," sponsored by the Banff International Research Station for Mathematical Innovation and Discovery, to be held at the Banff Centre, Alberta, Canada in January 2007. Thirty mathematicians, educators, and artists from four countries were invited, including Pete. Pete encouraged Phil to apply, but then could not go himself. The now-invited Phil ended up being responsible for presenting the ideas of the FP to the workshop participants. Although confident as a businessman, he felt the scope of the workshop was beyond his experience. Pete assured him of a receptive audience and enriched his PowerPoint talk with museum and art images.

Phil's obvious concern for students' math performance[5] made him an instant insider. FP was quickly identified as having significant potential and was chosen for review and development by a focus group, comprising Nat Friedman, Doris Schattschneider, and Stewart Craven. They recognized the opportunities in the Bay Area with its many museums of science, nature, and art, but they foresaw an even broader context for the development and distribution of FP techniques and materials. They perceived the consonance of FP and the goals of the Banff workshop. Applying their personal experience from a variety of school systems, they advised that we would not gain traction with teachers or administrators if the program were couched as reform or even enrichment. Such attitudes can be interpreted as elitist or as undermining established, even mandated, patterns. In particular, they warned against calling FP products *curricula*. Later, Doris suggested using words like *enhancement* and *encounter*, which we adopted. The group recommended concentrating on the middle school and tailoring the materials for the 7th grade, stressing that interest in math is often gained or lost at this level.

Since the workshop, the focus group participants have made vital contributions to the development of FP. We have consulted with them electronically and hosted Doris and Nat on visits to San Francisco.

The curious mascot. While at Banff, Phil's companions discovered an ingenious toy in a gift shop. Invented by the creator of the eponymous Hoberman Sphere, it is sold as the Switch-Pitch™. It can "switch phases" when tossed in the air with a slight spin (Fig. 1). Phil bought the shop's entire supply and later developed a steady source so we always have them on hand.

Figure 1. *Static and dynamic changes of the Switch-Pitch [4, 5]; check youtube.com*

We have shared this essential FP emblem as a gift on first contact and a "recognition token" to benefactors, rewarded wise children who helped us see math in art, stimulated an artist who speaks math to prisoners, and shared the balls with university executive officers. We always point out that the ball can be viewed as a self-dualizing tetrahedral compound, such as the stella octangula. The static shape was

already known to Neolithic Scottish stone carvers [6] (Fig. 2). Similar stone balls are a source of speculation that the Platonic solids were known well before the Greeks [7]. Although not art, this mascot fits our broader paradigm of communicating math via visually (and haptically) attractive representations.

Figure 2. *Neolithic Scottish type 2 stone balls (1, 2 University of Aberdeen Museum; 3, 4 famed Towie ball, and a drawing of it) [7, 8]. Note the chirality in the stone balls as well as in the mascot.*

2. FP Connects the Math and the Museum

Both FAMSF and FP felt that a strong correspondence between the art and the math was required for a successful collaboration. Shortly after the Banff workshop, the FAMSF Education Department received a grant from the Israel Family Foundation in Colorado. FAMSF then hired Pete to correlate works of art with target standards in the California 7th grade math curriculum. Two things made this feasible: his experience with aligning (matching) standards and problems, and identification of the crucial standards.

Pete had performed alignments for five years for the Center for Educational Policy Research at the University of Oregon. For example, their Standards for Success, a project of the Association of American Universities, produced a list of Knowledge and Skills for University Success [9] endorsed by 28 leading research universities. The project in which Pete participated aligned that list with state high school standards and assessments [10]. FP could reveal the art-math connections, if they were there.

Data difficulties. Identification of the crucial math standards proved to be a difficult process. Student performance data on individual test problems was virtually impossible to find. Although much in education in America, and particularly in California, currently depends on published test results, these are pooled, and actual student behavior on individual problems is zealously (maybe jealously) guarded. Apparently administrators are not eager to have that kind of detail revealed, even by averages. We were frustrated for months, but a contact through a local public TV math-tutoring show led to a teacher at a continuation school who obtained anonymous test-item score listings. Pete then aligned the test problems with the California state standards. That gave us a set of concepts to target in order to reach our goal of improving test scores. These we call the *target standards*.

Target standards. The California 7th grade content standards [11] list 46 items (including some from Mathematical Reasoning). Using the data on test performance, Pete classified ten items as primary targets and another ten as secondary. The following table summarizes these twenty, with the high targets in **bold**. Those marked with * are also designated as key standards for 7th grade in the Mathematics Framework for California Public Schools [12, p. 112]. It may be significant that only four strong targets are key standards, and another eleven key standards are not targets of either kind.

NS1.2*	**+, ×, –, / rational numbers (integers, fractions, and terminating decimals); $(a/b)^m$**
NS1.3	Convert fractions to decimals and percents; use in estimations, computations, applications
NS1.6	Calculate the percentage of increases and decreases of a quantity
NS2.2*	Add and subtract fractions by using factoring to find common denominators
AF1.2	**Use correct order of operations to evaluate algebraic expressions such as $3(2x + 5)^2$**

AF1.3* **Simplify numerical expressions by applying laws of rational numbers (assoc, etc.), and justify**
AF1.5 Represent quantitative relations graphically; interpret parts of a graph in the situation it represents
AF3.3* **Graph linear functions; note Δy is same for given Δx; rise/run = slope**
AF3.4* **Plot quantities whose ratios are constant (ft/in); fit line, interpret slope as ratio**
AF4.1* Solve 2-step linear equations and inequalities in one variable over the rationals; interpret
AF4.2* Solve multistep problems involving rate-speed-distance-time and direct variation
MG2.1 **Use formulas to find perimeter and area of elementary 2- and 3-dimensional figures**
MG2.2 Estimate and compute area of complex or irregular 2- and 3-dimensional figures by decomposition
MG2.3 Compute perimeter, surface area, volume of 3-dimensional objects obtained from rectangular solids; scale volume, surface area.
MG3.1 **Identify geometric figures; construct with compass and straightedge (altitude, midpoint, diagonal, bisectors, circle parts, etc.)**
MG3.2 Use coordinate graphs to plot simple figures; determine length, area; translated/reflected image
MG3.6* Identify elements of 3-dimensional objects; describe skew lines, 3-plane intersections
MR1.1 **Analyze problems from relationships, relevant/irrelevant and missing information, patterns**
MR2.3 **Estimate unknown quantities graphically; solve for them by using logic, arithmetic, algebra**
MR2.4 **Make and test conjectures by using both inductive and deductive reasoning**

Clustering art and standards into stories. In visits to the de Young Museum, Pete surveyed works from the permanent collection on display, teasing out their mathematical content. He also noted interior and exterior architectural details that would be useful to highlight. With target standards at hand, he matched artwork on his list with the relevant math standards. A 2D matrix emerged showing that most of the identified works and all the target standards (and more) were covered by each other. But how could we organize this diffuse information in a usable way? By clustering the art works and math topics, we found a natural decomposition of both into seven groups and called them Stories/Encounters. The resulting correlation convinced both parties that the de Young Museum was highly suitable for the purposes of FP. Here are the clusters (the first three are more elementary; the last, more exploratory):

Story/Encounter 1. Counting, adding, multiplying, grouping, distributing, and estimating
Story/Encounter 2. Fractions, percent, parts, and rhythm
Story/Encounter 3. Lines, slopes, intercepts, equations, and ramps
Story/Encounter 4. Edge lengths, surface area, and volume of various 3D objects
Story/Encounter 5. Lines and planes in space, ruled surfaces, and belts
Story/Encounter 6. Parallels, perspective, other projections
Story/Encounter 7. Uniformity, symmetry, chaos, confusion

Museum resources. To see how the art fits into the stories, we need to review the types of art resources that FAMSF has made available to FP:

(1) Works of art in the permanent collections—this restriction aids stability of instructional materials, and access to the art is more open (for example, nonflash photographs may be taken);
(2) Cultural artifacts in the ethnological collections;
(3) Site-specific works and exhibits commissioned by FAMSF;
(4) Architectural elements (e.g., windows, walls, pavers, rooflines, staircases, furniture);
(5) Poster-sized prints of any image in the museum's ImageBase or 4D electronic databases[6];

Each Encounter involves all of these: original paintings and sculpture, integral features of the building or its furnishings, ethnological artifacts, or posters to be printed by FAMSF for FP classrooms. Some works on paper, including all of FAMSF's holdings of Escher's work, are most easily accessed on the Internet.

Recruiting people and materials. Pete's report [13] on alignments and stories to FAMSF gave a skeletal structure to their involvement in the project, but FP needed more detailed materials before we could begin to think about how to build the school-end of the bridge. FAMSF sent invitations to a thousand Bay Area teachers on their mail list to join the FP Teachers Advisory Group (TAG). The Israel

Family Foundation provided another grant for TAG training and consultation. From the respondents, we chose five middle school math teachers in public, private, and parochial schools. We trained this group at the de Young Museum in late 2007, covering the FP/FAMSF report and giving a tour of major works included in it. Subsequently, the TAG communicated by email with us and with each other. These teachers were expected to develop the Story outlines into teaching materials. Story assignments were negotiated. On request, Pete offered a suggested outline [14, pp. 16–17] for expanding a Story into an Encounter—that is, a teacher-ready guide of questions and explorations that could be used in class and on museum visits. The teachers have submitted two to four sets of draft instructional materials that are currently being compiled and edited. The next section gives samples of three different levels and types of draft materials [13, 14] produced by the TAG and FP.

3. Sample Story/Encounter Materials

Story/Encounter 1: Example of a core cycle. The following problems form a *core cycle*, the essential element of the structure outline mentioned above. They center around *Strontium*, a huge photo array made up of identical rectangular panels containing large balls, small balls, and some partial balls.

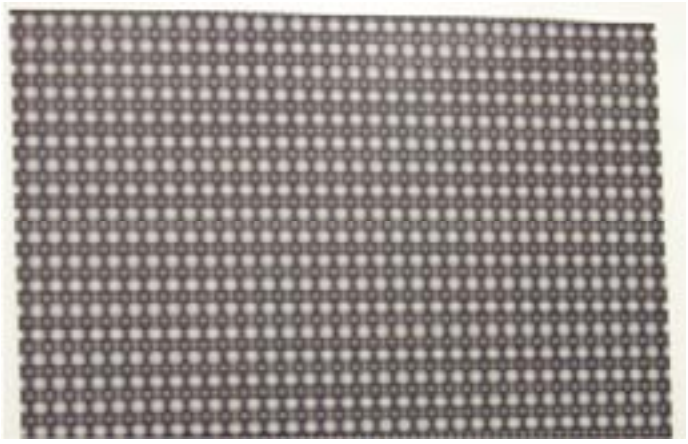

Figure 3. *Top half of* Strontium *by Gerhard Richter, a FAMSF site-specific commission*
Figure 4. Strontium *at opening of the new de Young Museum—October 15, 2005 ©Art Rogers*

Problem 1. Count the fuzzy balls in *Strontium* (Fig. 3).[7] We start with the large ones.

Concept/Technique A: (1) To count a rectangular arrangement of things, count one row and multiply by the number of rows. (2) How about counting one column and multiplying by the number of columns?

Concept/Technique B: (1) To handle split half balls, count them and divide by 2. (2) Quarter balls?

Concept/Technique C: (1) Count the small balls by using the same methods, as if the large balls weren't there. (2) Count the small balls by seeing how many belong to a large ball.

Application to Problem 1, and refinement: (1) How many rows are there in the full picture? Do they each have the same number of balls? Whole balls? (2) How many columns are there? Do they each have the same number of balls? (3) So how many balls are there, by counting a row? by counting a column? (4) Is there an easier way to handle the half balls? quarter balls? small balls? (5) What about counting by panel? How many panels are there by using the methods? Are all panels the same? Is it easier or harder?

Problem 2 (driven by math). Count the number of items in a three-dimensional array. Models of this can be a stack of cocktail sugar cubes, or Montessori cubes, but the abstract problem is the focus here.

Application to Problem 2, and generalization: Use the teaching and learning from Problem 1 to generalize to three dimensions. Develop the approach of multiplying rows, columns, and layers by seeing that we can already count in each layer, and that each layer is the same size as the others.

Problem 3 (driven by an image). How many people are there in front of *Strontium* (Fig. 4)?

Application to Problem 3, and review: The method of counting the fuzzy balls does not work immediately or directly here, because people are not standing in rows and columns (but, at a school assembly, that might work). But dividing the picture into rows and columns of boxes would make it something like the panels in Problem 1. What makes this work? What keeps it from working very well?

Story/Encounter 3: introduction and worksheet fragment. *(TAG member Claire Potter with Pete and Doris)* There are many paintings in the de Young Museum that have lines or suggestions of lines that the artist has included to draw our eye to a focal point, or to have us look at a scene from a special angle. The museum also has several staircases—their steepness, or pitch, makes them easier or harder to climb. We can describe how a line appears in a painting by its slope, and can calculate this by measuring. To find the pitch of a staircase, we can imagine it replaced by a ramp, and then calculate the slope of the ramp.

Figure 5. *Wayne Thiebaud,* Diagonal Freeway

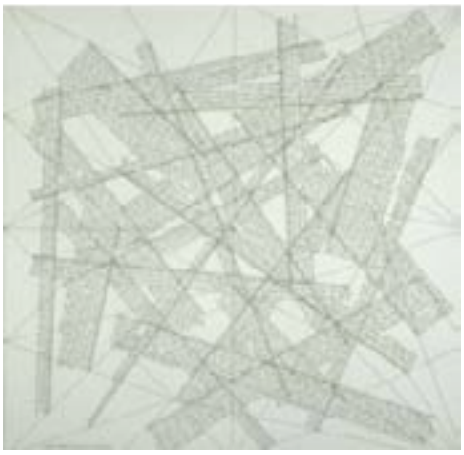

Figure 6. *Sol LeWitt,* Lines from Points to Points

How steep is this freeway (Fig. 5)? Notice there are several lines to consider. They appear to intersect outside the frame, somewhere below and to the left of it. Do they all intersect at the same place? How does this affect your answer?

Examine the picture by Sol LeWitt (Fig. 6). 1. Which lines [labeled in the handout] slope upwards from left to right? List them. Which labeled lines slope downward from left to right? List them.

2. In your list of upward sloping lines, which line is the steepest? Which line is the most flat? Now sort these lines according to steepness, with the most flat first, and list them in order by letter. In your list of downward sloping lines, which line is the steepest? Which line is the most flat? Now sort these lines according to steepness, with the most steep first, and list them in order by letter.

Definition: The slope of a line is the ratio of the vertical change to the horizontal change as you move from one point to another along the line. Note that as you move along the line from one point to another, if you move up, the vertical change is positive and if you move down, the vertical change is negative. The vertical change is called the *rise* and is the numerator of the ratio. As you move along the line from one point to another, if you move to the right, the horizontal change is positive and if you move to the left, the change is negative. The horizontal change is the *run*; it is the denominator of the ratio.

3. For each of the labeled line segments in the picture, use the coordinate grid superimposed on the picture to measure vertical and horizontal change between two points on the line where a grid line intersects the line. Your teacher will demonstrate how to do this. In measuring vertical and horizontal change, round your measurements to the nearest centimeter. Remember to include the sign of the change. Fill in Table 1 [to be supplied] with your measurements, and use them to calculate the slopes of the lines.

Here are some ideas for extension. These studies about slope can lead to practical representations of the Pythagorean Theorem and computing missing parts of right triangles. LeWitt's minimal, procedural art lends itself to reimplementation and elaboration. Students find it fun to make this sort of art.

Story/Encounter 4: sample tasks. *(TAG member Gail Purtell)*
To do in the classroom:

- Identify equilateral, isosceles, and scalene triangles; acute, obtuse, and right triangles.
- Find the area of triangles.
- Use pattern blocks to demonstrate how equilateral triangles can be tessellated various ways.
- Find the surface area of pyramids.

Figure 7. *Architects Herzog and de Meuron's eucalyptus benches*

Figure 8. *Kane Kwei,* Coffin in the Shape of a Cocoa Pod

To do at the museum:

- Notice that there are benches (Fig. 7) placed throughout the museum. Notice that each bench module covers a triangular area of floor space, and each one is made up of three smaller triangles tilted into a pyramid facing up toward the ceiling or down toward the floor.
- Identify the kind of triangle formed by the outside edges of the module. Measure the lengths of the sides of one bench module.
- Use the Pythagorean Theorem to find the height of the triangle.
- Find the floor area of the bench, i.e. the amount of floor space it covers.
- Notice the three smaller triangles that make up the pyramid within each bench module. Are the three triangles congruent? What kind of triangles are they? Measure the base and height of one.
- Compute the surface area of one bench module.

Strategies for finding the volume and surface area of the cocoa pod coffin (Fig. 8):

- To estimate the surface area, you could divide the cocoa pod into a cylinder with cones on each end. Find the surface area of each section and then add the three areas together.
- Another suggestion might be to consider each of the lengthwise strips separated by grooves that go from tip to tip. Estimate the area of each of these strips by dividing them into a rectangle with triangles at each end. Count the number of strips, then multiply to estimate the total surface area.
- The volume of the cocoa pod can be estimated by dividing it into a cylinder and two cones then finding the volume of each section. Add the volume of the three sections.

4. Next Steps at USF and Beyond

Teachers first; 7th graders next. The de Young Museum had provided a framework (literally, too; see Figs. 9, 10, which go with Story 6) and the TAG was producing material, but we had no model for the next step. A phone call to USF's School of Education led to a conversation and an ongoing collaboration with Caryl Hodges, their Associate Dean for Teacher Training. She proposed workshops for teachers and convinced us that it would be easy for FP to join Pete's College of Arts and Sciences and her School in a way that facilitated obtaining grants to pay teachers for FP training and implementation. We added Jeff Buckwalter, Associate Professor of Computer Science and Director of the two schools' Dual Degree in Teacher Preparation program. Then the de Young Museum offered facilities for the workshops and "Get Smart with Art" binders[8] for Fusion Project materials.

Figure 9. *The Hamon Tower at the de Young Museum*

Figure 10. *Its hyperbolic paraboloid sheath*

Interest in FP at USF has grown; in April, 2009, it is expected to move from Pete's personal research project to a program of the College of Arts and Sciences. We are still developing the proper structure at USF, but progress is steady. In particular, the Deans of the College have enthusiastically endorsed FP, and the TAG members have agreed to act as instructors for the first rounds of workshops. We'll use USF students and local peer teachers in FP-active classrooms. The Israel Family Foundation has renewed their grant, and we have a list of middle schools and teachers interested in our workshops. There has been no classroom testing of FP materials yet, but we expect that to change by the next school year. Best of all, we have found great resonance of FP with the USF Mission and Core Values [15].

FP Rev. 2.0. We are already thinking beyond the FP in the Bay area and collaboration with the de Young museum. We envision an enlarged Fusion Project concept that will:

- Identify State by State those standardized math questions most frequently answered incorrectly in that State. This will replicate the methodology used in the initial project to identify those math concepts most difficult for Bay Area students at risk to comprehend. We anticipate that discovery of this data will be successful but require effort and strategic alliances.
- Broaden the use of the term *art* to include animation, video games, or other media familiar to today's 7th graders. This extends the natural funding base to entertainment corporations as well as public and private sources.
- Target cities with major museums and evaluate and use their collections as we did at the de Young Museum. This will facilitate students' grasp of art in a museum setting outside the classroom.
- Use computer access to show works of art and enlarge them for the classroom, when no art museum is conveniently located near a school.

The creation of printed guides for teachers and students will further this dissemination. The portability or ability to adapt the program depends on having guides that can be retargeted to different art collections, preferably by Teachers' Advisory Groups at each location. Involvement in such a program must remain completely voluntary for schools and classes and be free to all students. Teachers electing to use this enhancement program would attend training workshops and would be compensated. As in the developing

USF pilot program, local college students and school students would be trained to assist in the classrooms utilizing the Fusion Project. Students in these roles would also be compensated.

It is essential that the programs be assessed, with the results (positive and negative) shared freely and used to make improvements.

Math, yes, but is it art? We would like to clarify the role of art in the Fusion Project. The evaluation of art in the de Young Museum's permanent collections was based on its potential for teaching math. Most of the site-specific commissions are especially appropriate, and the entire collection is world class. But the artistic values were not assessed, nor are they directly a part of FP methodology. Art teachers were excluded from the Teachers Advisory Group for much the same reason. Our math classroom teachers are not required, expected, or recruited to teach art. That said, the authors and our advisors love and appreciate art and are stimulated by the mathematics we see in art. This will be shared by those attracted to join FP.

All consultants feel that *the heart of the Fusion Project is the art*. Some of us are collectors, some have used art in math and science courses, some have taught art, and some have been founders of the Art & Math movement. We are sensitive to the needs of museums and of art programs in schools as well, and we intend to provide structural suggestions for including an art education aspect in the Fusion Project. In particular, although the workshops will not train the math teachers in art education, they will certainly introduce them to the artistic dimensions, through guided tours by museum docents and references to art interpretation. Of course, the reason we are at the de Young Museum is because they see us as an important activity for their own art education effort. Similarly, we endorse the collaborative involvement of schools' art teachers in FP classrooms. With no emphasis on the appreciation of the art, the works in the first stories become little more than mathematical tokens to be counted and measured (but see Stories 5–7 for surface development, perspective, and procedural art, which are topics in art school courses). That is far from our goal. In fact, we believe that the interest in the mathematics that flows from the art will make the art that much more interesting and significant to the students, and we intend to help that flourish. Obviously, this attitude extends beyond the pilot program and USF.

The future unfolding. Our future vision already verges on reality at USF. USF has always had inquiries about online, distant learning, including two recent ones to the School of Education. The developing USF Yale National Initiative offers innovation for school classrooms through the College of Arts and Sciences. A proposed Fine Arts Core course involving museum resources is about to be launched. USF Teacher Education and our joint Dual Degree Teacher Preparation program (especially in math) are open to testing materials and jump-starting the Fusion Project for new classroom teachers. The Fusion Project can work with all of these.

Student tours of art museums are typically reserved, hands-off, and distant. Our tours are planned to involve (polite) interaction with the art and hands-on activities with the architecture and furnishings. For example, the de Young Museum can become more like San Francisco's hands-on science museum, the Exploratorium. In fact, the de Young Museum already has a reputation of being kid-friendly [16, 17], and this congeniality will be a helpful characteristic for other FP placements or similar programs.

Finally, the extension to visual media beyond the traditional art museum (or even art and science museums like the Exploratorium) suggest opportunities at USF and far beyond. In particular, we have already had several areas of contact with Pixar Animation Studios in nearby Emeryville. As one of the authors has said explicitly (and the other agrees but never put it into words): "I was taught how to pass state exams and math SATs. The same test questions were frequently repeated year after year. But this is not 'learning.' Perhaps if the text or the teacher could have *shown* me the concepts visually, I would not have needed to memorize the answers. But there was no Fusion Project available to me." We think this speaks to the question of the value of art and visual media. Mathematicians—and math teachers—use "show" in a sense far removed from informed seeing. Even illustrated textbooks often do not make the pictures engaging.[9] Artists do.

References

[1] The Fusion Project, http://fusionprojectinfo.com/ —constructed by Cyndi Lott (Align PR Agency)
[2] L. Shlain, *Art and Physics*, William Morrow, New York, 1991; Harper Perennial, New York, 2007.
[3] California Department of Education, *2008 STAR program summary of results*, Sacramento CA, 2008.
[4] http://www.amazon.com/Hoberman-Switch-Pitch-Ball/dp/B000P13PL0/
[5] http://www.teachersource.com/Chemistry/MolecularModels/HobermanSwitchPitchBall.aspx
[6] http://www.georgehart.com/virtual-polyhedra/neolithic.html
[7] http://www.pballew.net/platonic.html, http://www.pballew.net/Towiestone.jpg
[8] http://www.abdn.ac.uk/virtualmuseum/pictures_db3.php?fieldsearch=stone+ball
[9] Center for Educational Policy Research, *Understanding University Success*, University of Oregon, Eugene, 2003.
[10] _____, *Mixed Messages: what state high school tests communicate about student readiness for college*, University of Oregon, Eugene, 2003.
[11] California Department of Education, *Grade Seven Mathematics Content Standards*, in Mathematics Content Standards for CA Public Schools, Sacramento CA, 1997, pp. 31–35.
[12] _____, *Mathematics Framework for California Public Schools*, Sacramento CA, 2006.
[13] B. Wells, *Math stories at the de Young Museum*, private report to FAMSF, 2007, rev. 2009. Contact author for a copy. Some materials used are not yet circulating.
[14] B. Wells, C. Potter, and D. Schattschneider, *Math encounters at the de Young Museum*, private report to USF College of Arts and Sciences, 2008. Contact author for a copy.
[15] http://www.usfca.edu/mission/
[16] D. Wood, *Kid-Friendly Art Museums: Three Places Where Children Can Look and Touch*, http://www.education.com/magazine/article/Art_Museums/
[17] M. O. Gorman, *The 10 Best Art Museums for Kids*, http://www.parents.com/family-life/travel/us-destinations/the-10-best-art-museums-for-kids/
[18] http://en.wikipedia.org/wiki/List_of _countries_by_GDP_(nominal), consulted 1/30/09;
[19] http://www.bea.gov/regional/gsp/, consulted 1/30/09.
[20] San Francisco Unified School District, *SFUSD exceeds state growth targets*, 9/04/08
[21] N. Asimov, *State schools' slow progress*, San Francisco Chronicle, August 16, 2006.
[22] E. Burger, M. Starbird, The Heart of Mathematics 2e, Key College Publishing, Emeryville CA 2005.

[1] Interestingly, the tests have no direct consequence for middle school students. Not until the California High School Exit Examination, first given in the 10th grade, is an individual student's score of personal importance. But receiving a diploma requires a passing score on this exit exam, which is based on *middle school math standards*.

[2] See [3] for 2008, and see previous Standardized Testing and Reporting (STAR) summaries for earlier years.

[3] According to the International Monetary Fund and World Bank (for countries' Gross Domestic Product) [18] and the US Bureau of Economic Analysis [19], California's 2007 Gross State Product of $\$1.8 \times 10^9$ would have put the state seventh in the list of countries by GDP, between Italy and Spain.

[4] According to a September 2008 San Francisco Unified School District press release [20], "SFUSD remains under NCLB program improvement status."

[5] There was objective evidence for the concern. At the time of Phil's talk, the most recent STAR summary showed that "In math, 40 percent of students scored at grade level or beyond this year." [21]

[6] ImageBase has public online access: http://www.famsf.org/fam/about/imagebase . 4D is a broader high-resolution image database internal to FAMSF.

[7] This is not an easy task. The photographic assembly of 130 identical panels is gigantic, and approaching it can be disorienting, because the image is deliberately fuzzy.

[8] Get Smart with Art @ the de Young: http://www.famsf.org/fam/education/subpage.asp?subpagekey=19

[9] A strong exception to this is [22], which Pete has used as a textbook in eight courses emphasizing math and art.

Combinatoria Poetica
Counting and Visualizing Rhyme Patterns in Sonnets

Hartmut F. W. Höft
Department of Computer Science
Eastern Michigan University
Ypsilanti, MI 48197, USA
E-mail: hhoft@emich.edu

Abstract

In this paper visualizations of end rhyme patterns of poems, including sonnet sequences, are studied. First, a notation for the grouping structure and end rhyme pattern types of poems and sonnet sequences is developed. Then the rhyme patterns of poems with even rhymes are constructed and their counts computed. Cascading this construction over rhyme groupings leads to counts for a variety of sonnet forms. The structure and counts are visualized for two types of sonnets, as trees that are drawn in a circularly symmetric manner. Finally, systematically generated rhyme patterns for sections of sonnets as well as rhyme patterns of sequences of sonnets from the literature are visualized as color bands. These bands provide a holistic visual overview that can give insight into the structure of poem sequences that may span hundreds of lines. Different color assignments can also be used to exhibit and enhance the visual beauty inherent in rhyme patterns (see website [6]). Mathematica 6 is used to create counts, summary tables and images of end rhyme patterns.

1. Introduction

In this paper principles and algorithms are described that can generate, count and visualize the number of possible end rhyme patterns for poems with paired rhyme patterns in general and sonnets in particular. Imposing different restrictions on the sound patterns for end rhymes and on the total number of end rhyme sounds in a poem allows counting and tabulation of a wide range of possible constructions of poems and sonnets that fit the specified end rhyme patterns. Even though a number of poets across the centuries have lamented the constrictions that the sonnet form places on their creative powers, it turns out that types of end rhymes for sonnets, even those close to the traditional forms, permit large numbers of patterns. Indeed the numbers are so large that they appear to contradict this sentiment expressed by some poets. Thus two complementary goals guide this paper: first to understand why the number of possible end rhyme patterns is so large when the rules governing sonnets seem so strict, and secondly to provide visualizations for types of sonnets generally and for sequences of sonnets in the literature that permit one to see at a glance end rhyme patterns used by poets. This may provide a new tool for literary criticism.

In Section 2 the underlying concepts for the structure types of poems that are the topic of this paper are introduced. I cite a number of sonnets that demonstrate the flexibility of this poetic form and provide a hint of the surprisingly large number of end rhyme patterns that 14 lines permit. The sonnet form also sets the stage for developing a notation for the structure types of poems that takes into account the grouping into subsections as well as conditions for the end rhyme sound patterns. I will discuss interrelationships and dependencies between some of the types.

Section 3 first considers poems with an even number of lines and paired end rhyme sounds. Since a poem of 2n lines can have between 1 and n end rhyme sounds, the counts of end rhyme patterns can be arranged to form a number triangle with rows denoting the length of a poem and columns denoting the

number of sounds occurring in the poem. I describe an algorithm to generate all end rhyme patterns for poems with even rhymes and show tables of end rhyme counts. Then I apply the algorithm to Shakespearean and Petrarchan sonnets and visualize their end rhyme structure and counts in trees.

Section 4 presents the visualization of end rhyme patterns as bands of gray scale strips. One end rhyme pattern is displayed on one line so that, for example, 14 horizontal squares visualize a sonnet, and the patterns of a sequence of poems are displayed as vertical columns of horizontal strips. I show bands for all possible patterns of three particular end rhyme pattern types as well as bands for the rhyme patterns of a sonnet sequence from the romantic period in English literature. These visualizations extend into greater depth the visualizations created in [3].

In Section 5 I list formulas related to the counts of end rhyme patterns for even rhymed poems and suggest directions for further investigations.

2. A Classification of End Rhyme Pattern Types in Poems and Sonnets

A sonnet is a poem of 14 lines. The analysis begins by assuming that an end rhyme sound is always paired with the end rhyme sound in another line. In some traditions end rhyme sounds may appear in triplets; we will consider those rhyme patterns also. I will follow the literary tradition that labels end rhyme sounds consecutively "a", "b", "c", etc., where "a" represents the first end rhyme sound in a sonnet, "b" the second, "c" the third, and so on.

While I show in this paper that the possible variations in the 14-line rhymed poem are immense it is useful to mention the two major types of sonnets described in standard accounts of this poetic form. In the **Petrarchan** sonnet pattern the 14 lines of the sonnet are commonly organized into a leading 8-line **octave** usually end-rhymed "abbaabba" followed by a final 6-line **sestet** that permits more variety but often is rhymed "cde cde" with three sounds or "ccd cdd" with two sounds. In the **Shakespearean** sonnet pattern the 14 lines of the sonnets are commonly organized into three 4-line **quatrains**, usually end-rhymed "abab cdcd efef", followed by a **couplet**, typically rhymed "gg". I will refer to the end rhyme patterns stated above, "abba abba cde cde" and "abab cdcd efef gg", as the standard patterns. If all poets adhered to these standards there would be no need for or interest in counting or studying all possible variations or actual poetic forms. However, a variety of rhyming patterns have been used in both traditions as well as patterns that depart sharply from these forms, demonstrating that there are venues of expression within the sonnet form that are not apparent at first sight. Indeed the number of possible rhyme patterns in a 14-line poem that a reader will recognize as a sonnet is surprisingly large as will become clear.

Despite conventional accounts of the two standard sonnet forms, in practice the rhyme patterns in sonnets have varied widely. A sonnet may not rhyme at all or use up to seven sounds. Each of these cases actually have been used by poets. Here are examples of each of the eight possible counts of end rhyme sounds with brief references:

No rhyme sounds:	abcdefghijklmn	Christian Gryphius	(see [1] p. 106)
One rhyme sound:	aaaa aaaa aaaa aa	Sir Philip Sidney	(see [2] p. 171)
Two rhyme sounds:	abba abba bba abb	Philander von der Linde	(see [1] p. 104)
Three rhyme sounds:	abab baba acca cc	Sir Philip Sidney	(see [2] p. 187)
Four rhyme sounds:	abba abba cdd ccd	William Wordsworth	(see [7] p. 187)
Five rhyme sounds:	abba abba cde cde	Wolfgang von Goethe	(see [1] p. 137)
Six rhyme sounds:	abba cdcd ebf ebf	Rainer Maria Rilke	(see [8] p. 30)
Seven rhyme sounds:	abab cdcd efef gg	William Shakespeare	(see [11] p. 387)

Some terminology is required in order to be able to classify different types within the sonnet form. The first quatrain in a sonnet will be called the ***leading quatrain*** and any subsequent quatrain will be called an ***interior quatrain***, even if it closes a sonnet. When a sonnet is structured into an octave and a sestet then the octave tends to be the leading section of the sonnet. Therefore, I will follow this literary preference and consider octaves as leading octaves. In order to understand the complexity of counting end rhyme patterns I start with a visual arrangement of rhyme patterns for leading and interior quatrains with two end rhyme sounds "a" and "b". The left half of the symmetric tree represents the three possibilities for a leading quatrain. Since an interior quatrain may start with sound designator "b" rather than "a" it is represented by six possibilities shown in the entire tree.

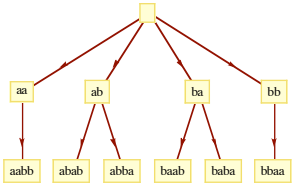

Figure 1: *Tree for Quatrains with Two End Rhyme Sounds.*

Counting possible end rhyme patterns for sonnets becomes much more intricate than the tree in Figure 1 may suggest since sonnets are divided into a number of sections of various lengths that determine the constraints on the end rhyme patterns. The following five examples of the leading octave sectioned into two quatrains or taken as a whole with two (Examples 1, 2 & 3) or with four (Examples 4 & 5) end rhyme sounds, respectively, demonstrate the structural possibilities and large variance in counts. The counts were computed using the algorithm described before Table 2 in the next section.

1:	two paired sounds in each quatrain:	18 possibilities from	"aabb aabb"	to	"abba bbaa"
2:	paired sounds in each quatrain:	31 possibilities from	"aaaa aabb"	to	"abba bbbb"
3:	two paired sounds across the octave:	63 possibilities from	"aaaaaabb"	to	"abbbbbba"
4:	two paired sounds in each quatrain:	9 possibilities from	"aabb ccdd"	to	"abba cddc"
5:	four paired sounds across the octave:	105 possibilities from	"aabbccdd"	to	"abcddcba".

As noted above, the 14 lines of a sonnet usually are divided into several sections, for example, into the 4-4-6 or the 4-4-4-2 groupings of the Shakespearean sonnet, or into the 8-6 or 4-4-6 groupings of the Petrarchan sonnet, and these divisions determine different kinds of rhyme patterns. In the remainder of this section I introduce a formal description for these (structured) divisions, count them and describe in more detail dependencies for those closely associated with sonnets.

A poem may be thought of as a sequence of groups where a ***group*** is a sequence of contiguous lines. For a sonnet specifically, each group may be of length 2, 3, 4, 6, 8, 10, 12, and 14 with the constraint that the sum of the group lengths adds up to 14, the length of a sonnet. I will refer to any such sequence of groups as a ***grouping type*** or, for short, a ***type*** for a sonnet. In mathematical terms, a type is a partition of the number 14 into a set of k positive numbers $\{g_1,\ldots, g_k\}$ such that their sum equals 14. For example, 4-4-4-2 and 8-3-3 as well as 7-7 or 9-5 are partitions of the number 14 that have been used by poets as groupings in sonnets although the last two appear only rarely, see ([5], pp.210-211 and 283-284).

Of specific interest are grouping types that contain group lengths from the set {2, 3, 4, 6, 8}. These five numbers represent group lengths that are commonly used in sonnets. The computational task is to produce all possible ways, subject to the constraints imposed by the set of group lengths to be used for a type, to partition the number 14 into groups of smaller numbers that add up to 14. In Table 1 the rows represent six sets of group lengths that may occur in a grouping type for a sonnet. The five columns represent the maximum number of groups that may occur in a type and the last column indicates that any number of groups is permitted. Each table entry is the number of different types for a given set of group

lengths and a maximum number of groups in a type. For example, there are 7 different types using lengths from the set {2, 4, 6, 8} and consisting of at most 4 groups such as 8-6, 6-4-4 and 4-4-4-2. Note that the counts of types in successive columns across a row from left to right subsume the counts from the previous column.

	1	<= 2	<= 3	<= 4	Any
4, 6, 8	0	1	2	2	2
3, 4, 6, 8	0	1	**3**	**4**	4
2, 4, 6, 8	0	1	**4**	**7**	11
2, 3, 4, 6, 8	0	1	**5**	**10**	17
2, 4, ..., 12, 14	1	4	8	11	15
1, 2, ..., 13, 14	1	8	24	47	135

Table 1: *Sonnet Types Classified by Groups.*

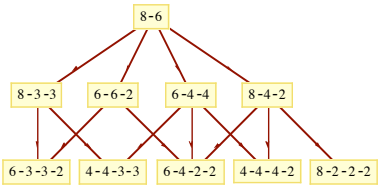

Figure 2: *Dependency Structure of Some Sonnet Types.*

In order to see the different structures in the sonnet form I visualize the 10 common grouping types for sonnets represented in row 4, column 4 of Table 1 through their dependencies. The fact that in this case there are 10 types of sonnets demonstrates the wide variety of structural constraints possible in this short poetic form. I will use the concept of partial ordering together with its standard pictorial representation in Hasse diagrams to render the 10 types as a directed graph in Figure 2. Grouping g_2 is said to be ***directly below*** grouping g_1 if g_2 can be obtained by partitioning one number of g_1 into two numbers. For example, grouping 4-4-4-2 is directly below 8-4-2, but it is not directly below 8-6, though it is below 8-6 in a two-step refinement. I normalize the notation for groupings so that the group lengths decrease or stay constant as one proceeds from left to right through the grouping type. Therefore, I write 6-4-4, the type of the Petrarchan sonnet, that is written more commonly as 4-4-6 indicating the actual quatrain-quatrain-sestet sequence of the poem. In the partial order of Figure 2 each vertex is labeled with its grouping pattern and the directed edges represent each direct refinement step.

3. Counting Rhymes in Poems and Visualizing Rhyme Count Structures through Trees

The central topic of this section is the generation and enumeration of end rhyme patterns of poems that have an even number of lines in which end rhyme sounds have ***even multiplicity***, that is, each sound occurs on some even number of lines in the poem. Such rhymes are called ***even rhymes***. When an end rhyme sound occurs exactly twice that rhyme sound is called a ***paired rhyme***. Using the grouping notation introduced in the previous section, the sets of poems of 2n lines, for some integer n, that have exactly k or at most k end rhyme sounds are denoted by $(2n)^e_k$ and $(2n)^e_{\leq k}$, respectively, where $1 \leq k \leq n$ and the upper index "e" denotes "even"; the absolute value expressions $|(2n)^e_k|$ and $|(2n)^e_{\leq k}|$ denote their counts. When k=n all rhymes must be paired and a numeric upper index is used such as $(4)^2_2$.

The grouping types in the center of the partial order in Figure 2, particularly the two dependency chains 8-6 to 6-4-4 to 4-4-4-2 and 8-6 to 6-4-4 to 4-4-3-3 have special significance since these end rhyme patterns for sonnet types include and generalize the Shakespearean and Petrarchan sonnet forms. Furthermore, many poets who write rhymed verse use even multiplicities of the rhymed sounds with pairs dominating. This suggests the following computing and visualizing tasks of possible end rhyme patterns in the sonnet form and their literary use:

(1) Generate all possible end rhyme sound patterns for all poems of 2n lines that contain between 1 and n end rhyme sounds of even multiplicity, that is, compute the set $(2n)^e_{\leq k}$ for $1 \leq k \leq n$, specifically for $n \leq 14$, and provide the associated counts for the end rhyme sound patterns.
(2) Generate all end rhyme patterns for the Shakespearean and Petrarchan sonnet forms. Visualize counts of end rhyme patterns for those sonnet forms in a structural manner by trees.
(3) Visualize all possible end rhyme patterns as colored bands for sections of poems such as sestets and

octaves as well as for end rhyme patterns of sequences of sonnets from the literature.

For the first task I begin with a description of the generating process of end rhyme patterns. The process starts with the set consisting of the single one-line pattern "a" and successively generates longer "partial" poems until the desired number of lines, 2n, for some chosen value of n is reached. The essential test for extendibility of a partial poem pp with sound s consists of checking that (i) sound s either already occurs in pp or that it is the (next alphabetic) sound after the maximum sound occurring in pp, and (ii) that adding sound s still permits matching evenly all sounds in pp and sound s when the designated maximum length 2n for the poem has been reached. For example partial poem "abba" may be extended with either "a", "b", or "c", but not with "d", while partial poem "abcadc" may be extended only with "b" or "d" if maximum length of the poem is 8 and end rhymes must be paired.

Implementation of this algorithm produces the list of all end rhyme patterns. Grouping the list by number of end rhyme sounds and counting the sizes of those lists creates the triangle of numbers displayed in Table 2. Since the numbers in the table represent poems of even length up to 14 lines the last row in the table includes most types of evenly rhymed sonnets. The entries in the last column of the table are the sums of all entries in the respective rows.

	1	2	3	4	5	6	7	sum
2	1	0	0	0	0	0	0	1
4	1	3	0	0	0	0	0	4
6	1	15	15	0	0	0	0	31
8	1	63	210	105	0	0	0	379
10	1	255	2205	3150	945	0	0	6556
12	1	1023	21120	65835	51975	10395	0	150349
14	1	4095	195195	1201200	1891890	945945	135135	4373461

Table 2: *The Triangle of Even Rhyme Patterns by Number of Distinct Sounds.*

A number of columns and diagonals in this Triangle of Even Rhyme Patterns are initial segments of sequences listed in The On-Line Encyclopedia of Integer Sequences (OEIS) [10]. If the entries in Table 2 are labeled w(n, k), where n represents poems of length 2n and k the number of sounds in the poems, correspondences between some number sequences in the triangle and initial segments of sequences listed in OEIS exist as follows:

column 2	w(n, 2) / 3	$4^{n-1} - 1$	sequence A002450,
column 3	w(n, 3) / 15		sequence A002451,
sum column	$\sum_{i=1}^{n} w(n,i)$		sequence A005046,
diagonal	w(n, n)	(2n-1)*(2n-3)*…*3*1	sequence A001147,
sub-diagonal	w(n+1, n)		sequence A001880.

For the remainder of this section I want to turn my attention to the rhyme pattern counts in the Shakespearean and Petrarchan sonnet forms. The next two tables show counts of rhyme patterns for poems such as sonnets that are constructed as sequences of blocks. The numbers were calculated by cascading the function that generates end rhymes patterns for a single group over the sequence of groups that form the indicated type of poem. The two tables demonstrate the huge variety of end rhyme patterns that are possible even under the constraints of quatrain and sestet sequences.

Table 3 shows the rhyme counts for poems that consist of sequences of quatrains $(4)_2^2$ that have two sounds in each quatrain with repetition of sounds across quatrains permitted, that is, the poems satisfy the grouping type 4-4-…-4. The rows in the table indicate the number of quatrains and the columns the number of end rhyme sounds in each grouping. The counts in the table are listed through sequences of four quatrains, that is, 16 lines at maximum, since the counts for rhyme patterns of Shakespearean and

Petrarchan sonnets will fall between these numbers. The columns in the table show the counts for 2 to 8 end rhyme sounds in the entire poem. The last column shows the sum of columns for the seven possible rhyme sounds. Note that the count for the number of sounds starts at 2 since the leading quatrain for this rhyme pattern type must have two sounds.

	2	3	4	5	6	7	8	Total
1	3	0	0	0	0	0	0	3
2	18	36	9	0	0	0	0	63
3	108	864	1026	324	27	0	0	2349
4	648	16 848	52 812	46 656	15 228	1944	81	134 217

Table 3: *The Triangle of Even Rhyme Pattern Counts for Sequences of Quatrains.*

Table 4 shows the total number of end rhyme patterns for five different grouping types that are related to various sonnet rhyme patterns and whose grouping types are shown in Figure 2. The columns of the table are arranged in the same manner as in Table 3. The rows represent five end rhyme pattern types: 1. the Petrarchan rhyme pattern $(4)^{e}_{\leq 2} - (4)^{e}_{\leq 2} - (6)^{e}_{\leq 3}$ which has between two and six rhyme sounds, 2. the Shakespearean rhyme pattern $(4)^{2}_{2} - (4)^{2}_{2} - (4)^{2}_{2} - (2)^{2}_{1}$ which has between two and seven rhyme sounds, 3. an alternate Petrarchan rhyme pattern type $(4)^{2}_{2} - (4)^{2}_{2} - (6)^{2}_{3}$ which has between three and seven sounds, 4. a more general Petrarchan rhyme pattern $(4)^{e}_{\leq 2} - (4)^{e}_{\leq 2} - (6)^{e}_{\leq 3}$, and 5. the most general rhyme pattern $(8)^{e}_{\leq 4} - (6)^{e}_{\leq 3}$ that is shown at the top of the partial ordering in Figure 2.

	1	2	3	4	5	6	7	Total
Petrarchan	0	360	2880	3420	1080	90	0	7830
Shakespearean	0	216	2700	4968	2646	486	27	11 043
Q - Q - S paired	0	0	4860	14 580	9990	2160	135	31 725
Q - Q - S even	1	1023	12 427	23 328	12 714	2385	135	52 013
Q - S even	1	2047	48 003	139 560	101 850	23 625	1575	316 661

Table 4: *Even Rhyme Pattern Counts for Five Grouping Types.*

A structural view of the numbers in the first two rows of Table 4 is presented in the next two figures.

Figure 3: *Rhyme Pattern Counts by Grouping in Petrarchan Sonnets (7,830)*

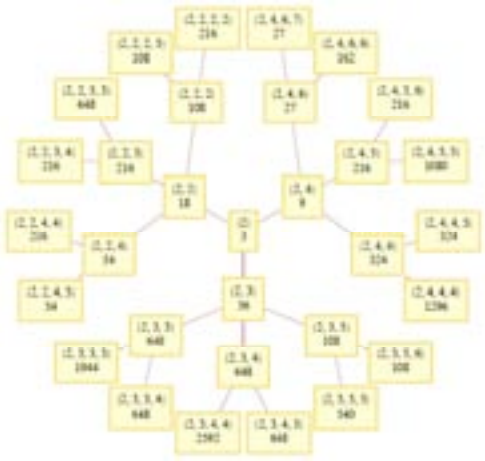

Figure 4: *Rhyme Pattern Counts by Grouping in Shakespearean Sonnets (11,043)*

They visualize the internal multiplicative and additive structure of the counts of the end rhyme patterns for the Petrarchan (4-4-6) and Shakespearean (4-4-4-2) sonnet forms. The images are drawn as concentric trees with the root in the center representing the leading quatrain and each ring representing the next group in the grouping type. Each node in the trees contains two indicators. The upper set denotes the number of end rhyme sounds occurring in the sequence of groups that the node represents and the lower number gives the respective total count of patterns for that sequence of groups. For example, the node $\left[\begin{smallmatrix}\{2,2,3\}\\ 720\end{smallmatrix}\right]$ in Figure 3 denotes a count of 720 for sonnets with two sounds in the leading quatrain, two sounds across the first two quatrains and three sounds total for the sonnet. Adding counts in appropriate nodes in the outermost rings of the two trees produces the counts in the first two rows of Table 4.

4. Visualizations of End Rhyme Pattern Types and Sonnet Sequences as Bands

In this section I show visualizations of two types of end rhyme patterns. In one visualization all possible patterns subject to stated constraints are shown side by side. The other visualization presents an actual sequence of sonnets from the literature to show how one poet used some of the rhyme patterns. Each end rhyme sound in a poem is associated with one color and the same color assignments for the sequence "a"-"g" of end rhyme sounds is used across sequences of poems. Each poem is shown as a horizontal strip of colored squares with the color for the end rhyme sound of the first line on the left and for the last line on the right. A sonnet will be represented as a strip of fourteen squares in at most seven colors. The visualization of a sequence of poems is a vertical band of these strips. Since the first end rhyme sound in a poem is always represented by sound symbol "a", a visualization of all poems in a sequence starts with the same color or gray tone when using a fixed color or gray scale assignment for each sonnet in a band.

Figure 5 shows the gray scale bands for three different end rhyme pattern types, arranged from smallest to largest number of possibilities. The left-most band represents the 27 possible rhyme patterns for sonnets of type $(4)_2^2 - (4)_2^2 - (4)_2^2 - (2)_1^2$ that have seven end rhyme sounds (see Table 4, row 2). The band shows the Shakespearean rhyme pattern "abab cdcd efef gg" right in its center as the 14-th strip. It is interesting to speculate why Shakespeare chose the middle pattern #14 in the lexicographic ordering of the band. One reason may be that it is the one pattern among the 27 rhyme patterns with the maximum number of 12 sound changes given the structural constraint of a final couplet in the sonnet. The middle band shows the 31 possible rhyme patterns for sestets of type $6^e_{\leq 3}$ with 1, 2 or 3 paired end rhyme sounds (see Table 2, row 3). The right-most band shows the 36 possible rhyme patterns for a pair of quatrains $(4)_2^2$ - $(4)_2^2$ with three rhyme sounds (see Table 3, row 2).

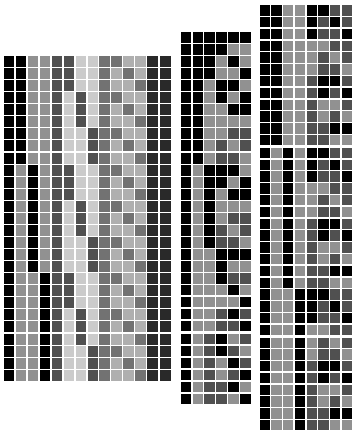

Figure 5: *7-Sound 4-4-4-2 Sonnets, ≤3-Sound Sestets & 3-Sound Quatrain Pairs*

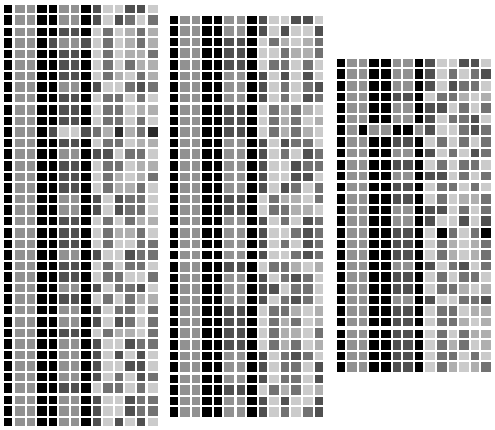

Figure 6: *Wordsworth's "Ecclesiastical Sketches" (as published in1822)*

Figure 6 shows the gray scale bands for the three parts of William Wordsworth's "Ecclesiastical Sketches", published in 1822 (see [7], pp. 137-204). The parts consist of 38, 36 and 28 sonnets, respectively, and the parts are shown as separate bands side by side. This image represents 102 x 14 = 1,428 lines of verse. It is immediately apparent that the poet used the same rhyme pattern, with a single exception (III.7), for the leading quatrain and two patterns, with three exceptions (I.4, I.12, III.7), for the second quatrain. The expressive rhyme variations occur in the concluding sestets of the sonnet sequence.

5. Further Work and Acknowledgements

In conclusion I would like to suggest two directions for further mathematical and literary inquiry. The first is motivated by the numbers w(i+k, k), 0≤i and 1≤k, in Table 2. The non-zero entries in the k-th column of that table appear as the initial values of the coefficients in the following power series:

$$G_k(x) = \prod_{j=1}^{k} \frac{2j-1}{1-j^2 x} = \frac{1}{2^{k-1}k!} \times \sum_{i=0}^{\infty} \left(\sum_{j=1}^{k} (-1)^{k+j} \binom{2k}{k+j} \cdot \left(j^2\right)^{k+i} \right) x^i = \sum_{i=0}^{\infty} w(i+k,k) x^i \quad \text{for all } 1 \le k.$$

For example, coefficient w(2+5, 5), that is, the value in row 7 and column 5 of Table 2 evaluates in closed form summation as: $w(2+5, 5) = \frac{1}{1920} (210 * 1^7 - 120 * 4^7 + 45 * 9^7 - 10 * 16^7 + 25^7) = 1{,}891{,}890$. The numbers of even rhymed patterns need to be related to the closed-form expressions for the coefficients in this power series by a combinatorial argument. The second direction would be to extract end rhyme words from poems and sequences of sonnets from a broad cross-section of the literature, to construct their associated colored bands and use the patterns evident in the bands as basis for comparative and interpretive studies.

Finally, I would like to thank the reviewers for their comments and suggestions that helped me improve this paper significantly.

References

[1] Jörg-Ulrich Fechner, *Das Deutsche Sonett,* Wilhelm Fink Verlag, München, 1969.
[2] Albert Feuillerat, editor, *The Complete Works of Sir Philip Sidney, Volume IV, The Countess of Pembrooke's Arcadia, being the original version,* Cambridge at the University Press, 1926.
[3] Laura J. George and Hartmut F.W. Höft, *Visualization of Rhyme Patterns in Two Sonnet Sequences,* Bridges Leeuwarden, Proceedings 2009, pp. 265-266.
[4] Günter Grass, *Selected Poems 1950 – 1993 (translated from the German by Michael Hamburger),* Hartcourt Brace & Company, New York, 1996.
[5] Edward Hirsch & Eavan Boland, editors, *The Making of a Sonnet, A Norton Anthology,* W. W. Norton & Company, New York, 2008.
[6] Hartmut F. W. Höft, *Mathematica Functions and Color Images for this Paper,* webpage: http://people.emich.edu/hhoft/bridges2009/.
[7] Geoffrey Jackson, editor, *Sonnet Series and Itinerary Poems 1820-1845 by William Wordsworth,* Cornell University Press, Ithaca and London, 2004.
[8] Rainer Maria Rilke, *Die Sonette an Orpheus,* Insel Verlag, Frankfurt am Main und Leipzig, 1930.
[9] Michael R. G. Spiller, *The Sonnet Sequence*, Studies in Literary Themes and Genres No. 13, Simon & Schuster Mcmillan, New York, 1997.
[10] Neil J. A. Sloane, *The On-Line Encyclopedia of Integer Sequences*, AT&T webpage: http://www.research.att.com/~njas/sequences/index.html.
[11] Helen Vendler, *The Art of Shakespeare's Sonnets*, The Belknap Press of Harvard University Press, Cambridge, Mass., 1999.

Tubular Sculptures

Carlo H. Séquin
CS Division, University of California, Berkeley, CA
E-mail: sequin@cs.berkeley.edu

Abstract

This paper reviews ways in which many artists have constructed large sculptures from tubular elements, ranging from single cylinders to toroidal or knotted structures, to assemblies of a large number of bent tubes. A few parameterized generators are introduced that facilitate design and evaluation of a variety of such sculptural forms.

1. Introduction

Artists like Charles O. Perry have been able to build very large scale sculptures filling volumes of more than 30 feet in diameter at an affordable price by assembling pre-cut and bent tubular pieces. Stellar examples are *Eclipse* in the Hyatt Regency lobby in San Francisco, or *Equinox* at the Lincoln Center, Dallas, Texas (Fig.1a). But even much smaller assemblies of tubular elements can make very attractive sculptures. At the small end of this spectrum we find sculptures by Max Bill, e.g., *Assembly of three equal cylinders* (Fig.1b) [2], or the elegant tubular loops by José de Rivera (Fig.1c) [4]. Additional "minimal sculptures" will be discussed in Section 3.

Figure 1: *(a) Charles O. Perry: "Equinox;" (b) Max Bill: "Assembly of 3 equal cylinder;" (c) José de Rivera: "Construction #35."*

With so many diverse ways of forming attractive sculptures from tubular elements, it seems worthwhile to try to compile an organized overview over the many possibilities and approaches used, and to explore in which ways computer-aided tools may be helpful to create additional, and potentially more complex, artistic structures. In addition, I have a personal, nostalgic reason to write this paper on *Tubular Sculptures*. It was the influence of Frank Smullin who started me a quarter century ago on this path of exploring "Artistic Geometry" at the intersection of computer science, mathematics, and sculpture.

2. Inspiration by Frank Smullin (1943 – 1983)

On June 30, 1981, Frank Smullin gave a keynote talk at the 18th Design Automation Conference in Nashville, Tennessee [19]. He showed pictures of his tubular sculptures, often celebrating simple knots (Fig.2a). He explained how he had created a program running on his Apple II computer to help him design these sculptures and to calculate the elliptical cut lines that resulted at the angled junction between two or more tubular elements. His program produced simple outline drawings, which he then colored in by hand (Fig.2b). In this talk he extolled the merits of the *Granny-knot*, which has an artistically much more interesting, 3-dimensional structure than the functionally preferred, but much flatter *Square-knot*. When he mentioned that in the *Granny-knot* the four ends of the cropped "shoe laces" would stick out in the 4 tetrahedral directions (Fig.2c), something clicked in my brain. Four arms sticking out in tetrahedral directions reminded me of a carbon atom and of the way such atoms readily assemble into a diamond lattice. I immediately saw the possibility of assembling a large number of *Granny-knots* in the same way into a *Granny-Knot Lattice* (Fig.2d). I left the conference with the firm goal that I wanted to create such a structure, and that I would use the emerging power of computer graphics to help me in that venture.

Figure 2: *(a) Sculpture by Smullin; (b) Smullin's design program; (c) Smullin: "Tetra-Granny;" (d) Séquin: "Granny-Knot Lattice."*

Over the following twelve months, Paul Strauss, a one-year-on-campus Master student from Bell Labs, developed a first version of a rendering program, called Berkeley *UNIgrafiX*, which was able to render such structures with proper hidden-surface elimination; thus there was no need to shade in the visible surfaces by hand. In parallel I developed a program *MakeWorm* that created the properly mitered and joined prismatic segments that would form tight, knotted or linked structures, and within a few months I had a dramatic visualization of the *Granny-Knot Lattice* displayed in the {1 1 0} direction of the diamond lattice structure to reveal the well-known channels that run in that particular direction (Fig.2d).

Figure 3: *Tubular sculpture models by Séquin: (a) "Standing Overhand Knot," (b) "Mitered Junction Models," (c) "Minimal Sticks Trefoil," (d) "Tetra-Tangle."*

Inspired by Smullin's sculptures, I also used this emerging programming environment to design some free-form knot models (Fig.3a), made from the 4-inch diameter cardboard tubes that carried the 3-foot wide Versatec printer paper. In that effort I used the mitering techniques explained by Smullin, and made many tutorial models (Fig.3b), which I then used in my class on *Creative Geometric Modeling*. Figure 3c

shows the 6-stick realization of the trefoil knot with shortest total axis length, which was obtained with a simple optimization procedure. I also was proud to discover a tight, highly symmetrical linkage of four mutually linked equilateral triangles (Fig.3d), but subsequently discovered that this link and many other, much more ingenious ones had already been described in the book *Orderly Tangles* [10].

3. Minimal Geometries – Cylinders

Trying to find a systematic approach to a classification of tubular sculptures, we start with the simplest tubular element: a straight, circular cylinder. In this raw form it shows up as an architectural element, e.g. in *La Défense*, near La Garenne-Colombes, France (Fig.4a) and in the chapel at MIT in Cambridge, MA (Fig.4b). When a single cylinder is used as a stand-alone sculpture, it normally is given some artistic enhancement. This may be achieved by painting its surface as in Max Bill's *Painting in form of a column* (Fig.4c) or by cutting off its ends in some special way as in Bill's *Cylinder as a right-angled volume* (Fig.4d). Alternatively only part of the cylinder surface may be retained, as in John Goodman's *Unicorn Spirit* (Fig.4e).

Figure 4: *(a) Cylinder in La Défense; (b) Chapel at MIT; (c) Bill: "Painting in form of a column;" (d) Bill: "Cylinder as a right-angled volume;" (e) Goodman: "Unicorn Spirit."*

Many large-scale sculptures are formed by groups of simple un-decorated cylinders, e.g., *FUNtain Hydraulophone* at the Ontario Science Centre [7] or Roger Berry's *Rising Wave* at Oyster Bay [1].

Figure 5: *(a) Hart: "72 Pencils – CMYK;" (b) Séquin: "Skewed Tangle of 12 Cylinders;" (c) Snoeyink: "30 Aluminium Tubes;" (d) Snelson: "Needle Tower."*

When cylinders are packed in tight, tangled configurations, we obtain very intriguing geometrical configurations. An example of such a cylinder packing, well known to Bridges attendees, is George Hart's *72 Pencils – CMYK* (Fig.5a) [8]. Figure 5b shows a tangle of 12 cylinders derived from the TetraTangle structure (Fig.3d). A more elaborate version of such a skewed arrangement has been constructed by Jack Snoeyink; it is made from 30 identical aluminum tubes, colored and grouped as five twisted, interlocking tetrahedral frames (Fig.5c). This sculpture celebrates a research result that shows

that this arrangement, made from simple straight cylinders, cannot be divided into two groups that can then be separated with a rigid-body motion [20]. In the context of cylinders used as sculptural elements, I would also like to reference the *tensegrity* structures pioneered by Kenneth Snelson (Fig.5d), which may be perceived as collections of cylinders seemingly floating free in space.

4. Tori and Chain Links

If we allow bending the tubular elements, then the simplest most regular shape we can form is the torus. Tori have been celebrated by many artists in many different ways. In the science museum in Vienna there is an archeological artifact in bronze representing a simple toroidal shape of more than a foot in diameter (Fig.6a), dating back about 5000 years! Given more than one torus – they just want to be interlinked. A beautiful tight linking of two tori has been created by John Robinson with *Bonds of Friendship* in Sydney Cove, Australia (Fig.6b). Three interlocking tori can be seen in a giant inflatable sculpture *Torus! Torus!* erected by Joseph Huberman (Fig.6c) [11].

Figure 6: *(a) 5000 year old bronze torus; (b) Robinson: "Bond's of Friendship;" (c) Huberman: "Torus! Torus!"*

Helaman Ferguson even has accomplished the feat of interlocking two tori made of different types of stone (Fig.7a). – Of course, they are not really complete tori, but rings with beveled gaps, depicting the self-intersecting surfaces of two Klein bottles; these two open chain links can then be assembled with a clever twisting maneuver. Stretched toroidal loops can readily be linked into longer chains. Tight-fitting plastic chain links have been assembled into deformable chains and then modeled into catenoids standing upside down in my sculpture model *Defying Gravity* (Fig.7b). Such tubular ovals are also the basis for a configuration of the Borromean rings cast by Alex Feingold (Fig.7c). In 1999 I created a Borromean tangle with five oval loops (Fig.7d). Interlinking ever more tubular loops in ever more intricate ways leads to a plethora of interesting configurations, as depicted in *Orderly Tangles* [10]. Some of these links would make quite dramatic large-scale sculptures. On a small scale (Fig.3a in [15]) they make bouncy dog toys or colorful "Nobbly Wobblys" [5].

Figure 7: *(a) Ferguson: "Four Canoes;" (b) Séquin: "Defying Gravity;" (c) Feingold: "Borromean rings;" (d) Séquin: "Borromean Tangle 5."*

5. Ruled Surfaces and Iterated Hula-Hoops

The simple geometrical elements that made up the sculptures discussed so far maintain some individuality. Now we look at configurations where the individual cylinder or torus has little meaning, and where it is a relatively large collection of such elements that then create the dominant form of the sculpture. As a first example we look at a large collection of long, skinny cylinders to form a more complex geometrical shape. Such geometry is reminiscent of *String Art* and of many mathematical models depicting hyperbolic paraboloids and other ruled surfaces. Tubular elements forming such ribbed surfaces are particularly useful when "transparency" is required. This is the case when we try to depict mathematical models with intersecting surfaces and would like to provide a look to the inside, to see interesting features such as triple points. Figure 8a and b show tubular models of a hemi-cube and of a hemi-dodecahedron. These are non-orientable, generalized polyhedra (or 2D cell-complexes) that can be obtained by taking surface elements of the cube or of the dodecahedron and identifying antipodal points, edges, and faces. Thus my model of the hemi-cube has just three bilinearly warped "squares," and the hemi-dodecahedron is composed of six (differently colored) warped pentagons forming a tetrahedral structure with six angled edges. The latter is the basic building block of the 4-dimensional 57-Cell [17].

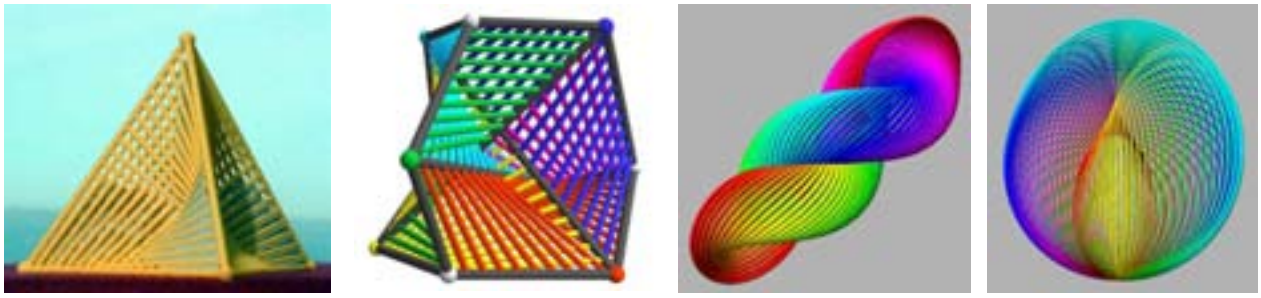

Figure 8: *Non-orientable 4-dimensional cells: (a) hemi-cube, (b) hemi-dodecahedron. Iterated circles: (c) twisted goblet, (d) cross-cap model of the projective plane.*

Similarly, a large assembly of skinny tori can produce interesting shapes. Just rotating such a "hula-hoop" around one of its diameters and simultaneously sweeping it along that diameter creates a twisted goblet (Fig.8c). If instead the hula-hoop is iteratively scaled from size 1.0 to size 2.0 and back to size 1.0 while we rotate the hoop through 180°, we obtain a rendering of a cross-cap – a model of the projective plane.

These iterative constructions, which are particularly amenable to generation with a computer program, can be generalized to *Ribbed Surfaces*, where the iterated ribs need not be straight cylinders nor tori, but may be a sequence of procedurally specified curves. One versatile approach first defines two *Guide Rails* and then suspends a collection of equally spaced Bézier curves or circular arcs between them.

6. Perry's Ribbed Sculptures

Charles O. Perry has created several large *Ribbed Sculptures* [14] that can be modeled with this paradigm; and his sculptures were the inspiration for this work and for this paper. A sculpture that is particularly fascinating to the mathematical mind is *Solstice* (Fig.9a) because its generating principle is so simple and elegant, yet the result is intriguing and spectacular in the variety of vistas it offers from different angles. *Solstice* has a thick rail that forms a (3,2) torus knot embedded in the surface of a fat virtual torus with a rather small central hole. Each minor circle of that torus has 3 symmetrically located points, 120° apart, through which the thick rail passes. These three points are connected with three thin ribs that form a "hyperbolic" triangle with inward-bending concave sides (Fig.9e). This triangular cross section now twists through 240° as it travels once around the major loop of the torus. (Helaman Ferguson has created a similar geometry in a bronze cast called *Umbilic Torus NC*; however, in his sculpture the twist of the triangular cross section is only 120°.)

Understanding the mathematics behind *Solstice* allows us to create a close computer emulation (Fig.9b). This generator program, written by James Hamlin, can now be parameterized so that we can readily change the number of ribs and their diameter or curvature to fine-tune the look and feel of the sculpture. But we can also introduce more dramatic changes by altering the integer parameters (*p*,*q*) that define the torus knot formed by the supporting rail. Figure 9c shows a sculpture that results from a (4,3) torus knot with all other parameters left unchanged. Figure 9d is yet another variation, based on a (2,3) torus knot; however, in this sculpture the ribs no longer lie in the planes of the minor circles of the torus, instead they are spiraling a significant distance forward or backward around the major loop of the torus. An additional parameter in the program allows us to control the amount of this angular offset around the major circle of the torus; in Figure 9d this value was –45 degrees.

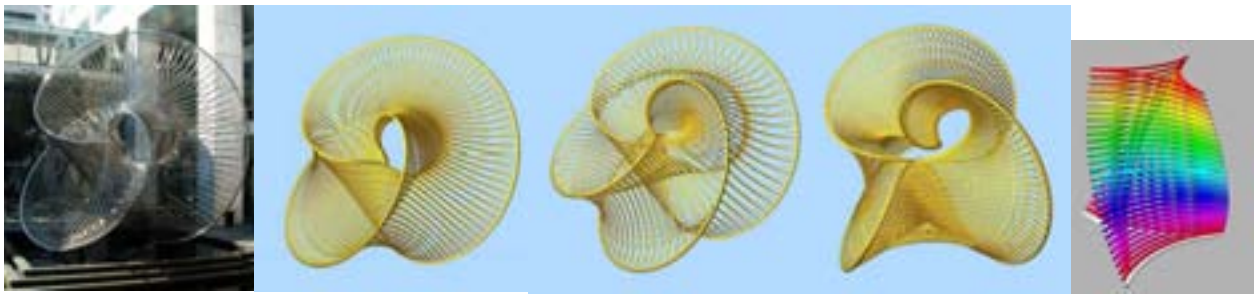

Figure 9: *"Solstice": (a) Perry's sculpture; (b) computer emulation; (c) (4,3) torus knot variation; (d) (2,3) torus knot variation. (e) Principle of swept 'hyperbolic' triangle.*

Early Mace (Fig.10a) is another sculpture by Charles O. Perry that uses ribs in the shape of circular arcs connecting two guide rails. In this case the rails are two pairs of (almost) great semicircles on an invisible sphere, held together by two small semicircles at both ends. The ribs form inwards-bending quarter arcs. Figure 10b shows an emulation of this sculpture with a program written by James Hamlin. Figures 10c and 10d then demonstrate what happens when the ribs are straightened and finally bent outward to follow the surface of the sphere.

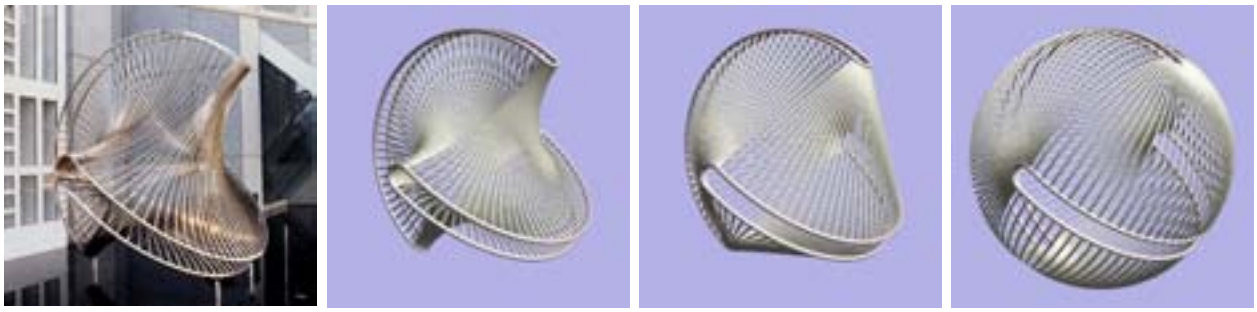

Figure 10: *"Early Mace": (a) Perry's sculpture; (b) computer emulation; (c,d) rib variations.*

7. Generalized Sweeps

Tubular elements provide broad artistic freedom of expression if free-form guide curves are used for the sweeps of circular or of more elaborate cross sections. Very simple free-form shapes have appeared as icons on musical album covers (Fig.11a) [13] or have been used by artists such as José de Rivera for 3D metal sculptures (Fig.11b). Free-form shapes typically need customized bending of tubes, and this may require tools and methods not readily accessible to many people. In 1982 Richard Zawitz introduced the *Tangle®-Toy*, a series of pipe segments, each curbed through 90°, connected into a loop and able to pivot at each joint (Fig.11c). This pliable assembly now allows anybody to become an instant tubular artist and to create attractive free form sculptures (Fig.11d).

Figure 11: *(a) "Tubular Bell" album cover; (b) de Rivera: "Construction #5B." (c) Zawitz: "Museum Tangle;" (d) modified shape by Séquin.*

Conceptually, a freeform sweep can use any cross section. Figures 12a and 12c show two wood sculptures by Brent Collins [3], where the cross section consists of the union of two overlapping discs. Figures 12b and 12d show emulations and further developments of this theme, modeled in the Berkeley SLIDE environment and fabricated on a rapid prototyping machine. As shown, these models do not use any standard tubular stock that could be readily bent in the way depicted, and thus they do not offer a ready pathway for making large-scale sculptures. One might perhaps try to start with just one tube and bend it in the required way. To this primary tube one would then add a second tube from which about one sixth of its mantle has been cut away. However, it is not clear how well such a cut-open cylinder could be bent into the exact shape required to make a good fit to the primary tube. Such sweeps can, of course, readily form knotted structures as depicted by Figures 12c and d.

Figure 12: *Sweep surfaces: (a) Collins: "Muscularity;" (b) Séquin: "Galapagos-6." Knotted sweeps: (c) Collins: "Trefoil;" (d) Séquin: "Figure-8 Knot."*

8. Knotty Sculptures

Figure 13: *Regular Knotty Sculptures: (a) "Hilbert Cube 512," (b) "DodecaPentafoil Tangle," (c) "Recursive Trefoil Knot 2D," (d) "Cubic Lattice of Figure-8 Knots."*

At other occasions I have talked extensively about *Knotty Sculptures* [16]. Conceptually most of my previously described knotty structures (Fig.13) belong to the family of tubular sculptures. But most of them were small-scale models that have been realized on different types of layered manufacturing machines, a process that is not amenable to fabricating large sculptures. However, these highly regular structures favor a modular approach. They each have just a few generic geometric elements, which could all be prefabricated individually and then assembled into the larger structure. In particular, "*Hilbert Cube 512*" (Fig.13a) only needs a single element: a 90° pipe elbow. The *Recursive Trefoil Knot 2D* also needs a small number of different elements (Fig.13c). The other two structures, however, may present some tough assembly problems, even though the number of individual types of elements is also rather low.

Figure 14: *Séquin: (a) "Chinese Button Knot" (copper tubing), (b) "Three Intertwined Loops," (c) "Chinese Button Knot" (drier duct), (d) "Glow-Worm."*

Another approach to make such knotty structures is to use some easily bendable material. Figure 14a shows a realization of the *Chinese Button Knot* (Knot 9_{40} in the standard knot tables) from thin copper tubing. For the three intertwined loops shown in Figure 14b, half-inch thick vinyl tubing has been used. The two structures shown in Figures 14c and 14d were realized with 6″-aluminum and 4″-vinyl drier duct; they depict again the *Chinese Button Knot* and a similar braided, but more complex 12-crossing knot (with internal lighting), respectively. A bigger challenge is posed by truly recursive knot structures such as the one presented by Robert Fathauer [6] where the pipe diameter is gradually reduced with subsequent recursion steps so as to allow arbitrarily many recursion steps without suffocating in the ensuing tangle.

9. Branching Tubular Assemblies

In the sculptures discussed so far, the assemblies of tubular elements followed individual poly-line paths or closed loops, and thus the mitering geometry at the "corners" was rather straightforward. But of course, tubular structures can have branches and may form much more complicated 3D graphs. If the tubular elements are skinny enough, then the details of the junctions escape the attention of the viewer; this is the case in Max Bill's *Construction with 30 Similar Elements* (Fig.15a) [12]. However, when tubes of larger diameter are joined, then careful attention has to be paid to the geometry of the mitered corners, as explained in Frank Smullin's keynote talk and demonstrated by the tutorial models shown in Figure 3b.

Figure 15: *(a) Bill: "Construction with 30 Similar Elements;" (b) Liberman: "Olympic Iliad;" (c) 'shade': "Steam pipe sculpture"; (d) Séquin: "Branching Drain Pipe."*

However, this kind of carefully calculated general mitering is rarely found in large-scale sculpture. Often large tubular elements are just left open-ended and connected to one another on their sides, as in Alexander Liberman's *Olympic Iliad* (Fig.15b). Another frequently found solution for creating tubular branches is to use the readily available "T"-junctions found in plumbing supply stores (Fig.15c) [18]. I have used more general and more complex junctions of three or more tubular elements in my *Branching Drain Pipe* (Fig.15d) and in my models of the projections of the 4-dimensional regular polytopes.

10. 3D Calligraphy

Figure 16: *(a) Serra: "Lead Piece;" (b) Hein: "Changing Neon Sculpture;" (c) RuBert: "Positronic Neural Net;" (d) Culbert: "SkyBlues."*

If the tubular material is thin and pliable enough, such as the lead pipe used by Richard Serra (Fig.16a), then it becomes a medium for "calligraphy" in 3-dimensional space. This becomes particularly apparent when neon tubes are used to form actual words as in large-scale advertisement and business logos. But neon tubes have frequently been used for purely artistic purposes. Since they can be turned on and off, they permit one to make dynamic time-varying sculptures, such as Jeppe Hein's *Changing Neon Sculpture* (Fig.16b), or Russ RuBert's *Positronic Neural Net* (Fig.16c) which changes in response to the viewers who walk around the sculptures. Neon tubes have also been used to make truly large-scale sculptures, such as Bill Culberts *SkyBlues* (Fig.16d), or Michael Hayden's installation at Chicago O'Hare airport [9].

11. Extensions to Organic Forms

Figure 17: *(a) 1994 Ad: "Absolut Scudera Vodka;" (b) Tunger: "Oh, Beautiful Life!" (c) Cragg: "Statue;" (d) Borofsky: "Dancers;" (e) Ochsner: "Libellotto".*

Most of the sculptures discussed so far have been completely abstract shapes. However, tubular elements can readily be used to approximate familiar natural shapes. Figure 17 shows a variety of sculptures that play with humanoid forms, ranging from advertisements of absolute vodka (Fig.17a) to John Tunger's

celebration of dance (Fig.17b). Tony Cragg has taken the modular approach one step further with his *Statue* (Fig.17c) in which he uses a large number of aluminum manikins made from tubular elements to assemble a giant sculpture in the shape of two persons, thus introducing an element of recursion. As the tubular elements become more varied or are blended together more smoothly, the resulting humanoid forms can be made ever more life-like, as in Jonathan Borofsky's *Dancers* (Fig.17d). At this end of the spectrum, tubular sculptures seamlessly transition into purely free-form shapes, as exemplified by Claire Ochsner's *Libellotto* (Fig.17e).

12. Conclusions

Tubular elements are a surprisingly expressive and cost-effective medium. Assembling stock elements, such as segments of rods, bands, or tubes is a much less expensive way to make large durable metal or plastic sculptures, than casting individual free-form bronze pieces, welding them together, and then smoothing the surfaces across the various joints. CAD tools are a big help in the conception, detailed design, and aesthetic optimization of any sizeable sculpture, and they play a crucial role in creating the necessary shop drawings. Parameterized procedural descriptions of such geometries can turn this domain into a fertile playground for artistic experiments.

Acknowledgments

Thanks are due to James Hamlin for coding the emulation programs for Perry's *Solstice* and *Early Mace*, and to John Sullivan who, once again, gave me the most critical-constructive feedback.

References

[1] R. Berry, *Rising Wave*. (2009): http://baytrail.abag.ca.gov/vtour/map4/access/OystrBay/OystrBay.htm

[2] M. Bill, in: *aus der sammlung theo und elsa hotz*, Museum Jean Tinguely, Basel, (1998), pp 62-69.

[3] B. Collins, *Geometric Curvature and their Aesthetics*. Proc. Bridges, Winfield, Kansas, 2001, pp 81-88.

[4] J. de Rivera, *Construction # 35*. in: *Modern Sculpture*, by H. Read, Thames and Hudson, Inc., NYC, Fig. 274.

[5] Doggie Solutions, *Nobbly Wobblys*. (2009): http://www.doggiesolutions.co.uk/dog-throw-toy-4364-0.html

[6] R. Fathauer, *Fractale Knots Created by Iterative Substitution*, Proc. Bridges, Donostia, 2007, pp 335-342.

[7] *FUNtain Hydraulophone*. Ontario Science Centre webpage (2009): http://wearcam.org/oscfuntain/

[8] G. Hart, 72 Pencils, webpage (2009): http://www.georgehart.com/sculpture/pencils.html

[9] Michael Hayden: *Sky's the Limit*. (2009): flickr.com/photos/good_day/129662479/

[10] A. Holden, *Orderly Tangles*. Columbia University Press, New York, (1983).

[11] J. Huberman, Treklite Ink, webpage (2009): http://treklite.com/products/art/torus.htm

[12] E. Huettinger, *max bill*, abc edition, Zürich, (1978).

[13] M. Oldfield, *Tubular Bells*. (2009): http://tubular.net/

[14] C. O. Perry, *Ribbed Sculptures*. webpage (2009): http://www.charlesperry.com/Ribbed.html

[15] C. H. Séquin, *Patterns on the Genus-3 Klein Quartic*. Proc. Bridges, London, 2006, pp 245-254.

[16] C. H. Séquin, *Tangled Knots*. Proc. Art+Math=X, Intnl. Conf., Boulder CO, June 2-5, 2005, pp 161-165.

[17] C. H. Séquin and J. F. Hamlin, *The Regular 4-Dimensional 57-Cell*. SIGGRAPH'07, Sketches and Applications, San Diego, Aug. 4-9, 2007.

[18] 'shade', *Steam Pipe Sculpture*. (2009): http://www.steampunkmagazine.com/forum/viewtopic.php?t=404

[19] F. Smullin, *Analytic Constructivism: Computer-Aided Design and Construction of Tubular Sculptures*. Luncheon Presentation, 18th Design Automation Conf., Nashville, TN, June 30, 1981.

[20] J. Snoeyink, J. Stolfi, *Objects that cannot be taken apart with two hands*. Proc. of the 9th ACM Symp. on Computational Geometry (1993).

Comic Books That Teach Mathematics

Bruce Kessler *
Ogden College Dean's Office
Western Kentucky University
1906 College Heights Blvd.
Bowling Green, KY 42101
E-mail: bruce.kessler@wku.edu
Illustrations by WKU undergraduate student Anne Erskine and the author.

Abstract

During the 2008–2009 academic year, the author embarked on an extremely non-standard curriculum path: developing comic books with embedded mathematics appropriate for 3rd through 6th grade students. With the help of an education professor to measure impact, an elementary-school principal, and talented undergraduate illustrators, this project came to fruition and the comics were implemented in elementary classrooms at Cumberland Trace Elementary in the Warren County School System in Bowling Green, Kentucky. This manuscript gives the history of this idea, the difficulties of developing the content of the comics and getting them illustrated, and the implementation plan in the school.

1 Introduction

In September 2008, I attended an Idea Kentucky meeting (www.ideakentucky.com) where the organizers had hired a professional cartoonist, Keith Bendis (keithbendis.com), to take notes of the meeting. He had three large pieces of white paper taped to the wall of the room, and a table full of markers. Throughout the meeting, he was taking in the salient points being made and then illustrating these points with small, humorous scenes capturing the essence of the conversation (Figure 1). When finished, I remember thinking that even people that did not care about the meeting would still be interested in the notes that he had crafted, and an idea was born. What if you could present mathematics in such a way that even people who did not care much about it would still be interested in the way it was presented, and take away the salient points?

Thus was born the idea of comic books that would teach mathematics. As a university mathematics teacher, I would develop the stories, embedding mathematics appropriate for the 3rd through 6th grade level, according to the National Council of Teachers of Mathematics (NCTM) standards. I contacted two graphic design/art professors that I knew at my university, Matt Tullis and Jeff Jensen, for help in identifying some students that could illustrate the comics. Determined to show that this approach had promise, I enlisted the help of an education professor at my university, Dr. Janet Tassell, to help measure the impact of the comics on the students who used them. I was lucky to find a elementary school principal, Dr. Mary Evans, who was supportive of the idea, and who agreed to involve her third grade through sixth grade teachers and students at Cumberland Trace Elementary in the project. And finally, I was able to wrangle $4,000 loose from my provost to cover printing costs. ***Operation Comics*** was in business.

In the interest of full disclosure, I must mention that this is not a completely original idea. Larry Gonick uses cartoons in his instructional books (see [2] as an example), Colin Adams has a comic book about knot theory [1], and mathematics (arithmetic, really) was a frequent antagonist in the *Calvin and Hobbes* comic

Figure 1: Cartoonist at the Idea Kentucky Think Tank.

strips by Bill Watterson, to name a few related works. Still, none of these works or any others I found were simultaneously plot-driven and instructional.

2 The Basic Premise of the Story Line

My basic idea for the story line in the comic was that we would have a superhero-type, ***Wonderguy***, who is super-strong, but not necessarily super-smart, and that two elementary school students, ***Claire*** and ***Dillon***, that he befriends will be the real heroes of the story. Having a superhero character helps disguise the fact that these are not standard comic books, and makes them look very much like a standard comic. Having the students be the real heroes gives the students positive role-models – one for each sex – who are good at mathematics, and a character through which they can "live vicariously".

Mathematics is not the driver of the main story line or even the individual stories in each episode of the comic. Rather, the stories are developed to stand on their own in terms of literary value. However, at some point during each of the stories, our heroes are able to "save the day" by knowing and applying mathematics. Developing stories for the different episodes where the use of mathematics is both plausible and necessary has been difficult, and has required some careful character development and planning. Having a character who can pick up a car eliminates situations where brute force removes the need for brains. And many situations are such that someone *could* use mathematics to resolve them, but they would not *have* to do so. I have had to be careful to develop situations where the use of brute force is irrelevant or even detrimental to the resolution of the situation.

The following is a description of the main characters that recur in each of the episodes, and some of the plot points I have added to make the addition of the mathematics content both plausible and entertaining. The line art in Figures 2, 3, 4, and 5 is the work of Anne Erskine, with the author taking partial credit for the drawing of Wonderguy in Figure 2.

*This work was made possible by a Provost's Initiatives in Excellence grant from the Western Kentucky University's Office of the Provost, PIE #O-09-039.

Figure 2: Cover to the first edition of Operation Comics.

Wonderguy. Wonderguy is the supposed "lead" character of each of the stories, which will be centered around his adventures in crime-fighting. Wonderguy is incredibly strong, but his brains do not match his brawn, a fact that is not part of his public perception. He is an immensely popular public figure, even perhaps a bit of a celebrity. His origins are left purposefully vague, although it is clear from the way that he carries himself that he has always had his super-powers.

Claire and Dillon. The real heroes of each story are the students, Claire and Dillon. Claire is an African-American student who is wise beyond her years, and not as star-struck with Wonderguy as Dillon is. Dillon looks studious and not too athletic. Both are on the school's academic team, and Principal Willoughby considers them the "best math students in the school".

Principal Willoughby. Miss Willoughby (she currently has no first name) is the principal at Best Elementary

Figure 3: Our "hero", Wonderguy.

Figure 4: The real heroes, Dillon (left) and Claire (right).

School, where Claire and Dillon are students. She acts as an enabler in the story line. She first introduces Claire and Dillon to Wonderguy when he needs mathematical assistance, and will provide them excused time out of class to help Wonderguy when he needs it. She has some connection to Wonderguy that is not immediately clear, but hints of how they know each other appear in the different episodes.

3 Sample Episode: Captain Confusion's Revenge

In Episode 1, we meet the diabolical Captain Confusion, who apparently was a student at Best Elementary School as a child. He had also been on the academic team at that time, and suffered an event that caused him embarrassment during a match. Extremely arrogant and condescending to those he perceives as not as smart as him, even as a child, he sees his chance to discredit Wonderguy, whom he abhors, and get back at the school that had treated him unfairly.

Captain Confusion, who is now an inventor, encloses the entire school, including the visiting Wonderguy, in an indestructible bubble of his own design. He threatens to expose everyone in the school to a lethal dose of confusion gas, also invented by him, if Wonderguy can not solve three elementary-level math problems in five minutes without giving any incorrect answers. His assessment of Wonderguy's mathematical abilities are not far from the truth, so Principal Willoughby decides to put Claire and Dillon "into the game" to help

Figure 5: Miss Willoughby, the principal of Best Elementary School.

the muscle-bound hero.

The three problems and the content that they illustrate are given below, along with sections of the script of the episode. All three problems address both the standard for problem solving and the standard for reasoning and proof, for all grade levels, as provided by the NCTM [3]. Additional standards addressed are given with each problem.

Number Sense and Divisibility Theorems. The first problem can be solved by trial-and-error, but given the fact that time is ticking away rapidly, the better path is a reliance on divisibility theorems. The stated problem is

"Insert a digit in the blank so that __4268 is divisible by 9."

The dialog that follows the introduction of the problem is given below.

Wonderguy: I have already ruled out 1. (Showing messy work on a sheet of paper.) I'll rework it for 2 and 3. You do 4, 5, and 6, and you do 7, 8, and 9. We've got to hurry!
Claire and Dillon: 7! The answer is 7!
Wonderguy: We can't guess, guys! Any wrong answer, and were in trouble.
Claire: We're not guessing! To be divisible by 9, the sum of the digits has to be a multiple of 9!
Dillon: (Showing his work on paper.) Think about the 3-digit number "*abc*", where the "*a*", "*b*", and "*c*" are the hundreds, tens, and ones digits, in that order. That means that

$$\text{“}abc\text{”} = (a \times 100) + (b \times 10) + (c \times 1).$$

Then pull one of each thing out of each place:

$$(a \times 99 + a) + (b \times 9 + b) + c.$$

Claire: So, put all of your singles together:

$$(a \times 99) + (b \times 9) + (a + b + c).$$

The first two parts are divisible by 9, so if the last part, the sum of the digits, is divisible by 9, then the whole thing has to be divisible by 9! $4+2+6+8 = 20$, so to get the next larger number that is divisible by 9, you have to add a 7.

Wonderguy: Great googly-moogly! Alright, here goes nothing! (Types in 7 and hits enter.)

This problem addresses the NCTM standard for numbers and operations for grades 3–5, which says that "in grades 3–5, all students should understand the place-value structure of the base-ten number system and be able to represent and compare whole numbers and decimals", "recognize equivalent representations for the same number and generate them by decomposing and composing numbers", and "describe classes of numbers according to characteristics such as the nature of their factors" [3].

Least Common Multiple The second problem has a similar bend, in that it can be solved by listing all factors of each number and comparing lists until a common number is found on each list, but there is a more efficient path to the correct solution using the prime factorizations of the numbers. The stated problem is

"What is the smallest number divisible by both 24 and 28?"

The dialog that follows the introduction of the problem is given below.

Wonderguy: Okay, I have a plan for this one. Brainy-Dude, you start writing out multiples of 24, and IQ-Girl, you start writing out multiples of 28. I'll watch both of you and wait for the same number to appear on both lists!
Claire: That would work, but given the shortage of time, can I suggest that we use the prime factorizations?
Wonderguy: (A very confused look on his face.) Er . . . , that could work . . . How exactly would that work?
Dillon: Break each number into its prime factors. 24 is 2 times 12, or 2 times 2 times 6, or 2 times 2 times 2 times 3. We write it like this.

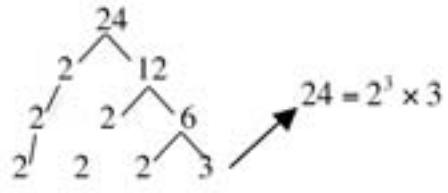

Claire: And 28 is 4 times 7, and 4 is 2 squared. You keep going until all of the factors are prime numbers.

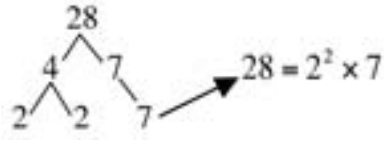

Dillon: Now, in order for our number to be a multiple of both, we have to have enough of each prime so that both of these numbers will divide into it, so we need at least 3 factors of 2, one of 3, and one of 7.
Claire: But to make it the least multiple of both, thats all of those factors that you want. So, the answer is

$$2^3 \times 3 \times 7 = 8 \times 3 \times 7.$$

Wonderguy: Okay, that's 24×7. (Starts working the multiplication problem on paper.)

$$\begin{array}{r} 24 \\ \times 7 \\ \hline \end{array}$$

Claire: Wait! It's quicker in your head: 8 times 7 is 56.
Dillon: Then 50 times 3 is 150, and 6 times 3 is 18, so . . .

Wonderguy: The sum is 168! Yeah, baby, . . . (entering the answer into the computer.)

This problem addresses the NCTM standard for numbers and operations for grades 3–5, which says that "in grades 3–5, all students should develop fluency with basic number combinations for multiplication and division and use these combinations to mentally compute related problems, such as 30×50" and "select appropriate methods and tools for computing with whole numbers from among mental computation, estimation, calculators, and paper and pencil according to the context and nature of the computation and use the selected method or tools". It also addresses the standard for numbers and operations for grades 6–8, which says that "in grades 6–8, all students should use factors, multiples, prime factorization, and relatively prime numbers to solve problems" [3].

Common difference. The last problem is an inverse problem, in that we are given a "black box" that outputs a number for each one that they enter, and they have to deduce what the formula is. The dialog that follows the introduction of the problem is given below.

Wonderguy: Holy moley, that could be anything!!
Claire: Wait. Remember that he said that only math taught at this school would be needed.
Dillon: Try a few numbers for x, and see what y is. And I recommend that you try some consecutive whole numbers, to help us see the pattern of the answers.
Wonderguy: Okay, when I give it "1", it gives me a "5". (Claire and Dillon are keeping track of the results on a piece of paper.) A "2" gives me a "7". A "3" gives me a "9". A "4" gives me an "11". This is going to take forever!
Claire: No, no! I see it! I see the pattern!
Dillon: Me, too! Each time we increase x by 1, the y is increased by 2. That means the formula has a "$2x$" in it.
Wonderguy: But its not "$2x$". Two times four is eight, not eleven.
Claire: Right, but if you notice, all of the values are three more than "$2x$". Check by putting a 0 in for x.
Wonderguy: Hey, you're right! Its a three! So the formula is . . . (Hesitates, looking at the kids.)
Claire and Dillon: (Together.) $2x+3$!!

This problem addresses the NCTM standard for algebra for grades 3–5, which says that "in grades 3–5, all students should describe, extend, and make generalizations about geometric and numeric patterns", "represent the idea of a variable as an unknown quantity using a letter or a symbol", "model problem situations with objects and use representations such as graphs, tables, and equations to draw conclusions", and "investigate how a change in one variable relates to a change in a second variable". It also addresses the standard for data analysis and probability for grades 3–5, which says that "in grades 3–5, all students should collect data using observations, surveys, and experiments" and "propose and justify conclusions and predictions that are based on data and design studies to further investigate the conclusions or predictions". It also addresses the algebra standard for grades 6–8, which says that "in grades 6–8, all students should represent, analyze, and generalize a variety of patterns with tables, graphs, words, and, when possible, symbolic rules" and "use symbolic algebra to represent situations and to solve problems, especially those that involve linear relationships" [3].

4 Usage and Measuring Impact

While I am comfortable developing mathematics curricula for elementary school students and teachers, elementary pedagogy and assessment are not something I feel qualified to address. Acknowledging my limitations, I have turned complete control of the classroom implementation of the comic books over to Dr.

Evans and her staff of teachers. Likewise, I have given Dr. Tassell complete control over the assessment of the effectiveness of the comics with the students.

Implementation in the classroom. At the time of this submission, the comics have not yet been introduced to the classrooms. My understanding of the implementation plan is that they will be introduced in a "fun and playful" context, perhaps as a part of center time or as a reward for good behavior or achievement. They will not be presented as a textbook – the whole idea is that the students see this as a comic first, that just happens to have some math ideas in it. I have been asked by Dr. Evans and members of her staff to develop some accompanying worksheets for students and teacher's guides to give an in-depth discussion on the mathematical content of the comics and how it relates to NCTM standards, which I will gladly develop. It has also been suggested that we let the students invent their own stories involving Wonderguy, Claire, and Dillon, and submit them to me for future comics, which I also believe is a marvelous idea. The back cover of each comic will solicit these types of ideas from the reader, and provide my contact information.

I am sure that actual classroom usage will suggest changes to improve the implementation plan. Again, I feel that giving my experts in elementary education control over this aspect of the project is crucial to its success.

Effectiveness of the Comics in the Classroom. While I or any other observer might think that this idea is innovative, "cool", etc., if it does not achieve the goals that we have set forth, then we need to either

- revise our product and/or its implementation, or
- let the project run its course and try something else.

We have Human Subjects Board approval for Dr. Tassell to have the students in the 3rd through 6th grade classes at Cumberland Trace Elementary take surveys, measuring their initial attitudes toward mathematics. Students will take a post-project survey at the end of the school year. We will also be collecting assessments from the teachers using comics to gauge their opinions about how well the comics were received by students and whether it helped and motivated their learning of mathematics. If these results are positive, then we may pursue funding to continue producing comic books on a larger scale.

5 Conclusion

Regardless of the outcome, I can truly say that this has been one of the most enjoyable grant projects I have ever undertaken. At present, that enjoyment comes from the artistic process of writing the stories, and then drawing out the scenes, and then turning them into the finished color comic books. The pride that I felt with the first completed comic is comparable to the pride I felt with my first accepted paper in a peer-reviewed journal. I hope to feel that same pride when the results from using the comics in the classrooms is known.

References

[1] C. Adams, *Why Knot? An Introduction to the Mathematical Theory of Knots*, Key College, 2004.

[2] L. Gonick and A. Huffman, *A Cartoon Guide to Physics*, Collins, 1992.

[3] "Principles and Standards for School Mathematics," National Council of Teachers of Mathematics, http://standards.nctm.org/document/chapter5/index.htm.

[4] B. Watterson, *The Complete Calvin & Hobbes*, Andrew McMeel Publishing, 2005.

Art and Nonlinear Projection

John Brosz*[1] Sheelagh Carpendale[1] Faramarz Samavati[1] Hao Wang[2]
Alan Dunning[2]

[1]Department of Computer Science, University of Calgary
[2]Alberta College of Art and Design

Abstract

Nonlinear projection is a current area of research in computer graphics. It provides a meeting place between science and art. After describing motivations for use of nonlinear projection, we provide a brief survey of different techniques for nonlinear projection described in computer graphics literature. We then examine several cases of how and when artists choose to use nonlinear projection, as opposed to perspective projection, and how these might be achieved with current computer graphics techniques. Lastly, we provide a synopsis of the Flexible Projection Framework and then describe how it was used in a collaborative project between an artist and a computer scientist.

1 Introduction

One of the most difficult aspects of creating images is determining how to represent three dimensional scenes on a two dimensional medium. This process of moving from three dimensions down to two dimensions is known as projection and it is not easy. The specific type of projection (if any) and our adherence to this type can drastically affect the impression an image makes. Some projections can make images seem very realistic; others can make the images surrealistic. Use of particular projections can create images that make you feel like you are within or close to the image; other projections create images that exaggerate a divide between you, the viewer, and the scene being portrayed [9].

Projection is an interesting meeting point between art and science. The scientific approach to projection is to view it as the mathematical reduction of dimension and organization of the reduced dimension's space. From here formulae, geometries, and spaces are theorized and derived. Artistically, projection is a means of organizing space, relationships between objects, and the observer's presence in an image.

By far the most familiar type of projection is perspective projection. This is the type of projection produced by most cameras and is seen widely in Western art. However, both before and after the discovery and formalization of perspective projection, artists have made use of other types of projection. The most prevalent examples are the many projections that have been developed to represent the earth on a flat surface. A long history of cartographic development has been explored by Snyder [15].

In computer graphics, projection has mostly been limited to projections that are linear in nature; that can be represented as linear transformations. The two common examples of such projections are perspective and orthographic. Recently a number of researchers have begun exploring other possibilities for nonlinear projection.

In this paper we begin with a brief survey of current computer graphics approaches to nonlinear projection. Then we look at some examples of the use of nonlinear projection in art and discuss how these might be reproduced with computer graphics techniques. We then describe our nonlinear projection technique, Flexible Projection [3] and how this technique was used in a collaborative art project.

2 Nonlinear Projection in Computer Graphics

Salomon [12] describes a wide variety of nonlinear projections including a variety of panoramas as well as fisheye, false perspective, telescopic, and microscopic projections. Wyvill and McNaughton [19] describe projections used in ray-tracing as a mapping between image space and rays that define and sample a volume. They demonstrate how this mapping can be defined to produce fisheye and panoramic projections. Similarly Glassner [6] defines ray tracing projections with two NURBS (Non-Uniform Rational B-spline) surfaces; one surface positioning the rays' origin, the other surface providing direction.

Nonlinear ray-tracing allows light to follow curved paths based on vectors fields [7, 18]. These projections have been used to visualize the behavior of dynamical systems [7] and to visualize relativistic effects [18].

Yu and McMillan [21] describe a framework capable of reproducing a wide variety of linear projections; that is, projections with linear equations. Linear projections such as orthographic and perspective have useful features such as mapping straight edges to straight lines in the image and are easily implemented in graphics hardware. Subsequently Yu and McMillan provide a framework [20] for creating nonlinear projections by using many of these linear projections together to create a single image. Image continuity is maintained by careful construction and selection of neighboring projections. A similar approach is that of Trapp and Döllner [16] where planar projections and non-planar projections are combined by placing tiles that cover the image. Each tile corresponds to a planar or non-planar projection that is used to fill in the area of the tile. These approaches can be considered multi-camera projections.

Multi-camera projections combine images produced by several cameras into a single image. The simplest example of this is putting together a collage of images such as that expertly done in David Hockney's *Pearlblossom Highway No. 2*, 1986 [9]. Examples in computer graphics that make use of this sort of technique include Cubist Style Rendering [5], Automating Joiners [22], and Photographing Long Scenes with Multi-Viewpoint Panoramas [1]. Rademacher and Bishop [11] provide an interesting variation where an image is created by moving a camera along a path. At regular points along this path columns of pixels are captured and placed beside one another to form an image.

A more advanced multi-camera approach, instead of combining images, is to combine objects in normalized device coordinates after projection. Agrawala et al. [2] do exactly this, allowing each object to be individually projected by a different perspective camera. These projections are then combined in normalized coordinates where depth testing and clipping operations occur. Singh [14] and Coleman and Singh [4] expand upon this, allowing objects to be projected by several cameras at once. Objects projected by more than one camera are only projected once, with a camera that interpolates between camera settings.

The Flexible Projection Framework [3], discussed in more detail in Section 4, operates by using parametrically modelled surfaces to define a viewing volume. We refer to Flexible Projection as a framework because it provides common techniques and tools for creating a wide variety of linear and nonlinear projections. This framework is able to reproduce all of the previously mentioned projections that incorporate a single viewing volume (excluding most multi-camera techniques). It also allows curved paths through the volume that allow for reproduction of the effects seen in nonlinear ray tracing.

Deformation is the manipulation, warping, or bending of the geometry of virtual objects. While often both nonlinear projection and deformation can be used to achieve the same result, the major difference is that nonlinear projection works with the camera; the geometry of the scene remains undisturbed and lighting features such as shadows remain true to the geometry. An interesting work halfway between nonlinear projection and deformation is that of Rademacher [10] where deformation is made dependent upon viewing

direction.

3 Nonlinear Projection in Art

Nonlinear projection has been used widely in art, beginning with cave art and continuing to the present day. In this section we investigate a few examples of nonlinear projection from the fine arts. We have chosen these examples as they provide insight into why and how artists choose to use nonlinear projection in their own creations.

Nonlinear Projection from Optics. In *Secret Knowledge* [9] David Hockney examines a variety of evidence that leads him to conclude that many artists used concave mirrors and later lenses to construct images from the early fifteenth century and onward. While these primitive lenses would allow artists to paint from a moving image, a key limitation was the small size of the projected images. In general these images could be no larger than 30 cm across.

As a consequence, if an artist wished to create a larger image, the artists would either have to try to repaint the image larger without aid of optics, or project the scene a piece at a time and then blend the pieces together into a unified whole. Images constructed in this fashion no longer strictly adhere to perspective projection. Rather each object appears to be directly viewed (i.e., projected as if positioned in the center of the field-of-view of a perspective projection). Hockney [9] points out that these composite projections present a compelling closer view of the world because all parts of the scene are viewed straight on.

It seems quite clear that this type of nonlinear projection performed by artists is the inspiration for the multi-camera projection systems discussed in Section 2. As this technique was originally created to bypass the technical restrictions of early optics, one wonders if this truly is a good technique for composing nonlinear projections. On the other hand, these techniques tie their approach to perspective projection, are based upon a clear, physical metaphor (that of constructing a collage) and, lastly, they allow the user to concentrate on a specific sections of the image, one at a time.

Van Gogh. Heelan [8] proposed that many of Vincent Van Gogh's paintings from 1888 onwards portray the subjective perception of constant curvature hyperbolic geometry; one such painting is that shown in Figure 1. In these paintings the projection is divided into three zones: near, intermediate, and far. In the near zone of Figure 1 vertical and horizontal surfaces such as the bed's footboard and the near chair appear to protrude in a convex bulge. In the intermediate zone, containing the bed and the nightstand, objects appear much as they do in a perspective image, while in the far zone, vertical and horizontal surfaces appear to be concave and depth differences (e.g., foreshortening) become less noticeable, as seen in the far chair and the back wall. Another difference is that the horizon will appears at a finite distance from the observer, rather than at infinity as in a perspective projection [8]. Heelan maintains that Van Gogh's paintings provide a visual embodiment of the subjective spatial perception of binocular vision.

To examine how this sort of projection could be handled with graphics techniques, the key point is that the projection changes as a function of the depth of the image, between the foreground, middle, and background. This is well suited to Flexible Projection where the viewing volume can be altered to produce these changes in projection at the desired depth in the scene. Additionally continuity of the viewing volume will ensure smooth changes between the differing areas seen in the painting.

Creative Perspective. Watson's book, *How to use Creative Perspective* [17] provides interesting insight into techniques used by illustrators to create perspective projections as well as to modify them for various

Figure 1: *Vincent van Gogh, Dutch, 1853-1890, The Bedroom, 1889, Oil on canvas, 29 x 36 5/8 in. (73.6 x 92.3 cm), Helen Birch Bartlett Memorial Collection, 1926.417, The Art Institute of Chicago. Photography © The Art Institute of Chicago.*

Figure 2: *Top: a painting for an advertisement for the Association of American Railroads. Image from [17]. Bottom: an image where we have extended lines from each pair of rails to examine the vanishing points. In a perspective projection, assuming that the rails are parallel, the rails should all converge to the same point; our drawn lines show that this is not the case.*

purposes. He calls such modified projections *creative perspective* and notes that an artist who uses "perspective creatively [can] bend it to his uses rather than be limited always to strict conformity" [17]. These manipulations are used: to allow the viewer to see structures that should be hidden, to change the scene (usually by manipulating vanishing points) and improve its overall composition, to allow the viewpoint to shift to more closely re-create human visual experience, and, lastly, to make the illustrations more dramatic and interesting. This last point, while somewhat vague, is important. Manipulating the projection allows illustrators to present objects in precisely the way they feel will have the desired impact.

We will examine two examples from this text. The first is the illustration of trains shown in the top of Figure 2. According to Watson [17] the artist has purposefully altered the vanishing point of the rails in the projection to compensate for eye movement across the picture; consequently this change makes the scene seem more natural.

The second example, shown in Figure 3, has a diagram showing how objects within the illustration have been moved and reoriented. In the diagram we can see that the illustrator has slightly altered the orientation of the wagon in relation to the horses, as well as the orientation of the horses to one another in order to present the most dramatic views of each [17]. With these subtle changes the illustrator has maintained realism while improving the produced image.

These two examples are difficult to describe as being best handled by any single computer graphics technique. The first example can be achieved with a multi-camera approach but care needs to be taken to achieve a smooth transition between changing viewpoints. Flexible Projection could also be applied as its parametric nature makes continuity easily achieved; however, adjusting the viewing volume to achieve the exact change in vanishing points requires finesse. The second example is interesting in that it could be achieved through a multicamera projection (one camera for the horses, the other for the engine), through Flexible Projection (where the viewing volume is shaped to produce a bend between the horses and engine), or through deformation of the models and then using perspective projection.

Figure 3: *Left: illustration by Fred Freeman. Middle: sketch by Watson presents the illustration as if wagon and horses are travelling in the same direction in perspective. Right: top down diagram of the horses' position relative to the wagon as interpreted from the left image, assuming it was created with a perspective projection. This diagram indicates how Freeman has positioned and adjusted the size of the horses from the expected orientation of parallel to the engine. All images from [17].*

4 Flexible Projection

This Section provides a synopsis of the Flexible Projection Framework as described in [3]. We have included this to assist in understanding of how Flexible Projection was used in the project described in Section 5.

Flexible Projection is unusual as it approaches projection, a rendering technique, with modelling tools. The primary concept is to define the viewing volume (the 3D volume that will appear in the 2D image) as a parametric volume $Q(u,v,t)$. This volume is defined so that the parameters u,v, and t correspond to the width, height, and depth positions that will result in the projected image. This volume can be stretched and reshaped to affect the projection and consequently the image.

While this volume can be defined in any manner whatsoever; we recommend using familiar surfaces to aid in the definition. For example, consider perspective projection. This projection uses a frustum as its viewing volume and is usually defined by an eye position, near surface, and far surface as shown. Such a frustum is shown in Figure 4 with the axes for the u,v,t parameters marked. Due to the familiarity of this construction, it makes sense to define Flexible Projections by defining a near and a far surface. We can then create our volume by interpolating between these two surfaces:

$$Q(u,v,t) = (1-t)S_0(u,v) + tS_1(u,v) \quad u_{min} \leq u \leq u_{max}, v_{min} \leq v \leq v_{max}, 0 \leq t \leq 1$$

where S_0 and S_1 are the near and far surfaces respectively. We do not include an eye position as many projections do not feature a single eye position.

Interesting variations on projection can be obtained by altering the interpolation between surfaces. For instance, by adding surface(s) between the near and far surfaces we can use Bézier curves to interpolate between the surfaces, consequently obtaining greater control over the volume, as is shown in Figure 5. This results in a definition of our volume as:

$$Q(u,v,t) = \sum_{i=0}^{n-1} B_{i,n-1}(t) S_i(u,v)$$

where $B_{i,d}(t)$ is the Bernstein polynomial $\binom{d}{i} t^i (1-t)^{d-i}$ and S_i is the ith surface (making S_{n-1} the far surface). Certainly other curve schemes could prove useful for this interpolation, however the ability of

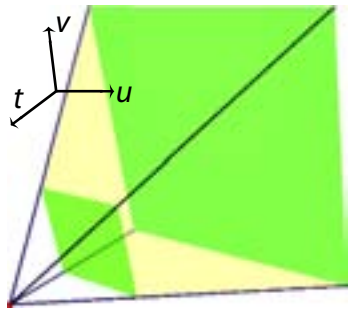

Figure 4: *A perspective projection's viewing volume. The volume is bounded by the near and far planes (green) and the sides of the frustum (yellow).*

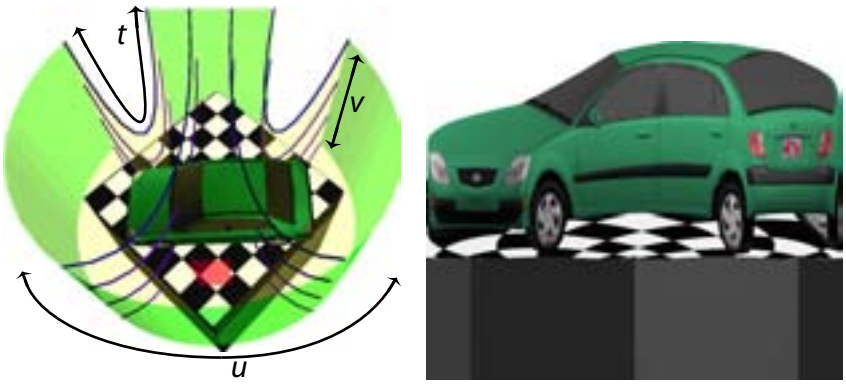

Figure 5: *Flexible projection using nonlinear interpolation. Left: the projection volume. The large green curved surface is the near surface, the red rectangle in front of the car is used to curve the volume, and the green rectangle behind the car is the far surface. Right: the projected result.*

Bézier curves to interpolate the near and far surfaces makes this curve scheme a useful place to start. Figure 5 shows how a curved volume can be created to show the front, back, and side of a car at the same time.

Projection in the volume occurs based on surface parameterization. We can imagine projection occurring by following light paths through the volume. The paths the light follows are iso-curves within the volume, known as *projectors*, that are defined by fixing u, v values $Q(u,v,t) = Q_{u,v}(t)$. For surfaces that flatten easily, image creation is a matter of scaling parameter values by the desired pixel dimensions of the image. For surface parameterizations that do not map directly to an image (i.e., the case of a hemisphere parameterized by polar coordinates) an additional step of reparameterization is necessary. This reparameterization step can additionally be used to apply distortions to the final image (e.g., zooming into particular areas, etc).

In implementation, projection of these viewing volumes occurs in one of two ways. The first and simplest is through ray tracing. Upon determining the parameter values u_0, v_0 that correspond to a particular pixel, the corresponding ray is the projector $Q_{u_0,v_0}(t)$. If the volume has not been linearly interpolated, the projector is not a linear curve and thus not suitable for the usual ray-tracing algorithm. There are two options to proceed, the first as Gröller [7] suggests, is to break the curve into linear pieces that approximate the curve and proceed with ray-tracing. The option suggested by Brosz et al. [3] is to limit our volumes to quadratic curves and compute object-quadratic intersections.

The other approach to implementation is to derive projection equations by finding the inverse of Q:

$$Q^{-1}(x,y,z) = (u,v,t).$$

While such an inverse is not always possible to derive analytically, there are several cases where analytical solutions are possible. Once a projection equation has been determined, projection can then be performed by vertex or geometry shaders in graphics hardware to achieve realtime rendering through rasterization. One last note is that rasterization makes use of linear interpolation, causing inaccuracies when triangles are deformed to curved shapes. These inaccuracies can be minimized with the use of high resolution models.

5 Using Flexible Projection in an Art Installation

As a part of a collaborative course between the Alberta College of Art and Design (ACAD) and the University of Calgary Hao Wang and John Brosz set out to complete a project combining artistic and scientific purposes. The project's goal became an art installation, *Perspectives*, that aimed to explore the 2008 confrontation between Tibetans and the Chinese authority. In particular, this project portrayed news images from distorted viewpoints representing the biases that exist in the media as well as between the involved parties. The produced images do not just represent pictorial organization but are instead intended to reflect different constructions of this issue and the world in general.

The scientific aspect of this project was the use of Flexible Projection to provide a variety of distorted outlooks in realtime. Flexible Projection was particularly useful in creating projections for this purpose in two ways. The first was that these projections could be adjusted to affect different depths of the scene differently; as a result, the background of the scene could feature a different kind of distortion than the foreground. Another aspect was that Flexible Projections can be animated by moving the projection surfaces over time. This added an extra impression of change and distortion. Together, this allowed creation of projections that provided very different outlooks into the 3d virtual world.

As our goal was to produce realtime renderings, we needed to derive projections equations (i.e., $Q^{-1}(x,y,z) = (u,v,t)$) allowing us to take an arbitrary point $p = (x,y,z)$ and then project it into device coordinates. As mentioned, for arbitrary volumes, finding Q^{-1} is difficult or impossible. To solve this, we limited ourselves to projection with viewing volumes where t (depth) can be easily calculated given p. With t determined in the viewing volume $Q(u,v,t)$ we can extract a parametric surface $Q_t(u,v)$. The next step is to find the specific values of (u,v) such that $Q_t(u,v) = p$. This leads to solve for two variables given three equations (one for each coordinate: x, y, and z). This can be solved for many parametric surfaces including the two that we made use of: parametrized spheres and bilinear patches.

To ensure we could calculate t, we relied upon two scenarios. The first is to define the viewing volume with surfaces that are pieces of spheres with a common center. Then t can be calculated by comparing the distance of p from this center, to the spheres' radii. The other scenario is to use surfaces that are planar and have a common surface normal. Then by projecting p onto this normal, and calculating distances between the surfaces, t can again be determined.

Sixteen different projections were developed. The only projection making use of parameterized spheres was a hemispherical projection (also known as fisheye) that was defined by a small hemisphere as the near surface and a larger one as the far surface. The other projections were defined by bilinear patches that, in turn, were defined by their corner points. The simplest projection recreated a perspective projection using two rectangular surfaces as shown in Figure 6(a).

The remaining fourteen projections were essentially chosen to be variations on perspective projection. This was a deliberate decision, made because it allowed the resulting projections to be different enough to be noticeable and eye-catching, but retain enough familiar characteristics to be intelligible. The modifications we made included: swapping the near and far surfaces to create an inverse perspective projection, moving the far surface relative to the near surface to create off-axis perspective projection, making the tops of the near and far surfaces narrower than the bottoms to expand the top of the image, and decreasing the height of the near surface as shown in Figure 6(b) to cause stretching of objects close to the near surface. More complex modifications were created by adding an intermediate surface between the near and far surfaces to allow for nonlinear projectors. In one projection, shown in Figure 6(c), this intermediate surface has been placed below the near and far surfaces causing projectors to travel downward before curving upward to reach

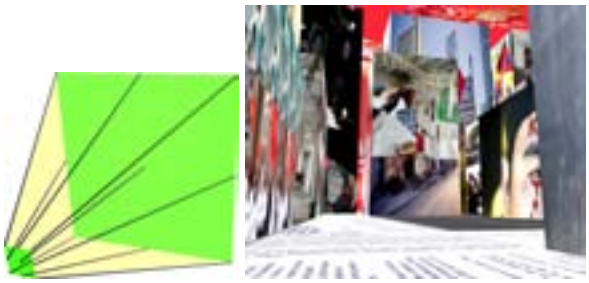

(a) Perspective projection (for comparison).

(b) A projection where the near surface is a line, same view position as (a).

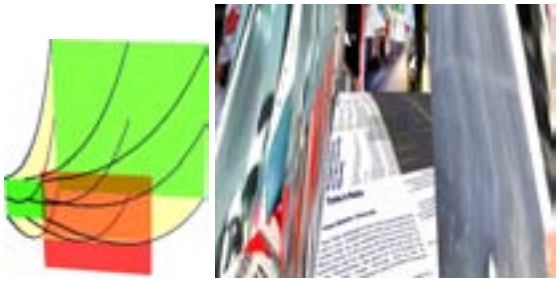

(c) Projection that causes the ground to appear to bulge upwards, same view position as (a).

(d) Twisted projection; causes rotation around the center of projection, view position near to that of Figure 7.

Figure 6: *Projection diagrams (left) and resulting images (right). In the diagrams the near and far surfaces are green, the viewing volume is yellow, and projectors are shown with lines. The red middle surfaces in (c) and (d) are used to curve the volume.*

the far surface. This produces an upward bulge in the midground of the produced images. A more exciting result is caused by introducing this intermediate surface and then rotating the far surface by ninety degrees. This, as shown in Figure 6(d), results in a twisting through the depth of the image.

Two animated projections were created. The first simply increased and decreased the size of the far plane over time. The second, shown in Figure 7, translated an intermediate surface around the center of projection.

The project itself made use of a game-like 3d environment with limited interaction. The environment, shown in Figure 8, was textured with news stories and images related to recent events in Tibet and related protests in Canada. Two modular ambient display screens [13] were used, each presenting a different virtual camera with a different projection of the environment. Each camera is then translated and rotated along a cyclical path through the environment. The interactive element of the projection was a button that randomly changed the projections used on both screens. Realtime rendering was at a rate of approximately 25 frames per seconds on two display devices of 1280 by 1024 resolution with an Intel Core2 6600 CPU, an NVIDIA 7800 video card, and 2 GB of system RAM. For the installation, the two displays with different projections were placed side by side at eye level. The installation setup is shown in Figure 9 and was presented at the ACAD graduation show in May 2008.

6 Conclusions and Future Work

In this work we have provided motivation for use of nonlinear projection. We have described specific examples where artists have used nonlinear projection. Additionally we have provided a short survey of current nonlinear projection techniques developed for computer graphics and shown how these technique could be

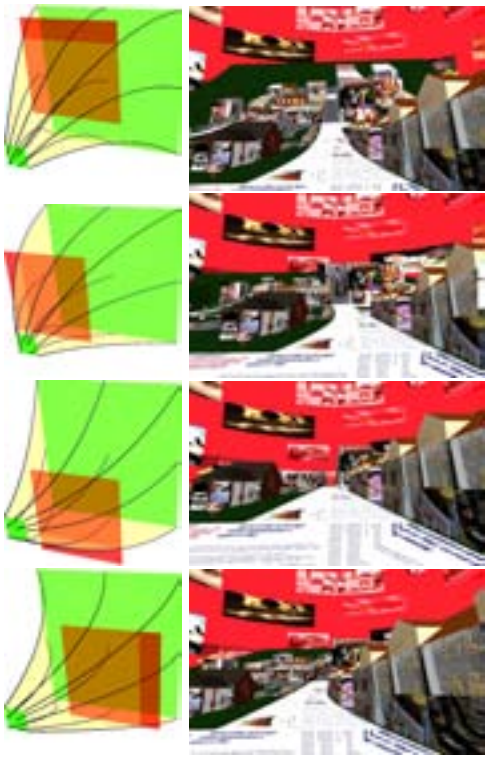

Figure 7: *Keyframes of an animated projection. The middle rectangle that controls the curving of the volume is moved in circles causing the middle ground of the produced images to bend in a circular motion.*

Figure 8: *The virtual environment used in the project.*

Figure 9: *The* Perspectives *installation.*

used to reproduce the artist created examples. We also have described a collaborative art and science project, describing how it made use of Flexible Projection to create a wide variety of visual effects.

In Section 5 we attempt to ensure that our projections are visually understandable by only introducing variations on perspective projection. This ensures that visual cues such as foreshortening and vanishing points are present (to some degree) in the resulting images. In particular we noted that the inverse perspective projection that causes a reversal of foreshortening, causing near objects to appear smaller than far objects, caused viewers of the installation difficulties. Further experimentation into restrictions or guidelines that allow freedom, while ensuring intelligibility of the resulting image, is a definite area for future study. Also of pertinence is that viewing of the animation (as opposed to a single image) as well as a known environment (such as city sidewalks) assists viewers in interpreting the images.

Another interesting area would be to further explor the use of animated projections; that is, projection where the projection surfaces move over time. One could imagine a camera rotation where near objects came into view first, followed by the appearance of objects further away. The could be achieved by rotating the far surface at a slower rate than the near surface. We were not able to achieve this in Flexible Projection due to the current limitation on calculating Q^{-1}. This is also an area of exploration for multi-camera projections.

Acknowledgements

We would like to thank the anonymous reviewers for their insightful and helpful comments as well as Ruth Hart-Budd for her editing assitance. This research was supported in part by the National Science and Engineering Research Council of Canada and the Informatics Circle of Research Excellence.

References

[1] Aseem Agarwala, Maneesh Agrawala, Michael Cohen, David Salesin, and Richard Szeliski. Photographing long scenes with multi-viewpoint panoramas. In *SIGGRAPH '06: ACM SIGGRAPH 2006 Papers*, pages 853–861. ACM Press, 2006.

[2] Maneesh Agrawala, Denis Zorin, and Tamara Munzner. Artistic multiprojection rendering. In *Proc. of the Eurographics Workshop on Rendering Techniques 2000*, pages 125–136. Springer-Verlag, 2000.

[3] John Brosz, Faramarz Samavati, Sheelagh Carpendale, and Mario Costa Sousa. Single camera flexible projection. In *Proc. of the 5th int. symp. on non-photorealistic animation and rendering*, pages 33–42. ACM, 2007.

[4] Patrick Coleman and Karan Singh. Ryan: rendering your animation nonlinearly projected. In *Proc. of the 3rd int. symp. on non-photorealistic animation and rendering*, pages 129–156. ACM, 2004.

[5] John P. Collomosse and Peter M. Hall. Cubist style rendering from photographs. *IEEE Transactions on Visualization and Computer Graphics*, 09(4):443–453, 2003.

[6] Andrew S. Glassner. Cubism and cameras: Free-form optics for computer graphics. Technical Report MSR-TR-2000-05, Microsoft, January 2000.

[7] Eduard Gröller. Nonlinear ray tracing: Visualizing strange worlds. *The Visual Computer*, 11(5):263–274, May 1995.

[8] Patrick A. Heelan. Towards a new analysis of the pictorial space of vincent van gogh. *The Art Bulletin*, 54(4):478–492, December 1972.

[9] David Hockney. *Secret Knowledge: Rediscovering the Lost Techniques of the Old Masters*. Viking Studio, 2 edition, 2006.

[10] Paul Rademacher. View-dependent geometry. In *SIGGRAPH '99: Proc. of the 26th annual conference on computer graphics and interactive techniques*. ACM Press/Addison-Wesley Publishing Co., 1999.

[11] P. Radmacher and G. Bishop. Multiple-center-of-projection images. In *SIGGRAPH '98: Proc. of the 25th annual conference on computer graphics and interactive techniques*, pages 199–206. ACM, 1998.

[12] David Salomon. *Transformations and Projections in Computer Graphics*. Springer Verlag, 2006.

[13] Ryan Schmidt, Eric Penner, and Sheelagh Carpendale. Reconfigurable displays. In *The ACM Conf. on Ubiquitous Computing, Workshop: Ubiquitous Display Environments*. ACM Press, 2004.

[14] Karan Singh. A fresh perspective. In *Graphics Interface*, pages 17–24, May 2002.

[15] John P. Snyder. *Flattening the Earth*. University of Chicago Press, 2 edition, 1997.

[16] Matthias Trapp and Jürgen Döllner. Generalization of single-center projections using projection tile screens. In *Advances in Computer Graphics and Computer Vision - VISIGRAPP 2008*, Communications in Computer and Information Science (CCIS). Springer, 2008.

[17] Ernest W. Watson. *How to Use Creative Perspective*. Van Nostrand Reinhold Company, 1955.

[18] Daniel Weiskopf. Four-dimensional non-linear ray tracing as a visualization tool for gravitational physics. *VIS*, 00:12, 2000.

[19] G. Wyvill and C. McNaughton. Optical models. In *Proc. of the 8th international conference of the Comp. Graphics Society on CG International: comp. graphics around the world*, pages 83–93. Springer-Verlag, 1990.

[20] J. Yu and L. McMillan. A framework for multiperspective rendering. In *15th Eurographics Symposium on Rendering (EGSR04)*, pages 61–68, 2004.

[21] J. Yu and L. McMillan. General linear cameras. In *Computer Vision - ECCV 2004*, volume 2, pages 14–27. Springer, 2004.

[22] Lihi Zelnik-Manor and Pietro Perona. Automating joiners. In *Proc. of the 5th int. symp. on non-photorealistic animation and rendering*, pages 121–131. ACM, 2007.

Aesthetically Pleasing Azulejo Patterns

Russell Jay Hendel
Mathematics Department, Room 312
Towson University
7800 York Road
Towson, MD, 21252, USA
E-mail: RHendel@Towson.Edu

Abstract

In [1], Fernandez outlined an algebraic approach to the construction of Azulejo patterns. An open problem listed in this paper is "to describe the geometric features of these designs that account for their aesthetic properties." This paper points to a direction to answer this problem. We identify *aesthetic pleasantness* with *aesthetic challenge* and present two definitions of *aesthetic challenge*: (1) *Aesthetic challenge* can be partially defined and quantified by the number of English phrases needed to describe an Azulejo pattern; (2) We can also define *aesthetic challenge* as equal to the number of primitive figures – isolated points and lines – in the *fundamental octant* of the Azulejo pattern. We show that these two definitions correlate and that they provide an alternative to Fernandez's purely algebraic approach for construction of Azulejo patterns. Several examples are presented showing that both approaches – the algebraic approach of Fernandez and the *aesthetic challenge* approach of the author - yield aesthetically pleasing designs. Future directions of research on the definition of *aesthetic challenge* are presented.

1. Azulejo Patterns

Azulejos are the traditional designs used by Spanish artisans for many generations. They typically have a blue and white design painted on a ceramic tile. Federico Fernandez, a professional architect, described the mathematical properties of these varied and beautiful designs in [1]. Some examples of Azulejo and related patterns are presented below in Figure 1 which the reader is encouraged to review now.

Intuitively, most people would consider the aesthetic pleasantness of the patterns in Figure 1 to increase as one goes from the two patterns in the leftmost column to the two patterns in the rightmost column. Fernandez's goal, in his paper, was to find an algorithm that would *exclusively* produce patterns considered aesthetically pleasing by most people. The Fernandez algorithm does not, for example, produce the two patterns in the leftmost column of Figure 1. There are however, two areas for improvement in the Fernandez algorithm: (1) The Fernandez algorithm may occasionally produce patterns that are not considered aesthetically pleasing; the algorithm user must simply discard those patterns and produce new ones. (2) The Fernandez algorithm simply produces patterns without in any way distinguishing those patterns that are *more* aesthetically pleasing than others. For example, the Fernandez algorithm does not distinguish between the aesthetic appeal of the patterns in the middle and rightmost columns of Figure 1.

In an attempt to remedy these problems, in Sections 3 and 4 we present two definitions of *aesthetic pleasantness* or *aesthetic challenge*, both definitions involving numerically quantifiable entities. We show that these two definitions highly correleate. Using these two definitions we proceed, in Section 4, to present an alternative to the Fernandez algorithm for producing Azulejo patterns. The patterns produced by the algorithm presented in this paper seem comparable in aesthetic pleasantness to the patterns

produced by the Fernandez algorithm. Nevertheless, as with the Fernandez algorithm, the algorithms presented in this paper occasionally produce patterns that most people would not consider pleasing.

In this introductory section, we briefly sketch some important features of the Fernandez algorithm and indicate major areas where the approach presented in this paper differs.

Fernandez *starts* Azulejo construction by computing the orbits of certain matrices acting on the integer lattice **Z x Z** and then extends the resulting sets by closing them under the actions of a subgroup of the dihedral group, $\mathbf{D}_4$. Fernandez's method also allows elimination of the "simplistic" patterns presented in the leftmost column of Figure 1. As already pointed out the resulting Fernandez algorithm occasionally produces patterns that are not considered aesthetically pleasing and which must be discarded and replaced

In a closing section of his paper Fernandez points to certain constructs, the *fundamental octant* and the *fundamental N-square,* which he says may point the way to a solution of the problem of defining *aesthetic pleasantness.*

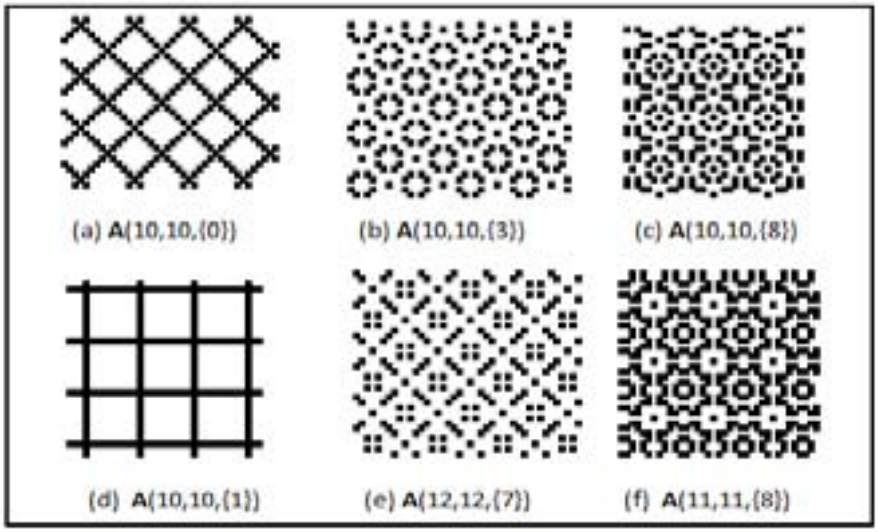

Figure 1: *Six patterns with varying levels of aesthetic challenge. Figures 1(b),(c),(e) and (f) follow the method in the Fernandez paper. Figures 1(a) and (d) are rejected as Azulejos by the Fernandez method but are brought here for purposes of contrast. More detail is presented in the text.*

The approach presented in this paper differs in two ways from the approach of Fernandez. First, in this paper we reverse the sequence in the Fernandez algorithm: Our approach to construction of Azulejo patterns, presented in Section 2, *starts* with the construction of a fundamental *octant*, a subset of $\mathbf{Z_n}$ **x** $\mathbf{Z_n}$, and then proceeds to extend this set of points by closing them under the actions of the dihedral group, $\mathbf{D_4}$. This gives us a *fundamental* **n x n** square from which we can build up the entire Azulejo pattern by a process of translation. The second and major innovation introduced in this paper is that we do not use algebraic methods to construct the *fundamental octant.* Instead, we use *complexity,* a numerical quantity, defined in Sections 3 and 4, that seems to correlate with *aesthetic pleasantness*.

2. The Azulejo Algorithm

In this section we present an algorithm for construction of Azulejo patterns that is equivalent to the Fernandez algorithm. We also indicate which algorithm steps are modified by our approach. To facilitate the readability of this section which is addressed both to mathematicians and to a less technical audience we first describe the algorithm visually and then present the algorithm formally.

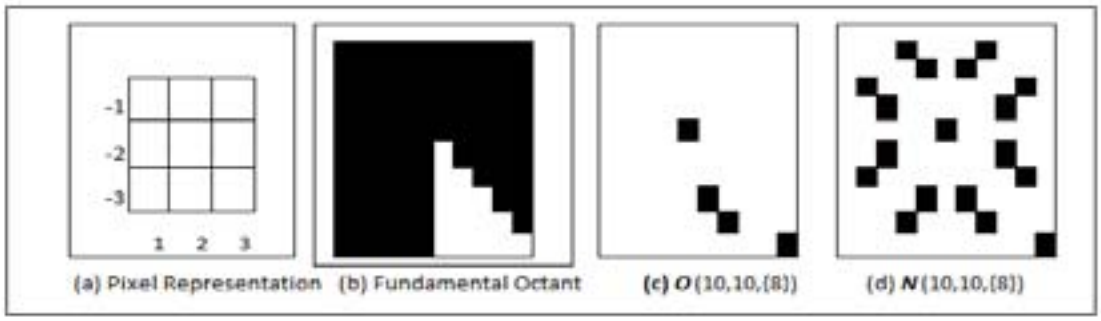

Figure 2: *Fundamental octant* (c) and *fundamental N-square* (d) *for the Azulejo presented in Figure 1(b)*.

Informal visual description. The Fernandez algorithm has five steps. They will be illustrated using the Azulejo presented in Figure 1(b). Figures supporting the algorithm description are presented in Figure 2.

1. Pixelation: It is important to emphasize that the Fernandez algorithm begins by perceiving the plane as represented by a grid of pixels. Each pixel has a unique address given by the Cartesian coordinates of its lower right corner. This is illustrated in Figure 2(a). As is traditional, we identify each pixel with its address. For example the pixel in the lower left corner in Figure 2(a) is identified with the "address" (1,-3). Fernandez introduced pixelation since it powerfully allows the description of complex figures and patterns using simply computed arithmetic functions. For computational reasons we use a square with positive x coordinates and negative y coordinates.
2. The fundamental octant: To begin Azulejo construction one starts with an n x n square of pixels as illustrated in Figure 2(a). Here, n is an arbitrary integer selected by the algorithm user. We then select the pixels in the lower half of the lower right quadrant, illustrated in Figure 2(b). We call this lower half of the lower right quadrant the *fundamental octant*.
3. The octant pattern: The Fernandez algorithm requires filling-in, or coloring black, certain pixels in the *fundamental octant*. The addresses of the pixels to be colored black are given by arithmetic functions. Figure 2(c) illustrates one such octant pattern. Details are provided in the next subsection.
4. The *N*-square pattern: If the reader carefully studies the relation between Figures 2(c) and (d) (s)he will see that the octant pattern in Figure 2(c) is simply reflected vertically, horizontally and diagonally in Figure 2(d). More precisely, Figure 2(c) consists of the pixel in the lower right corner, with an additional three-pixel pattern, while Figure 2(d) consists of the pixel in the lower right corner and an eight-fold repetition of the three-pixel pattern. This eight-fold repetition is accomplished by applying all combinations of horizontal, vertical and diagonal reflections. A formal description of the symmetries that transform Figure 2(c) into Figure 2(d) is given in the next subsection.
5. The Azulejo pattern: If the reader carefully studies the relation between Figure 1(b) and Figure 2(d) (s)he will see that the Azulejo presented in Figure 1(b) is simply a "translation" of Figure 2(d) throughout the plane.

Formal Description. The formal description of the five steps listed in the last subsection are as follows:

1. Pixelation: We use a traditional Cartesian system. The pixel associated with address (x,y) is the unique pixel whose lower right coordinates are (x,y) – e.g. (1,-3) is the lower left corner of Figure 2(a)
2. The fundamental octant: To formalize the algorithm we suppose that n is a positive integer with positive divisor d and k is an integer with $0 \leq k \leq d - 1$. The *fundamental octant* is defined as the collection of pixels whose addresses (x,y) satisfy the *fundamental octant inequality*, $n/2 \leq x,-y \leq n$. Throughout this section we illustrate with $n = 10$, $d = 10$ and $k = 3$.
3. The octant pattern:
    a. To describe the pixels that will be colored black in the *fundamental octant*, Fernandez begins with the function $x(d,0) + y(k, n/d)$ where x and y are arbitrary integers. For example, when

$x = 6$ and $y = 7$ this function equals $6(10,0) + 7(3,10/10) = (81,7)$.

b. We next introduce the function [ ] defined as follows: if x and y are integers, then we define $[(x,y)] = (a,b)$, with $1 \leq a,-b \leq n$ and $x \equiv a$, $y \equiv b \pmod{n}$. For example, $[(81,7)] = (1,-3)$. Heuristically, [ ] maps each pixel to its translate in the **[1,n] x [-1,-n]** square.

c. We need a function to take the pixel (1,-3) to its "related pixel" in the *fundamental octant*. Formally, for $1 \leq x,-y \leq n$, we define a function by $\langle(x,y)\rangle = (a,b)$, with $n/2 \leq a,-b \leq n$ and (a,b) is a member of $\{[(\pm x, \pm y)], [(\pm y, \pm x)]\}$; e.g., $\langle(1,-3)\rangle = (9,-7)$.

d. Summary: Fernandez, by applying the functions [ ] and < > to the function $x(d,0) + y(k, n/d)$, where x and y are arbitrary integers, associates each x and y with a pixel in the *fundamental octant* which is to be colored black.

4. The *N*-square pattern: Finally, we need an arithmetic method to take each pixel in the *fundamental octant,* and give all "related pixels" in the *fundamental N-square*. Formally, for $n/2 \leq x,-y \leq n$ we define $\langle\langle(x,y)\rangle\rangle = \{(a,b): \langle(a,b)\rangle = \langle(x,y)\rangle$ and $1 \leq a,-b \leq n\}$. For example, $\langle\langle(1,-3)\rangle\rangle = \{(1,-3), (1,-7), (9, -3), (9, -7), (7,-9), (7,-1), (3,-1), (3,-9)\}$. The mathematical reader will recognize << >> as giving the *orbit* of a pixel modulo n under the actions of the dihedral group, $\mathbf{D_4}$. Heuristically, the dihedral group takes the pattern in the *fundamental octant* and reflects it in all 8 combinations of vertical, horizontal and diagonal symmetry.

5. The Azulejo pattern: Let $\boldsymbol{O(n,d,k)}$ denote the set of pixels in the *fundamental octant*. We define the *fundamental N-square*, $\boldsymbol{N(n,d,k)} = \langle\langle\boldsymbol{O(n,d,k)}\rangle\rangle$. Here the function << >> applied to a set is simply the union of << >> applied to all members of that set. Heuristically, $\boldsymbol{N}$ is the orbit of $\boldsymbol{O}$ under the actions, modulo n, of the dihedral group, $\mathbf{D_4}$, and consequently $\boldsymbol{N}$ lies in the rectangle of pixels **[1,*n*] x [-1,-*n*]**). Finally, we define, $\boldsymbol{A(n,d,k)} = \bigcup \{\boldsymbol{N(n,d,k)} + \boldsymbol{(x,y)}\}$: ***x* and *y* varying over all integers,}** (that is, $\boldsymbol{A}$ is the union of all integral translates of the $\boldsymbol{N}$ square)

To increase richness and variety of patterns Fernandez allowed construction of Azulejos based on a set of integers *K*. Here, $\boldsymbol{O(n,d,K)}$ is simply the set-theoretic union of the $\boldsymbol{O(n,d,k)}$ as k varies over members of *K*. We then define $\boldsymbol{N(n,d,K)}$ and $\boldsymbol{A(n,d,K)}$ in the obvious ways. Examples are given in later sections.

The author's algorithm: The author's algorithm differs from the Fernandez algorithm only in step 3: Whereas Fernandez used the function $x(d,0) + y(k, n/d)$ to generate the pixels in the *fundamental octant* pattern, the author allows a random selection of pixels to be colored black provided the selected set of pixels has sufficient *complexity*. *Complexity* is defined in the next two sections.

3. Aesthetic Pleasantness

In this and the next section we outline our approach to the definition of *aesthetically pleasing*. We first identify *aesthetic pleasantness* with *aesthetic challenge.* In this section we explore the informal heuristic that the *aesthetic challenge* of an Azulejo pattern can be numerically quantified by *the number of English phrases needed to describe it*. We illustrate this approach using the three columns of Azulejo patterns presented in Figure 1:

- The leftmost column has aesthetic challenge 1: This corresponds to the fact that we would describe Figure 1(d) as a *lattice of squares* and Figure 1(a) as a *lattice of diamonds*. The numerical value of *aesthetic challenge* equal to one comes from the single underlined term needed to describe the figure. (Fernandez ruled out these patterns as Azulejo patterns by using algebraic criteria. However our approach will be to allow all patterns, classify them, and then only use the more *complex* ones.)
- The middle column has aesthetic challenge 2: This corresponds to the fact that we would describe Figure 1(b) as an *alternating lattice of circles and points,* or as an *alternating lattice of octagons and points,* and we would describe Figure 1(e) as *a lattice of diamonds with inscribed squares*.

The numerical value of *aesthetic challenge* equal to two comes from the two underlined terms needed to describe the figure. Notice that these descriptions are not complete. For example, the diamonds in Figure 1(e) use punctured lines for their sides. However, the basic bird's-eyeview description of the figure is *diamonds with inscribed squares*. As indicated above, this method of measuring *aesthetic pleasantness* by counting phrases, is informal.

- The rightmost column has aesthetic challenge 3+: To describe either pattern in the rightmost column we need at least three descriptors, possibly more. For example, Figure 1(c) has the following subthemes: (1) octagons of points with a point in the center, (2) four sets of a pair of solid rectangles surrounding a blank square and (3) two opposing sets of solid rectangle pairs surrounding a point. There are of course other ways of describing the Azulejo pattern but they all involve a reference to at least three subthemes. Similarly Figure 1(f) may be described using the following subthemes: (1) A white square with a central dot, (2) two opposing solid rectangles with a white slit separating them and white center, (3) a white dot, inscribed in a black square, inscribed in a rounded white square with ornaments. Again, other descriptions are possible but they all would use at least three basic subthemes. Also note that the above descriptions of Figure 1(c) and Figure 1(f) are informal in the precise sense that an outside person could not *reproduce* the Azulejo pattern from the three subthemes because there is *further richness* to the pattern.

Frequently, in a mathematics paper, definitions are presented as is without further defense. However, in this paper we are using a definition to capture a human concept - *aesthetic pleasantness.* We therefore review the heuristic arguments for *number of English phrases* capturing *aesthetic pleasantness*:

The basic psychological assumption used is that *the challenge to the viewer to identify patterns in a figure creates a sense of accomplishment, satisfaction, and aesthetic pleasantness*. The viewer of Figures 1(a), (b), (d), and (e) can instantly recognize and understand these patterns; there is no further challenge; hence these patterns are not aesthetically challenging. By contrast, Figures 1(c) and (f) are more challenging, since more sub-patterns must be identified. Note particularly that a random array of dots would not be as challenging. The important point to emphasize is that there is *challenge coupled with partial accomplishment.* Consequently, Figures 1(c) and (f) are *very* challenging because the viewer trying to discern the multiple underlying patterns only achieves a partial success by identifying several various subthemes which however only cover a significant part of the pattern.

For purposes of this paper we will suffice with (arbitrarily) categorizing *challenge levels* as equal to 1, 2 and 3+. In the next section, we continue our attempt to numerically quantify *aesthetic challenge*.

4. Fundamental Octant Complexity

As explained in the last section, Figure 1(b) requires two English keywords to describe the pattern. Heuristically, we would like to argue that the *fundamental octant* for this figure, exhibited in Figure 2(c), is overly simplistic, containing one line segment and 2 pixels; this octant simplicity gives rise to the simplicity of Figure 1(b). To facilitate formalizing this intuition of *octant complexity* we first present a simple lemma describing the relation between the *fundamental octant* and the full Azulejo pattern.

Lemma 1**:** Let $\boldsymbol{O}$ be the fundamental octant with fundamental square $\boldsymbol{N}$**,** of an Azulejo pattern, $\boldsymbol{A}(\boldsymbol{n,d,K})$.

(a) A singleton pixel, $(n,-n)$ in the set $\boldsymbol{O}$ gives rise to one pixel in $\boldsymbol{N}$. Similarly if n is even then $(n/2, -n/2)$ in the set $\boldsymbol{O}$ gives rise to one pixel in $\boldsymbol{N}$.
(b) A singleton pixel $(m,-m)$ in the set $\boldsymbol{O}$, with $m \neq n$, $m \neq n/2$, gives rise to 4 pixels in $\boldsymbol{N}$.
(c) A singleton pixel $(n,-k)$ in the set $\boldsymbol{O}$, with $k \neq n$, $k \neq n/2$ gives rise to 4 pixels in $\boldsymbol{N}$**.**
(d) A singleton pixel $(j,-k)$ in the set $\boldsymbol{O}$, with $j \neq k$, $j,k \neq n$, $j,k \neq n/2$, gives rise to 8 pixels in $\boldsymbol{N}$.

(e) If n is even then the singleton pixel (n, $-n/2$) in $\boldsymbol{O}$ gives rise to 2 pixels in N.

Proof**:** Parts (a) - (e) all follow from the the definition of << >> and the *fundamental octant inequality*. For example $\langle\langle(n,-n)\rangle\rangle = \{(n,-n)\}$ since $[(\pm n, \pm n)] = (n,-n)$ by our conventions of representatives of $\mathbf{Z_n}$. Similarly for case (d) the << >> function produces the orbit of $(j,-k)$ under the dihedral group, $\mathbf{D_4}$, which has 8 pixels.

We now define, $\boldsymbol{C} = \boldsymbol{C}(\boldsymbol{n,d,K})$, the octant *complexity* level, as follows:

a) For each vertical, horizontal, diagonal and anti-diagonal "line" with two or more pixels in $\boldsymbol{O} - \{(n,-n)\}$ we assign a value of one; (if a pixel in $\boldsymbol{O} - \{(n,-n)\}$ is shared by two such lines then both lines are assigned a value of one); here, by the term "line" we mean *any* collection of filled-in pixels, not necessarily consecutive, whose addresses satisfy a linear equation (note, since we only allow horizontal, vertical and (anti)-diagonal lines the slope must be 0,1,-1, or infinity).

b) For each remaining pixel not on any of the lines enumerated in (a) we assign a value of one.

$\boldsymbol{C}$ is defined as the sum of assigned values.

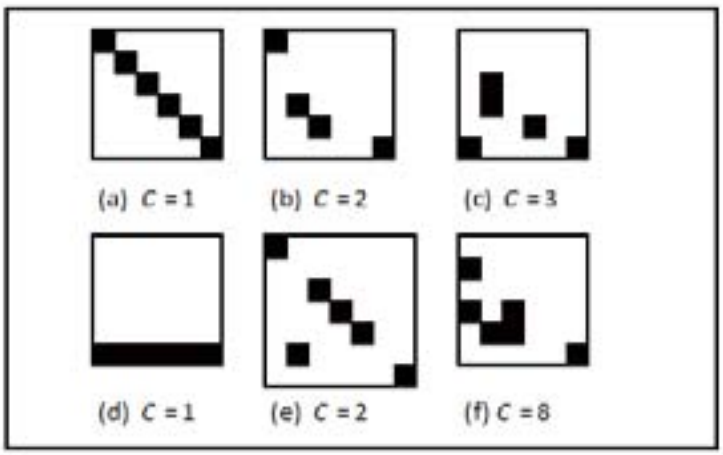

Figure 3: *The fundamental octants and their complexities, for the six Azulejo patterns in Figure 1. The verification of the numerical complexities is left as an exercise for the reader.*

Three points should be noted about our definition of *complexity*: (1) The numerical *complexity, C,* increases as one goes from the leftmost column to the rightmost column in Figure 1. (2) The octant complexity, C, correlates with the *number-of-English-phrases* complexity introduced in the last section. (3) Our definition of complexity surprisingly avoids any mention of symmetry! The Section-2 description of the Fernandez algorithm shows an ingenious separation of a symmetry component (Step 4) from a non-symmetry component (Step 3). That is, the octant pattern (Step 3) *need not* have any symmetry since by applying the dihedral group symmetries (Step 4) the resulting Azulejo will have symmetry.

We are now ready to identify the non-algebraic criteria used in this paper for constructing octants.

Definition: An octant is said to be *minimally aesthetically challenging* if its *octant complexity* is at least 3. An octant is said to be *very aesthetically challenging* if its *octant complexity* is at least 10 (this choice of 10 in the definition is somewhat arbitrary). The corresponding Azulejo pattern is said to be *minimally* or *very aesthetically challenging* if its octant is *minimally* or *very aesthetically challenging*.

As already indicated at the end of Section 2, Fernandez constructed the fundamental octant using certain simple linear arithmetic functions. The position of the author is that a random approach to octant pattern construction is *equally* capable of producing aesthetically pleasing patterns.

5. Aesthetically Pleasing Azulejos Based on Random Octants

The goal of this section is to compare the *aesthetic pleasantness* of Azulejos whose octant construction is based on *complexity* vs. an algebraic definition. The octants and corresponding Azulejos are presented in Figures 4 and 5 respectively which the reader is invited to review now. The reader can readily compare the aesthetic pleasantness of these Azulejos to verify the thesis of this paper that a *complexity* approach to octant construction is a viable alternative to Fernandez's algebraic approach. The following additional points should be made:

Figures 5(a) and 5(d) use Fernandez's algebraic approach. The octants each have $C > 20$. As can be seen the Azulejos are indeed *very aesthetically challenging*. By contrast, Figures 5(b), (c), (e) and (f) use a pure *complexity* approach without an underlying algebraic generation. Figures 4(b), (c), (e) and (f) should be approached as follows:

Figure 4(b) was a first attempt at aesthetic challenge without algebra. The octant has one pixel, one diagonal (left to right upward) and one vertical line. Its complexity is five (there are two extra downward diagonals (left to right). Figure 5(b) shows the corresponding Azulejo. It can be described with three English phrases: (1) a pixel (2) inscribed in a diamond, (3) inscribed in a 4-corner-square. The three English phrases needed to describe the Azulejo clearly correspond to the three connected components of the octant: by lemma 1, the pixel in the lower right corner remains a pixel in the Azulejo, the upward (left to right) diagonal becomes a diamond, and the vertical line becomes a 4-corner-square.

Figure 5(b) is only *minimally aesthetically challenging*. It can be *completely described* with three English phrases. Figures 4(c), (e), and (f) are attempts to remedy this simplicity.

- Figure 4(c) "fixes" Figure 4(b) by adding an extra dot and an extra upward diagonal. The resulting Azulejo now requires five English phrases to describe it: a (1) pixel (2) inscribed inside a diamond (3) inscribed in a 4-pixel square (4) inscribed in a 4-corner square. Each set of four of these four-fold nested patterns forms a square with (5) a diamond in the center. Although this Azulejo has complexity nine it is too transparent in the precise sense that it can be *completely* described by the five phrases.
- Figure 4(e) "fixes" Figure 4(b) by adding a "random" assortment of dots. The resulting Azulejo pattern, Figure 5(e), is more aesthetically challenging in the precise sense that it can't be *completely described.*
- Figure 4(f) goes one step beyond Figure 4(e) by providing a pure random assortment of dots without any lines. Although $\boldsymbol{C} = 5$, this pattern appears more aesthetically challenging than Figure 5(c) whose complexity equals 9. The observation that many people consider Figure 4(f), with $C = 5$, more aesthetically challenging than Figure 4(c), with $C = 9$, strongly suggests that the definitions of *aesthetic challenge* presented in this paper are only useful approximations and that further research into a better definition of aesthetic challenge is needed.

The above remarks suggest the following future directions of research, which were already raised in [1]. (1) Do random dot assortments which miss lines produce aesthetically pleasing Azelujos? – if so, is there a way of numerically quantifying the complexity of random dot patterns? (2) When there are competing lines, diagonals and pixels in an octant which ones will stand out in the resulting Azulejo? (3) What algebraic and graph theoretic properties of octants result in Azulejos that are *completely describable*? (4) Figures 4(e) and 4(f) use *knight* jumps (1 diagonally down and 1 over) to produce the *random* dot configurations; is this method generalizable?

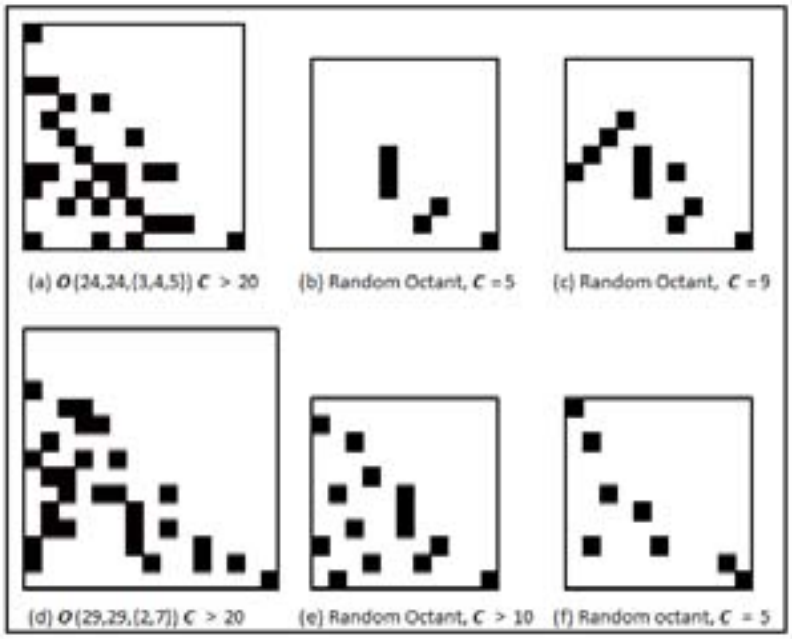

Figure 4: *Comparison of octants based on an algebraic definition (Figures a,d) vs. a complexity approach (Figures b, e, c, f). The corresponding Azulejos are presented in Figure 5.*

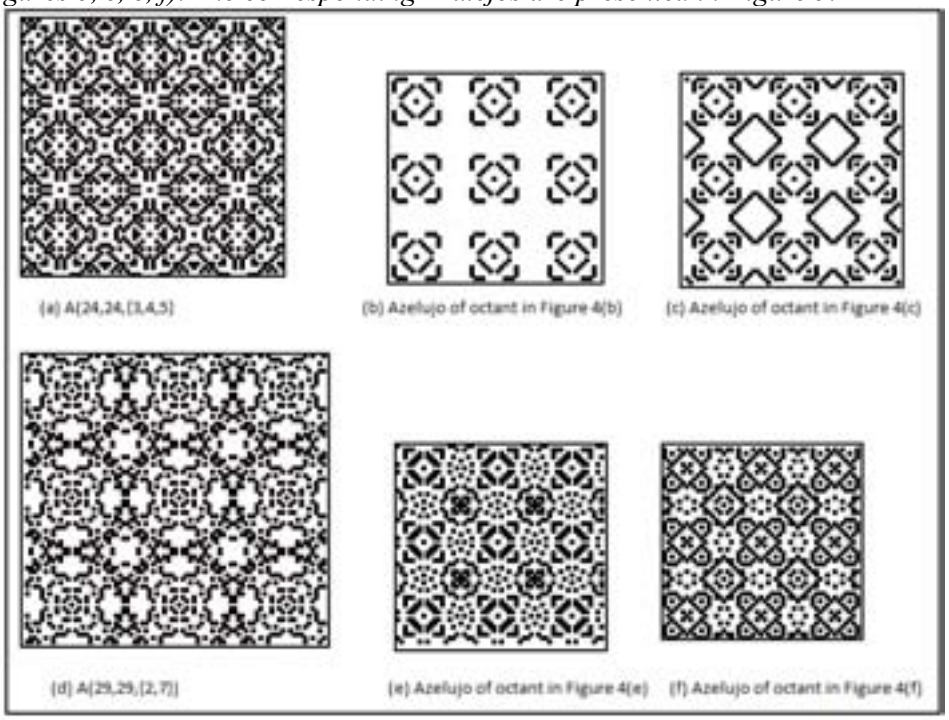

Figure 5: *Azulejo patterns for the fundamental octants of Figure 4.*

References

[1] Federico Fernandez, *A Class of Pleasing Periodic Designs*, The College Math Journal, Vol. **29.1**, pp. 18-26. 1998.

Marking a Physical Sphere with a Projected Platonic Solid

C. A. Yackel*
Mathematics Department
Mercer University
1400 Coleman Ave.
Macon, GA 31207-0001, USA
E-mail: yackel_ca@mercer.edu

Abstract

Although mathematicians often use coordinates for the vertices of the Platonic solids, a physical sphere is not a priori situated within this same coordinate system. In this paper, we describe how to locate points relative to one another on the surface of a sphere, in order to mark vertices and edges of each of the spherically projected Platonic solids without first coordinatizing. While certain methods for the cube and octahedron are standard and the tetrahedron method is known in the temari community, and is clear to any mathematician, in this paper, one procedure that leads to all three is given as a necessary first step to finding the dodecahedron. The author believes the dodecahedron and icosahedron procedures to be original to Western language scholarship. While some steps are theoretically exact, others only approximate; however at one step the approximation can be made as exact as one desires. Furthermore, the procedures allow for making adjustments to account for the fact that physical balls always fail to be perfect spheres.

1. Art---Motivation and Applications

Humans are drawn to the spherical form and to symmetrical division. What could be more natural than artists wishing to divide spheres into congruent regions for the purpose of decoration? Indeed, this occurs across media with wood, ceramics, painting, and embroidery to name but a few. This author can imagine many other applications. For examples of existing artwork incorporating exact subdivision of spheres, see Figure 1.

Figure 1: *From left to right---Roads Untaken, by George Hart, wood tiled fiberglass sphere [3]; Sphere of Influence, by Richard Weber, carved ceramic spherical rattle [11]; Which Way, by Dick Termes, painted sphere [7]; temari ball with cube/octahedral symmetry, by the author.*

Only one of the pieces in Figure 1 was divided into a projected Platonic solid. Yet Hart's piece is fundamentally based upon a truncated Platonic solid. [4] Termes' piece comes from taking a projected icosahedron, dividing each triangle into three subtriangles by connecting the incenter with the vertices, and then forming diamonds by pairing triangles across the original trianglar boundaries. Auxiliary triangles have been drawn that obscure this construction. To learn about his multiperspective technique, consult his website. [8] Weber's ceramic sphere relies only on sectors, but one can imagine him using

Platonic projection to inform future designs, given the large variety of divisions he has already employed. [11]

This author frequently works within the medium of wrapped and embroidered Japanese thread balls, called temari balls. The inspiration for this paper came from the mathematical impurity of the standard method for dividing the sphere for a projected dodecahedral/icosahedral subdivision, known as a C10 subdivision in the temari literature. Hence, the goal was to find a simultaneously theoretically more exact and technically purer method for making this subdivision. The techniques used here are derived from the traditional Japanese techniques of measuring with paper tape, and directions are given as though pins can be pushed into the sphere, as if it were made of Styrofoam. If this is not possible, such as if the sphere is made of glass or metal, perhaps the pinheads can be affixed to the sphere pointing outwards with glue. However, with smooth media it may be easiest to use only one pin (the North Pole on which the paper tape swivels) and to mark all other pinpoints and edges with pencil or other erasable marker. Nonetheless, any artist interested in dividing his or her spherical region into those given by a projected Platonic solid will be able to do so by following the essence of these directions.

2. Geometric Applications---Math in the Wild

Imagine holding in your hand a ball, or better yet, go get a ball---a super ball, tennis ball, Styrofoam ball, metal ball, or any other ball. Notice that what you have is round, but not a perfect sphere. Observe that finding the diameter is not immediate. Finding the circumference is much more natural, but this too poses a challenge. How will you know when you have the circumference rather than something close? What will you use to find the circumference? A rubber band? A piece of string? A paper tape? Using our methods, we will not need to measure distances per se, but will use only relative distances. Therefore, we will not need a ruler. However, we will need to be able to record distances for future reference, such as for division. Therefore, a rubber band will not work for our purposes. The string will only work if it has no elasticity. A paper tape, a thin strip of paper, will work best, because it has no elasticity, and we will be able to record our observations directly onto our measuring device with a pen or pencil.

In what follows, we describe a procedure to divide a ball into sections defined by the central projection of an inscribed Platonic solid onto the surface of the ball. With paper tape, origami techniques, two colors of pins (black and white), a pen, and thread, we can mark the surface of a ball with the vertices and edges of any Platonic solid. We make no attempt to use the known coordinates of the Platonic solids or to situate the ball within a coordinate system.

3. Finding the Circumference of the Sphere

How do we determine the circumference of the given sphere? Near one end of a paper tape, place a black pin through the paper tape and into the ball. Wrap the tape around the sphere, attempting to form a great circle, and make a fold in the tape where the paper meets the pin. If the paper really constitutes a great circle at this point, then this is the longest the tape will be and still lie flat around the ball. If not, then when the loop of tape is swiveled around the ball, there will be some other position at which the tape will need to be longer in order to reach the pin while lying flat around the ball. So, to check that the paper is the right length from pin to fold, turn the ball around the pin, holding the paper tape fixed and reflattening the tape as the ball is turned. If the tape continues to just reach the pin exactly, then the initial circumference estimate was correct. However, if the length of tape undershoots the pin at some points as the ball is turned, then make sure to straighten the tape and refold it to lengthen the distance to the fold so that the new distance just reaches the pin. Remember that because we want a great circle, the tape will always be lengthened, never shortened.

4. Marking a North/South Pole Pair on the Sphere

All of the Platonic solids except for the tetrahedron have antipodal vertex pairs. Therefore, we wish to mark one such pair. We may rename the pin already placed through the paper tape (used to find the circumference of the ball) the North Pole. The antipodal point to this is the South Pole, which is halfway around the ball. To find this new point, fold the distance on the paper tape measuring the circumference in half, and then we can easily measure the distance from the North Pole to the South Pole. Swiveling the tape any direction is valid, as all great circles should have the same length. Place a black pin, not through the paper tape, at the South Pole, as shown in Figure 2. Because the ball is not perfectly spherical, prudence suggests checking pin placement by measuring the half circumference from the North Pole by swiveling the ball and holding onto the paper tape, as before. The South Pole pin may have to be moved slightly a few times until it is in a suitable spot from all directions, that is, it is close to being equidistant from the North Pole measured in all directions. This adjustment may be necessary be due to thickness of the paper obfuscating initial pin placement as much as ball defect.

Figure 2: *Fold the circumference length in half, flatten the tape against the sphere, and place the South Pole pin at the center end of the tape.*

5. Marking a Projected Cube, Octahedron, or Tetrahedron

In the temari literature, the projected octahedron marking, known as C6 is commonly marked separately from the projected cube marking, known as C8. However, because our ultimate goal is to mark the projected dodecahedron, for which we will need to know the cube side length, we will not mark these separately here. Rather we refer the reader to standard sources. [1,2,6,9,10,13] Nevertheless, to begin the construction process, consider the six vertices of the octahedron shown in Figure 3: there are three antipodal pairs, one of which we have already placed. The other two pairs, made up of four points, we call equator points.

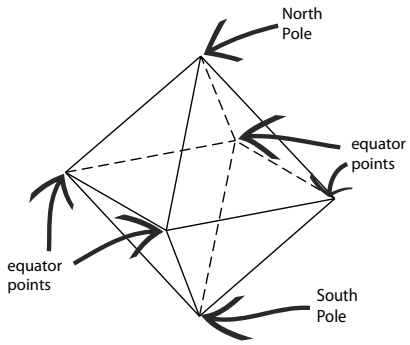

Figure 3: *Octahedron with vertices marked as pole or equator points.*

To place equator points, first fold the circumference tape (which should still be securely anchored at the North Pole) into fourths, and measure one half distance down the ball, placing eight to ten pins approximately equally spaced around the equator of the ball---that is, on the great circle lying equidistant between the North and South poles. See Figure 4(a). Now make a small cut through one half of the paper tape to the pin at the North Pole allowing removal of the paper tape without requiring disturbance of the pin placement. Divide the circumference length into eights by folding. This will be most accurate if halving folds are made one at a time rather than allowing paper thickness to build up. Using the equator pins as a guideline, place the paper tape around the equator, abutting each pin from the same side of the ball, with circumference ends matching up, as in Figure 4(b).

(a)  (b) 

Figure 4: *(a) Place equator pins by measuring one fourth of the distance down from the North Pole. (b) After placing a number of equator pins, use these arbitrarily spaced pins as guides to place the circumference tape around the middle of the sphere, like a belt. This tape, divided into eighths, will be used to repositions the pins equally around the equator of the sphere.*

Place a pin at every fold mark, alternating colors (black and white), simultaneously removing the pins used simply to mark the equator. (It is helpful to simply move the pins that do not correspond to a fold mark to a point rather than introducing a whole new set of pins.) We now have ten pins on the ball---the six black vertices correspond to the six vertices of the octahedron, and the four white vertices further divide the equator.

Next choose a pair of opposite black vertices on the equator and reconceptualize the ball so that those are the poles. Use the four pins already lying on the equator with respect to the new poles to place the paper tape around the new equator. Keeping those pins in place, use the paper tape to place four more (white) pins on the equator, dividing it into eighths. Finally, locate the unique pair of (black) antipodal pins on the initial equator that can be used as poles so that the equator corresponding to this pair will be perpendicular to both of the other equators. Then repeat the procedure of putting in four additional (white) pins to divide this third equator into eighths.

Both the vertices and the edges of the cube can now be marked by strategically wrapping thread around the ball, guided by the pins. For each pole pair, one at a time, tightly wrap all four great circles passing through both poles and one pair of opposing equator points. See Figure 5(a). From the perspective of the pole, doing so divides the ball into eight equal sectors, looking something like an orange. As this division is completed for the three pole pairs, the sector lines cross. Indeed, at eight points on the ball, three sector lines cross at the point, as exhibited in Figure 5(b). These points are the vertices of the cube. They may be marked with a pin, if desired. Note also that the points are already joined by sectors, which form the edges of the cube. Hence, the cube has been completed, and the octahedron has been completed, as well.

(a)  (b) 

Figure 5: *(a) Four great circles pass through each octahedral vertex guided by the marking pins. (b) As a result, three great circles meet in the center of each octahedral triangle to form the vertices of the cube.*

To make a tetrahedron, note that by taking alternating upper and lower vertices of a cube you have an inscribed tetrahedron, and this remains true when projected onto the sphere. Simply join the vertices to obtain the edges.

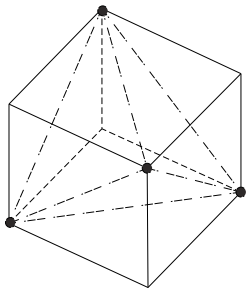

Figure 6: *Tetrahedron lying in cube. Six tetrahedral edges are marked with irregular dotted lines and four tetrahedral vertices are marked with small circles.*

6. Marking a Projected Dodecahedron or Icosahedron

To make a projected dodecahedron or icosahedron is slightly more difficult. On your existing paper tape, mark off the side length of the cube you have made. The paper tape is now spent in terms of folding, but it contains important distance information. So cut a new tape, longer than the ball circumference, marking the new tape with the circumference length approximately one centimeter from one of the ends. We now divide the circumference into tenths, which can be done in several ways. Use the Fujimoto approximation technique, an origami technique beautifully described by Hull [3], to divide the circumference into fifths. Repetition of the technique allows for as much accuracy as one desires. Or, use a ruler and compass construction to divide the length into fifths. After satisfactory division into fifths, use folding to further subdivide the circumference into tenths. Choose an existing pole pair and use its equator pins to accurately wrap the newly divided paper tape circumference around the equator. Repin the equator so that pins mark each tenths subdivision. Remove all pins other than these twelve (poles and equator) and all marking threads. Now wind threads to mark five new great circles through the five pairs of antipodal points on the equator and passing through the poles. This divides the ball into ten equal sectors from the perspective of the poles, as in Figure 7(a).

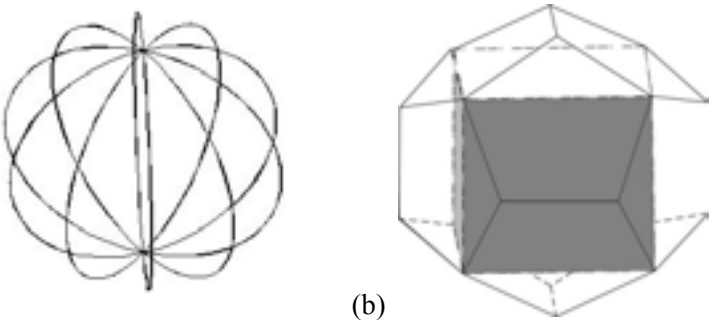

(a) (b)

Figure 7: (a) *Five equally spaced great circles placed around an invisible sphere; (b) The solid cube, two grey faces and one white, inscribed in the dodecahedron. The fact that one edge of the cube spans two edges of the dodecahedral pentagon is key to the construction.*

The two poles represent centers of two projected pentagonal faces of the dodecahedron. The other ten centers of the faces of the dodecahedron will lie on the sector lines, but they alternate up and down some distance from the equator. Thus knowing the distance between two adjacent projected centers is essential to marking the remainder of the ball.

Now choose any one of the sector lines and go up near a pole. Using your paper tape, marked off with half of the edge of the cube length, measure orthogonally over from your latitude line until your length hits the latitude line two over, as shown in the middle of Figure 8. Do so by moving the straight folded edge of the paper tape nearer or farther away from the pole on the latitude line, not by changing the angle of the tape! Note that the ninety degree angle here is local, and originates from the interaction of the folded edge of the paper tape with the straight guideline (marking thread). Mark the intersection point of the mark on the tape with the latitude line two over with a pin. See Figure 9(a).

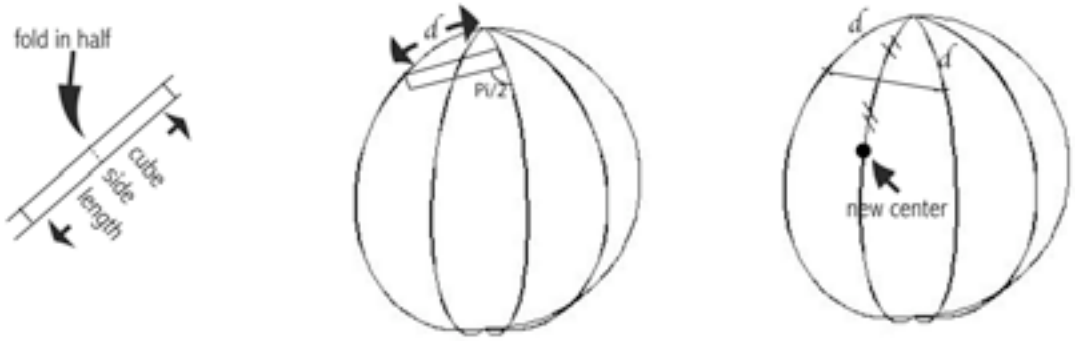

Figure 8: *Diagrams for steps involved in locating adjacent centers on the dodecahedron.*

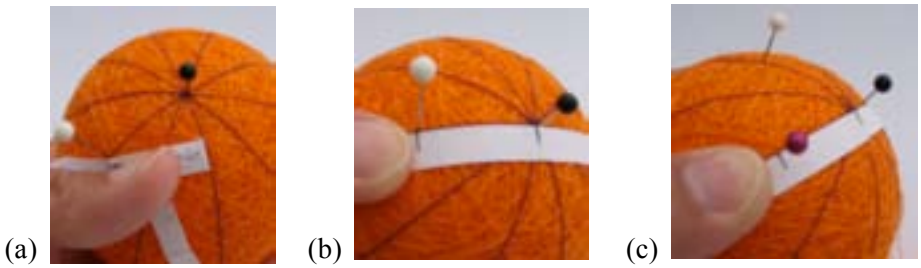

(a) (b) (c)

Figure 9: *(a) Using the half cube side length tape; (b) Determining distance d; (c) Marking off a new distance d.*

If the most recent step has been done accurately, the new pin is at one of the vertices of the pentagon surrounding the pole. Now mark the distance from the pole to this pin on a piece of paper tape and call the distance *d*, as depicted in Figure 9(b). Mark the distance *d* with a pin on a second latitude line two over from the one already marked off by the pin. This is illustrated in Figure 9(c). This marks off a second vertex. Use these two vertex pins and either a piece of paper tape or a piece of string pulled tight to mark off (with a pin) the intersection of the line segment they generate, which is an edge of the dodecahedron, with the latitude line between them, shown on the right side of Figure 8. Now measure the distance between the pole (one center of the dodecahedron) and this latest pin. This distance is the projected perpendicular distance between the center of a pentagonal face and one of its edges. Then double that distance along that same latitude line and place another pin, also shown on the right side of Figure 8. This new pin represents the center of an adjacent face on the dodecahedron. Now that we have solved the problem of finding the distance between adjacent centers on the projected dodecahedron, we have theoretically completed our solution.

Practitioners may like to have the steps for marking the dodecahedron and icosahedron spelled out; therefore, we do so below. Begin by measuring and copying the distance between two adjacent centers onto a piece of paper tape. Mark this distance from the North Pole on every other sector line. Next mark the same distance, but this time from the South Pole, on the remaining sector lines. Now all centers have been marked onto the ball. See Figure 10(a). Checking that the distance between the centers is indeed constant can ensure accuracy. Ten of the centers do not have five great circles emanating from them, namely the ten just placed on the sector lines. However, for symmetry of the ball, and to mark edges, these great circles should be marked with thread. Choose any one of these ten centers and its antipodal pin. One of the great circles is already present---the sector line upon which the pin lies. The other four great circles will be guided by the eight remaining centers, divided into antipodal pairs. Continue for each of the other four pairs, noticing that fewer and fewer great circles are needed at each next pin pair to complete the five great circle set. When each center has 10 sector lines equally dividing the ball from the perspective of the center, the entire ball will appear to be divided up into twelve pentagons. This is the projection of the dodecahedron. These twelve pentagons will be themselves divided up into 10 triangles. Alternately, the ball could be seen as being divided into 20 triangles, which are subdivided into six subtriangles. This is the icosahedron, as depicted in Figure 10(b).

(a)  (b) 

Figure 10: *(a) Pins on spindle lines repositioned; (b) Completely marked projected dodecahedron and icosahedron.*

7. Notes on the Procedures

The methods in this paper extend those given in the temari sources available to the author [1,2,6,9,10,13,14] and are analogous in many ways to straight edge and compass constructions rather than ruler use. The author's goal was to find a way to make a C10 subdivision using "rules" of temari, which she took to mean measuring with paper tape and using traditional paper folding techniques. As a mathematician, she was also prepared to use straightedge and compass techniques. She did not, however, allow herself rulers or protractors. This eliminated the usual techniques for C10 subdivisions. The methods for the octahedron and cube are standard and available in any book on making temari balls (cf. [2,6,10,13]), as well as on temari websites (cf. [1,9]) Less common, but obvious to any mathematician, is the method given for the tetrahedron, which was included in the author's previous work. [14] The methods for the first three Platonic solids were collapsed here for brevity, but included as a necessary step to making the projected dodecahedron/icosahedron. Via the method in this paper the most multifaceted of the Platonic dual pairs is marked simultaneously, but the edge length of the cube projected onto the same sphere is needed in order to complete the construction.

The existing temari literature contains two other techniques for marking the projected dodecahedron/icosahedron. The first accepted technique is based on using the radius times an approximation of the radian measure of the $\arccos\left(\frac{1}{\sqrt{5}}\right)$ as the distance between centers. The second ordinary technique involves using a v-ruler (a special tool combining a protractor constantly set at seventy-two degrees with metric rulers on its sides) and an approximation of side length from a chart, which essentially does the same as the first approximation, though possibly more accurately. As much as possible, the method set forth in this paper is akin to a classical construction—it may not always be the fastest, but it exhibits a purity of form.

References

[1] Deborah Abolt. http://www.temarimath.info/about.html, last viewed 2/2/09.

[2] Anna Diamond. *The Temari Book*, Lark Books, New York, NY 2000.

[3] G. Hart. http://www.georgehart.com/sculpture/roads-untaken.html, last viewed 4/17/09

[4] G. Hart. Sculpture based on Propellorized Polyhedra, Proceedings of MOSAIC 2000, Seattle, WA, August, 2000, pp. 61-70. Online at http://www.georgehart.com/research/hart.html

[5] Tomas Hull. Project Origami, A K Peters Ltd, Wellesley, MA 2006.

[6] Barbara B. Seuss. *Japanese Temari,* Breckling Press*,* Elmhurst, IL 2007.

[7] D. Termes. http://www.termesphere.com/gallery-1.html, last viewed 4/17/09.

[8] D. Termes. http://www.termesphere.com, last viewed 4/17/09.

[9] G. Thompson. http://www.temarikai.com/, last viewed 2/2/09.

[10] Diana Vandervoort. *Temari: How to make Japanese Thread Balls*, Japan Publications Trading Co., Ltd. 1992.

[11] R. Weber. http://www.silverhawk.com/artisan/clay/weber-r/index.html, last viewed 4/17/09.

[12] Eric W. Weisstein. "Dodecahedron." From MathWorld—A Wolfram Web Resource. http://Mathworld.wolfram.com/Dodecanedron.html last viewed 2/1/09.

[13] Mary Wood. *The Craft of Temari*, Search Press, Tunbridge Wells, Kent 1991.

[14] C. A. Yackel. Embroidering Polyhedra on Temari Balls, Proceedings of Math+Art=X 2005, Boulder, CO, June, 2005, pp. 183-187.

Coloring Uniform Honeycombs

Glenn R. Laigo, glaigo@ateneo.edu
Ma. Louise Antonette N. De las Peñas, mlp@math.admu.edu.ph
Mathematics Department, Ateneo de Manila University
Loyola Heights, Quezon City, Philippines

René P. Felix, rene@math.upd.edu.ph
Institute of Mathematics, University of the Philippines
Diliman, Quezon City, Philippines

Abstract

In this paper, we discuss a method of arriving at colored three-dimensional uniform honeycombs. In particular, we present the construction of perfect and semi-perfect colorings of the truncated and bitruncated cubic honeycombs. If G is the symmetry group of an uncolored honeycomb, a coloring of the honeycomb is *perfect* if the group H consisting of elements that permute the colors of the given coloring is G. If H is such that $[G : H] = 2$, we say that the coloring of the honeycomb is *semi-perfect*.

Background

In [7, 9, 12], a general framework has been presented for coloring planar patterns. Focus was given to the construction of perfect colorings of semi-regular tilings on the hyperbolic plane. In this work, we will extend the method of coloring two dimensional patterns to obtain colorings of three dimensional uniform honeycombs. There is limited literature on colorings of three-dimensional honeycombs. We see studies on colorings of polyhedra; for instance, in [17], a method of coloring shown is by cutting the polyhedra and laying it flat to produce a pattern on a two-dimensional plane. In this case, only the faces of the polyhedra are colored. In [6], enumeration problems on colored patterns on polyhedra are discussed and solutions are obtained by applying Burnside's counting theorem. The works [14, 19] highlight edge-colorings of the platonic solids. There are studies on colorings of three-dimensional space using an algorithm that makes use of the group structure of the Picard group [1, 2, 21]. Cross sections of the colored three-dimensional patterns were used to produce colored two-dimensional Euclidean patterns.

We find the occurrence of colored *honeycombs* (space filled with polyhedra) in different places; for instance, as representations of geometric constructions, or as models of chemical structures. Shown in Figures 3(a), 3(b) and 4(b) are illustrations of colored honeycombs. Interestingly, the colorings shown are representations of three different uniform constructions of the bitruncated cubic honeycomb, a honeycomb consisting of truncated octahedra. For example, the coloring with two colors in Figure 3(a) represents two types of truncated octahedra: half are obtained from the original cells of the cubic honeycomb and the other half are centered on vertices of the original honeycomb. In Figure 4(b), this colored honeycomb is referred to as the cantitruncated alternate cubic – there are 3 types of truncated octahedra in 2:1:1 ratios. In Figure 3(b) there are 4 types of octahedra in 1:1:1:1 ratios; each type is represented by a different color. In [18], a bitruncated honeycomb is used to represent a spongy graphite network of carbon atoms in 3-dimensional space.

In this paper, we present the construction of colored honeycombs where an entire cell gets one color.

In recent works [8, 16], a method for determining subgroups of three-dimensional symmetry groups in spherical, Euclidean or hyperbolic 3-space was discussed. The approach, based on concepts on color symmetry theory, allows for the characterization of each subgroup in terms of the symmetries it contains. This development is helpful in the construction of colorings of honeycombs especially in hyperbolic space, since the subgroup structure of hyperbolic symmetry groups is not widely known. As will be seen in this work, the subgroup structure of the symmetry group of a given honeycomb plays a significant role in arriving at colorings of the honeycomb.

Uniform honeycomb

We start the discussion by defining uniform honeycombs. A polyhedron is called *uniform* if its faces are regular polygons and it satisfies the property that its group of symmetries acts transitively on its vertices. A *uniform* honeycomb is a three dimensional honeycomb with uniform polyhedra as its cells and where the symmetry group of the honeycomb acts transitively on its vertices. Uniform honeycombs are also called *Archimedean* honeycombs.

In three-dimensional Euclidean space, twenty-eight such honeycombs exist: the cubic honeycomb and seven truncations thereof; the alternated cubic honeycomb and four truncations thereof; ten prismatic forms based on the uniform plane tilings (eleven if including the cubic honeycomb); and five modifications of some of the mentioned by elongation or gyration [11, 13]. In this paper, we illustrate the concept of arriving at colored honeycombs using two examples of uniform honeycombs, the truncated and the bitruncated cubic honeycombs, shown in Figures 1(a) and (b) respectively. Both of these honeycombs are directly constructed from the only regular honeycomb in three-dimensional Euclidean space – the regular space filling of cubes [4]. Interestingly, the centers of the cells of the bitruncated cubic honeycomb coincide with the body centered cubic (BCC) lattice.

The symmetry group of both the truncated and bitruncated cubic honeycombs is the group [4, 3, 4] generated by four reflections P, Q, R and S satisfying the following relations

$$P^2 = Q^2 = R^2 = S^2 = (PQ)^4 = (QR)^3 = (RS)^4 = (PR)^2 = (PS)^2 = (QS)^2 = e\ .$$

The planes of reflections P and Q, R and S intersect at an angle of $\pi/4$; the planes of reflections Q and R intersect at an angle of $\pi/3$ and the planes of reflections P and R, P and S, Q and S intersect at an angle of $\pi/2$. The planes of the reflections P, Q, R and S are shown in Figures 1(a) and (b), respectively, for the truncated and bitruncated honeycombs.

A method for coloring symmetrical patterns

The following method given in [12], will be applied to arrive at colorings of uniform honeycombs.

Let G denote the symmetry group of the uncolored honeycomb and X the set of cells in the honeycomb. If $C = \{c_1, c_2, \ldots, c_n\}$ is a set of n colors, an onto function $f: X \rightarrow C$ is called an *n-coloring* of X. To each $x \in X$ is assigned a color in C. The coloring determines a partition $\mathcal{P} = \{f^{-1}(c_i): c_i \in C\}$ where $f^{-1}(c_i)$ is the set of elements of X assigned color c_i.

Let H be the subgroup of G which consists of symmetries in G that effect a permutation of the colors in C. Then $h \in H$ if for every $c \in C$, there is a $d \in C$ such that $h(f^{-1}(c)) = f^{-1}(d)$. This defines an action of H on C where we write $hc := d$ if and only if $h(f^{-1}(c)) = f^{-1}(d)$.

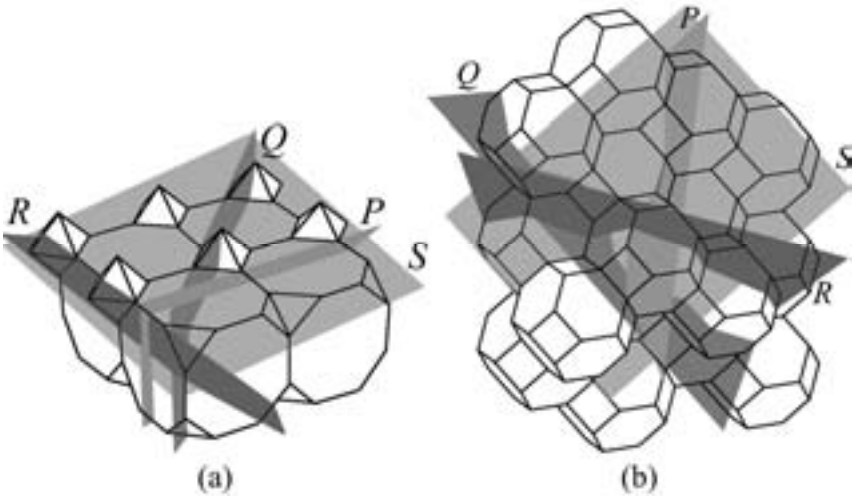

Figure 1: *The* (a) *truncated and* (b) *bitruncated cubic honeycombs with the planes of the reflections P, Q, R and S.*

Since H acts on the set C of colors of X there exists a homomorphism σ from H to Perm(C) where Perm(C) is the group of permutations of C.

Let $c_i \in C$ and denote by O_i the H-orbit of c_i, that is $O_i = Hc_i$. Suppose $J_i = \{h \in H : hc_i = c_i\}$ is the stabilizer of c_i in H. From each H-orbit of X with an element colored c_i, pick one such element. Put these elements together in a set X_i. Then the set of all elements of X that are colored c_i is $J_iX_i = \{jx : j \in J_i, x \in X_i\}$, that is, $f^{-1}(c_i) = J_iX_i$. A one-to-one correspondence results between the sets $O_i = Hc_i$ and $\{hJ_iX_i : h \in G\}$ where hJ_iX_i denotes the image of J_iX_i under h.

As a consequence of the orbit-stabilizer theorem given the assumptions above, we have the following:

Theorem:

1. The action of H on O_i is equivalent to its action on $\{hJ_i : h \in H\}$ by left multiplication.
2. The number of colors in O_i is equal to $[H : J_i]$.
3. The number of H-orbits of colors is at most the number of H-orbits of elements of X.
4. If $x \in X_i$ and $\text{Stab}_H(x) = \{h \in H : hx = x\}$ is the stabilizer of x under the action of H on X then
   (a) $\text{Stab}_H(x) \leq J_i$.
   (b) $|Hx| = [H : J_i] \cdot [J_i : \text{Stab}_H(x)]$

Thus, using the above framework, we outline the steps to obtain a colored uniform honeycomb, where H permutes the colors of the resulting coloring.

1. Pick a cell t from an H-orbit of the elements of X.
2. Determine the finite group S^* of isometries in H which stabilizes t, that is, $S^* = \text{Stab}_H(t)$.
3. Choose a subgroup J of H such that $S^* \leq J$.
4. Apply color c to cell t and to all the cells in the set Jt. If $[H : J] = k$, then Jt is $1/k$ of the cells in the H-orbit where t belongs.
5. Assign a color to every element of the set $\{hJt : h \in H\}$. The set Jt is given color c and each of the remaining $k - 1$ elements of the set gets a different color. In this coloring of the given H-orbit of cells, J will be the stabilizer in H of color c.

To obtain a coloring of a given uniform honeycomb, we consider each H-orbit of cells separately, coloring each orbit with a given set of colors such that H permutes the colors. If two H-orbits of cells are to have a color in common, the subgroup J used should contain the stabilizers of representative tiles from the two H-orbits. Combining the colored orbits of cells will give a colored honeycomb where all elements of H effect a permutation on the set of colors.

Constructing perfect colorings of the truncated and bitruncated cubic honeycombs

In this part of the paper, we discuss the construction of perfect colorings of the truncated and bitruncated cubic honeycombs. Given either a truncated or bitruncated cubic honeycomb, we apply the framework to arrive at colorings where the symmetry group $G = [4, 3, 4]$ of the honeycomb effects a permutation of the colors in the coloring.

In coloring the honeycombs, we will make use of the subgroups of G. (Table 1 gives a list of low index subgroups of G up to conjugacy in G obtained from [8, 16]). In this work, we obtain all perfect colorings where the number of colors used for each G-orbit is at most 4. Any other perfect coloring satisfying the given restriction on the number of colors may be obtained by a symmetry of the honeycomb, a one-to-one change of colors or a combination of both. We consider those colorings where a G-orbit of tiles gets at most 4 colors.

Index	Generators of the subgroup	Index	Generators of the subgroup
2	$A = \langle Q, R, S, PQP \rangle$	4	$F = \langle P, RQ, SRSQ \rangle$
2	$E = \langle P, RQ, S \rangle$	4	$B = \langle Q, R, S, PQRPQP \rangle$
2	$\langle P, RQ, SQ \rangle$	4	$\langle Q, R, PQP, SRS \rangle$
2	$C = \langle P, Q, R, SRS \rangle$	4	$\langle Q, R, PSQP, SRQP \rangle$
2	$\langle Q, R, SP \rangle$	4	$\langle QP, RP, SRSP \rangle$
2	$\langle QP, RP, S \rangle$	4	$\langle RQ, S, PRQP \rangle$
2	$\langle QP, RP, SP \rangle$	4	$\langle RQ, SP, PRQP \rangle$
3	$\langle RPR, RQR, RSR, S, QPQ \rangle$	4	$\langle RQ, SQ, PRQP \rangle$
4	$D = \langle P, Q, R, SRSQRS \rangle$	4	$\langle RQ, PQS \rangle$

Table 1: *The index* 2, 3, 4 *subgroups of* $G = [4, 3, 4]$ *up to conjugacy in G.*

Perfect colorings of the truncated cubic honeycomb. The truncated cubic honeycomb has two G-orbit of cells: the orbit X_1 of octahedra and the orbit X_2 of truncated cubes. The perfect colorings that we will discuss first will involve those colorings where the G-orbits of cells do not share a color; that is, a color that is used in X_1 will not be used in X_2. We will color X_1 first, then X_2.

In coloring X_1, we start with the cell labeled t in Figure 2(a). The stabilizer of t in G, $\mathrm{Stab}_G(t)$, is the group generated by Q, R, S, a group of type $\mathbf{O_h}$, also known as the octahedral group. We need to select a subgroup J_1 that satisfies the condition that $\mathrm{Stab}_G(t) \leq J_1$. Using Table 1 we find that the groups $A = \langle Q, R, S, PQP \rangle$ and $B = \langle Q, R, S, PQRPQP \rangle$ are suitable choices for J_1.

To obtain a perfect coloring of X_1 using A, we assign At the color light grey. To color the rest of the orbit, we apply the 2-fold rotation $(PQ)^2$ about x on At to obtain a coloring of two colors shown in Figure 2(a). A perfect coloring of X_1 using $B = \langle Q, R, S, PQRPQP \rangle$ is given in Figure 2(b). The coloring is obtained by assigning all cells in Bt light grey. Then we assign the colors grey, black and white to the other cells by applying the 4-fold rotation PQ about x.

Next, we color the orbit X_2 of truncated cubes. We start with the cell labeled t' in Figure 2(c). The stabilizer of t' in G, $\text{Stab}_G(t')$ is the group $\langle P, Q, R \rangle$ of type $\mathbf{O_h}$. From Table 1, the groups $C = \langle P, Q, R, SRS \rangle$ and $D = \langle P, Q, R, SRSQRS \rangle$ contain $\text{Stab}_G(t')$, thus either C or D may be used to color X_2. Using C and D, we obtain the colorings shown in Figures 2(c) and (d) respectively.

Note that the group G can also be used to color X_1 or X_2 since it contains the stabilizer of every cell. Consequently, all the octahedra or the truncated cubes, respectively, will get one color.

The perfect colorings of the truncated cubic honeycomb where the two G-orbits of cells do not share colors will be obtained by considering the perfect colorings of the octahedra in orbit X_1 and the perfect colorings of the truncated cubes in orbit X_2. Using G, A and B, there are 3 colorings of orbit X_1 and using G, C and D, there are 3 colorings of orbit X_2 that will give rise to 9 perfect colorings of the truncated cubic honeycomb where the orbits X_1, X_2 do not share colors and both X_1 and X_2 get at most 4 colors.

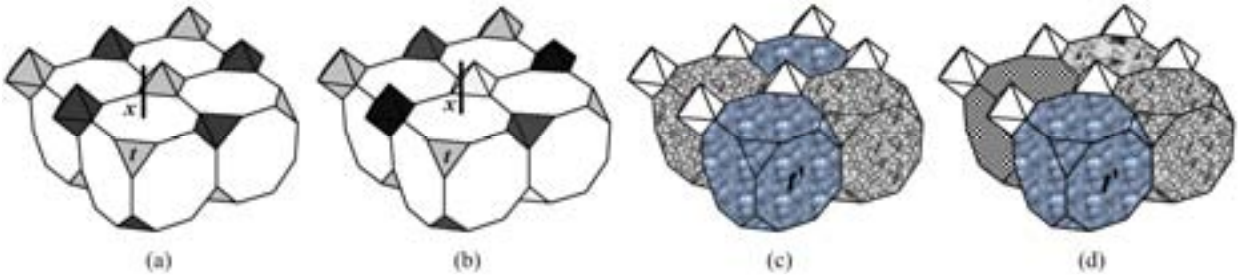

Figure 2: *Perfect colorings of X_1 using*: (a) A and (b) B; *perfect colorings of X_2 using*: (c) C and (d) D.

Perfectly colored honeycombs may also be arrived at by constructing colorings where the G-orbits of cells share colors. If a subgroup J_i is used to color one orbit of cells X_i, it can be used to color another orbit X_j as long as J_i contains the stabilizer of a tile in X_j. Moreover, if a color used to color cell $t \in X_i$ is used to color cells in X_j then the tile $t' \in X_j$ that will be assigned the same color as tile t should have a stabilizer contained in J_i.

We wish to remark that in constructing non-trivial perfect colorings of the truncated cubic honeycomb, the G-orbits of cells X_1 and X_2 cannot share colors. The subgroups A and B, for example cannot be used to color cells in X_2 since these groups do not contain a stabilizer of a cell in X_2. Similarly, the subgroups C and D cannot be used to color cells in X_1 since these groups do not contain a stabilizer of a cell in X_1.

Perfect colorings of the bitruncated cubic honeycomb. To color the bitruncated cubic honeycomb, we first note that this honeycomb has only one type of cell – the truncated octahedron. The symmetry group G of the bitruncated cubic honeycomb is cell-transitive. This means that we only have one G-orbit of cells to color. Since the symmetry group of the uncolored bitruncated cubic honeycomb is also $G = [4, 3, 4]$, we will use the list provided in Table 1 to choose the subgroups that we can use to color.

First, consider the truncated octahedron labeled t in Figure 3(a). The stabilizer of t in G is $\langle P, Q, R \rangle$ a group of type $\mathbf{O_h}$. Aside from G, the groups $C = \langle P, Q, R, SRS \rangle$, $D = \langle P, Q, R, SRSQRS \rangle$ contain $\langle P, Q, R \rangle$ and may be used to arrive at perfect colorings of the bitruncated cubic honeycomb. The colorings of the entire honeycomb using C and D are given in Figures 3(a) and (b), respectively.

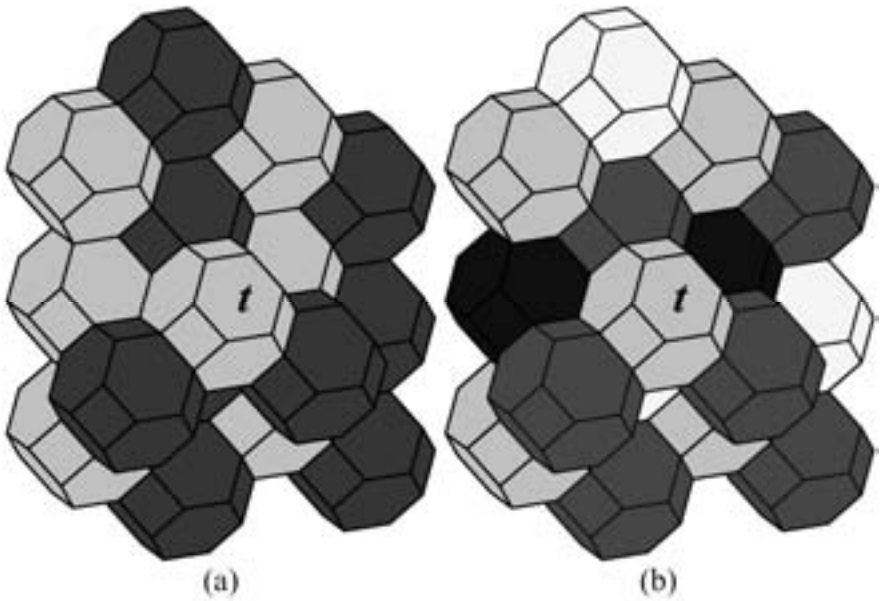

Figure 3: *Perfect colorings of the bitruncated cubic honeycomb using* (a) *C and* (b) *D.*

Semi-perfect colorings of the bitruncated cubic honeycomb

In this part of our work, we illustrate the construction of semi-perfect colorings of the bitruncated cubic honeycomb. In this case, the group H consisting of elements that permute the colors in a given coloring is an index 2 subgroup of G. Following the framework presented earlier, the first step is to choose an index 2 subgroup H and determine the H-orbits of cells. Then we proceed by coloring each H-orbit of cells separately.

For our first example, let us construct a semi-perfect coloring where in particular the subgroup $C = \langle P, Q, R, SRS \rangle$, permutes the colors in the given coloring. There are two C-orbits of cells. As shown in Figure 4(a), the set of "patched" cells is the C-orbit X_1, while the set of white cells is the C-orbit X_2.

To color X_1, we first choose our starting cell t labeled in Figure 4(a). Note that $\text{Stab}_C(t) = \langle P, Q, R \rangle$ of type $\mathbf{O_h}$. The subgroup $D = \langle P, Q, R, SRSQRS \rangle$ of C contains $\langle P, Q, R \rangle$, so that we let $J_1 = D$. We assign the color light grey to the set Dt and black to the set aDt, to obtain the coloring shown in Figure 4(b) (a is the two-fold rotation with axis x labeled in Figure 4(b)).

To color X_2, note that if $t' \in X_2$ then $\text{Stab}_C(t') \leq C$, so we can use C to color X_2 and X_2 gets a single color. Assuming the color white is used to color X_2, the semi-perfect coloring we obtain is the coloring given in Figure 4(b).

As a second example, let us construct a semi-perfect coloring where $E = \langle P, RQ, S \rangle$ is the group consisting of elements that will permute the colors of the coloring. In this case, all the truncated octahedra in the honeycomb will form one orbit of cells under E, so we only have one E-orbit to color. Consider the cell labeled t in Figure 4(c) where $\text{Stab}_E(t) = \langle P, RQ \rangle$. The subgroup $F = \langle P, RQ, SRSQ \rangle$ of E has $\langle P, RQ \rangle$ as a subgroup, so that we may use F to color the honeycomb semi-perfectly. The resulting semi-perfect coloring is shown in Figure 4(c).

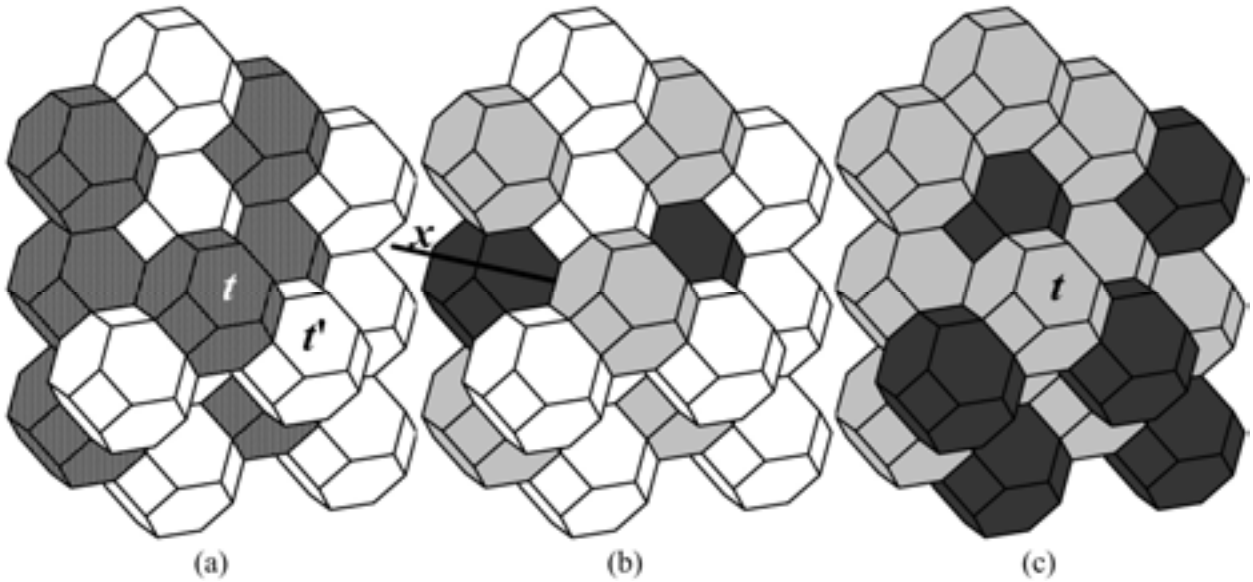

Figure 4: (a) *Two C-orbit of tiles of the bitruncated cubic honeycomb* ($C = < P, Q, R, SRS >$); (b)-(c) *Semi-perfect colorings of the bitruncated cubic honeycomb.*

References

[1] Chung, K.W., H.S.Y. Chan, and B.N. Wang. *Tessellations in three-dimensional hyperbolic space from dynamics and the quaternions*, in Chaos, Solitons & Fractals, Vol 12, Issue 7, 1181 – 1197 (2001).
[2] _____. *Tessellations with symmetries of the wallpaper groups and the modular group in the hyperbolic 3-space from dynamics*, in Computers & Graphics, Vol 25, Issue 2, 333 – 341 (2001).
[3] Conway, J.H., H. Burgiel, and C. Goodman-Strauss. *The Symmetry of Things*. USA: A. K. Peters. (2008).
[4] Coxeter, H.S.M. *Regular Polytopes*. New York: Dover Publication, Inc. (1973).
[5] Coxeter, H.S.M. *Wythoff's Construction for Uniform Polytopes*, in Beauty of Geometry: Twelve Geometric Essays. Dover Publications, Inc.(1999).
[6] Cromwell, P.R. *Polyhedra*. Great Britain: Cambridge University Press (1997).
[7] De Las Peñas, M.L.A.N., R. Felix, and G. Laigo. *An Approach in Coloring Semi-Regular Tilings on the Hyperbolic Plane*, in Renaissance Banff, Bridges: Mathematical Connections in Art, Music and Science Proceedings 2005, R. Sarhangi, ed. USA: Central Plain Book Manufacturing (2005).
[8] De Las Peñas, M.L.A.N., R. Felix, and G. Laigo. *On Subgroups of Tetrahedron Groups*. In print.
[9] De Las Peñas, M.L.A.N., R. Felix, and G. Laigo. *Colorings of Hyperbolic Plane Crystallographic Patterns*, in Z. Kristallogr 221, 665 – 672 (2006).
[10] De Las Peñas, M.L.A.N., R. Felix, and M.V.P. Quilinguin. *A Framework for Coloring Symmetrical Patterns*, in Algebras and Combinatorics: An International Congress, ICAC '97 Hong Kong. Singapore: Springer-Verlag (1999).
[11] Deza, M and M. Shtogrin. *Uniform partitions of 3-space, their relatives and embedding*, in European Journal of Combinatorics Vol 21, Iss 6, 807 – 814 (2000).
[12] Felix, R.P. *A General Framework for Coloring Planar Patterns*, a paper presented in National Research Council of the Philippines Symposium, February 7, 2004.
[13] Grunbaum, B. *Uniform Tilings of 3-space*, Geombinatorics 4, 49-56, 1994.
[14] Jablan, S. *Edge Bi-Colorings of Regular Polyhedra*, in Z. Kristallogr 210, 173-176, 1995.

[15] Laigo, G. *On the Construction of Perfectly Colored Semi-Regular Tilings on the Hyperbolic Plane*, a masters thesis, Ateneo de Manila University, Philippines. (2005).
[16] Laigo, G. *On Tetrahedron Groups and their Subgroups*, a PhD dissertation, Ateneo de Manila University, Philippines (2008).
[17] Meenan, E.B. and B.G. Thomas. *Pull-up Patterned Polyhedra: Platonic Solids for the Classroom*, in Sarhangi, R. et al (Editors), Bridges Leeuwarden: Mathematical Connections in Art, Music and Science, Tarquin Publications, Hertfordshire, 109 – 116 (2008).
[18] Umeda, T. and M. Fujita. *Polymorphism of Carbon Forms*: *Polyhedral Morphology and Electronic Structures*, in Phys. Rev. B Vol 51 No 19, (1995).
[19] Walo, L. *On* (*k,l*) - *chromatic colorings of the edges of platonic solids*, a masters thesis, University of the Philippines – Diliman, Philippines (2003).
[20] Walo, L. *Images of orbits and orbits of images in symmetry groups*, a PhD dissertation, University of the Philippines – Diliman, Philippines (2008).
[21] Ye, R.S., J. Ma, and H.L. Li. *Symmetric Tiling Patterns with the Extended Picard Group in Three-Dimensional Space*, in Advances in Computer Graphics, Lecture Notes in Computer Science Vol 4035/2006. Berlin: Springer Berlin / Heidelberg. 486 – 493 (2006).

Map-Colored Mosaics

Robert Bosch
Oberlin College
Oberlin, OH 44074
(bobb@cs.oberlin.edu)

Andrew Pike
Michigan State University
E. Lansing, MI 48824
(pikeand1@msu.edu)

Abstract

We describe how to construct map-colored mosaics. When viewed from afar, they resemble familiar images. When viewed from up close, they look like properly colored maps.

1 Introduction

After a long day of coloring maps, a cartographer might view a grid of squares (Figure 1(a)) as an uncolored map. To color this map, the cartographer would follow the traditional map-coloring protocol and assign colors to countries in such a way that no two countries (squares) that share a border (edge) receive the same color. The Four Color Theorem states that, at least in the plane, four colors suffice; never will the cartographer need more. When coloring a grid of squares, one needs only two colors, as in Figure 1(b). But with four (or more) colors, much more interesting and aesthetically pleasing results can be achieved. For example, with four colors a grid of squares might take on the likeness of the Mona Lisa's right eye, as in Figure 1(c).

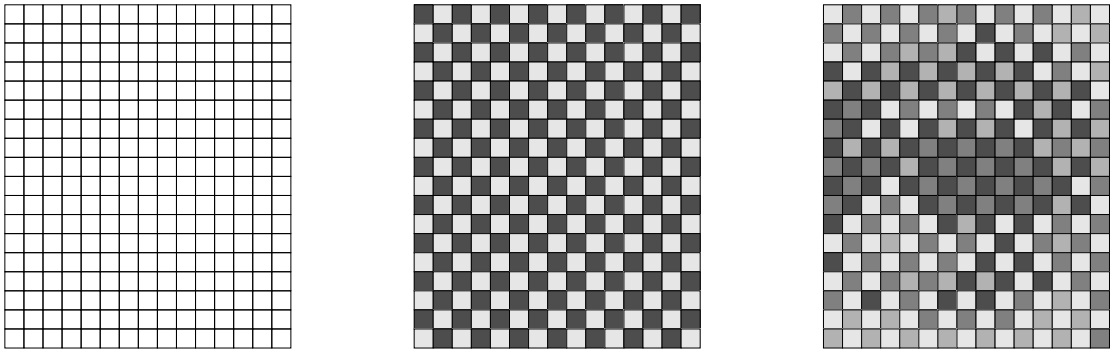

Figure 1: (a) an uncolored map, (b) colored with two shades of gray, (c) colored with four shades of gray

In this paper, we describe how to produce pictures like Figure 1(c). We call them *map-colored mosaics*. When viewed from afar, they resemble familiar images. When viewed from up close, they look like properly colored maps. In a properly colored map, no two countries that share a border can share a color. In a map-colored mosaic, no two tiles that share an edge can share a color.

2 The Map-Colored Mosaic Design Problem

We begin with a user-supplied target image, a map (a tiling of the plane with copies of one or more tiles), and a small set of colors (usually between four and eight). We first assume that our target image is in grayscale, our map is a grid of squares, and all of our colors are different shades of gray.

Furthermore, we assume that our target image consists of m rows and n columns of pixels and that our map is a grid that consists of m rows and n columns of squares. We denote the brightness of the row i, column j pixel—pixel (i, j)—by $\beta_{i,j} \in [0,1]$, where 0 stands for completely black, 1 stands for completely white, and intermediate values stand for intermediate shades of gray.

Finally, we assume that we only have χ colors. (We refer to them as colors even though they are just shades of gray.) We denote the brightness of color $c \in \{1,\ldots,\chi\}$ by b_c, using the same 0-to-1, black-to-white scale we use for the pixel brightnesses.

Our goal is to construct an $m \times n$ mosaic that (1) when viewed from afar, resembles the target image as much as possible, and (2) when viewed from up close, looks like a properly-colored map. To attain this goal, we use integer programming formulations as in [2-4].

3 A Simple Integer Programming Formulation

For each square (i, j) and each color c, we must decide if we will paint square (i, j) with color c. We model this with binary variables, setting $x_{i,j,c}$ equal to 1 if we do indeed paint square (i, j) with color c, and setting $x_{i,j,c}$ to 0 if we don't. We need a total of χmn such variables.

Given that we want our mosaic to resemble our target image as much as possible, we need to be able to measure our mosaic's "goodness of fit" with our target image. Our strategy is to compute a separate error term for each square of the mosaic and then add them all up. If we paint square (i, j) with color c, then it will have brightness b_c, whereas pixel (i, j) has brightness $\beta_{i,j}$. So one possible error term for square (i, j) is

$$\sum_{c=1}^{\chi} \left|b_c - \beta_{i,j}\right| x_{i,j,c},$$

and another is

$$\sum_{c=1}^{\chi} (b_c - \beta_{i,j})^2 x_{i,j,c}.$$

We use the first one, which gives us the goodness-of-fit measure

$$\sum_{i=1}^{m}\sum_{j=1}^{n}\sum_{c=1}^{\chi} \left|b_c - \beta_{i,j}\right| x_{i,j,c}$$

for our model's objective function.

To force ourselves to paint square (i, j) with precisely one color c, we incorporate the following equation into our model:

$$\sum_{c=1}^{\chi} x_{i,j,c} = 1.$$

We need a total of mn such equations.

To force ourselves to paint squares (i, j) and $(i, j+1)$ with different colors, we introduce, for each color $c \in \{1,\ldots,\chi\}$, the inequality

$$x_{i,j,c} + x_{i,j+1,c} \leq 1.$$

This inequality prohibits us from painting both square (i, j) and its right neighbor, square $(i, j+1)$, with color c. We need a total of $\chi m(n-1)$ such inequalities.

Similarly, to force ourselves to paint squares (i, j) and $(i+1, j)$ with different colors, we introduce, for each color $c \in \{1,\ldots,\chi\}$, the inequality

$$x_{i,j,c} + x_{i+1,j,c} \leq 1.$$

This inequality prevents us from painting both square (i, j) and its lower neighbor, square $(i+1, j)$, with color c. We need a total of $\chi(m-1)n$ such inequalities.

We end up with the following integer programming formulation:

$$\begin{aligned}
\text{minimize} \quad & z = \sum_{i=1}^{m} \sum_{j=1}^{n} \sum_{c=1}^{\chi} \left| b_c - \beta_{i,j} \right| x_{i,j,c} \\
\text{subject to} \quad & \sum_{c=1}^{\chi} x_{i,j,c} = 1 && \text{for each } 1 \le i \le m,\ 1 \le j \le n \\
& x_{i,j,c} + x_{i,j+1,c} \le 1 && \text{for each } 1 \le i \le m,\ 1 \le j \le n-1,\ 1 \le c \le \chi \\
& x_{i,j,c} + x_{i+1,j,c} \le 1 && \text{for each } 1 \le i \le m-1,\ 1 \le j \le n,\ 1 \le c \le \chi \\
& x_{i,j,c} \in \{0,1\} && \text{for each } 1 \le i \le m,\ 1 \le j \le n,\ 1 \le c \le \chi.
\end{aligned}$$

This formulation is simple and fast but yields low quality mosaics for small values of χ. Each of the mosaics displayed in Figure 2 was produced in a fraction of a second by CPLEX [8] on a 3.2 GHz Pentium IV PC.

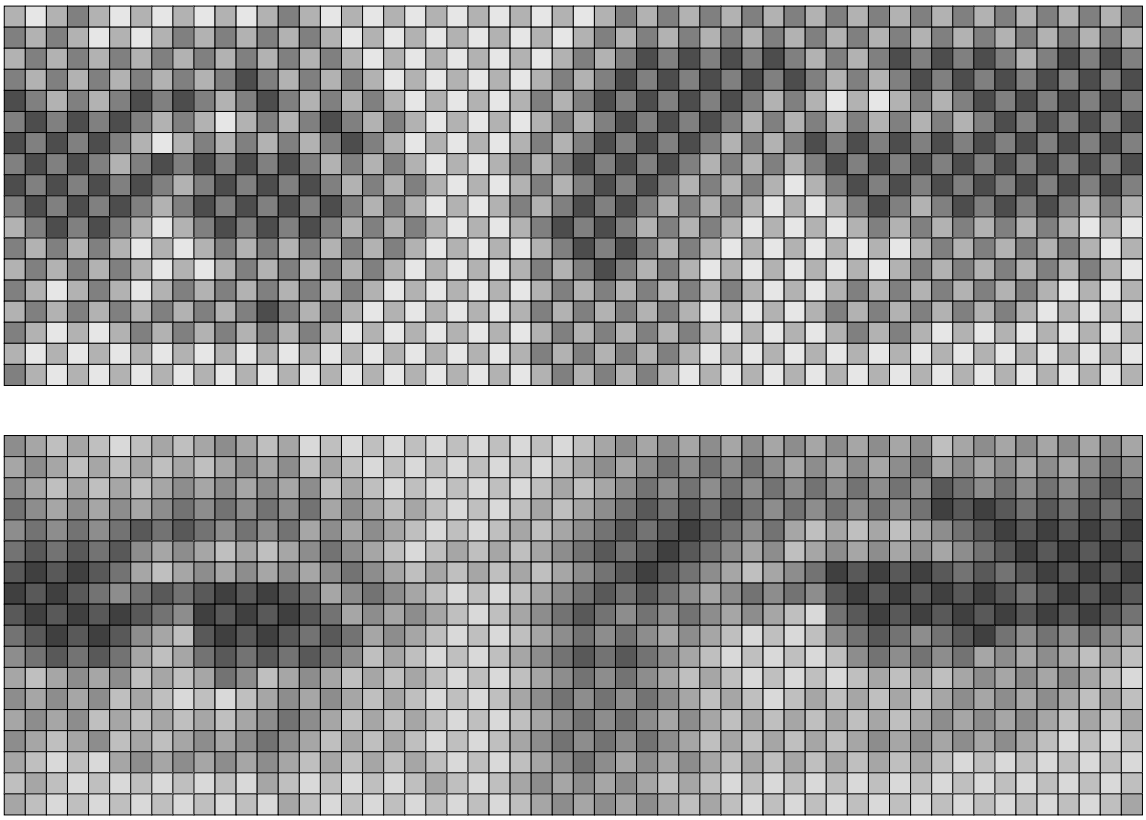

Figure 2: The Mona Lisa's Eyes, simple formulation ($m = 18$, $n = 54$) (a) $\chi = 4$, (b) $\chi = 8$

The four-color mosaic (Figure 2(a)) is recognizable, but crude. The eight-color mosaic (Figure 2(b)) achieves a better likeness. We encourage the reader to view both of these mosaics (and all of the others displayed in this paper) from two vantage points: from up close and from afar (e.g., from across the room).

4 An Alternate (Block) Formulation

The problem with the simple integer programming formulation is that it measures the mosaic's goodness of fit by comparing each individual square with its corresponding pixel. Recent research on matrix rounding and digital halftoning [1,5] suggests another approach: comparing each two-by-two block of squares with its corresponding two-by-two block of pixels.

Consider the $m \times n$ matrix M whose row-i, column-j entry gives the number of the color in the row-i, column-j position of our mosaic. Let $\mathscr{Q}$ equal the set of all 2×2 matrices that *could be* a 2×2 block of M. Note that $Q = \binom{q_{11}\ q_{12}}{q_{21}\ q_{22}} \in \mathscr{Q}$ if and only if each entry of Q belongs to $\{1, \ldots, \chi\}$ and no two adjacent entries are equal (in other words, $q_{11} \neq q_{12}$, $q_{11} \neq q_{21}$, $q_{12} \neq q_{22}$, and $q_{21} \neq q_{22}$).

In this formulation, for each $1 \leq i < m$, each $1 \leq j < n$, and each $Q = \binom{q_{11}\ q_{12}}{q_{21}\ q_{22}} \in \mathscr{Q}$, we set $y_{i,j,Q}$ equal to 1 if we place the upper-left corner of block Q in square (i, j), painting square (i, j) with color q_{11}, square $(i, j+1)$ with color q_{12}, square $(i+1, j)$ with color q_{21}, and square $(i+1, j+1)$ with color q_{22}. So, in this formulation, setting a variable equal to 1 paints an entire two-by-two block of squares. It turns out that we need a total of $[\chi(\chi-1)^2 + \chi(\chi-1)(\chi-2)^2](m-1)(n-1)$ such variables.

Here is our alternate (block) formulation:

$$\min \quad z = \sum_{i=1}^{m-1} \sum_{j=1}^{n-1} \sum_{Q \in \mathscr{Q}} \left| (b_{q_{11}} + b_{q_{12}} + b_{q_{21}} + b_{q_{22}}) - (\beta_{i,j} + \beta_{i,j+1} + \beta_{i+1,j} + \beta_{i,j+1}) \right| y_{i,j,Q} \tag{1}$$

$$\text{s.t.} \quad \sum_{Q \in \mathscr{Q}} y_{i,j,Q} = 1 \qquad \text{for each } 1 \leq i \leq m-1,\ 1 \leq j \leq n-1 \tag{2}$$

$$\sum_{\substack{Q \in \mathscr{Q}: \\ q_{12}=u,\, q_{22}=v}} y_{i,j,Q} = \sum_{\substack{R \in \mathscr{Q}: \\ r_{11}=u,\, r_{21}=v}} y_{i,j+1,R} \qquad \begin{array}{l}\text{for each } 1 \leq i \leq m-1,\ 1 \leq j \leq n-2, \\ \quad \text{and } 1 \leq u, v \leq \chi : u \neq v\end{array} \tag{3}$$

$$\sum_{\substack{Q \in \mathscr{Q}: \\ q_{21}=u,\, q_{22}=v}} y_{i,j,Q} = \sum_{\substack{R \in \mathscr{Q}: \\ r_{11}=u,\, r_{12}=v}} y_{i+1,j,R} \qquad \begin{array}{l}\text{for each } 1 \leq i \leq m-2,\ 1 \leq j \leq n-1, \\ \quad \text{and } 1 \leq u, v \leq \chi : u \neq v\end{array} \tag{4}$$

$$y_{i,j,Q} \in \{0,1\} \qquad \text{for each } 1 \leq i \leq m-1,\ 1 \leq j \leq n-1,\ Q \in \mathscr{Q}.$$

The objective function, (1), measures goodness of fit by comparing the total brightness of each two-by-two block of squares ($b_{q_{11}} + b_{q_{12}} + b_{q_{21}} + b_{q_{22}}$) with the total brightness of the corresponding two-by-two block of pixels ($\beta_{i,j} + \beta_{i,j+1} + \beta_{i+1,j} + \beta_{i,j+1}$). The type (2) equations make sure that we paint each and every two-by-two block of squares, and the type (3) and (4) equations make sure that we paint the two-by-two blocks in such a way that they overlap with each other both horizontally and vertically.

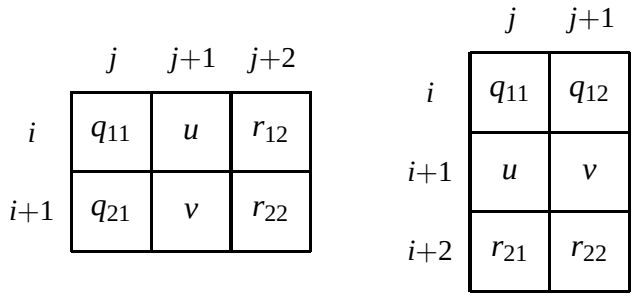

Figure 3: (a) horizontal overlapping, (b) vertical overlapping.

When thinking about the type (3) equations it helps to consider Figure 3(a), and when thinking about the type (4) equations, it helps to consider Figure 3(b). The left-hand side of a type (3) equation counts how many blocks Q of the form $\binom{q_{11}\ u}{q_{21}\ v}$ we place in square (i, j). The right-hand side counts how many blocks R of the form $\binom{u\ r_{12}}{v\ r_{22}}$ we place in square $(i, j+1)$. Note that each side is either 0 or 1 (due to the type (2)

equations and the fact that the variables are binary.) By setting the left-hand and right-hand sides equal, we force the blocks to overlap horizontally.

The block formulation does have its drawbacks. It is certainly harder to understand. It has many more variables and constraints than the simple formulation (on the order of χ^3 times the number of variables, and on the order of χ times the number of constraints). And it is slow. It is so large that to solve it, we had to divide the problem into sections, creating a dozen columns of the mosaic at a time. Still, the advantage of the block formulation is that it produces high quality mosaics even for small values of χ. The four-color mosaic displayed in Figure 4 (which required about a minute for CPLEX) is much nicer than the one in Figure 2(a). In fact, we strongly prefer it to the eight-color mosaic displayed in Figure 2(b). It uses half the number of colors, yet when viewed from a distance, it still achieves a better likeness of the target image.

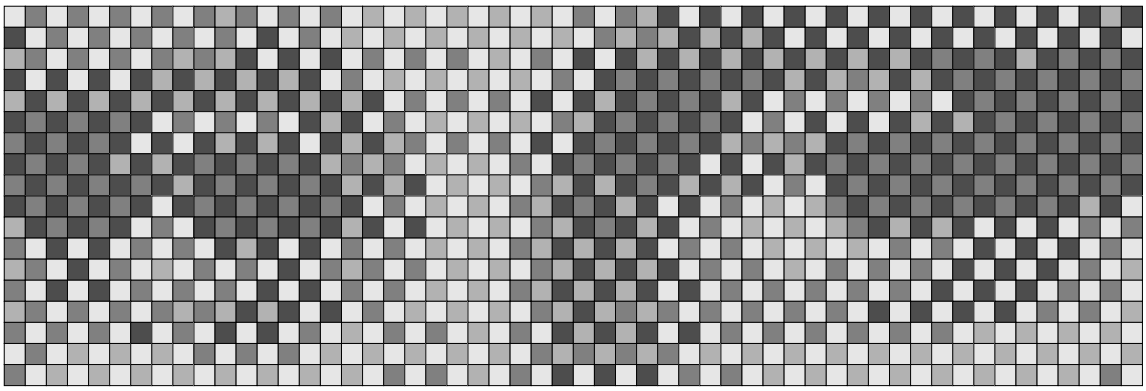

Figure 4: The Mona Lisa's Eyes, block formulation ($m = 18$, $n = 54$, $\chi = 4$)

5 Modifying the Mosaic

Once we have created a map-colored mosaic that pleases us, we can modify it by replacing its square tiles with other tiles that behave like squares. By doing this, we obtain images that are reminiscent of Escher-like tessellations [6,10] or Huff-like parquet deformations [7,9] when viewed from up close, yet still look like familiar images when viewed from a distance. See Figures 5 and 6.

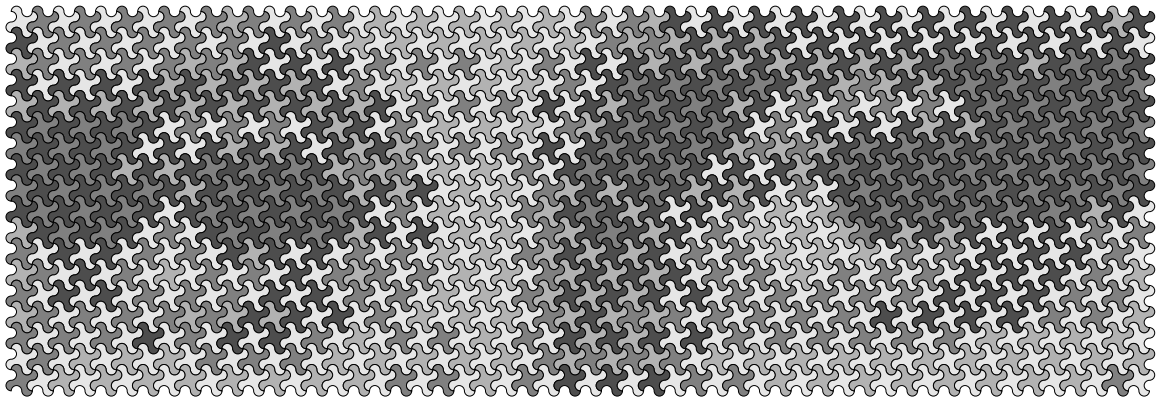

Figure 5: The Mona Lisa's Eyes, block formulation, propeller tiles ($m = 18$, $n = 54$, $\chi = 4$)

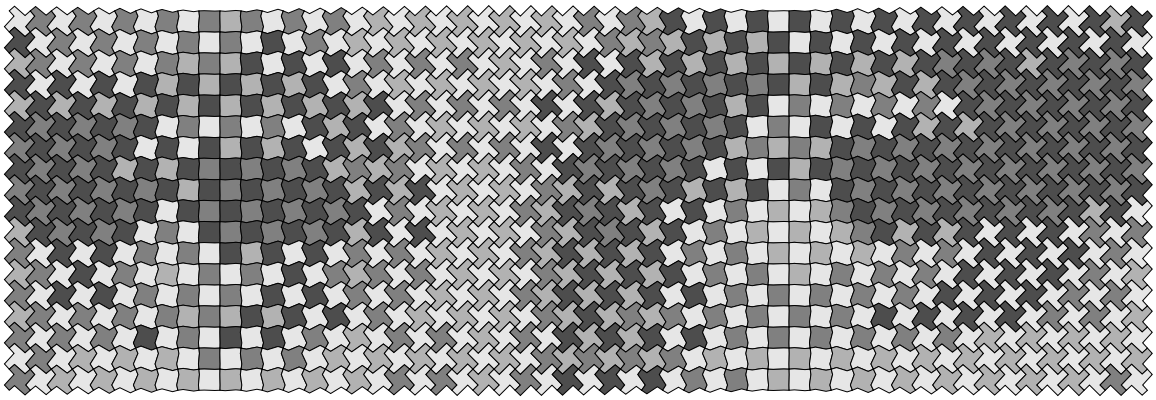

Figure 6: The Mona Lisa's Eyes, block formulation, parquet deformation ($m = 18$, $n = 54$, $\chi = 4$)

6 Other Tilings

One can adapt both the simple and block formulations for non-square tilings based on hexagons, equilateral triangles, rhombuses, etc., but it is usually much easier to adapt the simple formulation. Figure 7 displays a six-color map-colored mosaic, based on a hexagonal tiling, that we created by solving a hexagonal version of the block formulation. Figures 8-10 display what happens when we replace the hexagons with pinwheels, a Mongolian three-pronged arrow design, and Escher-like lizards.

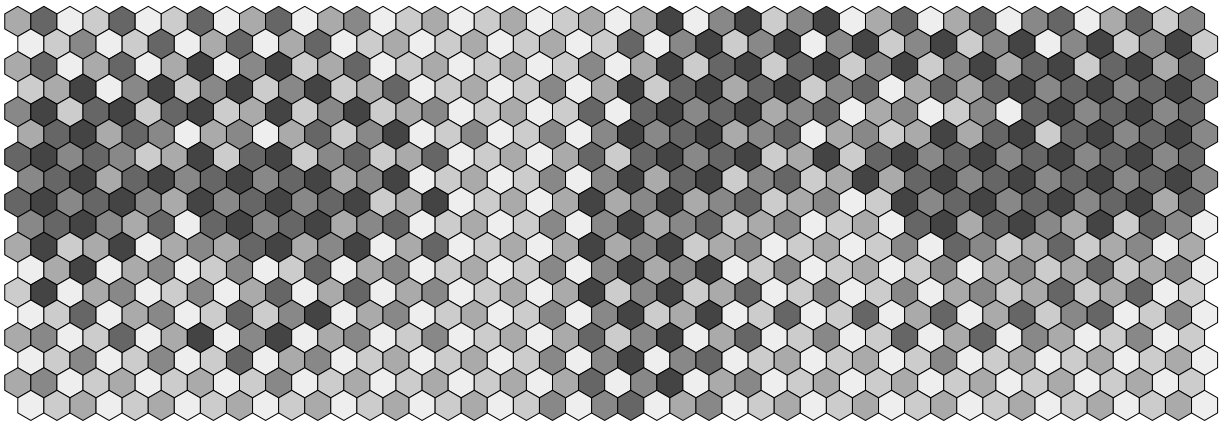

Figure 7: The Mona Lisa's Eyes, block formulation, hexagons ($\chi = 6$)

7 Color

It is also possible to adapt the formulations so that they work with different color palettes. The main difficulty is that the user needs to specify the color palette in advance. A palette that works well for one target image may fail spectacularly for another. See Figure 11 for a successful example.

References

[1] Tetsuo Asano, Naoki Katoh, Koji Obokata, and Takeshi Tokuyama. Matrix rounding under the L_p-discrepancy measure and its application to digital halftoning. *SIAM Journal on Computing*, 32: 1423-1435, 2003.

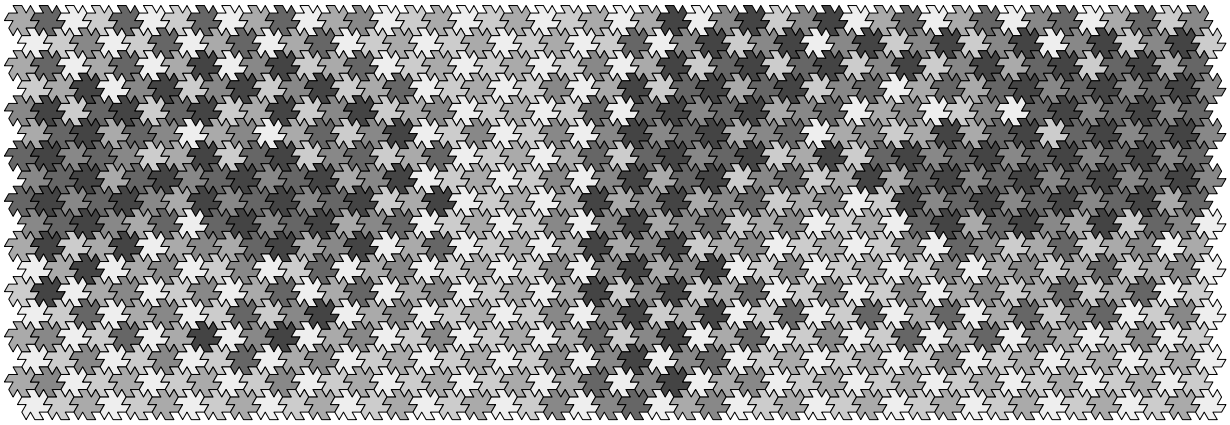

Figure 8: The Mona Lisa's Eyes, block formulation, pinwheels ($\chi = 6$)

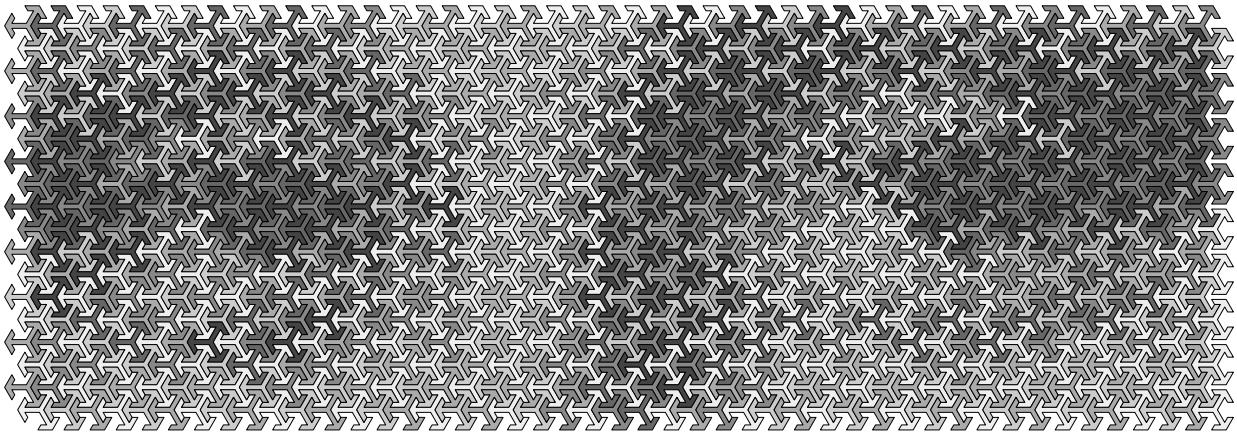

Figure 9: The Mona Lisa's Eyes, block formulation, arrows ($\chi = 6$)

[2] Robert Bosch. Constructing domino portraits. In B. Cipra et al., editor, *Tribute to a Mathemagician*, pages 251-256, A.K. Peters, 2004.

[3] Robert Bosch. Opt Art. *Math Horizons*, pages 6-9, feb 2006.

[4] Robert Bosch. Edge-constrained tile mosaics. In *Bridges Donostia: mathematical connections in art, music, and science*, pages 351-360, 2007.

[5] Benjamin Doerr. Nonindependent randomized rounding and an application to digital halftoning. *SIAM Journal on Computing* 34: 299-317, 2004.

[6] M.C. Escher. *Escher on Escher: Exploring the Infinite.* Henry N. Abrams, 1989.

[7] Douglas R. Hofstadter. *Metamagical Themas: Questing for the Essence of Mind and Pattern.* Basic Books, 1985.

[8] ILOG CPLEX. High-performance software for mathematical programming and optimization. `www.ilog.com/products/cplex/`.

[9] Craig S. Kaplan. Metamorphosis in Escher's art. In *Bridges Leeuwarden: mathematical connections in art, music, and science*, pages 39-46, 2008.

[10] Doris Schattschneider. *M.C. Escher: Visions of Symmetry.* Henry N. Abrams, second edition, 2004.

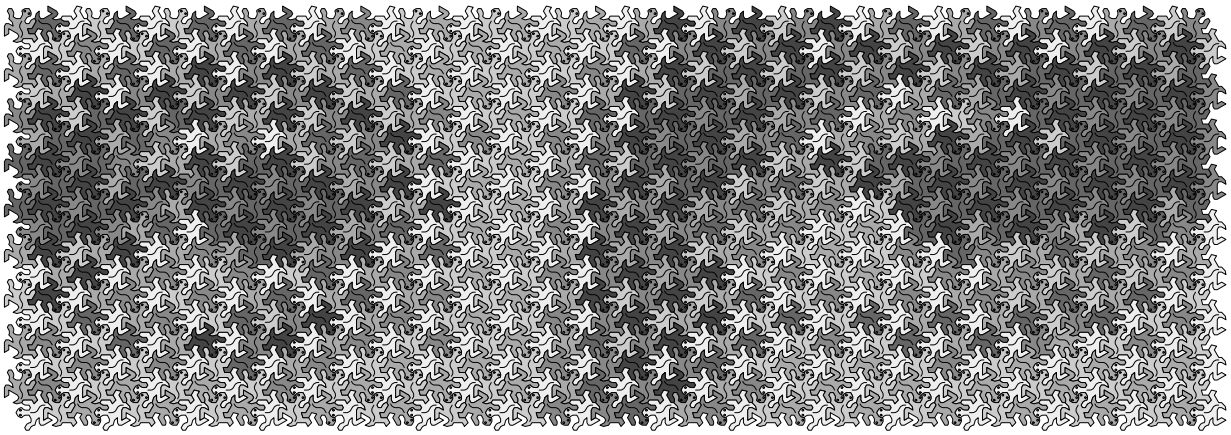

Figure 10: The Mona Lisa's Eyes, block formulation, lizards ($\chi = 6$)

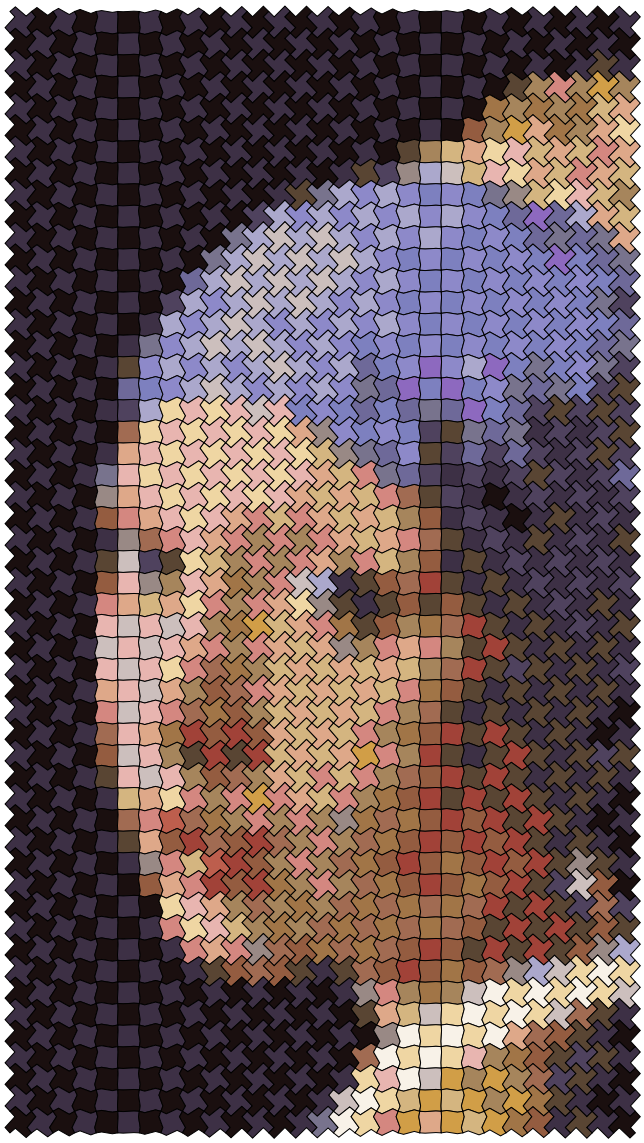

Figure 11: Girl With A Pearl Earring, simple formulation, parquet deformation ($\chi = 25$)

The Eleven–Pointed Star Polygon Design of the *Topkapı Scroll*

B. Lynn Bodner
Mathematics Department
Cedar Avenue
Monmouth University
West Long Branch, New Jersey, 07764, USA
E-mail: bodner@monmouth.edu

Abstract

This paper will explore an eleven-pointed star polygon design known as Catalog Number 42 of the *Topkapı Scroll*. The scroll contains 114 Islamic architectural and ornamental design sketches, only one of which produces an eleven-pointed star polygon. The design also consists of "nearly regular" nine-pointed star polygons and irregularly-shaped pentagonal stars. We propose one plausible "point-joining" compass-and-straightedge reconstruction of the repeat unit for this highly unusual design.

Introduction

The *Topkapı Scroll,* thought to date from the 15th or 16th century (and so named because it is now housed at the Topkapı Palace Museum Library in Istanbul), is a 96-foot-long scroll containing 114 Islamic architectural and ornamental design sketches. Believed to be the earliest known document of its kind (and also the best-preserved), most of the sketches in this manual show only a small portion, or *repeat unit,* of an overall pattern, contained, for the most part, within a square or rectangle. Thus, to achieve the entire pattern, these repeat units may be replicated by reflection across the boundaries of the rectangles or by rotation about the vertices of the squares. Since this scroll contains no measurements or accompanying explanations for the creation of these idealized Islamic patterns, it is believed by Harvard professor Gülru Necipoğlu, the recognized authority on the scroll and the author of *The Topkapı Scroll – Geometry and Ornament in Islamic Architecture: Topkapı Palace Museum Library MS H. 1956,* that the drawings most likely "served as an *aide-memoire* for architects and master builders who were already familiar through experience with the coded graphic language used in them" [1, pages 10-12].

How, then, using only the traditional drafting tools of the medieval period – the compass, straightedge, and set square [1, page 138] – were the original patterns (from which the repeat units were generated) conceptualized and created? More specifically, how did the designer of the only eleven-pointed star polygon pattern of the *Topkapı Scroll* (known as Catalog Number 42 or CN42 for short) determine, without mensuration, the proportion and placement of the polygons comprising the design? Some hints for answering this question are provided by the scroll itself. This paper will explore these and propose one plausible "point-joining" compass-and-straightedge reconstruction of the repeat unit for this very rare design.

Topkapı Scroll, Catalog Number 42

The original repeat unit for CN42 was drawn in black ink on cream-colored rag paper [1, page 29], a facsimile of which is reproduced in [1, page 309]. The author's reproduction of CN42, made by tracing the image and producing its copy using the *Geometer's Sketchpad* software program [2]), is shown in

Figure 1a. The repeat unit contains two halves of eleven-pointed star polygons along its vertical edges and two halves of nine-pointed star polygons along its horizontal edges. Between the half-star polygons are eight irregularly-shaped pentagonal stars and two arrow-like polygons. Underlying the black-inked drawing of CN42's repeat unit are faintly embossed "dead" construction lines, scratched on the paper with a pointed tool such as a compass or stylus "so as not to detract from the inked patterns they generate" [1, page 31]. **Figure 1b,** which is a reconstruction of what appears on page 255 of [1], shows the inked pattern (as dashed line segments) superimposed on the uninked "dead" construction lines (in bold). Note that all of the star polygons (the "nearly regular" nine- and eleven-stars as well as the irregularly shaped pentagonal ones) drawn in black ink in Figure 1 are constructed using inscribed and circumscribed circles. The remaining polygonal shapes may be achieved by joining certain intersection points with line segments in such a way that the uninked "dead" lines do form the basis for most of the pattern. Also, notice that the pattern in the repeat unit has 180 degree rotational symmetry about the center of the rectangle. This is useful in the construction of the pattern.

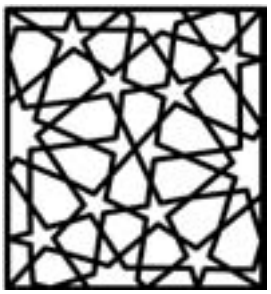

Figure 1a. *Author's reconstruction, of CN42 [1, p 309] produced using the Geometer's Sketchpad software*

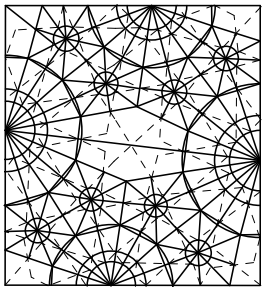

Figure 1b. *Author's reconstruction of the overlay for CN42 [1, p 255] produced using the Geometer's Sketchpad*

The repeat unit of the *Topkapı Scroll's* only eleven-pointed star polygon design is extraordinary for several reasons. First, the vast majority of Islamic star designs have an even number of points, and CN42 has none of these. Second, the repeat unit contains both nine- and eleven-pointed star polygons, presumably created from an underlying grid consisting of nine-gons and eleven-gons. As discussed in more detail in the next section, neither nine-gons nor eleven-gons are *constructible* using the traditional drafting tools of straightedge and compass, so most likely an approximation was utilized to create them. Third, the position of the stars in the repeat unit is remarkable as well. Usually the major stars appear centered at either corner vertices or at the midpoints of the edges in the repeat units of Islamic star patterns in the *Topkapı Scroll*. But for CN42, the centers of the large stars are not located in these standard positions.

Constructing Star Polygon Designs Inscribed within Regular Polygons

One of the most straightforward techniques for creating geometric "heavenly star" patterns found throughout the Islamic world (and for which there is evidence that this method was used [3]) is to initially construct an n-gon (a polygon with n sides) and then draw in the corresponding regular n-pointed star polygon by methodically joining the vertices of the n-gon with line segments (diagonals) or by methodically joining midpoints of the n-gon's edges. For example, every second vertex of a regular pentagon is connected with line segments to form the regular pentagonal star polygon shown in **Figure 2a** on the following page. By connecting alternate midpoints of edges of the same regular pentagon, a smaller regular pentagonal star polygon is formed, as shown in **Figure 2b**. Similarly, star polygons with n points may be created within any n-gon, where every second (or third or fourth or k^{th}, where $2 \le k \le n/2$) vertex (or midpoint) is connected.

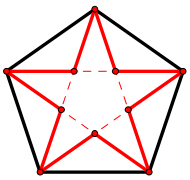

Figure 2a.

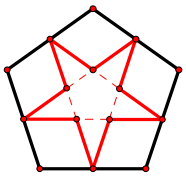

Figure 2b.

The most common geometric regular star polygon designs have n points where, n is 4, 5, 6, 8, 10, 12, 15, 16, 20, 24, and so on. It should be noted that these regular n-gons are *constructible* in the Euclidean sense; that is, they may be constructed using only a compass and straightedge. For n = 7, 9, 11, 13, 14, 18…, the regular n-gons (and likewise, the corresponding regular n-star polygons) may only be constructed approximately using these tools. Of these *non-constructible* star polygons, master builders in the eastern regions of the Islamic world did regularly create star patterns with n = 7, 9, 14 and 18.

Construction of a Nearly Regular Eleven-Sided Polygon and its Inscribed Star Polygon

One way to construct a very good approximation of a regular eleven-gon is to follow the method that the author adapted from an origami folding procedure [4]. (For those interested in the mathematics behind this construction, the angle constructed may be calculated to be 0.4 arctan(7), based on a double approximation – first that π is approximately equal to 22/7 and second, that tan (π/22) is approximately 1/7 for small angles. For more information see [4].)

Starting with a square, construct a diagonal and its midpoint. Then draw a line segment from the midpoint to one of the remaining vertices of the square (**Figure 3a**). Bisect this segment with a perpendicular line segment that terminates on the edges of the square (**Figure 3b**). Repeat this procedure twice more so that there are now three perpendicular segments parallel to the diagonal as shown in **Figure 3c.** Now draw a line segment from the midpoint of the square's diagonal to one of the endpoints of the perpendicular line segment constructed last. This segment and one of half of the square's diagonal form an obtuse angle, shown in **Figure 3d**. Bisect this angle as shown in **Figure 3e**. This angle bisector and the line segment that is the other half of the square's diagonal form a second obtuse angle (**Figure 3f**).

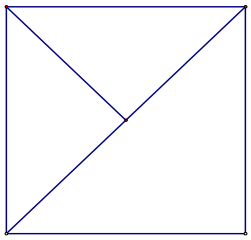

Figure 3a.

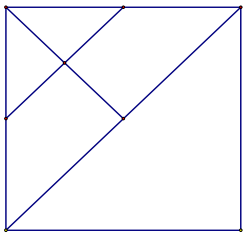

Figure 3b.

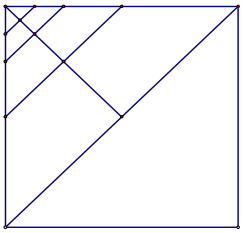

Figure 3c.

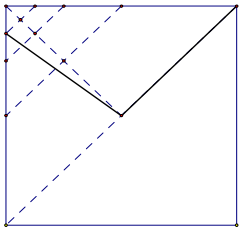

Figure 3d.

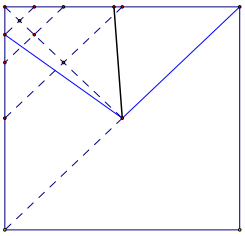

Figure 3e.

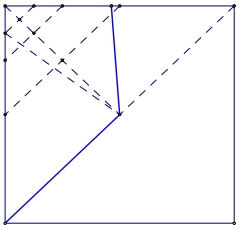

Figure 3f.

Bisect this angle as shown in **Figure 3g,** then bisect the angle that is formed by this second angle bisector and the same segment of the square's diagonal, as shown in **Figure 3h.** The resulting angle (shown in **Figure 3i**) measures approximately 32.733 degrees (as measured by the *Geometer's Sketchpad* software program), which is roughly one-eleventh of a circle's angular measure. (One-eleventh of 360 degrees is exactly 32.727272… degrees, or approximately 32.723 degrees, hence the measure of this constructed angle differs by only one hundredth of a degree from the exact central angle measure.)

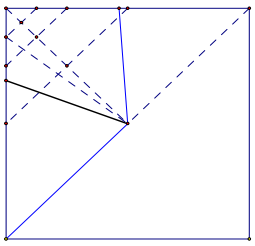

Figure 3g.

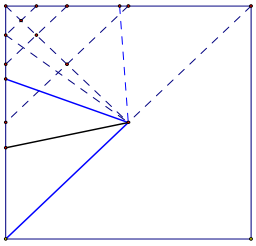

Figure 3h.

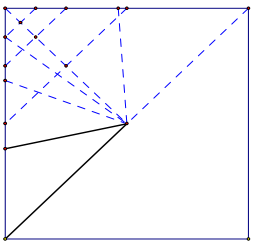

Figure 3i.

Once we have the requisite angle we may replicate it to form an eleven-spoked circle (**Figure 4a**) which leads to the construction of the inscribed eleven-gon (**Figure 4b**). Constructing the midpoints of the eleven-gon's edges (and erasing the circumscribing circle) yields the image in **Figure 4c**.

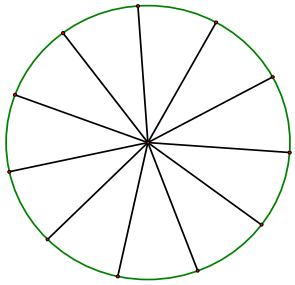

Figure 4a.

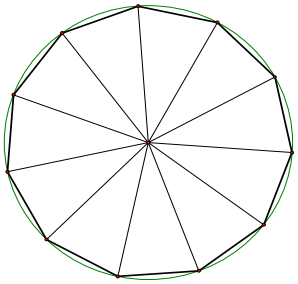

Figure 4b.

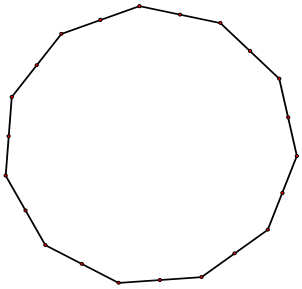

Figure 4c.

The construction of the eleven-pointed star polygon is now straightforward. Connect every 9th point along the perimeter (there are 22 points – 11 vertices and 11 midpoints) as shown in **Figure 4d**. This produces a 22-pointed star, but highlighting every other point, as shown in **Figure 4e** and erasing the remaining dashed line segments yields the eleven-pointed star polygon with the same proportions as those found in the repeat unit of CN42 (**Figure 4f**).

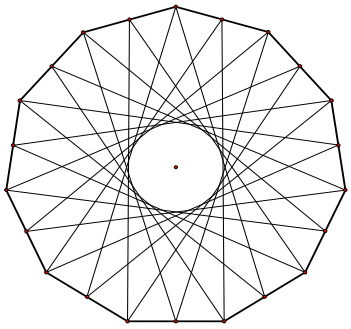

Figure 4d.

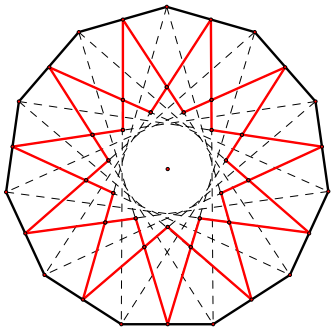

Figure 4e.

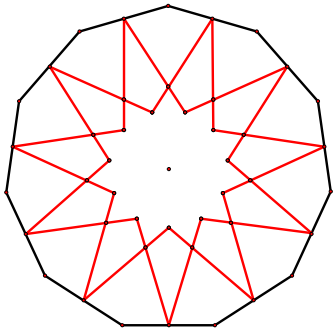

Figure 4f.

A Plausible Construction of the Original Eleven- and Nine-pointed Star Polygon Design

Now that we have constructed a "nearly regular" eleven-pointed star polygon inscribed within an eleven-gon and a circle, we may use this to recreate a very close approximation of the repeat unit shown in CN42 of the *Topkapı Scroll*. Start with a horizontal ray and a vertical ray meeting at a common vertex. These rays will define the top and right edges of the repeat unit rectangle. Construct two congruent circles of any radius, the first centered at the top right corner of the rectangle, and the second tangent to the first circle and centered on the right edge of the rectangle, shown in **Figure 5a**. Construct the eleven-pointed star polygon within the second circle using the method described previously (**Figure 5b**). Now construct three equispaced rays emanating from the center of that polygon by using existing intersection points, as shown in **Figure 5c**.

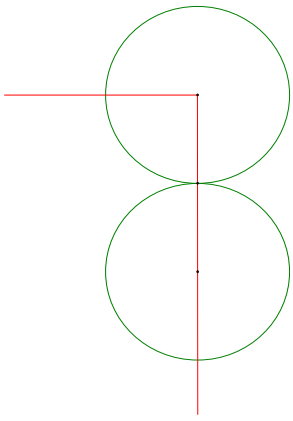

Figure 5a.

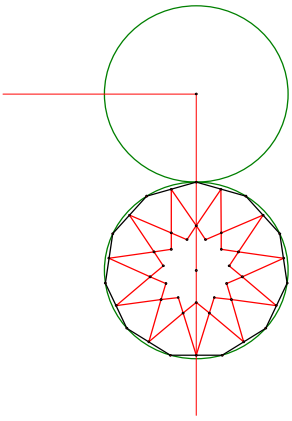

Figure 5b.

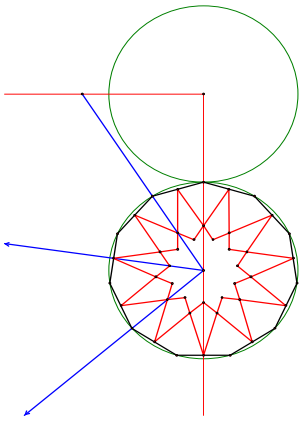

Figure 5c.

The top constructed ray intersects the top of the rectangle. From that intersection point, construct a line perpendicular to the constructed middle ray, as shown in **Figure 5d**. This perpendicular line segment intersects both the middle and lower constructed rays. At the lower intersection point, construct a line parallel to the top edge of the rectangle; this defines the lower edge of the rectangle. The intersection of the perpendicular with the middle ray is the center of the rectangle. With this point as center, construct a circle through the center of the eleven-gon; this circle intersects the middle ray. At that point of intersection, construct a line parallel to the right edge of the rectangle, completing the rectangle (**Figure 5e**). This point of intersection is also the center of the second star eleven-gon, which can be constructed as before (**Figure 5f**). These last two steps exploit the 180 degree rotation symmetry of the repeat unit.

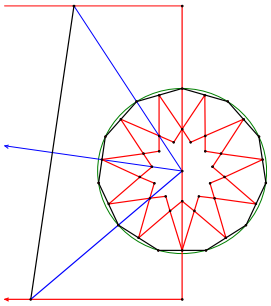

Figure 5d.

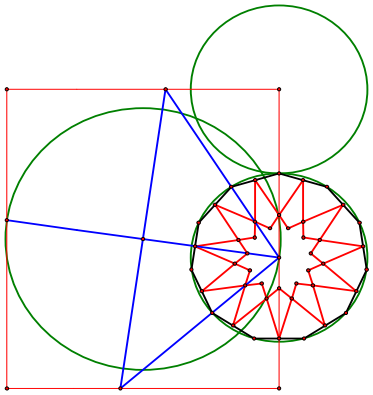

Figure 5e.

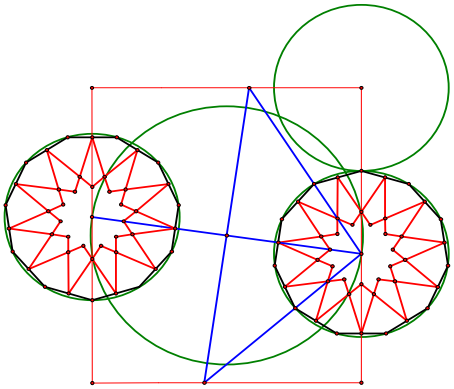

Figure 5f.

Erasing the circles, their inscribed eleven-gons, and the halves of the star eleven-gons outside the repeat unit and constructing two additional line segments from the center of the left eleven-star to the points of intersection of the diagonal with the upper and lower edges of the rectangle yields a repeat unit partially filled with two halves of star eleven-gons and a large rhombus touching each side of the rectangle (**Figure 6a)**. Next bisect the four angles that are formed by the upper edge of the rectangle, the two upper edges and the diagonal of the rhombus (**Figure 6b**). Extend the upper edges of the eleven-stars that are parallel to the edges of the rhombus until they intersect the upper edge of the repeat unit. The point where these lines intersect the long diagonal of the rhombus define the radius of a semicircle centered at the endpoint of that diagonal (**Figure 6c**).

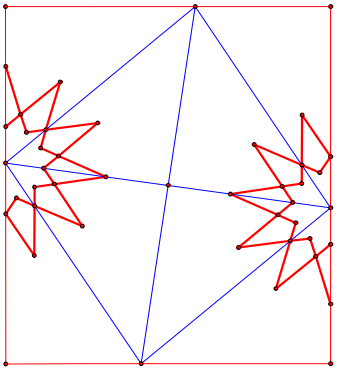

Figure 6a.

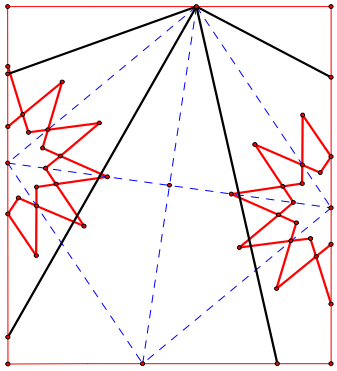

Figure 6b.

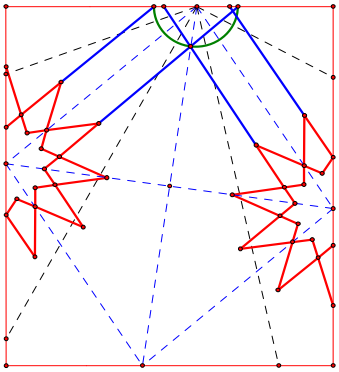

Figure 6c.

The points where the angle bisectors intersect these new line segments define the radii of two additional semicircles, both concentric with the one just created (**Figure 6d**). These three semicircles will be used to construct half of the nine-pointed star polygon. Constructing line segments between certain points on the three semicircles and extending two existing segments that are parallel to the diagonal of the rhombus yields two half nine-star polygons, one within the other (**Figure 6e**). After erasing these semicircles and some segments, construct a line segment from the upper right corner of the rectangle to the midpoint of the long diagonal of the rhombus. The point where this segment intersects the right upper edge of the rhombus defines the radii of two new tangential semicircles, a large one centered at the eleven-star and the smaller one centered at the nine-star. The smaller semicircle also intersects the upper left edge of the rhombus thereby defining the radius of a second larger semicircle centered about the other eleven-star. Construct a line segment through this new point from the midpoint of the long diagonal to the edge of the rectangle. The point where this line intersects the upper segment parallel to the upper left edge of the rhombus defines a second semicircle centered about the nine stars, but slightly smaller (**Figure 6f**).

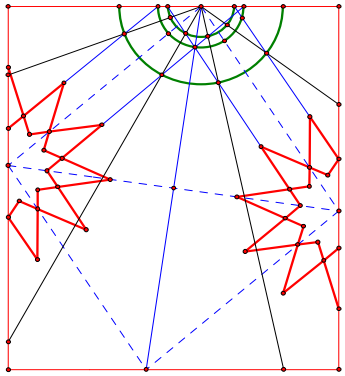

Figure 6d.

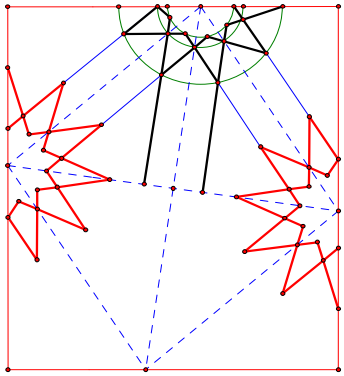

Figure 6e.

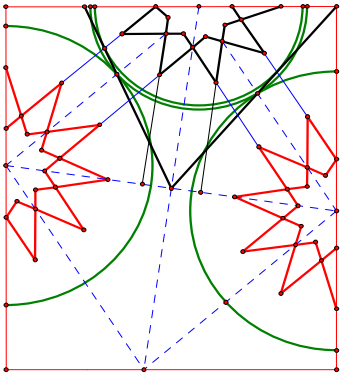

Figure 6f.

To complete the rosettes of the nine-star construct a line from the center of the right eleven-star to the upper left corner of the rectangle. Construct a second line from the center of the left eleven-star through the point of tangency between the two semicircles to the right of the diagonal. Join existing points of intersection between segments and semicircles and extend line segments to produce half of the nine-star rosette (**Figure 7a**). After erasing the now-dispensable semicircles and line segments, construct an additional semicircle, centered about the right eleven-star and defined by the point of intersection between the segment connecting the upper right corner with the midpoint of the rectangle and the innermost segment parallel to the upper right edge of the rhombus. Similarly, a congruent semicircle may also be constructed centered about the left eleven-star. By extending segments and joining existing points, the outlines of the pentagonal stars and the rosettes of the eleven-star rosettes begin to form (**Figure 7b**). Extend two additional segments to construct the upper halves of the two arrow-shaped polygons in the center of the rectangle (**Figure 7c**).

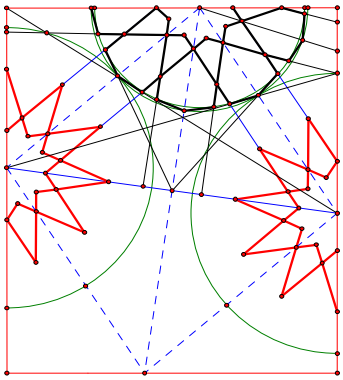

Figure 7a.

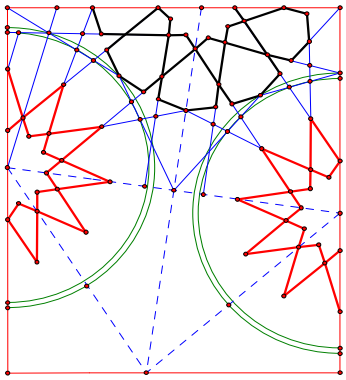

Figure 7b.

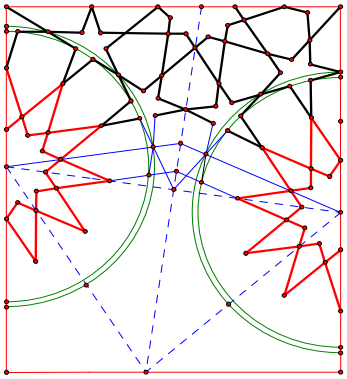

Figure 7c.

Figures 7d and **7e** show the upper half of the repeat unit before and after the now unnecessary semicircles and line segments are erased. To construct the lower half of the repeat unit, replicate the procedure previously described and illustrated by **Figures 6b – 7e,** thereby taking advantage of the two-fold rotational symmetry of the repeat unit. The completed repeat unit design is shown in **Figure 7f**.

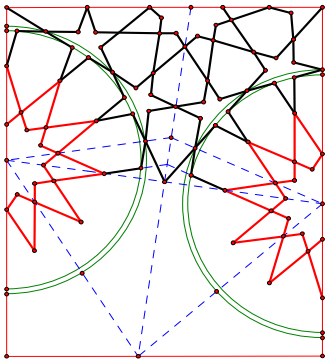

Figure 7d.

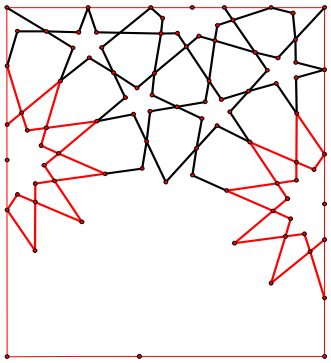

Figure 7e.

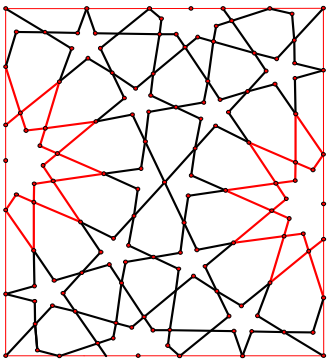

Figure 7f.

A colored rendition of sixteen copies of the repeat unit, replicated by reflection across the rectangle's edges, is provided in **Figure 8** on the next page. The symmetry of the pattern is unusual, with obvious vertical reflection mirrors bisecting the large eleven-stars, and horizontal reflection mirrors bisecting the smaller nine-stars. But, the 180 degree rotation centers at the corners and the center of the repeat units induce horizontal and vertical glide-reflections as well. The symmetry group of the pattern is *cmm*.

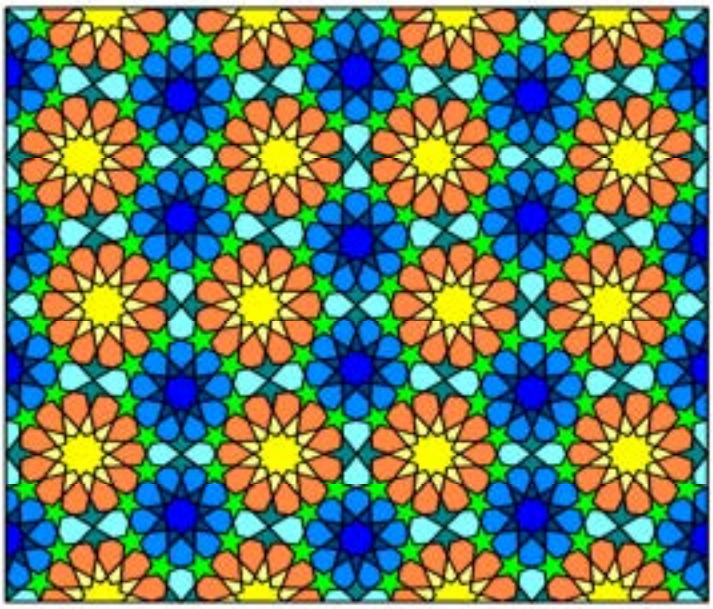

Figure 8. *Sixteen copies of the repeat unit, colored and replicated by reflection across the rectangle's edges*

Discussion

CN42 is the only idealized recorded pattern in the *Topkapı Scroll* containing eleven-pointed star polygons; there are no other such recorded pattern templates of which the author is aware. There are no eleven-pointed star polygons to be found in two rich published sources of Arabic geometric designs: Bourgoin's manual of 190 Islamic patterns, *Arabic Geometrical Pattern and Design* [5], and David Wade's collection of over 4000 images, now online [6]. Clearly CN42 is a very rare pattern.

Acknowledgements

The author is indebted to the reviewers for their useful comments and suggestions for improvement.

References

[1] Necipoğlu, Gülru (1995). *The Topkapı Scroll – Geometry and Ornament in Islamic Architecture: Topkapı Palace Museum Library MS H. 1956,* Santa Monica, California: The Getty Center for the History of Art and Humanities.
[2] The *Geometer's Sketchpad* software program, available at http://www.keypress.com.
[3] Bodner, B. L. (2008). "Hankin's 'Polygons in Contact' Grid Method for Recreating a Decagonal Star Polygon Design," *Bridges: Mathematical Connections in Art, Music, and Science Conference Proceedings*.
[4] Dutch, Steven. (2009) *11-Pointed Star: Approximate,* available at http://www.uwgb.edu/DutchS/RECMATH/Star11Approx.HTM.
[5] Bourgoin, J. (1973). *Arabic Geometrical Pattern and Design,* Dover Publications. Original 1879.
[6] Pattern in Islamic Art: The Wade Photo Archive, available at http://www.patternsinislamicart.com

Composite Digital Mosaics using Duotone Tiles

Gary R. Greenfield
Department of Mathematics & Computer Science
University of Richmond
Richmond, VA 23173, USA
ggreenfi@richmond.edu

Abstract

We describe a method for combining a foreground image and a background image to make digital mosaics using duotone tiles. Unlike the tiles of thumbnail images used in photomosaics, our duotone tiles each consist of precisely two colors. Our method uses diffusion limited aggregation (DLA) to approximate via a curve the foreground image which is then composited over a pixellated enlargement of the background image.

1 Introduction

The current popularity of digital mosaics is surely due to the success of Silvers' well publicized, and widely marketed, Photomosaic technique [11]. Computer generated mosaics such as those by computer artist Robert Bosch that rely on sophisticated optimization algorithms [1] continue to advance the state of the art.

An ongoing challenge in digital mosaics is to make the resulting imagery more visually exciting by, for example, embedding messages, motifs, or subliminal images. The original Photomosaic technique of Silvers accomplishes this to a limited extent by (1) constructing high resolution mosaics, (2) using a large database of tiles, and (3) using a database all of whose images have the same thematic content. However, if we restrict ourselves to working with small sets of tiles as in the case of the domino mosaics of Knowlton [5], Knuth [6] and Bosch, or the automatically generated sets of grayscale tiles used in the photomosaics of Sah et al. [10], this issue becomes more problematic. Figure 1 shows two examples using small sets of tiles: a Mona Lisa domino mosaic portrait by Robert Bosch, and Andrew Pike's 2007 "Sierpinski Carpet", a high resolution portrait mosaic whose tiles were induced from gray scale versions of the Sierpinski carpet. Our goal is composite a background image and a foreground image into a digital mosaic in such a way as to make the background image almost subliminal. Further we would like to reduce the number of colors, and hence tiles, required.

Our approach to bringing multiple images into play for digital mosaics while simultaneously restricting the set of tiles that can be used is new in two significant ways. First, rather than drawing from only a small set of tiles, we use *duotone* tiles meaning each tile contains a pair of distinct colors. Second, the foreground image overlaid on our background image is approximated thanks to the use of simulated diffusion limited aggregation (DLA) by a continuous curve. Thus our overlay technique bears some similarity to the TSP art of Kaplan and Bosch [4], or the space filling curve mosaics of Knowlton (see http://www.knowltonmosaics.com/). We remark at the outset that the inspiration for our technique stems from a series of prints by I. Orosz exhibited at Bridges 2008 and reproduced in that exhibition pamphlet [9]. Online examples [12] of Orosz' prints of this type include the etchings "Dürer in the Forest" and "Dalí and the Holy Family." The most closely related work to ours that we are aware of appears in the thesis of Long [8]. Long explored the use of diffusion limited aggregation for special effects in commercial and representational imagery.

Stated formally, our task is to digitally composite two low resolution identically sized $m \times n$ images — a background image and a foreground image — in such a way as to produce a duotone tile digital mosaic. Since our results are reproduced here in grayscale we will focus on a limited number of examples. Figure 2 shows the Tanzanian sunset image, East African giraffe image, and author's portrait image we will use in

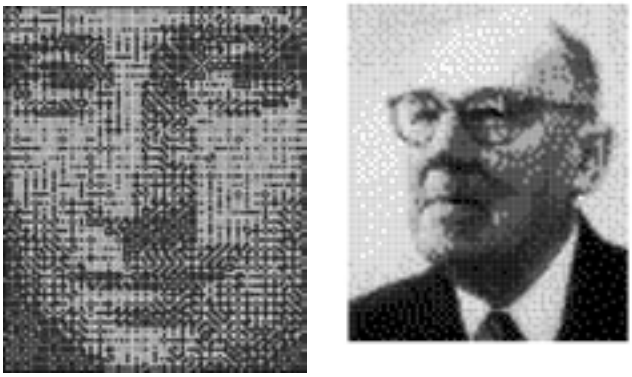

Figure 1: Left: Domino mosaic portrait of the Mona Lisa by Robert Bosch. Right: "Sierpinski Carpet" by Andrew Pike. Reprinted with permission.

this paper. Figure 3 shows the two duotone composites we obtained with the sunset and giraffe alternating as both foreground and background. To create them we cropped and downsampled the sunset and giraffe images to yield low resolution 70×52 pixel images. Downsampling reduces the number of colors we have to work with. Each duotone tile in these two composites is 21×21 pixels.

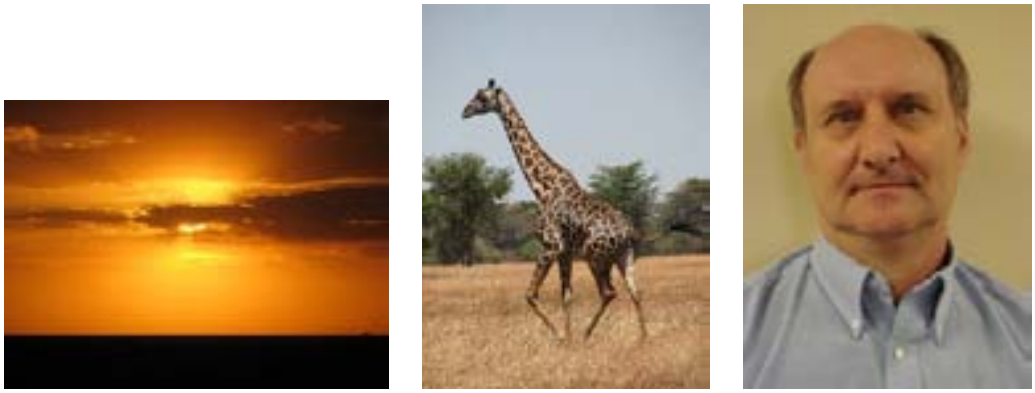

Figure 2: Left: Tanzanian sunset image. Center: East African giraffe. Right: Author's portrait.

2 Overview of the method

The "background mosaic" is simply a pixellated version of the background image. It is obtained by expanding each pixel of the low resolution background image to a block of pixels of the appropriate size. This yields a digital mosaic of the background image where each tile has a single color. To accomplish our overlay process, we rely on a modification of a simulated diffusion limited aggregation (DLA) technique for image *magnification* that was previously described by Greenfield [3]. We want to ensure that the DLA image that represents the foreground image will be perceived as a continuous curve so that much of the blockiness that normally arises when trying to expand our foreground image is suppressed. As a consequence both the low resolution background mosaic and the effectively higher resolution DLA foreground image can reinforce one another. To manage this we glue together several DLA structures deposited on each background tile in such a way that all tiles remain duotone. To this end, we invoke a three pass algorithm involving the

foreground image. The first two passes deposit DLA structures on each background tile of the same color as the unique corresponding pixel of the foreground image. This second color makes every tile a duotone tile. The third and final pass glues these DLA structures together using additional DLA structures in such a way as to preserve the duotone nature of the tiles.

3 An example using the method

We provide details by working through an example. We will choose the sunset image and the author's portrait. To help reveal composite image detail, these images are first cropped and downsampled to yield 30×22 pixel images and the tiles in the resulting 30×22 duotone composite mosaics will each be 41×41 pixels. Figure 4 shows the results following the initial step where each image in turn is treated as the background image. It clearly reveals how each pixel in the background image is expanded into a monochrome tile that is a 41×41 block of pixels.

The first two of the three passes that use the foreground image aggregate a DLA structure within each tile by placing a seed particle at the center of each tile and then generating a DLA structure for the tile whose color corresponds to that of the associated pixel of the foreground image. The two structures are generated independently. The DLA aggregation method of Kobayashi et al. [7] as further refined by Greenfield [2] is invoked. To briefly review the aggregation process, for these two passes the center of the tile serves as the local origin, and one at a time additional particles are released and subsequently undergo a random walk until they either encounter the existing structure and adhere, or their time limit expires. When the structure grows to the appropriate size (here extending out to within one pixel of the tile's border), this process stops.

The third and final pass involving the foreground image again considers each pixel of the foreground image in turn. But now after it identifies the tile in the mosaic corresponding to the pixel it performs a search near the boundaries of the neighboring tiles looking for an aggregated particle. Finding such a particle means we have located the extremity of one of the DLA structures in some neighboring tile. If such a particle is found, then it serves as the local origin for a third DLA structure to be aggregated. This time we must be more careful. The purpose of this third structure is to glue existing aggregated structures together. Thus, in order to preserve the duotone property of the tiles, we must check before aggregating any subsequent particle to see which color must be assigned to it, i.e., to which tile it actually belongs. The other subtle point is that the search along the borders of neighboring tiles must be done pseudorandomly to ensure that no visual artifacts or biases will result. Figure 5 shows the results of these three aggregation passes by focusing on six foreground pixels. Notice in Figure 5 how in the last pass the three tiles on the left are joined to neighboring tiles that are not shown, but the three tiles on the right are joined to each other. Figure 6 shows the results using the sunset as the background and the giraffe as the foreground after each of the first two foreground passes. The results following the last pass are shown in Figure 7. For the sake of completeness, and for side by side comparison, in Figure 7 we show both duotone composites, i.e., the composites with foreground and background roles reversed.

4 Discussion

There are three key points that should be raised. First, because of the blockiness of the background image in the composite mosaic, care must be exercised when choosing background versus foreground to achieve an effective result. Second, we trust the reader realizes that we have used duotone tiles in order to eventually facilitate the construction of actual *physical* mosaics. At worst, if all the pixels in the downsampled $m \times n$ images had distinct colors, we would need sufficient quantities of $2mn$ distinct smaller tiles on hand to construct our composite mosaics. This is because the $p \times p$ enlarged duotone tiles that make up the composite can then each be formed using p^2 tiles selected from our repository of smaller ones. Of course, in practice it would be rare for all $2mn$ pixels to be be distinct. Third, there is no guarantee our search for a neighboring

particle to serve as the seed during the final pass will be successful for every foreground image pixel, nor that all the structures aggregated during the first two DLA passes will be joined during this last pass. Empirically we have observed that the search for a suitable neighboring seed is almost always successful and that there is usually a large connected component that forms in the composite during this pass [3]. We have not taken the extra trouble to correct for these two possible shortcomings because it does not appear that the human eye is that discerning.

5 Conclusions and future work

We have shown that our method for generating duotone composite mosaics is viable. Clearly, some skill is required in selecting, cropping, and downsampling source imagery in order to achieve superior results. Future work should be directed towards mitigating the effects of the blockiness of the background image in the composite and developing methods for handling imagery with different height and width dimensions.

6 Acknowledgment

This work was supported in part by a University of Richmond 2008 Arts & Sciences Summer Fellowship.

References

[1] Bosch R., Constructing domino portraits, *Tribute to a Mathemagician*, Cipra B. (Ed.), 2004, 251–256.

[2] Greenfield G., Composite diffusion limited aggregation paintings, *Bridges Donostia: Bridges 2007: Mathematical Connections in Art, Music and Science*, Sarhangi R. and Barrallo J. (Eds.), 2007, 15–20.

[3] Greenfield G., Connectivity and a diffusion limited aggregation digital image magnification technique, *Proceedings of the 13-th International Conference on Geometry and Graphics*, Weiss G. (Ed.), CD-ROM (ISBN 978-3-86780-042-6), 2008.

[4] Kaplan C. S. and Bosch R., TSP art, *Renaissance Banff: Bridges 2005: Mathematical Connections in Art, Music and Science*, Sarhangi R. and Moody R. V. (Eds.), 2005, 301-308.

[5] Knowlton, K., Knowlton Mosaics: Computer Assisted Portrait Art, http://www.knowltonmosaics.com/ (accessed 1 April 2009).

[6] Knuth, D., The Stanford GraphBase: A Platform for Combinatorial Computing, *ACM Press*, New York, 1993.

[7] Kobayashi Y., Niitsu T., Takahashi K., and Shimoida S., Mathematical modeling of metal leaves, *Mathematics Magazine*, Volume 76, Number 4, 2003, 295–298.

[8] Long J., Modeling dendritic structures for artistic effects, *M.Sc. Thesis*, University of Saskatchewan, 2007.

[9] Orosz I., Istvan Orosz Bridges 2008, *Exhibition Publication*, Utisz Bt., 2008.

[10] Sah S. B., Ciesielski V., Sousa D., and Berry M., Comparison between genetic algorithm and genetic programming performance for photomosaic generation, *Simulated Evolution and Learning 2008 Proceedings*, Li X. et al. (Eds.), Springwer Verlag LNCS 5361, 2008, 259–268.

[11] Silvers R., *Photomosaics*, Henry Holt and Company, New York, NY, 1997.

[12] UTISZ, The homepage of Istvan Orosz, http://web.axelero.hu/utisz/page.htm (accessed March 2009).

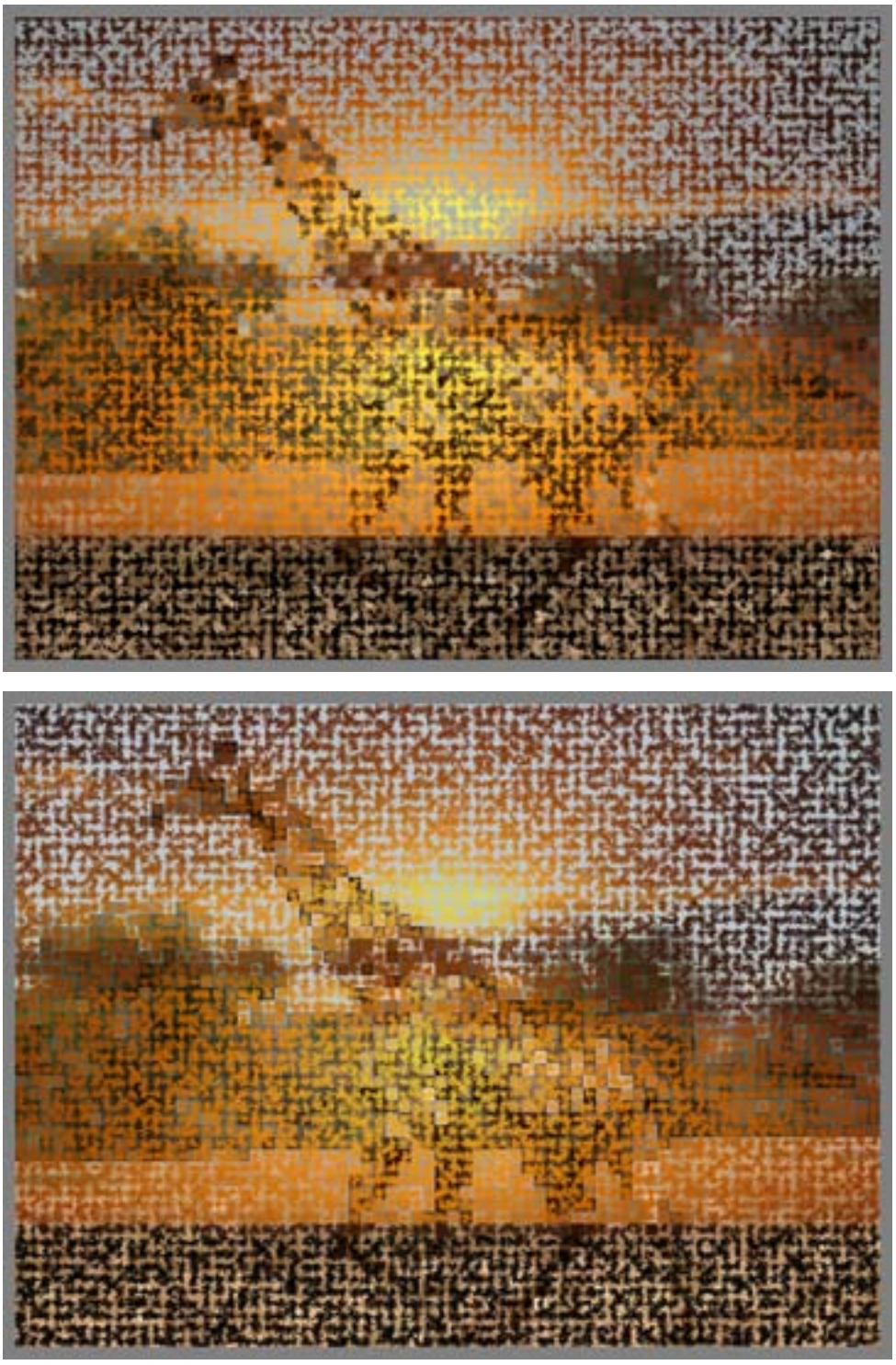

Figure 3: Our 72×52 duotone composite mosaics. Top: Sunset as background, giraffe as foreground. Bottom: Sunset as foreground, giraffe as background.

Figure 4: Initial pass for the background images yielding 30×22 mosaics with 41×41 tiles.

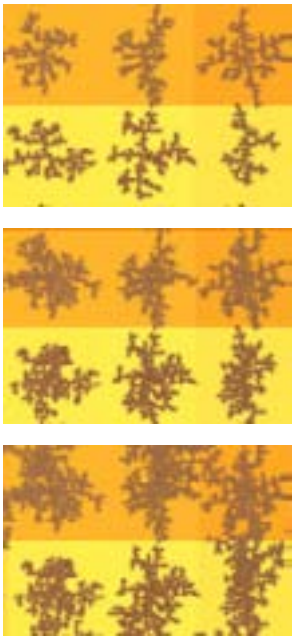

Figure 5: An example of the cumulative aggregation of the DLA structures used to construct the foreground image after each of the passes.

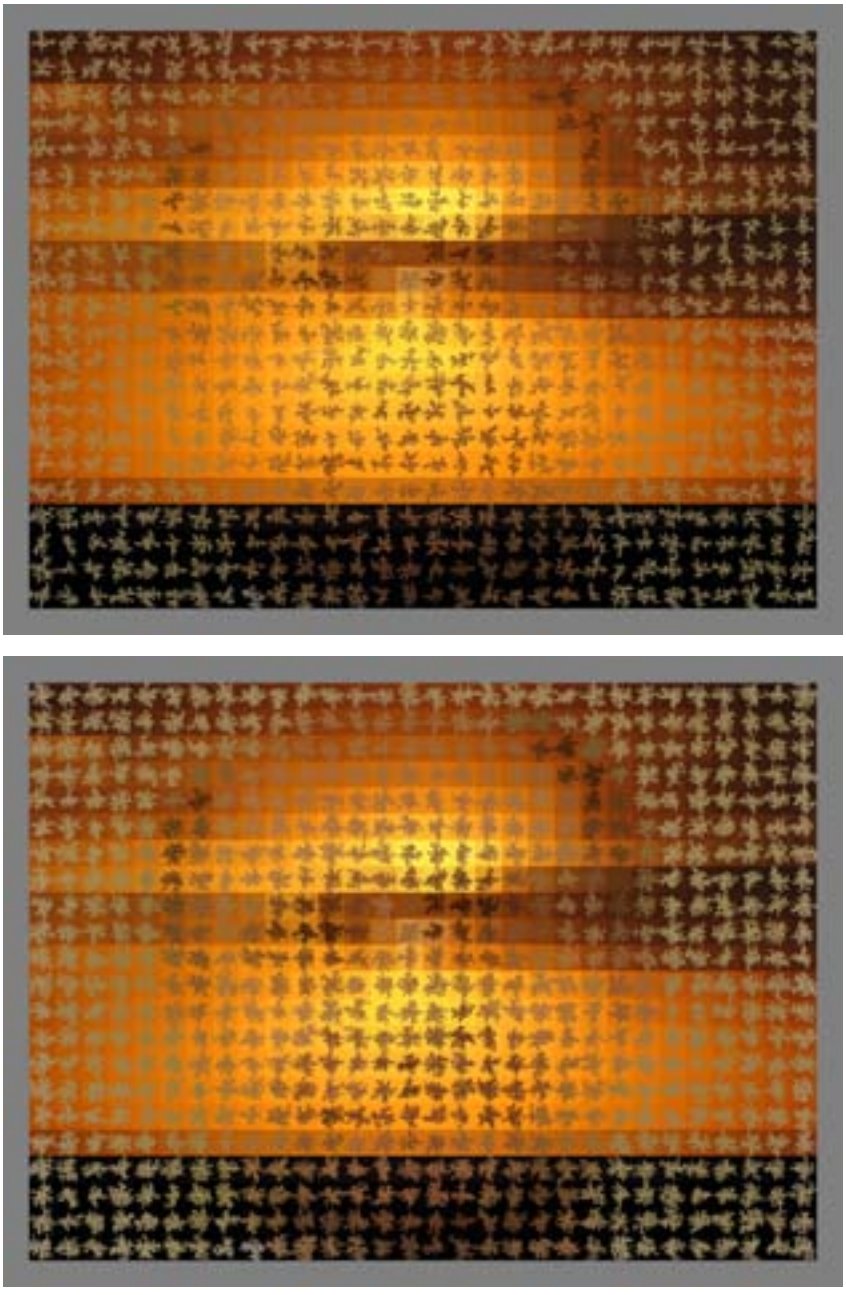

Figure 6: The first two passes used to build up the DLA structure for the foreground portrait image over the background sunset image.

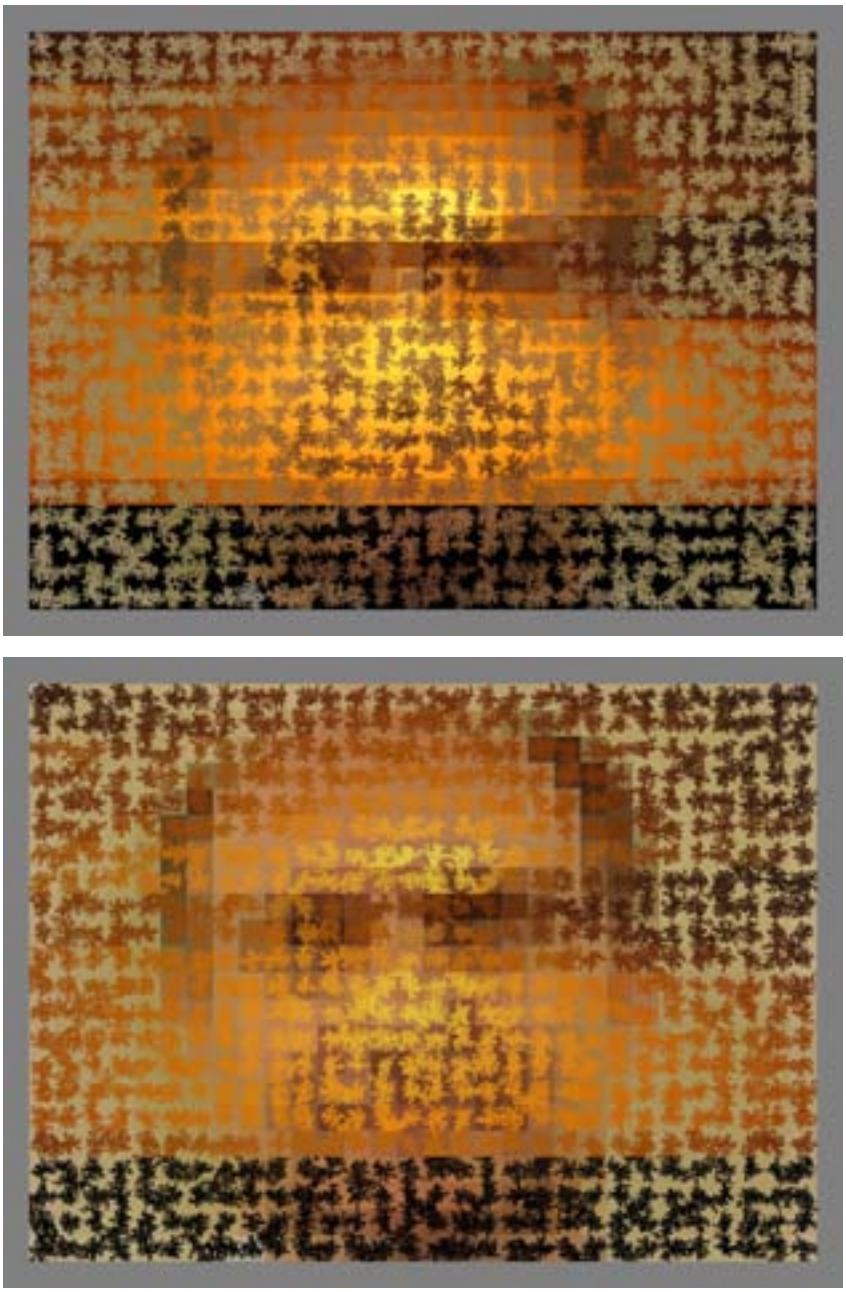

Figure 7: Top: Final pass gluing previously aggregated DLA structures of the foreground portrait together over the background sunset while preserving the duotone nature of the 41×41 enlarged tiles. Bottom: The result obtained by reversing the roles of foreground and background.

The Symmetry of "Circle Limit IV" and Related Patterns

Douglas Dunham
Department of Computer Science
University of Minnesota, Duluth
Duluth, MN 55812-3036, USA
E-mail: ddunham@d.umn.edu
Web Site: http://www.d.umn.edu/~ddunham/

Abstract

M.C. Escher's print *Circle Limit IV* is the last of his four "Circle Limit" patterns. There are two questions one can ask about the symmetry of *Circle Limit IV.* First, what is the correct orientation in which to display the print? Second, what is the symmetry group of the pattern? We answer those questions and show some new patterns related to *Circle Limit IV.*

1. Introduction

M.C. Escher's print *Circle Limit IV* [1] was the last of his four "Circle Limit" patterns. Figure 1 is an early computer generated pattern inspired by that print. It has more symmetry than Escher's pattern, which is

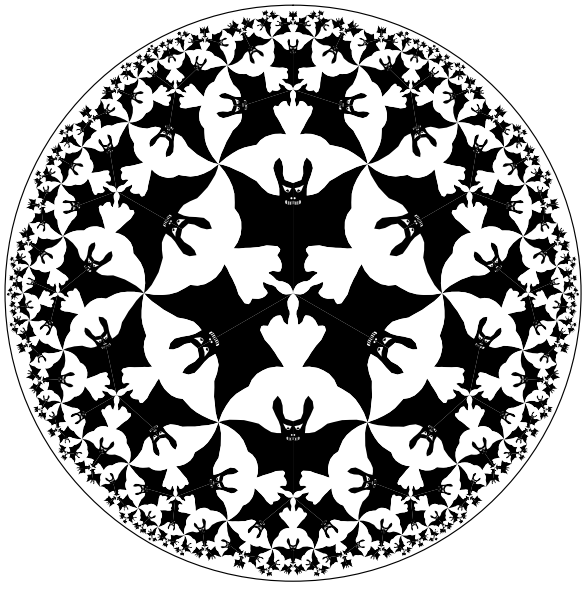

Figure 1: A pattern based on M.C. Escher's print *Circle Limit IV.*

shown in Figure 2 below with Escher's initials circled. The angels and devils motif was also the only one that Escher realized in each of the classical geometries: Euclidean, spherical, and hyperbolic.

The *Circle Limit IV* pattern seems to have confused some people in that it has appeared rotated from its correct orientation. In the next section we will explain how to determine the correct orientation. In the following section, we review the Poincaré disk model of hyperbolic geometry and use it to analyze the

[1] M.C. Escher's *Circle Limit IV*

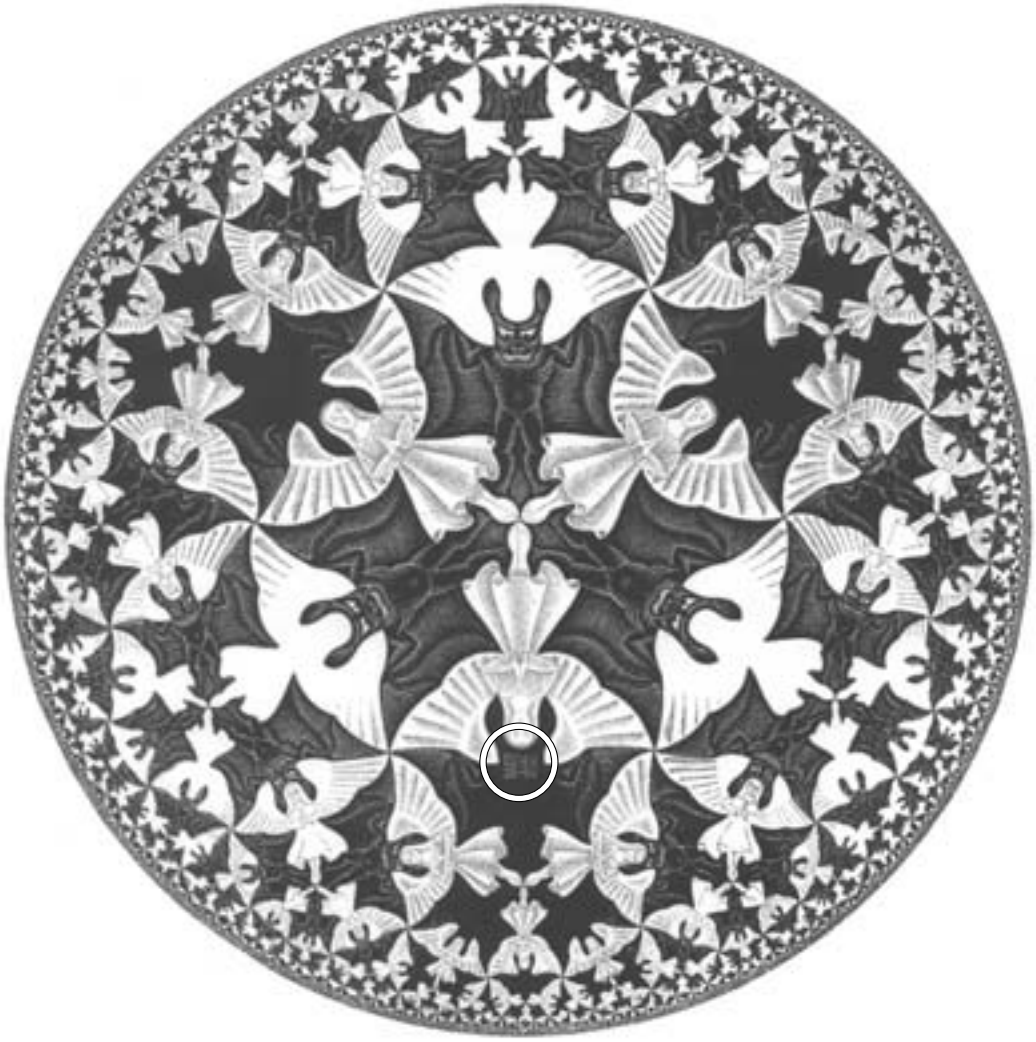

Figure 2: M.C. Escher's print *Circle Limit IV* with his initials circled.

symmetry group of *Circle Limit IV,* which can also be a source of confusion — for many years I thought the symmetry group was different from what it actually is. We also show new patterns related to *Circle Limit IV,* including one with my imagined symmetry group.

2. The Correct Orientation of *Circle Limit IV*

Recently, four books have been published that show *Circle Limit IV* with incorrect orientations, on pages 224 and 166 of [1] and [8] respectively, and on the covers of [6] and [7]. Interestingly, the previous edition of [6] also used *Circle Limit IV* on its cover — correctly oriented [5].

However, the mis-orientation of *Circle Limit IV* is not just a recent phenomenon. In one of the definitive books on Escher, *M.C. Escher, His Life and Complete Graphic Work* [9], a large version of the print is correctly oriented on page 98, yet a small view of it is incorrectly oriented on page 322.

How is the correct orientation determined? In fairness to the books mentioned, it is a bit subtle. It is determined by Escher's initials (MCE in block letters) and the date, which he placed on many of his prints. The problem is made more difficult in some reproductions by very faint intials. Figure 3 shows those initials and date as they appear on *Circle Limit IV.* Escher dated his prints by month and year. At first he used

Figure 3: Escher's initials and date on *Circle Limit IV.*

Arabic numerals for the months, but switched to Roman numerals in 1937. Thus, *Circle Limit IV* is dated `VII-'60`, indicating that it was completed in July, 1960. Escher's block letter initials look almost the same upside down. However, the requirement that the date be upright establishes the correct orientation of the print. There are three each of fully developed angels and devils in the center. Outward from the center and adjacent to each angel, is a devil shown mostly in black background. The initials and date appear in the head of the bottom "background" devil.

Here is a question for the reader. To print a copy of *Circle Limit IV,* did Escher use two black woodblocks — one with the initials (for the bottom) and one without initials (for the top left and for the top right)? If not, how did he get by with just one woodblock? Here is the answer.[2]

3. The Symmetry Group of *Circle Limit IV*

Though Escher considered his "Circle Limit" patterns to be just patterns with a circular limit, they can also be viewed as repeating patterns in the Poincaré disk model of hyperbolic geometry. The points of that model are just the (Euclidean) points within a Euclidean bounding circle. Hyperbolic lines are represented by circular arcs orthogonal to the bounding circle (including diameters). Figure 4 shows some hyperbolic lines over an angels and devils pattern. The measure of an angle between hyperbolic lines is the same as the Euclidean measure of the angle between their arcs; however, equal hyperbolic distances correspond to ever smaller Euclidean distances toward the edge of the disk. Thus all angels are the same hyperbolic size, as are all devils. A hyperbolic reflection across a hyperbolic line is represented by inversion in the circular arc representing that line (reflection across a diameter is just a Euclidean reflection). As in Euclidean geometry, successive hyperbolic reflections across two intersecting lines results in a hyperbolic rotation about the intersection point by twice the angle between the lines.

Using this hyperbolic interpretation, we can analyze the symmetries of the *Circle Limit IV* pattern. If we only look at the outlines of the angels and devils, the reflection axes of the pattern coincide with

[2]There was just one woodblock — with initials. After making three impressions with that woodblock, Escher took a small plain block of wood slightly larger than the initials, inked it, and blacked out two of the initials/dates.

bilateral symmetry axes of the angels and devils. These axes divide the hyperbolic plane into hyperbolically congruent "squares", that is equilateral, equi-angular quadrilaterals, as in Figure 4. The outlines also have 4-fold rotation centers at the centers of the squares where wing tips of the angels and devils meet. Thus, the outline pattern has symmetry group $4 * 3$ in orbifold notation, or $[4^+, 6]$ in H.S.M. Coxeter's notation [2]. Escher's first angels and devils pattern, the Euclidean periodic Drawing 45 (page 150 of [10]) created in 1941, has symmetry group $4 * 2$ (or $[4^+, 4]$ in Coxeter's notation).

However, in *Circle Limit IV* some of the angels and devils are have been filled in with interior detail, others are just background with no interior detail, and yet others are partially filled in. If this were done in such a way that maintained the reflection symmetries across the edges of the "squares" mentioned above, yet destroyed any rotational symmetry about their centers, the symmetry group would be $*3333$. Such a pattern is shown in Figure 5 in which different colors destroy the rotational symmetry. In fact I erroneously

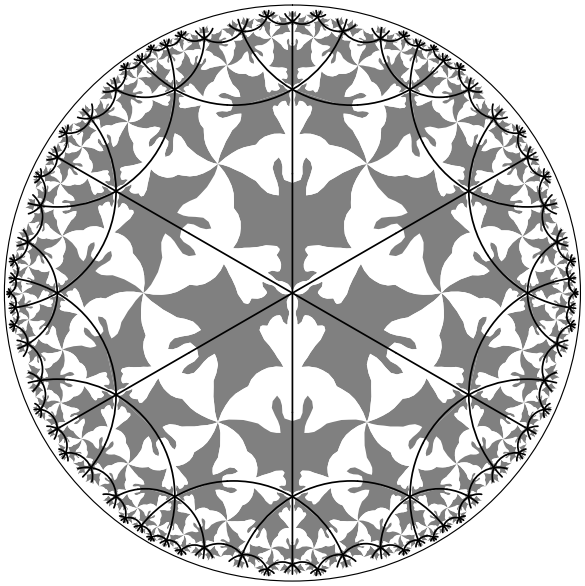

Figure 4: The hyperbolic plane divided into "squares" by the bilateral symmetry axes of the angels and devils.

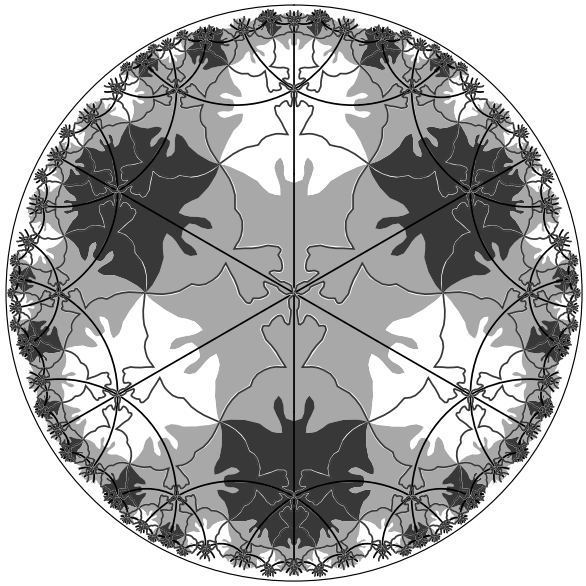

Figure 5: A pattern based on *Circle Limit IV* with symmetry group $*3333$

thought that the symmetry group of *Circle Limit IV* was $*3333$ until very recently.

What is the actual symmetry group of *Circle Limit IV*? First, we ignore Escher's initials and date, otherwise the only symmetry would be the identity. Then there are three reflection axes through the center of the circle. It turns out that those reflections and the rotations they generate (by ± 120 degrees and the identity) are the only symmetries. Careful inspection reveals that the devils are fully developed and the angels are just background on the upper end of the vertical reflection axis and the reverse is true at the lower end of that axis. The same switching of roles occurs on the other two reflection axes. Thus the symmetry group is just D_3, the Euclidean dihedral group about the center of the circle.

This was Escher's intention as he explained on page 10 of [3]:

> Here too, we have the components diminishing in size as they move outwards. The six largest (three white angels and three black devils) are arranged about the centre and radiate from it. The disc is divided into six sections in which, turn and turn about, the angels on a black background and then the devils on a white one gain the upper hand. In this way, heaven and hell change place six times. In the intermediate, "earthly" stages, they are equivalent.

Escher had previously used this idea in 1942 when he carved a maple ball with angels and devils on its surface. Here is his description of it in a letter to the collector C.V.S. Roosevelt ([10] page 245):

> It has two poles and an equator. One pole represents "heaven," with only white angels on a black background, which I carved much deeper than the angel figures. The other pole shows "hell," with only black devils on a deeply carved white background. At the equator both angels and devils are visible and equivalent, carved at the same sphere-level.

So, due to the relative indentations of the angels and devils, the symmetry group of the carved ball is just D_2, generated by orthogonal reflections through the poles. There is a picture showing this relative indentation on page 244 of [10]. If all the angels and devils were on the same sphere-level on the ball, the symmetry group would be 3*2 in orbifold notation (or $[3^+, 4]$ in Coxeter's notation). Such balls (without the relative indentation of Escher's original) are available from the M.C. Escher web site [4].

So Escher's first angels and devils pattern was the Euclidean Notebook Drawing 45 done in 1941, and was followed by the carved sphere in 1942. Almost 20 years passed before he completed the classical geometry series with his hyperbolic *Circle Limit IV.*

4. Other Angels and Devils Patterns.

We have already seen in Figures 4 and 5 two hyperbolic patterns with more symmetries than *Circle Limit IV.* If we left out the interior details of all angels and devils as in Figure 4, or filled in those details for all the figures as in Figure 6 below, there would be 4-fold rotations about the meeting points of wing tips in addition to the reflections in the sides of the "squares" of Figure 4. As mentioned above, the symmetry group would be $4 * 3$ or $[4^+, 6]$ in Coxeter's notation.

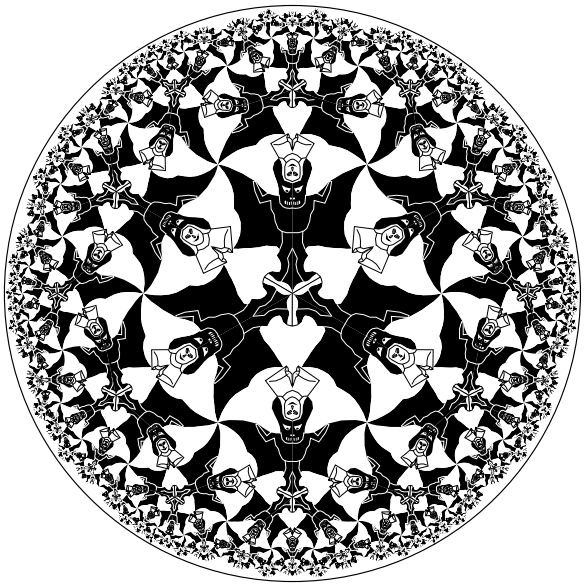

Figure 6: An angels and devils pattern with the interior details filled in for all the figures.

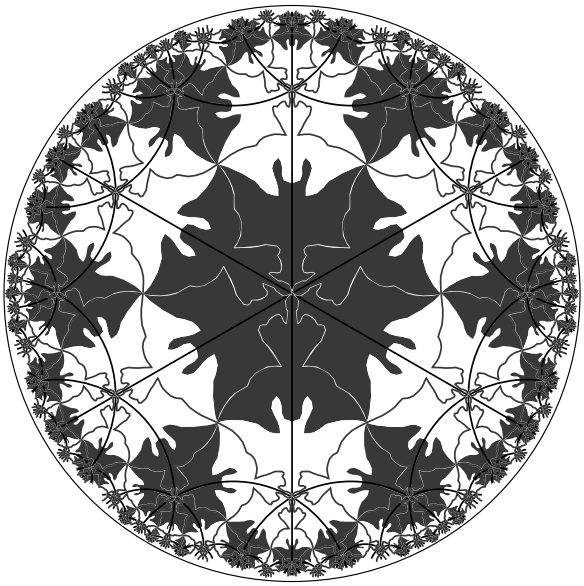

Figure 7: A pattern based on *Circle Limit IV* with symmetry group $2 * 33$

In Figure 5, following Escher's lead, we can interpret the black and white areas as places where the devils and angels dominate respectively. The gray areas represent "earthly" places where the angels and devils hold equal sway. As mentioned above, by taking into account the different colors, the symmetry group does not have rotational symmetries about the centers of the "squares" and is therefore $*3333$.

Figure 7 shows a pattern with 2-fold rotational symmetry about the centers of the "squares" of Figure 3, and thus has intermediate symmetry between that of Figures 4 and 5. The symmetry group of this pattern is $2 * 33$ or $cmm_{3,3}$ using a notation suggested by Coxeter. Again, following Escher's lead, we may interpret the white areas as places where the angels dominate, and the dark areas as places where the devils dominate. In this case there are no intermediate "earthly" regions.

5. Conclusions and Future Work

We have explained how to determine the correct orientation for *Circle Limit IV* and analyzed its symmetries. We have also shown angels and devils patterns with other symmetries.

For future work it would be useful to extend the current version of our hyperbolic pattern program so that it can draw patterns with symmetries like *Circle Limit IV* — it can currently only draw patterns that repeat the same way in all directions. We are just starting the process of converting this C program, which is not very portable, to Java so that others may use it.

Also, it would be interesting to use 3D printing technology to create a "heaven and hell" disk pattern with areas where angels are raised and devils are recessed, areas where the opposite is true, and intermediate areas where neither is dominant, in the manner of Escher's carved maple ball. It is likely that the techniques developed by Yen and Séquin for spherical geometry [11] would be useful for this task.

Acknowledgments

I want to thank Lisa Fitzpatrick, director, and the staff of the Visualization and Digital Imaging Lab at the University of Minnesota Duluth. I also want to thank the reviewers for their helpful suggestions.

References

[1] J. Conway, H. Burgiel, C. Goodman-Strauss *The Symmetries of Things,* A.K. Peters, Ltd., Wellesley, MA, 2008. ISBN 1-56881-220-5

[2] H.S.M. Coxeter and W.O.J. Moser, *Generators and Relations for Discrete Groups* Springer-Verlag, Berlin, 1972. ISBN: 3540058370

[3] M.C. Escher, *M.C. Escher The Graphic Work,* Barnes & Noble/TASCHEN, New York, 2007. ISBN 0-7607-9669-6

[4] Official Escher web site: `http://www.mcescher.com/`

[5] M. Greenberg, *Euclidean & Non-Euclidean Geometry, Third Edition: Development and History,* 3nd Ed., W. H. Freeman, Inc., New York, 1993. ISBN 0716724464

[6] M. Greenberg, *Euclidean & Non-Euclidean Geometry: Development and History,* 4th Ed., W. H. Freeman, Inc., New York, 2008. ISBN 0-7167-9948-0

[7] P. Henry-Labordère, *Analysis, Geometry, and Modeling in Finance: Advanced Methods in Option Pricing,* Chapman & Hall/CRC Press, 2008. ISBN 1-4200-8699-5

[8] S. Kalajdzievski, *Math and Art: an Introduction to Visual Mathematics,* Chapman & Hall/CRC Press, 2008. ISBN 1584889136

[9] J.L. Locher (ed.), *M.C. Escher, His Life and Complete Graphic Work* (English edition), Harry N. Abrams, Inc., New York, 1982. ISBN 0-8100-0858-1

[10] D. Schattschneider, *M.C. Escher: Visions of Symmetry,* 2nd Ed., Harry N. Abrams, Inc., New York, 2004. ISBN 0-8109-4308-5

[11] J. Yen and C.H. Séquin, Escher Sphere Construction Kit, *Proceedings of the 2001 ACM Symposium on Interactive 3D Graphics,* (2001) 95–98. `http://portal.acm.org/citation.cfm?id=364371`

Symmetry and Transformations in the Musical Plane

Vi Hart
http://vihart.com
E-mail: vi@vihart.com

Abstract

The musical plane is different than the Euclidean plane: it has two different and incomparable dimensions, pitch-space and time, rather than two identical dimensions. Symmetry and transformations in music have been studied both in musical and geometric terms, but not when taking this difference into account. In this paper we show exactly which isometric transformations apply to musical space and how they can be arranged into repeating patterns (frieze patterns and variations of the wallpaper groups). Frieze patterns are created intuitively by composers, sometimes with timbral color patterns or in sequence, and many examples are shown. Thinking about symmetry in the musical plane is useful not just for analysis, but as inspiration for composers.

Introduction

Composers have been using symmetry for hundreds of years. Sometimes this is done on a small scale, such as when the notes in one measure of a Bach fugue are found repeated upside-down within the next measure, or when an arpeggio is played going up and then back down. On a large scale, one can find examples of constructions such as crab canons—where the same notes are played forwards and backwards at the same time (most famously in Bach's *A Musical Offering*)—or table canons—where the same sheet music is played by two instrumentalists looking down at it from either side of a table, so that their notes are upside-down and backwards (examples can be found by Bach, Mozart, and others). These simple geometric transformations, containing just one mirror or point of rotation, are well studied and understood by both mathematicians and music theorists.

When looking at a piece, music theorists are interested in following the development of themes and motives. A motive (here used to mean a set of notes) can be found repeated (translated horizontally), transposed (translated vertically), inverted (horizontal mirror), in retrograde (vertical mirror), or in retrograde inversion (180° rotation). We show that these transformations and three other combinations are all of the possible isometries in the musical plane. We precisely characterize which patterns are symmetric under one or more musical transformations: the seven frieze patterns, each mapped horizontally or vertically, and the 14 musical wallpaper groups (not all of the Euclidean wallpaper groups appear, and some appear twice—once horizontally and once vertically). We also account for the symmetry found when passing a motive back and forth between instruments through color patterns, and we analyze sequences by thinking of them as a frieze pattern on a diagonal and relating them to color patterns.

Knowledge of these patterns may be useful for music analysis, but more importantly it is helpful for composers to be aware of the symmetries that we are already using intuitively, so that we can have conscious control over our work.

Related Work. Connections between mathematical and musical symmetry have been studied before [2, 3]. They focus on the basic musical transformations and on frieze patterns, but they do not look

systematically at all transformations and combinations of transformations that are possible in the musical plane—in particular, they do not consider color patterns, sequences, or wallpaper groups.

Transformations in Unequal Dimensions

Transformations. A set of notes can be thought of as a set of points in 2-dimensional space. The musical plane, however, has a very important difference from the usual geometric plane: the two dimensions are not the same. Time is seen horizontally while pitch space is mapped vertically, and the fact remains that time is different from space, not just in physics (as in General Relativity's spacetime), but most strongly in our perception. The musical plane therefore has less symmetry than the Euclidean plane—for example, rather than having symmetry at any mirror line, the musical plane only has horizontal and vertical axes of symmetry. However, this very limitation also splits most Euclidean transformations into two unique musical transformations, one horizontal and one vertical.

Isometries. In the Euclidean plane, there are three types of transformations that preserve the distances between all points or notes (isometries): translations, reflections, and rotations. In the musical plane, all transformations must treat each of the two dimensions separately, leaving these possible isometries: horizontal translation (repetition), vertical translation (transposition), horizontal reflection (retrograde), vertical reflection (inversion), and combinations thereof. A rotation of 180° can be done, though in music terms this is thought of as a combination of the two mirrors and called a retrograde inversion. Likewise, the horizontal and vertical translations can be combined to repeat a motive in a different key (also called transposition). The last combination is the glide reflection (a translation plus reflection), which also comes in two types: if the glide reflection axis is horizontal, an inversion follows the motive, while if it is vertical the motive is followed by its retrograde in transposition. Any two isometric instances of a motive are related by exactly one of these eight geometric transformations.

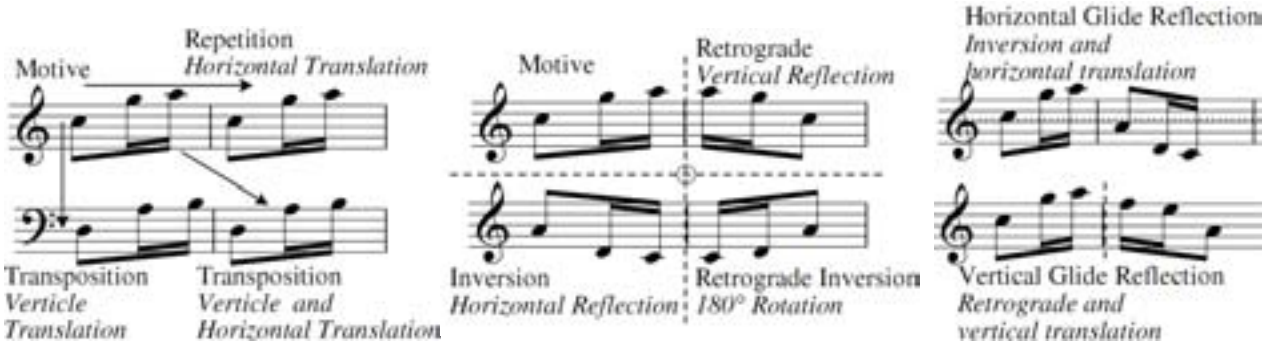

Figure 1: *All Eight Isometric Transformations in Musical Space*

Choosing a scale for pitch. Pitch, aside from being wholly different from time, can be measured in various ways. Most music is written tonally within some scale, and so it makes sense to use one step of that scale as one unit of pitch when applying transformations. In music, this is called a *tonal* transformation. This is the metric used in the examples in this paper because it is most common and easiest to see visually in music notation. On the other hand, a *real* transformation uses each step of the chromatic scale as one pitch unit. There are comparatively fewer musical examples of this second type (though still very many, especially in 12-tone music).

Frieze Patterns

Frieze patterns. Frieze patterns are the seven symmetry groups of patterns that repeat infinitely in just one dimension in the Euclidean plane. These patterns often appear as borders in art and architecture, and are especially well suited to music because they share the property that their two dimensions are not equal

(one is infinite and one is not). Like music, frieze patterns can contain only repeating symmetries that use translation, glide reflection, horizontal mirrors, vertical mirrors, and 180° rotation, in various combinations. If you count time as possibly infinite and audible pitch space as limited, then frieze patterns exactly match the symmetric capabilities of a repeating phrase of music. Of course, no music can really repeat endlessly in one dimension, just as no frieze patterns in architecture do either, so a few repetitions will have to do.

Frieze patterns are so natural to music that a composer can unknowingly use all seven groups within a single piece. Below, we illustrate each of the seven frieze patterns with an example from Debussy's *Three Nocturnes* on the right, as well as a simple example using the motive from Figure 1, on the left. The seven frieze patterns have various notations, but we find Conway's footprint analogies to be intuitive and easy to use as names [1]. We also give the orbifold notation and describe the groups using both mathematical and musical terms. The analogous feet are included above the corresponding notes.

Hop ∞∞. The hop has translational symmetry only. In music, it is repetition. Repeated motives, bass lines, choruses, chord progressions, and melodies are so common that hops are difficult to avoid in music.

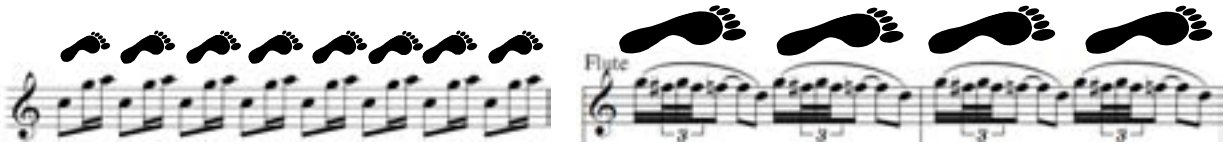

Figure 2: *Hops.*

Step ∞x. The step is a glide reflection—a pattern of a motive and its inversion. Bach was especially fond of glide reflections and they can be found in much of his work

Figure 3: *Steps.*

Jump ∞*. A hop with a horizontal mirror makes a jump. A motive and its inversion are played simultaneously, and repeated. Jumps are a difficult frieze pattern to find in music, perhaps because horizontal mirrors do not sound very subtle. Some Bach pieces, for example, contain a horizontal mirror at the end of a piece or section which had many glide reflections, bringing closure to the motive and its inversion by calling attention to that they are really the same under transformation.

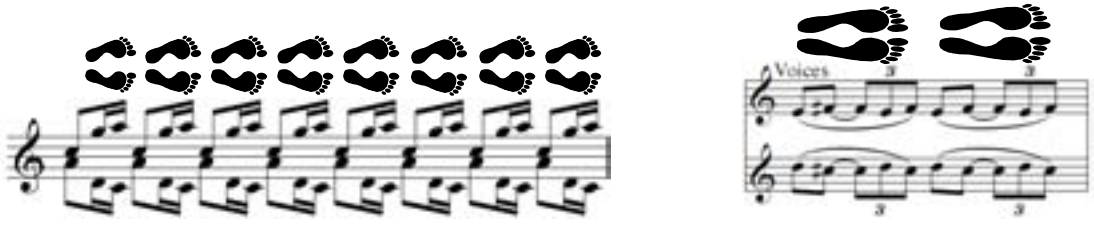

Figure 4: *Jumps.*

Sidle *∞∞. A sidle contains two vertical mirrors, alternating a motive with its retrograde. They are commonly found in arpeggios, especially piano accompaniment.

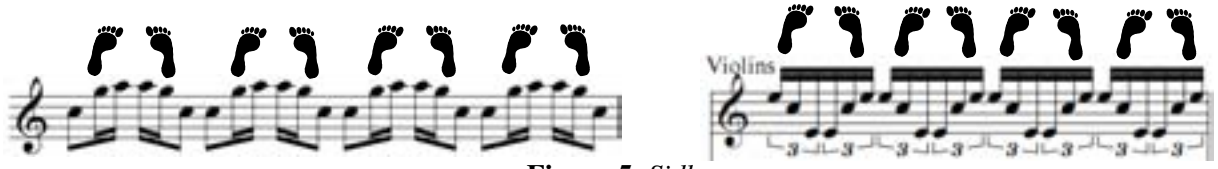

Figure 5: *Sidles.*

Dizzy hop 22∞. The dizzy hop, or spin hop, has two points of 180° rotation. In music, this alternates a motive with its retrograde inversion. There are many frenetically dizzying dizzy hops in Stravinsky's music.

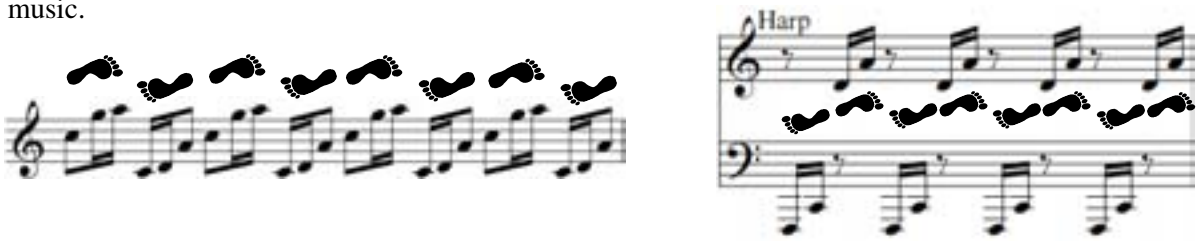

Figure 6: *Dizzy hops.*

Dizzy sidle 2*∞. A sidle with a twist yields the dizzy sidle—one vertical mirror and one point of 180° rotation. It contains all four transformations of a motive in order: a motive, its retrograde, the inversion, and the retrograde inversion, repeated indefinitely. Traditional Alberti Bass has this symmetry (in which the mirror lines go through the top and bottom notes).

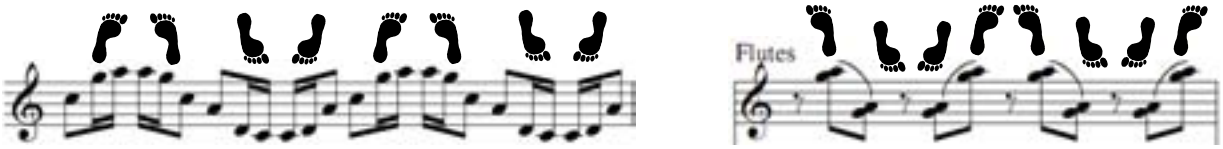

Figure 7: *Dizzy sidles.*

Dizzy jump *22∞. The dizzy jump has all possible symmetries: one vertical and one horizontal mirror, which create a point of rotation where they meet. A motive and its inversion are played simultaneously, and then the retrograde and retrograde inversion played simultaneously as well. Like jumps, this is a less common frieze pattern in music—except for music where the horizontal mirror sound is used purposely, such as Philip Glass's music in which dizzy jumps are quite commonplace.

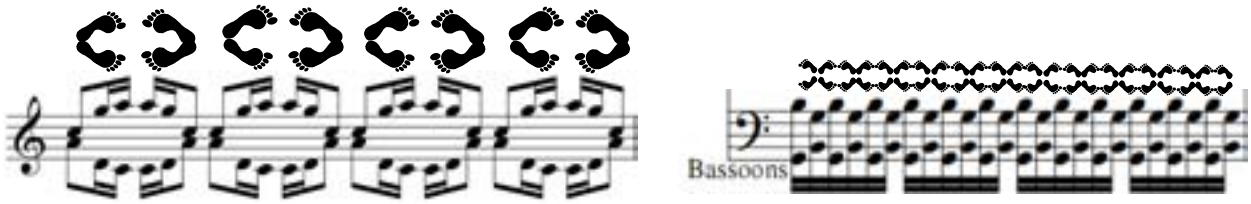

Figure 8: *Dizzy jumps.*

The other seven musical frieze patterns. Though it is intuitive to map frieze patterns to the musical plane in the horizontal (time) dimension, it is still geometrically sound to map a piece of a frieze pattern vertically (pitch). The aesthetic problem with this mapping is that an infinitely long pattern must be suggested within a very short amount of time through the use of a large range of pitches. Time can feel infinite from the perspective of one moment, but pitch-space is severely limited by the amount of information the ear can perceive at once. While examples can be found in music where many instruments in different octaves play the same thing, this is usually done for timbre or volume. We hear all the octaves together as one melody rather than as a repeating pattern through pitch-space, making these vertical frieze patterns not as useful from an analysis or composition viewpoint. Still, it is worth noting that there are actually 14 types of frieze patterns in the musical plane.

Color

In mathematics, the word "color" refers to a labeling. In music, "color" refers to the timbre, or sound quality, of an instrument or set of instruments. Just as a color labeling differentiates sets of points in mathematics, sound color is what lets us hear the difference between sets of notes played by one instrument rather than another. Frieze patterns, both musical and mathematical, have color patterns associated with them [1]. Most frieze patterns can be colored in more than one way. For example, a jump could alternate each set of footprints between two colors, or it could have all the left feet one color and all the right feet another. There are 17 different 2-color frieze patterns [1], many of which—if not all—can be found in existing music, including the previous example of Debussy's *Nocturnes* as shown in Figure 9.

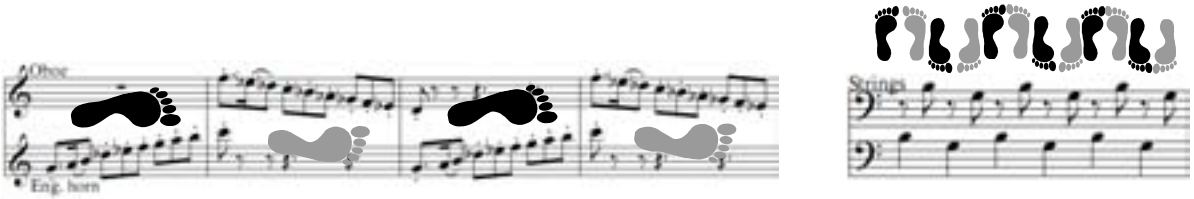

Figure 9: *Debussy Nocturne I has a 2-color step and a 2-color dizzy sidle.*

Sequences

The frieze patterns above are missing one of the most common musical transformations: transpositions involving both vertical and horizontal translation. All frieze patterns contain horizontal translations by definition, and all of the other musical isometries are accounted for as well. But what if each repetition of a motive were translated not just horizontally, but also vertically? In music this is called a sequence, and they run rampant in classical styles. Just as an arithmetic sequence adds a fixed number to each successive number, a musical sequence adds a fixed interval to each successive repetition of a motive.

A sequence can be thought of as a slanted frieze pattern. By normalizing the sequence (vertically translating each repetition to have the same vertical extent), one can then analyze the frieze pattern. The difficulty lies in picking the repeating unit. In the second example in the figure below, one can normalize each triplet in order to get a sidle. However, if instead of taking the first three notes, one took three notes starting with the second, then the sequence would normalize to a dizzy hop. It is usually easy to find the musical cues necessary to decide what the motive is.

Figure 10: *Three sequences from Mozart's Piano Sonata in C: a walk, sidle, and dizzy hop.*

The repeating unit of a frieze patterns consists of one, two, or four transformed instances of the motive (feet). When creating a sequence from a frieze pattern, the vertical shift can be applied every one, two, or four instances of the motive (up to the length of the repeating unit), and each choice will create a unique symmetry group. (One could apply the shift to a larger set of instances, but the result would fall into one of the other groups.) There are eleven different kinds of frieze pattern sequences, a subset of 2-color patterns where each time the color changes, a transposition occurs (the missing six of the seventeen color patterns are the ones where two colors occur at the same point in time—once again the difference between time and space creates a difference between the geometry of music and of the usual plane—and

the ones where the color change is at a point where there is a built-in vertical translation through glide reflection or rotation, making it impossible to tell whether there is an extra translation or not). The figure below shows the two different ways of sequencing a sidle.

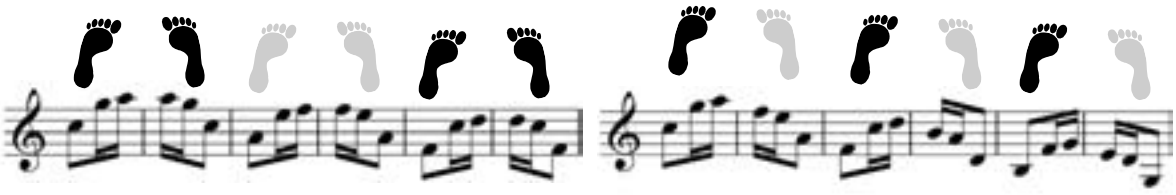

Figure 11: *The two ways of sequencing a sidle, related to the two possible 2-colorings.*

Color and Sequences Together: A Bach Example

Bach's Invention 14 is a great example of color and sequence: it contains hops and steps of the same motive in all possible 2-color patterns between the right and left hand, in sequence. The piece also contains both hops and steps in just one hand and in both hands at once.

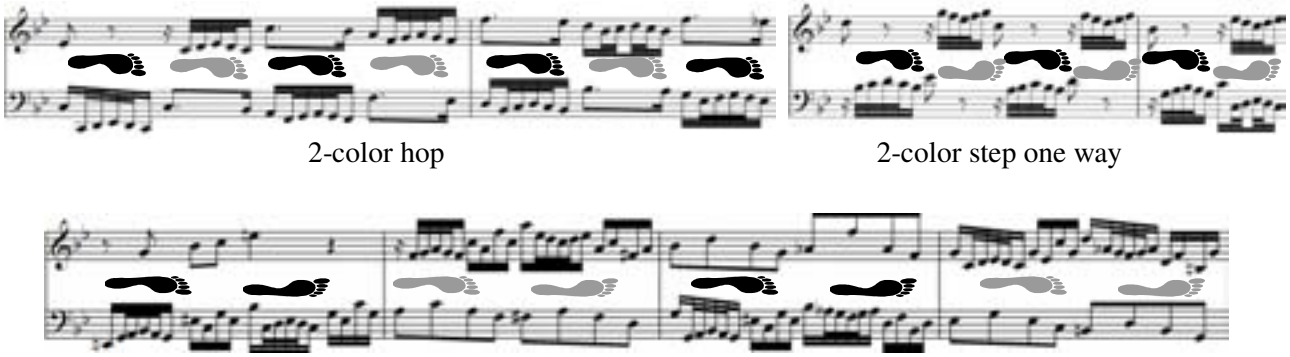

Figure 12: *2-color hop and step sequences in Bach's Invention 14.*

Wallpaper Patterns

The wallpaper groups are the symmetry groups of patterns that repeat in two dimensions. There are 17 of them, but not all can be naturally mapped to the musical plane because many contain rotations other than 180° or have mirror and glide-reflection lines which meet at angles other than 90°. The following eight patterns (in orbifold notation [1]) do work: o, **, xx, *x, *2222, 2222, 22*, and 2*22, because they can be mapped onto the musical plane with all mirror lines and glide-reflection axes going either horizontally or vertically, and do not contain rotations other than 180°. Interestingly, just as with the Euclidean isometries, this limitation also splits some wallpaper groups into two unique musical wallpaper groups, because they can be mapped onto the musical plane in two different ways at 90° from each other. *2222 and 2*22 fit just one way each. 22*, xx, *x, and ** find two distinct ways to map themselves to the staff. Patterns o and 2222 can both fit at any angle, though they fit into two classes: the way that makes repetitions play in parallel, and the infinite possible offsets.

To give these pairs distinct names, we add a "V" for vertical mirror, glide-reflection axis, or parallel repetitions, and add "H" for horizontal mirror, glide-reflection axis, or nonparallel repetitions. Figure 13 illustrates swatches of the 14 groups, showing just one vertical repetition.

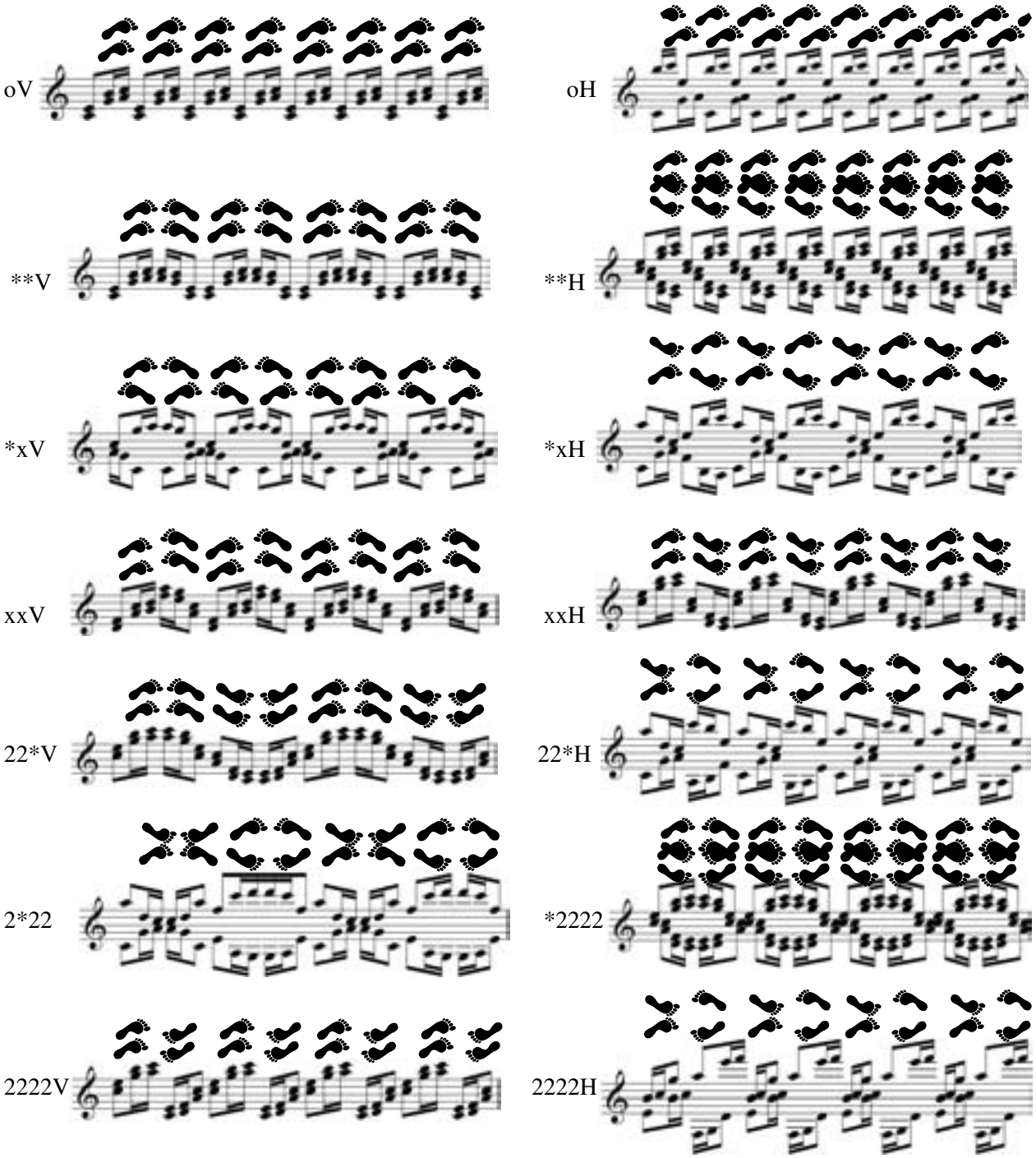

Figure 13: *The 14 musical wallpaper groups*

There is the same number of musical wallpaper groups as musical frieze patterns, but the wallpaper groups cannot all be constructed by simply repeating frieze patterns in the second dimension. However, if one repeats each of the 14 musical frieze patterns with either a translation in the second dimension, a translation in the second dimension followed by reflection, or a translation in both dimensions, the set of possibilities (removing duplicates) is the 14 musical wallpaper groups. Interestingly, though there are

many duplicates, both horizontal and vertical frieze patterns are required under these transformations to get all 14 wallpaper groups.

Use in Composition

The author finds these ideas particularly inspiring for use in composition. For example, it seemed obvious to begin a seven-movement piece with one movement dedicated to each of the seven horizontal frieze patterns. This piece, as of yet untitled, is a set of variations where one motive is transformed as it travels through the different symmetries of the movements. The mathematics is used to inspire and inform the pieces rather than to generate them, and so the frieze patterns are used in the melody and accompaniment when it is musical to do so but not conformed to when the author finds it beautiful to do otherwise.

The figure below contains excerpts from the first four movements to show how the motive evolves as it finds itself in different frieze patterns.

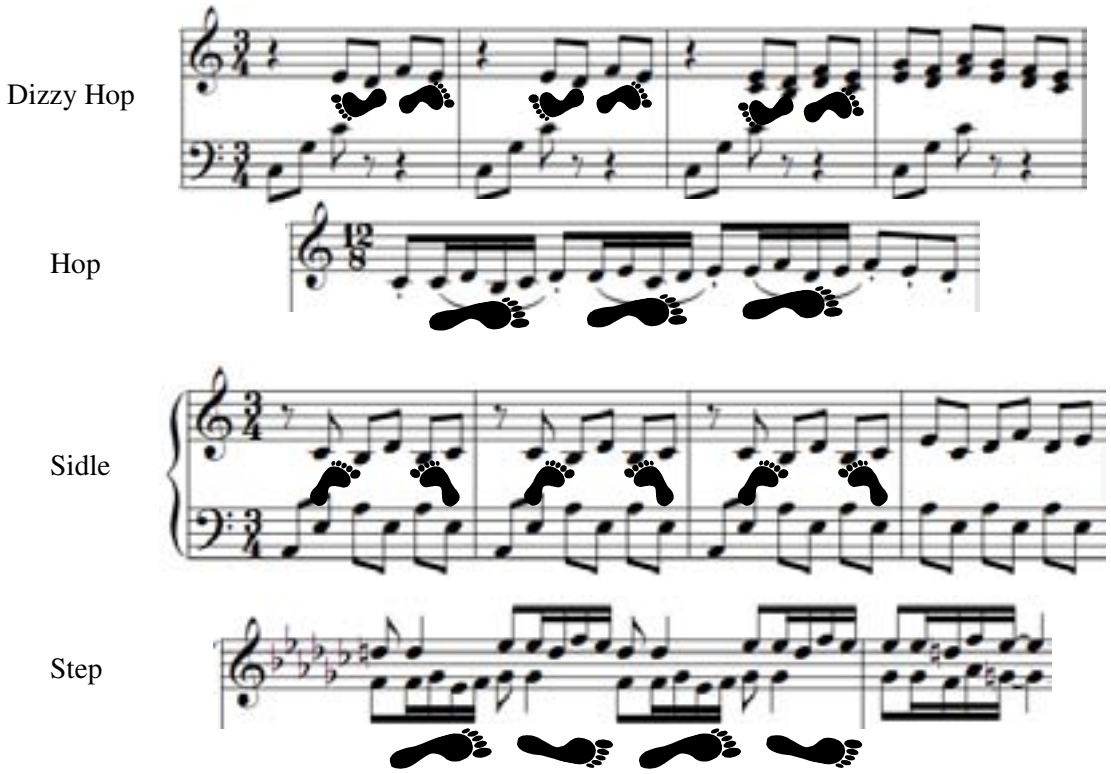

Figure 14: *Four frieze variations.*

For recordings and more, see http://vihart.com/papers/symmetry/

References

[1] John H. Conway, Heidi Burgiel, and Chaim Goodman-Strauss, *The Symmetries of Things*, A K Peters, 2008.

[2] Colleen Duffy, "Symmetrical musical pieces," Manuscript, 2001. http://www.math.rutgers.edu/~duffyc/research/SymmetricalMusical2b.doc

[3] Wilfred Hodges, "The geometry of music," in *Music and Mathematics: From Pythagoras to Fractals*, Oxford University Press, 2003, pp. 91–111.

Counterchange Patterns and Polyhedra

B.G. Thomas
School of Design, University of Leeds
Leeds LS2 9JT, UK
b.g.thomas@leeds.ac.uk

Abstract

Recent research has examined the difficulties encountered when attempting to apply two-dimensional repeating designs to wrap around the surface of polyhedra. The study was concerned with symmetry in pattern but did not consider symmetries that involve a color change. A pattern is said to have color symmetry when it exhibits, as a minimum, one symmetry that is color-changing. Counterchange designs are produced when the color-changing symmetries of a pattern involve only two colors. This paper discusses the problems involved in the application of counterchange patterns to polyhedra, focusing particular attention on the icosahedron.

Introduction

Recent investigations have explored the problem of patterning certain polyhedra in a systematic and complete way [1, 2, 3]. The initial inquiry identified which of the seventeen two-dimensional repeating pattern classes are capable of regular repetition around the Platonic solids, applying only the restriction that the pattern's unit cell must repeat across the surface of the polyhedron in exactly the same manner as it does in the plane [1, 2]. Focusing on the application of an area of the pattern's unit cell to act as a tile on the faces of the polyhedra, it was shown that only certain pattern classes are suited to the precise patterning of each Platonic solid. The investigation highlighted the importance of the pattern's inherent lattice structure and the symmetry operations of both the pattern and the polyhedron that were most significant to the process. The application of pattern to the dodecahedron required a different approach due to the impossibility of a regular five-sided figure tiling the plane [2, 3]. Through the exploitation of the concept of duality, a method was presented by which pattern can be applied to the dodecahedron through projection from a related patterned polyhedron. This projection method can also be used to pattern other solids dependant on their inter-relationships [3].

The work outlined above was concerned only with pattern symmetries that do not involve color change. This paper will explore the problems associated with the application of color counterchange patterns to polyhedra. Specific attention will be focused on the difficulties encountered when pattern is applied to the icosahedron in such a way that pattern's unit cell (and constituent coloring) repeats in exactly the same manner around the solid as in the plane.

Counterchange Patterns

A *color symmetry* of a tiling or pattern, with two or more colors, is a symmetry of the (uncolored) pattern that induces a permutation of the colors. Symmetries that consistently interchange or preserve color, are said to be *consistent with color* [4]. A color-changing symmetry that systematically interchanges only two colors is known as *counterchange symmetry*. This characteristic is also known as *antisymmetry* [5]. An infinite checkerboard is a typical example of a pattern that exhibits counterchange symmetry. The elements of the pattern of the one color and the elements of the pattern of the other color are exactly the

same. The pattern is therefore made up of two identical components and at least one symmetry of the pattern interchanges the two parts. These patterns are often referred to as *counterchange patterns* in art and design literature [6, 7, 8].

The classification of patterns and tilings, taking into account their color symmetry, is comparatively recent in relation to the classification of designs by geometric symmetry. H.J. Woods [7] was the first to produce complete enumerations the 17 one-dimensional counterchange patterns and the 46 two-dimensional counterchange patterns. This visionary work anticipated the later theoretical developments of crystallographers and mathematicians worldwide [9]. An array of literature has since been published on the subject of color symmetry. Schwarzenberger [10] identified over 100 research papers or other publications dealing with color symmetry from a mathematical perspective. The works of Washburn and Crowe [4] and Schattschneider [11] are more readily accessible to a non-mathematical audience.

Although there is no universally accepted notation, the *type/sub-type* notation developed by Coxeter [12] is currently the most commonly used amongst mathematicians and is the notation used throughout this paper. The pattern *type* is determined by considering all the symmetries of the pattern, both those that preserve color and those that interchange color. The pattern *subtype* is determined by the symmetry formed by one of the colors alone. Another modified form of the *pxyz* notation, proposed by Belov and Tarkhova [13], is commonly used by artists and designers. In this notation a prime (') is attached to the symbol if the corresponding operation is associated with a color change, although there are several exceptions to this rule.

Counterchange Patterns on Polyhedra

Mathematical coloring problems relating to polyhedra are usually concerned with the minimum coloring requirements, the number of distinctly different coloring solutions and coloring to preserve certain color combinations. The problem proposed in this paper refers to coloring a polyhedron through the application of a two-dimensional counterchange pattern to repeat across the faces and edges of the solid, rather than the application of color directly to the polyhedron's faces. A pattern must be wrapped around a polyhedron in such a way that the unit cell of the underlying (uncolored) pattern repeats across the polyhedron's faces in exactly the same manner as it does in the plane. In addition to this, the counterchange symmetry, indicated by the pattern's subtype, must also correspond and repeat in an identical way as in the two-dimensional pattern. This allows for color-changing and color-preserving translations of the unit cell in accordance with the symmetries of the plane pattern. The difficulties encountered primarily relate to the removal of certain areas within the pattern when it is folded into different planes to wrap around the solid. In some cases, the removal of prescribed areas within the pattern cause adjacent motifs and/or color not to register at the polyhedron's edges.

Previous studies [1, 2] have shown that it is possible to pattern the icosahedron with two-dimensional pattern classes p6 and p6m. These patterns are constructed on a hexagonal lattice in which the unit cell comprises of two equilateral triangles. When the patterns are wrapped around the icosahedron, an area equivalent to half the unit cell is applied to each face, ensuring repetition across each of the solid's edges and vertices in exactly the same manner as in the planar pattern. The difficulties encountered with the application of counterchange patterns, based on the two-dimensional pattern classes p6 and p6m, to wrap around the icosahedron are discussed and illustrated below.

Symmetries of the Patterned Icosahedron

When considering the systematic application of two colors to pattern classes p6 and p6m, there is only one possible counterchange coloring of class p6 (p6/p3), while class p6mm offers three possible counterchange colorings (p6m/p3m1, p6m/p31m and p6m/p6). Of these counterchange pattern classes only class p6m/p6 is capable of patterning the icosahedron in such a way that the pattern, and its constituent color symmetries, repeat in the same manner as in the plane (see Figures 2, 3 and 4). The difficulties encountered when applying counterchange patterns p6/p3, p6m/p3m1 and p6m/p31m are indicated in Figure 1. The edges of the patterned net that will not correspond, and do not maintain the color symmetry of the plane pattern, are indicated with an asterisk (*).

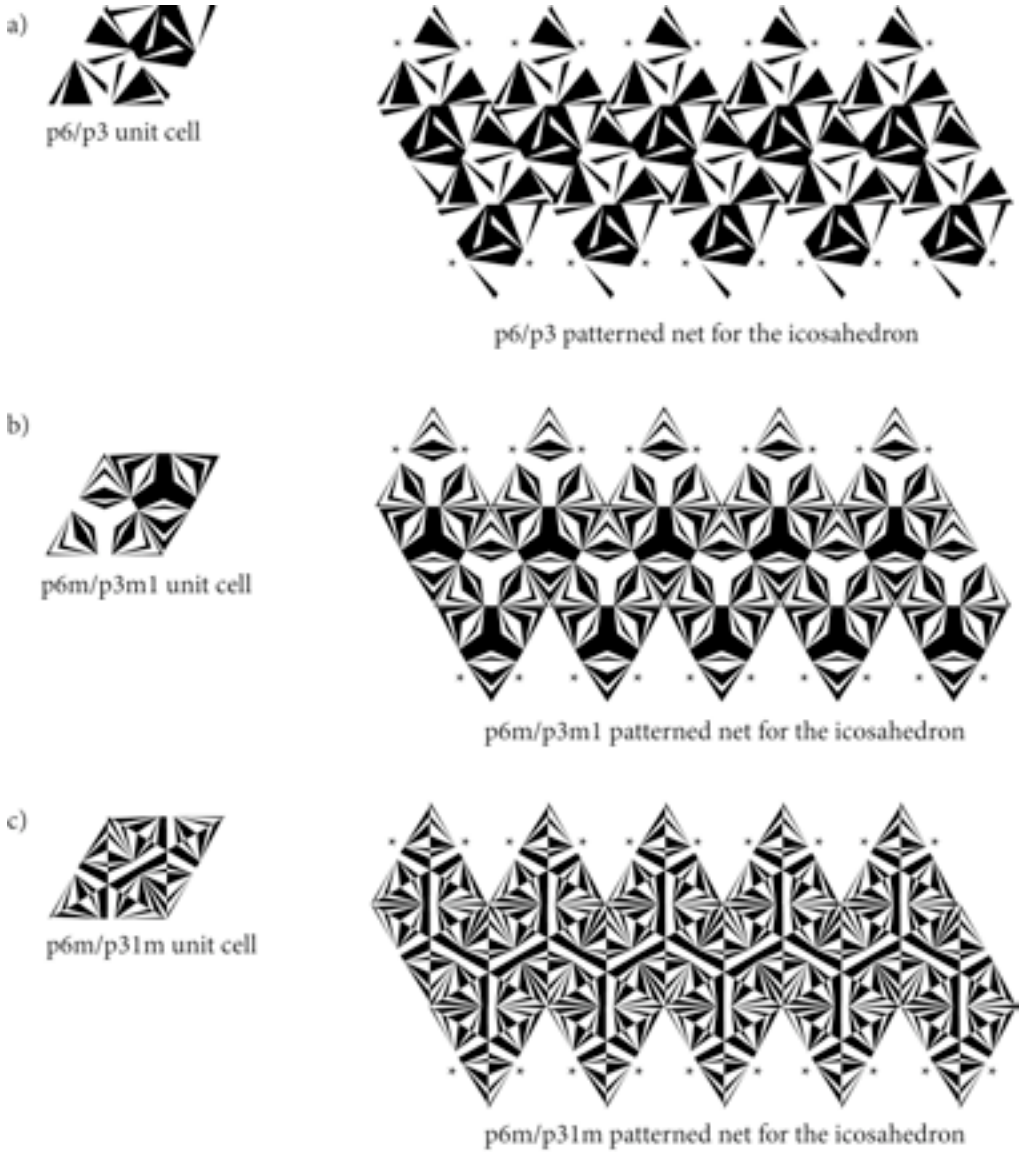

Figure 1 *Nets for the icosahedron patterned with counterchange classes a) p6/p3, b) p6m/p3m1 and c) p6m/p31m, indicating the edges of the patterned polyhedron where the two-dimensional color symmetries are not maintained*

Whilst the underlying symmetry of two-dimensional pattern classes p6 and p6m allow these patterns to be successfully wrapped around the icosahedron, the introduction of color restricts the patterning possibilities. Axes of two-fold and six-fold rotation in pattern p6/p3, shown in Figure 1(a), interchange color in the two-dimensional pattern and the translation of the unit cell preserves color. The removal of 10 prescribed areas of pattern, each equivalent to half the unit cell, is necessary to allow the plane pattern to repeat around the five-fold rotation axes present at the vertices of the icosahedron. As a result, the color symmetries of pattern p6/p3 not corresponding at edges where areas of pattern have been removed. The application of counterchange pattern p6m/p3m1 to the icosahedron presents a similar difficulty, as shown in Figure 1(b). A comparable problem also occurs with the color-preserving reflection planes of two-dimensional pattern p6m/p31m, shown in Figure 1(c). The reflection planes coincide with the edges of the icosahedron, causing the color symmetry of the pattern to conflict at the 10 edges where areas of the pattern have been removed.

The successful patterning of the icosahedron with counterchange pattern class p6m/p6 is illustrated in Figures 2 – 4 and the symmetries of the patterned solid described below.

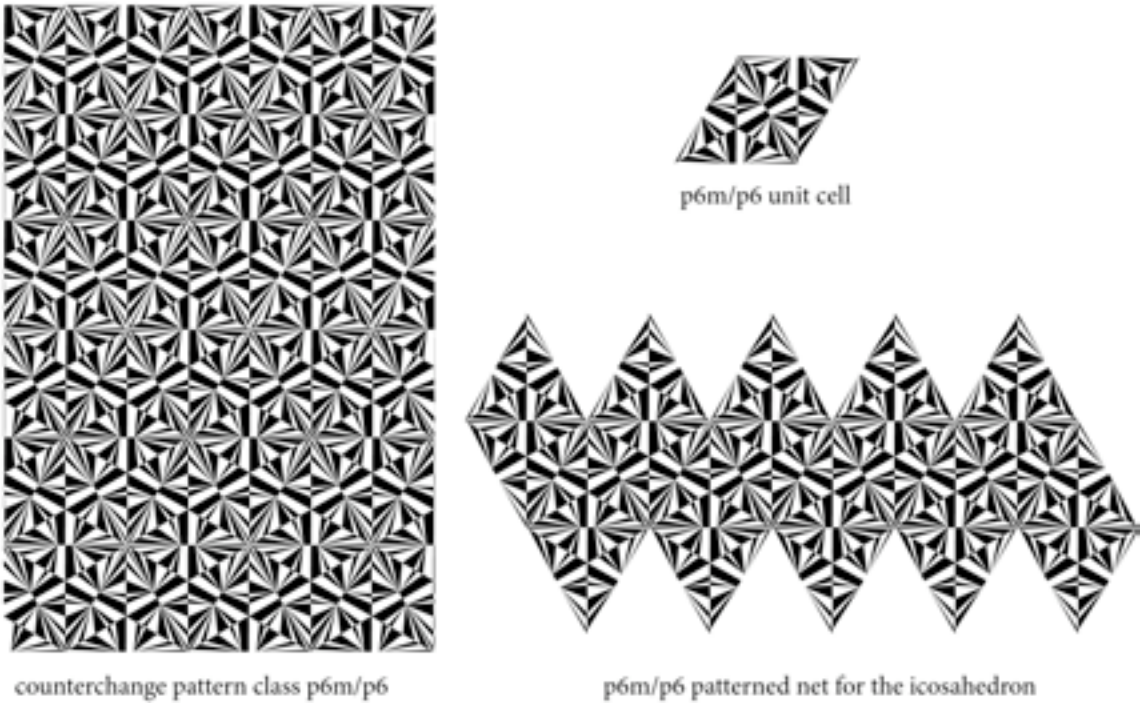

Figure 2 *Counterchange pattern class p6m/p6 applied to a net for the patterned icosahedron*

Full icosahedral symmetry (or *achiral icosahedral symmetry*), I_h, exhibits 120 symmetries including transformations that combine reflection and rotation. The archiral icosahedral symmetries are: identity; 12 axes of five-fold rotation; 12 axes of two-fold rotation about a five-fold axis; 20 axes of three-fold rotation; 15 axes of two-fold rotation; 12 axes of rotoreflection by 108 degrees; 12 axes of rotoreflection by 36 degrees; 20 axes of rotoreflection by 60 degrees and 15 planes of reflection.

As the reflection axes of the plane pattern coincide with the 15 reflection planes of the icosahedron, all three-dimensional reflection symmetries are preserved in the patterned solid. Color is interchanged across these reflection planes in the same manner as in the two-dimensional counterchange pattern. Icosahedral axes of two- and three-fold rotation correspond with centers of two- and three-fold rotation in the plane pattern. Centers of six-fold rotation in the plane pattern correspond with axes of five-fold

rotation at the patterned solid's vertices, where areas equivalent to half the unit cell are removed as the pattern is wrapped around the polyhedron. All five-fold, three-fold and two-fold axes of rotation on the patterned icosahedron preserve color, whereas all axes of rotoreflection interchange color. It should be noted that while, in this instance, the three-dimensional symmetries of the icosahedron are also symmetries of its patterned faces, it has been shown that in many cases [1, 2] there are two-dimensional symmetries of the plane pattern that are not three-dimensional symmetries of the patterned polyhedron. It is the manner in which a polyhedron is wrapped with a pattern that determines which planar symmetries coincide with the symmetries of the solid.

Figures 3 and 4 show illustrations of the icosahedron patterned with counterchange class p6m/p6. The model shown in Figure 3 is based on the design previously illustrated in Figure 2, where the area of the pattern that is applied to each face is equivalent to half the unit cell. In Figure 4 an area of patter equivalent to two unit cells is applied to pattern each face. In both instances, all faces are identical.

Figure 3 *The icosahedron patterned with counterchange pattern class p6m/p6 (created from laser-etched and painted acrylic)*

Figure 4 *The icosahedron patterned with counterchange pattern class p6m/p6 (created from laser-etched wood composite)*

In Conclusion

This paper builds on knowledge from previous research that presented a method by which appropriate pattern types can be identified and applied to the Platonic solids [1, 2, 3]. The systematic addition of color to a pattern, in association with its symmetries, introduces additional restrictions to the pattern classes that are capable of wrapping the icosahedron in such a way that the pattern repeats in an identical manner as in the plane. The introduction of color symmetry increases the importance of the operations of rotation and/or reflection that coincide at the edges of a patterned solid. It is the color-change associated with these symmetry operations that determines whether color interchanges, or is preserved, correctly between the faces and in exactly the same manner as in the plane pattern.

Further investigation into the application of counterchange patterns to the remaining four Platonic solids should be undertaken to enable a complete analysis of the symmetries of importance to the patterning process. Further research should be undertaken to identify additional areas within the unit cell that are capable of patterning polyhedra in a similar manner as in the plane. Particular attention should be focused on developing methods to apply counterchange patterns to tile the dodecahedron. This inquiry could also be extended to take account of the Archimedean solids and more complex polyhedra, experimenting with patterning through projection [3] and investigating other patterning methods. Future research could also take into account patterns with higher color symmetries.

References

[1] B.G. Thomas and M.A. Hann, *Patterned Polyhedra: Tiling the Platonic Solids*, in R. Sarhangi and J. Barrallo (eds.) Bridges Donostia: Mathematical Connections in Art, Music, and Science, pp.195-202. 2007.

[2] B.G. Thomas and M.A. Hann, *Patterns in the Plane and Beyond: Symmetry in Two and Three Dimensions*. Monograph no. 37 in the Ars Textrina series, The University of Leeds International Textiles Archive (ULITA). 2007.

[3] B.G. Thomas and M.A. Hann, *Patterning by Projection: Tiling the Dodecahedron and other Solids*, in R. Sarhangi and C. Séquin (eds.) Bridges Leeuwarden: Mathematical Connections in Art, Music, and Science, pp.101-108. 2008.

[4] D.K. Washburn and D.W. Crowe, *Symmetries of Culture: Theory and Practice of Plane Pattern Analysis*. Seattle, University of Washington Press, chapter 3. 1988.

[5] I. Hargittai and M. Hargittai, *Symmetry: A Unifying Concept*, Bolinas, California, Shelter Publications, p.116. 1994.

[6] E.H. Gombrich, *The Sense of Order,* Oxford, Phaidon Press Ltd. 1979.

[7] H.J. Woods, *The Geometrical Basis of Pattern Design. Part 4: Counterchange Symmetry in Plane Patterns*, Journal of the Textile Institute, Transactions, 27, T305-T320. 1936.

[8] M.A. Hann and G.M. Thomson, *The Geometry of Regular Repeating Patterns,* The Textile Institute, Manchester. 1992.

[9] D. Schattschneider, *Visions of Symmetry. Notebooks, Periodic Drawings and Related Works of M.C. Escher,* New York, Freeman, p.100. 1990.

[10] R.L.E. Schwarzenberger, *Color Symmetry*, Bulletin of the London Mathematical Society, 16, pp. 209-240. 1984.

[11] D. Schattschneider, *In Black and White: How to Create Perfectly Colored Symmetric Patterns*, Comp. & Maths. with Appls. 12B, 3/4, pp.673-695. 1986.

[12] H.S.M. Coxeter, *Colored Symmetry*, in H.S.M. Coxeter et al. (eds.) *M.C. Escher: Art and Science*, Amsterdam and New York, Elsevier, pp.15-33. 1986.

[13] N.V. Belov and T.N. Tarkhova, *Dichromatic Plane Groups*, in A.V. Shubnikov and N.V. Belov (eds.) *Colored Symmetry*, New York, Pergamon. 1964.

Non-Flat Tilings with Flat Tiles

Rinus Roelofs
Sculptor
Lansinkweg 28
7553AL Hengelo
The Netherlands
E-mail: rinus@rinusroelofs.nl
www.rinusroelofs.nl

Abstract

In general a tiling is considered to be a set of tiles placed next to each other in a flat plane. The tiles are placed in the plane in such a way that there are no gaps and no overlaps. But what if we leave out the condition that the plane has to be flat? For when there are no gaps and no overlaps between the tiles we still can call it a tiling. The consequences for the possible shapes of the tiles in non-flat tilings as well as the possible symmetrical structures that can be used are discussed in this paper.

1. Tilings

1.1. Definition. A tiling, or tessellation, is a covering of a plane without gaps or overlaps by polygons, all of which are the same size and shape. That is one of the definitions of a tiling. Another definition is the following: Tiling: a pattern made of identical shapes; the shapes must fit together without any gaps and the shapes should not overlap. Although the second definition doesn't speak about a plane, it is mostly assumed that the tiles do cover a plane. But we can take the definition literal, and then the only conditions are that the tiles do not overlap and do not leave gaps. Tilings in which all the tiles have the same shape are mostly called monohedral tilings [1]. In this paper all the tilings will be monohedral. In the example of Figure 1 we see a set of identical L-shaped tiles. With these tiles we can make a tiling as a covering of a plane. And there are several ways to do this.

Figure 1: *L-shaped tiles.*

Figure 2: *A non-flat tiling.*

Figure 3: *Cylindrical tiling.*

1.2. Non-flat tilings. Besides the possibility shown in Figure 1, where the tiles are put together in such a way that they cover a flat plane, there are a few more ways to put the tiles together under the condition that we do not want overlaps or gaps in the construction. In Figure 2 the L-shaped tiles are set up in such a way that we can make a three dimensional construction. As you can see the structure is made out of identical shapes. The tiles do not overlap and there are no gaps in the structure. To call it a tiling in the

traditional way, the only remark one can have is that it is not a covering of a flat plane. But it still is a tiling. Also when we combine the tiles in the way shown in Figure 3, the resulting structure is a tiling.

1.3. Squares. There are more shapes that can be used to create non-flat tilings and some of them are well known. The square can be used to tile a flat plane, but we can also make non-flat tilings using the squares (Figure 4), again there are no overlaps and no gaps in the structure. The most well known way to combine the squares in a three-dimensional way is the cube (Figure 5), although in general we do not call this a tiling.

Figure 4: *Non-flat tiling with square tiles.*

Figure 5: *Non-flat tiling: the cube.*

1.4. Polyhedra. Just as the cube also the other Platonic solids can be interpreted as non-flat tilings (Figure 6). In fact the standard term for “non-flat tiling” is “polyhedron”. And because all the tilings in this paper are monohedral we can call these tilings “monohedra”. So in non-flat tilings the regular pentagon can be used as a tile, which is not possible in the plane.

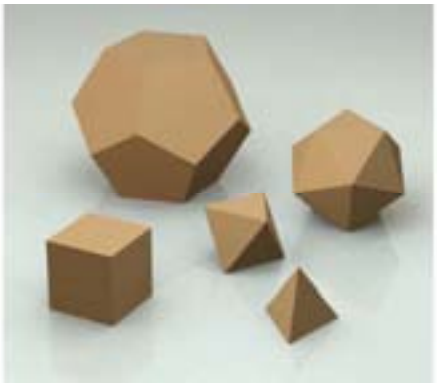

Figure 6: *Platonic solids.*

Figure 7: *Platonic solids.*

1.5. Duals of the Archimedean Solids. The Archimedean solids all have two or more different faces, or tiles. For a monohedral tiling the pattern has to be made with identical shapes, so therefore the Archimedean solids can not be seen as monohedral tilings. But when we look at the dual of an Archimedean solid then we see that such an object is built with all identical shapes. Figure 7 shows the complete collection of the thirteen duals. Seven of them are built with triangle-shape tiles, in four duals

you will find quadrangle tiles and in two cases pentagonal tiles are used. And because each dual is made out of identical shapes, they can be seen as non-flat tilings.

2. Elevation

2.1. Leonardo da Vinci. In the illustrations that Leonardo da Vinci made for Luca Pacioli's book "La Divina Proportione" [2], we can find a remarkable step towards non-flat tiling. This step is called Elevation and Leonardo da Vinci applied this on almost every regular and semi-regular polyhedron. What we mean with Elevation can be comprehended when we look at Figure's 8, 9 and 10.

Figure 8: *Tetrahedron elevated.*

Figure 9: *Cuboctahedron elevated.*

Figure 10: *Rhombic cuboctahedron elevated.*

2.2. The Elevation Process. The process of elevation of a polyhedron can be described as follows: from a face of the polyhedron we take the midpoint and we move this point away from the centre of the polyhedron until the distance between this point and the corner points of the face equals the length of the side of the face. After that we draw a line between the elevated point and each of the corner points of the face. When we do this for each face of the polyhedron the result will be the elevation of the polyhedron.
In Figure 8 we can see the result of this process when we start with the tetrahedron. Because the new faces are all equilateral triangles it is clear that this process only works on triangular, quadrangular and pentagonal faces. In Leonardo's drawings we can find eight of the fourteen possible elevations of regular and semiregular polyhedra. Two of the elevated Archimedean solids are shown in Figure 9 and 10.

2.3. The Elevation of flat tilings. The process of elevation that Leonardo used to create a new set of monohedra can also be applied on flat tilings in which triangles, squares or pentagons are used. In Figures 11 and 12 we can see the non-flat tilings that we will get when we apply the elevation process on the regular tilings with respectively triangles and squares. The resulting tiling is always a non-flat tiling in which only one type of tile is used, which is the equilateral triangle. The possibilities to make non-flat tilings with this tile, the equilateral triangle, are overwhelming. Therefore in this paper we will limit ourselves mainly to cylindrical shapes. When we make a small change with some of the tiles in the tiling of Figure 12, we get the tiling shown in Figure 13. Because this structure is bendable we can transform it into a cylindrical shape (Figure 15). Because all the tiles in these examples areequilateral triangles the tilings belong to the group of "deltahedra".

Figure 11: *Eelevation of 3,3,3,3,3,3.*

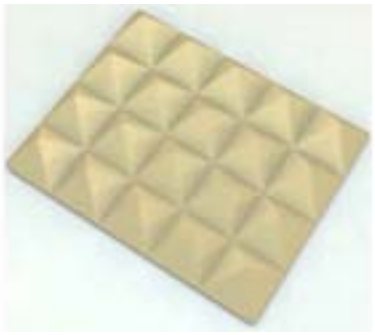

Figure 12: *Squares elevated.*

Figure 13: *Transformation.*

Figure 14: *Bending.*

Figure 15: *Cylindrical tiling with equilateral triangles.*

2.4. Cylinders – folding/unfolding. The method used in Figures 13 to 15 is just one way of creating cylindrical non-flat tilings with equilateral triangles.

Figure 16: *Tetrahelix.*

Figure 17: *Unfolding: plane.*

Figure 18: *Unfolding: strip.*

In Figure 16 we see the tetrahelix, one of the most simplest cylindrical non-flat tiling with equilateral triangles. The tetrahelix can be fold from the normal flat tiling with triangles (Figure 17), but we can also start with a strip of triangles. Just spiralling around as in Figure 18, the strip of triangles will become a tetrahelix. A lot of interesting new shapes can be made by using this way of building non-flat tilings. Especially when we do not just use the simple strip but also allow adding extra triangles at each side, as in Figure 19. This strip is used to produce spiralling cylindrical shape of Figure 20.

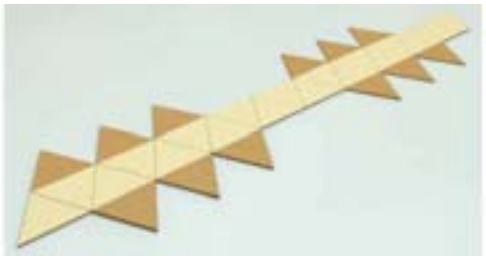

Figure 19: *Strip of triangles.*

Figure 20: *Spiralling cylinder.*

Many variations are possible. The examples shown in Figure 20 to 22 are all created while starting with a simple strip of triangles on which we add some extra triangles on each side.

Figure 21, 22: *Spiralling cylindrical tilings.*

3. Twisted Elevation

3.1. Twisting. Until now the tiles we have used can also be applied for flat tilings, or tiles that we knew as faces of the regular solids, the semi-regular solids and their duals. So we can ask ourselves whether it is possible to find other shapes of tiles that only can be used for non flat tilings. To study this we first go back to one of Leonardo da Vinci's drawings of an elevation of a polyhedron, the elevated icosahedron of Figure 23. The step we will now use by making a change in the shape of the tiles is called twisting. The elevated icosahedron can be seen as a set of twenty triangular pyramids. When we rotate each pyramid on it's own axis with the same angle we will get a new object, like the one in Figure 24 and 25. We will call this process twisting. In every stage the object we get is built out of (twenty times three) sixty faces, or tiles. The shape of the tile has changed from an equilateral triangle into a non-convex pentangle. And in every stage the shape of the tiles is the same. The object in Figure 25 can be recognized as a compound of five tetrahedral, but here it just is a set of sixty equal tiles that makes a non-flat tiling.

Figure 23: *Elevated icosahedron.*

Figure 24: *Twisting – first step.*

Figure 25: *Twisting – final step.*

3.2. New shapes. With twisting we have found a method to create new shapes that can be used for non-planar tilings. In general the shape of the resulting tile will be a non-convex polygon. The result of twisting applied on the non-planar tiling, that we created by elevating the planar tilings with squares is shown in Figure 26. And in this case it is clear that the tiles can not be used to make flat tiling. There is no way to fill the plane with these tiles without leaving gaps or without overlaps.
Two more examples can be seen in Figure 27 and 28. The non-flat tiling of Figure 27 is derived from the elevation of the flat tiling of equilateral triangle.

Figure 26: *Twisted elevation.* **Figure 27**: *Non-flat tiling.* **Figure 28**: *Non-flat tiling.*

4. Spiral Cylinders

4.1. New shapes for cylindrical tilings. To create new shapes of tiles for cylindrical tilings the method used to generate new tiles described in chapter 3 didn't turn out to be very successful. Therefore a new approach was developed. First a normal spiral curve is drawn. This curve is divided in equal parts. After that a straight line is drawn from the start point of the first part to the start point of the next part. And so on. These straight lines are then extruded downwards to the axis of the spiral, as in Figure 29. This is the basic shape that is needed to construct the shape of the tiles for the cylindrical tiling. The shape of Figure 29 is now turned upside down and added to the original shape (Figure 30). Both shapes do intersect, and from the intersection lines we can derive the final shape of the tile. The completed tiling is shown in Figure 31. The shape of the tile is a non-convex hexagon and can not be used to tile a flat plane. New tilings are created this way.

Figure 29: *Extruded spiral sections.* **Figure 30**: *Intersecting 'spirals'.* **Figure 31**: *Non-flat cylindrical tiling.*

4.2. Variations. The method described in chapter 4.1 allows many variations: the distance between the point on the spiral, the angle of the extrusion, and the position of the second spiral shape (height as well

as rotation angle) may vary. Each set of values will present another shape of tile. In Figures 32 to 34 just a few of the possibilities are shown.

Figure 32: *Cylindrical tiling..*

Figure 33: *Cylindrical tiling.*

Figure 34: *Cylindrical tiling.*

4.3. Unroll. Just like the spiralling cylinders in chapter 2, also the objects shown in Figures 31 to 34 can be unrolled into a simple strip of tiles. As an example the object of Figure 34 is unrolled here (Figure 35).

Figure 35: *Plan for cylindrical tiling of Figure 34.*

5. Classification

5.1. Glide Rotation. For the classification of tilings we make use of the symmetry operations that are needed to map one tile of the tiling onto another tile. In flat tilings these operations are called translation, rotation, reflection and glide reflection. When we want to map a tile onto another tile in one of the cylindrical tilings shown in Figure 31 to 34, none of the operations will give the result that we want. Translation, nor rotation, nor reflection, nor glide-reflection will map one tile onto another. What we need here is a combination of two operations, which are translation and rotation. While also glide reflection is a combination of two operations (translation and reflection), the most logical solution seems to be that we introduce a new operation: Glide Rotation, in literature often referred to as “screw rotation”.

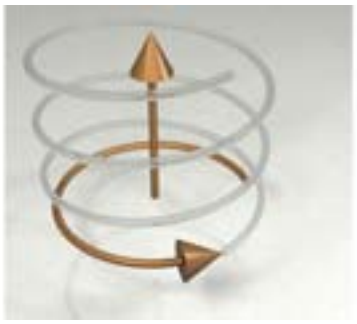

Figure 36: *Glide Rotation.*

Figure 37: *Pentagonal tiles.*

5.2. Polygons. In non-flat tilings all the tiles are polygons. Curved edges is not possible because of the use of flat tiles. An edge between two flat tiles, not laying in a plane is part of the intersecting line of the two planes in which the tiles are laying. And therefore the edge is always a straight line. So another property that we could use for classification might be the number of sides of the polygon. And because convex as well as non-convex polygons can be used, also the position of the non-convex angle can also be used for classification. In Figure 38 some of the main types of tiles for non-flat cylindrical tilings are put together. The notation is according the way it's being described in Heesch's and Kienzle's book Flächenschluss [3] in which they present the types for normal flat tilings.

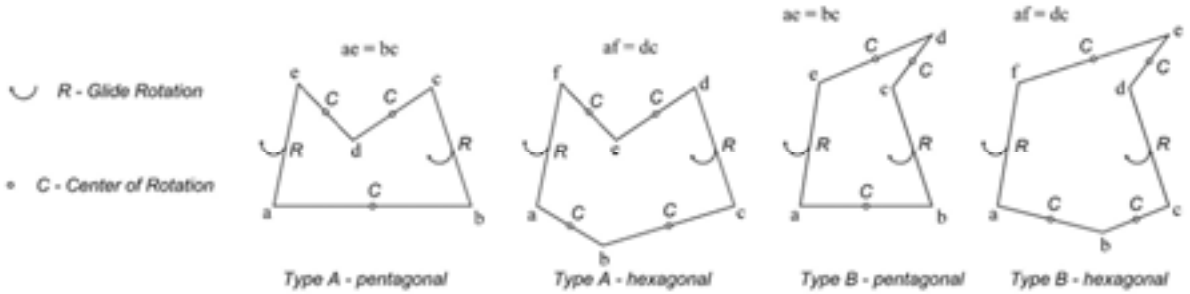

Figure 38: *Classification.*

5.3. Type B. In the pictures 39 to 41 you can see examples of the use of tiles B-pentagonal (Figure 39, 40) and tile B-hexagonal (Figure 41). The concept of non-planar tilings leads to new interesting structures. The method to create cylindrical tilings with flat tiles described in chapter 5.1 is one of the methods I found. To create the tilings shown in Figure 37 and Figures 39 to 41 other methods had to be used.

Figure 39: *Cylindrical tiling - pentagons.*

Figure 40: *Top view.*

Figure 41: *Cylindrical tiling – hexagons.*

Figure 42: *Convex pentagons - Type C.*

We will use the classification 'Type C' for tilings in which the tiles are convex polygons. Figure 42 shows a cylindrical tiling of Type C with the use of convex pentagons.

5.4. Triangular tiles. In normal flat tilings it is not required that all the corner points of the tiles meet in one point. In 'Tilings and Patterns'[1], page 475-481 we can see many examples of polygonal isohedral tilings in which the corner point of one tile touches another tile somewhere at the edge in between two corner points. In Figure 43 such a tiling is shown made by M.C. Escher [4]. Also in non-flat tilings this way of connecting the tiles can be used. In the examples (Figure 44 and 45) the constructions are tilings with Glide Rotation.

Figure 43: *M.C. Escher.*

Figure 44: *Triangular tiles (1).*

Figure 45: *Triangular tiles (2).*

5.5. Quadrangular tiles. For convex quadrangular tiles we now have two different ways of using them in non-planar tilings with Glide Rotation as can be seen in Figure 46. In Figure 46 also the triangular tile used in Figures 44 and 45 is shown.

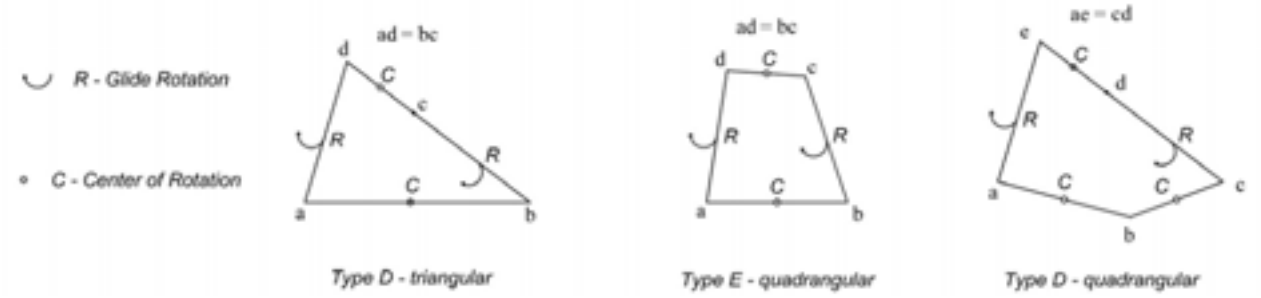

Figure 46: *Classification – convex triangular and quadrangular tiles.*

The use of quadrangular tiles leads to nice constructions. Many variations are possible as can be seen in the examples of Figures 47 to 49.

Figure 47: *Type E - quadrangular.*

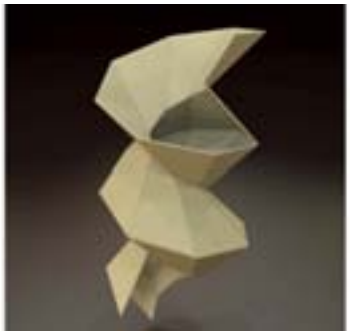

Figure 48: *Type E – quadrangular.*

Figure 49: *Type D – quadrangular.*

5.6. Special cases. Finally I want to show some special cases of the spiral cylinders with quadrangular tiles. For the tile of Type E we can change the shape of the quadrangle in such a way that it becomes a rectangle. And now the top view of the construction shows an equilateral triangle as the shape of the hole.

Figure 50: *Quadrangular tiles.*

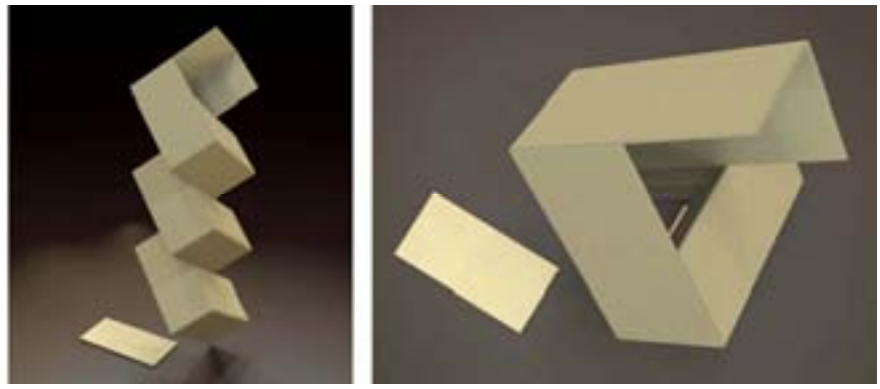

Figure 51, 52: *Rectangular tiles.*

And when we use a trapezoid with angles 60-60-120-120 degrees we will get a square hole.

Figure 53, 54: *Trapezoids.*

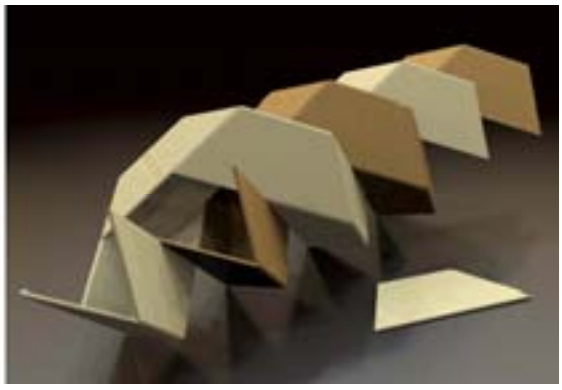

Figure 55: *Two entwined spirals.*

A special case of such a trapezoid is the tile used in the construction of Figure 55. The tile is the exact half of a regular hexagon, and it leads to a non-flat tiling that also can be seen as a combination of two entwined spirals.

6. Conclusion

6.1. Non-flat Tilings. I think the field of non-flat-tilings with flat tiles is interesting and needs further exploration. Especially the use of Glide Rotation leads to interesting new constructions which can be used as designs for sculptures. In other words, it is a topic which can bring art and mathematics together in an elegant way.

References

[1] Grünbaum and Sheppard, *Tilings and Patterns*, W.H. Freeman and Company, New York, 1987.
[2] Luca Pacioli, *La Divina Proportione*, Edicione Akal, Madrid, 1991 (first published in 1509).
[3] Heesch und Kienzle, *Flächenschluss*, Spinger-Verlag, Berlin, 1963.
[4] Doris Schattschneider, M.C. *Escher: Visions of Symmetry*, Harry N. Abrams, 2004 (2nd ed.).

Using Polyhedral Stellations for Creation of Organic Geometric Sculptures

Vladimir Bulatov
2970 Christine Street
Corvallis, OR, 97330, USA
E-mail: vladimir@bulatov.org

Abstract

We describe the process of making metal sculptures starting from geometric constructions based on stellation of polyhedra. Symmetry transformations and various algorithms of mesh subdivision are used to convert straight edges and planes of stellated polyhedra into smooth organic shapes.

Stellation of Polyhedra

Stellation is a process of extending the faces of a polyhedron in all directions to infinity. These extended faces divide the space into convex polygonal cells. In general, any subset of these cells may be called a stellation of the original polyhedron. Typically, only the most symmetric subsets are considered [1], but stellations with lower symmetry [2] are interesting as well. Figure 1 shows the steps of making the first stellation of icosahedron by attaching triangular pyramids to each face of the original icosahedron. Figure 2 shows the final step of this process - first stellation of icosahedron.

Figure 1: *First steps in stellation of icosahedron. The final shape is shown in Fig. 2*

The calculation of intersections of extended polyhedron faces is a tedious process to do by hand, but it can be easily done using interactive computer programs such as Stellation Applet [3] or Great Stella [4].
One can view the first stellation of icosahedron in Fig. 2 as a combination of the original icosahedron and 20 triangular pyramids attached to each of its 20 faces. However, we adopt here a different view: it is a surface consisting of 20 identical convex flat hexagons. One such face is marked with the bold outline in Fig. 2. These faces intersect along the edges of the original icosahedron and meet each other along the side edges of the triangular pyramids. We would like to build a surface with the same overall topology, but which has no intersections between the faces. One way to construct such a surface is to make deep cuts in each hexagonal face as shown in Fig. 3.

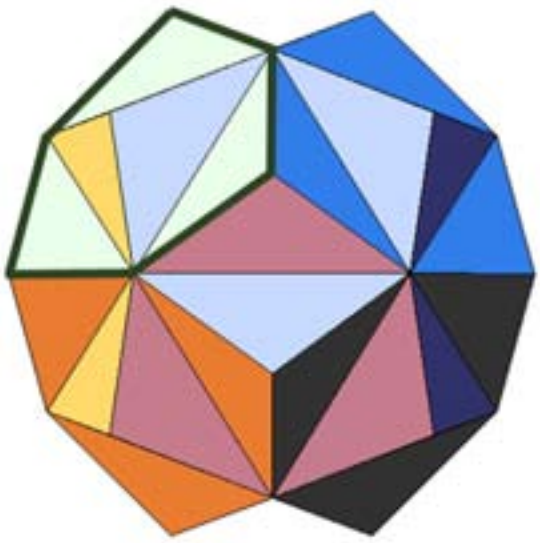

Figure 2: *Complete first stellation of icosahedron with one hexagonal face outlined.*

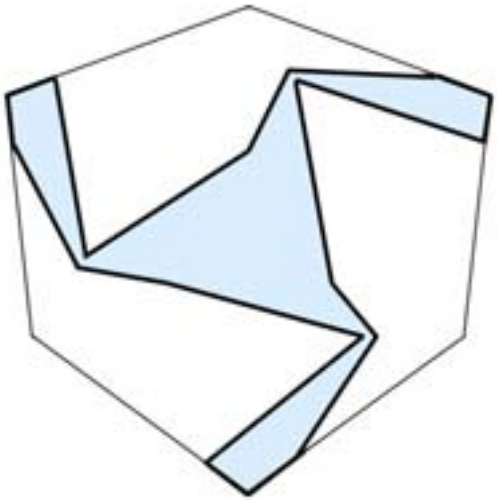

Figure 3: *A face of the first stellation of icosahedron with deep cut-outs.*

The complete surface composed of such prepared faces is shown in Fig.4. In order to make a real solid object one can assign to that surface some finite thickness as shown in Fig.5.

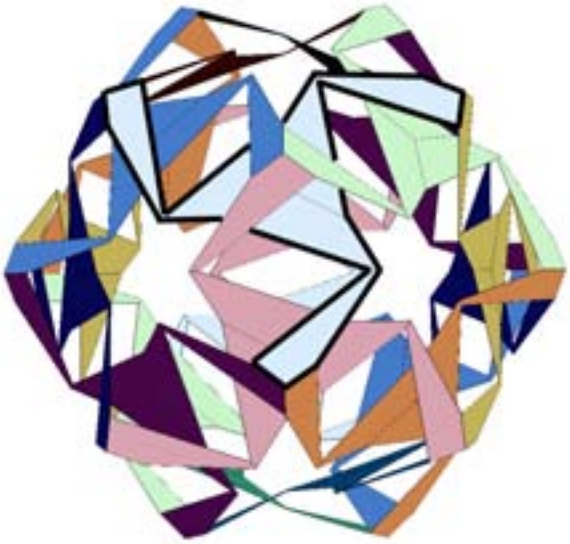

Figure 4. *The first Stellation of Icosahedron with cut out faces.*

Figure 5: *The faces are given some thickness.*

Subdivision

The object in Fig.5 possesses multiple sharp edges, and as such is far from our goal of an organic-looking shape. However, one can apply well-developed computer graphics algorithms known as surface subdivision, to smoothen the surface [5,6]. These algorithms refine a low-resolution mesh into a high-

resolution smooth mesh. The general idea of subdivision is to replace each polygonal face of the existing mesh with several smaller polygons, and then shift the vertices to new positions to make the new mesh smoother. The procedure is repeated several times until the surface is smooth enough. The result of this algorithm is shown in Fig. 6 for two simple initial shapes: the cube and a toroidal shape. One can observe that just a few subdivision steps result in very smooth looking surfaces.

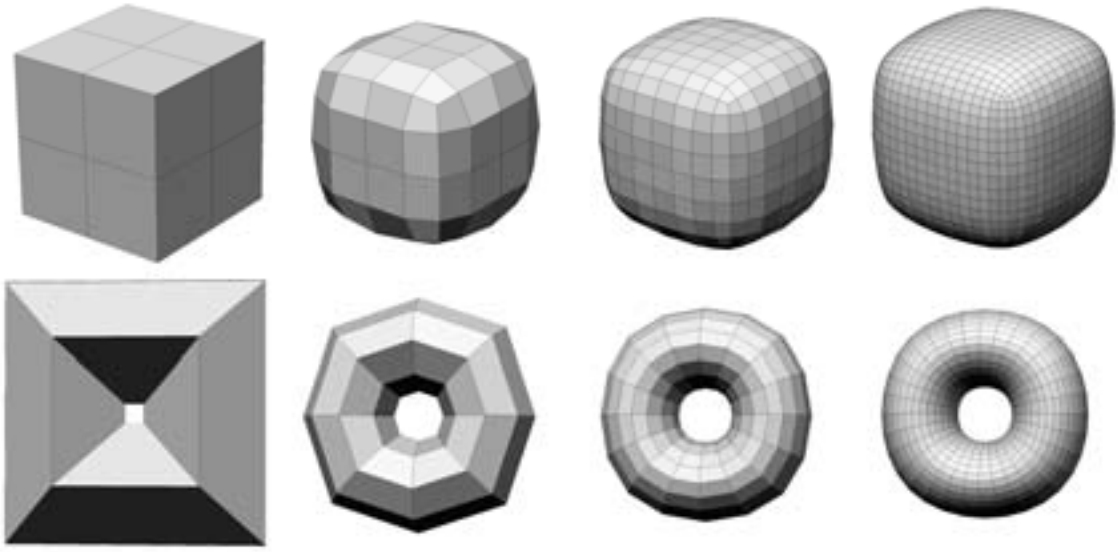

Figure 6: *Examples of mesh subdivision applied to the two simple shapes.*

Application of the subdivision algorithm to the first icosahedron stellation of Fig. 5 produces the sequence shown in Fig.7. The object becomes very smooth already after 3 subdivision steps.

Figure 7: *The subdivision sequence for the icosahedron stellation of Fig. 5.*

One more trick needs to be added to the algorithm. Real organic objects seldom have absolutely smooth surfaces. Typically, they have folds and creases of various types. The subdivision algorithms have been generalized to create such discontinuities in surface derivatives [7]. The idea is to mark some edges of the initial mesh as "crease edges" and then modify the shift rules for the vertices that belong to the crease edges. The result of the application of the modified algorithm to the mesh of Fig. 5 is shown in Fig. 8.

Metal Sculptures

There exist several fabrication technologies that can transform a 3D computer model into a real-world metal object. We have used Selective Laser Sintering (SLS) from 3D Systems [8] and Direct Metal Printing from ProMetal [9]. Both technologies make parts from stainless steel powder infiltrated with molten bronze. The first method produces more precise shapes with finer surface finish, but it has problems with larger pieces. They have the tendency to break during late stages of processing. In addition, the second method can make parts with copper and gold. Figure 9 shows a photo of sculpture "*Icosahedron I"* made using SLS technology. Outer corners of the sculpture have been polished. Polishing creates a pleasing combination of rough and smooth surfaces.

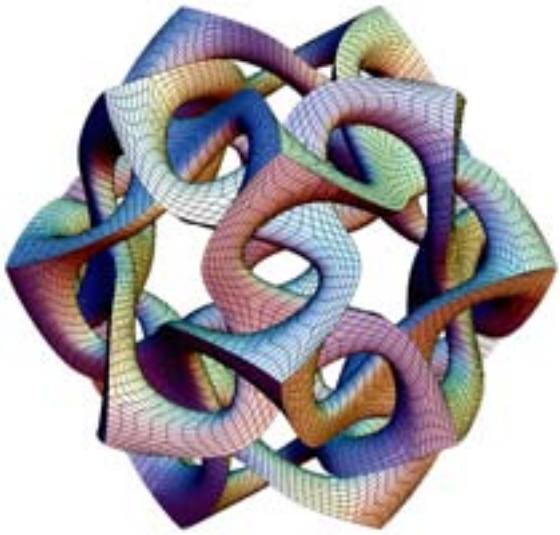

Figure 8. *A subdivision mesh with creases.*

Figure 9. *Icosahedron I.*
Steel and Bronze. Diameter is 4 inches.

Figure 10. *A subdivision mesh based on great stellated dodecahedron.*

Figure 11. *Dodecahedron X.*
Steel and Bronze. Diameter is 4 inches.

Figures 10-15 show additional examples of author's sculptures based on polyhedra stellations.

Figure 12. *Dodecahedron IX. Steel and bronze. Diameter is 4 inches. Based on Small stellated dodecahedron (the first stellation of Dodecahedron).*

Figure 13. *Dodecahedron IV. Diameter is 4 inches. Based on Great Dodecahedron (the second stellation of Dodecahedron)*

Figure 14. *Rhombic Triacontahedron III. Diameter is 4 inches. Based on stellation of Rhombic Triacontahedron.*

Figure 15. *Dodecahedron IV.* Diameter is 4 inches. Based on Great Dodecahedron.

Conclusion

Modern technology provides an artist with new tools and possibilities to make the art forms he or she wants. However, this raises the question: Can we call objects made with help of computer controlled machines art? Shouldn't art be hand made? Well, art is impossible without use of technology. No "*hand made*" art is truly hand made and modern technology is always used to some degree. The artist in his art work is entitled to use any tools he can get his hands on.
Other artists used stellations in the way similar to the author's. Most notable are M.C. Escher's *Double Planetoid (1949)* and *Gravity (1952),* and many sculptures of George Hart [10]. The original contribution of the author is application of subdivision algorithms to polyhedra stellations. The author writes his own software in Java and C.

The author is very grateful to Bathsheba Grossman [11] for inspiration and help in mastering the metal printing technology.

References

[1] *H. S. M. Coxeter, Patrick du Val, H. T. Flather, and J. F. Petrie.* The Fifty-Nine Icosahedra**.** Springer-Verlag, 1982. Originally published by Univ. of Toronto Press, 1938.
[2] *V. Bulatov.* An interactive Creation of Polyhedral Stellations with Various Symmetries. *Proceedings of Bridges 2001,* Winfield, Kansas, 2001. pp. 201-212.
[3] *V. Bulatov.* Stellations Applet software. http://bulatov.org/polyhedra/stellation_applet/
[4] *R. Webb.* Great Stella software. http://www.software3d.com/
[5] *Catmull, E., and Clark, J.* Recursively generated B-spline surfaces on arbitrary topological meshes. Computer Aided Design 10, 6 (1978), pp. 350–355.
[6] *Loop, C.* Smooth spline surfaces over irregular meshes. In Computer Graphics Proceedings (1994), Annual Conference Series, ACM Siggraph, pp. 303–310.
[7] *Henning Biermann, Adi Levin, Denis Zorin,* Piecewise Smooth Subdivision Surfaces with Normal Control. Computer Graphics (SIGGRAPH 2000 Proceedings), pp. 113-120.
[8] 3D system http://www.3dsystems.com/
[9] ProMetal http://www.prometal.com/
[10] *G. Hart*, "Sculpture from Symmetrically Arranged Planar Components", *Proceedings of ISAMA-Bridges 2003* Granada, Spain.
[11] *Bathsheba Grossman*, Sculpture http://bathsheba.com

Polyhedra Through the Beauty of Wood

Bob Rollings
883 Brimorton Drive
Scarborough, ON, M1G 2T8, Canada

Abstract

This paper has been prepared to demonstrate how I have used the geometry of polyhedra and my chosen medium of lathe turned wood to present the models shown in an aesthetically pleasing and artistic way. Each of the five platonic solids (tetrahedron, hexahedron, octahedron, docedahedron and icosahedron) has been interpreted through the eyes of a woodturner allowing the viewers alternate perspectives of these classic polyhedra. The description of each model includes details such as the type of wood used, dimensions and the process of fabrication.

Introduction

My interest in geometry stems no doubt from a lifetime spent in the cabinet making industry. Initially I worked as a hands-on craftsman and then later in a supervisory position which consisted of interpreting designer/architectural concepts and turning them into practical and beautiful pieces. After my retirement in 1996, I turned my interest in geometry into a hobby, using wood as a medium and a lathe as one of my many tools. I started a second journey of discovery as a wood turner/artist.

My investigation and interpretation of the platonic solids has been influenced by Johannes Kepler, Luca Pacioli, Leonardo De Vinci, M. C. Escher, and later by Buckminster Fuller and Donald Coxeter. After exhibiting some of my work at the Fields Institute I was invited to share space in Donald Coxeter's showcase in the math department at University of Toronto where I currently have four pieces on display.

The five platonic solids are the tetrahedron, hexahedron (cube), octahedron, dodecahedron and icosahedron. The properties of the platonic solids are that each of the faces is regular, the faces are identical, and at each vertex the same number of faces meet. Each pair of adjoining faces meet at the same angle and the vertices lay on the surface of a sphere.

Tetrahedra

Figure 1 is a simple tetrahedron model, which has been made of pear wood. Each of the faces is an equilateral triangle of about 2 inches long. The faces were cut using a template on a table saw with the mitre angle being 35.264 degrees. The angle was originally obtained from Table 8 [1] and then adjusted if required based on dry fitting the pieces. The piece was then glued and the holes were cut only to show that it is a hollow form.

Figure 1: *A simple tetrahedron*

The two tetrahedra shown in Figure 2 have turned spindles representing the edges. This type of model can be referred to as the web of the polyhedral form. The spindles,

which are 5/16” in diameter, have tenons turned on each end fitting into holes drilled into the ½ inch spheres representing the vertices.

The angle and the spacing of the three drilled holes is critical. The angles were approximated and then confirmed using cardboard models and a master block was produced. The holes were then drilled using the angled block and an indexing system to ensure equal spacing of the holes. This process was used to create other polyhedral spindle figures by producing other master blocks of appropriate angles and indexing.

Figure 2: *Two web tetrahedral*

The tetrahedron in Figure 3 was initially turned as a 6 inch walnut sphere. The four vertices were located using a compass. The compass is set using the diameter of the sphere divided by 1.25, which in this case is 4.8 inches. The first vertex was used as the starting point and a circle was scribed on the sphere. The second vertex is any point on the scribed circle. By rotating the compass left and right, the third and fourth vertices are established. If the setting on the compass is correct, this line will have been divided into three equal parts and you have located the four vertices of a tetrahedron.

The sphere was then hollowed out to a wall thickness of about ¾ inch, leaving enough wood to carve the double twists, which connect the vertices. The twists were cut freehand using a dremel burr.

Figure 3: *Artistic tetrahedral*

Hexahedra

The 6 inch cube in Figure 4 is a hexahedron designed to be a secret box. Made of applewood, its six faces are identical and one of them is also a screw-in panel. Each face is inscribed with two logarithmic spirals textured with a rotary burr prior to being highlighted with black acrylic paint. The logarithmic spirals were developed by repetitive division of a rectangle conforming to the proportion of the golden mean [2]. The spirals were transferred to the figure by rotating the template 180 degrees around the centre of each face.

Figure 4: *Hexahedron box*

Octahedra

The grouping shown in Figure 5 was one of my first attempts at working with platonic solids. Although they appear to be one octahedron and three spheres, all four started as octahedra each having eight equilateral triangular faces. The name “The Family” comes from the idea that all the boxes come from the same original form.

Three of the octahedra were lathe turned to their spherical shapes What sets them apart is the species of wood and the manner in which the lids are oriented. For the lower box I used becote and divided it at the equator; four sections for the lid and four sections for the bottom. For the middle box I used laurel and used two sections for the lid and six sections for the bottom. For the upper box I used wenge. Again, there were four pieces for the lid and four pieces for the bottom, the difference being the orientation of the triangles, which produces the zig-zag edge when the lid is removed

Figure 5: *The Family*

This octahedron in Figure 6 was inspired by a traditional quilting design known as tumbling blocks. The technique used is referred to as stickware or Tunbridgeware as it has been made up from a bundle of sticks. In this case, the sticks are rhomboids cut at 30 degrees with each of the faces being of equal length. A group of three made of three different colours of wood can be bundled together, the end view creating the optical illusion of a cube. The next step is to rebundle them together to make a triangular stick, which can then be cut into identically patterned slices. Eight of the resulting equilateral triangles are mitred and glued together to produce an octahedron. The woods in this case are holly, white oak and cocabola.

Figure 6: *Stickware octahedron*

Dodecahedra

The dodecahedron in Figure 7 came about when I made stickware for some spinning tops. Having enough left over for 12 faces, I decided to make this dodecahedron. I took the ten sided stick and clad it with five pieces of oak to construct the pentagonal stick. From this stick I cut 12 panels, each 3/16 inches thick, to make the dodecahedron. The woods used are holly, cocabola, pear, white oak, and maple, and it is about 7 inches in diameter.

Figure 7: *Stickware dodecahedron*

Figure 8 is titled Piece-Peace Suspended. This title is intended to be a play on words. As you can see, the dodecahedron box is suspended. Each face of the dodecahedron is a pentagon, which is a symbol of peace. The box was intended to symbolically contain George's weapons of mass destruction but when you look inside, the box is empty. The web, made of ebony, represents the web of evil. The handle, which is a dove, but not the white dove of peace, is made from the same black ebony.

Figure 8: *Piece-Peace Suspended*

Figure 9 is a stellated dodecahedron. The term stellated was coined by Johannes Kepler [3]. Stellation is a process that allows us to derive a new polyhedron from an existing one by extending the faces until they re-intersect.

Figure 9: *Stellated dodecahedron*

The flat planes, which emerge from these figures, enable this piece to be produced using the lathe or the bandsaw; I opted for the latter. The first step is to create a sphere and then locate the 12 vertices. The compass setting is calculated using the diameter of the sphere times 0.526 [4] and an initial circle is scribed on the sphere. Choosing any point on the initial circle, a second circle is scribed creating two intersection points. Circles are drawn from each point where two circles intersect. Each point of intersection becomes a vertex. At the end of this process, the twelve vertices will have been located.

Holes were drilled at each of the vertices and a temporary rod was inserted to act as a pivot while cutting the faces on the bandsaw. A jig was used to control the depth of cut on all 12 axes and as the wood fell away a dodecahedron emerged. The holes were plugged using contrasting coloured wood for emphasis.

Figure 10: *Web icosahedron*

Icosahedra

The simple web of the icosahedron (Figure 10) emphasizes the symmetry and balance of all of the platonic solids. The web is created using spindles and spheres for the vertices as previously described with the only difference being the angles at which they are drilled and the number of holes drilled. The spindles are made from rose wood and the spheres at the vertices are boxwood. The piece is about 12 inches in diameter.

Figure 11: *Spherical icosahedron*

The sphere in Figure 11 was initially a faceted icosahedron made from curly maple. The joints have been emphasized with a laminate of black, white, and black veneer. The vertices were drilled out and replaced with black inserts. Centered on each insert are hand turned flowers of several designs and a variety of woods.

Figure 12 is a stellated icosahedron, which began as a solid sphere made from madrone. The faces were then cut on the bandsaw using a similar technique described for Figure 9. In this case there are 12 pivot points of rotation located in the valleys, which can be seen as the black caps of ebony. The base is made of walnut and was made on the lathe, using a swing pivot router, then painted black. The finished piece is 9 inches high.

Figure 12: *Stellated icosahedron*

Figure 13 is a combination of a stellated and a concave icosahedron. All of the panels used to make this piece are 1/8 inch thick. There are 120 flat panels required to construct the piece. It is about 8.5 inches from point to point. The panels are mitre cut using a template and glued together.

Figure 13: *Stellated and concave icosahedron*

Hybrids

In the following pieces I have used the solid faces of the platonic solids surrounded by web models. I call these designs hybrids.

In Figure 14 we have compounds of two tetrahedra constructed from eight minor tetrahedra; four of which are walnut, and the other four are maple. One of the vertices of each of the eight minor tetrahedrons becomes the corners of a hexahedron. I have joined these together using applewood spindles to reinforce the relationship.

Figure 14: *Tetrahedron-hexahedron hybrid*

This stellated dodecahedron in Figure 15 has been made up of 3/16 inch babinga panels; five panels for each pyramid with a total of 60 panels. The 12 vertices give us the framework for the web, which as you can see is an icosahedron. The 30 spindles and spheres are rosewood.

Figure 15: *Dodecahedron-icosahedron hybrid*

The piece shown in Figure 16 was completely turned on the lathe. It was inspired by Wenzel Jamnitzer who was a German etcher/goldsmith and drew this piece in 1568 [5]. I can only assume it was never made and that it was only a graphic design as the main body only hovered above the base. The wood for the core icosahedron is honey locust and the web and base were made in cocabola.

Web Models

The following four pieces have been modelled using a web design. They consist of more artistic interpretations of the platonic solids and were done using webs so that the entire shape, as in line drawings, are visible from a single perspective.

Figure 16: *Totally Turned*

This is a web model of a stellated icosahedron (Figure 17). It is interesting to see that when the 20 faces are stellated to create 20 new vertices we begin to see a relationship between the icosahedron and the dodecahedron. There are 12 planes where pentagons are formed. The vertices of the stellated icosahedron are created by extending the edges of these pentagons. The ratio of the length of the spindles to the length of the base conforms to the golden mean.

Figure 17: *Stellated icosahedron*

After completing the work shown in Figure 17, I saw further possiblilities and so created Metamorphosis (Figure 18). The relationship between the dodecahedron and icosahedron fascinated me. It began with a central dodecahedron. In the centre of each of the 12 faces, spindles were projected to create the 12 vertices of the icosahedron. Finally the icosahedron was stellated to create the 20 vertices of the outer dodecahedron. The web was then connected between these vertices completing the metamorphosis.

Figure 18: *Metamorphosis*

Johannes Kepler lived from 1571 to 1630, had a great interest in the platonic solids, and was the inspiration for this piece. It was his contention that the orbits of the planets are related to the platontic solids. In Figure 19, each of the platonic solids are contained within one another and each rotate on their own axis. From the centre working out we have the tetrahedron, hexahedron, octahedron, dodecahedron and then finally the icosahedron. Each rotates, as do the heavenly bodies. This piece has a total of 90 spindles and 40 vertices. The spindles and the circular frame are Brazilian rosewood, the vertices are boxwood and the base is black painted hardwood.

Figure 19: *Kepler Theory*

Figure 20 is an example of a progressive web transformation. The centre is an octahedron, which has been converted by making each of the eight faces into tetrahedrons. Four were made from ebony and four from holly. These not only express two major intersecting tetrahedrons, but also indicate the eight vertices of the hexahedron. The various woods used here are pear, ebony, holly, and satinwood. The circular frame is walnut and the base is black-painted hardwood. This piece has found a home in Donald Coxeter's showcase of models, at the University of Toronto's math department.

Figure 20: *Transformation*

The following two pieces have been inspired by Luca Pacioli's publication of De Divina Proportiona, published in 1509 in which Leonardo De Vinci drew the illustrations of the regular solids. Leonardo's drawings are probably the first illustrations of skeletonic solids.

Figure 21 is similar to De Vince's model and my interpretation of the piece is constructed of 84 individual frames mitred together. The side angles had to be cut prior to assembly. After the first row of 12 frames had been glued together the other rows could be glued and assembled until the sphere was closed. All faces of the strips used for the frames were prefinished prior to assembly as all faces can be seen. The sphere was made from babinga wood and has a 10 inch diameter. The base is turned from walnut and has been weighted with lead shot to permit the piece to be shown in an offset position.

Figure 21: *De Vinci model 1*

The second of Leonardo's pieces is a torus. This is his mazzocchio which he drew in solid edge form. It consists of 32 sections around the circumference (Figure 22). Each section contains eight frames for a total of 256 frames, each with specific side angles. This model is made from zebra wood and is 14 inches in diameter.

Figure 22: *De Vinci torus*

Figure 23 shows a web model of Buckminster Fuller's Vector Equilibrium [6], which is a polyhedron. It is a cuboctahedron with all the vertices connected to the centre.

It has many unique properties; it has 12 vertices, which lie on the surface of a sphere. It contains 24 edges as well as 14 faces. Vector equilibrium is comprised of eight tetrahedrons and six half octahedrons. Finally, the distance from any two adjoining vertices is identical to the distance from any vertices to the central sphere. The piece rotates within its circular oak frame, which in turn pivots in the base.

Figure 23: *Vector equilibrium*

This article has described many of the polyhedra and platonic solids I have worked on in the past few years and is also the result of much reading on the subject. The journey is endless and the variables infinite.

References

[1] J. Cox, *Beyond Basic Turning*, pp. 209. 1993.
[2] R. Lawlor, *Sacred Geometry*, pp. 64-70. 1982.
[3] P. Cromwell, *Polyhedra*, pp. 168-171. 1997.
[4] D. Sprigett, *Woodturning Wizardry*, pp. 20-22. 1993
[5] P. Cromwell, *Polyhedra*, pp. 288. 1997.
[6] R. Buckminster Fuller in collaboration with E.J. Applewhite, *Synergetics*, pp. 118. 1982.

Growth Forms

George W. Hart
Computer Science Dept.
Stony Brook University
Stony Brook, NY 11790 USA
george@georgehart.com

Abstract

This paper presents work-in-progress on techniques for procedurally "growing" organic-looking forms. The goal is to design and implement techniques for expressing simple algorithmic operations that can be combined in various ways to produce forms that develop from an amorphous blob to a structured cellular assemblage. Growth "buds" in a cellular assemblage each execute short programs that determine local parameters of growth, e.g., directionality, branching, cell size, cell shape, and color. These are executed in a software simulator package that generates both graphical (2D) and geometric (3D) output. Every step along the way determines a triangulated manifold boundary that can be fabricated by solid freeform fabrication equipment. I plan to incorporate these techniques into future sculpture that combines mathematical ideas with organic sensibilities.

Introduction. Nature provides an enormous range of attractive organic forms which have inspired artists through the ages [2]. In previous work, I have created simulated organic forms reminiscent of underwater sea life via mathematical models of an entire organism's static structure [3]. This paper explores simple techniques for mimicking various organic forms via a simple dynamic growth process, e.g., Figure 1. The goal is to create organic-looking geometric sculpture which can be built on 3D printing machines. It relates to well-known techniques of L-Systems [6] but is designed to create smooth surfaces with a triangulated manifold boundary that can be fabricated by solid freeform fabrication equipment.

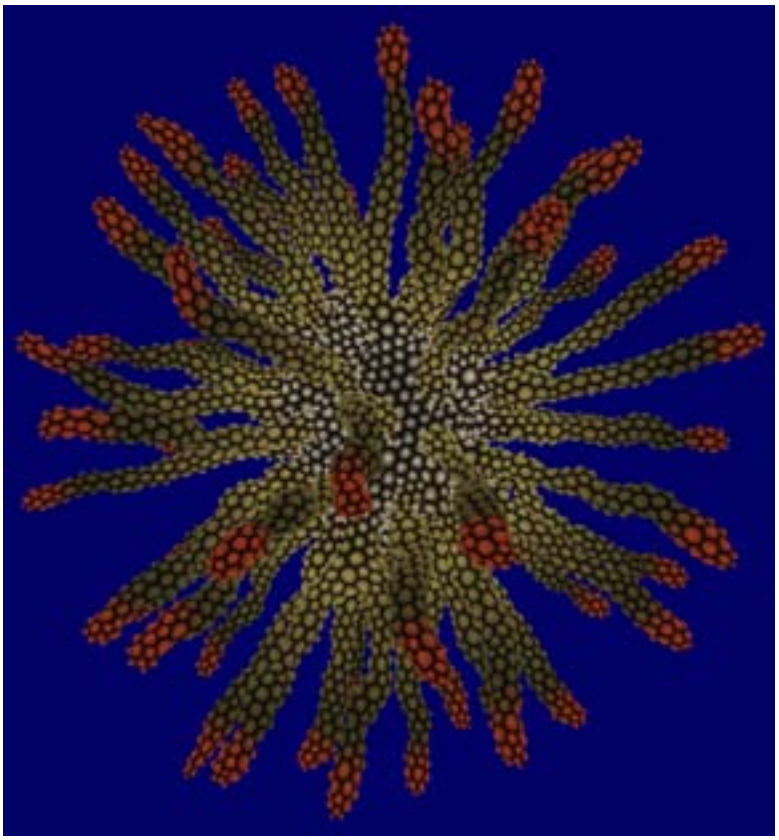

Figure 1: *A cellular form that develops by outward growth at the tip of each arm.*

A form here is represented as a network of "cells" on its surface, analogous in some ways to skin cells on an organism. Each cell has properties assigned to it, including size, color, and texture (e.g., bumpy or smooth). A cell may divide into two cells, which are topologically connected into the space that the single cell formerly occupied. Their geometry is then determined by a spring energy relaxation model that calculates new positions for the cells so all are the appropriate distance from their neighbors. As a consequence, after cell division the surface bumps out slightly to accommodate the additional cell. Some cells contain a special entity, called a "bud" that controls the growth and cell properties in their local area. Each bud follows an algorithmic program, allowing it to control how nearby cells divide, to change its growth properties over time, to split into two or more new buds, to check for collisions, and to do other simple operations. There may be several different bud types and any number of buds, each independently following the program for its bud type. The behavior for each bud type is specified in advance using a simple programming language. The growing areas around the various buds develop and interact to result in complex, visually attractive overall structures. Due to many random choices of exactly which cell divides when, the same program when executed repeatedly gives output that appears like different individuals of a single species. The project is not intended as a simulation of particular organisms or natural mechanisms. The goal is simply to produce sculptural forms that mimic the forms of various natural biological processes. The best means to understand the growth dynamics is to view the screen-capture videos at [4].

Origins: Symmetry via Growth. I began this project when thinking about how icosahedral symmetry rarely appears in nature. Certain microscopic viruses and radiolarians have icosahedral forms but, to my knowledge, no larger multicellular organisms do. As a fan of icosahedral symmetry, I could envision a simple growth process that in principle could lead to larger scale icosahedral organisms. The mechanism appears similar to natural biological growth processes, and nature has an enormous range of techniques, so why does this not appear in nature?

The proposed growth mechanism involves buds that promote growth in their local area. It is apparent from observing the type of apical growth one observes, e.g., in trees, that there is something special at the tip of each branch causing it to elongate. Suppose twelve such buds were randomly positioned in a small spherical blob of cells, each causing growth in their local area, perhaps by producing some sort of "growth hormone" that diffuses away from them and causes nearby cells to divide. If two buds happened to be very close to each other, the area between them should receive twice the dose of hormone and so grow faster than average, pushing the two buds away from each other. Conversely, if buds are very far from each other, most of the area between them has little hormone so does not grow. This appears to provide a stabilizing feedback mechanism that would, after some time, cause buds to be roughly equally spaced from their neighbors. So if twelve buds started out randomly distributed in a spherical ball of cells, I envision this mechanism producing an even distribution of buds, i.e., positioned as the vertices of an icosahedron. If the bud regions continued to grow, I would expect a kind of 12-armed almost-regular icosahedral "starfish" to result. But I know of no such biological organism. So I decided to "play god" and see if I could create one. And while I was at it, I made an environment for creating a range of other organic-looking forms that develop by bud-based growth.

Local cell division. In this model, cells are like small balls that stick to their neighbors in a monolayer surface or skin. Each is surrounded by a small number of adjacent cells, most typically five, six, or seven. This adjacency relation determines a graph I call the "cell graph." Each cell is represented by a vertex. When cells are adjacent, there is an edge connecting the corresponding vertices. In most examples below, the skin has no "donut holes," i.e., it is of genus zero, so the cell graph is planar, but that is not essential to the method. One example is shown of a process in which holes are grown, making high-genus forms.

The growth algorithms below ensure that the cell graph always corresponds to a triangulated surface. This simplifies some of the algorithms and makes it easy to convert to the STL file format for 3D printing machines. Furthermore, it corresponds visually to what one finds in nature, where cells in surfaces usually meet in groups of three [7]. However, unlike most real organisms, these forms are empty of all structure.

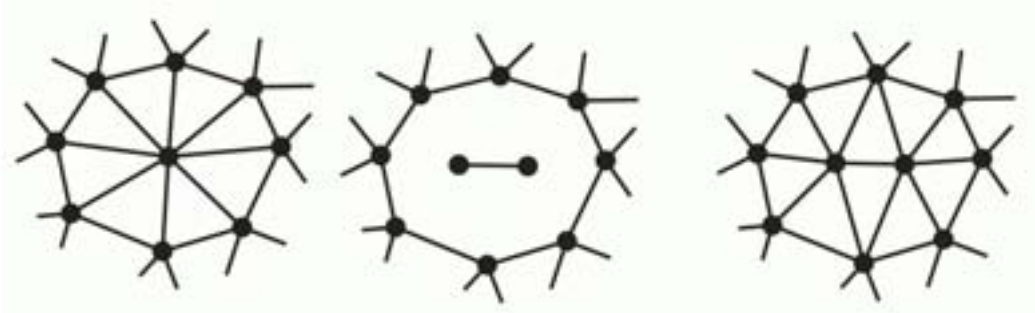

Figure 2: *Cell division process. If the center cell at left is chosen for division, it is temporarily removed and replaced with two cells that join each other. The surrounding n cells (here, n=8) connect via n+2 edges to the two new cells, to make a triangulated graph. Here, the topmost and bottommost of the eight surrounding cells each end up with one more edge than they began with.*

Given a cell graph and a cell to divide, we apply the procedure illustrated in Figure 2. It is a special type of "vertex splitting" designed to maintain a triangulated graph of approximately balanced degree. The vertex corresponding to the cell that divides is removed, temporarily creating an n-gon face if the cell had n neighbors. Two new vertices are placed in this face and connected to each other. These two cells are then connected to the n surrounding vertices, using exactly n+2 edges so that the result is triangulated. This means that most of the surrounding vertices connect to just one of the two new cells, but two of the surrounding vertices connect to both of the new cells. For those two surrounding vertices, their neighbor count will increase by one. As we do not want vertices of very high degree, we choose the surrounding vertex of lowest degree for one that will increment. The other is chosen to be opposite the first in the n-gon, as otherwise the two new cells would have unbalanced degrees. (If n is even, this completely determines the opposite vertex, but if n is odd we can round up or down, and do so in a way that increments the degree of the one with lower degree if they are not equal, otherwise randomly.)

Position determination. Cell division, as described above, is a topological operation on the cell graph. To form a geometric surface, we need to embed this graph in 3D space by assigning a position to each vertex. This is accomplished here by a "spring embedder" algorithm which treats each vertex as a massless node and each edge as a spring with a preferred length. We define an energy function associated with vertex pairs that is quadratic in the difference between the actual length and the preferred length. We choose coordinates for each node to minimize the sum of these spring energies. The actual global minimum is difficult to compute, but a simple iterative algorithm can repeatedly adjust one node at a time to minimize its contribution to the energy. This can be accomplished with a straightforward Newton-Raphson numerical method which converges very quickly. The actual method applied is similar to the method of [5] but adapted for 3D. (Another difference from [5] is that we use a spring for each pair within a distance of at most four hops, taking the shortest distance in the graph as the target distance. This is fast and seems to work because of the triangulated nature of these graphs.)

After a cell divides and the cell graph is updated, the spring embedder algorithm is used to locate the positions in space of the two new cells and relocate their surrounding n-gon. Assuming all edges are specified to be of unit length, this requires that the surface bump out to accommodate two cells where there was formerly one. (The preferred edge lengths can be specified to be any positive length, not just unity, as discussed below. Whatever they are, the algorithm seeks an embedding with actual lengths that closely match them.)

Bud behavior. Our forms are represented by a cell graph (its topology) and a position for each cell (its geometry). Given a form, the cell division and spring embedder mechanisms above are applied to produce a slightly modified form whenever a cell divides. The overall process begins with a small blob of cells, e.g., a tetrahedron of four cells, as that is the simplest triangulated polyhedral manifold. One possible mode of behavior is to allow any cell to divide, perhaps choosing at random repeatedly. We call this method "general growth" and starting from a tetrahedron, it produces "blobs" of arbitrary size.

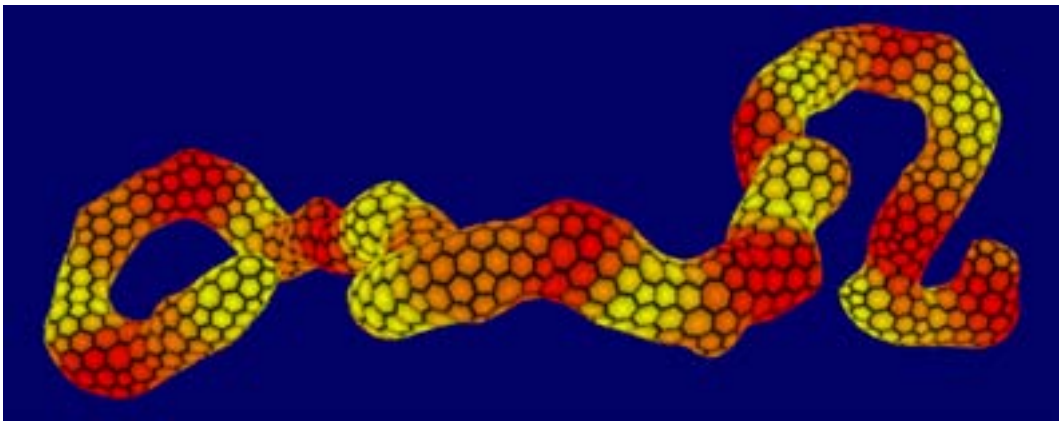

Figure 3: *Having just a single bud results in a snake-like form. If no specific tropism is specified, it wanders in a type of self-avoiding random walk in 3D.*

To control the form, we introduce *buds*, which may be thought of as small microcontrollers that sit inside some cells. In the examples below, there may be ten thousand or more cells, but at most a few dozen of them contain a bud. Each bud has a set of parameters that control which nearby cells should divide and how frequently. Currently this is specified in terms of the number of "hops" in the cell graph, i.e., a bud may specify that a randomly chosen cell within distance three of it is to divide. As nearby cells divide, the bud-containing cell is pushed along, like the tip of a growing plant. By restricting the hop distance to be small, a thin tube is formed. By allowing it to be larger, a fatter branch is generated. Conceptually, this corresponds to the bud producing "growth hormone" that diffuses either to only the adjacent cells or more widely to a larger neighborhood of cells.

If a bud-containing cell divides but the bud does not divide, the bud may end up in either of the two children cells. Generally, this is done at random, but it is natural to allow for a number of variations on this idea. For example, the bud may also split, so it becomes two independent buds, one in each of the two cells. In that case the two buds each continue independently to make nearby cells divide. They soon are pushed away from each other and become two independent branches. Continuing in this way, with repeated bud division, results in fractal branching structures.

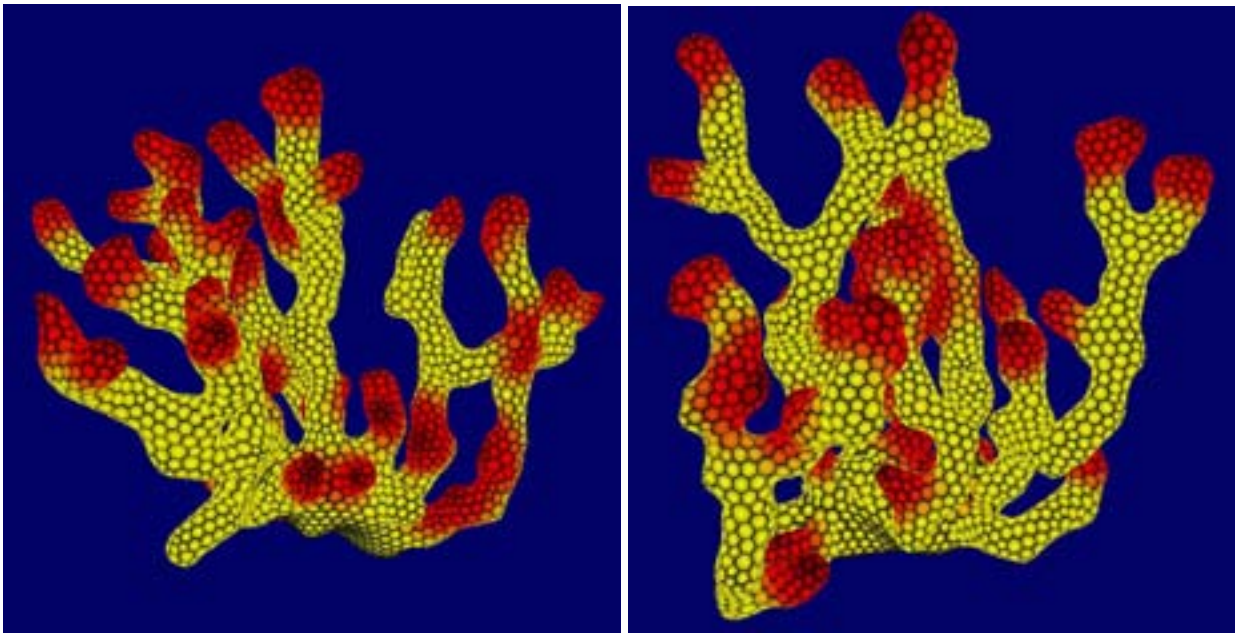

Figure 4: *Allowing buds to occasionally split into two buds gives a branching fractal form. Due to randomness of which cell is chosen to divide, one script run twice produces different "individuals" within a "species".*

When a bud-containing cell divides, we can take that opportunity to introduce a gentle steering mechanism. If we place the bud in the higher of the two cells, as measured by Z coordinate, the net effect is to introduce a vertical tropism. Without such a tropism, the tube takes a kind of a random walk through space, as in Figure 3. This is because the cell with the bud is "pushed forward" by nearby cell divisions, which depend on a pseudorandom number generator, sometimes favoring left or right, etc. With the vertical tropism, as in Figure 4, there is a feedback mechanism that encourages the bud to be at the top of the growing region. (One may think of this physically as floating buoyantly within the cell before division, so it ends up in the upper of the two children cells, or perhaps as attracted to light trickling down to the seafloor from the sea surface, but I can avoid biology and think of it merely in terms of which cell's position maximizes a dot product with a target heading.)

Other bud properties control cell color and cell texture. When a bud causes a cell to divide, the two new cells are assigned the color and texture specified in the bud. So for example, if this bud color is gradually changing over time, the branch will have a gradient of colors along its length. The colors can be used artistically in computer graphics output. But for physical fabrication, I do not have access to a color 3D printer, so I introduced some parameters of cell texture to appear in uncolored fabricated output. For example, each cell can be flat, a bump, indented like a dimple, spiked with a hair, or any shape in between. As the position data for each cell is converted to an STL file for 3D printing, these parameters are used to determine the exact cell geometry. Details are omitted here, as techniques for geometrically texturing small regions are well-known [1].

Another variation on bud division is that buds contain a "line flag" which if set to *true* specifies they should maintain a connected line with neighboring buds. If before cell division a bud is in a cell adjacent to another cell containing the same kind of bud, but after cell division it is no longer adjacent, insert a new bud in the cell that separates the previous neighbor. The effect of this is that there is always an unbroken line of these buds. This can be used to create growth along an edge of a leaf-like form. Such a line can be seen in Figure 5, producing a negatively curved surface.

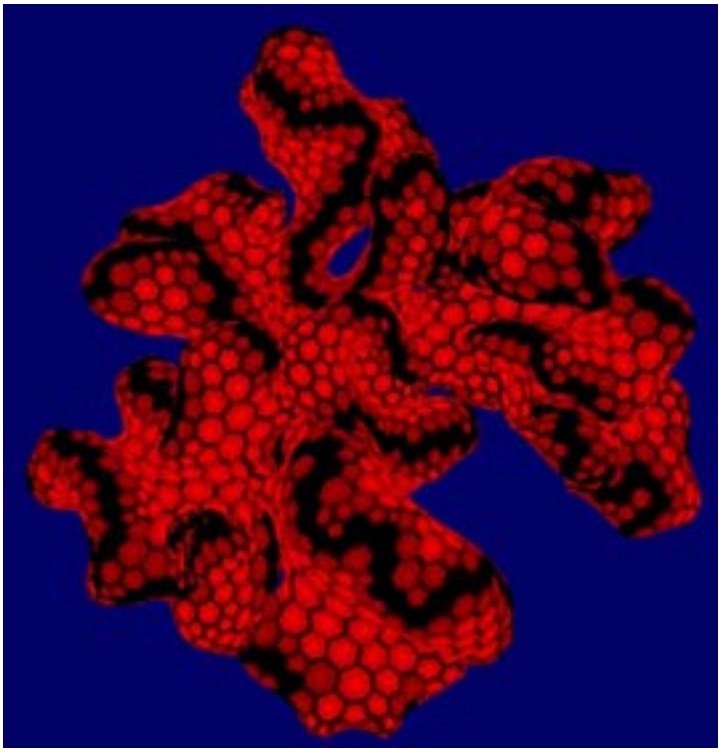

Figure 5: *The result of keeping a single line of buds (dark) is a negatively curved form.*

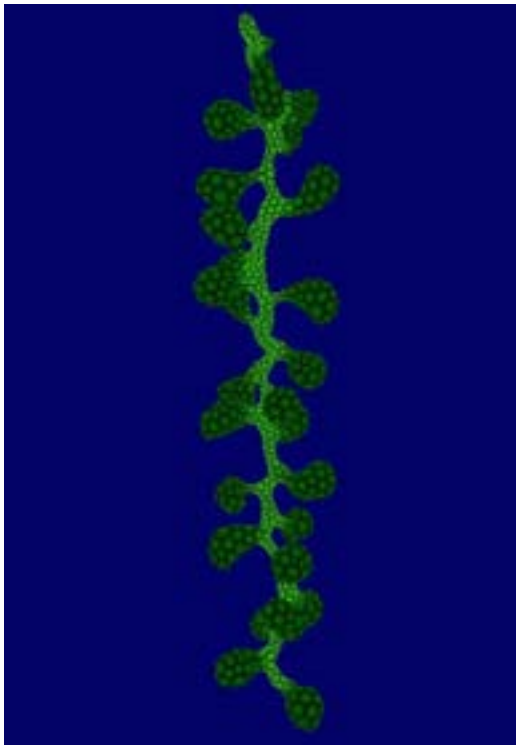

Figure 6: *Result of a program with two bud types, one for stem and one for pods.*

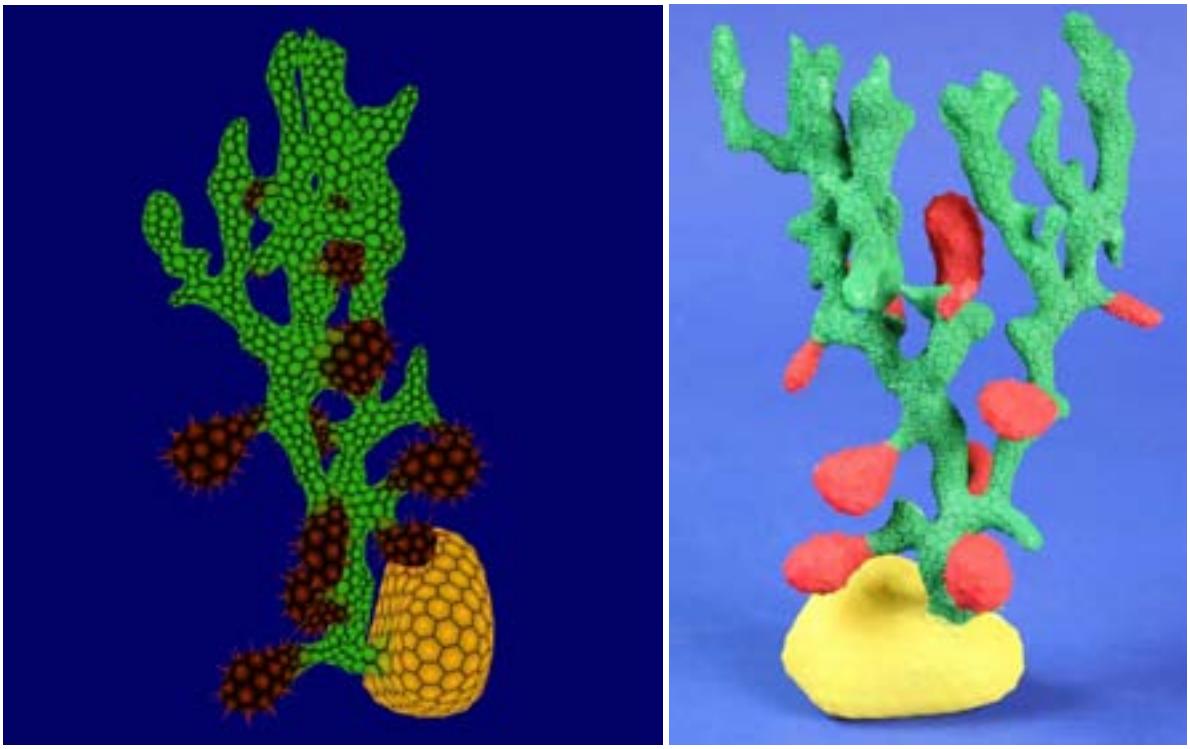

Figure 7: *Three types of buds allow a form with a blobular root, a branching stem, and spiky fruits, which are older and riper at the bottom. At right is a 3D printed model (hand painted) based on a similar run of the same program.*

Buds can also specifically create new buds of other bud types in nearby cells. The new bud then starts following its own program to control the region around it. For example, to produce Figure 6 a single "stem" bud grows upwards forever to make the main branch. At intervals, it produces a "pod" bud that grows out from the stem into a pod. The pod bud is programmed to make larger cells of a different color, and after a finite number of cell divisions it dies. In Figure 7, the program is very similar, except the program for the stem bud splits into two after a certain period of growth and the pod bud specifies a spiky texture.

In physical organisms, a growing region may collide with another so each is constrained in shape by the other. Here, a bud will "freeze," i.e., stop executing its program, if the region it controls is about to collide into other parts of the form. This is checked after each cell division by standard software techniques, using a specifiable tolerance of closeness. As a result, a branch will not grow into or through others, and the surface remains a triangulated manifold.

Syntactic representation. Bud behavior has a temporal component. At any moment, there can be different buds following the same program, but at different steps in the process. For example, a pod bud which was created early on a stem may have completed the pod program, while another pod bud higher up the stem is half complete, and another near the newest part of the stem is just beginning. This sort of behavior is naturally accommodated by having a syntactic representation for the bud behavior and what is effectively a time sharing operating system which keeps track of the "program counter" for each bud.

A typical program looks like Figure 8, which is read and interpreted by the software (described below) to produce the form in Figure 7. This program defines three bud types, called `Base`, `Stem`, and `Pod`. Each is processed in a procedural manner; the lines are executed in order. By convention, the form always starts as a tetrahedron of four cells with one bud of the first type given in the program. In this case, there will be a bud of type `Base` which creates the blob at the bottom of the form. The `yellow` and `flat` commands set parameters for color and texture, then the `blob 300` command results in general growth for 300 steps. In the third line, a bud of type `Stem` is created and inserted into an adjacent cell. As that is the end of the

`Base` program, the `Base` bud then dies. Meanwhile, the `Stem` bud sets its parameters to head upwards and make green cells with a bumpy texture. The `fat 0` command sets its "growth hormone diffusion radius" to be small. It grows a thin tube for 40 cells, leaving a pod bud in one of them three quarters of the way along. It reaches the last line of its program and dies just after it creates two new `Stem` buds, which will follow the same `Stem` program from the beginning. Finally, the `Pod` buds at first grow like a stem for ten cells, and then become red with a spiky texture. The `size 1.3` command overrides the default cell size of 1, making longer edges in the spring embedding algorithm, and the `fat 4` command leads to a blobbier shape. Figure 7 shows a seven-inch plastic model of the result, which was produced by fused deposition modeling, then hand painted.

```
Base:                Stem:                Pod:
  yellow, flat         head up              grow 10
  blob 300             green, bumpy         red, spiky
  create Stem          fat 0                size 1.3
                       grow 30              grow 20
                       create Pod           size 2.0
                       grow 10              fat 4
                       create Stem 2        grow 20
```

Figure 8: *Program to create branching stem with spiky red pods seen in Figure 7. These programs are usually written linearly, but this is broken into three columns for exposition.*

When writing a time-sharing computer operating system, there are many details of synchronization and fairness to be worked out, e.g., what portion of the machine's CPU cycles should be assigned to each user, job, and thread. There are analogous issues here, to specify the relative growth rates of each bud's area. I have temporarily addressed this by giving each bud an equal share of the growth but allowing a `sleep` command (not shown) which I can use to slow down a bud's program in places. Future work should address this more systematically, as the balance of growth rates strongly affect the form's appearance.

Software. The images here and the videos on the web page [4] show the output of software I have written which implements all the above ideas. It is currently about 2000 lines of Java code and generates any of these forms in real time, in under a minute. A parser interprets the bud code and a time sharing scheduler puts each bud in control briefly in an interleaved manner. Meanwhile a separate graphics thread continually displays the current state of the form and allows it to be rotated on the screen under mouse control. It is very much experimental software, with various additional algorithmic ideas implemented or partially implemented and still being explored, which may or may not survive my testing. In addition, there are user interface functions for reading and saving the bud programs, executing programs one step at a time, outputting STL files for 3D printing, and various options for coloring, smoothing, and filtering the final output. I am exploring many experimental features, so the program is not in a stable enough state to make it publicly available any time soon. For example, Figure 9 shows the result of an experimental process that grows holes. Two cells near a bud are removed and the resulting boundaries are stitched together with a tunnel through the interior, which takes the form of an antiprism joining the temporary boundaries. This operation produces holes in many random directions and increases the genus by one each time it occurs. This does not correspond to any biological process I know of, but makes for interesting sculptural surfaces.

Conclusions and Future work. The forms presented here are inspired by nature, but the mechanisms do not necessarily simulate nature. I'm not a biologist, just an algorithm designer attempting to find simple ways to derive a wide range of interesting 3D organic forms. These forms may appear very different from the geometric style of my main body of sculptural work, but my intention is to use them as components and/or ornaments in larger structures that express an overall geometric aesthetic. That larger plan will hopefully be presented in future work, but must remain vague for the moment as I focus on this subproblem.

Rapid prototyping models of forms shown here are easily made. I am working on additional types of simple bud behavior which I expect will result in other visually interesting patterns of growth and form. These will be coded and tested with the intention to produce a large variety of forms from a small inventory of mechanisms. In addition, because the bud programs are syntactic, one might use genetic or evolutionary algorithm techniques to evolve them according to some fitness criterion, e.g., to maximize subjective beauty.

Finally, I can sometimes grow an icosahedral form, but it happens rarely. My 12-armed blobs usually have a less regular set of directions, so the icosahedral ones appear to be mostly due to luck. In the context of these growth mechanisms, it seems there is nothing particularly stable about the icosahedral form, as opposed to other 12-vertex forms such as the cuboctahedron.

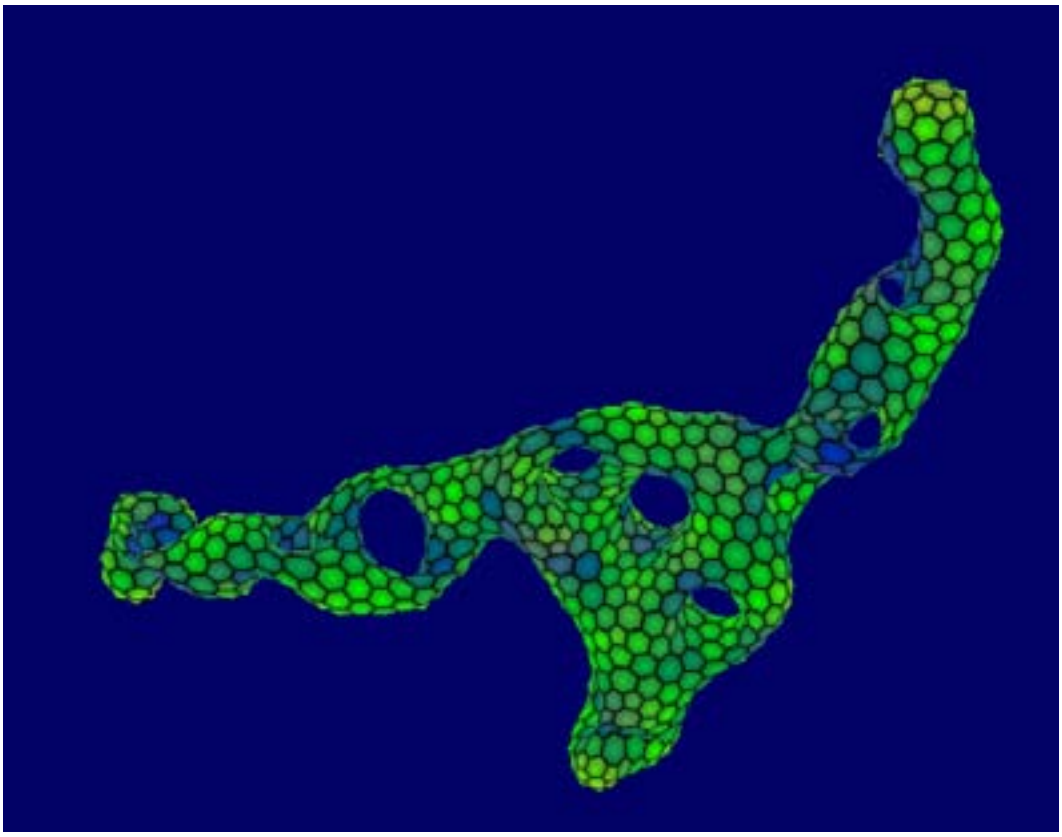

Figure 9: *High-genus form results from growing holes.*

References

[1] Kurt Fleischer et al., “Cellular Texture Generation,” SIGGRAPH 1995.

[2] Ernst Haeckel, *Artforms in Nature,* Verlag des Bibliographischen Instituts, 1904.

[3] G. Hart, "An Algorithm for Constructing 3D Struts," *Journal of Computer Science and Technology*, 24:1, 2009, pp. 56-64.

[4] G. Hart, videos at **`http://www.georgehart.com/Growth/growth.html`**

[5] Tomihisa Kamada and Satoru Kawai, “An Algorithm for Drawing General Undirected Graphs,” *Information Processing Letters*, 31:7-15, 1989.

[6] Przemyslaw Prusinkiewicz and Aristid Lindenmayer, *The Algorithmic Beauty of Plants,* Springer, 1991.

[7] D’Arcy Wentworth Thompson, *On Growth and Form,* Cambridge, 1952.

Using Works of Visual Art to Teach Matrix Transformations

James Luke Akridge*, Rachel Bowman*, Peter Hamburger, Bruce Kessler
Department of Mathematics
Western Kentucky University
1906 College Heights Blvd.
Bowling Green, KY 42101
E-mail: james.akridge620@wku.edu, rachel.bowman708@wku.edu,
peter.hamburger@wku.edu, bruce.kessler@wku.edu
Undergraduate students.

Abstract

The authors present a modern technique for teaching matrix transformations on $\mathbb{R}^2$ that incorporates works of visual art and computer programming. Two of the authors were undergraduate students in Dr. Hamburger's linear algebra class, where this technique was implemented as a special project for the students. The two students generated the images seen in this paper, and the movies that can be found on the accompanying webpage **www.wku.edu/~bruce.kessler/**.

1 Introduction

As we struggle to increase the number of students succeeding in the science, technology, engineering, and mathematics disciplines, it is the opinion of the authors that

- we must find ways to motivate a larger audience as to the importance and relevance of these disciplines, and
- once we have convinced students to invest in a discipline, we must then be innovative in the ways that we engage the students in learning, so that they stay in the discipline.

The second of these ideas was put into practice in Dr. Hamburger's Fall 2008 linear algebra class, in such a way that both the scientifically-minded and artistically-minded students were actively engaged in the course, and eventually learned a great deal about the topic.

Matrix multiplication has a number of applications that can attract the interest of students, but as we move to a more abstract understanding of matrices as generators of transformations, we sometimes lose the interest of the more application-driven students. In general, multiplying an $m \times n$-matrix (that is, a matrix with m rows and n columns) on the right by an n-vector (column), generates an m-vector, so it can be interpreted as a transformation from $\mathbb{R}^n$ to $\mathbb{R}^m$. We generally illustrate this type of transformation in $\mathbb{R}^2$ with rather dull diagrams, such as the ones shown in Figure 1. If the matrix causes the same change with every vector in $\mathbb{R}^2$, then the effect of the matrix multiplication would be shown on one vector, as on the left in Figure 1, where $R(x,y)$ is a counterclockwise rotation about the origin of 60°. If the matrix has varying effects depending on the choice of the vector, then perhaps two vectors are shown under the transformation, as on the right in Figure 1, where $T(x,y)$ stretches vectors horizontally by a factor of 2 and vertically by a factor of 1.5. (See sample college-level linear algebra texts [1, 2, 3, 4], where [3] probably comes closest to the work illustrated in this paper with its visual interpretation of matrix transformations.)

This method of showing the effects of matrix multiplication is antiquated and goes back to a time when computers were not available. A better understanding of the effect of the matrix multiplication would be

*The authors would like to thank the four anonymous reviewers for their valuable suggestions which improved the manuscript.

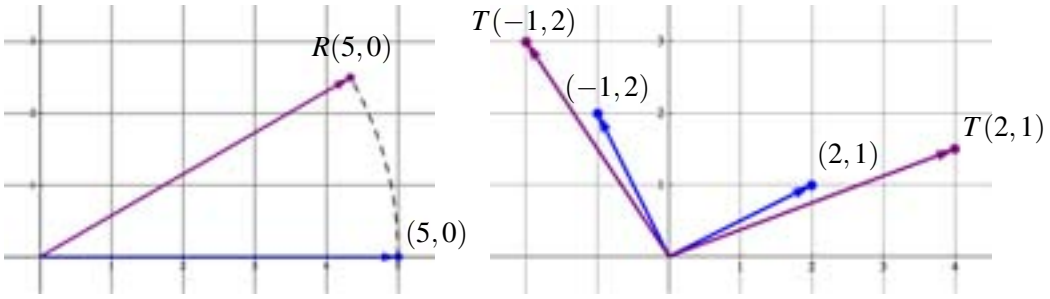

Figure 1: Typical diagrams illustrating the effects of matrix multiplication.

gained by applying the matrix to every point in $\mathbb{R}^2$, an impossibility. However, we can look at a large number of regularly-spaced vectors in the plane, but drawing all of the vectors would cause an undecipherable mess. Instead, we start with a digital image that we recognize, so that we can tell the effects of the matrix transformation on each pixel of the image. This could be a digital portrait of anyone, but given that some people might object to having their portrait warped, we decide instead to use famous works of visual art. This gives the observer an original image to which they can compare, and has the added bonus of capturing the interest of students that have an affinity to the visual arts.

The following section provides a brief introduction to matrix transformations in general, and to the specific code that was used to generate the examples in this paper.

2 Definitions and Code Used

Terminology. A ***transformation on*** $\mathbb{R}^2$ is any mapping T that takes a point in $\mathbb{R}^2$ to a point in $\mathbb{R}^2$. Any transformation on $\mathbb{R}^2$ that can be expressed in the form

$$T\begin{pmatrix}x\\y\end{pmatrix} = \begin{bmatrix}a(x,y) & b(x,y)\\ c(x,y) & d(x,y)\end{bmatrix}\begin{bmatrix}x\\y\end{bmatrix}, \tag{1}$$

where a, b, c, and d are real-valued functions dependent upon x and y, is called a ***matrix*** transformation on $\mathbb{R}^2$. Note that we use the short-hand notation $T\begin{pmatrix}x\\y\end{pmatrix}$ in place of the bulky, but more accurate, notation $T\left(\begin{bmatrix}x\\y\end{bmatrix}\right)$. For example, the transformation T defined by

$T\begin{pmatrix}x\\y\end{pmatrix} = \begin{bmatrix}x^2+y^2\\ 2xy\end{bmatrix}$ can be considered a matrix transformation, since $T\begin{pmatrix}x\\y\end{pmatrix} = \begin{bmatrix}x & y\\ y & x\end{bmatrix}\begin{bmatrix}x\\y\end{bmatrix}$.

Not all transformations are matrix transformations. As an example, the transformation T defined by

$$T\begin{pmatrix}x\\y\end{pmatrix} = \begin{bmatrix}a & b\\ c & d\end{bmatrix}\begin{bmatrix}x\\y\end{bmatrix} + \begin{bmatrix}e\\f\end{bmatrix}, \quad a,b,c,d,e,f \in \mathbb{R}, \tag{2}$$

called an ***affine*** transformation, is defined for all $(x,y) \in \mathbb{R}^2$ and always maps to a point in $\mathbb{R}^2$, but it does not fit the form of (1) unless $\begin{bmatrix}e\\f\end{bmatrix} = \begin{bmatrix}0\\0\end{bmatrix}$. In that case, the transformation is said to be a ***linear*** transformation.

Programming the Transformations. The code used for this project was written by the author Kessler for the algebraic manipulation software package *Mathematica*™, due to the ease in generating graphics and movies, and due to our students' familiarity with the software from their prerequisite coursework. The

code is presented here in the syntax of the *Mathematica*™ programming language, which is very readable since the commands are usually full English words. The code generates an animation of the transformations applied recursively, which we obviously can not show here. In our illustrations, we show selected frames from the animations. The full animations are available for download at **www.wku.edu/˜bruce.kessler**.

We opted to center the digital images on our coordinate axes, as shown in Figure 2. This allows us the best "viewing window" with which to watch the effects of the matrix transformation on the image when using our choices of matrices. The units on the axes are pixel-widths. The size of the images were not standardized, as our code adjusts for the size of the image.

Figure 2: Placement of the coordinate axes with respect to the digital images.

While we want to give the appearance that we are moving the pixels to different locations in the plane, we are actually considering each pixel as a fixed location. Thus, instead of changing the location of a pixel P by repeated multiplying by a matrix A, we apply the inverse matrix A^{-1} to each pixel P, and note the color of its resulting pixel P'. We then recolor each pixel P to that color, giving the illusion of applying the transformation to each pixel. The *Mathematica*™ code is given below, with the matrix set to $\begin{bmatrix} \frac{79}{80} & 0 \\ 0 & \frac{39}{40} \end{bmatrix}$.

```
(* The following command inputs the image file.  You supply the
 file name. *)
temp = Import["31PersistenceOfMemory.jpg"];
colors = Reverse[temp[[1, 1]] / 255.];
(* Scales the RGB values for Mathematica. *)
{rows, cols, check} = Dimensions[colors];  (*Sets the dimensions. *)
countermax = Max[rows, cols];
rmax = rows / 2.; cmax = cols / 2.; max = Max[rmax, cmax];
centers = Table[{-max + j - .5, -max + i - .5}, {i, countermax}, {j, countermax}];
(* The following command inputs the matrix that will be used to
 generate the graphics. *)
matrix[x_, y_] := {{79/80, 0}, {0, 39/40}} // N;
imat[x_, y_] = Inverse[matrix[x, y]];
f[{x_, y_}] := imat[x, y].{x, y};
```

```
(* The following two commands put the original picture into the
 list of frames, as the initial frame. *)
newcolors =
  Table[If[1 ≤ Floor[centers[[i, j, 1]] * cmax * .50000001] ≤ cols &&
     1 ≤ Floor[centers[[i, j, 2]] * rmax * .50000001] ≤ rows,
    colors[[Floor[centers[[i, j, 2]] * rmax * .50000001],
     Floor[centers[[i, j, 1]] * cmax * .50000001]]], {.5, .5, .5}],
   {i, countermax}, {j, countermax}];
frames = {Graphics[Raster[Reverse[newcolors]]]};
Print["0"];
(* The following do-loop generates the frames for the animation.  You
  specify how many frames past the original that are generated
  by changing the value after "n," in the last line. *)
Do[(
  centers = Map[f, centers, {2}];
  newcolors =
   Table[If[1 ≤ Floor[centers[[i, j, 1]] * cmax * .50000001] ≤ cols &&
      1 ≤ Floor[centers[[i, j, 2]] * rmax * .50000001] ≤ rows,
     colors[[Floor[centers[[i, j, 2]] * rmax * .50000001],
      Floor[centers[[i, j, 1]] * cmax * .50000001]]], {.5, .5, .5}],
    {i, countermax}, {j, countermax}];
  AppendTo[frames, Graphics[Raster[Reverse[newcolors]]]];
  Print[n];
 ), {n, 100}]
Export["WM_stochastic.avi", frames]
```

3 Examples

The students experimented with a number of different types of 2×2 matrices. The following sections and figures show some of the more interesting results from this experimentation. The still figures show the effects of the various matrix transformations much more effectively than the vector diagrams shown in Figure 1, and the animations are even more illustrative.

Dilations. Matrix transformations with matrices of the forms

$$\begin{bmatrix} k & 0 \\ 0 & 1 \end{bmatrix} \quad \text{and} \quad \begin{bmatrix} 1 & 0 \\ 0 & k \end{bmatrix}$$

are called ***horizontal*** and ***vertical dilations***, respectively. If $0 < k < 1$, the dilation is a ***contraction***. If $k > 1$, then the dilation is called an ***expansion***. The effects can be combined into one dilation matrix, since

$$\begin{bmatrix} k_1 & 0 \\ 0 & 1 \end{bmatrix} \begin{bmatrix} 1 & 0 \\ 0 & k_2 \end{bmatrix} = \begin{bmatrix} 1 & 0 \\ 0 & k_2 \end{bmatrix} \begin{bmatrix} k_1 & 0 \\ 0 & 1 \end{bmatrix} = \begin{bmatrix} k_1 & 0 \\ 0 & k_2 \end{bmatrix}.$$

The images shown in Figure 3 were generated by applying the dilation matrix $\begin{bmatrix} \frac{79}{80} & 0 \\ 0 & \frac{39}{40} \end{bmatrix}$ to a 580 pixel wide by 418 pixel tall digital image of Salvador Dali's painting "Persistence of Memory". This causes a horizontal contraction, and a slightly faster vertical contraction.

Shears. Matrix transformations with matrices of the forms

$$\begin{bmatrix} 1 & k \\ 0 & 1 \end{bmatrix} \quad \text{and} \quad \begin{bmatrix} 1 & 0 \\ k & 1 \end{bmatrix}$$

Figure 3: The original picture at left. Ten applications of the contraction matrix at center. Fifty applications of the matrix at right.

are called ***horizontal*** and ***vertical shears***, respectively. The sign of the value k determines the direction of the shear.

The images shown in Figure 4 were generated by applying the shear matrix $\begin{bmatrix} 1 & 0.01 \\ 0 & 1 \end{bmatrix}$ to a 563 pixel wide by 705 pixel tall digital image of one of Van Gogh's self-portraits. This causes a horizontal shear, with the top moving to the right and the bottom moving to the left. Figure 5 shows the effects of a vertical shear with the matrix $\begin{bmatrix} 1 & 0 \\ -0.02 & 1 \end{bmatrix}$ applied to the same image.

Figure 4: The original picture at left. Twenty applications of the horizontal shear matrix at center. One hundred applications of the matrix at right.

Rotations. Matrix transformations with a matrix of the form

$$\begin{bmatrix} \cos\theta & -\sin\theta \\ \sin\theta & \cos\theta \end{bmatrix}$$

are called ***rotations***. Multiplication by this matrix causes a counterclockwise rotation by θ degrees about the origin.

The images shown in Figure 6 were generated by repeatedly applying the rotation matrix $\begin{bmatrix} \cos(1^\circ) & -\sin(1^\circ) \\ \sin(1^\circ) & \cos(1^\circ) \end{bmatrix}$ to a 400 pixel wide by 572 pixel tall digital image of Leonardo daVinci's painting "Mona Lisa".

Figure 5: The original picture at left. Twenty applications of the vertical shear matrix at center. One hundred applications of the matrix at right.

Figure 6: The original picture at left. Twenty applications of the rotation matrix at center. One hundred applications of the matrix at right.

Distance-dependent rotations. Matrix transformations with a matrix of the form

$$\begin{bmatrix} \cos(f(d)) & -\sin(f(d)) \\ \sin(f(d)) & \cos(f(d)) \end{bmatrix},$$

where f is a function defined on non-negative real numbers and d is the Euclidean distance from the origin $\sqrt{x^2+y^2}$ for the pixel with coordinates (x,y), are called ***distance-dependent rotations***. The images shown in Figure 7 were generated by repeatedly applying the distance-dependent rotation matrix

$$\begin{bmatrix} \cos\left(2\sqrt{\frac{x^2+y^2}{rmax^2+cmax^2}}\,1^\circ\right) & -\sin\left(2\sqrt{\frac{x^2+y^2}{rmax^2+cmax^2}}\,1^\circ\right) \\ \sin\left(2\sqrt{\frac{x^2+y^2}{rmax^2+cmax^2}}\,1^\circ\right) & \cos\left(2\sqrt{\frac{x^2+y^2}{rmax^2+cmax^2}}\,1^\circ\right) \end{bmatrix},$$

where *rmax* and *cmax* are as defined in the *Mathematica*™code, to a 400 pixel wide by 572 pixel tall digital image of Leonardo daVinci's painting "Mona Lisa".

Stochastics. Matrices of the form

$$\begin{bmatrix} a & 1-b \\ 1-a & b \end{bmatrix},$$

Figure 7: The original picture at left. One application of the distance-dependent rotation matrix at center. One hundred eighty applications of the matrix at right.

where $0 \leq a \leq 1$ and $0 \leq b \leq 1$, are called ***stochastic*** matrices. Stochastic matrices are used to calculate probabilities, and are usually thought of in the context of Markov chains or random walks. While not generally thought of in the context of matrix transformations, we can certainly define matrix transformations using these matrices.

The images shown in Figure 8 were generated by applying the stochastic matrix $\begin{bmatrix} \frac{29}{30} & \frac{1}{60} \\ \frac{1}{30} & \frac{59}{60} \end{bmatrix}$ to a 750 pixel wide by 652 pixel tall digital image of James Whistler's painting best known as "Whistler's Mother".

Figure 8: The original picture at left. Five applications of the stochastic matrix at center. Twenty-five applications of the matrix at right.

Other Matrices. The undergraduate students went through their own type of transformation – from being mathematics students using matrices on art, to "matrix artists" using mathematics to generate their pieces. The students involved in this project were very creative in developing matrices, other than the types described above, that generated beautiful animations, using time and distance dependencies in their matrices. In order to increase computation efficiency, they replaced the pictures with grids of points in the plane, colored according to their initial quadrant as shown at the top left in Figure 9, thereby allowing the students to run experiments more quickly. Figure 9 shows selected frames from animations created by the students, using the transformations

$$T\begin{pmatrix} x \\ y \end{pmatrix} = \begin{bmatrix} 1-\frac{1}{xy} & -\frac{1}{xy} \\ \frac{1}{xy} & 1-\frac{1}{xy} \end{bmatrix} \begin{bmatrix} x \\ y \end{bmatrix} \quad \text{and} \quad T\begin{pmatrix} x \\ y \end{pmatrix} = \begin{bmatrix} \cos\left(\frac{n\sqrt{x^2+y^2}}{200}1^\circ\right) & -\sin\left(\frac{n\sqrt{x^2+y^2}}{200}1^\circ\right) \\ \sin\left(\frac{n\sqrt{x^2+y^2}}{200}1^\circ\right) & \cos\left(\frac{n\sqrt{x^2+y^2}}{200}1^\circ\right) \end{bmatrix} \begin{bmatrix} x \\ y \end{bmatrix}.$$

at top and at bottom, respectively, where n is the iteration number. Again, the still frames do not do the animations justice, and we encourage readers to view the animations on the previously mentioned website.

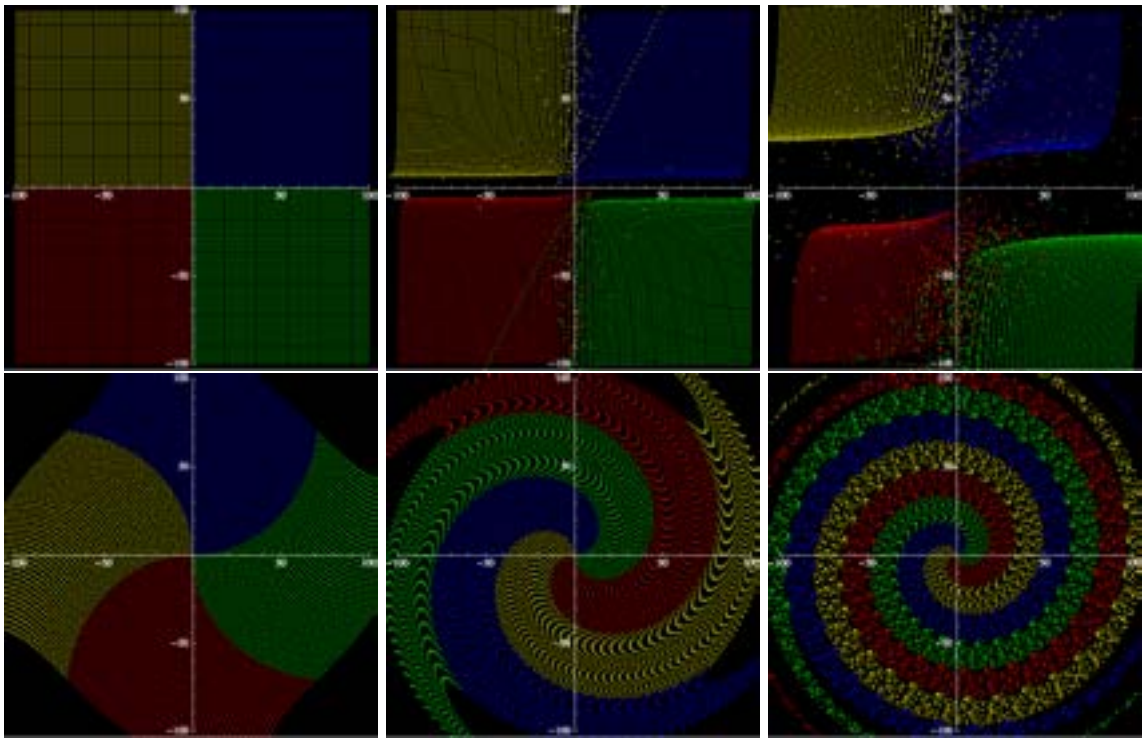

Figure 9: The original picture at top left. Progressive frames of one animation, top center and top right. Progressive frames of another animation, bottom row.

4 Conclusion

It has often been said that "A picture is worth a thousand words." In our cases illustrated here and on the fore-mentioned webpage, this idea could be extended to say "An animation is worth a thousand diagrams." While the idea of using matrix transformations to create art is not new, it was definitely a new approach to learning linear algebra for our students. There can be little doubt that the students who worked on this project now have a better understanding of the effects of these matrices on points in the plane than they would have ever had just looking at vector diagrams. In the course of analyzing the results, they have also touched upon other seemingly unrelated topics, like vector norms, eigenvalues, and matrix limits. In the course of doing so, they have broadened their recognition of art, and have learned how to create their own "masterpieces".

References

[1] H. Anton, "Elementary Linear Algebra", 8th edition, John Wiley & Sons, 2000.

[2] R. Larson, B. Edwards, and D. Falvo, "Elementary Linear Algebra," 5th edition, Houghton Mifflin Company, 2004.

[3] G. Strang, "Introduction to Linear Algebra", Wellesley-Cambridge Press, 1998.

[4] D. Wright, "Introduction to Linear Algebra", The McGraw-Hill Companies, 1999.

Regular 3D Polygonal Circuits of Constant Torsion

Tom Verhoeff *
Faculty of Mathematics and CS
Eindhoven University of Technology
Den Dolech 2
5612 AZ Eindhoven, Netherlands
Email: T.Verhoeff@tue.nl

Koos Verhoeff
Valkenswaard, Netherlands

Abstract

We explore a special class of regular 3D polygonal circuits, that is, of regular non-planar polygons. In these circuits, all segments (edges) have the same length, all corner angles are equal, and all torsion angles have the same (absolute) value. We also show some artwork based on these constant-torsion circuits.

1 Introduction

Consider the polygonal circuit[1] in Figure 1. Although not immediately obvious from the pictures, this is a highly regular 3D structure. It consists of 16 *equal-length segments*. The 16 *angles between adjacent segments* are all *equal* (viz. to 49.94°). We call these the **corner angles** or **joint angles**. Finally, the 16 *dihedral angles between adjacent corner-spanning planes* are *equal* (viz. to 90°). Figure 2 shows these planes explicitly. We call the latter angles the **torsion angles**, as explained further below.

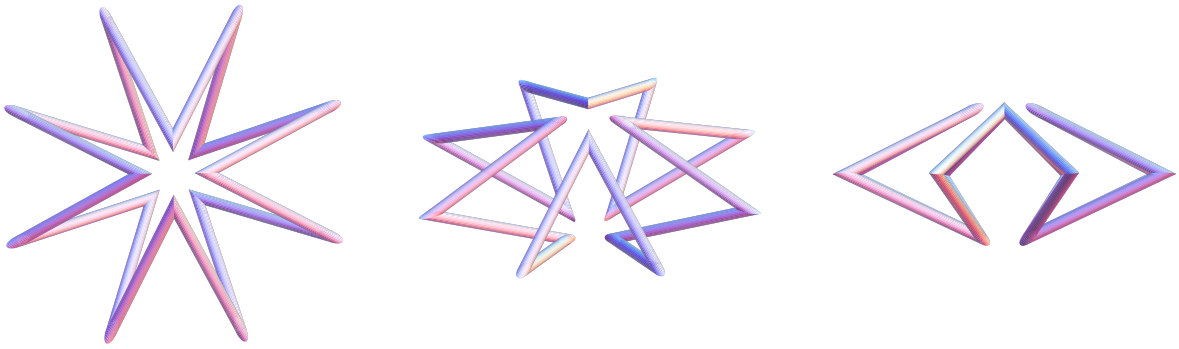

Figure 1: *Regular 3D polygonal circuit of constant torsion (top view, halfway view, side view)*

In this article, we explore 3D non-planar polygons[2] having constant segment lengths, constant corner angles, and constant torsion angles. We refer to these polygons briefly as **regular constant-torsion polygons**. Section 2 explains why these structures raised our interest. In Section 3, we precisely define this class of polygons, using 3D turtle graphics, and in Section 4 we provide some theoretical analysis results. We address the issue of finding such constant-torsion polygons in Section 5. In Section 6 we show some artwork that involves constant-torsion polygons. Section 7 concludes the article.

[1] The circuit's line segments are infinitely thin, but they have been thickened for the sake of visualization.

[2] Traditionally, a polygon is a planar figure; we also use the term polygon for arbitrary (possibly non-planar) polygonal circuits.

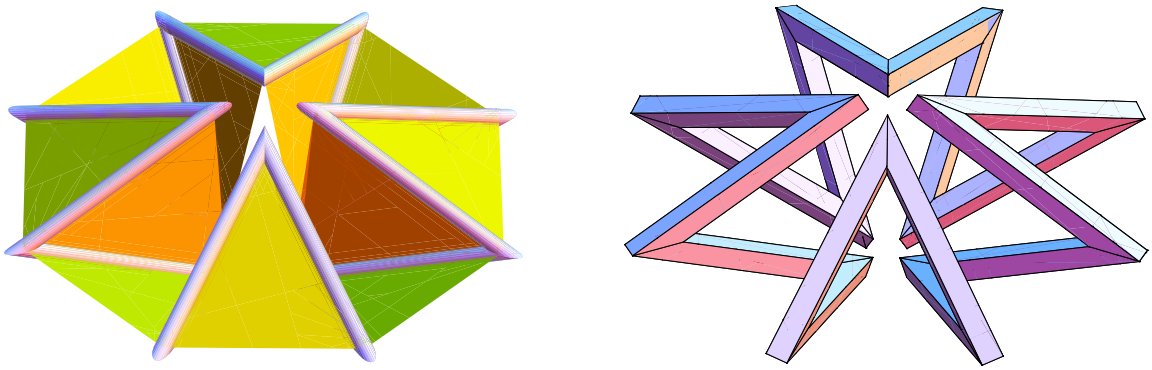

Figure 2: *Polygon of Figure 1 with corner-spanning planes (left) and mitered with a square beam (right)*

2 Motivation

In a polygonal circuit, the line segments can be thickened to beams that all have the same cross section and that have the segments as center line. It is most elegant when the edges of adjacent beams nicely match, yielding (regular) miter joints. Figure 2 (right) shows the polygonal circuit of Figure 1 with its line segments thickened to beams having a square cross section. Here, the beam edges match properly at all miter joints.

When a polygonal circuit is thickened to a beam, it is always possible to have beam edges match properly at all joints *but one*. Hence, open polygonal chains are not so interesting, because they pose no mitering challenge. As explained in [2] and demonstrated in [3], it depends on the geometric details of the circuit, whether the final joint will match as well. Traveling along the circuit, you accumulate a certain amount of *torsion*. The final joint matches properly, if and only if the total amount of torsion is a symmetry of the cross section. Note that the total torsion of a planar polygon is always zero.

A mitering artist has an interest in circuits that can be "mitered all the way round", that is, circuits whose total torsion corresponds to the cross section. There are several techniques available to obtain such circuits:

1. Exploit some freedom in the choice of the vertices to tweak the circuit such that an appropriate total amount of torsion is obtained. For aesthetic reasons, certain relationships between the vertices may need to be kept invariant, such as the knot type. This typically leads to beams with *ad hoc* dimensions (lengths, bevel angles, and torsion angles), which complicates the actual construction of artwork.
2. Restrict the circuit's vertices and segments to a pre-defined 3D-embedded graph with suitable torsion properties. Two special cases are regular polyhedrons and 3D lattices. For example, take a Hamilton path on a cuboctahedron, or a trefoil knot in the cubic lattice.
3. Restrict the torsion changes at each joint. This generalizes the preceding technique, by retaining what is valuable (torsion control) and dropping the (sometimes overly restrictive) pre-defined graph.

   In Figure 2 (right), the miter joints match all the way round, because the beam cross section is a square and the accumulated torsion at each joint changes in steps of 90° (remember that adjacent corner-spanning planes are perpendicular).

The second technique can be compared to walking in a city along the streets. Given the road map, it is easy to make a closed tour, but there is little freedom. The third technique resembles walking in the desert, with a compass and no landmarks. There is more freedom, but then it is a challenge to walk a closed tour.

By the way, [2] also presents *skew miter joints* as a way of making more interesting objects based on lattices, such as the face-centered cubic lattice. However, we will not employ skew miter joints in this article. Here, we pursue the third technique with classic miter joints.

3 Definitions

We will define the circuits of interest using a 3D variant of *turtle graphics* [1]. Turtle graphics were introduced by Seymour Papert as a simple way of producing graphics by a robot turtle, and later by a virtual turtle in the Logo programming language. It is based on self-relative operations, rather than absolute coordinates. At any moment, the turtle has a position and a heading. The turtle walks in the plane and can be instructed to activate (lower) or deactivate (raise) its pen; to move forward or back a given distance; to rotate left or right through a given angle, around its center. This way, many figures can be described through simple programs that control the operation of the turtle.

Our 3D variant of turtle graphics [4] involves a flying turtle whose **state** is defined by its **position** and **attitude** in 3D space. The turtle's attitude is determined by its **heading** (a vector) and its **normal** (a vector perpendicular to the heading, defining the relative up direction). The plane that contains the heading and is perpendicular to the normal is called the turtle's **base plane**.

The turtle starts in the origin heading along the positive x-axis and with the positive z-axis as normal (see Figure 3, left), so that the (x,y)-plane is its base plane. For our purposes, the pen is always active. The flying turtle obeys these commands:

$Move(d)$ moves distance d in the direction of the current heading;

$Turn(\varphi)$ turns clockwise about the current normal by angle φ, changing the heading but not the normal;

$Roll(\psi)$ rolls clockwise about the current heading by angle ψ, changing the normal but not the heading.

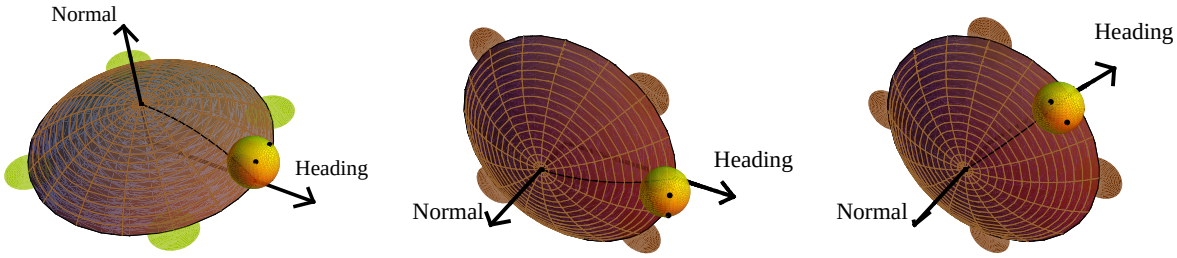

Figure 3: *3D flying turtle in initial state (left); after* $Roll(90^\circ)$ *(middle); after* $Roll(90^\circ)$, $Turn(45^\circ)$ *(right)*

By suitably combining *Turn* and *Roll* commands, the turtle can head in any direction and produce 3D paths.

We define $Segment(d,\psi,\varphi)$ as the sequence of the three commands $Move(d)$, $Roll(\psi)$, $Turn(\varphi)$, where d, ψ, and φ are given parameter values. A sequence of *Segment* commands describes a 3D polygonal path.

The **torsion angle** of an internal segment in a directed polygonal path is defined as the directed dihedral angle between the plane spanned by the segment and its predecessor segment, and the plane spanned by the segment and its successor segment. Note that the torsion angles are the same as the roll angles in paths produced by a sequence of *Segment* commands.

We call a turtle program, typically consisting of *Segment* commands, **closed** when it returns the turtle to its initial position, and we call it **properly closed** when it returns the turtle to its initial *state*. That is, in order to be properly closed, not only should the turtle's final position equal its initial position, but also its final attitude must equal its initial attitude.

A **polygonal path of constant torsion**, or CT path in short, is a path P produced by a sequence of $Segment(d_i,\psi_i,\varphi_i)$ commands that all have the same value for $|\psi_i| = \psi$, with all $d_i > 0$ and $\varphi_i \neq 0$ modulo 180°. Path P is called **regular**, when all $d_i = d$ and $\varphi_i = \varphi$ for $0 < \varphi < 180^\circ$. P is called a polygonal circuit of constant torsion, or briefly a **CT polygon**, when it is a *properly* closed CT path. A *regular CT polygon* is completely determined by the constants d, ψ, and φ, and the sequence of roll signs for ψ. All its segments have the same length, all corner angles are $180^\circ - \varphi$, and all torsion angles are $\pm\psi$.

The regular CT polygon of Figure 1 has $\varphi = 130.06°$, $\psi = 90°$, and ψ-signs ++−−++−−++−−++−−. With $\psi = 90°$, $\varphi = 120°$, and sign sequence +−−++−−++−−++− one obtains a circuit (see Figure 4, left), but the angle at the origin is clearly less than 60° (the final and initial heading are not equal, and the torsions of the two segments at the origin is much less than 90°. The turtle program is closed but not properly closed.

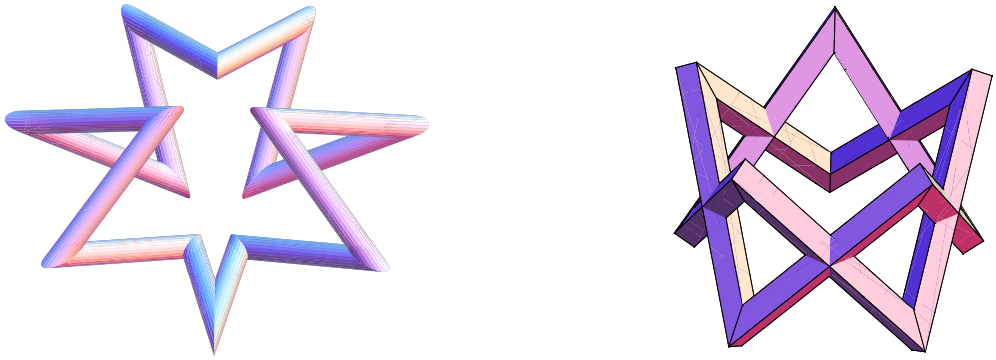

Figure 4: *CT path that is not properly closed (left); regular CT polygon with self-intersection (right)*

Taking $\psi = 90°$, $\varphi = 112.456°$, and the sign sequence +−+−+−+−+− yields a regular CT polygon that exhibits self-intersection (see Figure 4, right). Even if the abstract (infinitely thin) circuit does not self-intersect, this may still happen when thickening the segments (too much).

4 Analysis

In this section, we present some theorems about 3D turtle geometry (we are not aware of a good reference). Two turtle programs are called **congruent** when they trace out congruent paths, and **path-equivalent** when they trace out identical paths. We call them **equivalent**, denoted by $\equiv$, when they are path-equivalent *and* lead to the same *final state* (especially, the same final attitude).

Every turtle program defines a 3D polygonal path. Every 3D polygonal path starting in the origin with its first segment aligned along the positive x-axis can be described by a suitable sequence of *Segment* commands with $d > 0$, $0 < |\varphi| \leq 180°$, and $0 \leq |\psi| \leq 180°$.

We mention a few basic properties of 3D turtle commands. Adjacent *Move* and *Roll* commands commute:

$$Move(d),\ Roll(\psi) \quad \equiv \quad Roll(\psi),\ Move(d)$$

Note that, in general, the other pairs do not commute.

Every program consisting of *Turn* and *Roll* commands only, i.e. without *Move* commands, has an equivalent program of the form $Roll(\psi_1),\ Turn(\varphi),\ Roll(\psi_2)$.

Concerning adjacent *Segment* commands, we have

$$Segment(d_1, \psi_1, \varphi_1),\ Segment(d_2, \psi_2, \varphi_2) \quad \equiv \quad Segment(d_1, \psi_1 \pm 180°, -\varphi_1),\ Segment(d_2, \psi_2 \pm 180°, \varphi_2)$$

This way, all turn angles φ_i in a properly closed turtle program consisting of *Segment* commands can be made positive, by compensating 180° in both adjacent roll angles. A *Segment* program with all turn angles positive is said to be in **normal form**. This is especially interesting for properly closed circuits that have $\psi_i = \pm 90°$, because in that case $\psi_i \pm 180°$ has the same absolute value as ψ_i, and hence the normal form is a CT polygon.

For a properly closed turtle program consisting of *Segment* commands, the total amount of torsion (as needed to determine closure of the mitering [2]) equals the sum of all roll angles (taking signs into account).

Consequently, if the roll angle of each segment is a symmetry of the cross section, then the circuit can be constructed with miter joints that match all the way round. For instance, with $\psi = \pm 90^\circ$ a square beam will always work.

As observed in the preceding section, a closed turtle program (final position = initial position), in general, need not be properly closed (also, final attitude = initial attitude). However, for every closed turtle program there exists a congruent properly closed turtle program consisting of *Segment* commands. Note that the *Roll* and *Turn* at the (end of the) last segment are not relevant for closure. They can always be adjusted to roll the turtle such that the last turn can make the final heading coincide with the initial heading. An extra *Roll* may be needed to align the final normal with the initial normal. This extra *Roll* command can then be merged into the first *Segment* command, thereby effectively rotating the entire path about the first segment, to bring its last segment in the (x,y)-plane.

Note that when a closed constant-torsion program is made properly closed by the preceding transformation, the resulting congruent program possibly no longer is a constant-torsion program! In that case, its path is (rightfully) not a CT polygon (cf. Figure 4, left).

By definition, the distance between adjacent vertices in a regular CT polygon is constant. Furthermore, because all corner angles are equal as well, we also have that distances between vertices that are *two segments apart* are equal. But it is even the case that distances between vertices that are *three segments apart* are equal, because all torsion angles are equal in absolute value.

The special case $\psi = 0$ modulo 180° yields planar figures. The regular CT polygons with $\psi = 0$ are the classic regular (planar) polygons. In order to close, φ must divide a multiple of 360°, in which case closure is proper as well. When $\psi = 180^\circ$, constant-torsion paths will zig-zag and never close.

In the remainder, we mostly restrict ourselves to regular CT polygons with $\psi = 90^\circ$.

5 Constructions

We already exhibited some regular CT polygons. Can all regular CT polygons be characterized? What combinations of corner and torsion angles, and sign sequences produce regular CT polygons?

There are some obvious regular sign patterns to try. For instance, a zig-zag obtained by repeating `+-`. Figure 5 (left) shows `+-+-+-`, which happens to close properly for $\psi = \varphi = 90^\circ$ (it is a path on a cube). In general, these zig-zags are Hamilton paths on antiprisms (including tetrahedron and octahedron, which have $\psi \neq 90^\circ$). When allowing self-intersection, they traverse the diagonals on the vertical faces of prisms (cf. Figure 4, right). In this family the vertices lie in two planes (layers).

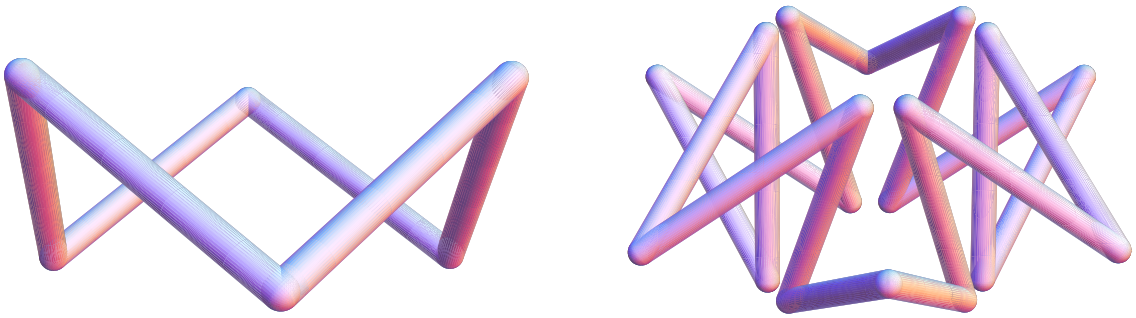

Figure 5: *Regular CT polygons with sign patterns `+-+-+-` (left) and `+++---+++---+++---` (right)*

There is also a three-layer family constructed by repeating `++--`, of which Figure 1 shows an example. The vertices now lie in three layers. Although it is possible to give a formula to determine the corresponding φ for given ψ, we have used numerical approximation techniques. Figure 6 shows a plot of

the distance between initial and final position of the turtle for the regular CT paths with $\psi = 90°$, signs ++−−++−−++−−++−−, and φ ranging from 0 to 180°. There are three solutions for φ, where the distance is zero, that is, where closure occurs, viz. around 50°, around 130° and at 180° (in the latter case, the path degenerates because all segments align). In fact, it came as a delightful surprise when we first discovered that this path closed properly for non-trivial φ.

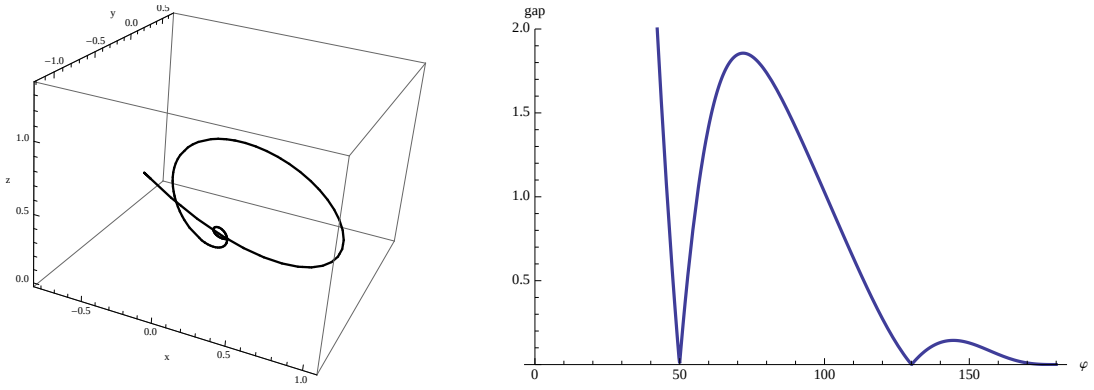

Figure 6: *Final position (left) and gap between initial and final position (right) for torsion signs ++−−++−−++−−++−− as function of corner angle φ*

A four-layer family is obtained by repeating +++−−−; see Figure 5 (right) for an example (it also appears in Figure 8, left). More complicated patterns also exist.

So far we have no clear insight into what patterns work. We only have many examples, found by exhaustive checking of short sign patterns, and interactive exploration of promising longer sign patterns. It is interesting to note that among all the examples, there are none that have a Möbius twist or that are knotted.

6 Artwork

The pieces of artwork shown in this section are all based on regular constant-torsion polygons with torsion angles $\psi = \pm 90°$. The beams have a square cross section, which makes it relatively easy to cut the beams appropriately, and it ensures that all joints are matching classic miter joints. A nice property of these beams is that they are all congruent (identical or mirror images).

Figure 7: *Artworks based on regular CT polygons with three layers (12, 16, 20 segments, wood)*

Figure 7 presents three instances of the three-layer family described in the preceding section. The one in the middle is also featured in Figures 1 and 2. Their roll sign patterns consist, respectively, of three, four,

and five repetitions of the sequence ++−−. The corresponding corner angles $180^\circ - \varphi$ are 90°, 49.94°, and 38.17° respectively. Note that the bevel angles are half the corner angle, and thus quite acute. For the object on the left, the cross section was rotated over 45°, so that the faces of adjacent beams do not lie flush at the joints, in contrast to the other two.

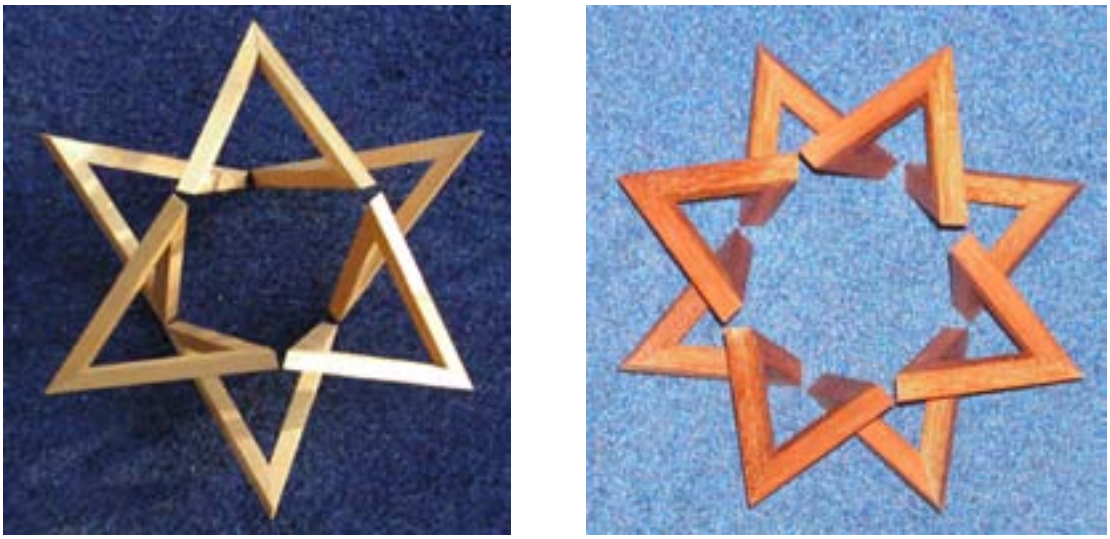

Figure 8: *Artworks based on regular CT polygons with four layers (18, 24 segments, wood)*

The two objects in Figure 8 are instances of the family of four-layer regular CT polygons. Their roll sign patterns consist, respectively, of three and four repetitions of the sequence +++−−−. The corresponding corner angles $180^\circ - \varphi$ are 40.99° and 52.85° respectively.

The object in Figure 9 is based on three repetitions of ++−++−−+−− with corner angle 48.62°. This sign pattern also closes properly with $\varphi = 90^\circ$, in which case it stays in the cubic lattice.

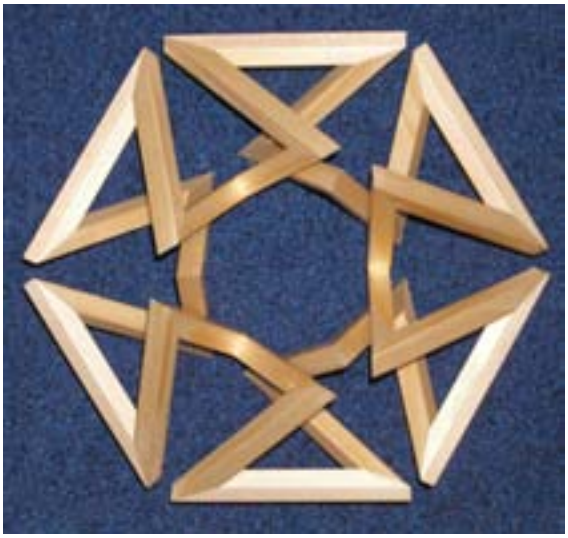

Figure 9: *Artwork based on regular CT polygon with signs* $(++-++-+--)^3$ *(30 segments, wood)*

The object in Figure 10 uses four repetitions of +++−−++−−− and a corner angle of 44.43°. It is less symmetric than the others, since it lacks an up-down symmetry, as the pictures corroborate.

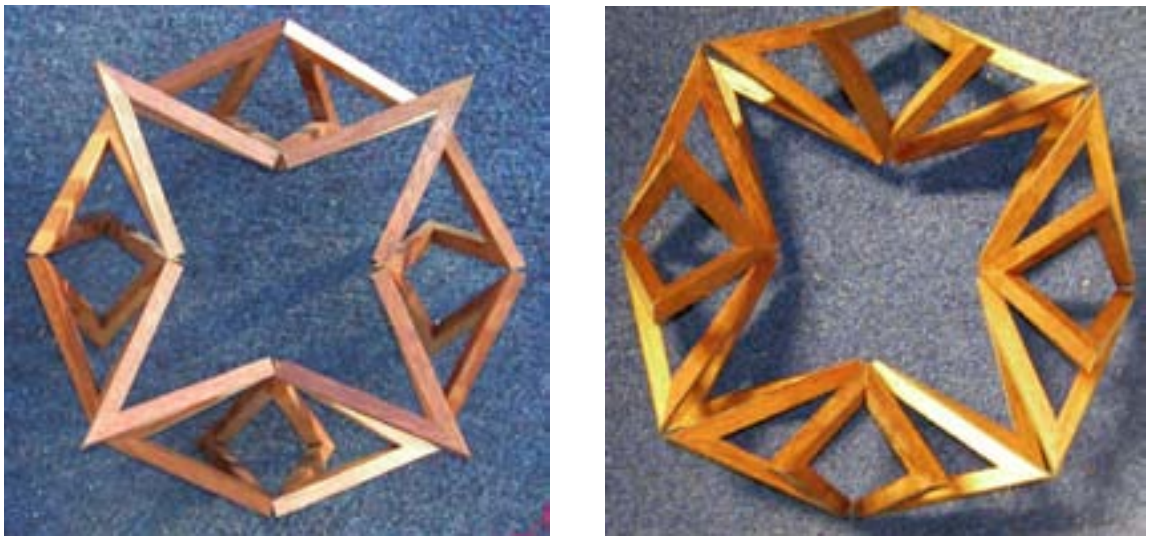

Figure 10: *Artwork based on regular CT polygon with signs* $(\texttt{+++--++---})^4$ *(40 segments, wood)*

7 Conclusion

We have defined and explored regular constant-torsion polygons, as a fruitful inspiration for artwork. The advantage of using constant-torsion circuits is that it gives the mitering artist control over the total amount of torsion, and hence over making all miter joints match properly. In the case of constant-torsion polygons, whose torsion is $\pm 90^\circ$ per segment, it is convenient to construct such artwork with beams having a square cross section: there are only two mirror-image pieces. Using regular CT polygons does raise the problem of finding appropriate angles and torsion signs to ensure that the polygonal chain properly closes onto itself.

We have exhibited several infinite families of regular CT polygons, but the characterization of all regular CT polygons is still an open problem. In our searches, no knots were encountered, nor regular CT polygons that have a Möbius twist. The use of skew miter joints and (skew) fold joints (cf. [2]) in constructing regular CT polygons also offers interesting opportunities for future research.

Acknowledgments All artwork and pictures were made by the second author. The illustrations were made with Mathematica and OmniGraffle. We would like to acknowledge the helpful feedback from the reviewers.

References

[1] Seymour Papert, *Turtle Graphics*, `http://en.wikipedia.org/wiki/Turtle_graphics` (accessed 13 January 2009)

[2] Tom Verhoeff, Koos Verhoeff. "The Mathematics of Mitering and Its Artful Application", *Bridges Leeuwarden: Mathematical Connections in Art, Music, and Science, Proceedings of the Eleventh Annual Bridges Conference, in The Netherlands*, pp. 225–234, July 2008.

[3] Tom Verhoeff. "Mitering a Closed 3D Path". From *The Wolfram Demonstrations Project*, `http://demonstrations.wolfram.com/MiteringAClosed3DPath/` (accessed 13 January 2009).

[4] Tom Verhoeff. "3D Flying Pipe-laying Turtle". From *The Wolfram Demonstrations Project*, `http://demonstrations.wolfram.com/3DFlyingPipeLayingTurtle/` (accessed 30 January 2009).

A Garden of Statistically Self-Similar Plants

Anne M. Burns
Mathematics Department
Long Island University, C.W. Post Campus
Brookville, NY 11548, USA
E-mail: aburns@liu.edu

Abstract

A simple fractal tree has the property of self-similarity, meaning it can be subdivided into parts, each of which is a reduced copy of the whole tree; its fractal dimension can be calculated from the scaling factor. Trees in nature exhibit an "approximate self-similarity". Using discrete time steps and probabilities, an algorithm for drawing plants that are not strictly self-similar, but that appear to belong to the same family, is described. The algorithm is based on a thesis of de Reffye and can be used in artwork and teaching. It has no claim to botanical accuracy, but creates images of purely decorative plants.
.

1. Modeling the growth of trees using probabilities and random numbers

The basic idea behind this model of plant growth is as follows: a tree is created from scratch, starting with a single node called the root *node*. The tree grows in a sequence of discrete time steps according to a set of probabilities. We start with simple rules; later, in order to more closely mimic nature, we will make these numbers functions of time. I encountered the basic idea in an article based on a thesis by Philippe de Reffye [2]. The article presents a method of modeling plants and trees faithful to their botanical nature; the figures in the paper are rendered on sophisticated computers using complicated rendering techniques and advanced data structures so as to obtain images with great realism. My goal is to distill and simplify the underlying mathematical ideas from articles like this and to cast them in a way that can be understood by undergraduate students. Inventing data structures and algorithms for modeling plant growth presents an interesting challenge for students in mathematics and computer science. The plant models described in this paper are purely imaginary.

A simple fractal tree has the property of self-similarity, meaning it can be subdivided into parts, each of which is a reduced copy of the whole tree; small portions of the tree when magnified look exactly like the whole tree. Its fractal dimension can be calculated from the scaling factor. In Figure 1 the binary trees look as if they might belong to the same "family" even though they are not identical. We might call them *statistically self-similar*. Several mathematical definitions of statistical self-similarity can be found in [1].

Figure 1: *Statistically self-similar binary trees*

2. A Simple Binary Tree

Our first tree is a *binary tree*. A binary tree is a finite set of nodes that is either empty, or consists of a *root* and two disjoint binary trees called the *left subtree* and the *right subtree*. A node contains information. The roots of the subtrees of a node are called its left and right *children*. If node A has node B as a child, then A is the *parent* of B. A node that has two empty subtrees is called a *leaf* or *terminal node*.

We assign to each node in the tree a positive integer called the *level* of the node. The root node has level 1; if the level of a node is *n*, the level of its child nodes will be *n*+1. Each parent node will be connected to its child nodes by *edges*, which will be interpreted as branches. Several examples of binary trees are rendered in Figure 1. The terminal nodes are rendered as disks.

Starting at the root node the tree grows in discrete time steps, $t_1, t_2,\ldots t_n$. At each time step a node in the tree can do one of three things: (i) ramify (create two child nodes), (ii) die and flower (that is, it cannot produce any more child nodes) or (iii) "sleep" for one time period. If a node dies it will become a terminal node. In a first simplified version we assign three nonnegative real numbers p_1, p_2 and p_3 whose sum is 1. These numbers represent the probabilities that a node (1) ramifies (creates two child nodes), (2) flowers (and dies), or (3) sleeps for one time period.

What information should each node contain? In our first attempt, in order to keep things simple, when a node is created it is assigned a positive integer representing its level. We also need to keep track of its (*x*, *y*) coordinates and the angle θ, the angle at which the line connecting its parent node to itself is drawn, so that if it has child nodes we know where to place them. And, finally, we need to know whether a node is capable of bearing child nodes; I use a Boolean variable, *alive*, to indicate that it is or is not able to ramify.

Before entering the loop that draws the tree, one node is created, the root node; it is assigned level 1, an initial point (x_0, y_0), and an initial angle θ_0 such as $\pi/2$. The Boolean variable, *alive*, is set to true. We also initialize three nonnegative real numbers whose sum is 1: p_1, p_2 and $p_3 = 1- (p_1+p_2)$.

The program enters a loop where each pass through the loop represents a tick of the clock or time period; initially we specify the number of stages, t_{max}, that the algorithm is carried out. At each pass we examine the list of nodes that have been created in previous passes through the loop whose *alive* status is true. For each live node we generate a random number *r* between 0 and 1.

Figure 2: *Three binary trees generated with the same program;* p_1=.5, p_2=.15 *and* p_3= .35. *Nodes are connected by lines; flowers are represented by disks,* $\theta_0 = \pi/2$ *and if a parent node's angle is* θ*, its child nodes are assigned* $\theta = \theta \pm \pi/12$.

Case 1: If $r < p_1$ the node ramifies and two new nodes are created. The information for the child nodes is entered into the new nodes. For each of the two new child nodes we assign: its level (the level of its parent plus 1), and its (x, y, θ) coordinates (if (x_p,y_p,θ_p) are the coordinates of its parent, then $x = x_p+l*\cos(\theta_p)$, $y = y_p+l*\sin(\theta_p)$ where l is the length of the connecting segment, also a function of the level), and set its *alive* status to true.

Case 2: If $p_1 \leq r < p_1+ p_2$ the node dies and flowers. We place a "flower" (a disk in Figure 1) at the node's (x,y) position and set its *alive* status to false.

Case 3: If $p_1+ p_2 \leq r \leq 1$ the node "sleeps" for one time period, so we leave it alone and proceed to the next node in the list.

Notice that if $p_1= 1$ then every node ramifies and we produce a *perfect* (and self-similar) binary tree.

Figure 2 illustrates the result of this simple program with the probabilities constant: $p_1=.5$, $p_2=.15$ *and* $p_3= .35$.

3. Probabilities as a function of time

Although I am not a botanist, it seems reasonable to me to expect that the probability of a node ramifying would be higher in the initial stages of growth of a plant. So to make the plants look more realistic we might consider making the probabilities a function of the time steps. We might want the probability of ramifying to be 1 at the beginning of the plant's life and the probability of flowering to be 1 in the last stage (call it t_{max}). Figure 3 shows three parabolic functions with this property and Figure 4 shows four trees using these probabilities with $t_{max} = 10$.

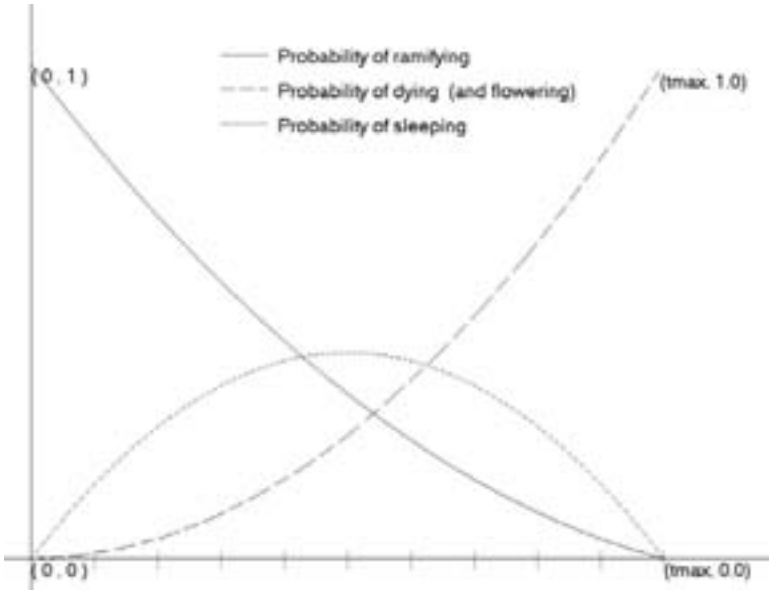

Figure 3: $p_1(t) = \frac{2t^2}{3(t_{\max})^2} - \frac{5t}{3(t_{\max})} + 1$, $p_2(t) = \frac{t^2}{(t_{\max})^2}$, $p_3(t) = 1 - p_1(t) - p_2(t)$

Figure 4: *Using the functions described in Figure 3 with t_{max} = 10.*

4. Other enhancements

There are many ways to modify the original model to achieve different styles of plant growth. In the original model if a node has level *n*, when it ramifies we assign level *n*+1 to its two child nodes. Instead we can assign level *n* to one of the child nodes (randomly) and level *n*+1 to the other. Then, when rendering the plant, we draw the child branch that has the same level as its parent at the same angle as its parent, as in Figure 5. This yields a "trunk" and alternate branching. In Figure 5 some curvature has been introduced into the segments connecting nodes whose level is greater than 1 and we have made the thickness of the connecting segments depend on the level of the parent node.

Figure 5: *A variation on assigning level to a child node.*

The tree in Figure 6 is drawn from the same program as the trees in Figure 5, but the parameters have changed; the curvature and thickness of the branches has been increased and includes the trunk, and a different rendering of the branches is shown. The coloring of the branches is achieved by a simple trick. Each branch is a curve drawn as a sequence of very short line segments whose width depends upon the

level of the parent node, and the RGB value of the color of each segment changes slightly from that of the previous segment. Flowers have been placed at the terminal nodes.

Figure 6: *A fanciful tree*

Figure 7 shows colorful versions of the tree in Figure 6. The short segments that make up the branches are colored randomly rather than "continuously" as they are in Figure 6.

Figure 7: *Trees from a Star Trek planet*

Another variation can be seen In Figure 8. It is an easy task to modify the program so that when a node ramifies it gives birth to 3, 4 or more child nodes.

Figure 8: *Each node gives birth to three child nodes.*

Figure 9: *A more realistic looking plant.*

In Figure 9 a more realistic-looking plant is achieved by allowing the branching angles to vary with controlled randomness and inserting leaves along the branches that connect the nodes.

Once the basic structure of a plant has been created the fun begins. Now the imagination takes over. We can experiment with different branching angles and different flower and leaf shapes. We can go outside and look at the incredible variety of shapes found in nature and try to imitate them or to make up our own. To create these shapes we use basic mathematical functions like lines, polynomials or trigonometric functions. For example, a leaf shape can be defined by a pair of parametric equations: $x = a*t^2$, $y = b*\sin(\pi t)$, $-1 \leq t \leq 1$. Knowledge of the math in a basic pre-calculus course is sufficient to program these shapes. And a bonus is that often one's mistakes turn out to look better than what was originally intended.

Figure 10 shows a garden of statistically self-similar plants.

Figure 10: *A garden of statistically self-similar plants.*

5. Future work

Animation of scenes created from computer graphics is one of my projects for the future. The method of generating plant growth described in this paper may be useful for producing animations.

Recall that in the algorithm that created the tree, when a node dies (flowers) the node is not deleted, but merely has its *alive* status changed to false. Initially I had the program delete a node from the list after it died and flowered. Allowing each node to remain in the list after it dies but changing its status from *alive* = true to *alive* = false means that at the end of the algorithm we have a record of the age (level at which the node died) and coordinates of each of the nodes. Thus there is the possibility of animating the nodes; one

idea for an animation is to incrementally change the position of the nodes and their connecting branches in order to simulate trees blowing in the wind. Another idea is to create an animation of changing seasons. Figure7 depicts four frames of a crude attempt at an animation of falling leaves. I have rendered the nodes as leaves (originally green). As the animation progresses the leaves gradually change color from green to red, yellow and brown, and eventually fall from the trees and drift slowly to the ground.

Figure 11: *Four frames from an animation of falling leaves.*

References

[1] Heinz-Otto Peitgen and Dietmar Saupe, Editors, *the Science of Fractal Images*, Springer-Verlag, New York, 1988.

[2] Philippe de Reffye, Claude Edelin, Jean Françon, Marc Jaeger, Claude Puech, Plant Models Faithful to Botanical Structure and Development, *Computer Graphics*, Volume 22, Number 4, August 1988

Real Tornado

Akio Hizume, Yoshikazu Yamagishi
Department of Applied Mathematics and Informatics
Ryukoku University
Seta, Otsu, Shiga, Japan

E-mail: akio@starcage.org
yg@rins.ryukoku.ac.jp

Abstract

The continued fraction expansion of a real number $R > 0$ generates a family of spiral triangular patterns, called "tornadoes." Each tornado consists of similar triangles, any two of which are non-congruent.

Basic Operation

Let $R > 0$ and $0 < s < 1$. In the plane, the sequence of points $V(j) = (s^j \cos 2\pi jR, s^j \sin 2\pi jR)$ for $j = 0,1,\cdots$, which we call the 'vertices', naturally converges to the origin. Fix an integer $k > 0$, which is called the 'modulo' or the 'step size', and join the vertex $V(j)$ with $V(j+k)$ by the line segment $\overline{V(j)V(j+k)}$ for $j \geq 0$.

Fibonacci Tornado

The Fibonacci numbers f_n are defined by $f_1 = f_2 = 1$ and $f_n = f_{n-2} + f_{n-1}$, $n > 2$. In the previous paper [2], we showed that if $k = f_{n-1}$ and $R = \tau$, where $\tau = (1+\sqrt{5})/2$ is the golden ratio, there exists a $0 < s < 1$ such that the vertex $V(j + f_{n+2})$ lands on the line segment $\overline{V(j + f_{n+1})V(j + f_n)}$ for each $j \geq 0$. By the Basic Operation above, we obtain the spiral pattern of similar triangles as shown in Figure 1 ($k = 2$), which is called a "tornado". As k gets larger, we could see that the tornado comes out like a blooming flower, while the argument jR of each vertex $V(j)$ remains unchanged.

Remark that the well-known spirals as in Figure 2 are different from our tornadoes because they have congruent triangles.

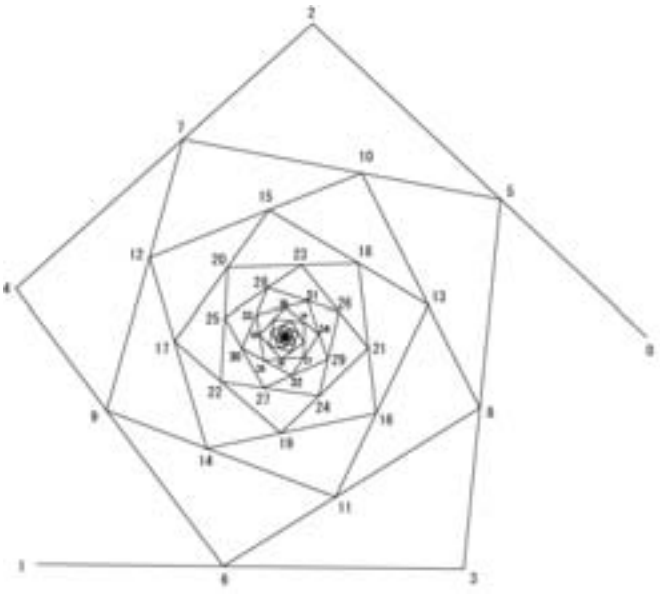

Figure 1: *Fibonacci Tornado.* [τ,3,5]

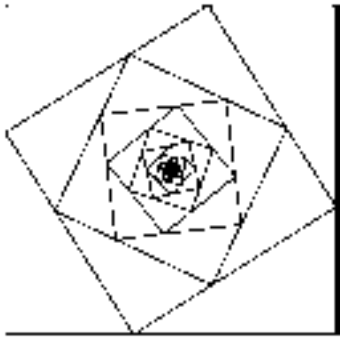

Figure 2 : *A Non-Fibonacci Tornado.*

$$R = C_0 + \cfrac{1}{C_1 + \cfrac{1}{C_2 + \cfrac{1}{C_3 + \cfrac{1}{\ddots + \cfrac{1}{C_n + \cfrac{1}{\ddots}}}}}}$$

p_0/q_0	0th	convergent
p_1/q_1	1st	convergent
p_2/q_2	2nd	convergent
p_3/q_3	3rd	convergent
p_n/q_n	n-th	convergent

Figure 3 : *Continued Fraction and Convergents*

Real Tornado

A generic real number R also generates a family of tornadoes. As is well-known (see [1]), the continued fraction expansion of R as in the Figure 3 is defined by $R = C_0 + \varepsilon_0$, $0 \le \varepsilon_0 < 1$, and $1/\varepsilon_n = C_{n+1} + \varepsilon_{n+1}$, $0 \le \varepsilon_{n+1} < 1$ for $n \ge 0$, where C_n are called the partial denominators. If R is rational, it is related to the Euclidean algorithm and stops when $\varepsilon_n = 0$. The n-th convergent p_n / q_n is defined by $p_0 = C_0$, $q_0 = 1$, $p_1 = C_1 p_0 + 1$, $q_1 = C_1$, and $p_{n+1} = C_{n+1} p_n + p_{n-1}$, $q_{n+1} = C_{n+1} q_n + q_{n-1}$ for $n > 0$. It is known that p_n / q_n are the best approximations of R, where

$$\frac{p_0}{q_0} < \frac{p_2}{q_2} < \cdots < R < \cdots < \frac{p_3}{q_3} < \frac{p_1}{q_1}, \text{ and } \left| \frac{p_n}{q_n} - R \right| > \left| \frac{p_{n+1}}{q_{n+1}} - R \right| \text{ for } n \ge 0 .$$

For example, the convergents of $R = \sqrt{3}$ are 1/1, 2/1, 5/3, 7/4, 19/11, 26/15, 71/41, ... The denominators q_n and q_{n+1} are coprime.

Choose any pair of consecutive convergents p_n / q_n and p_{n+1} / q_{n+1}, and denote by $q = q_n$ and $q' = q_{n+1}$. Define the step size by $k = q' - q$. Then there exists a unique $0 < s < 1$ such that under the Basic Operation the vertex $V(j+q+q')$ lands on the segment $\overline{V(j+q)V(j+q')}$ and we obtain a spiral pattern named as the tornado $[R, q, q']$, consisting of similar triangles $T_j = \Delta V(j)V(j+q)V(j+q')$ for $j \ge 0$. Figure 4 presents the tornadoes $[R, q, q'] = [\sqrt{3}, 3, 4]$ and $[\sqrt{3}, 4, 11]$.

The basic idea of the Real Tornado was originally published in Japanese in [3]. Here we show how to find a $0 < s < 1$. Denote the length of the three edges of T_j by

$$a(j) = \left| V(j+q)V(j+q') \right|,$$
$$b(j) = \left| V(j)V(j+q) \right|,$$
$$c(j) = \left| V(j)V(j+q') \right|.$$

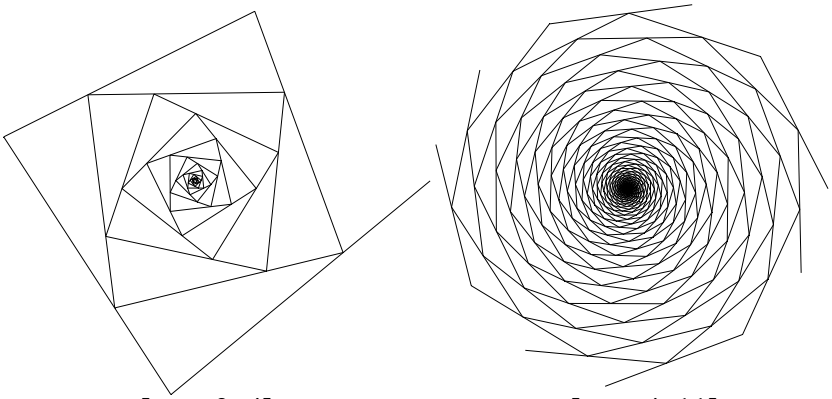

$[\sqrt{3}, 3, 4]$ $[\sqrt{3}, 4, 11]$

Figure 4 : $\sqrt{3}$ *Tornado.*

By Figure 5 we can see that

$$\begin{aligned} & a(j) \\ &= |V(j+q)V(j+q')| \\ &= |V(j+q)V(j+q+q')| + |V(j+q+q')V(j+q')| \\ &= s^q |V(j)V(j+q')| + s^{q'} |V(j)V(j+q)| \\ &= s^q c(j) + s^{q+k} b(j). \end{aligned}$$

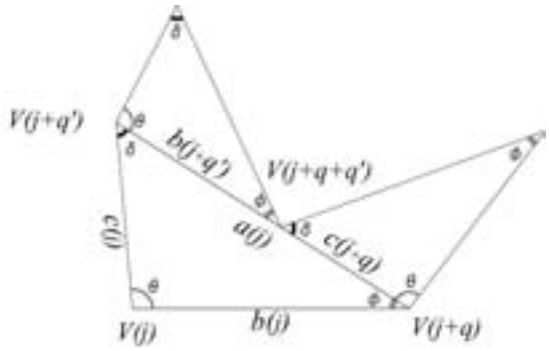

Figure 5 : *Principle.*

The three angles of T_j are

$\phi = 2\pi Rq' = 2\pi R(q+k)$, $\delta = -2\pi Rq$, and $\theta = 2\pi Rk$

or

$\phi = -2\pi Rq' = -2\pi R(q+k)$, $\delta = 2\pi Rq$, and $\theta = -2\pi Rk$,

where the signs are chosen to satisfy that $\sin\phi, \sin\delta$ and $\sin\theta$ are all positive. The law of sines is expressed by

$$\frac{a(j)}{\sin\theta} = \frac{b(j)}{\sin\delta} = \frac{c(j)}{\sin\phi},$$

and we obtain the equation

$$s^{q'} \sin(2\pi Rq) - s^q \sin(2\pi Rq') + \sin(2\pi Rk) = 0.$$

It is easy to see that this equation has a unique solution $0 < s < 1$.

Additional Results

Conversely, we can also prove that any possible tornado $[R, q, q']$ with q, q' positive is related to the continued fraction expansion of R.

Theorem: Let R be a real number and q, q' positive integers. There exists a tornado $[R, q, q']$ if and only if R has a convergent $\frac{p_n}{q_n}$ and an (intermediate) convergent $\frac{cp_n + p_{n-1}}{cq_n + q_{n-1}}$, $0 < c \le C_{n+1}$, where we denote by $p = p_n, q = q_n, p' = cp_n + p_{n+1}$ and $q' = cq_n + q_{n+1}$, such that

(1) R is distinct from $\frac{p}{q}$ and $\frac{p'}{q'}$, that is, $\frac{p}{q} < R < \frac{p'}{q'}$ or $\frac{p'}{q'} < R < \frac{p}{q}$, and

(2) $|\{qR\} - \{q'R\}| > 1/2$, where $0 \le \{x\} = x - \lfloor x \rfloor < 1$ denotes the fractional part.

See [4] for the proof and further discussions. Note that the golden ratio τ is a special irrational number which has no intermediate convergents.

Acknowledgements

The authors would like to thank the reviewers for their helpful comments and suggestions. They suggested to consider the equation $z^{q+k} = \alpha z^k + (1-\alpha)$ with $0 < \alpha < 1$ given, where q and k are relatively prime. By experiments, they claim that the tornado $[R, q, q+k]$ is obtained by using the root

$z = se^{2\pi iR} \neq 1$ of the largest magnitude. Note that in our setting above, the ratio α tends to 0 or 1 as R approaches to p/q or p'/q' respectively.

References

[1] G. H. Hardy and E. M. Wright, *An introduction to the theory of numbers*, fifth edition, Oxford, 1979.
[2] Akio Hizume, *Real Tornado*, MANIFOLD #17, pp. 8-11. 2008. (in Japanese)
[3] Akio Hizume, *Fibonacci Tornado*, Bridges Proceedings, pp. 485-486. 2008.
[4] Akio Hizume and Yoshikazu Yamagishi, *Monohedral similarity tilings*, in preparation.

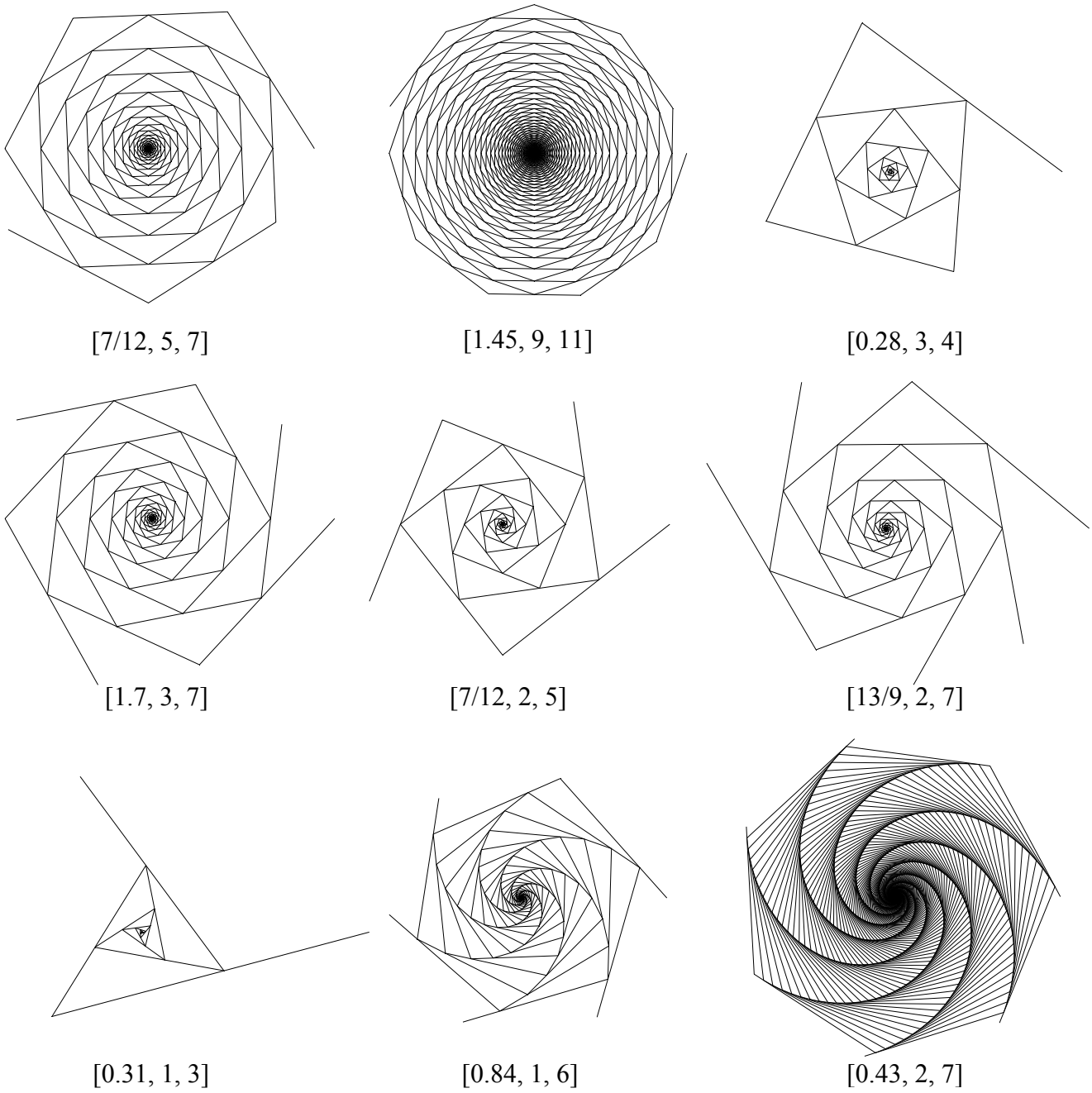

Figure 6 : *Real Tornado Samples.*

Concave Hexagons

Paul Gailiunas
25 Hedley Terrace, Gosforth
Newcastle, NE3 1DP, England
email: p-gailiunas@argonet.co.uk

Abstract

The tilings (*n*.3.*n*.3) exist in the spherical, Euclidean or hyperbolic plane, depending on whether *n* is less than, equal to, or greater than 6. In all cases the dual tiling consists of rhombi, which can be taken in pairs to form "regular" concave hexagons. In the case of the spherical examples the tilings can be illustrated by colouring the faces of rhombic polyhedra. In the Euclidean plane "regular" concave hexagons allow tilings that cannot be constructed from the dual (6.3.6.3) tiling, some of which allow analogous tilings of non-"regular" concave hexagons. Some Escher-like designs are derived from such tilings.

Some of the possibilities in the hyperbolic plane are briefly considered.

Some Concave Spherical Hexagons

Previously [1] I described polyhedra that can be produced by removing parts of the small stellated dodecahedron, having fifteen faces that are equilateral triangles, and fifteen that are concave pentagons (figure 1). The two types of face are always paired, and it is convenient to think of a pair as some kind of irregular folded hexagon, which can be projected onto the surface of a sphere with centre coincident with the centre of the original small stellated dodecahedron.

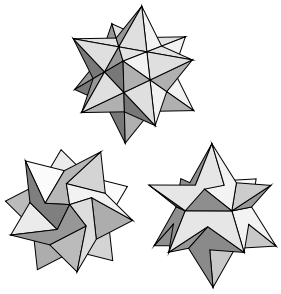

Figure 1: *The small stellated dodecahedron, and two views of a polyhedron derived from it that has five-fold symmetry.*

These polyhedra have two types of vertex, twelve that are vertices of the convex hull (a regular icosahedron), and twenty that are vertices of the regular dodecahedron from which the original stellation is derived. It follows that in the projection they are the vertices of a spherical triacontahedron, and the spherical hexagons consist of pairs of spherical rhombi. The resulting spherical tilings can be conveniently indicated by colouring faces of the triacontahedron in pairs (figure 2).

Figure 2: *Two polyhedra with triacontahedra coloured in corresponding ways. One pair has 5-fold symmetry, the other has 3-fold symmetry.*

Since there are fifteen hexagons the only possible symmetrical polyhedra have 3-fold or 5-fold symmetry, as illustrated in figure 2. In both cases the hexagons around a symmetrical vertex can be arranged in either

sense, so each polyhedron exists in four forms (two enantiomorphic pairs). Mirror symmetry is not possible since any plane would have to bisect at least one hexagon, because fifteen is an odd number, and it would cut adjoining hexagons non-symmetrically. There is a large number of non-symmetrical arrangements.

The triacontahedron is the dual of the icosidodecahedron, with vertex symbol (5.3.5.3). There are two other face-regular rhombic polyhedra, the rhombic dodecahedron, the dual of the cuboctahedron, (4.3.4.3), and the cube, the dual of the octahedron, (3.3.3.3). In both of these cases the rhombic faces can be taken in pairs corresponding to tilings of concave hexagons on the sphere.

In the case of the rhombic dodecahedron there are six concave hexagons so that, although it is possible to place four hexagons symmetrically around a 4-valent vertex, this leaves only two hexagons, so that complete 4-fold symmetry is impossible. There is a natural arrangement with 3-fold symmetry that corresponds to Coffin's "pennyhedron puzzle" [2].

It is easy to make three pairs of adjacent cubic faces, in only one way, with 3-fold symmetry.

Euclidean Tilings

Since the Euclidean plane is infinite there is no limit to the number of ways edges can be removed from the dual (6.3.6.3) tiling to produce concave hexagons, even if we consider only periodic tilings with rotational symmetry. It is instructive, however, to consider analogues of the symmetrical polyhedra in figure 2. A general strategy is to start at a symmetrical vertex and to add successive rings of hexagonal tiles, noting that the 3-valent vertices occur at the concave vertex and at the two off-centre 120• angles. At the local level the main difference is the addition of extra tiles at the 5-fold vertices to make them 6-fold.

In the lower half of the right-hand illustration in figure 1 the hexagons (concave pentagon + triangle) in the second (equatorial) ring have their two concave edges meeting edges of one hexagon in the first (lower) ring. The third (upper) ring is like the first ring: five hexagons around a symmetrical vertex. The Euclidean analogue (figure 3) consists of six concave hexagonal tiles combined to form a regular hexagon (the first ring) with tiles at its corners (the second ring). Regular hexagons corresponding to the third ring meet the tiles of the second ring in the same way as those in the spherical case, with convex 3-valent vertices.

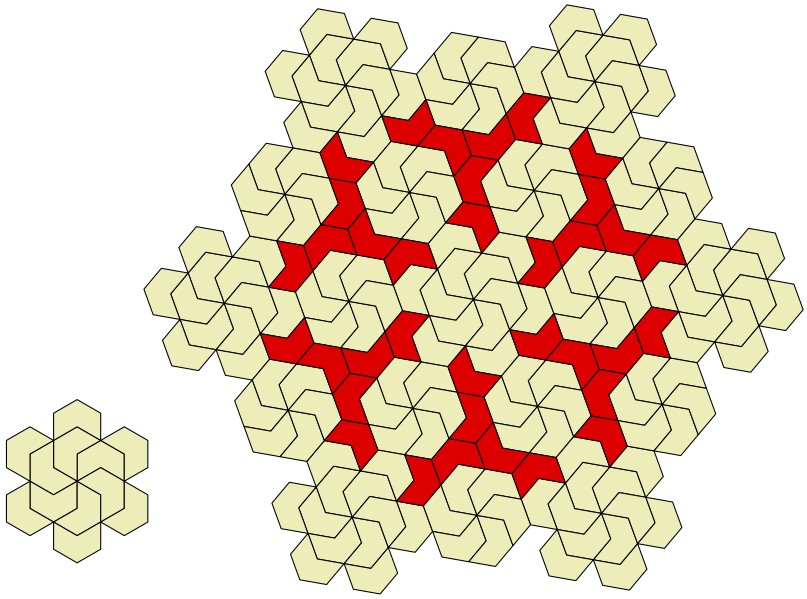

Figure 3: *A Euclidean analogue of the spherical tiling with 5-fold symmetry.*

There is only one hexagonal plane symmetry group without mirrors, p6, or **632** in orbifold notation. The patches corresponding to the first two rings are centred on 6-fold axes, but the patches corresponding to the third ring, which also have local 6-fold symmetry, are centred on 2-fold axes of the tiling. The patches formed by the tiles that must be added (red in the figure) are centred on the 3-fold axes of the tiling.

Applying the same process from the top of the right-hand illustration of figure 1, so the order of rings is reversed, generates a different tiling pattern (figure 4).

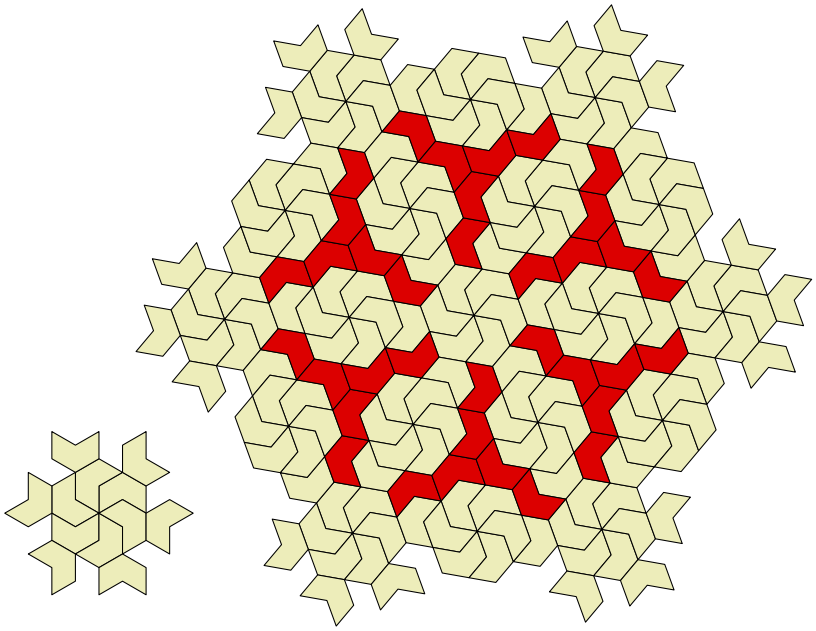

Figure 4: *An alternative Euclidean analogue of the spherical tiling with 5-fold symmetry.*

Spiral Tilings

All of the tilings considered so far are derived from duals of (*n*.3.*n*.3), and no alternative is possible on the sphere. In the Euclidean plane, however, the angles of the concave hexagons are commensurable, so it is possible to disregard the distinction between 3-valent and 6-valent vertices. In particular chevron arrangements are possible, which allows the two spiral tilings described towards the end of [3] (figure 5).

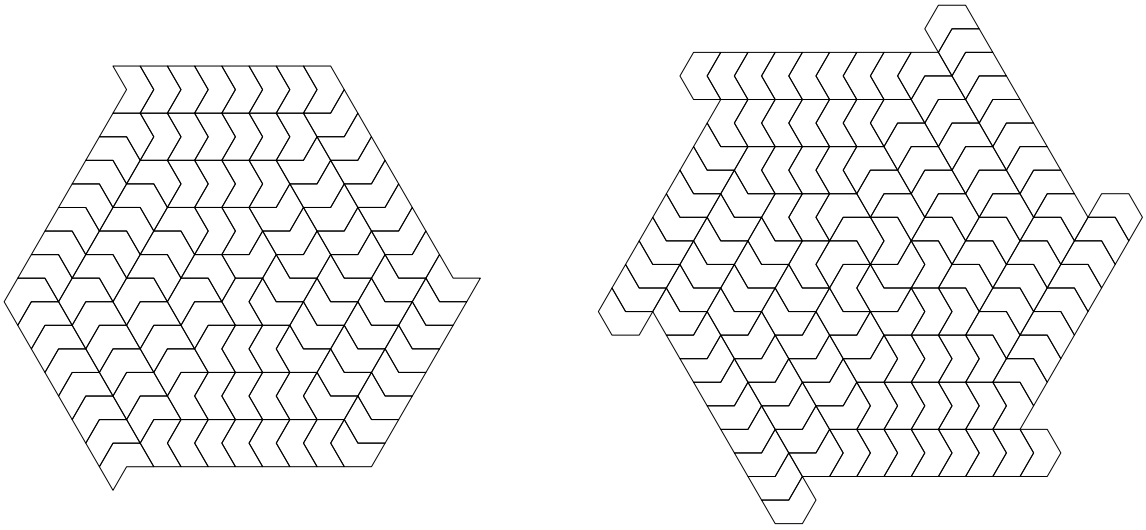

Figure 5: *The two spiral tilings possible with 60• concave hexagons.*

The patches of tiles around the central vertex, six in the 3-armed example, eighteen in the 6-armed example, observe the vertex restrictions, and can be seen as Euclidean analogues of some symmetrical patches that occur in spherical tilings. The straight sections of the spiral paths, however, do not fit on the dual (6.3.6.3) tiling, and it is not possible to identify vertices as either 3- or 6-valent. The pairs of tiles at the corners of the spiral paths, where there is a 60• turn, are the only neighbours that preserve vertex type in this way.

Edge-deformation

The tiling patterns of M.C.Escher are all periodic, or derived from periodic drawings [4] (obviously apart from those that involve no element of symmetry at all and the spherical examples), and the standard methods of construction rely on periodicity to ensure that complicated shapes will fit together properly. Inspection of the spiral tilings in [1] suggests that the usual techniques of edge-deformation will not work with them, since edges meet copies of many other edges, which in turn meet copies of many edges, so that there is no consistent way to deform the edges without generating a large number of differently shaped tiles. There are some circumstances. however, in which spiral tilings can form the basis of Escher-like patterns with only two shapes of tile.

If an edge is a straight line segment it has two lines of (local) symmetry, itself and its perpendicular bisector (and, of course, together they generate a rotational symmetry of order 2). The symmetry can be broken by losing either line of symmetry, or both. Breaking the symmetry along the line of an edge, for example by the edge becoming a concave or a convex circular arc, is considered in [5]. Figure 6 shows a modification of the 3-armed spiral in figure 5 with edges that are all circular arcs.

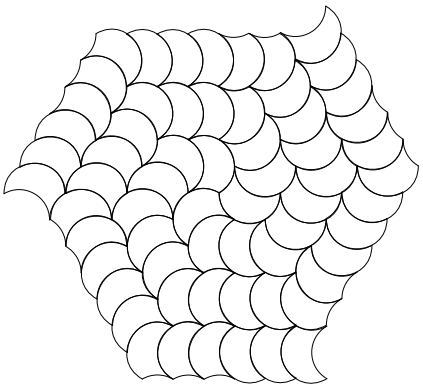

Figure 6: *A modified version of the 3-armed spiral in figure 5, having edges that are circular arcs.*

Such local symmetry-breaking of the edges of a tile derived from a regular polygon is possible only when the tiling does not rely on special circumstances, for example the tile having only one concave vertex (see [5] for details). The 6-armed spiral in figure 5, and the periodic tilings in figures 3 and 4 depend on particular properties of hexagons, so there is no equivalent edge-deformation that preserves the monohedral tilings.

If edges are replaced by a line of arbitrary shape we need to consider its orientation between vertices as well as its orientation between faces (concave/convex in figure 6, for example). The local symmetry of the edges in a perpendicular line could, in principle, be broken in tilings such as those in figures 3 and 4, where there is a consistency in the way vertices are arranged. For example edges could be labelled with arrows directed from 3-valent vertices to 6-valent vertices.

Figure 7 shows the 3-armed spiral of figure 5 with the edges replaced by arbitrary curves. Two shapes of tile are needed because there is no way to direct the edges between vertices in a consistent way. Notice that the shapes of tile alternate along the spiral path, except at the corners, where there are pairs of the same shape, as expected from the earlier observation about vertex type in spiral tilings. In fact spiral tilings of this type exist for all orders of rotational symmetry, since the "regular" concave hexagons that consist of two 60• rhombi can be transformed into non-"regular" concave hexagons that consist of two

different rhombi, that will still tile an infinite wedge that can form the fundamental domain of some rotational symmetry. Figure 7 also shows a 4-armed spiral, previously described in [1], with edges substituted by the same arbitrary curve. Tiles of the same shape form v-shaped zones, and the structure is closely related to the way this 4-armed spiral is coloured in [6].

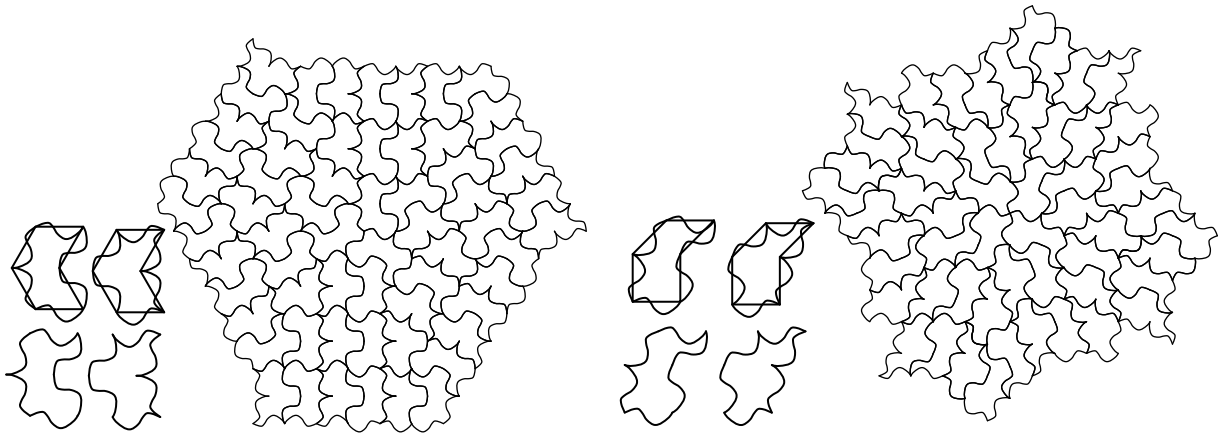

Figure 7: *A modified version of the 3-armed spiral in figure 5, and an analogous 4-armed spiral.*

While one of the tile shapes, especially in the 3-armed case, could make quite a convincing bird, the other does not suggest any realistic form, however stylized. In the case of the 60• concave hexagon it is possible to arrange the curved edges so that they start and finish with straight sections that are coincident in some parts of the tile boundary (figure 8).

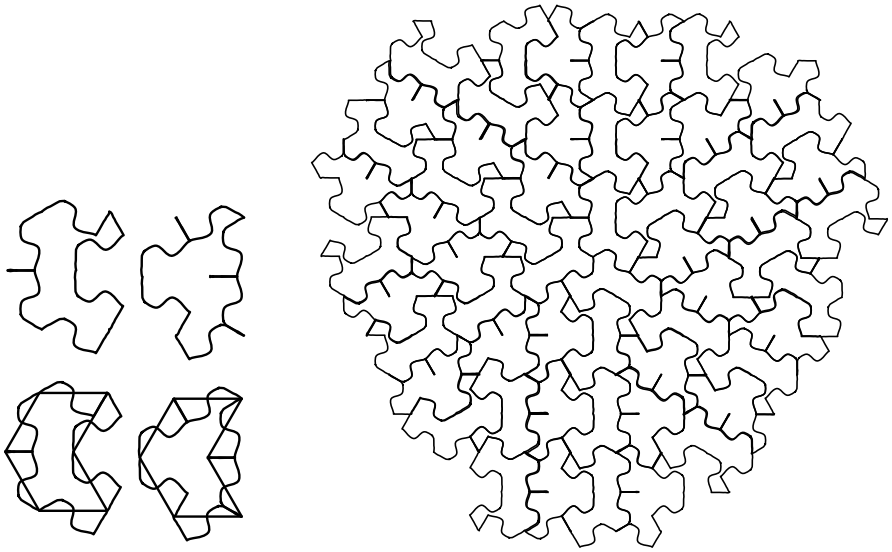

Figure 8: *An alternative version of the 3-armed spiral.*

This change converts the "awkward" tile into quite a reasonable bird, and the bird tile into a more-or-less dog shape (figure 9). The problem with these substitutions is that the same shape must be substituted for every edge (although in different orientations) so that there needs to be a compromise: what produces a better shape at one place makes a worse one at another. The dogs in figure 9, for example, do not bear close scrutiny, although the birds (doves maybe?) are reasonably convincing.

In a tiling such as that of figure 6 the concave edge of one tile coincides with the convex edge of its neighbour. This is the same as the relationship between directed edges if they are considered in an intrinsic way, i.e. clockwise or anticlockwise around the tile. A directed edge in a tiling is clockwise around one of its tiles and anticlockwise around the other. This observation suggests another kind of edge-deformation, where the orientation of an edge is either clockwise and concave, or anticlockwise and

convex. A consequence is that all the edges in the tiling are related by direct isometries, and there are no mirror images.

Figure 11 shows an example of this type of edge-deformation applied to the tilings in figure 5. The edges are directed in the same way as those in figure 7 (alternately), and this determines their orientation with respect to faces ("concave" or "convex"). Again there are two shapes of tile, for the same reason as before. Since the central patch of the 6-armed spiral tiling can be derived from the dual (6.3.6.3) tiling, and the rest of the tiling consists of chevron elements, they are consistent with it.

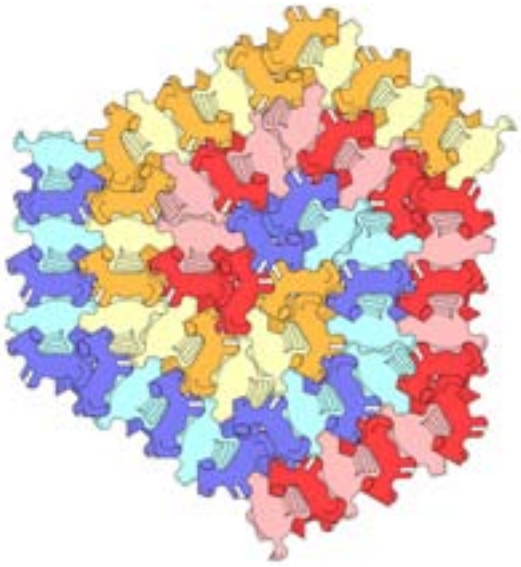

Figure 9: *Figure 8 with designs added to the tiles, and coloured to show the spirals.*

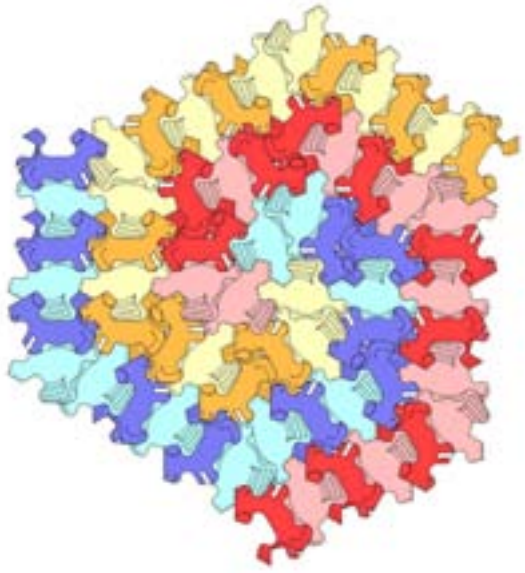

Figure 10: *Interchanging tile shapes still gives a consistent tiling.*

In general spiral tilings of the type described in [1] require mirror-image copies of tiles, but if all the edges are deformed so that they are related by direct isometries, mirror image copies will not fit. In this case four different shapes of tile are needed: a pair where corresponding edges are rotated by 180• with respect to each other, and a pair based on the mirror image but with edges that are direct copies from the

first pair, again where corresponding edges are rotated by 180• with respect to each other. The 3-armed spiral in figure 11 is a special case, because it is based on "regular" concave hexagons that have mirror symmetry, so the two pairs are the same.

The same idea can be apppied to the tiling illustrated in figure 6. Edges that are some random shape are directed according to whether the the circular arc is concave or convex. This time in general two shapes of tile are sufficient, and figure 12 is equivalent to figure 7, but with tiles related by direct isometries only.

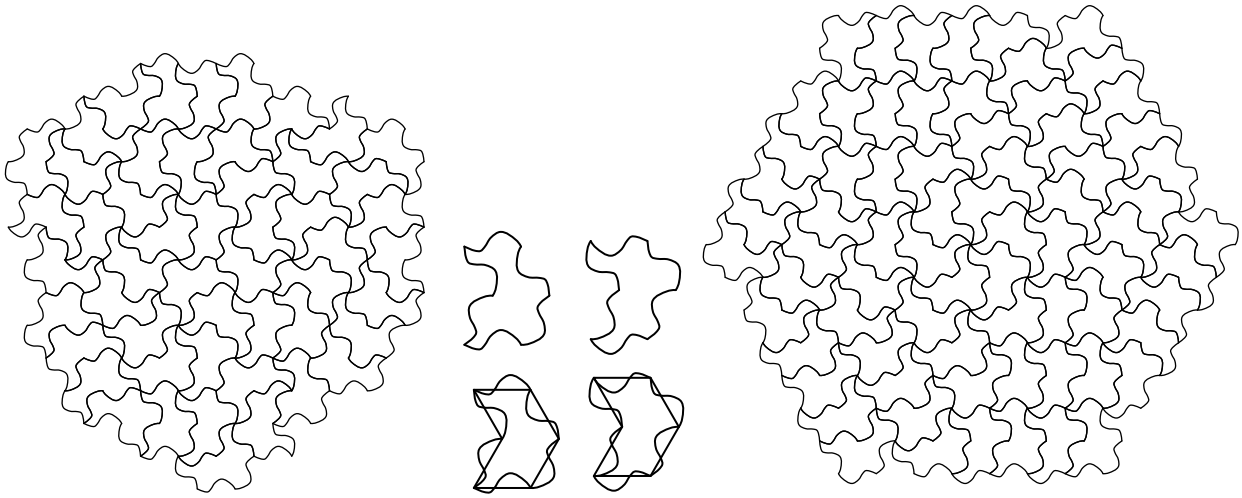

Figure 11: *Modified versions of the spiral tilings in figure 5.*

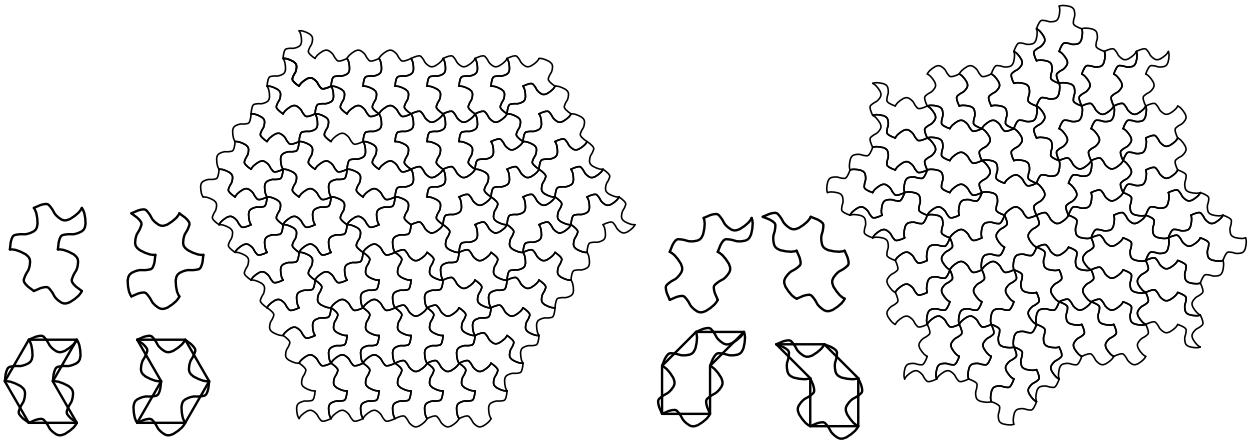

Figure 12: *A different edge-deformation of the tilings in figure 7.*

Hyperbolic Tilings

The tilings (n.3.n.3) lie in the hyperbolic plane if n>6, and once again tilings of concave hexagons can be produced by removing edges from the dual tilings. As with spherical geometry the size of polygons depends on the sum of their internal angles, and a problem with images of these tilings, which is worse for higher values of n, is that most of the interesting structure gets pushed to the edges, whichever projection is used.

When n=7, the image is not too distorted, and Douglas Dunham has presented a tiling of butterflies that indicates how the tiles might look, although he uses edge-deformations that are less restricted than the ones needed for spiral tilings [7]. In this case the angles of the concave hexagons are incommensurable, so that there is a distinction between 3-valent and 7-valent vertices in any tiling. Commensurable angles

occur whenever n is divisible by 3, so the smallest value in the hyperbolic plane is 9. Analogues of the Euclidean 3-armed spiral should be possible, although extra tiles must be fitted into the equivalent of the rows of chevrons. When n=12 two tiles will fit into the concave angle, and it seems that some kind of branching spiral tiling might be possible. Even when n=9 projections of hyperbolic tilings are pushed quite far to the perimeter, so it is likely that images of these tilings will be quite disappointing.

Not a lot of software exists for investigating hyperbolic tilings, and what is available is designed around full symmetry, typically isohedral tilings. The spiral type of tilings have a single centre of symmetry, and they are not easily investigated. The best strategy seems to involve colouring tilings of triangles manually. Very little has been attempted, and there is much to be discovered, but the results are unlikely to lead to striking images for the reasons already discussed.

Conclusion and Further Possibilities

Tilings of concave hexagons exist in spherical, Euclidean and hyperbolic geometries, and they provide a range of decorative possibilities. The technique of edge-deformation has been used in all three geometries by Escher [4], and it can be applied in these examples. Grünbaum and Shephard's classification of isohedral tilings [8] can be used to find possibilities in the Euclidean plane that can be produced by deleting edges from IH30-37.

There are more constraints on edge-deformations to ensure they will work with spiral tilings of concave hexagons. In particular every edge must be the same shape. Some possibilities have been described, and they illustrate aspects of structure that are not apparent in the examples previously described in [3] that have edges that are straight lines. There are related tilings described in [5], with more illustrated in the extended online version [9], to which the technique of edge-deformation could be applied, providing further decorative possibilities, and maybe additional insight into their structures.

All of the tiles considered are compounds of two rhombi, so they have special properties, being zonogons. There are other classical tilings and polyhedra that have quadrilateral faces that are not rhombi. It is unlikely that they will provide such a rich source of possibilities, but some other tilings of concave hexagons can be generated by deleting edges from them, with properties yet to be investigated.

References

[1] P.Gailiunas, *A Polyhedral Byway*. Bridges Proceedings 2001, pp.115-122.
[2] S.T.Coffin, *The Puzzling World of Polyhedral Dissections*, OUP, 1990, pp.126−7.
[3] P.Gailiunas, *Spiral Tilings.* Bridges Proceedings 2000, pp.133-140, available online at http://www.mi.sanu.ac.yu/vismath/gal/index.html
[4] D.Schattschneider, *Visions of Symmetry*, W.H.Freeman and Company, 1990.
[5] P.Gailiunas, *Some Monohedral Tilings Derived from Regular Polygons*, Bridges Donostia Proceedings 2007, p.11.
[6] http://www.bridgesmathart.org/art-exhibits/bridges2007/gailiunas.html
[7] D.Dunham, *168 Butterflies on a Polyhedron of Genus 3*, Bridges Proceedings 2002, pp.197-204.
[8] Grünbaum and Shephard, *Tilings and Patterns, W.H.Freeman and Company*, 1987, p.289.
[9] http://www.mi.sanu.ac.yu/vismath/gailiunas2008/index.html

A New Method for Designing Iterated Knots

Robert W. Fathauer
Tessellations Company
3913 E. Bronco Trail
Phoenix, AZ 85044, USA
E-mail: tessellations@cox.net

Abstract

A new method for designing iterated knots is described. The method utilizes a starting curve in which smaller copies of the curve are embedded. Points along the curves are connected by strands to form a knot, which is iterated by replacing the contents of the smaller curves with the contents of the larger curve. The method possesses considerable design flexibility, allowing the creation of stylized and esthetically pleasing iterated knots.

1. Introduction

Fractals and knots are popular topics at Bridges Conferences, both being mathematical objects with considerable visual appeal. In 2005, Carlo Séquin showed a couple of examples of iterated knots, created by applying the iterative substitution concept of fractals to knots [1]. The basis for this approach is Conway's notion of a tangle, a portion of a knot isolated by a boundary that is crossed four times by the strands [2]. Descriptions of knots and operations on knots are facilitated by the use of tangles.

At Bridges 2007, Robert Fathauer presented a paper that described a widely-applicable method for creating fractal knots by iterative substitution [3]. In that method, the starting point is a knot from the Knot Table [2]. The knot is rearranged to have holes that are similar in shape to the overall knot. It is then iterated by substituting copies of the current knot for the holes. While it is relatively straightforward to apply this method to any knot in the Knot Table, the method does not allow much flexibility in guiding the design to result in esthetically pleasing knots.

In this paper, a new method is described that allows greater flexibility in the esthetics of the design. The starting point is not the Knot Table, however. If desired, one can work backwards from the chosen starting knot to determine the knot in the Knot Table to which it corresponds. The work presented here is a recreational and artistic endeavor that makes use of established knot theory.

2. Description of the Method

The method is described below and illustrated in Figure 1. More concise and rigorous mathematical language could be used, but the language chosen should be accessible to a wider audience.

1. Create a "starting knot interior" as follows:
   a. Create a simple closed curve C_0 within the plane.
   b. In the interior of C_0, embed one or more smaller curves C_1^1, C_1^2, ... that are similar to C_0 within a set of operations that include scaling, rotation and reflection, as desired.

c. Within each C_1^i, draw strands with one or more crossings, terminating at points P_1^{i1}, P_1^{i2}, … on C_1^i. Each group of strands and points should be similar (identical except for the differences in scaling, rotation, and reflection used in Step 1b). There should be at least four points P on each curve, and the number of points must be even. I.e., each curve bounds an n-strand tangle with $2n$ endpoints.

d. Create a set of points on C_0 that is similar to the set of points on each C_1^i. Connect the loose strands terminating at the points P_1^{i1}, P_1^{i2}, … on the each C_1^i either with points on other C_1^i or with the points P_0^1, P_0^2, … on C_0.

2. Outside of C_0, join the loose strands terminating at points P_0^1, P_0^2, … in such a way as to obtain a unicursal (single-strand) knot with alternating over/under weave. These strands, the "exterior strands", together with the starting knot interior, constitute the starting knot. Check to be sure that this starting structure really is a knot; i.e., that it is unicursal and that it isn't actually the unknot (that it can't be reduced to a simple loop with no crossings). The signs of some of the crossings in one or more of the C_1^i may need to be flipped in order to maintain an overall over/under weave.

3. In the starting knot interior, replace each C_1^i and it's interior with a scaled-down copy of the starting knot interior, created according to the sets of operations used in Step 1b. Check to be sure that this new knot is unicursal. Change the sign of the crossings with each C_1^i as needed to maintain an overall under/over weave when the exterior strands are included. Call the resulting structure, exclusive of the exterior strands, the "current knot interior".

4. Replace each C_1^i and it's interior with a scaled-down copy of the current knot interior, created according to the sets of operations used in Step 1b. Check to be sure that this new knot is unicursal. Change the signs of the crossings with each C_1^i as needed to maintain an overall under/over weave when the exterior strands are included. Call the resulting structure, exclusive of the exterior strands, the "current knot interior".

5. Repeat step 4 as desired. After all repetitions, the strands defined in Step 2, together with the current knot interior, constitute the final iterated knot. The exterior strands may be modified if desired, as may the strands within the smallest generation of curves.

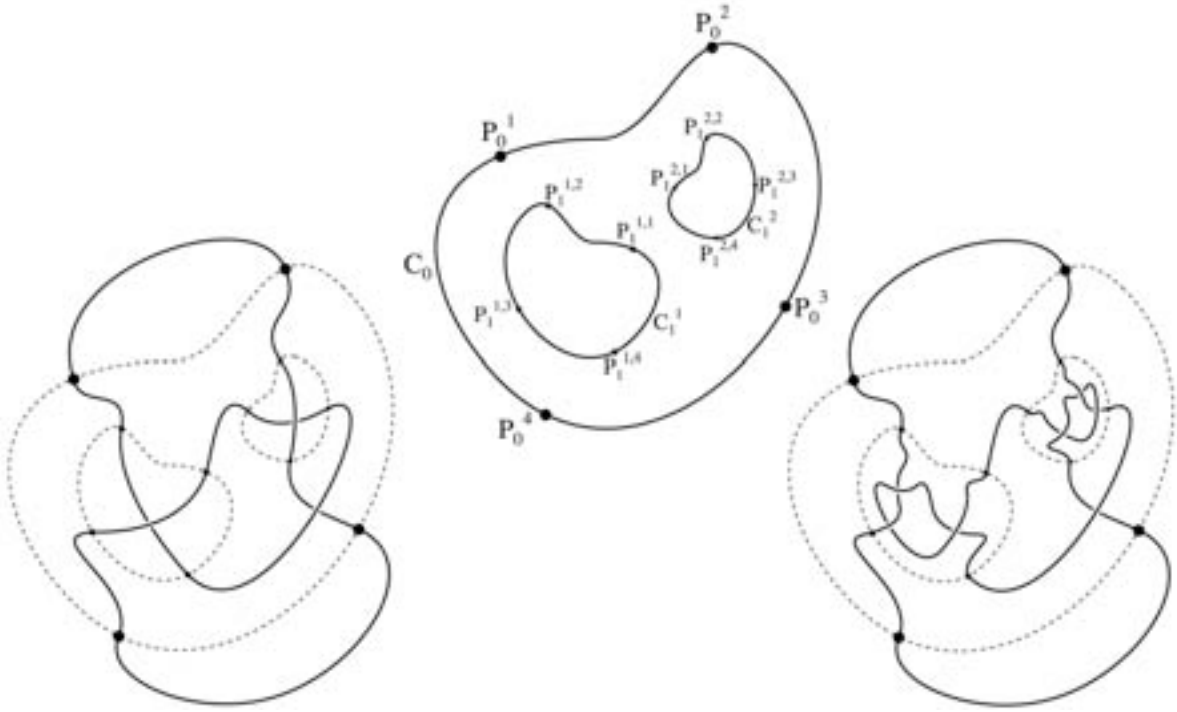

***Figure 1**: An illustration of the method for creating an iterated knot, showing the starting curves and points at top, the starting knot interior plus exterior connections at bottom left, and the knot after a first iteration at bottom right.*

An example of an iterated knot designed according to the method outlined above is shown in Figure 2. The starting curve is a square, and there are two smaller curves, both of which are scaled by 1/3 and neither rotated nor reflected. There are four points on each square at which strands connect, located at midpoints of the edges. The starting knot, shown at top left in Figure 2, has 7 crossings. There is one crossing that is exterior to the largest square, a single crossing within each smaller square, and four crossings in the space between the large and smaller squares. After one iteration, shown at top center in Figure 2, the knot has 17 crossings. The second and third iterations are shown at top right and bottom in Figure 2. The knot is sufficiently complex and the smallest features so small that additional iterations are not shown here. The number of crossings for the second through fifth iterations is 37, 77, 157, and 317. Note that the increase in the number of crossings from one iteration to the next is 10, 20, 40, 80, 160, … The number of crossings N in the jth knot (where $j = 1$ corresponds to the starting knot) is given by the following expression:

$$N(j) = 7 + 10 \sum_{i=0}^{j-1} 2^i = 7 + 10\,(2^j - 1)$$

A general formula can be written for the number of crossings in an iterated knot of this sort. If there are k smaller curves C_1 within C_0, l crossings outside C_0, m crossings in the volume between C_0 and the C_1, and n crossings within each C_1, then the number of crossings in the starting (first) knot is $l + m + kn$. In the iterated (second) knot, the number of crossings is $l + m + k(m + kn)$. In the jth knot, the number of crossings is $N(j) = l + (m + km + k^2m + \ldots + k^{(j-1)}m) + k^jn$. The geometric series in parentheses can be summed, giving for the number of crossings in the jth knot $N(j) = l + m(1 - k^j)/(1 - k) + k^jn$.

3. Design Considerations

Keeping some design guidelines in mind will in general lead to more esthetically pleasing iterated knots. Four general guidelines follow.

A. Keep it simple.

Knots become complex and confusing very quickly. As a result, it is usually a good idea to use a simple starting curve, such as a circle or a polygon possessing symmetry and not too many sides. In addition, keeping the number of curves k small (≤ 5) will also keep things simple. Using the same scaling factor for all of the C_1 will also simplify the construction, but it may be desirable to vary the scaling factor to achieve a particular visual effect.

B. Having some sort of overall symmetry will in general be pleasing to the eye.

Both rotational symmetry and mirror symmetry (one or multiple lines) work well. Note that while the strand positions may obey some symmetry, the signs of the crossings may be reversed from one region of the knot to another and therefore not obey that symmetry.

C. Keep the scaling factor s as close to unity as possible, and the number of iterations small.

This will allow the eye to take in a few iterations at once. After three iterations, the smallest regions will have features only $1/s^3$ as large (linearly) as the largest similar regions. If a scaling factor $s = 1/3$ is used, for example, features in the smallest regions will be 1/27 as large as the similar features in the largest regions.

D. A style should be selected for the finished knot.

One possibility is smooth curves that call to mind rope knots in the real world, as in the knot of Figure 2. It is also possible to use some sharply angled features in otherwise curved strands; this is often employed in Celtic knot designs and was employed in the knot of Figure 3 below. Relatively wide strands are often used in Celtic designs, as in the final knot of Figure 3. Crosses are a design element often found in Celtic knots, and these were used in the knot of Figure 4 below. Islamic style can also be intentionally used to guide the shape of strands, in which case the strands will mostly consist of straight lines and openings in the knot could include characteristic shapes like star polygons. More generally, styles could include bold

and forceful, playful (see Figure 5), delicate, etc. Effectively employing a particular style generally requires the reshaping of strands after construction of the basic iterated knot.

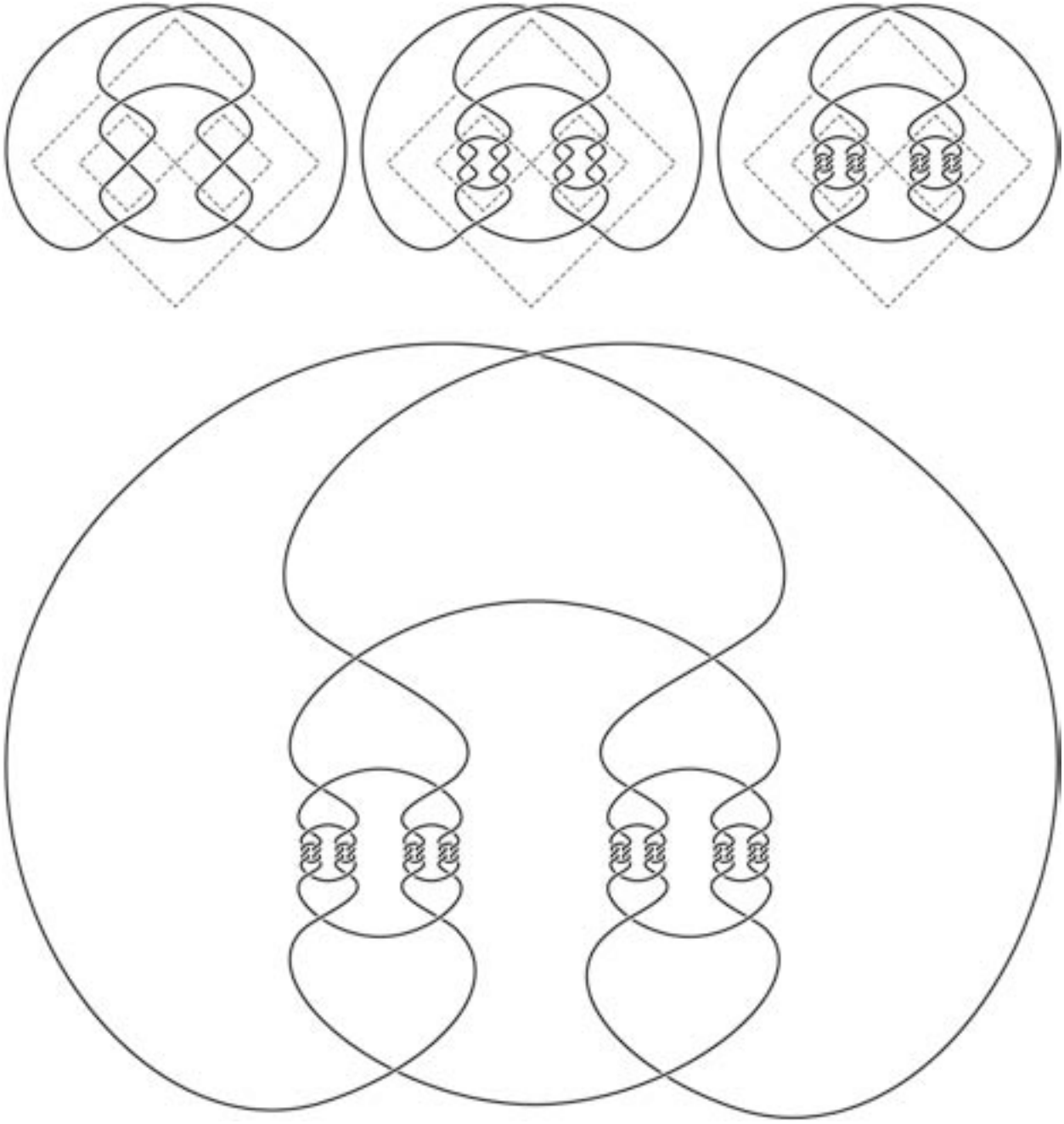

***Figure 2**: A simple example of a knot iterated using the method described above. The starting knot and first three iterations are shown. The dashed lines indicated the starting curves described in the method.*

4. Further Examples

Three additional iterated knots designed using the method described above are shown here. The knot of Figure 3 employs a rectangle as the starting curve. Two smaller rectangles are arranged within it, with a rectangular space of the same size and shape between them. The smaller rectangles are rotated 90° with respect to the starting rectangle, and the scaling factor for this arrangement is easily calculated to be $1/\sqrt{3} \approx 0.577$. The starting knot, shown at top left in Figure 3, has three crossings. Since there is only one knot with three crossings, it must be a trefoil knot. The first and second iterations are shown next to it, and the knot after five iterations is shown at the bottom of Figure 3, with gray shading. The number of crossings for the starting knot and first four iterations are 3, 7, 15, 31, and 63, and the increase in the number of crossings with each successive iteration is 4, 8, 16, 32, 64, …

The knot of Figure 4 employs a square as the starting curve, with five smaller squares embedded within it. This was derived from a fractal tiling created *via* dissection of a polyomino that leads to a scaling factor of $1/\sqrt{17} \approx 0.243$ and a rotation angle of $\tan^{-1}(1/4) \approx 14°$ for each of the smaller squares [4]. The starting knot (near top center in Figure 4) has nine crossings, five of which are within the five smaller curves. It has two-fold rotational symmetry and would have four-fold symmetry if not for the exterior strands. Note that some artistic license was taken in connecting points on the smaller squares, with pointed loops that extend well outside the large square. The first iteration is show at upper right in Figure 4, and the second iteration is blown up to overfill the page, in order to make the smallest features clear. In this case, due to the rather severe scaling factor, two iterations already leads to small features. The quintupling of features with successive iterations leads to a rapid increase in the number of crossings, from 9 for the starting knot to 49 for the first iteration to 249 for the second iteration. A third iteration would have 1,249 crossings! The increase in the number of crossings with each successive iteration is 40, 200, 1000, …

The knot of Figure 5 employs a hexagon as the starting curve, with three smaller hexagons embedded within it. The scaling factor is $1/3 \approx 0.333$, and the smaller knotted regions are rotated 60° with each iteration. The strands were given arrow-like shapes in order to create a whimsical design that seems to possess a lot of energy. The starting knot has 15 crossings, and the first two iterations have 30 and 75 crossings. The increase in the number of crossings with each successive iteration is 15, 45, 135, …

5. Conclusions

We have presented a new method for designing iterated knots. In contrast to the previously described method, in which holes in a starting knot are replaced with scaled down copies of the knot, holes in the starting structure in the current method are filled with crossing strands. Several examples have been presented. These illustrate the greater degree of design flexibility in this method, which allows the creation of more stylized and esthetically pleasing iterated knots.

References

[1] Carlo Séquin. *Tangled Knots*, presented at the Art+Math=X conference in Boulder, Colorado, June, 2005. Paper available at http://www.cs.berkeley.edu/~sequin/PAPERS/ArtMath05_TangledKnots.pdf, and PowerPoint presentation at http://www.cs.berkeley.edu/~sequin/TALKS/AM05_TangledKnots.ppt.
[2] See, for example, Colin C. Adams, *The Knot Book,* The American Mathematical Society, Providence, RI, 2004.

[3] Robert Fathauer, *Fractal Knots Created by Iterative Substitution,* Bridges Donostia Conference Proceedings, edited by Reza Sarhangi and Javier Barrallo, pp. 335-342, 2007.
[4] Robert Fathauer, *Fractal Tilings Based on Dissections of Polyominoes,* Bridges London Conference Proceedings, edited by Reza Sarhangi and John Sharp, pp. 293-300, 2006.

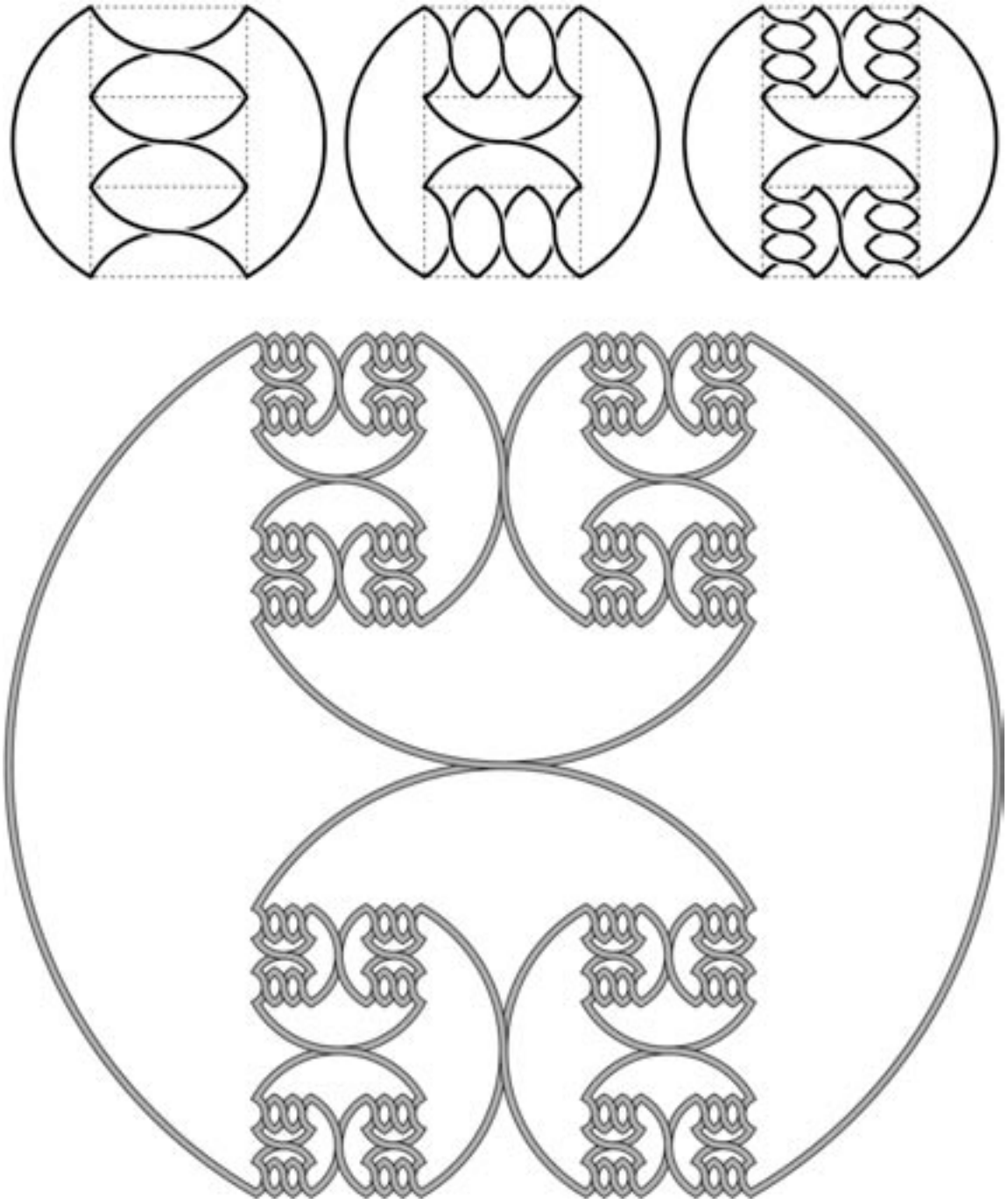

Figure 3*: An iterated knot in which the smaller copies of the current knot are rotated 90° before being substituted in the smaller rectangles. The top line show the starting knot and first two iterations, while the bottom figure shows the knot after five iterations.*

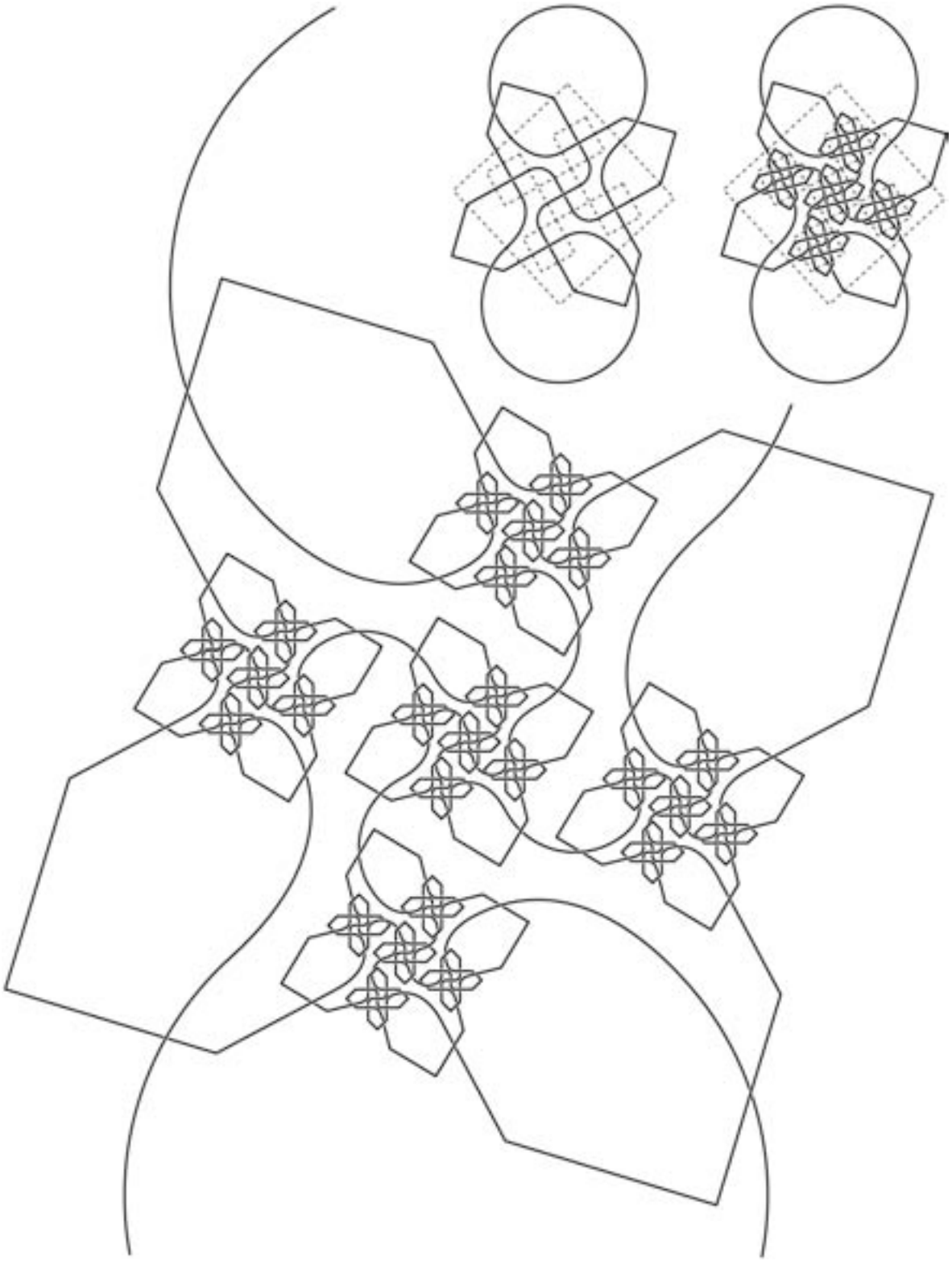

Figure 4: *An iterated knot in which five smaller copies appear with each successive iteration. The starting knot is show at top center, with the first iteration next to it. The knot after two iterations is blown up, with the outer loops cut off, in order to better shown the smallest features.*

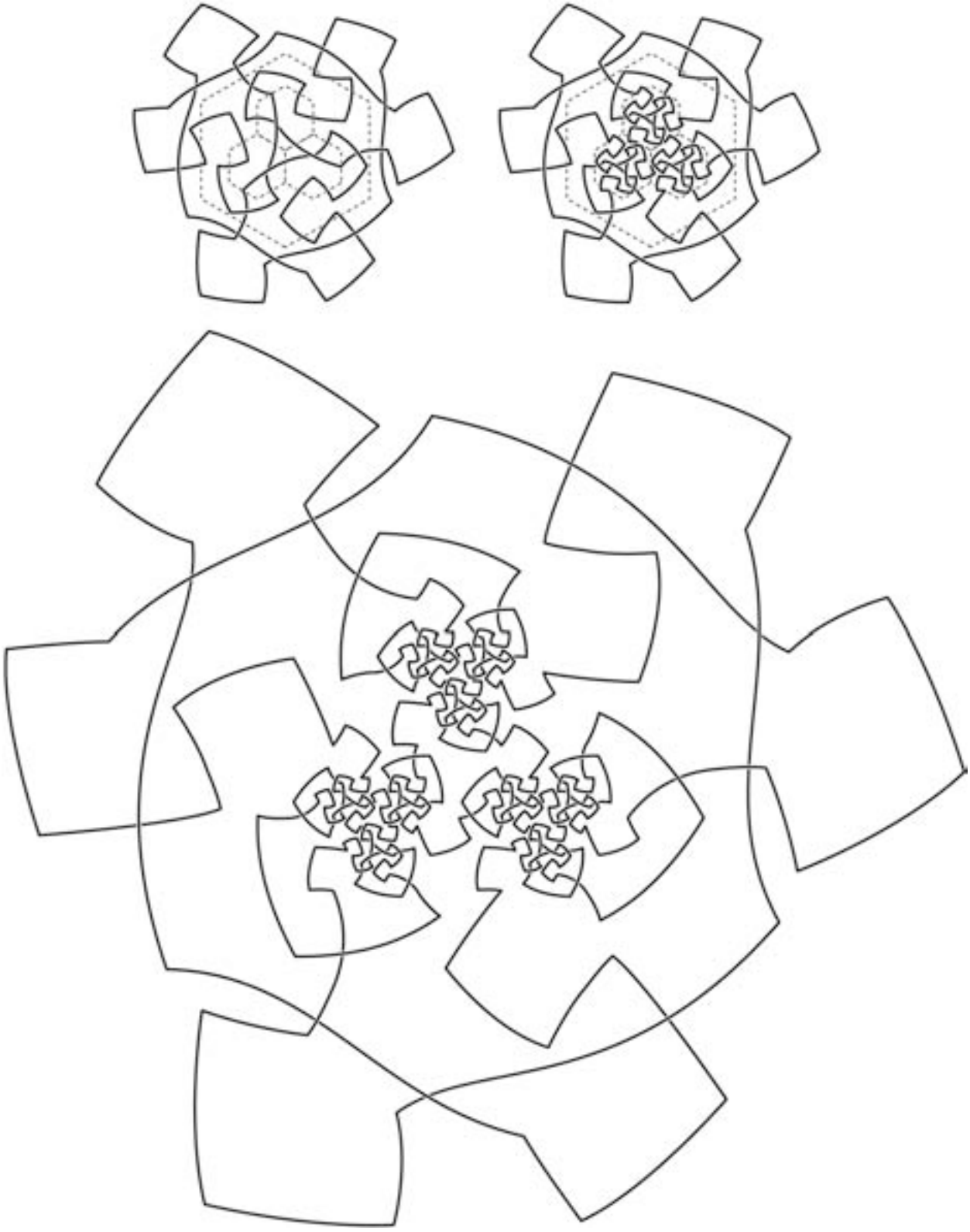

***Figure 5**: An iterated knot with three-fold rotational symmetry. Arrow-like strands were employed to give the knot a vibrant and whimsical character.*

A Group Portrait on a Surface of Genus Five

Jay Zimmerman
Mathematics Department
Towson University
8000 York Road
Towson, MD 21252, USA
E-mail: jzimmerman@towson.edu

Abstract

This paper represents a finite group with 32 elements as a group of transformations of a compact surface of genus 5. In particular, we start with a designated pair of regions of this surface, and each region is labeled with the group element, which transforms the designated region into it. This gives a portrait of that finite group. These surfaces and the regions corresponding to the group elements are shown in this paper. William Burnside first gave a simple example of such a portrait in his 1911 book, "Theory of Groups of Finite Order". This paper is the third paper in a series which models groups as groups of transformations on a compact surface in the style of William Burnside.

Introduction and Historical Perspective

A group is a set and an associative binary operation which contains an identity such that each element has an inverse element in the group. Therefore, a group is an abstract object. Groups were originally thought of as permutations of some other mathematical structure, such as a set of points. This permutation group idea comes very naturally from the set of symmetries of physical objects. Thus the symmetries of an equilateral triangle are a group with six elements. It follows that groups can be both abstract objects and real physical motions of a symmetric object.

A group can also be thought of as a set of transformations of a "plane" into itself that is closed under composition. Some groups of transformations can be realized on the Euclidean plane and these give rise to the tessellations of the plane. Many groups need to be realized on the hyperbolic plane and give rise to tessellations of it. A finite group is a finite set of transformations which is closed under composition. If a finite group were represented on an infinite plane, then the fundamental region would have to be infinite. Therefore, a finite group is represented as a set of transformations of a compact two dimensional surface, such as the sphere or the torus. These surfaces must become more complex in order to contain the portraits of some groups.

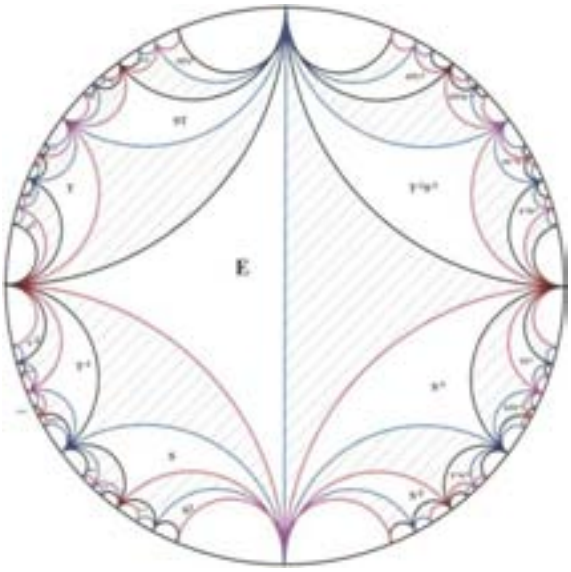

Figure 1, Portrait of a Free Group

This paper is part of a series of papers on how to draw a portrait of a finite group, in the style of Burnside [1]. Burnside started with circles in the plane and used inversion in the circle as the transformation. The relationship between circles determines the group generated by these transformations. When we look at the regions this generates inside of a circle we get Figure 1. Burnside [1, p. 379] constructed a free group on 2 generators, F_2, using two mutually tangent circles and the line tangent to them (a circle centered at

infinity). We only need to picture the part of each region inside the circle through the three points of tangency. Like Burnside, the initial region is the "triangle" labeled E and its corresponding shaded region. Each “triangle” is bounded by arcs colored red, blue or black in our sketch. Inversion in any single arc will take a shaded region into a non-shaded region and vice- versa. Each region can be labeled by the transformation needed to get from E to that region. Since we are interested in orientation-preserving transformations, each group action is represented by the composite of two such inversions. Inversion through first a red arc and then a blue arc corresponds to multiplying on the left by the generator S. Multiplying on the left by the generator T corresponds to inversion through black and then red. Multiplying on the left by ST corresponds to inversion through black and then blue. If we considered inversion through a black arc first and then a blue arc as the inverse of a single generator, R, then we could interpret this picture as a portrait of a group with presentation $T_2 = \langle R, S, T \mid RST = 1 \rangle$. This construction fills up a unit disk with black and white regions and the transformations are given in the same way. We have used Geometer’s SketchPad [4] to reconstruct this portrait of a free group on two

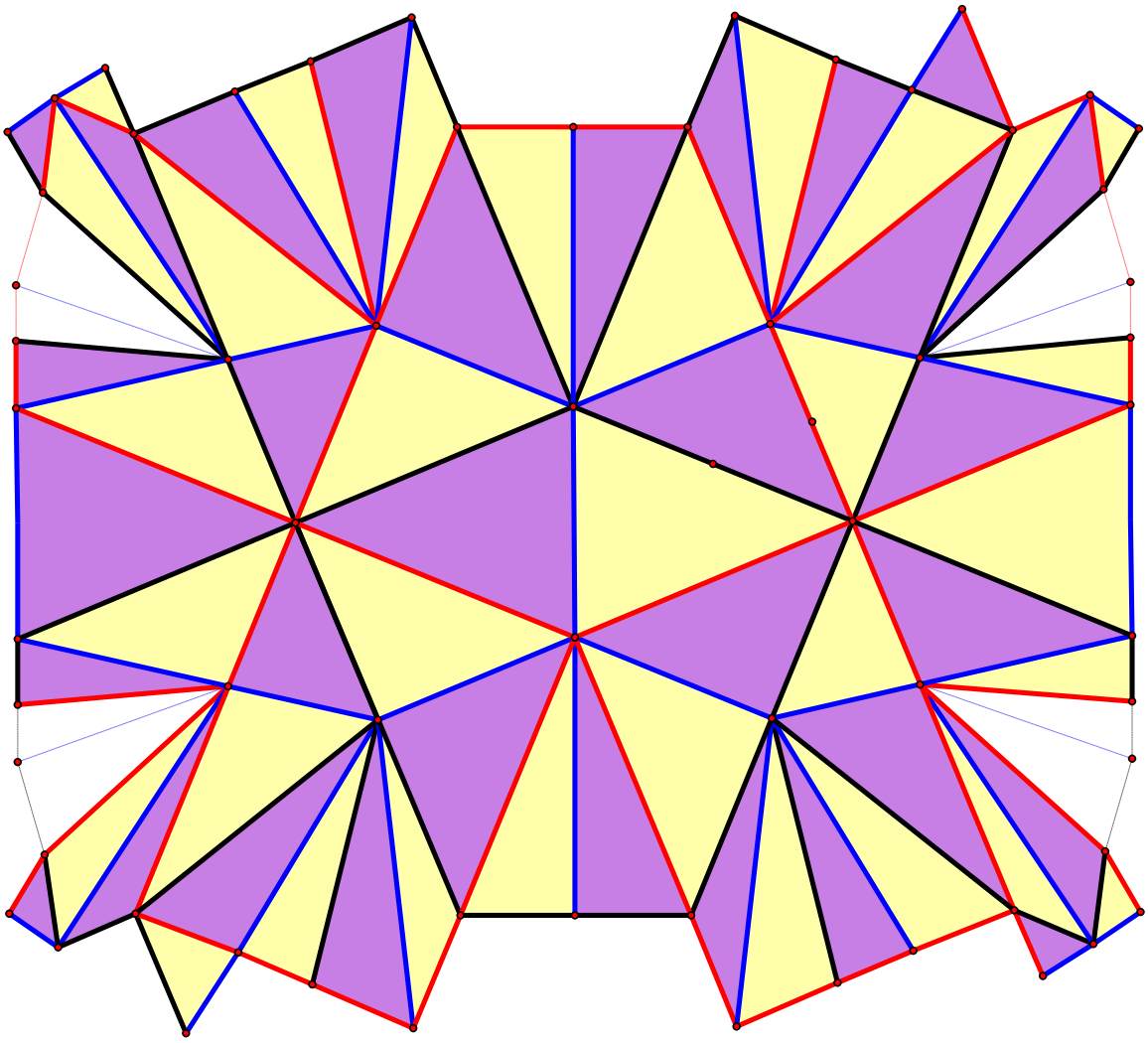

Figure 2 - The Fundamental Region for SG(32,2)

generators (Figure 1), similar to a figure in Burnside [1, p. 380].

Now suppose that we have a finite group, G, generated by 2 generators. The group G is the image of F_2 by a normal subgroup N. Specifically, two strings of generators represent the same element of the

group if the product of one string and the inverse of the other string is in the subgroup N. One example of this is that a rotation of 120º clockwise is the same as two rotations of 120º counterclockwise. After associating an element of F_2 to each region, the final step is to identify all regions with labels from the subgroup N. After this identification, we have the finite group G. However the circle in Figure 1 still has an infinite number of regions labeled with elements from the presentation T_2. This circle can be thought of as the Poincare disk model of hyperbolic space. At this point, we choose a connected set of regions which contains a single region for each group element and whose label corresponds to that group element. This set of regions is called the Fundamental Region for the finite group. Any region outside of the fundamental region is equivalent to some region within the fundamental region. Therefore, the compact two dimensional surface is derived by folding the fundamental region in certain ways. This is the same idea as constructing a torus by taking a rectangle and identifying the top and bottom as connecting to each other and the two sides as connecting.

In the diagram in Figure 1, each element has infinite order and the curvilinear triangles get smaller and smaller as they approach the boundary of the circle. This means that the connected region in Figure 1 would have a ragged boundary with parts of the boundary intersecting each point. This can be fixed by picturing a different tiling of the hyperbolic plane or by drawing a polygonal region with the same relationship between the triangles. The second approach has the advantage that the triangles remain easily visible as they get near the boundary of the polygonal region and this portrait is pictured in Figure 2. The portraits developed are topologically equivalent to the model that we want, but even the areas of the regions are changed.

Compact surfaces are classified topologically by genus and orientability. Every compact orientable surface with genus g is topologically equivalent to a sphere with g handles. Very roughly, the genus is the number of "donut" holes that a surface has. This is why a donut and a coffee cup are topologically equivalent. Thus, every compact surface of genus g may be constructed in many different, but topologically equivalent ways. We will pick a symmetric way of representing the surface and use it. This surface may be drawn and colored with each face composed of one white and one black region. These faces represent a finite group of transformations, which act on the surface in the style of Burnside [1]. The choice of surface is made arbitrarily with the correct orientability and genus.

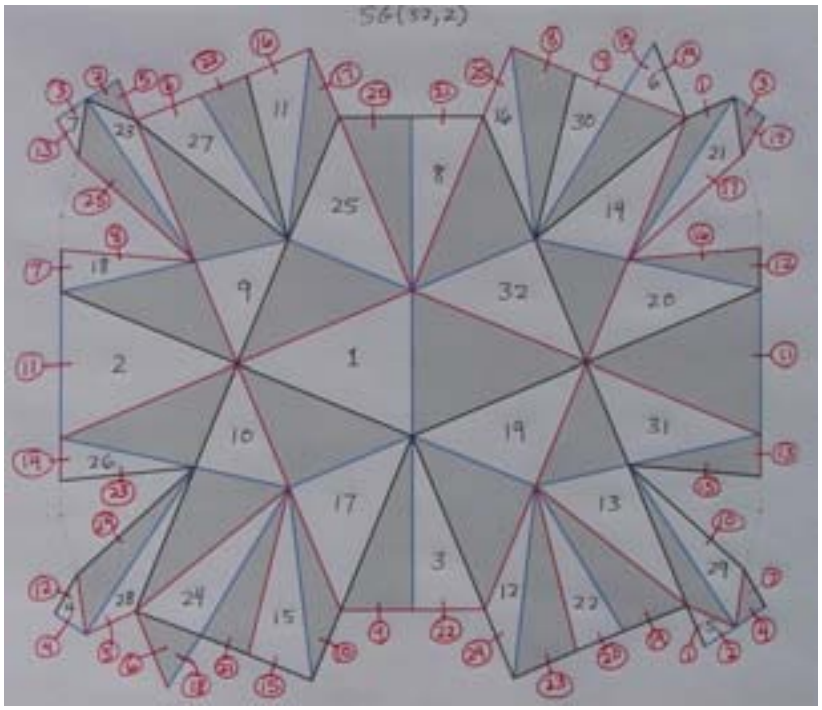

Figure 3 - Connectivity of the Fundamental Region

There have been several Bridges papers which pictured regular maps on surfaces of genus 3 to 7 (for example [3] and [7]) and their associated tilings and the related topic of portraits of groups using techniques in this paper ([9] and [10]). The automorphism groups of these tilings are the groups PSL(2,7) (in [3]) and S_5 (in [7]). The portraits in [9] are of the dicyclic group of order 12 and the group of order 16 with notation < 2, 2 | 2> (see [2, p. 134]) acting as orientation-preserving transformations and the group P_{48} = SG(48, 33) pictured as a group where some transformations are orientation-reversing.

Group Portraits

Let G be a finite group. There is a set of orientable surfaces on which G can be represented as a group of transformations. One of these surfaces has the smallest possible topological genus of all surfaces in this set. The genus of this surface is defined to be the symmetric genus of the group. If the group can only be represented by transformations that preserve the orientation of the surface, then the genus of the surface of smallest genus is called the strong symmetric genus of the group.

The group that we will be considering is a group of order 32 with symmetric genus 5 (see [6]). The genus action is given as a quotient of the triangle group $\Gamma(4,4,4) = \langle S,T \mid S^4 = T^4 = (ST)^4 = 1 \rangle$ and these transformations preserve the orientation of the surface, its strong symmetric genus is also 5. This group is SmallGroup(32,2) in the Magma Library of groups (see [5]). We denoted this group by $SG(32,2)$. It has a presentation $\langle S,T \mid S^4 = T^4 = (ST)^4 = ([S,T])^2 = [S,[S,T]] = [T,[S,T]] = 1 \rangle$ as the image of $\Gamma(4,4,4)$. This presentation is extremely symmetrical. We know that this group can be drawn as a group of transformations of a compact surface with five "donut holes" and that it cannot be

Figure 4 - The model of SG(32,2) on a surface of genus 5

drawn on a compact surface with any fewer than five "donut holes". The polygonal region for the group $SG(32,2)$ is given in Figure 2.

In Figure 3, each of the thirty two faces is labeled with a number which corresponds to a group element. Remember that each "face" is a paired white and black region separated by a blue curve. Each region on the border of the plane figure connects to another region on the border of the plane figure. Theoretically, this tells us how to fold the fundamental region to get a compact surface with genus five. The faces are split into white and black parts simply because this is the way that Burnside constructed his original diagram. This portrait consists of 32 white and 32 black triangles. Each of the 64 regions is bounded by 3 edges and each edge bounds 2 regions. So a simple combinatorial argument gives that there are 96 edges. The faces that meet at a vertex are labeled in such a way that each face is related to the adjoining face by multiplication on the left by either S, T, ST or its inverse. For example, two regions *M* and *N* are both incident to the same S vertex if and only if $N = S^k M$ for some *k*. Therefore, each vertex could be classified as an S-vertex, a T-vertex or an ST-vertex depending on the labeling of its bounding regions. Since S, T and ST have order 4, each S, T or ST vertex has degree 8. This gives 24 vertices. Therefore, the Euler characteristic is $\chi = V - E + F = -8$. Since $\chi = 2 - 2g$, where g is the genus of the surface, this portrait is drawn on a surface of genus five. Therefore, the portrait in Figure 4 gives the genus action for this group (see [6]).

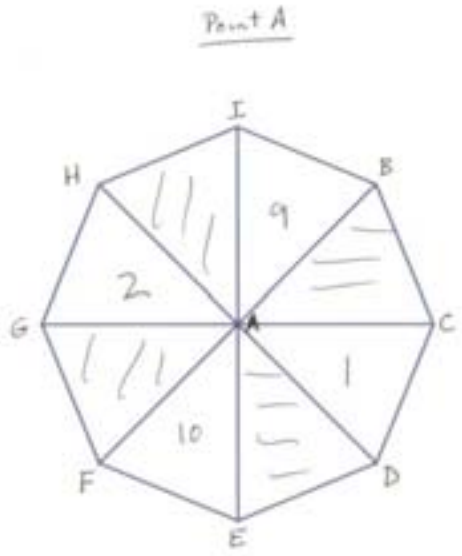

Figure 5 - Local information about a point

Finally, we construct a model of the surface and of the transformations in this group. This model is in Figure 4. Notice that this is a model where each transformation is represented as a word in the generators of a particular presentation. Therefore, one could say that this is a model of the particular presentation of this group. I would point out that this presentation was chosen as the one which can be drawn on a surface of smallest genus. In this particular case, the Cayley graph of this presentation is the dual of this model where each region consists of a paired white and black region. However, in general Cayley graphs can be embedded in surfaces of smaller genus than can be done with this technique (see [8]).

Construction of the Model

Finding a blueprint for the model is the hardest part of this process. A graph is constructed from the data in figure 3. This graph is a regular map, but unfortunately this fact is not useful in finding the model. The basic idea is to construct a model of a genus five surface and try to fit the points of the graph on the model in the proper way. The first step is to get the information about the points and faces that are adjacent to a point. An example of this is shown in Figure 5 for the point labeled A. Diagrams like this one are constructed for each point in the graph. Notice that although Figures 2 and 3 distort the angles, in the final model the triangular regions which have point A as a vertex, all have vertex angle 45º. In Figure 5, the points H, A and D are on a straight line and in the model this is a black curve. We can extend this "straight line" to a closed curve on the model. These curves are referred to as "straight line curves".

There are 24 straight line curves in the model, eight each of black, red and blue curves. Each straight line curve contains four vertices. Each vertex is on four straight line curves, two of one color and two of another color. The two straight line curves of the same color which intersect in a point are at right angles. If you start at any point in the model and pick a color incident to that point, the two straight line curves intersect in exactly two steps. For example, the two black straight line curves incident to point A are $H \to A \to D \to L$ and $F \to A \to B \to L$ and they intersect again at point L. The two red straight line curves incident to point A are $G \to A \to C \to P$ and $E \to A \to I \to P$ and they intersect again at point P.

Two white regions *M* and *N* both bound a straight line curve of the same color if and only if

$N = S^2 \cdot M$. The same is true for T and ST vertices. Thus, a straight line curve contains directed edges that are two steps apart if and only if these edges are incident to the white regions F and x^2y^2F where $x, y \in \{S, T, ST\}$ are different generators. Two steps preserve the direction of the directed edge along the straight line curve. The elements S^2, T^2 and $(ST)^2$ are in the center of $SG(32,2)$. So if $N = z^k \cdot M$ for $z \in \{S, T, ST\}$, then both images x^2y^2M and x^2y^2N have the same initial vertex because they satisfy the equation $x^2y^2N = x^2y^2z^k \cdot M = z^k x^2y^2M$. This is why the straight line curves above always intersect in 2 steps. It is also clear, since these elements have order 2, that four steps gets you back to the initial point.

There are 24 points and since there are 5 holes and the outer rim, each one of these has a straight line curve on its rim. Now we find a way to connect these points. There are in fact multiple ways to do this, but one constraint used is that the front and back side of the models must be symmetrical. This gives a pleasing symmetry to the whole construction and makes it easier to see how it fits together.

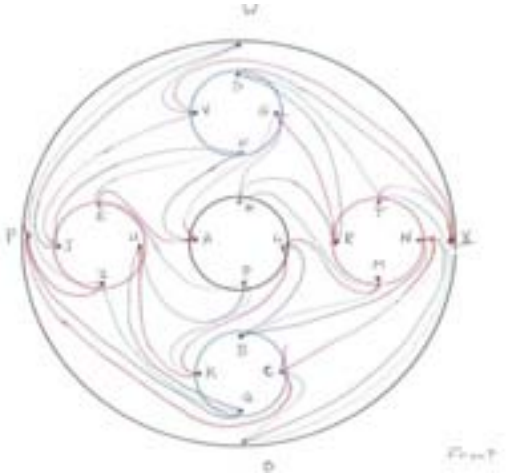

Figure 6 - Blueprint of the Model

Figure 7 - Model with graph on it.

Finally, the front face of the blueprint for the model is included in Figure 6, and the actual model with the graph drawn on it is in Figure 7. Note that even though the graph was embedded on the model first, it is easily checked that the faces are properly positioned.

References

1. W. Burnside, *Theory of groups of finite order*, Cambridge University Press 1911.
2. Coxeter and Moser, *Generators and Relations for Discrete Groups*, Springer 1984.
3. D. Dunham, *168 Butterfies on a Polyhedron of Genus 3*, Proc. Bridges 2002, Baltimore, USA, 197 – 204.
4. The Geometer's Sketchpad (Software), http://www.dynamicgeometry.com/.
5. Magma Computational Algebra System, http://magma.maths.usyd.edu.au/magma/.
6. C. May and J. Zimmerman, The groups of symmetric genus $\sigma \leq 8$, Communications in Algebra 36, No. 11 (2008), p. 4078 –4095.
7. C. Sequin, *Symmetric Embeddings of Locally regular Hyperbolic Tilings*, Proc. Bridges 2007, Donostia, Spain, 379 – 388.
8. A. T. White, Graphs of Groups on Surfaces, North-Holland Mathematics Studies 188, 2001.
9. J. Zimmerman, Portraits of Groups, Proceedings 2006, Bridges London: Mathematics, Music, Art, Architecture and Culture, London, England, 131 - 134.
10. J. Zimmerman, Portraits of Groups II, Orientation Reversing Actions, Proceedings 2007, Bridges, Donostia: Mathematical Connections in Art, Music and Science, San Sebastian, Spain, 109 - 114.

Tiling the Musical Canon with Augmentations of the Ashanti Rhythmic Pattern

Carl Bracken[1], Gary Fitzpatrick[2], Nadya Markin[3]
[1]Department of Mathematics
National University of Ireland Maynooth
Co. Kildare, Ireland
Email:carlbracken@yahoo.com
[2]Email:garyfitz@dublin.ie
[3]Claude Shannon Institute
School of Mathematical Sciences
University College Dublin
Bellfield, Dublin 4, Ireland
Email:nadyaomarkin@gmail.com

Abstract

We discuss the problem of constructing a tiling of the musical time-line with a number of instruments (called voices) all of which are playing according to variations of a particular rhythmic pattern. We show that the Ashanti rhythmic pattern allows a tiling in six voices.

1 Introduction

The term rhythmic canon was coined by the composer Olivier Messiaen (1908-1992). The rhythmic canon dictates when each instrument in a composition may play a note or be silent. Each instrument should play the same rhythm but start at a different time. If the rhythmic canon is such that at every time interval exactly one instrument can be heard, then the canon is said to be tiled. Messiaen himself referred to the sound of a rhythmic canon as "organised chaos" [5]. In his composition *Harawi*, Messiaen uses a three voice canon with each voice playing according to the following rhythmic pattern.

1001000010000000100001001000100100000010010001010101001000010 0

A 1 indicates that the instrument plays a note, while a 0 means it is silent. When the three voices play together they play with the same rhythm but start at different times to give the following rhythmic canon.

V_1 : 1001000010000000100001001000100100000010010001010101001000010 0
V_2 : 0010010000100000001000010010001001000000100100010101010010000100
V_3 : 0000100100001000000010000100100010010000001001000101010100100001 00

This canon has the property that there is an instrument playing on almost every beat and with just a few exceptions there is only one instrument playing, so it is almost perfectly tiled. In this article we are concerned with perfectly tiled canons, i.e., canons in which there is one and only one instrument playing at every time interval. Today there are many musicians who use tiled canons in their compositions. In particular we would refer the reader to the work of Tom Johnson [4].

2 Polynomial Representation of the Rhythmic Canon

The binary representation of rhythmic patterns used above is useful to anyone wanting to analyse a pattern or compose a piece of music based on the described rhythm. However, if we wish to construct a rhythmic canon with particular properties or check whether a given set of patterns tile the musical time-line, then polynomial representation is more useful.

The polynomial that represents a given rhythmic pattern is simply a polynomial in x with integer coefficients 0 or 1. If in the binary representation the pattern has a 1 in the i^{th} position, then the coefficient of x^i is 1, otherwise it is zero. Note that for a rhythmic pattern of period n (i.e., one that repeats every n beats) we consider the binary representation as starting at position 0 and finishing at position $n-1$. This means the binary pattern of Messiaen

$$1001000010000000100001001000100100000010010001010101001000010 0$$

will be written as

$$1+x^3+x^8+x^{16}+x^{21}+x^{24}+x^{28}+x^{31}+x^{38}+x^{41}+x^{45}+x^{47}+x^{49}+x^{51}+x^{54}+x^{59}.$$

We shall refer to polynomials which have 0 and 1 as coefficients as $0-1$ polynomials. As each rhythmic pattern has some period n, the powers in its polynomial representation are reduced modulo n. Therefore its corresponding polynomial can be regarded as an element of the ring $\mathbb{Z}[x]/(x^n-1)$. Multiplication of a polynomial by x^i will shift the rhythm by i positions, meaning it will start i beats later. Let $P(x)$ be a $0-1$ polynomial that describes a rhythm to be used in a canon. If there exists another $0-1$ polynomial say $Q(x)$ such that $Q(x)P(x) = 1+x+x^2+...+x^{n-1}$, then the canon can be tiled with the pattern $P(x)$. We refer to $P(x)$ as the inner rhythm and the polynomial $Q(x)$ is called the outer rhythm. Each voice plays according to inner rhythm, while the outer rhythm determines when each voice starts.

3 Examples of Tiled Canons

3.1 A Simple Tiling

Consider the rhythmic pattern of period 12 described by the polynomial $P(x) = 1+x^5+x^7$. We choose the outer rhythm $Q(x)$ to be $1+x^3+x^6+x^9$. As the period is 12, all powers of x will be reduced modulo 12. It can be easily verified that

$$Q(x)P(x) = (1+x^3+x^6+x^9)(1+x^5+x^7) = 1+x^2+x^3+x^4+...+x^{11},$$

hence the time-line is tiled with four voices, one for each term of $Q(x)$. The rhythmic patterns are periodic, so in the binary representation we may write the following canon.

V_1 : 100001010000100001010000100001010000
V_2 : 000100001010000100001010000100001010
V_3 : 010000100001010000100001010000100001
V_4 : 001010000100001010000100001010000100

Here each voice repeats the pattern three times. It can be seen from above we have a perfect tiling of the time-line.

As $Q(x)P(x) = P(x)Q(x)$, we can obtain another tiling by interchanging the roles of the outer and inner rhythms. That is, we can obtain the following canon in three voices.

$$V_1 : 1001001001001001001001001001001001001001$$
$$V_2 : 0100100100100100100100100100100100100100$$
$$V_3 : 0010010010010010010010010010010010010010$$

3.2 Vuza Canons

In the above example we see that the rhythm $1+x^3+x^6+x^9$ has a smaller period than 12. It repeats every three beats. If a polynomial is invariant under multiplication by x^k, then the polynomial's rhythm has period k. If a tiling has no period smaller than n in either the inner or outer rhythms then it is said to be of *maximal category*. It was shown by Vuza [6] that there exists no tiled canon of maximal category with period less than 72. He also provided an algorithm for producing canons of maximal category of period 72 and 120. Much work has been done by both mathematicians and musicians on canons of maximal category, or as they are now called Vuza canons. One example of a Vuza canon is given by polynomials

$$P(x) = 1+x+x^5+x^6+x^{12}+x^{25}+x^{29}+x^{36}+x^{42}+x^{48}+x^{49}+x^{53},$$

$$Q(x) = 1+x^8+x^{18}+x^{26}+x^{40}+x^{58}.$$

As mentioned earlier this will allow for two tilings of the time-line. For more on this topic we refer the reader to [1] and references there in.

3.3 Augmented canons

Another class of tiled rhythmic canons are the augmented canons. In an augmented canon different voices will still play the same rhythmic pattern but some may be stretched by a factor r so that they take longer to complete their cycles, while the non-stretched voices will be repeated r times so that the canon can be tiled. In terms of polynomials, an augmentation of $P(x)$ by a factor of r corresponds to the polynomial $P(x^r)$.

Let k be the period of a rhythm represented by $P(x)$. Suppose we wish to tile the canon with two versions of the same rhythm say $P(x)$ and $P(x^r)$. Note that the augmented pattern $P(x^r)$ is periodic in kr. We can fill kr time intervals with r copies of the pattern corresponding to $P(x)$. In polynomial notation the r copies are created by the polynomial

$$(1+x^k+x^{2k}+x^{3k}+...+x^{(r-1)k}).$$

Now, to complete a tiling we would have to find two outer rhythms $Q_1(x)$ and $Q_2(x)$ such that

$$Q_1(x)(1+x^k+x^{2k}+x^{3k}+...+x^{(r-1)k})P(x)+Q_2(x)P(x^r) = 1+x+x^2+...+x^{rk-1}.$$

The polynomials $Q_1(x)$ and $Q_2(x)$ determine when the voices $P(x)$ and $P(x^r)$ start. The number of terms in $Q_1(x)$ will be the number of voices playing the faster rhythm $P(x)$, while the number of terms in $Q_2(x)$ will be the number of voices playing the slower rhythm $P(x^r)$. We could, of course, try to tile the canon with many different augmentations of the same rhythm, but for the purpose of this article we will consider just one augmentation along with the original pattern.

3.4 Augmented Canons from Traditional Patterns

The purpose of this collaboration (between two mathematicians and a musician) was to try to tile the time line with augmentations of an existing traditional rhythmic pattern and to compose a piece of music on this tiling. Of the large number of (mathematically) possible rhythm patterns that could be used for a given rhythm period only a small number of these are used in practice [3]. It is believed that a rhythmic pattern that has been used for generations probably has some aesthetic quality that a pattern chosen just to satisfy an equation does not. Using a list of traditional African patterns (from [2]), for each period 12 pattern on the list we attempted to solve the equation

$$Q_1(x)(1+x^{12}+x^{24}+\ldots+x^{(r-1)12})P(x)+Q_2(x)P(x^r)=1+x+x^2+\ldots+x^{12r-1},$$

for some small value of r. That is we had to find $0-1$ polynomials $Q_1(x)$ and $Q_2(x)$ such that the above equation holds. We were able to solve this equation for just one of the patterns. In the next section we show how we derived the solution and demonstrate the resulting tiling.

4 The Ashanti Rhythmic Pattern

4.1 Background

The Ashanti people make up 14% of the population of modern day Ghana. The basic rhythmic pattern behind much of their traditional music is the following period 12 pattern with four onsets

$$100101001000.$$

As a polynomial we would write this as

$$P(x)=1+x^3+x^5+x^8.$$

Before attempting to tile with a polynomial it is a good idea to note all the possible differences of the powers of x. This will rule out some shifts by revealing which shifts induce overlap. For example, two of the powers that occur in the Ashanti polynomial are 5 and 3, which have a difference of 2. So a shift by 2 places will cause an overlap. The differences are all calculated modulo 12 and no shift greater than 6 need be considered, as this is just a smaller shift in the other direction. The set of all differences of the powers in the Ashanti polynomial is $\{2,\ 3,\ 4,\ 5\}$, so the only possible shifts that can be used in a tiling are 1 and 6. This means that $Q_1(x)$ has to be of the form $x^i(1+x)$ or $x^j(1+x^6)$.

4.2 An Augmented Tiling

To tile the Ashanti pattern with augmentations by a factor of two we are required to find $0-1$ polynomials $Q_1(x)$ and $Q_2(x)$ such that,

$$Q_1(x)(1+x^{12})P(x)+Q_2(x)P(x^2)=1+x+x^2+\ldots+x^{23}.$$

Using the restriction derived above we may assume that $Q_1(x)$ is either $1+x$ or $1+x^6$. From here we can rule out the remaining possibilities for $Q_2(X)$ by hand without too much difficulty (or with ease on a computer). We concluded that the above equation has no solutions for $Q_1(x)$ and $Q_2(x)$ that are $0-1$ polynomials, therefore a tiling with the augmentation by two is not possible. We can similarly rule out augmentations by a factor of three.

We proceed to look for a tiling with the Ashanti pattern using augmentations by a factor of four. As before we are required to find polynomials Q_1 and Q_2 such that,

$$Q_1(x)(1+x^{12}+x^{24}+x^{36})P(x)+Q_2(x)P(x^4)=1+x+x^2+...+x^{47}.$$

Again, we know that $Q_1(x)$ is either $1+x$ or $1+x^6$. We found a solution for $Q_1(x)=1+x$. What follows is a summary of the computations that lead to the finding of a viable $Q_2(x)$.

Assuming $Q_1(x)=1+x$ we must find $Q_2(x)$ such that

$$(1+x)(1+x^{12}+x^{24}+x^{36})(1+x^3+x^5+x^8)+Q_2(x)(1+x^{12}+x^{20}+x^{32})$$
$$=1+x+x^2+...+x^{47}.$$

This implies

$$(1+x^{12}+x^{24}+x^{36})(1+x+x^3+x^4+x^5+x^6+x^8+x^9)+Q_2(x)(1+x^{12}+x^{20}+x^{32})$$
$$=(1+x^{12}+x^{24}+x^{36})(1+x+x^2+x^3+x^4+x^5+x^6+x^7+x^8+x^9+x^{10}+x^{11}).$$

A simple rearrangement yields

$$Q_2(x)(1+x^{12}+x^{20}+x^{32})=(1+x^{12}+x^{24}+x^{36})x^2(1+x^5+x^8+x^9),$$

while factoring $(1+x^{12}+x^{20}+x^{32})$ will give

$$Q_2(x)(1+x^{12})(1+x^{20})=(1+x^{12}+x^{24}+x^{36})x^2(1+x^5+x^8+x^9).$$

To facilitate finding a $Q_2(x)$ that would obey the above expression we assume that $Q_2(x)$ has the form $Q_2(x)=x^2(1+x^{24})R(x)$. The equation above turns into the following equation in $R(x)$

$$x^2(1+x^{24})R(x)(1+x^{12})(1+x^{20})=(1+x^{12}+x^{24}+x^{36})x^2(1+x^5+x^8+x^9).$$

It implies

$$(1+x^{24})(1+x^{12})(1+x^{20})R(x)=(1+x^{24})(1+x^{12})(1+x^5+x^8+x^9).$$

Note, we are careful not to say that we divide across by $(1+x^{24})(1+x^{12})$ as the elements $(1+x^{24})$ and $(1+x^{12})$ are not invertible in $\mathbb{Z}[x]/(x^{48}-1)$.

Since all the powers are reduced modulo 48, the polynomial $1+x^{12}+x^{24}+x^{36}=(1+x^{24})(1+x^{12})$ is invariant under multiplication by x^{12}. Therefore we can replace $1+x^5+x^8+x^9$ with $1+x^{41}+x^{20}+x^{21}=(1+x^{20})(1+x^{21})$, since the powers in these polynomials are the same modulo 12. We may now write

$$(1+x^{24})(1+x^{12})(1+x^{20})R(x)=(1+x^{24})(1+x^{12})(1+x^{20})(1+x^{21}).$$

The polynomial $R(x)=1+x^{21}$ satisfies the equation. This gives us the solution

$$Q_2(x)=x^2(1+x^{24})(1+x^{21})=x^2+x^{23}+x^{26}+x^{47}$$

and we now have a tiling.

In the binary notation we may write this tiling as follows.

V_1 : 100101001000100101001000100101001000100101001000
V_2 : 010010100100010010100100010010100100010010100100
V_3 : 001000000000001000000010000000000010000000000000
V_4 : 000000010000000000000000100000000000010000000010000
V_5 : 000000000010000000000000001000000000001000000010
V_6 : 000000000001000000010000000000010000000000000001

What follows is an excerpt from a piece of music composed on the above tiling. We can see from this section of the score that all the instruments have been introduced and that at every beat one and no more than one instrument is playing.

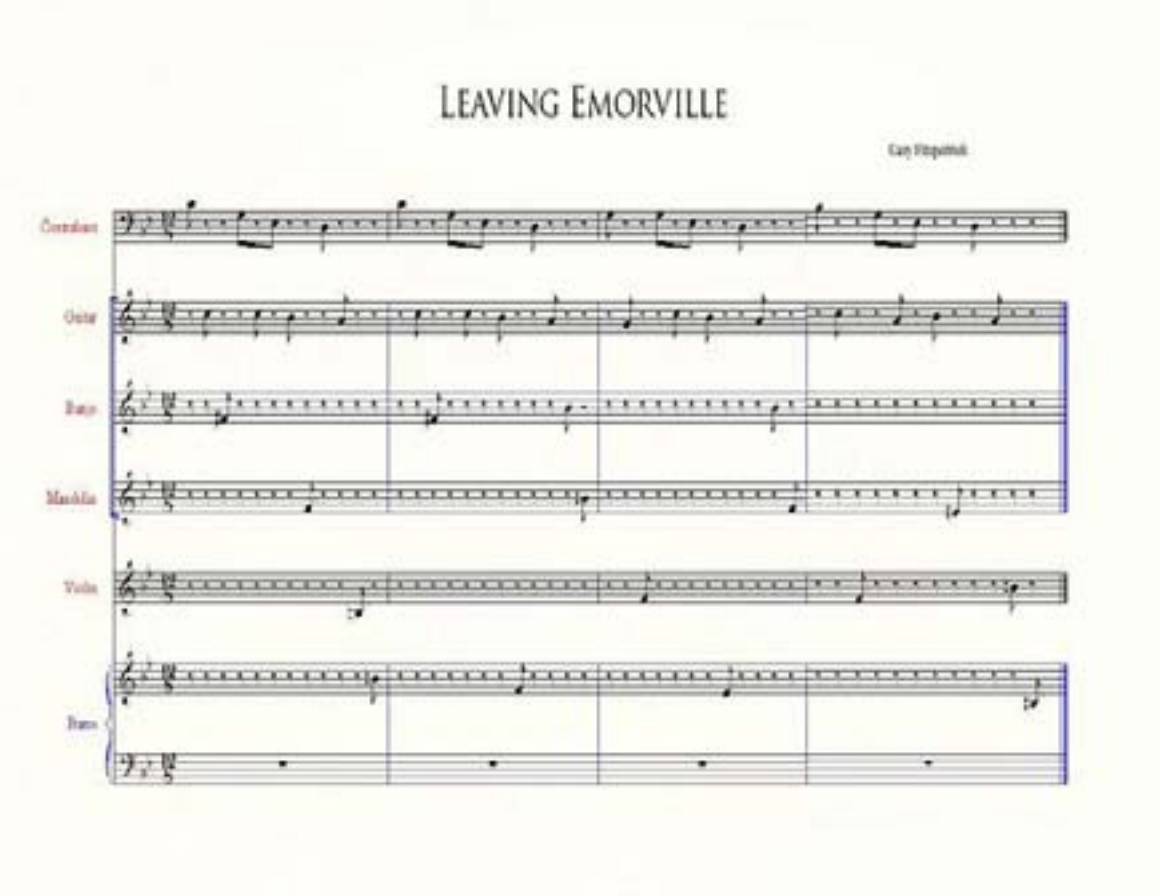

References

[1] M. Andreatta, C. Agon, E. Amiot, "Tiling problems in music composition: Theory and Implementation", *Proceedings of the ICMC, Goteborg*, pp. 156-163, (2002).

[2] E. Thul, G. Toussaint, "A comparitive phylogenetic-tree analysis of African timelines and North Indian talas ", *Proceedings of the* 11^{th} *Bridges Conference on Mathematical Connections in Art Music and Science*, pp. 187-194, (2008).

[3] G. Toussaint, "Mathematical features for recognizing preference in Sub-saharan African traditional rhythm timelines", *LNCS, Pattern Recognition and Data Mining, 3686*, pp. 18-27, (2005).

[4] Tom Johnson, Wikipedia pages on Tom Johnson, $http://en.wikipedia.org/wiki/Tom_Johnson_{(composer)}$.

[5] O. Messiaen, "Traité de rhythme, de couler, et d'ornithologie", *Editions mysicales Alphonse Leduc*, Paris, (1992).

[6] D.T. Vuza, "Supplementary sets and regular complementary unending canons", *Perspectives of New Music*, Nos. 29(2) pp. 22-49; 30(1) pp.184-207; 30(2) pp.102-125; 31(1), pp. 270-305, (1991).

Spidronised Space-Fillers

Walt van Ballegooijen
Parallelweg 18
4261 GA Wijk en Aalburg
The Netherlands
waltvanb@xs4all.nl

Paul Gailiunas
25 Hedley Terrace, Gosforth
Newcastle, NE3 1DP
England
p-gailiunas@argonet.co.uk

Dániel Erdély
31. Batthyány
1015 Budapest
Hungary
edan@spidron.hu

Abstract

Saddle polyhedra have faces that are skew polygons, with edges that do not lie in one plane. The surface of a face can be undefined [1], a minimal surface [2], triangulated [3], or filled using a spidron nest [4,5]. Identifying circuits in three dimensional periodic networks of vertices and edges [6] with saddle faces generates space-filling saddle polyhedra, described in [2]. We consider these space-fillers, and by extending the concept of a spidron so it can be applied to the faces create forms that are visually interesting, both as individual polyhedra and in aggregations.

Spidrons and Spidron Nests

A spidron was originally defined as a particular infinite set of triangles that tiles the plane, and a spidron nest as a combination of semi-spidrons that form a hexagon [4]. This idea can be extended in a fairly natural way to work with any regular polygon with an even number of sides, but there are problems if the polygon is not regular (see later for more detailed discussion).

Throughout this paper a polygon is considered, as in [1], as a closed circuit of edges, meeting at vertices. In particular a polygon is considered to be distinct from its interior. A polyhedron is considered to be a surface distinct from its interior. Only two faces of a polyhedron meet at any edge, but they can share more than one edge.

Dániel Erdély discovered that the interior of a hexagon divided into an infinite series of similar rings, each consisting of six equilateral and six 120° isosceles triangles (a spidron nest), can fold so that the hexagons become non-planar. By noticing that a cube can be dissected along a skew hexagon he was then able to construct a space-filling octahedron [7]. If the skew hexagons are simply triangulated then the polyhedron that is generated is the first stellation of the rhombic dodecahedron, which is a well-known space-filler [8]. If a minimal surface is used it corresponds to Pearce's #40, figure 8.55 in [2], which is used in his space-filling #4, illustrated in his figure 8.68.

In fact spidron nests can be folded in many different ways, since each ring can turn either clockwise or counter-clockwise. Usually the choices are made in a consistent way so that the spidronised polygon appears as a many-armed spiral in relief. However the choices are made, in a space-filling, faces that coincide must correspond, so that a clockwise ring matches a counter-clockwise ring. This has important consequences.

In order to make spidronised versions of the faces of the saddle polyhedra used by Pearce we need to consider their edges, which are usually skew polygons. As long as the skew polygon is regular (equilateral and equiangular) it is not too difficult to construct a corresponding spidron nest. In fact, within certain limits, there are two degrees of freedom, which can be thought of as the angles of one of the triangles in the dissection.

Unfortunately it is more usual to need skew polygons that are not regular, even to make a single polyhedron before the constraints of space-filling are considered. There is an obvious construction that generates visually satisfying forms, but in general the spidron nests produced cannot fold.

Start with a polygon, which may be skew. Usually it will have some rotational symmetry, so there is an obvious centre, but it may be necessary to make some more or less arbitrary decision about which point to take as the centre. Make a copy of the polygon, scale it down by some factor towards the centre and rotate it by some angle. Triangulate the region between the two polygons by joining every point on the original (outer) polygon to the images of its two neighbouring vertices. Apply the similarity transformation (scale + rotation) to the resulting surface, which, by construction, will fit inside. The transformation can be repeated indefinitely to give a series of rings that converge towards the centre. The set of images of any point lies on a logarithmic spiral.

Constructing Space-filling Polyhedra

The faces of any polyhedron can be spidronised using this construction, and because the (arbitrary) rotation around the axis can be in either direction, there are clockwise (CW) and counter-clockwise (CCW) versions of the nests. For a single polyhedron there is no restriction on how these versions are chosen, but in a space-filling, faces that meet must match. Looking from the outside of the polyhedra a CW face is matched by a CCW face. We want to choose these orientations so that the number of different spidronised polyhedra is minimised, if possible with a single spidronised form for every copy of a polyhedron in a space-filling. This is often quite difficult to achieve, and sometimes impossible.

Pearce [2] lists 42 space-filling systems using a total of 54 polyhedra with 34 different polygons as faces, but he acknowledges that this list is not exhaustive. Figure 1 shows all these faces, with the skew polygons spidronised. For each space-filling a *translational unit* can be identified that generates the complete space-filling by translations only. The translational unit consists of one or more *basic repeat units,* which are the smallest aggregations of spidronised polyhedra that fill space by themselves. Generally the numbers of polyhedra in the repeat unit are given in space-filling ratio listed in Pearce, but there are circumstances when twice as many are needed because of the requirement for equal numbers of CW and CCW versions of a face, for example in a space-filling that uses a single type of polyhedron with an odd number of faces.

The situation that can occur when (unspidronised) faces are enantiomorphic is rather less obvious. An enantiomorphic face is a three dimensional object, rather like a helix, so that right-hand, R, and left-hand, L, forms can be interchanged by reflection, but in no other way. The process of spidronisation is essentially two dimensional, and CW and CCW forms can be interchanged by a 180° flip. Since R faces must meet with R faces (and L with L) we can consider each type separately, so a polyhedron with an odd number of R faces behaves like a polyhedron with an odd number of identical faces, and the requirement for an equal number of CW and CCW versions implies an even number of different spidronised forms of the polyhedron.

Some space-filling polyhedra listed in Pearce have faces that are not enantiomorphic, having mirror symmetry, but they are two-sided, in the sense that their appearance is not conserved under a 180° flip. Such polygons can be spidronised in two ways, either with the “A” side CW, or the “B” side CW. Since in a space-filling the “A” side of a polygon must meet the “B” side of its mate, all that is needed is to use the same spidronisation throughout, and CW will always meet CCW.

All of the saddle polyhedral space-fillers in Pearce can be constructed applying these general principles, but they can have different consequences. Two examples illustrate the main points.

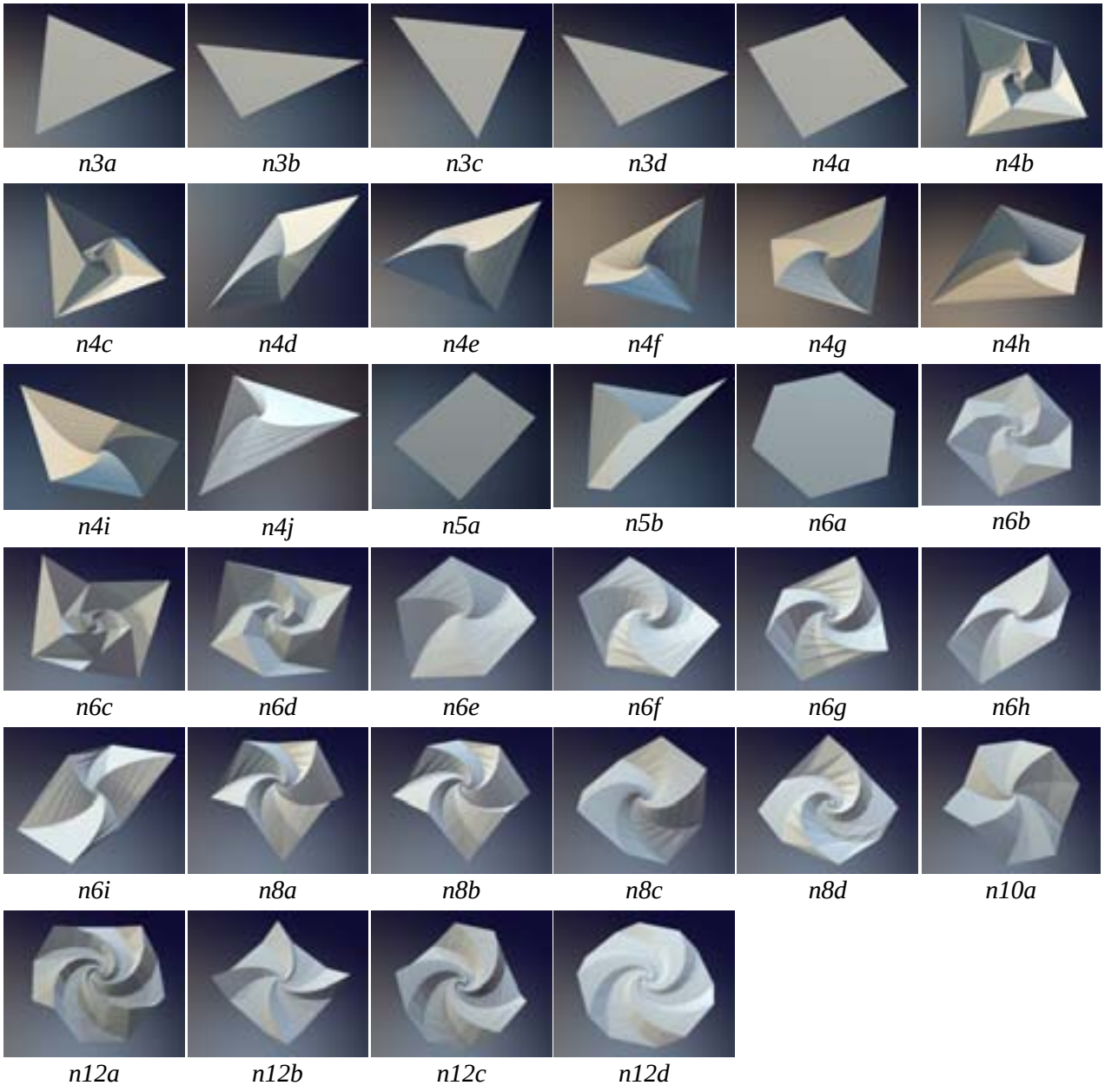

Figure 1: *Total set of 34 nests for spidronised space-filling polyhedra*

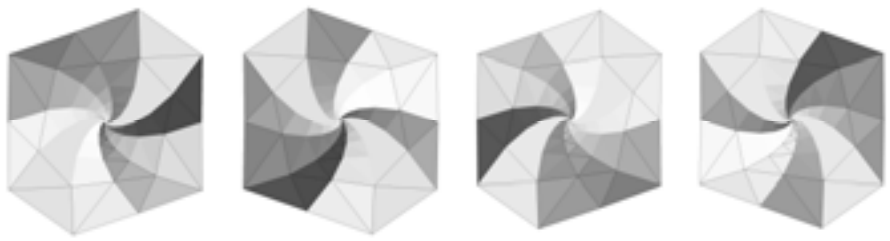

Figure 2: *Two sides and the chiral versions of the decagonal spidron-nest (n10a)*

Example 1 - The Decatrihedron (The Triamond Space-filling)

Pearce's first space filler has three skew decagonal faces, hence his name of *decatrihedron*. The decagons are circuits in the *triamond* lattice [9], hence its classification as [10, 3]. Although the decagons are equiangular, with an included angle (G-angle) of 120°, they are not regular, so the spidronised version is rather different from previously published examples (Figure 2).

The polyhedron faces come very close to each other so some care is needed in choosing the parameters (scale factor and rotation angle) to construct the spidron-nest so that intersections are avoided.

Since the polyhedron has an odd number of faces two different spidronised forms are needed, and the basic repeat unit consists of two polyhedra with four external faces (Figure 3). There are three ways to achieve this. The two external CW faces can be from the same polyhedron, or there can be one face from each. In the latter case moving between faces of the same type (CW or CCW) involves a screw rotation of 90° along a helix that can be of either sense. Of course there is further variation if we consider the two possible alternatives for the internal faces. As Figure 2 indicates the decagon is chiral, so it has two enantiomorphic forms, either of which can be used to construct the polyhedra, so the final space-filling can be of two forms.

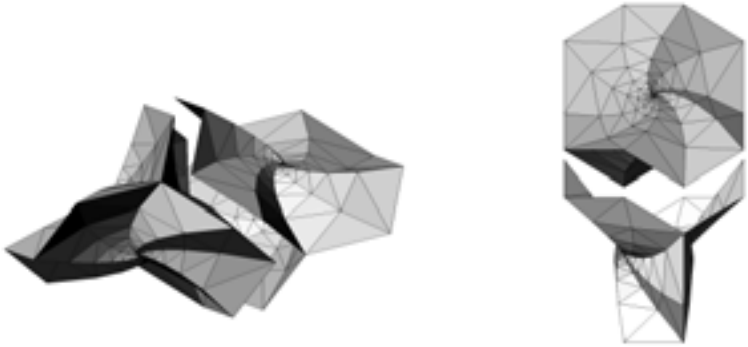

Figure 3: *Joining two spidronised decatrihedra (one of the three possibilities). Middle faces omitted.*

Example 2 - A More Complicated Example

One of the most complicated examples is Pearce's #41, which has a basic repeat unit consisting of ten polyhedra. Finding the correct orientation for each spidron-nest is far from easy. In one sense the internal faces are easier since they could be oriented randomly and the basic repeat unit would still work, but they should be chosen so that each polyhedron appears as only one spidronised form. There are 16 such internal face to face meetings. The basic repeat unit has 60 outer faces, and there are seven different directions of translation to neighbouring repeat units.

Four of the nests are of the "mirror" type with "A" and "B" sides described above. This makes things slightly easier, since the unspidronised structure determines the orientations of the spidrons.

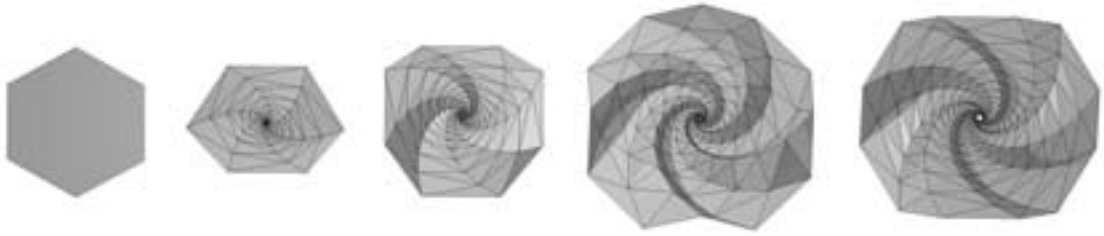

Figure 4: *The spidron nests used in making Pearce's space-filling #41.*

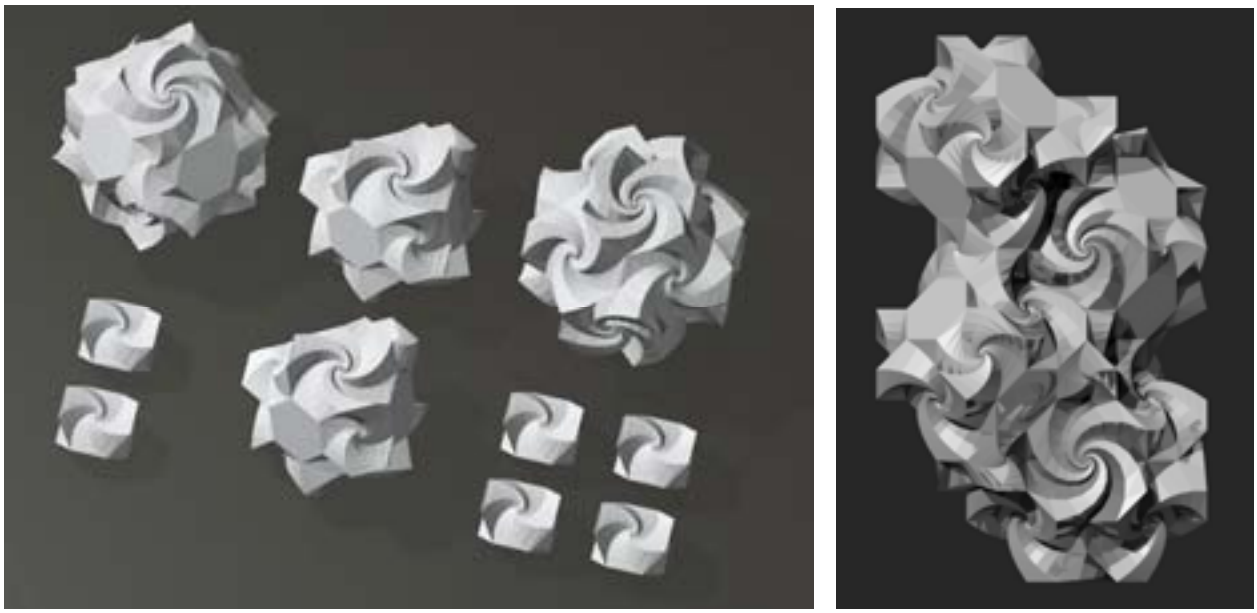

Figure 5: *The spidronised polyhedra used in a basic repeat unit of #41, and the assembled unit*

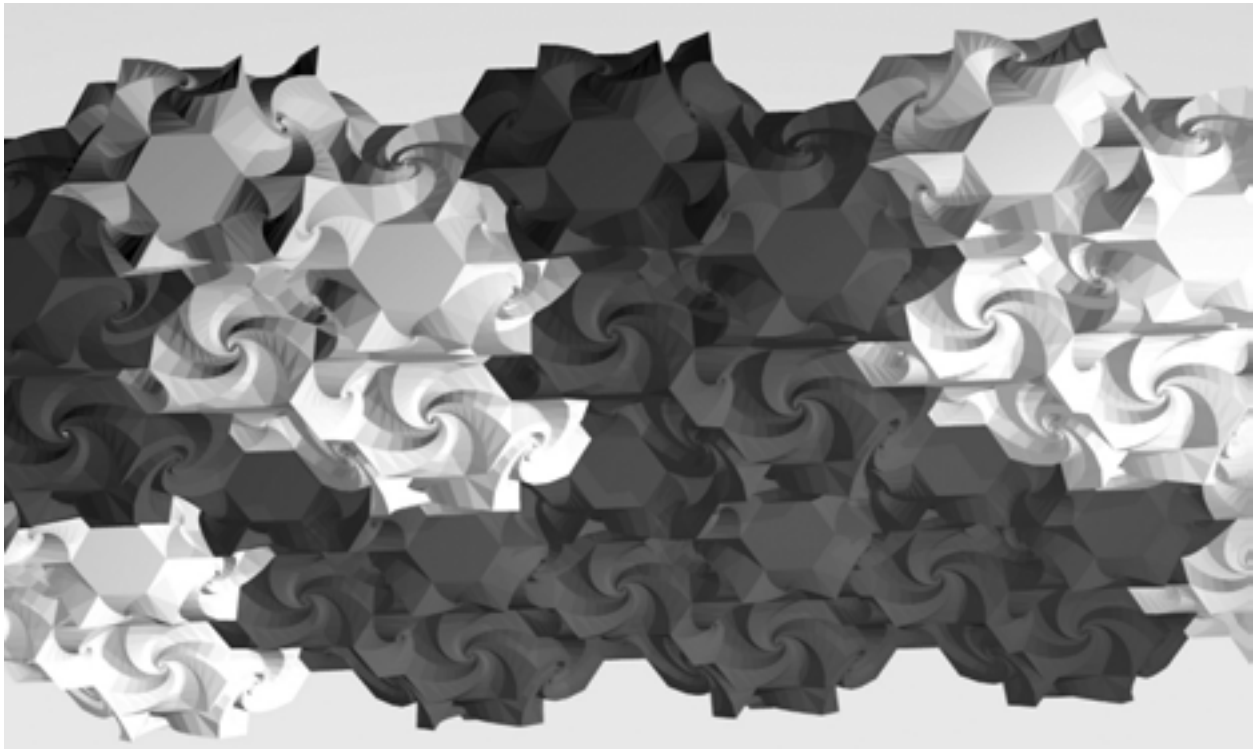

Figure 6: *A piece of Pearce's space-filling #41, coloured to show the basic repeat units*

Tables

The following tables summarise all 34 nests and 42 space-fillings described by Pearce, and provide details of spidronised versions. There are two errors in Pearce's space filling ratios which have been corrected *(marked with *)*.

Nest code	Used in polyhedra	Used in spacefillers	Polygon	Group	Symmetry	G-angles	Zome Code
n3a	52 cubocta	36	3-gon	flat	3-fold	3x60	GGG
n3b	02 09 26	24 29 32	3-gon	flat	no symm	90;54.7;35.3	BG2Y
n3c	04 07 09	08 13 32	3-gon	flat	mirror	54.7;70.5;54.7	YYB
n3d	10	32	3-gon	flat	mirror	45;90;45	BBG
n4a	30 33 34 cubocta	17 20 21 36 37 38	4-gon	flat	4-fold	4x90	BBBB
n4b	12 35 36	03 15 19	4-gon	regular	2-fold	4x70.5	YYYY
n4c	14 43	05 16 42	4-gon	regular	2-fold	4x60	GGGG
n4d	02 15 28	24 27	4-gon	enantio	2-fold	2x(45;90)	BGBG
n4e	03 13 14 26 32 44 51	16 23 26 29 37 39 42	4-gon	mirror	2-fold	2x(60;90)	GGGG
n4f	04 27	06 08	4-gon	enantio	2-fold	4x54.7	BYBY
n4g	03 05 24	18 39	4-gon	mirror	mirror	60;90;90;90	BBGG
n4h	08 20	28	4-gon	mirror	mirror	109.5;54.7;90;54.7	BBYY
n4i	07 16	09 13	4-gon	enantio	no symm	90;54.7;54.7;90	BBB2Y
n4j	09 10 23 39	32 33	4-gon	enantio	no symm	90;45;54.7;54.7	B2Y2BG
n5a	18 22	12 31	5-gon	flat	mirror	90;90;180;90;90	GBBG2B
n5b	21 22 42	30 31	5-gon	mirror	mirror	5x90	BGGB2B
n6a	19 46 53	07 14 25 41	6-gon	flat	6-fold	6x120	6xG
n6b	11 25 38 47	02 10 15 22 34 35	6-gon	regular	3-fold	6x109.5	6xY
n6c	24 43 49	05 18 20 42	6-gon	regular	3-fold	6x60	6xG
n6d	24 40	04 18	6-gon	regular	3-fold	6x90	6xB
n6e	17 30 31 52 53	17 25 36 38 41	6-gon	mirror	2-fold	2x(90;120;120)	6xG
n6f	06 25	22 34	6-gon	mirror	2-fold	6x109.5	no zome!
n6g	18 41	11 12	6-gon	mirror	mirror	6x90	2x(GGB)
n6h	19	14	6-gon	mirror	mirror	2x(90;90;120)	2x(GGY)
n6i	38	10	6-gon	mirror	mirror	2x(70.5;70.5;109.5)	6xY
n8a	32 33 49 51	20 26 37 42	8-gon	mirror	4-fold	4x(60;90)	8xG
n8b	29 35 37 47	15 35 40	8-gon	mirror	4-fold	4x(70.5;109.5)	8xY
n8c	17 46	07 17 41	8-gon	mirror	2-fold	8x120	8xG
n8d	37 45	40	8-gon	mirror	2-fold	2x(90;144.7;109.5;144.7)	2x(GGYY)
n10a	01	01	10-gon	enantio	2-fold	10x120	10xG
n12a	31 34 50 53	21 25 38 41	12-gon	mirror	4-fold	4x(90;120;120)	12xG
n12b	36 48	19	12-gon	mirror	4-fold	4x(70.5;144.7;144.7)	4x(YYG)
n12c	46 50	07 21 41	12-gon	mirror	3-fold	12x120	12xG
n12d	48	19	12-gon	mirror	3-fold	12x144.7	6x(YG)

Table 1: *The 34 nests*

Nest Code: an identifier based on the number of edges.
Used in polyhedra: referred to Pearce's table 8.1, also used in Table 2.
Used in spacefillers: referred to Pearce's table 8.2, also used in Table 2.
Polygon: taken from Pearce.
Group: there are 4 kinds of nests: flat, regular, mirror and enantiomorphic.
Symmetry: taken from Pearce.
G-angles: between adjacent edges (rounded to 1 decimal place).
Zome Code: Zometool [10] struts used to make a model. 2Y means two Yellows in the same line.

Space-filler	Polyhedra	Ratio	Nests classified per type				Symmetry	Factor SF	Outer Nests	Types	Factor Unit
			Flat	Regular	Mirror	Enanthio-morphic					
1	1	1				n10a	E	2	**4**	4	4
2	11	1		n6b			R	1	**4**	4	2
3	12	1		n4b			R	1	**4**	4	6
4	40	1		n6d			R	1	**8**	8	1
5	43	1		n6c n4c			R	1	**10**	4,6	2
6	27	1				n4f	E	2	**10**	6+4	8
7	46	1	n6a		n12c n8c		M	1	**14**	4,4,6	2
8	4	1	n3c			n4f	E	2	**4**	2,2	12
9	16	1				n4i	E	1	**4**	2+2	12
10	38	1		n6b	n6i		M	2	**10**	4,6	1
11	41	1			n6g		M	1	**8**	8	1
12	18	1	n5a		n6g		M	1	**4**	2,2	4
13	7	1	n3c			n4i	E	2	**4**	0,2+2	4
14	19	1	n6a		n6h		M	2	**6**	0,6	2
15	47 35	1 3		n4b n6b	n8b		M	1	**26**	12,8,6	1
16	13 14	1 2 *		n4c	n4e		M	1	**8**	4,4	1
17	30 17	1 2 *	n4a		n6e n8c		M	1	**10**	2,6,2	1
18	5 24	1 1		n6c n6d	n4g		M	2	**10**	8,2,0	1
19	48 36	1 3		n4b	n12b n12d		M	1	**26**	12,6,8	1
20	49 33	1 3	n4a	n6c	n8a		M	1	**26**	12,8,6	1
21	50 34	1 3	n4a		n12a n12c		M	1	**26**	12,6,8	1
22	6 25	1 1		n6b	n6f		M	1	**6**	2,4	2
23	13 44	3 1			n4e		M	1	**18**	18	1
24	15 2	1 4	n3b			n4d	E	1	**8**	8,0	6
25	53 31	1 3	n6a		n6e n12a		M	1	**38**	8,24,6	1
26	51 32	1 3			n4e n8a		M	1	**30**	18,12 or 24,6	1
27	28 15	2 3				n4d	E	1	**14**	8+6	2
28	8 20	4 3			n4h		M	1	**12**	6+6	4
29	13 26	1 4	n3b		n4e		M	1	**14**	10,4	6
30	21 42	2 1			n5b		M	1	**12**	6+6	1
31	21 22	1 2	n5a		n5b		M	1	**8**	2,6	1
32	9 10	2 1	n3b n3c n3d			n4j	E	1	**6**	2,0,2,2	12
33	23 39	3 2				n4j	E	1	**14**	8+6	4
34	6 25 11	1 1 2		n6b	n6f		M	1	**10**	6,4	2
35	47 29 11	1 1 2		n6b	n8b		M	1	**22**	12,10	1
36	52 30 cubocta	1 3 1	n3a n4a		n6e		M	1	**38**	14,6,18	1
37	33 32 13	1 1 1	n4a		n4e n8a		M	1	**12**	4,6,2	1
38	31 34 30	1 1 1	n4a		n6e n12a		M	1	**14**	6,6,2	1
39	13 5 3	3 8 12			n4e n4g		M	1	**24**	0,24	1
40	29 37 45	1 3 1			n8b n8d		M	1	**24**	6,18	1
41	53 46 50 17	1 2 1 6	n6a		n6e n8c n12a n12c		M	1	**60**	12,14,10,10,14	1
42	49 51 43 14	1 1 2 6		n4c n6c	n4e n8a		M	1	**46**	12,12,12,10	1

Table 2: *The Space-fillers*

Space-filler: an identifier, taken from Pearce table 8.2.

Polyhedra: as in Table 1.

Ratio: space-filling ratio as in Pearce.

Nests: classified by type.

Symmetry: minimal symmetry, where E is **"**smaller**"** or lower symmetry than M, so E < M < R < F.

Factor SF: multiplication needed to match nests.

Outer Nests: number of outer faces in the spidronised repeat unit.

Types: numbers of each kind of nest (in corresponding order). A + sign means there are chiral versions.

Factor Unit: multiplication needed to create a translational unit.

Further Work

The similarity transformation method has been used to construct the faces of almost all of the polyhedra considered. This is satisfactory so long as computer images, or models produced by rapid prototyping are adequate, but it would be more convenient, and cheaper, to be able to make the faces from single sheets of material. This means that the faces need to fold, and the behaviour of spidrons as foldable linkages, apart from the regular examples, is at present poorly understood. We do not even know very much about the way regular spidrons behave when folded in non-symmetric ways. Much remains to be discovered.

In order to make progress through a large number of examples we have proceeded by trying to find the smallest aggregation of spidronised polyhedra that will fill space on its own periodically. A different approach would be to start from particular spidronised forms of known space-filling polyhedra, and determine whether they will fill space, and how.

More detail about the 3D structure of edges and their projections will be shown on the a special CD that will be made available during Bridges 2009. It will also contain further Excel tables and coloured pictures and animations of all the spidronised space-fillings.

References

[1] Grünbaum B. *Polyhedra with Hollow Faces*, Proc. NATO-ASI Conference on Polytopes: Abstract, Convex and Computational, Toronto, 1993. pp. 43–70.

[2] Pearce, P. *Structure in Nature is a Strategy for Design*, The MIT Press, 1978.

[3] Gailiunas, P. *Some unusual space-filling solids*, The Mathematical Gazette, 88**,** 512, July 2004, pp. 230–241.

[4] Erdély, D. *Some Surprising New Properties of the Spidrons*, Renaissance Banff, Bridges Proceedings 2005, pp, 179–186.

[5] http://www.spidron.hu

[6] Wells, A.F. *The Third Dimension in Chemistry*, OUP, 1956.

[7] Erdély, D. *Spidron System: A Flexible Space-Filling Structure*, POLYHEDRA; Symmetry, Culture and Science, volume 11. Numbers 1–4, 2000, pp. 307–316, published in 2004, Symmetry Foundation.

[8] Holden, A. *Shapes, space and symmetry*, Dover, 1991, p.165.

[9] Conway, J.H, Burgiel, H, Goodman-Strauss, C. *The Symmetries of Things*, A.K. Peters, 2008, pp. 351–352.

[10] http:/www.zometool.com

Spirograph Patterns and Circular Representations of Rhythm: Exploring Number Theory Concepts Through Visual, Tangible and Audible Representations

Susan Gerofsky[1], Francisco Gomez[2], David Rappaport[3], Godfried Toussaint[4]
[1]University of British Columbia, Vancouver BC susan.gerofsky@ubc.ca
[2]Polytechnique University of Madrid, Madrid, Spain, fmartin@eui.upm.es
[3]Queen's University, Kingston ON daver@cs.queensu.ca
[4]McGill University, Montréal, PQ godfried@cs.mcgill.ca

Abstract

This paper offers connections between representations in a number of multisensory modes – visual, tactile and audible/musical – that explore a single underlying conceptual structure of periodicity and factorization. A number line is explored in visual, musical and tactile modes with regard to the relationship between regular periodic rhythms; then spirographic geometric patterns and the visual and musical patterns produced by the use of circular representations of musical rhythms are used to develop initial intuitions and observations. Throughout the process, the concept of conceptually-related multiple (multisensory, multimodal) representations is invoked as a way for mathematics learners to feel, hear and see mathematical concepts in depth.

Introduction

Mathematics has special status in terms of theories of embodied knowing because it seems to be the most abstract and conceptual of all fields, ostensibly having little necessary connection to physical experience – or at least, it has come to be considered so in modern times. Historically, mathematics originated with the need to solve very specific, practical problems [9], using a mode of thought essentially visual and kinesthetic. This approach predominated in mathematics until the Enlightenment, when abstraction, conceptualization and formal notation gradually displaced sensory approaches to mathematical reasoning and teaching. By the end of 19th century, mathematics had become highly formal and abstract, and this change of mentality has affected the way mathematics is taught at all levels. We may consider the Bourbaki group as being the greatest representative of abstraction and formalization in mathematics (see [1] and the references therein). While their idea of introducing utmost rigour in the mathematical practice is generally accepted, there has been criticism regarding its introduction at the early levels of mathematical education. Common criticisms to Bourbaki approach are its disregard of discrete aspects of mathematics (algorithms, combinatorial characterizations), its lack of emphasis on logic, and excessive emphasis on exact problem-solving versus exploratory, intuitive heuristics [23].

However, recent work in cognitive science and mathematics education has begun to show that mathematics, far from being disembodied and wholly cerebral, has both roots and expression in bodily knowing [2, 7, 8, 10, 14, 15, 16, 17, 18, 19, 20, 21, 22, 29]. Mathematics education is at the intersection of embodiment and abstraction, physicality and symbolization, where systems of abstract conceptualization are in the process of development. Multisensory, multimodal explorations and the use of physical objects as material anchors and 'tools for thinking' give insight into the details of this cognitive development [11]. Explorations of multimodal possibilities for the embodiment of abstract mathematical structures offer the basis for innovations in the teaching and learning of mathematics. The mathematical explorations introduced below would be appropriate for students learning basic concepts related to fractions, divisibility and factorization; these explorations could be adapted to suit learners and fit curriculum from Grade 5 (age 10) to Grade 10 (age 15) in North American school systems (and the equivalent elsewhere).

Exploring periodicity with rhythms on a number line

Imagine a number line on a long sheet of paper, with numbers starting from zero, increasing in unit increments. If we were interested in exploring the relationship of any two or more numbers, we could use the number line as a way of representing the multiples of those numbers and their relationship to one another, visually, sonically and kinesthetically. For example, if we wanted to explore the relationship between the numbers 3 and 4, we could mark the multiples of 3 on the number line with one symbol or colour, and the multiples of 4 with another one.

Counting up three at a time, we would obtain the numbers 3, 6, 9, 12, 15, 18, 21, 24, 27, 30, 33, 36,…; counting four at a time, we would get 4, 8, 12, 16, 20, 24, 28, 32, 36,… . Now imagine a group of three students working with this marked-up number line as if it were a musical score. One student might play the role of time-keeper or metronome, and count aloud steadily ("one, two, three, four,…) while tapping successive numbers on the number line. The second student could clap hands (or alternatively stamp a foot or make a sound on a musical instrument) whenever the timekeeper reached a multiple of three. The third student could do the same every whenever the timekeeper reached a multiple of four. If we represent the second student's clap as **S** and the third student's clap as **T**, the resulting sound pattern up to the number 24 could be represented as follows:

S1	***1***	***2***	***3***	***4***	***5***	***6***	***7***	***8***	***9***	***10***	***11***	***12***
S2			**S**			**S**			**S**			**S**
S3				**T**				**T**				**T**
S1	**13**	**14**	**15**	**16**	**17**	**18**	**19**	**20**	**21**	**22**	**23**	**24**
S2			**S**			**S**			**S**			**S**
S3				**T**				**T**				**T**

Figure 1: *Charting the relationship between a 3- and a 4- rhythm through two periods.*

A pattern begins to emerge. First of all, the second student (counting by threes) and the third student (counting by fours) clap together on the numbers twelve, twenty-four, and continuing the pattern, every multiple of twelve. I would argue that this gives a compelling, embodied demonstration of part of the concept of LCM (Least Common Multiple). Students can feel and hear the necessity of 3 and 4 coinciding at 12. Rather than learning a rule that is applied without sense-making ("if the two numbers are relatively prime, multiply them together to find the LCM"), students would have visual, tactile and auditory sensory representations that demonstrate the least common multiple of two numbers. (Note that Klöwer [4] suggests a similar exercise for a slightly different purpose; Klöwer suggests that percussion students learn rhythmic independence experientially by simultaneously clapping one rhythm with hands and stamping another with feet.)

What is more, it is not only the LCM that is demonstrated, but also the periodically recurring patterns that relate the multiplicative patterns of these two numbers. Going back to the figure, students can start to notice that at the beginning, the third student claps one beat later than the second student (since four is one higher than three). At the next iteration, Student 3 claps *two* beats later than Student 2,

and at the following iteration, S3 claps *three* beats later than S2 – at which point the two students' claps coincide, because three beats after one of S2's claps comes the next of S2's claps.

The same pattern repeats over the next twelve beats, from numbers 13 to 24 (or *1* mod *12* to *0* mod *12*) and it can be seen, heard and felt that the pattern will continue its periodic repetition indefinitely. Students can begin to feel, hear and make claims of a more profound *understanding* of the multiplicative relationship between 3 and 4.

Adding a tactile element: rolling a polygonal "wheel" to explore rhythms

A related additional tactile/kinetic representation of the periodicity of 3 and 4 can be made using the same number line. Say the original number line is marked with hatch marks 5 cm apart. Groups of students could be instructed to cut out an equilateral triangle and a square, each with base 5cm, using compass and straightedge constructions and heavy cardboard. The vertices of the triangle and the square could be numbered sequentially counterclockwise (from one to three or four), with the highest-numbered vertex marked in a distinctive colour. If the number line is laid flat on a tabletop or the floor, students can then "roll" the triangle and square simultaneously or sequentially, clockwise along the number line, with vertices hitting the number line on the numbered hatch marks. The effect would be like rolling a square and a triangular wheel along a numbered path. The highest-numbered vertex (3 or 4) will hit the number line at exactly the same spots that have been marked for clapping – that is, the multiples of 3 and 4. (Note that a similar effect, and one that is easier to roll, could be achieved by constructing circles of circumference equal to the distance of 3 or 4 hatchmarks respectively, but that this would have the effect of losing the visual emphasis on 'three' and 'four' that is so obvious when working with the triangle and square – and the construction of circles with precise circumferences is not trivial.)

Students can use tactile, kinetic materials that they produce themselves to demonstrate the logic of periodic multiplicative patterns of 3 and 4, including their LCM. Patterns with numbers other than 3 and 4 can be explored using other regular polygonal "wheels" (pentagons, hexagons, etc.). Note that if a heptagon were desired, then methods other than classic straightedge-and-compass would have to be used – see < http://mathworld.wolfram.com/Heptagon.html> for a reference to knotting methods for this construction.

Exploring the rhythms of related spirographic patterns

Yet another visual/tactile representation of the periodic relationship between two numbers is offered by the toy originally called the Spirograph (and now produced as a dollar-store toy). (A "spirograph algorithm" and the use of spirograph equations and graphics to solve higher-degree polynomials are illustrated at < http://documents.wolfram.com/mathematica/Demos/Notebooks/Spirograph.html>).

A spirograph is a geometric drawing toy made up of plastic gears and shapes (for example, rings and oval bars), all fitted with interlocking teeth. A selected shape can be pinned or taped to a sheet of paper and one of several different-sized gears selected to be rolled along the inside or outside of the shape. A pen point slotted into a hole near the edge of the moving gear traces out a curve on the paper.

A virtual Java-based spirograph is available at: <http://wordsmith.org/anu/java/spirograph.html>, and the reader may wish to visit this site to help visualize the scenarios described in the following paragraphs. A related interactive rhythm/drumming site at <http://www.philtulga.com/unifix.html> may also be of interest here.

Consider just the case of a hollow ring with a smaller gear traveling around its interior as an example. (Other configurations of the spirograph produce similar results in the terms discussed here.) The number of teeth on the inside of the ring and the number of teeth on the smaller gear determine the geometric pattern made by the moving pen.

For example, to take a simple case, imagine a hollow ring with twelve gear slots numbered one to twelve like a clock, and a smaller gear with four teeth. If the tip of a pen is placed in a slot near the edge

of the gear as it is rolled along the gear slots on the inside of the hollow ring, starting at 12, it will trace a vertex at each of 4, 8 and 12; the next place the pen will "hit" will be at 12 again, and the pattern will repeat. No matter how many iterations are carried out, and no matter what the offset of the pen placement on the gear, the pattern will have the same three vertices, since 4 is a factor of 12, and 12/4 = 3. (There are three other possible initial placements for the pen tip – at 1, 2 or 3 – which will yield congruent figures with three vertices, offset by one, two or three slots. Figure 4 shows this kind of pattern as part of a brief discussion of necklaces.)

If we continued to use the hollow ring with twelve gear slots, but selected a gear with, say, 10 teeth (a number not a factor of 12 nor relatively prime with 12, but sharing a factor of 2), the pen would trace out a figure with 12/2 = 6 vertices – one vertex each at 10, *20* mod *12* = 8, *30* mod *12* = 6, *40* mod *12* = 4, *50* mod *12* = 2, and *60* mod *12* = 0 (ie. 12). Notice that, while the small gear with 4 teeth traced all four vertices in one revolution of 2 pi radians, the small gear with 10 teeth took 5 revolutions (ie: 10 pi radians) to trace all its 6 vertices, ending up at the top of the "clock" at the zero mark (also called 12).

A small gear with a number of teeth relatively prime to 12 will trace out a figure with vertices at all 12 marks around the "clock". The number of revolutions needed to trace out all 12 vertices will vary. For example, if the small gear had 5 teeth, it would take 5 revolutions (10 pi radians) to complete all twelve vertices (at 5, 10 [end of first revolution], *15* mod *12* = 3, *20* mod *12* = 8 [end of second revolution], *25* mod *12* = 1, *30* mod *12* = 6, *35* mod *12* = 11 [end of third revolution], *40* mod *12* = 4, *45* mod *12* = 9 [end of fourth revolution], *50* mod *12* = 2, *55* mod *12* = 7, and *60* mod *12* = zero or 12 [end of fifth revolution]). Similarly, a small gear with 7 teeth would take seven revolutions to complete all 12 vertices, and one with 11 teeth would take eleven revolutions to complete all 12 vertices. (In fact, since 5 and 7 are co-prime to 12 they act as "generators"-- that is all numbers 0 .. 11 can be generated by a product of *7* mod *12*, or a product of *5* mod *12*.)

Here, in chart form, is the pattern for all the numbers of small gear teeth < 12 for a hollow ring with 12 gear slots:

# of teeth	Relative to 12	Number of vertices	Number of revolutions	Outer ring/inner ring
1	A factor	12	1 (2 pi radians)	12/1
2	A factor	6	1 (2 pi radians)	12/2 = 6/1
3	A factor	4	1 (2 pi radians)	12/3 = 4/1
4	A factor	3	1 (2 pi radians)	12/4 = 3/1
5	Relatively prime	12	5 (10 pi radians)	12/5
6	A factor	2	1 (2 pi radians)	12/6 = 2/1
7	Relatively prime	12	7 (14 pi radians)	12/7
8	Has shared factor(s)	3	2 (4 pi radians)	12/8 = 3/2
9	Has shared factor(s)	4	3 (6 pi radians)	12/9 = 4/3
10	Has shared factor(s)	6	5 (10 pi radians)	12/10 = 6/5
11	Relatively prime	12	11 (22 pi radians)	12/11

Figure 2: *Charting spirographic patterns.*

It is easy to generalize these results to any hollow ring with *M* gear slots and any smaller gear with *n* teeth (where *n* < *M*, and *n, M* are whole numbers):

> Given *M/n* in its most reduced form, the resulting figure has *M* vertices and is produced by *n* complete revolutions (or in 2*n* pi radians).

Thinking through this general result, there are three cases possible:

a) if n is a factor of M, M/n will reduce to a denominator of 1. The figure will have M/n vertices, produced by one complete revolution.
b) if n and M are relatively prime, M/n will be irreducible. The figure will have M vertices, produced by n complete revolutions.
c) if n is not a factor of M, but neither are the two numbers relatively prime, then M/n will be reducible, but the denominator will be greater than 1. The reduced form of M/n will give the number of vertices as its numerator and the number of complete revolutions necessary to complete the figure as its denominator.

Circular representation of musical rhythms

Observations about periodicity and the relative factorization of two whole numbers, (demonstrated above using a number line and periodic clapping, marking, or rolling of regular polygons, or with a spirograph, using graphic images) can also be experienced and explored using circular representations of musical rhythms.

Toussaint [25, 26, 27] has explored relationships between musical rhythms and geometry using circular representations of musical rhythms. I will borrow Toussaint's representation of rhythms here to offer a further, musical and auditory means of exploration of periodicity and factorization complementary both to linear and to visual representations of the same phenomena. (Note that although Toussaint independently invented the circular representation of rhythms, he later discovered a similar representation used by Persian scholar Safi Al Din in the year 1250 [28, 31]. A similar idea, representing the notes of a scale by a polygon, appears in a Krenek's paper [13] published in 1937, and earlier in Vincent's 1862 publication [30].)

Toussaint describes his circular representations of musical rhythms in terms of a clock with only a rapidly-sweeping second hand [27]. The clock may have any number of numbers or hatchmarks on its face, depending upon the number of beats in a measure of the musical rhythm in question. The numbers marked on the face of this imagined clock correspond to the number of gear slots in the outside hollow ring of the spirograph in our earlier example, but where the gear slots represented a physical mechanism made to produce a graphic pattern, the numbers on the musical rhythm 'clock' represent evenly-spaced rhythmic 'beats' in a musical pattern.

It is interesting that these two different kinds of 'clock charts' (the spirograph and the circular representation of musical rhythm) can use the same form to represent widely divergent phenomena which might share similar structures of pattern and periodicity. The number line referred to earlier in this paper is also homologous to these 'clock charts'; imagine choosing a number from the number line and then wrapping the number line into a loop of concentric circles, all with that circumference. The resulting circle would look very much like one of the clock diagrams used to represent musical rhythms or the patterns of the spirograph.

Let us return to the 'clapping on a timeline' example given earlier in this paper. In this example, one student marked out points on the timeline that were evenly spaced three apart, and the other student marked points space four apart, and then clapped their two rhythms to a third student's 'metronome' beat. It was found that every twelve beats, the two students would clap at the same moment, and that the 'four-beat' person would clap at first one, then two, and then three beats after the 'three-beat' person (at which point they would coincide). The pattern would repeat indefinitely with a period of twelve beats.

Converting the timeline to a rhythm circle with a circumference of 12 (marked out as a clock with twelve hatchmarks, but numbered for convenience with the '1' at the top of the clock since, by convention, music time is beaten starting with a downbeat on '1'), the four-beat and three-beat patterns would look like this:

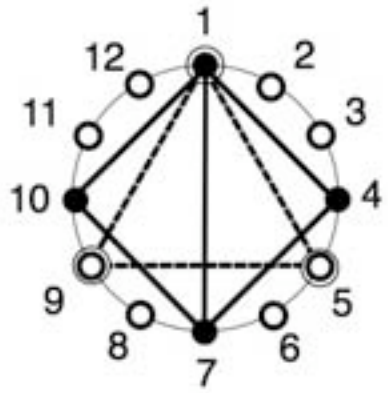

Figure 3: A 3- and 4-rhythm on a clock of 12

Note that the 'every-three-beats' rhythm lands on beats 1, 4, 7, 10, and then 1 again, yielding a square with four vertices; the 'every-four-beats' rhythm lands on beats 1, 5, 9, and then 1 again, yielding an equilateral triangle with three vertices. This effect is homologous to the pattern yielded by rolling an equilateral triangle and a square along the number line – but when the line is 'rolled up' into a circle, the triangular gear yields a square, and the square gear yields a triangle! On the number line, we used a triangle and a square with bases of equal length. Here, the square created within the circle of twelve has a base length of three units, while the equilateral triangle has a base length of four units. This allows space to contemplate the fact that 3 and 4 are complementary modulo 12.

Another interesting observation that can be made using three-beat and four-beat patterns on a circle of twelve are the possible so-called 'necklace patterns'. Toussaint describes a necklace as "the inter-onset duration interval pattern that disregards the starting point in the cycle…If a rhythm is a rotated version of another we say that both belong to the same *necklace*." [26, p. 5]

The following figures give all the possible patterns in the necklace of two-beat intervals on a rhythmic clock of six (figure (a)) and of three-beat intervals on a rhythmic clock of twelve. The figures created are rather beautiful star shapes made up of overlaid discrete regular polygons (equilateral triangles in figure (a) and squares in figure (b)).

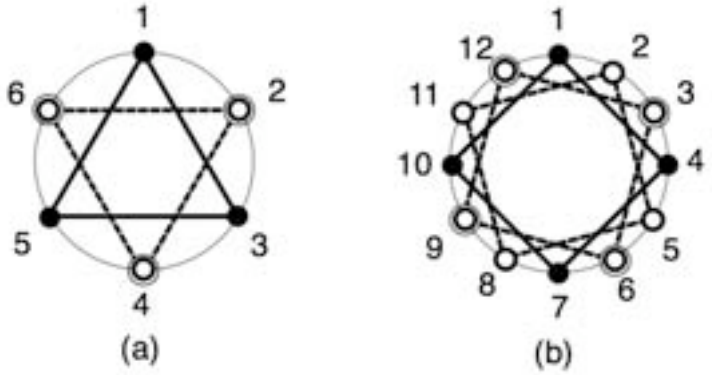

Figure 4*: Necklaces of a 3-rhythm on a clock of 6 and a 4-rhythm on a clock of 12*

It is important to note that, as these are images of rhythmic patterns, the rhythms are meant to be both sonic and visual. The visual representations of these rhythms can be treated as structurally equivalent to the *sonification* ("the use of nonspeech audio to convey information" http://www.icad.org/websiteV2.0/References/nsf.html) of the pattern. So these visual representations are meant to be sonic and kinesthetic – meant to be clapped, drummed, played on other musical instruments, stamped, even danced [3, 4, 5, 6, 29].

A different kind of star pattern can be created in sonifications of regularly-spaced rhythmic patterns. In a pattern exactly parallel to the one discussed previously with reference to the spirograph, the number of a rhythmic 'clock' may be overlaid with a regular 'beat' that is (a) a factor of the number of the clock, (b) relatively prime with regard to the clock, or (c) one which is neither relatively prime nor a factor, but which shares one or more prime factors with the number of the clock. The clock of twelve overlaid with a beat of three or four, and the clock of six overlaid with a beat of two are examples of (a), beats which are factors of the clock (since 3 and 4 are factors of 12, and 2 is a factor of 6).

Here, in contrast, is the visual representation of a beat of 3 on a clock of 7:

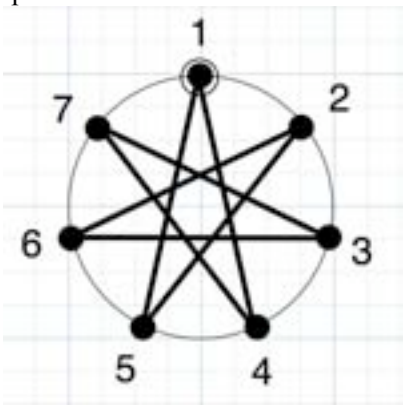

Figure 5: *A 3-rhythm on a clock of 7, forming a star polygon*

Since 3 and 7 are relatively prime, the beats fall on the clock at 1, 4, 7, *10* mod *7* = 3, *13* mod *7* = 6, *16* mod *7* = 2, *19* mod *7* = 5, *22* mod *7* = 1. The resulting figure is an aesthetically-pleasing regular star polygon with 7 vertices – a figure very much like those produced on a spirograph. As predicted by our earlier observations of the spirograph, the pattern of *M/n* with *M* = 7 and *n* = 3 yields a figure with 7 vertices that takes 3 full rotations to complete. In musical terms, this translates to a pattern that has salient beats that eventually hit all seven beats of the 7-beat bars, and repeats after every three full bars or measures.

Conclusion

The exploration above of visual, sonic and kinesthetic representations of aspects of multiplicative relationships and factorization offers a starting point for the development of innovative teaching and learning activities in mathematics education. It is hypothesized that students engaged in making multiple, multimodal representations of mathematical relationships as well as learning to make sense of equivalent structures represented in different sensory modes develops deeper understandings of those mathematical structures and patterns [24]. Here we have presented an approach to teaching concepts of periodicity and factorization that incorporates visual, tangible and audible representations.

References:

[1] Armand, B. (1998). Twenty-five years with Nicolas Bourbaki, (1949-1973). *Notices Amer. Math. Soc*. 45 (3), 373-380.

[2] Arzarello, F. (2006). Semiosis as a multimodal process. *Revista latinoamericana de investigación en matemática educativa*, Número Especial, pp. 267-299.

[3] Bamberger, J. (1991/95). *The mind behind the musical ear*. Cambridge, MA: Harvard University Press (Paperback Edition, 1995).

[4] Bamberger, J. (1996). Turning Music Theory On Its Ear: Do We Hear What We See: Do We See What We Say? *International Journal of Computers and Mathematics Education*, 1.

[5] Bamberger, J. (1998). Action Knowledge and Symbolic Knowledge: The Computer as Mediator. In D.Schon, B.Sanyal & W.Mitchell (Eds.), *High Technology and Low Income Communities*. Cambridge, MA: MIT Press.

[6] Bamberger, J. (2000a). *Developing musical intuitions: A project-based approach to making and understanding*

music. New York: Oxford University Press.
[7] Bamberger, J. (2000b). Music, math and science: Towards an integrated curriculum. *Journal for Learning Through Music*, Summer 2000, 32-35.
[8] Bamberger, J. & Disessa, A. (2003). Music as embodied mathematics: A study of a mutually informing affinity, *International Journal of Computers for Mathematical Learning* 8: 123-160.
[9] Boyer, C. B. & Merzbach, U. C. (1991). *A history of mathematics*. Hoboken, NJ: Wiley.
[10] Gerofsky, S. (2008). Gesture as diagnosis & intervention in the pedagogy of graphing: Pilot studies & next steps. In *International Group for the Psychology of Mathematics Education: Proceedings of the Joint Meeting of PME 32 and PME-NA XXX*, July 17-21, 2008, Morelia, Mexico.
[11] Hutchins, E. (2005). Material anchors for conceptual blends. *Journal of Pragmatics, 37*(10), pp. 1555-1577.
[12] Klöwer, T. (1997). *The joy of drumming: Drums and percussion instruments from around the world.* Haarlem, NL:Binkey Kok.
[13] Krenek, E. (1937). Musik und Mathematik, in *Uber neue Musik*, pp. 71–89. Vienna: Verlag der Ringbuchhandlung.
[14] Lakoff, G. & Núñez, R. (2001). *Where mathematics comes from: How the embodied mind brings mathematics into being*. New York: Basic Books.
[15] Nemirovsky, R. & Borba, M. (2003) Perceptual-motor activity and imagination in mathematics learning. In Pateman, N., Dougherty, B. & Zilliox, J. (Eds). *Proceedings of the 27Th Conference of the International Group for the Psychology of Mathematics Education held jointly with the 25th Conference of PME-NA*. Honolulu, HI: University of Hawaii.
[16] Nemirovsky, R., Noble, T., Ramos-Oliveira, D., & DiMattia, C. (2003, April). The symbolic body. Paper presented at the Annual meeting of the American Educational Research Association, Chicago.
[17] Nemirovsky, R., Tierney, C. & Wright, T. (1998). Body motion and graphing. *Cognition and Instruction*, 16(2), pp. 119-172.
[18] Núñez, R. (2000). Mathematical idea analysis: What embodied cognitive science can say about the human nature of mathematics. *Proceedings of the 24th International Conference for the Psychology of Mathematics Education*, Vol 1. 1, pp. 3–22. Hiroshima, Japan
[19] Núñez, R. (2004a). Do real numbers really move? Language, thought, and gesture: The embodied cognitive foundations of mathematics. Reprinted in R. Hersh (Ed.), *18 Unconventional Essays on the Nature of Mathematics*, pp. 160-181. New York: Springer.
[20] Núñez R. (2004b). Embodied cognition and the nature of mathematics: Language, gesture, and abstraction. In K. Forbus, D. Gentner, and T. Regier (Eds.) *Proceedings of the 26th Annual Conference of the Cognitive Science Society*, pp. 36-37. Mahwah, NJ: Erlbaum.
[21] Núñez, R., Edwards, L.D., & Matos, J.F. (1999). Embodied cognition as grounding for situatedness and context in mathematics education. *Educational Studies in Mathematics,* 39(1-3), pp. 45-65.
[22] Sellares, J. A & Toussaint, G. T. (2003). On the role of kinesthetic thinking in computational geometry. *Journal of Mathematical Education in Science and Technology*, 34(2), 219-237.
[23] Senechal, M. (1997). The continuing silence of Bourbaki— An interview with Pierre Cartier. *The Mathematical Intelligencer.* June 18.
[24] Tall, D. (2007). Developing a theory of mathematical growth. *ZDM* 39 (1-2).
[25] Toussaint, G. T. (2002). A mathematical analysis of African, Brazilian, and Cuban *clave* rhythms. *Proceedings of BRIDGES: Mathematical Connections in Art, Music and Science,* Townson University, Towson, MD, July 27-29, 2002, pp. 157-168.
[26] Toussaint, G. T. (2005a). The Euclidean algorithm generates traditional musical rhythms. *Proceedings of BRIDGES: Mathematical Connections in Art, Music, and Science*, Banff, AB, July 31 to August 3, 2005, pp. 47-56.
[27]Toussaint, G. T. (2005b). The geometry of musical rhythm. *Proceedings of the Japan Conference on Discrete and Computational Geometry,* J. Akiyama et al. (Eds.), LNCS 3742, Berlin: Springer-Verlag, pp. 198-212.
[28] Toussaint, G. T. (April 2009). Computational geometric aspects of rhythm, melody and voice-leading. *Computational geometry: Theory and applications.*
[29] Upson, R. (2002). Educational sonification exercises: Pathways for mathematics and musical achievement. In *Proceedings of the 2002 International Conference on Auditory Display*, Kyoto, Japan, July 2-5, 2002, pp. ICAD02-1 to ICAD02-6.
[30] Vincent, H. (1862). *Die Einheit in der Tonwelt*. Leipzig: Verlag von Heinrich Matthes.
[31] Wright, O. (1978). *The modal system of Arab and Persian music AD 1250-1300.* Oxford: Oxford University Press.

On Constructing a Virtual Loom

Susan McBurney
Western Springs, IL USA
E-mail: smcburne@iit.edu

Abstract

This paper explores the simulation of the weaving process on a computer with a simple graphic language. Details of some of the commands serve to illustrate general programming techniques which could be applied elsewhere. Then specific math-related designs are explored and finally, a reference is made to the history of both weaving and computer development and a connection between the two.

The weaving of textiles is nearly as old as mankind and today is found throughout the world. The process itself, as practiced on hand looms, is very slow and labor intensive.

It is interesting to wonder if this pattern-making could be simulated on a computer. The process to do so evolved in a very modular, ordered and structured manner, and it soon became evident that this could serve also as a good example of programming techniques. This paper will present the development of the process in a manner suitable to be used for teaching in a classroom or for self-study. In particular, the following topics are introduced in a logical order that lends itself to beginning programming studies.

The outcome is not intended at all to be used on a professional level or as a general-purpose program. Rather, it is the process and programming strategies that are the most important product of the paper. Ready-to-use applications can be referenced on the web [1, 2, 3].

General Outline of Method

Roughly speaking, the topics should be introduced in the following order.

1. Analysis of the problem
2. Identification of data structures
3. Basic language commands
4. Looping and subroutine implementation. This would include passing parameters, the concept of global and local variables and nesting subroutines.
5. Modular construction of the program
6. Refinements

Basic Language Commands

The LOGO programming language is a very simple language designed to be easily learned by beginners while at the same time being powerful enough for advanced use in more complex applications. It is free for downloading from multiple sites [4, 5, 6]. Additionally, there are many other versions available. Although programming books are scarce, a helpful reference can be found on Wikipedia [7] and in the program's own help menu.

The most fundamental commands are those that move the drawing point (forward, back) and those that rotate the drawing direction of the point (right, left). Other commands used here are pen up (move without drawing), pen down, set pen color, set fill color, and fill (flood an enclosed area with specified

color). Subroutines can be defined as needed and nested which facilitates a modular design which is more easily designed, debugged, and understood. Comments begin with a semi-colon and variable names within an instruction must be preceded with a colon.

Beginning the Process

Examination of a basic under-and-over weave sample such as shown in Figure 1, suggests the fundamental unit should be a square.

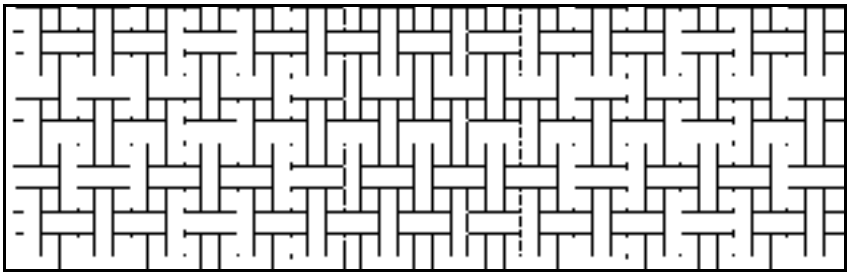

Figure 1: *Basic under-and-over weave*

Writing in the simple language called LOGO, where the basic commands are "forward", "back", "right" and "left", a subroutine named (SQ) to draw a square and fill it with color is shown below.

```
to SQ :size :color  ;Draw a Square--comments begin with semi-colons
   setpc 0              ;set pen color
   repeat 4 [forward :size   right 90]   ;repeat instructions inside [  ] Draw line, turn
   setfc :color         ;set fill color
;pu = pen up (do not draw)  pd = pen down   move inside square and fill with color
   pu   right 45  forward  2   fill   back  2  left 45   right 90   forward :size    left 90   pd
end
```

It is easy to anticipate needing to move right at each step without drawing a line, and since subroutines can be nested, it is efficient to create a **"Move Right" (MR)** and corresponding **"Move Up" (MU)** subroutine (not shown). With both of them, a negative number will indicate a move in the opposite direction.

```
to MR :amount        ;Move right without drawing
;pen up, turn right, move forward, turn left, pen down
   pu    right 90   forward :amount   left 90   pd
end
```

Finally, a pattern could be specified with two colors, one indicating the warp (vertical) thread is on top at a particular junction, and the other showing the weft (horizontal) thread is on the top. For a repeated pattern, only the fundamental portion needs to be specified. For instance, the unit in Figure 2, when repeated, results in the textile shown in Figure 3. Red indicates the *warp* thread is on top and white specifies that the *weft* thread is on top.

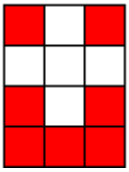

Figure 2: *Basic weave pattern*

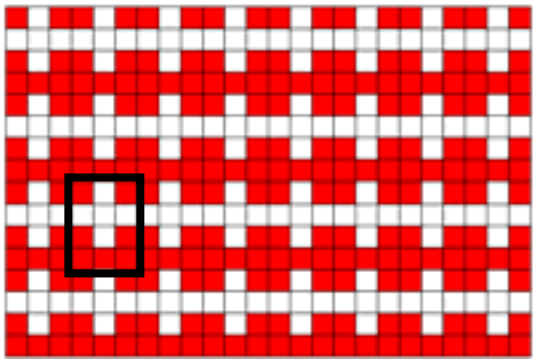

Figure 3: *Resulting textile weave*

The program that draws one row of the basic pattern is as follows:

```
to pat2 :size :number      ;size of individual squares    number of repeats of pattern
;color   4 = red   7 = white
repeat :number[ sq :size  4   sq :size  7   sq :size  4]  right 180   ; red  white  red
repeat :number[ sq :size  7   sq :size  7   sq :size  7]  right 180   ; all white
repeat :number[ sq :size  4   sq :size  7   sq :size  4]  right 180   ; red  white  red
repeat :number[ sq :size  4   sq :size  4   sq :size  4]  right 180   ; all red
end
```

The weave patterns have an attractive quality of their own, but of course in a real example the fibers are narrower and show more texture. What we need now is a variation of the SQ routine which will show both fiber width and color as in Figure 4.

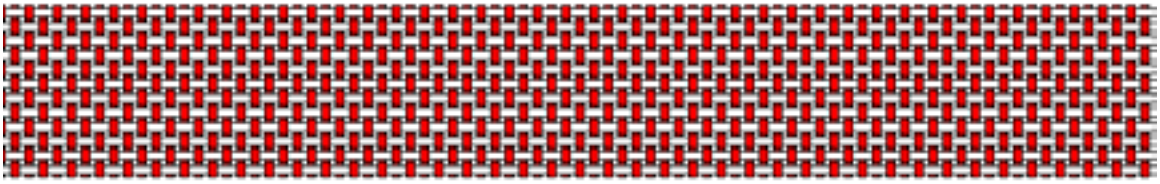

Figure 4: *Basic weave showing fiber width and color*

Again two basic routines are called repeatedly depending on whether the warp or weft thread should be on top. The procedure for the first case is to calculate the difference (d) between the width of the fiber and the size of the square, move right half that amount, draw a rectangle and move to the bottom right of the square. Then go up d/2, turn, draw the weft fiber underneath the warp and return to the bottom right of the square. See Figure 5. An analogous routine draws a square with the weft thread on top. Color fill is also added in each case (not shown). The black outline is actually not drawn.

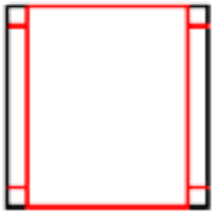

Figure 5: *Show fiber widths in square*

```
to jsq5 :a  b                          ;subroutine to draw Figure 5
;a = size of stitch square  b = width of thread
;mr = move right,  pu = pen up,  pd = pen down
;warp thread over
  mr (:a - :b)/2   forward :a   mrd :b   back :a     ; mrd moves right with the pen down
  mrd   -:a      mr :a     mr (:a - :b)/2        ; draw bottom of rectangle, move to bottom right corner
;weft thread under
  pu    forward (:a - :b)/2    left 90   pd    ; move up to begin weft and rotate 90° to left
; draw left side of weft, move under warp, continue weft
        forward (:a - :b)/2   pu     forward :b    pd    forward    (:a - :b)/2
        mrd :b   back (:a - :b)/2              ; move right with pen down and start right side of weft
  pu     back :b    pd   back (:a - :b)/2      ; go under warp, continue drawing right side of weft
  right 90    pu    back (:b + (:a - :b)/2)    ; rotate 90° to right, pen up, move to bottom right corner
end
```

Now we have the ability to "weave" patterns from a small initial diagram.

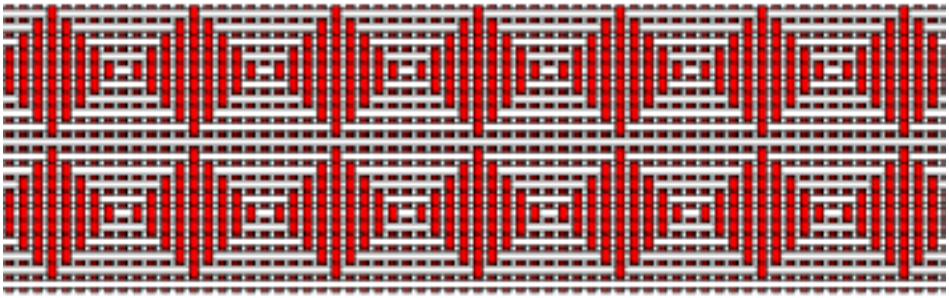

Figure 6: *Woven Diamond pattern*

We can change the orientation of the basic motif.

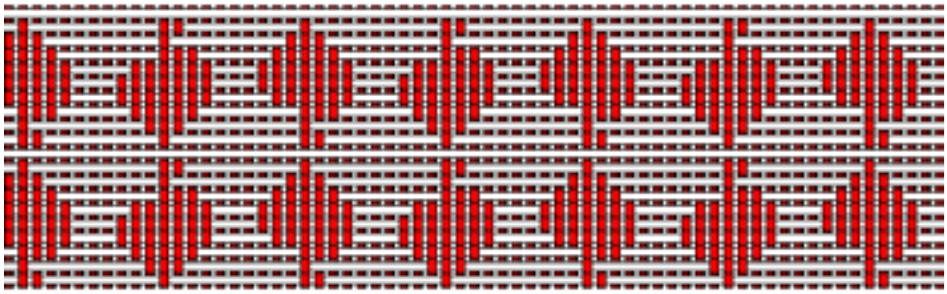

Figure 7: *Free-form object with glide reflection*

Weaving Mathematical Themes

Searching for mathematical themes to incorporate into our designs can proceed along two different tracks. First, we can look for those items which fit naturally into our binary woven structures. For instance, cellular automata and binary truth tables both have characteristics which can be easily adapted to a woven structure.

A	B	A×B
0	0	0
0	1	0
1	0	0
1	1	1

Figure 8: *Truth Table*

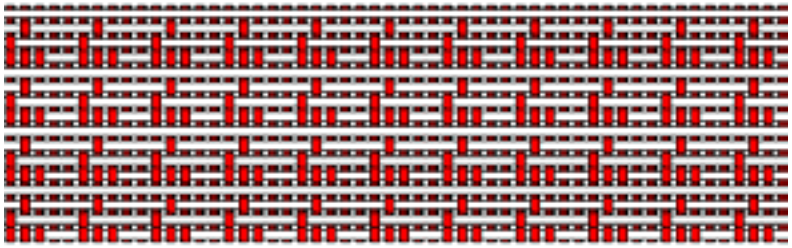

Figure 9: *Pattern woven using Figure 8*

A 9x9 cellular automata is shown in Figure 10 with two similar starting conditions, the only difference being a small hole in the center of the second one. The rule governing each state is that a square with 3, 4 or 8 red neighbors will be red in the next step. Otherwise it will be white. One of the patterns has been used in the design of Figure 11.

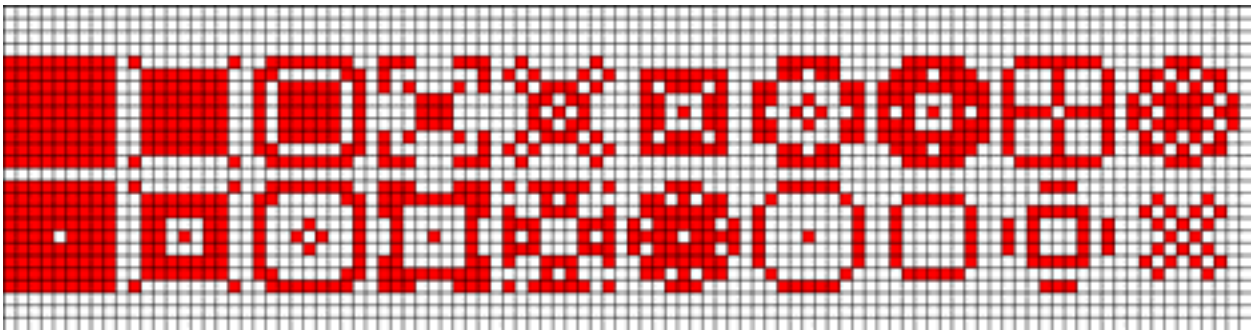

Figure 10: *A cellular Automata with two similar starting states*

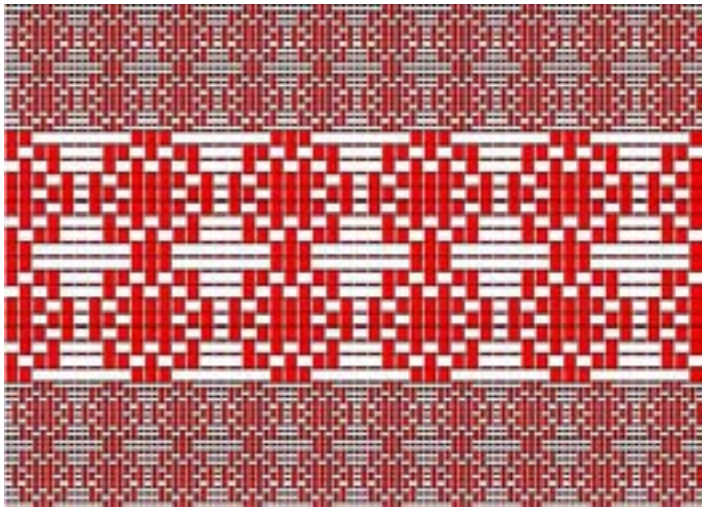

Figure 11: *Design from last state of top row in Figure 10*

Secondly, we can look at less obvious mathematical items and try to find characteristics which can be expressed on the "loom". For example, even multiples of seven appear in this pattern in Pascal's triangle [7].

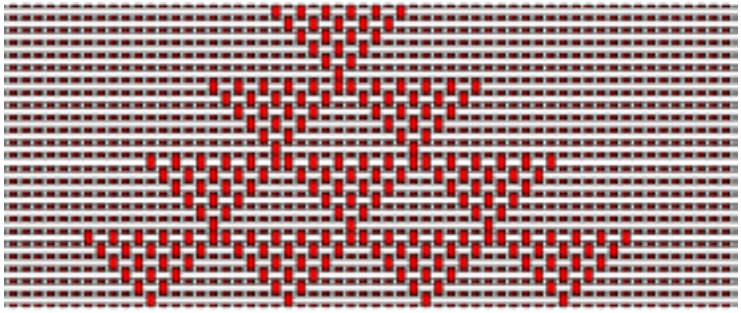

Figure 12: *Even Multiples of seven in Pascal's Triangle*

7		21		35		35		21		7
	28		56		70		56		28	
		84		126		126		84		
			210		252		210			
				462		462				
					924					

Figure 13: *Rows 8 - 13 of Pascal's Triangle (partial)*

Refinements

Additional programs come readily to mind for the development of designs. Specifically, we could use subroutines which rotate a design by 180°, allow a design to be copied and saved, allow motifs to be varied within a row, add a border, and so on. The direction of enhancement can be tailored to the specific interests and abilities of the students as well.

Historical Note

Finally, it would be remiss to not comment on the connection this theme has to computing history [8]. The mechanical Jacquard Loom (patented in 1804) revolutionized the weaving industry and the key idea behind it was the use of punched cards to control the lifting of particular warp threads at each passage of the weft. The use of punched cards was carried forward in other applications (Babbage's Analytic Engine, Hollerith's census-counting machines) and eventually appeared as input devices to early computers. Now we have used the modern computer to simulate weaving on a loom, bringing the process full circle. It seems especially appropriate to celebrate the progress made over the years by recreating the output of one of the early starting points in the computer's developmental history.

References

[1] Fiberworks PCW, www.fiberworks-pcw.com
[2] Winweave 1.1, Free downloadable software, www.softronix.com
[3] Interweave Press, Article on weaving software, www.interweave.com/weave
[4] MSW Logo (Free download), http://www.softronix.com/logo.html
[5] UCB Logo, http://www.eecs.berkeley.edu/~bh/
[6] Logo instructions, http://en.wikipedia.org/wiki/Logo_(programming_language)
[7] David Wells, *Dictionary of Curious and Interesting Geometry*, Penguin Books, 1991
[8] James Essinger, *Jacquard's Web*, Oxford University Press, 2004

ShamsehTrees: Providing Hierarchical Context for Nodes of Interest

Katayoon Etemad and Sheelagh Carpendale
Department of Computer Science
University of Calgary

Abstract

Visualizations of hierarchical data usually focus on conveying structure. However, with really large hierarchies, layouts tend to become overcrowded, making it difficult to see details about specific nodes. In contrast, ShamsehTrees focus on layouts centered on a node of interest, provide interactive nested layouts that were inspired by artistic and natural floral patterns, and make use of the natural symmetries in phyllotactic patterns. Instead of emphasizing overall tree structure, these layouts are created to make the most space available for the node of interest. The basic layout is comprised of nested circles that are centered on the node of interest. After selecting a new node of interest, the resizing and repositioning of nodes is animated as they transition to the new layout.

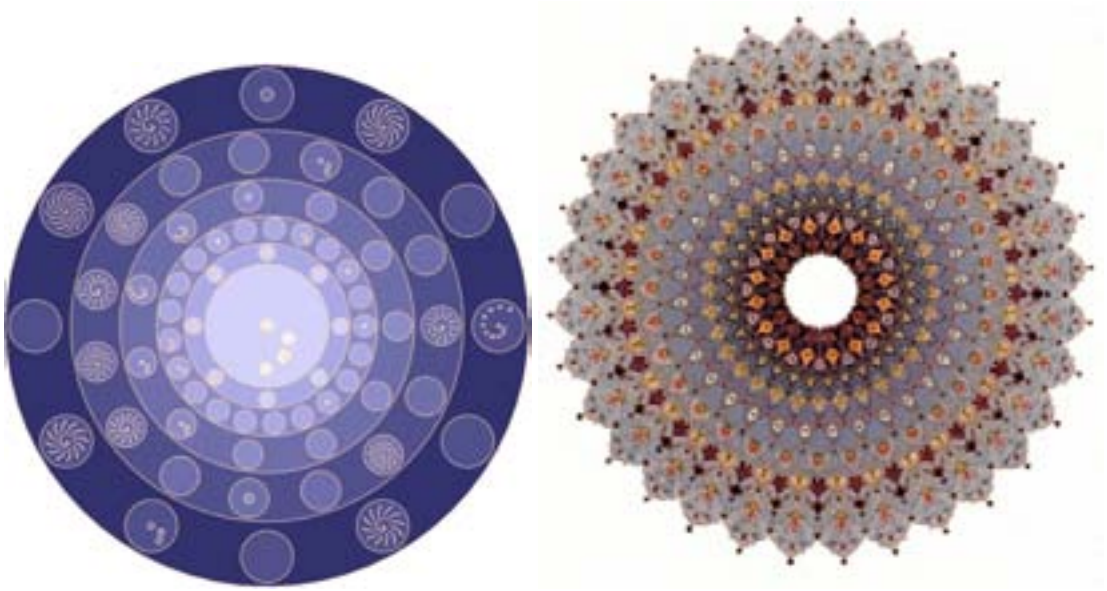

Figure 1: *Left: ShamsehTree, symmetric representation of the hierarchical context of the node of interest. Right: Traditional design of Shamseh, a circular shaped Persian Floral Pattern.*

1 Introduction

Many types of data in science, engineering and social sciences can be characterized as hierarchical. This hierarchical or tree structured data can be represented in a variety of layouts, which are usually designed to emphasize the structure and to show the relationships between parent, child, and sibling nodes. Hierarchically structured data occur sufficiently frequently that tree visualization continues to be an active research topic. However, as the data being represented becomes huge the resulting tree layouts can easily become too dense to be readable. While many tree visualizations exist (for surveys see [1, 5]) increasingly massive data sets, expanding computational power and still relatively limited display space makes this a topic of ongoing

interest. The problem of visualizing tree layouts can be more challenging when it comes to representing huge trees in a clear and aesthetically pleasing layout.

In extremely large trees, representing overall structure can make access to and discovery of individual nodes difficult due to limitation of available space. To address this, the ShamsehTree layouts presented in this paper emphasize a node of interest (NOI) by making the most space available for the chosen node and by displaying the hierarchical structure of the tree around the NOI.

Our node focused layouts are based on inspiration from Persian floral patterns and spiral arrangement of phyllotactic patterns. In Persian floral patterns plant elements have been symmetrically arranged to form a beautiful and complex concentric circular pattern (Figure 1) [3]. We also make use of the natural symmetries and spiral arrangements of phyllotactic patterns [6, 11] to develop concentric, node-focused layouts (Figure 1).

Symmetry can be an important factor for recognizing elements within an image [13]. Symmetrically arranged elements can create a strong holistic impression and may be a useful feature for grouping individual elements with the same properties. In general, symmetry is a pervasive phenomenon in both natural and constructed environments. It has long been recognized as playing an integral role in geometry and architecture [13]. Symmetry is an important factor for harmony, balance, and proportion used in nature, art, mathematics and computational sciences [7]. A symmetric representation of information is usually more aesthetically appealing, and aesthetically appealing objects have been shown to better engage and motivate viewers [7]. Symmetry can be simple when the elements of an image are repeated by translation, rotation and reflection (translational symmetry) or can be more complex and dynamic when scaled repetition is used (dilational symmetry) [3]. In dilational symmetries, suitable scale factors and appropriate arrangements of the copies (e.g. spirals) can create an aesthetically appealing and proportionally pleasing final composition. Some use of symmetry has been explored in human perception [10] and graph layout [2, 8]. However, the full potential and power of symmetry, most notably dilational, in terms of layout and interactive exploration methods, has not yet been fully explored. The potential for a positive role of dilational symmetry in information visualization is partially evidenced by PhylloTrees [9] and Botanical trees [8].

Since ShamsehTrees are intended for large real world trees, the images used for illustration in this paper are ShamsehTree views of WordNet [4]. WordNet is a human-constructed lexical database in frequent use by many Natural Language Processing (NLP) techniques. WordNet has a hierarchical structure that has been created based on the IS-A relationship. For example, a cat IS-A mammal and a mammal IS-A animal. The WordNet is a collection of English noun synsets (groups of synonyms) rooted at the word *entity* using the IS-A relation (called hyponomy). The hierarchy consists of 73,736 synsets with a maximum depth of 14. The data identifies a synset by the first word in the set, creating a hierarchy of words related by IS-A. Figure 2 shows a ShamsehTree view with the WordNet with labels in place. For the other figures in the paper, we have not displayed the labels as the discussion is about the structure of visualization of ShamsehTrees not about WordNet.

2 Representation

Our nested ShamsehTrees use a circle as the basic shape for their nodes. Although, our method can work for any convex shape, the circle has a simple but rich geometry and is frequently found in nature and art. Also, it has been suggested that circles make it easier to see groupings and structural relationships [12]. We use a nested layout to visualize parent/child relationships without direct use of lines or curves. Wang et al. [12] also describe a method for a nested tree layout where tree nodes at different levels are displayed by using 2D nested circles with variable sizes. Unlike the available nested layouts such as those presented by Wang et al. [12], in our representation we use nodes with the same size in each level which creates more symmetrical patterns (Figure 1). The inspiration for the underlying layouts comes from the symmetric structure of Persian Floral Patterns [3] especially the circular shaped known as *Shamseh* which means sun in Arabic language

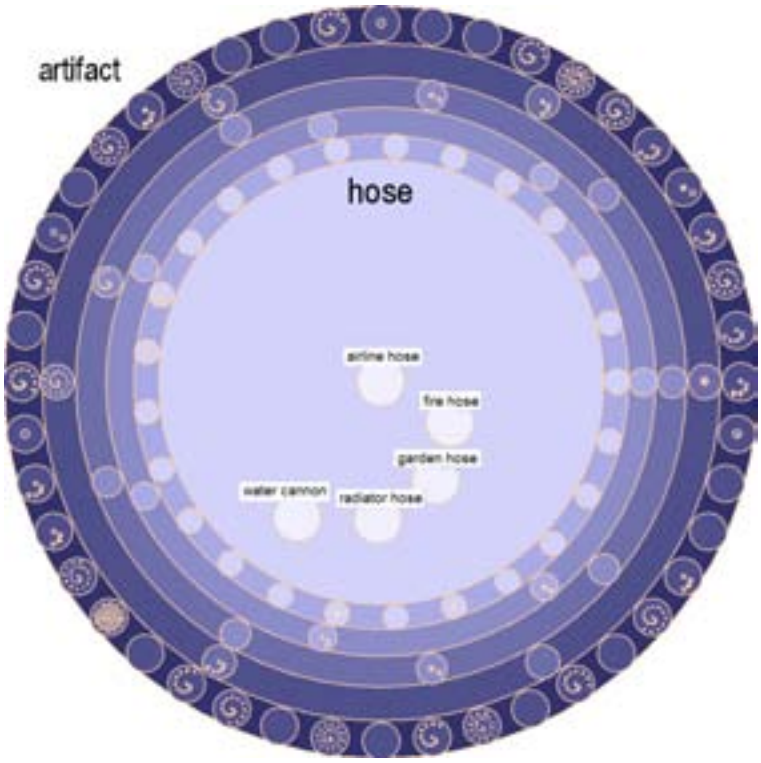

Figure 2: *The ShamsehTree view of WordNet with the NOI set at hose. The five children of the NOI are all a type of hose and a hose is a type of artifact.*

(Figure 1) and provides the name for our layout.

In our representation, if node A is inside node B then A is a child of B. ShamsehTree layout shows a subset of the tree. Figure 3 illustrates this in comparison with a more traditional, node-link, tree layout. The red circle in the node-link tree layout on the left shows the NOI (node of interest). This same node is also outlined in red in the ShamsehTree (right). In the node-link tree, children of the NOI are shown in blue lines. In the ShamsehTree the children of the NOI are nested inside the NOI, and contain the NOI's children's children. The ancestors of the NOI are shown in green lines in the node-link tree, and are shown as progressively larger circles encasing the NOI in the ShamsehTree. In addition, two levels of children are shown for each ancestor of the NOI. In ShamsehTrees the NOI is central and nested inside all of its parents and contains two levels of its children. ShamsehTrees only display two levels of children in the NOI, however, if further levels of children exist, they can be reached interactively. Our approach is an abstraction that provides both ancestor and descendant context for an NOI. This dual context abstraction enables quick exploration around NOI and ready access to the rest of the tree via the root's children while keeping the entire tree in a traceable and interactive size.

Nested layouts may address edge congestion, however, new challenges arise. For instance, one issue is how to arrange sub-nodes. If $A_1, A_2, \ldots, A_n$ are all children of B, then all these nodes must be inside of B but their arrangement needs to be organized, if possible, to enhance the clarity of visualization. Our layout is based on a node of interest (NOI), which is drawn as a circle and is nested within concentric circles that represent its ancestors. The outer most circle is the *root* of the tree. In the initial layout the node of interest would be the *root*. If the NOI has children, they are laid out inside the NOI using phyllotactic patterns. If the NOI has siblings, they are evenly spaced in the NOI's parent's ring. This is repeated until the outer ring is the tree's root. The NOI and any drawn ancestor node will display its children, and its children's children depending on how much space it has. For the NOI this creates both an ancestrally-

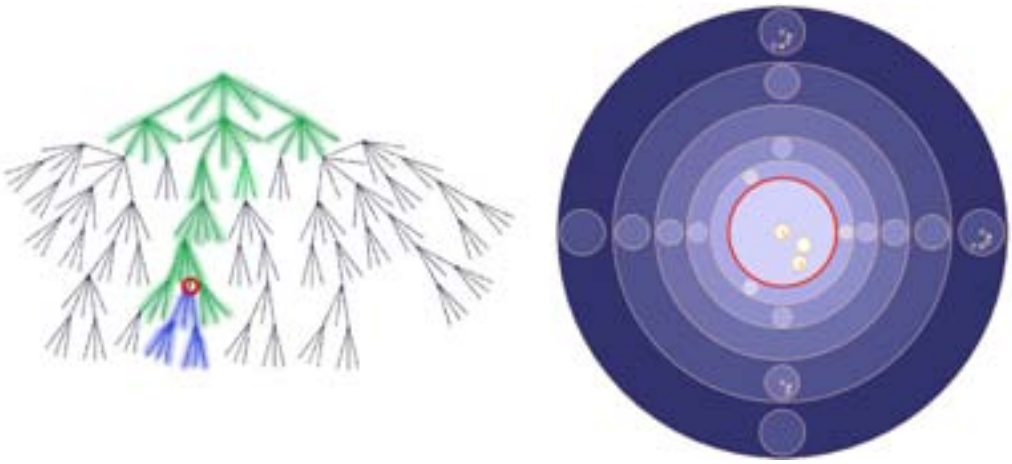

Figure 3: *Comparing the circular node focused tree layout with a traditional tree layout.*

based and a descendant-based context. For the layout of a node's children, we use spiral patterns based on basic phyllotactic arrangements. Suppose that (ϕ_n, r_n) is the polar coordinate of the center of child n for $n = 1, 2, \ldots, n_{max}$ where n_{max} is the number of children. We distribute the centers on spirals from inside out. Therefore, both ϕ and r are increasing functions in term of n. In our implementation, we use:

$$\begin{aligned} \phi_n = n\,\alpha \quad &, \quad r_n = c(n_{max})\,\sqrt{n} \\ n \quad &= \quad 1, 2, \ldots, n_{max} \end{aligned}$$

where the constant α controls the angular increment between successive nodes and $c(n)$ is used to control the radius of the spiral. Figure 4 shows how changing α affects the layout.

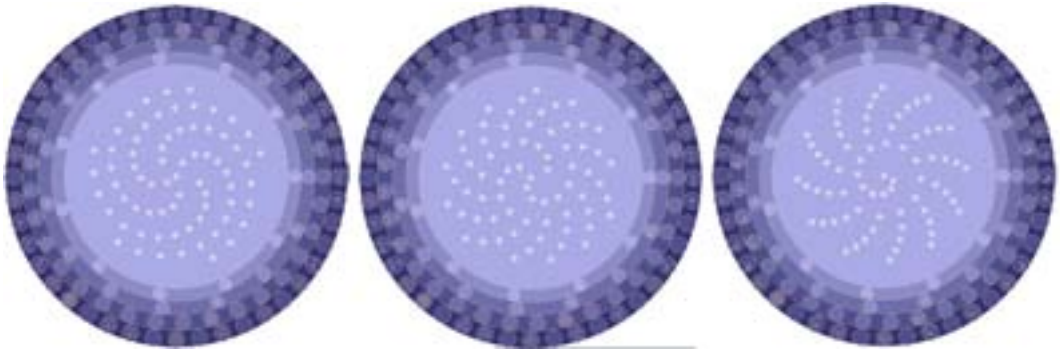

Figure 4: *Change of α creates different patterns. From left to right: $\alpha = 10, \alpha = 130, \alpha = 100$.*

The function $c(n_{max})$ controls the increment factor for the radius. To keep the symmetry of layout, maintaining all siblings as the same size, we reduce the effect of $c(n_{max})$ when there are more children. In our implementation we have used $c(n) = \frac{1}{\sqrt{n_{max}}}$ to normalize r_n in the range between 0 and 1. Therefore, changing n_{max} results in different layouts as demonstrated in Figure 5.

When a node A is selected that node becomes the NOI and moves dynamically to the center of the layout and its size is appropriately increased. Following this action, the NOI's children are recursively resized and re-positioned. Since the NOI's siblings are to be arranged within the NOIs parent node B, the size of the NOI must be slightly smaller than its parent to leave enough space for the siblings. We uniformly space the

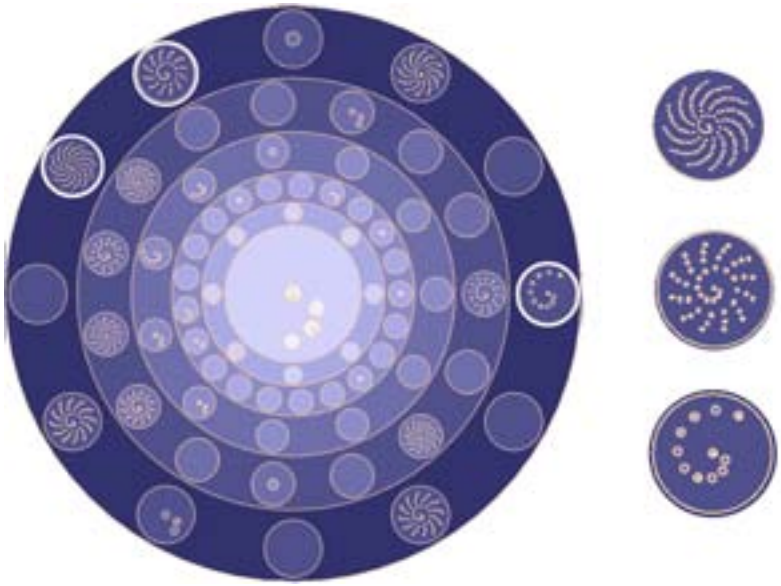

Figure 5: *The effect of n in the layout. The three nodes shown on the right have from top to bottom 156, 50, and 11 children, all of which have been laid out in the same size parent. For all three nodes α is the same. Note how in the node with 11 children only the inner part of the spiral is used.*

siblings of A in the space around A and inside B as demonstrated in Figure 5 (left side). The NOI and its siblings are displayed with the same color. To describe these operations more precisely, let (x_A, y_A) be the center of A (NOI) and r_A be its radius. The new position of the NOI can be obtained by:

$$(x_A, y_A) = (x_B, y_B).$$

And the size of the NOI is increased by:

$$r_A = d\, r_B,\ 0 \leq d \leq 1$$

where d is a constant that controls how much smaller the NOI is than its parent. As illustrated in Figure 6, larger values for d (left) provide more space for the NOI and smaller values for d (right) provide more space for ancestors and their children. However, for really deep trees large values of d do not provide enough space for the NOI. In addition, extremely small or large values for d do not produce proportional and aesthetically appealing layouts. Setting d to the values near to the golden ratio (the right layout in Figure 6) seems to make better layouts.

During the transition from one NOI to another, the NOI's siblings and their children are dynamically repositioned and resized as shown in the Figure 7. Assume $S_1, S_2, \ldots, S_k$ are siblings of NOI. As a simple solution, we distribute these nodes in a circle uniformly around the NOI and within their parent. More precisely, we use the new NOI's parent's center (x_B, y_B) as the new NOI center and to obtain the position of the sibling's centers we calculate a sibling-base circle upon which all siblings will lie. The radius of the sibling-base circle is

$$\rho = \frac{1}{2}(r_A + r_B)$$

where r_A is the NOI radius and r_B) is the NOI's parent's radius. For each sibling, we use a circle whose center is on the sibling-base circle and whose radius will keep the sibling inside the parent and outside the

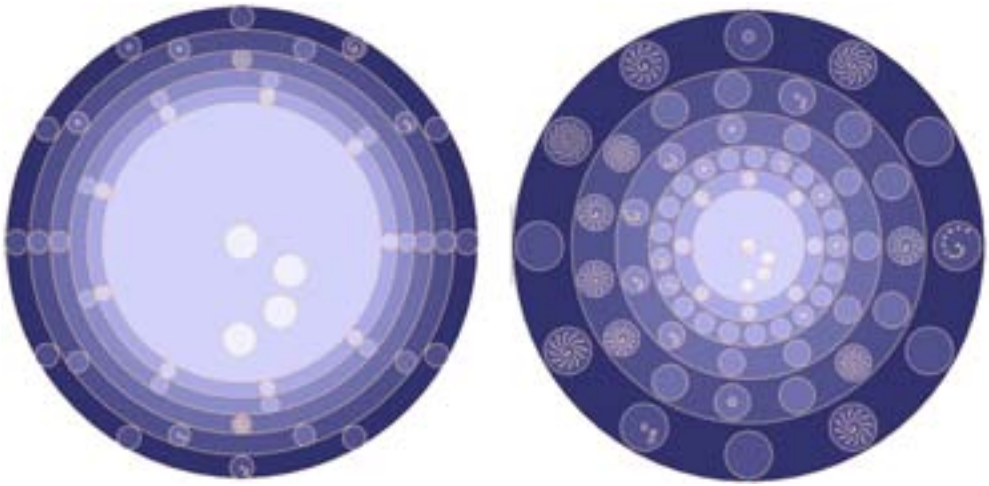

Figure 6: *Left: larger values for d gives more room for an NOI deeply nested in the tree; Right: smaller amounts for d provides more space for the ancestors and their children.*

NOI. To do this, we set the sibling-radius as

$$r_{s_k} = w\,(r_B - r_A)$$

where w is a contraction factor sufficient to keep the edges of the sibling's circle just clear of both the parent and NOI circles (see Figure 7).

Figure 7: *Left: A node is selected node to be the next NOI; Left, middle: the new NOI's children encircle the new NOI; right, middle: the NOI starts to expand; Right: the new NOI and its siblings in their new positions. To make a smooth transition for animation position and radius are functions of time*

When an NOI is selected, the sibling nodes of the selected node are clustered around the new NOI. These new positions are in a flower-petal arrangement around the NOI and as the NOI expands, the sibling nodes spread apart similar to flower petals Figure 7. Animation plays an integral role in our interactive system. All of the repositioning and resizing is done dynamically as demonstrated in Figure 7. Starting from the left, the first image shows that the fourteenth of twenty-two siblings has been selected. The second and third images show the transition in progress. The newly selected NOI is expanding, moving towards the center, and its 21 siblings have arranged themselves around its edge. In the fourth (right-hand) image the new NOI is in place, centered in its ancestors and ringed by its siblings. To effect this transition, we change the center position (x_o, y_o) and the radius r_o of node S to a new position (x_f, y_f) and final size r_f in a continuous manner. To

make a smooth transition for animation, we make position and radius functions of time t

$$(x_t, y_t) = (1-t)(x_o, y_o) + t(x_f, y_f)$$
$$r_t = (1-t)r_o + t r_f$$
$$0 \leq t \leq 1$$

Color shades are used to show the hierarchy. The selected node can be seen as a circle with its children inside it and all of its parents with their hierarchy relationships are shown as circular layers with different shades of blue. Each circle in the hierarchy includes its children which are evenly and symmetrically positioned around the circle. The presentation shows the NOI with its children and its ancestors and their children through to the root of the tree.

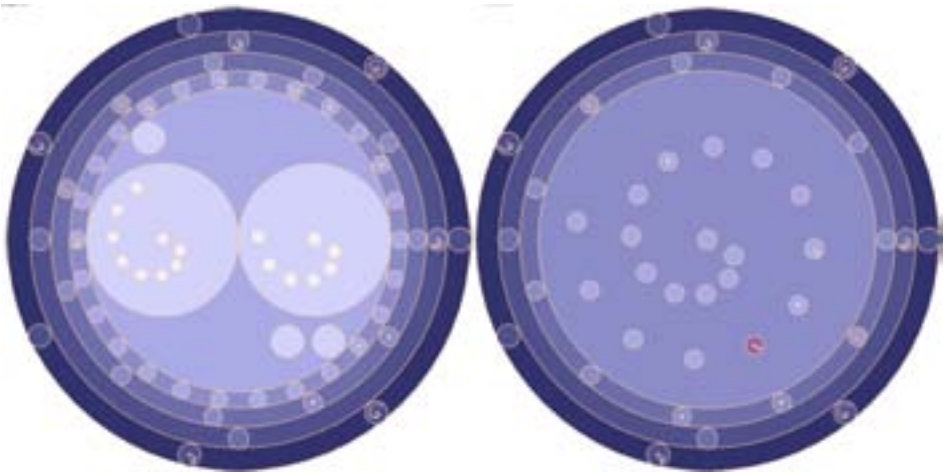

Figure 8: *Left: Comparing nodes. Right: Searching for a node with its label.*

3 Interactive Exploration

It is also possible to compare two different sibling nodes in our interactive system. The two nodes that are being compared are drawn the same size and are positioned inside their parent's node. All of their siblings are positioned around them inside their parent's node (Figure 8). While nodes can be dynamically selected node search is also supported. A search for a specific node can be conducted by entering the label of the node. The node related to the label will be highlighted using a contrasting color (Figure 8). The relation between the selected node and the root still stays visible. The tree can also be edited by adding and removing the nodes. During exploration, the tree can be modified by interactively adding and removing nodes in any desired level.

4 Conclusion and Future Work

In this paper, we introduced an interactive tree layout that makes some use of dilational symmetry and was inspired by natural and artistic floral patterns. This tree layout provides a node-focused approach that centers the node of interest and sets it in its symmetrically drawn context. Nodes of interest can be interactively changed and the transitions are animated. In a given layout the subset of the tree that contains the node of interest's ancestors and all of its immediate children. The whole tree can be explored interactively. Further

investigations into the type of interactivity provided and the effectiveness of this type of contextual layout are underway.

Acknowledgments: Thanks to iLab members' useful advice and discussions. Further thanks to Dr. Samavati for his insightful input. The funding for this research is from NSERC, iCORE, and SMART Technologies.

References

[1] G.D. Battista, P. Eades, R. Tamassia, and I.G. Tollis. *Graph Drawing: Algorithms for the Visualization of Graphs*. Prentice-Hall, 1999.

[2] P. Eades and X. Lin. Spring algorithms and symmetry. *Theoretical Computer Science*, 240(2):379–405, 2000.

[3] K. Etemad, F.F. Samavati, and P. Prusinkiewicz. Animating persian floral patterns. In *CAe'08: Proceedings of Computational Aesthetics in Graphics, Visualization, and Imaging*, pages 25–32, 2008.

[4] C. Fellbaum. *(Ed.): WordNet: An Electronic Lexical Database*. MIT Press, Cambridge, MA, USA, 1998.

[5] I. Herman, G. Melancon, and M.S. Malshall. Graph visualization and navigation in information visualization: A survey. *IEEE Transactions on Visualization and Computer Graphics*, 6(1):24–43, 2000.

[6] R.V. Jean. *Phyllotaxis: A Systematic Study in Plant Morphogenesis*. Cambridge University, Cambridge, UK, 1994.

[7] Z. Kang. From abstract painting to information visualization. *Visualization Viewpoints: IEEE Computer Graphics and Applications*, 27(3):12–16, 2007.

[8] E. Kleigerg, H. Van De Wetering, and J. Van Wijk. Botanical visualization of huge hierarchies. In *INFOVIS'01: Proceedings of the IEEE Symposium on Information Visualization*, pages 87–94, Washington, DC, USA, 2001. IEEE Computer Society.

[9] P. Neumann, S. Carpendale, and A. Agarawala. Phyllotrees: Phyllotactic patterns for tree layout. In *EUROVIS'06: Proceedings of Eurographics / IEEE VGTC Symposium on Visualization*, pages 59–66. Eurographics, 2006.

[10] J. Thorpe and P.C. Oorschot. Graphical dictionaries and the memorable space of graphical passwords. In *Proceedings of the 13th USENIX Security Symposium*, pages 10–17, Berkeley, CA, USA, 2004. USENIX Association.

[11] H. Vogel. A better way to construct the sunflower head. *Mathematical Biosciences*, 44(3-4):179–189, 1979.

[12] W. Wang, H. Wang, and G. Dai. Visualization of large hierarchical data by circle packing. In *CHI'06: Proceedings of the Conference on Human Factors in Computing Systems*, pages 517–520, New York, NY, USA, 2006. ACM.

[13] C. Ware. *Information Visualization: Perception for Design*. Morgan Kaufmann Publishers Inc., San Francisco, CA, USA, 2004.

Talking About Math/Art: The Long Pause

Bathsheba Grossman
Bathsheba Sculpture LLC
3127 Branciforte Drive
Santa Cruz, CA, USA
E-mail: b@bathsheba.com

Abstract

Thoughts on discussing mathematical art, concerning the appreciative yet tongue-tied lay viewer.

Apologia

After much thought, I've decided not to add here to the literature on the production of geometrical art. The mathematical techniques I use are neither technically difficult nor conceptually deep, and anyone who is interested will find no obstacle to reverse engineering them should that be desired, or better, developing their own directions to a greater degree. Nor do I wish to repeat an introduction to the use of 3D printing technology, which is now widely known and well documented. What concerns me here is the central transaction of art: what happens when someone not the maker, be they naive or mathematically sophisticated, sees a sculpture. I can speak of this only from personal experience and opinion, so this paper – essay, rather – must stand unsupported by citation.

Enthusiasm, Interrupted

I'll guess that everyone who has made a piece of math/art has had the experience of showing it eagerly to a layperson and hearing the response "Neat!" followed by a long silence. This is characteristic: the work is well liked almost universally, and the market for it is strong, but viewers are at sea on how to discuss it. I wish to begin exploring what happens after the "Neat!". How can we get rid of the pause, and what is it hiding?

This is not entirely a matter of personal egotism, for it seems to me that a lack of clarity about how to discuss this art form is a real obstacle to its wider spread. As we – researchers, popularizers, artists, educators – create this field, we must also create a climate for discourse, in which the viewing public can build a language and context to discuss it. Although math/art is ancient, it has never been commonplace or mainstream, and certainly has not received the mass-pop currency which the new technologies are now enabling. Thus there is little historical precedent or culture in which to evaluate these works.

Artspeak

The literature of the history, appreciation, and criticism of art must, a fortiori, be applicable to math/art. We are accustomed to hearing nonmathematical sculpture evaluated in terms of expressiveness of line, composition of mass and void, balance and variety of viewpoints, choice of color and material, and so forth. It is vital to the development of this artistic movement that viewers have permission to discuss math/art in identical language. A blobby, insensitive or misbalanced sculpture has problems whether it is

a Muse or a minimal surface, and it is not crass or uninformed to say so, regardless of the delicacy or abstruseness of any mathematical concept involved. I submit that as creators and informed mediators, we must explicitly give permission for this type of comment.

In particular, it's necessary to resist any tendency to assert that conceptual or technical considerations may override those of good taste. To do so is analogous to stating that a work can be immunized against aesthetic criticism because it carries a moral or political message, and that dog won't hunt: viewers, and still less history, cannot be constrained to evaluate a work conditionally on terms set by its author or presenter. If we don't wish to remain marginal to the wider practice of art, we must accept its criteria fully, in addition to those peculiar to this form.

Cloak of Invulnerability

In math/art, the subject matter carries an intellectual authority that is widely perceived as impeccable, to the point of being overbearing. Mathematically naive viewers, even those knowledgeable about art, tend to feel disqualified from applying ordinary artistic criteria to the work, or indeed having any reaction but awe. They perceive the entire edifice of mathematics to inhere in each piece, and are cowed. It's an odd phenomenon as art goes – no one feels bashful opining about landscapes for lack of geological or botanical knowledge, and why should they? But I believe that this is the source of most of the pause, and that it must be specifically denatured before useful commentary can occur.

This is difficult. The temptation to the creator is powerful: the impervious aura I've described is about as unfair an advantage as a piece of art can have, and it is correspondingly difficult to resist leveraging it as a potent marketing tool. What is worse, the aura becomes viewer-driven. In my own presentation I take pains to distinguish works of my authorship from those that illustrate preexisting ideas, but I find that it's very difficult to make this message stick. Although my site says otherwise, many customers believe that I invented the gyroid, and that my own works illustrate deep, complex geometrical truths. (Neither is the case.) It's understandable that buyers and presenters should prefer that the work remain unassailable, but this confusion acts strongly to stifle even the limited level of comment that is normally made to an artist about their own work – I've led an astonishingly criticism-free artistic life – let alone thoughtful discourse. Before the pause can end, the aura must be exploded.

Approaching the Divine

Should math/art then be spoken of exactly as other art? Is it merely a style – a style so constraining that in many instances the usual decisional process of art-making is subsumed almost entirely into the requirements of the form? Haiku is a free format compared to what we do when trying to create a credible, informative physical representation of a polytope of dimension >3, and also make it beautiful.

This art is not abstract in the sense of being idiolectic; obviously it refers to the shared language and experience of mathematics. Thus it is representational, an interpretive form, but one whose subjects are objects and experiences unfamiliar to most viewers. Perhaps one productive way to look at it is as a stop on the path toward mysticism, which translates ineffable experience. In speaking of mystical art, the crucial thing is that it cannot be evaluated in terms of that original experience, which is by definition inaccessible. In encouraging speech about math/art we need not go quite this far – there is some evidence that mathematicians exist – but it is necessary that we strongly resist conflation of the inspiring subject matter, which is as immune to criticism as rocks and trees, with the present object. An artwork is an evocative lump of material, a single data point in art history, and for the pause to end, we must give permission for ours to be approached on exactly those terms. And for this field to become a full part of art culture and history, the pause must end.

The Whitney Music Box

Jim Bumgardner
10066 Orcas Ave
Shadow Hills, CA, 91040, USA
E-mail: jbum@jbum.com
Website: krazydad.com

Abstract

I describe my musical realization of the motion graphics of experimental animation pioneer John Whitney. The Whitney Music Box casts John Whitney's visual idea of "incremental drift" into musical form.

About John Whitney

John Whitney (1917-1995) was an innovative filmmaker who pioneered a number of methods for producing experimental animations based on precisely defined motions. All his life, perhaps beginning with his youthful obsession with the Mount Palomar telescope, Whitney was especially interested in the mathematics of circles, including polar coodinates and sine waves. Whitney's earliest films, made with his brother James during the 1940s, used a pendulum device to produce music and graphics simultaneously.

In the 1950s, Whitney converted a surplus World War II analog computer, originally used in the sighting mechanism of an anti aircraft gun into a versatile and accurate motion control rig, the first of its kind. This "cam machine," was used by the Whitney brothers to realize a series of commercial film effects as well as more personal experimental films all featuring elaborate and fluid abstract motions. In their films, they used multiple exposures while rotating both the camera and a variety of photographed objects and light sources, all moving in complex paths, such as nested arcs. The striking spiraling figures in the Saul Bass designed opening credits of *Psycho*, were animated by Whitney on this equipment, as well as James' most successful movie, the mandala-like *Lapis*.

In the early 1960s, Whitney changed his medium from analog to digital, and began making a series of pioneering computer graphics shorts, including his 1968 film, "Permutations". Whitney continued working in the computer graphics field until his death in 1995, making the film *Arabesque* and the film series *Moon Drum*.

Whitney's films were highly geometrical in nature, often consisting of nothing more than colored points of light, moving over mathematically defined paths, such as sine waves, controlled by either electro-mechnical or digital computation. Whitney was principally interested in the cumulative effect of these motions on the viewer.

Incremental Drift. The motions of the objects in Whitney's mid to later films often were based around a type of mathematically choreographed motion Whitney called "incremental drift." Whitney described incremental drift in his 1980 book, *Digital Harmony*, in which he elaborated on his belief that the the mathematical properties of music could be applied to motion graphics on a computer.

> *An early intuition about how to control total dynamics led me to activate all graphics elements through a motion function that advances each element differentially. For example, if one element were set to move at a given rate, the next element might be moved two times that rate. Then the third would move at three times that rate and so on. Each element would move at a different rate and in a different direction within the field of action. So long as all elements obey a rule of direction and rate, and none drifts about aimlessly or randomly, then pattern configurations form and reform. This is harmonic resonance and it echoes musical harmony, stated in explicit terms. I tried this procedure in several films, and was gratified by the consistency of the confirmation it demonstrated.*
>
> – John Whitney, *Digital Harmony*, pp. 38

The Whitney Music Box

In the book, Whitney goes on to describe a few simple examples of this type of motion. The book contains sample code in the back, in the BASIC programming language. One of those examples is constructed of points moving around a series of increasingly wider concentric circlular paths.

I noticed the resemblence of the circular paths to the dots on the disc of a music box, and thought it would be interesting to use Whitney's dots to trigger a series of notes on a chromatic scale. Although this arrangement is very similar to a regular music box equipped with chromatically tuned tines, the rotational speed of the dots differs in a way that can't be produced with a single disc - rather such a music box would require a single disc or cylindar for each dot, each moving at a slightly faster speed.

Much like Whitney, I was "gratified" by the quality of the music this system generated, and even more so by the effect of listening to the music while watching the animation that triggered it [Figure 1]. What to the ear sounds like a complex piece of music becomes more lucid when the eyes are confronted with the evidence of a relatively simple and predictable system of motions triggering those sounds. The overall effect can produce a strong sense of wonderment in the listener / viewer, which I found pleasing.

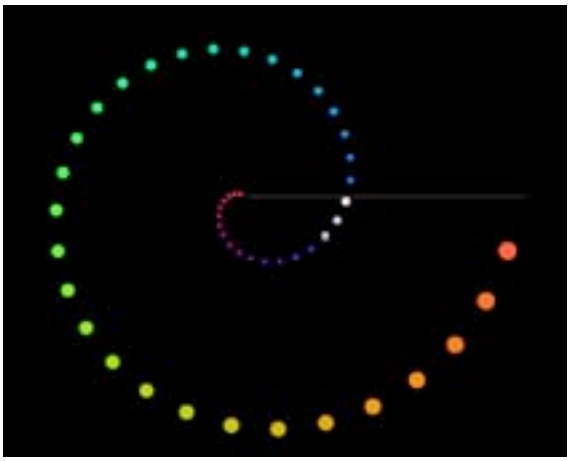

Figure 1 :
The Whitney Music Box

I went on to produce a series of variations of this basic experiment, using different numbers of dots, tunings (both chromatic, harmonic, and modal, with forward and retrograde assignments) as well as a few different methods of sound production.

A close inspection of Whitney's writings reveals that he was much more of an artist than a mathematician. The mathematics of Whitney's movies can be quite simple, based on nothing more than the simple integer ratios of Pythagoras. Like medieval music theorists, Whitney believed that the appeal of his animations, like the appeal of tonal music, was based on these simple ratios.

For the casual mathematician, and casual listener, the Whitney Music Box provides a beautiful and fascinating introduction to some elementary and beautiful mathematical ideas.

For more information about this project, including an online Flash demonstration, visit
http://www.coverpop.com/whitney/

Mathematical Experiments with African Sona Designs

Darrah Chavey
Department of Mathematics & Computer Science
Beloit College
700 College St.
Beloit, WI, 53511, USA
E-mail: chavey@beloit.edu
Web: <http://math.beloit.edu/chavey/>

Abstract

The sona designs of the Chokwe people of Angola/Congo are a particularly attractive form of "mirror curves," which can be visualized as a curve drawn through a lattice of dots, bouncing off the edges of the lattice and off "mirrors" placed between some of those dots. Most such designs are drawn as a single, uninterrupted line, and most contain symmetries of some type. The mathematics of the designs reflect issues of common divisors of numbers, Eulerian cycles, and symmetry groups. This talk will investigate ways to use a sona-drawing program to investigate these topics with students from middle school through college, with particular emphasis on the experimental discovery of mathematical facts. The sona program developed by the author is cross-platform and free.

Introduction

The Chokwe people of Angola and Congo have a drawing tradition, done both in sand drawings and on more permanent objects, that has attracted a substantial amount of mathematical attention (e.g. Ascher [1], Gerdes [4], Jablan [5]). Although their sona (singular "lusona") drawings arise in several different forms, one of the more common, and the most mathematical, can be viewed as a grid of dots with a curve passing through the grid, "bouncing" off the boundary and off internal "mirrors," to create a single continuous curve. The "Leopard with Cubs" lusona shown in figure 1 is an example of such a drawing without internal mirrors. This sand drawing includes a few features added to the fundamental design to indicate the heads and tails of the mother leopard (vertical) and her two cubs (horizontal). Figure 1 shows it in three forms: a photograph of the drawing made in the sand, a computer rendition of the drawing showing it with the heads and tails of the leopards, and a computer drawn form of the underlying Eulerian drawing, as the sona drawing program draws it, without the artistic additions to personify the animal forms the artist has seen in the principal monolineal drawing.

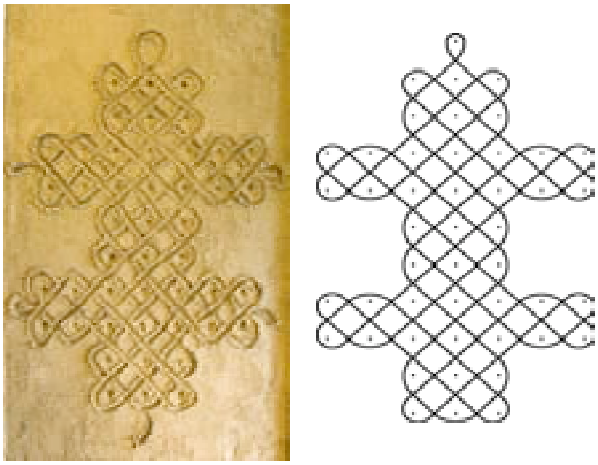

Figure 1: *The "Leopard with Cubs" lusona drawn in the sand, with additional heads and tails of the mother leopard and her two cubs. On the right is the underlying monolineal curve, as drawn by the sona program.*

The "Leopard with Cubs" is a sona example with no internal "mirror" walls for the curve to bounce off. A classic example of a sona that uses such mirrors is the "Chased Chicken" of figure 2, so called because it seems to capture the path that a chicken might take if you were trying to catch it.

Figure 2 shows both the sona as it would be drawn by a Chokwe artist, and the "hidden" walls that help to define the shape. The artist making this drawing lays down the grid of dots shown, does *not* draw the walls, but draws the Chased Chicken sona directly on the dot grid. There is some evidence that the Chokwe artist envisions the walls as they draw the sona. In many cases, the wall layouts help us to see more clearly the symmetries within the sona design. Both parts of figure 2 were drawn by the sona program.

The range of sona designs gives rise to many types of investigations, both mathematical and artistic. The use of the computer program to try different layouts of dots and walls allows a student to imitate what might be months worth of work by a Chokwe artist looking for interesting designs. A fundamental challenge is that not all grids lead to acceptable sona drawings: they may not be monolineal, or to make them monolineal may require extra walls that disrupt the symmetry or aesthetic appearance of the design. Our experience, with students from 4th grade through college, is that these experiments and open-ended design questions are enjoyed greatly by the students, many of whom continue to work on designs well after the assignments have been completed.

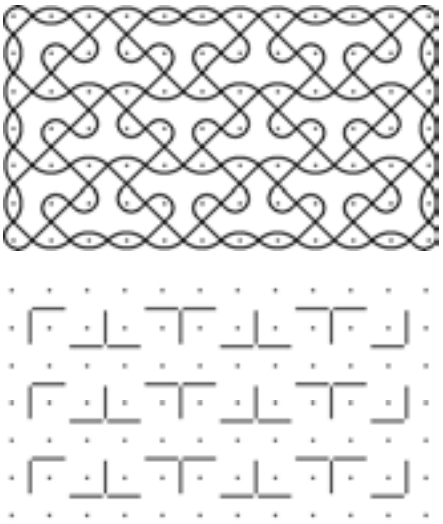

Figure 2: *The "Chased Chicken" lusona, on a 7 × 12 grid, along with the mirror walls that define the curve. The design has pmg symmetry.*

Some Mathematical Investigations

Greatest Common Divisor Investigations. A basic experiment with sona is to determine for what dimensions an $m \times n$ rectangle, with no walls, will give a monolinear sona. The answer is "when m and n have no common factor," i.e. when $\gcd(m, n) = 1$. In most cases, the students' original hypothesis is that it happens whenever one of m and n are odd. A little experimentation, occasionally with suggestions of rectangles to try, generally leads students to the correct answer. (For young students, this is especially true if they have recently been simplifying fractions.) A similar investigation is to ask "If a rectangle does not give a monolineal sona, how many lines does it take to draw the sona?" (Answer: It takes $\gcd(m, n)$ lines.)

Some African sona designs are built from combinations of rectangles, such as *abutting rectangles* or *overlapping rectangles*, as shown in figure 3. This leads to easy extensions of the basic rectangle investigation just mentioned. For example, we can ask "When do rectangles abutting (i) along a single dot, or (ii) abutting along two dots, give monolineal sona?" (Answer: (i) If both rectangles have dimensions with gcd's of 1; (ii) If one rectangle has a gcd of 1 and the other has a gcd of 2.) Similar, but slightly more complicated answers, apply to rectangles overlapping by 1 or 2 dots.

Additional GCD Investigations: The exercises below have answers that can be discovered through experimentation, and which are simply enough to be found empirically. As with the examples above, these investigations are usually too tedious to do by hand, but fairly easy to do with computer assistance from the sona drawing program. Additional exercise are online at <http://math.beloit.edu/chavey/Sona>.

1) If a single dot is erased from a corner of a rectangle, when will the resulting sona be monolineal? (Answer: If, and only if, the rectangle dimensions have a gcd of 2.)

2) If a rectangular grid has dimensions with a gcd of r, $r > 1$, can you erase dots along one edge, starting from the corner, to create a layout with a monolineal sona? If so, what is the smallest number of dots you need to erase? (Answer: Yes, by erasing $r-1$ dots.)

3) If two rectangular grids with gcd's of r and s respectively are aligned so as to overlap at one corner dot, can you tell how many lines the resulting sona will need? (Answer: $r + s - 1$.)

4) If you have two identical rectangular grids, with a gcd of r, can you overlap them in a $1 \times n$ rectangle so the resulting sona is monolineal? (Yes; they should overlap in a $1 \times r$ rectangle.)

5) By starting with a monolineal rectangle sona, and then attaching squares of dots, what interesting sona (e.g. animal or naturalistic shapes) can you construct? Look at examples of authentic Chokwe sona for ideas of shapes that might be appreciated by those artists.

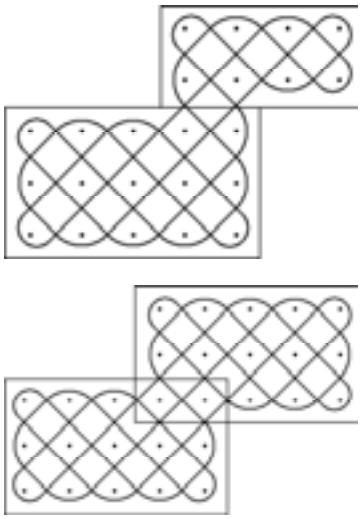

Figure 3: *Monolineal sona built from abutting and overlapping rectangles. On the top, two rectangles "abut at two dots," while on the bottom they "overlap at two dots."*

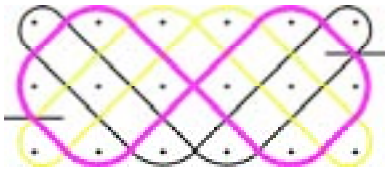

Figure 4: *The tri-lineal sona constructed on a 3×6 rectangle grid. This sona can be made monolineal by many different choices of 2 symmetrically placed mirror walls.*

Mirror Investigations. An important result about mirrors (see [3]) is that if a sona with one or more lines has a mirror added where two different lines cross, those lines will merge into one, while adding a mirror where a line crosses itself splits that line into two. The sona drawing program draws multiple lines in separate colors, so it's easy to locate places where adding mirrors will reduce the number of lines. We can use this idea to construct monolineal sona while meeting the Chokwe symmetry aesthetic. For example, in figure 4 there are many ways to find symmetric placements of two walls so that each wall merges two of the three colors, resulting in a monolineal sona. One such placement, with rotational symmetry, is indicated. In open-ended investigations, students can construct a tentative sona, then use this technique to change it to be monolineal.

Symmetry Group Investigations. To imitate the Chokwe aesthetic, we want to build symmetric sona. Many authentic sona have bilateral or rotational symmetry, although often with disruptions to the symmetry from adding animal or natural features. Creating such symmetric sona is an enjoyable investigation by itself. One particular area for interesting, open-ended artistic exploration is the construction of sona with wallpaper pattern symmetries. The Chased Chicken design of fig. 2 is one such example. Figure 5 shows another. Several other examples can be found in Chavey [2]. This suggests several options for investigation of new designs that the Chokwe would likely appreciate:

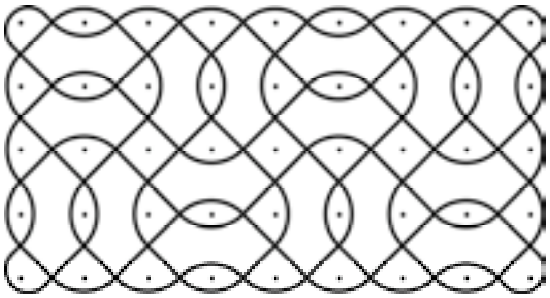

Figure 5: *A monolineal sona with p4g symmetry, This sona uses a wall motif of the form:* | - | *This design will be monolineal for all dimensions of the form $(4m+1) \times (4n+1)$.*

1) The design of figure 5 uses a pair of walls (┃ ┃) as a building block to construct a 2-dimensionally symmetric pattern, while the Chased Chicken design uses a T shape (truncated on the sides) to construct such designs. What types of simple building blocks can we use to construct such designs? Some students have found examples answering this in 40–60 minutes, but I think of this type of question as part of a longer exploration. I generally have students work in pairs.

2) For a given building block (a.k.a. "fundamental region"), what wallpaper symmetry groups can be applied to that design to give monolineal sona? With what types of spacing between the wall motifs? And for what sizes of rectangles will that building block and symmetry group generate such designs?

The Sona Program

The sona program itself allows the user to place rectangles of dots in a grid on the screen, and construct more complicated layouts from unions of such rectangles. A *wall tool* allows the user to place walls at any location within the grid layout. The *draw tool* then initiates the process of drawing a sona line from a user-specified point as defined by the grid layout and the walls. If a sona configuration requires multiple lines to complete the sona, each successive line will be drawn in a new color (within limits). The scale of the drawing, the pen width, the speed of the drawing, and whether the walls are shown or hidden are each adjustable by the user. Designs can be printed or saved to a file, e.g. to be turned in to the instructor. The instructor can also use these files to demonstrate interesting sona, without constructing them in real time, or as starting points for student investigations. The program is written in Java, hence should be fully cross-platform, and is freely available from <http://math.beloit.edu/chavey/Sona>.

Summary

Sona are useful designs to show students at many levels some of the interactions between mathematics and patterned artwork. They allow students to do both directed experimental investigations, or more open-ended investigations. Explorations topics include common divisors, the Euclidean algorithm for common divisors, and implementations of many types of symmetry groups. The students are challenged to find patterns that would be appreciated by the Chokwe artists, while using the mathematical properties to direct their explorations. Many years of experience by the author, and others, with the software used to construct these sona show the topic to be interesting and exciting to students of various ages, including some who have discovered original results through its use. We will demonstrate several of these explorations in the process of showing the functions and capabilities of the Sona drawing software.

References

[1] M. Ascher, Ethnomathematics, Wadsworth, Inc., Belmont, California, 203 pp, 1991.

[2] D. Chavey, *Symmetry Groups of Chokwe Sand Drawings*, to be submitted to J. of Math & Art.

[3] D. Chavey & P. Straffin, *The Analysis of Chokwe Sand Drawing Grids*, to appear.

[4] P. Gerdes, *Sona Geometry Vol. 1*, Maputo, Mozambique: Ethnomathematics Research Project Instituto Superior Pedagógico, 200 pp, 1994.

[5] P. Gerdes, Sona Geometry from Africa, Polimetrica, Milano, Italy, 2006.

[6] S. Jablan, *Mirror Curves*, < http://members.tripod.com/~modularity/mirr.htm>.

Honors Seminar: A Creative Interdisciplinary Approach for Student Exploration

Gail Kaplan
Department of Mathematics
Towson University
8000 York Road
Towson, Maryland 21252, USA
E-mail: gkaplan@towson.edu

Abstract

This paper describes how atypical assignments in a mathematics seminar encourage students to explore mathematical ideas through multidisciplinary lenses. Students enjoy an extraordinary journey on a remarkable mathematical road with astonishing curves and twists from art, music, writing, and more.

Philosophy of the Seminar

The focus of the seminar is on classroom strategies including seminar discussions and small group work that encourage students to creatively engage in mathematical investigations. The student is expected to take a dynamic role in all parts of the class, including classroom discussions and presentations. The assignments and activities both in and out of class are designed for active student participation and to enhance each student's understanding, appreciation, and practical experience of the bridges connecting mathematics to the world around us. The role of the instructor is merely to provide questions and suggestions to facilitate a student centered classroom. The course focuses on classroom strategies that encourage students not only to enjoy exploring mathematical connections to other disciplines, but also to learn how to creatively engage in investigations linking mathematics to those disciplines. In this article we will explore a selection of activities and projects to achieve this goal. We only begin the journey; it is never ending.

The First Class

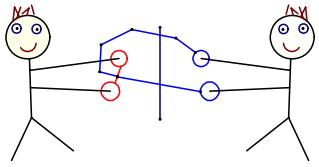

Tie a piece of yarn around each of your wrists. Tie another piece of yarn around your twin's wrist and overlap your yarn as shown in the picture. Separate yourselves without taking the string off of your wrists, without breaking the string, and without untying the knots.

Figure 1: *Siamese Twin Challenge*

As students enter the room the first day of class, they are immediately given pieces of yarn and presented with the above challenge. As they contort their bodies, searching for a solution, the atmosphere vibrates with laughter and discussions of how to find the solution. Sometimes a pair of students shouts with glee as they solve the puzzle. Sometimes frustration mounts, and after a reasonable period of time, I lead the students to the solution which is rather simple. Person A takes their yarn and pulls it through the wrist yarn of person B from the inside to the outside. It is really neat to see that, almost magically, the yarn separates! Of course, there is no magic involved, just knot theory. The class begins to hear about an unusual area of mathematics and a particular application.

Toothpick challenges are next. Students are given six toothpicks and must create designs you consisting only of **equilateral** triangles. The **entire** toothpick must be the side of the triangle. Design 1: Use five toothpicks to make two identically sized equilateral triangles. Design 2: Use six toothpicks to make two identically sized equilateral triangles. Design 3: Use six toothpicks to make four identically sized equilateral triangles. The first two designs are readily found. Design 3 is impossible in two dimensions, but easily solved in three by a triangular pyramid. As one student commented "I learned about people's natural assumption of "flatland." As we discuss the problem, we talk about how the problem itself was not particularly hard, but many made it not only harder, but impossible, to solve because they added an assumption that was not there. This helps students to recognize that we need to keep ourselves from making such assumptions.

In a reflection, one student commented that he had always thought "that all math was a series of steps to obtain a solution. That is, until I reached this class. The first class we were already forced to think outside the box." This sets the tone for the semester. Students anticipate an intriguing adventure to examine mathematics in an unusual fashion.

The Mathematical Autobiography

Good teaching orchestrates the learner's experience so that all aspects of brain operation are addressed such as analytical thinking, imagination, and emotions. The first assignment in the seminar is to write a mathematical autobiography. The goal of the project is to share glimpses of one's life through the lens of mathematics. There are many options for this project ranging from a writing an essay to composing a song. Students are limited only by their imagination. The work must be **creative**, **lively**, and **engaging**. Interestingly, students are generally uncomfortable with the freedom to make interesting choices. Yet the results are utterly amazing. The words of one student illustrate how many view the world of mathematics, "My first reaction was, "is this even possible?" On top of having to write an autobiography we were told to be creative. This is way outside my realm. I always thought there was no room for creativity in math." As you consider the following examples, each unique in its own way, observe how the students created links from their mathematical lives to literature, geometric shapes, and music.

Example #1 is a wonderful illustration of using literature to describe the nature of mathematics.

> Imagine a vast nation that stretches from sea to sea, with terrain as varied as the personalities of its citizens. Most people spend at least thirteen years of their life here, sprinting for the borders as soon as their paperwork clears. Others, however, are willing to give everything they have to stay, fearing what lies abroad. This country is made up of an almost uncountable number of states; some with mountains that stretch past the capacity of most climbers, others with barren uninteresting desert. This country, of course, is the United States of Academia.
>
> Although I currently live in the state of Mathematics, I have spent time all over the country. As a young man, I moved around a lot. Many of my favorite places included my current home state, English, Physics, History, Chemistry, and even Music Theory. At one time or another, I thought I could find a home in each one of these states, going from one to another on a daily basis (gas was cheaper back then). After spending thirteen years as a vagabond in the USA, it was about time for me to find a permanent residence.

Example #2 shows how one student uses geometric shapes as symbols of her personality.

I am a square. With its four right angles and equal sides it is truly symbolic of my perfectionist nature.

I am a sphere. It takes great artistic talent to be able to shade a drawn circle properly so that it appears to the viewer as a sphere. Therefore, it is symbolic of my creative talent.

I am a rectangle, standing proud and confident. Once becoming comfortable with those around me, I tend to voice my opinion without concerns of what those around me will think of me because of it. . . . However, I am not a towering rectangle looking to be in the spotlight, but one that prefers to get silently recognized for my accomplishments.

Example #3 illustrates how one student uses music to show "a glimpse of musical, mathematical, authorial "me." She cleverly creates a miniature story book accompanied by an audio CD containing "musical interludes from . . . my favorite artists." For example, one segment contains an illustration of the Beatles Yellow Submarine and reads "The fun simplicity of 'All Together Now' with its 1, 2, 3, 4" lyrics reminds me (in hindsight) of the relaxed, happy math of elementary school. Math was no longer my address or my telephone number – it was counting the little girls in my Madeline book, timing my friends in races around . . ."

Brain Teaser Leads to a History/Mathematics Connection

Brain teasers delight students of all ages. The following helps to introduce students to mathematical history.

The Initial Question: Consider the first five entries in a sequence of letters. Can you determine the pattern? What are the next five letters? **O T T F F**

The Solution: Consider the numbers we count with, 1, 2, 3, 4, 5, etc. Take the first letter from each number to form the sequence. The next five letters come from 6, 7, 8, 9, and 10, S, S, E, N, T. Students enjoy this challenge and frequently work together in their search for the answer.

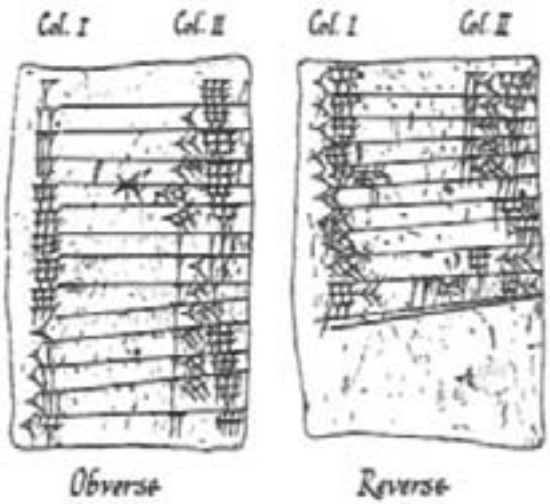

Figure 2: *An Ancient Clay Tablet*

After solving the brain teaser, students are informed that they will be playing the role of mathematical archeologist for the day by exploring the Babylonian cuneiform symbols found on a clay tablet from ancient Babylonia. The tablet was likely the equivalent of a worksheet from an elementary level classroom. The obverse is the front side of the tablet and the reverse is the back side of the tablet.

The clay was often well preserved so by putting pieces together, mathematical historians have been able to uncover and understand the world of ancient Babylonian mathematics.

Each group of students is given a copy of the tablet shown in figure 2. The first challenge is to examine only the first column and determine how the symbols represent numbers. As each group hunts for the solution, intense discussions on individual theories echo through the class. Since they have just solved the brain teaser, counting is in their minds. Quickly, almost all students conjecture that the vertical triangle represents the numeral 1 and the horizontal triangle represents the numeral 10. As the students decode the first column, a stumbling block frequently occurs after the numbers one through twenty. The next symbol consists of three horizontal triangles, which represents thirty, not the expected twenty-one. But further examination shows that the writer is now counting by tens until fifty is reached. Another curiosity – the last line doesn't fit the pattern. This is called the catch line and really belongs to the next topic to be covered. Thus, it does not need to be considered for our work.

Next, students are asked to find the relationship between the first column entry and the second column entry. After many conjectures and directed questions, students conjecture that the table appears to a multiplication table for 9. However, their original conjecture for the meaning of the symbols breaks down in line 7 because the symbols for 63 are one vertical triangle followed by a group of three vertical triangles. Why is this 63 and not 4? We then discuss that the vertical triangle represents a 1 or a 60 or a 60^2 or a 60^3, similar to how in the following numbers the digit 1 can stand for a unit, ten, hundred, or a thousand depending on its location. 1, 15, 132, 1987. The excitement in figuring out how the number system works arouses student curiosity. We use the Babylonian sexagesimal number system today when we refer to time; there are 60 seconds in a minute and 60 minutes in an hour.

This project connects mathematics, history, and archeology; it begins to help students recognize the interdisciplinary nature of mathematics.

More Mathematics Connections

During the seminar, students are expected to engage in scholarly discourse that focuses on expanding awareness of how mathematics relates to our lives. Here are brief descriptions of some of the other areas we explore. A colleague from the art department visits to provide a workshop on the use of the golden ratio in artwork. Students explore paintings using a ruler and a calculator to discover how the golden ratio appears when examining important locations on paintings. The world of art becomes intertwined with mathematics. Another colleague presents a workshop on mathematics and makeup, describing how makeup is applied to provide the illusion of the golden ratio for various facial measurements. Students are amused with the unexpected makeup and mathematics connection. Through a guided discovery project, students investigate the symmetries of a square to learn the basic concepts of group theory. Strangely enough, this abstract mathematical theory explains why particular items cause a cash register to bleep, how the machine knows a UPC code is not being read correctly, why passports have particular ID numbers, and how the ISBN number of a book is constructed. All of these experiences illustrate how mathematics is intricately woven into the fabric of our lives.

Conclusions

Students delight in the variety of mathematics used to explore a smorgasbord of disciplines in an engaging, hands on fashion. By the conclusion of the course, students see mathematics not only as numbers and symbols, but as a means to link disciplines as varied as music, art, literature, and more.

Realistic Image Making with Mandelbrot Set

Mehrdad Garousi
Freelance fractal artist
No. 153, Second floor, Block #14
Maskan Apartments, Kashani Ave
Hamadan, Iran
E-mail: mehrdad_fractal@yahoo.com
http://Mehrdadart.deviantart.com

Khalil Taleslami
Bu-Ali Sina University
Hamadan, Iran
E-mail: tale@basu.ac.ir

Abstract

Fractal images enjoy a great deal of abstraction and are very wonderful and out of expectation for observers. These mathematical paintings are clear exposures of complexity, all-scale features and self similarity which are presented simultaneously and provide unique views. On the other hand, fractals are representations of the nature behaviors and rise from nature. Therefore, it must be possible to use these fractal properties and images in the creation of natural and realistic phenomena and landscapes. In this article, I am going to briefly explain the way of creating an absolutely realistic painting, as real as nature landscapes, called *Sea at the sunset* only by means of Mandelbrot set.

Process of Creating a Realistic Painting with Mandelbrot Set

To create a realistic illustration, it is not absolutely essential to obtain a fractal exactly similar to our subject, instead we should try to exploit the properties of the nature that are presented in that fractal and apply them in our image making process. So, we ought to produce an image according to properties like self similarity, complexity, chaos which the last years` artists were disappointed with in creation of their artworks. The Mandelbrot set has no similarity to any imaginable natural phenomenon, but contains a great deal of nature traits; therefore this fractal can be used to create a perfectly realistic painting including many nature qualities. There will be no difference by which program or software we do the processes of our image making. We only use Mandelbrot fractal with some magnifications and sometimes color transparencies. Therefore, never do we use any distortion, erasing or any image processing software like Adobe Photoshop. Here, I have used Ultra Fractal software [1] to create my piece and started with this basic formula:

Initial Condition: z = 0 Loop: z = z * z + #pixel Bailout Criterion: |z| < 2

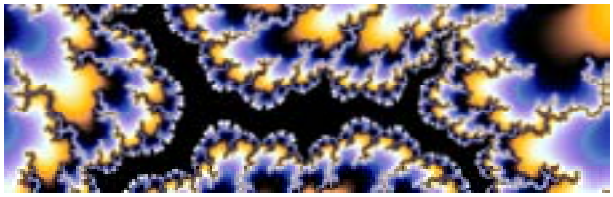

Figure 1: *A close-up view of the Mandelbrot set, zoomed in by a factor of 5.8x10^7 relative to the bounding box of the entire fractal.*

Figure 2: *Our painting with 11 separated layers of Mandelbrot set.*

We use our Mandelbrot set to create our painting and zoom in a piece of its outer border until we attain an image which can be seen in Figure 1. Afterwards, we change our point of view to the image by

changing angle of the image from horizon to make it flat and provide ten other different layers of this image, each of which has only a little difference in zoom and transparency from the previous ones. The result of over punching these ten layers on the first layer is observed in Figure 2.

Now we arrive at the phase that we should control the dispersion of the painting's colors. Accordingly, we can change and regularize the colors near what we want by putting nine other layers of Mandelbrot set with more blue, red, yellow and white colors on previous ones. It should be mentioned that in most stages of the color control process I have not changed the color of Mandelbrot fractal, but I zoomed in the suitable color I needed. After adding another layer that present the sun in the painting (by changing the amount of z in Initial Condition to 1 and in the Loop to #pixel), we obtain the complete landscape (Figure 3). What you can watch is the magic of fractals. However, our painting now consists of 21 layers of complex and disordered views of Mandelbrot fractal, but by managing the convolutions of different layers and controlling the dispersion of colors in the whole image, we have obtained an evidently ordered painting representing a blue sea at a reddish and yellowish sunset.

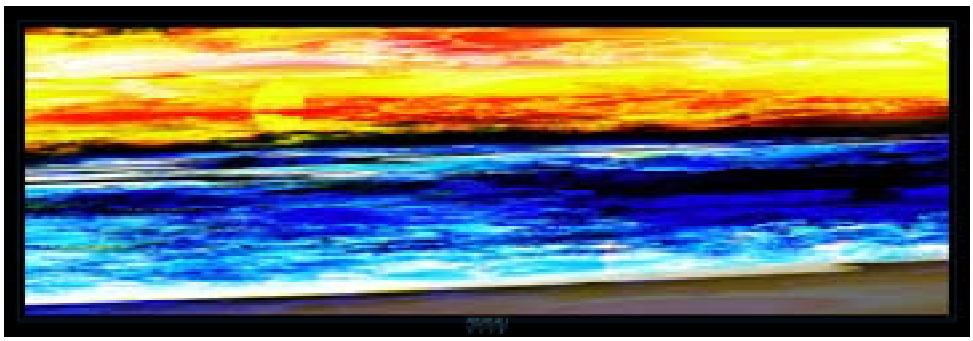

Figure 3: *Completed "Sea at the sunset" with 21 layers (2008; © Mehrdad Garousi).*

Now we have a 21 layer landscape in which every part of the canvas is covered with detail, just like a real landscape, which faces to more and more complexities. If we have a look at the space between two waves, we will observe other more irregular waves that sequentially continue towards the infinity and clouds of the painting similar to real clouds in the sky which do not have any clear border with sky. Now, we have a perfect and exclusive sunset painting which would not be created on any canvas or in any photograph. Its creation is dependent on computer assistance and on exploiting advanced fractal mathematics and geometry. To have a better look at the images I invite you to watch the color version of the paper on the CD-ROM.

Conclusion

Not all fractals provide an artistic and aesthetic image, but they present us several properties and behaviors of the nature, however rarely do some of their raw abstract formats have eye catcher beauties, too. It is the creative artist that, by enjoying and applying these properties, should create an artistic and aesthetic work of art. I hope fractal image making goes further than limited boarders of abstract images and some professional painters will be interested in realistic painting by using fractals. Mandelbrot says [2]: "For many years I had been hearing the comment that fractals make beautiful pictures, but are pretty useless. I was irritated because important applications always take some time to be revealed."

References

[1] Slijkerman, F., http://www.ultrafractal.com/.
[2] Brockman, J., 2004, *A THEORY OF ROUGHNESS:* A Talk with Benoit Mandelbrot. Available at http://www.edge.org/3rd_culture/mandelbrot04/mandelbrot04_index.html (accessed 5 November 2008).

An Interdisciplinary First Seminar on Symmetry

Tamara J. Lakins
Department of Mathematics
Allegheny College
Meadville, PA 16335, USA
tamara.lakins@allegheny.edu

Abstract

The concept of symmetry, including what it means in mathematics, how it occurs in other disciplines, and how the mathematical ideas are applied to symmetry in art and architecture, is investigated in an interdisciplinary first seminar at Allegheny College.

The Freshman-Sophomore Program at Allegheny College

Allegheny College requires each of its students to complete a sequence of three First-year/Sophomore seminars that emphasize writing and speaking. Each faculty member who teaches a first-year seminar may choose his or her own topic, and interdisciplinary topics are encouraged. My course, "Symmetry through the Eyes of Mathematics", investigates the interdisciplinary nature of symmetry.

What is Symmetry?

On the first day, I begin with an exercise asking students to define what it means for a figure to possess symmetry. While most students begin by focusing on bilateral symmetry, the discussion naturally leads to an introduction of the four rigid motions of the plane.

I also assign for reading and discussion the introduction to *Patterns of Symmetry* [3], which is the proceedings of the 1973 "Symmetry Festival" held at Smith College. The reading foretells many of the ideas we discuss in my course: the universal nature of symmetry, the rigid motions, groups, the idea of analyzing symmetries in a pattern, and the fact that there are only finitely many possible symmetry types.

The reading also primes students for the first major paper and speech assignment, which asks them to investigate how symmetry occurs in any discipline other than art and architecture (which is discussed later in the course). Examples of possible subject areas include biology, chemistry, physics, dance, music, neuroscience, psychology, theatre performance, and literature. Students address, for their chosen field, what the concept of symmetry means, where and how symmetry occurs, the significance of symmetry (its purpose or how it is interpreted), and how and why symmetry is broken.

The Mathematics: Rigid Motions and Symmetry Groups

The major mathematical goals of the course are to understand how rigid motions are combined (multiplied), the concept of a mathematical group, and how we can describe the symmetry type of a figure in the plane. Many of the activities I use in class are, or are inspired by, tasks in Chapters 2-5 in Farmer's book *Groups and Symmetry* [2].

I begin with worksheets that I developed which ask students first to determine where a particular combination of rigid motions moves a given triangle, and then to conjecture a general result. My primary goal is to investigate what happens when a reflection is followed by another reflection. We discuss why any translation and rotation can be described as a product of reflections.

The language of rigid motions provides us with the usual mathematical definition of what it means for a figure in the plane to possess symmetry. Beginning with regular polygons and other simple finite shapes, the students investigate the multiplication (or group) tables of the symmetries of the figures and classify figures as having either cyclic or dihedral symmetry type.

Moving on to strip (or frieze) patterns and wallpaper patterns, the students discover why there are at most $2^4 = 16$ possible symmetry types of strip patterns. After some experimentation, they conjecture that only 7 of the 16 apparent possibilities actually occur. The facts about rigid motions investigated earlier in the course enable us to explain why some of the other possibilities cannot occur. Students classify a variety of strip patterns, using IUC notation. Since working out why certain combinations of symmetries cannot be present in a wallpaper pattern is mathematically very difficult, we focus on using the standard flow chart to analyze the symmetry types of these patterns.

Connections

As mentioned earlier, the first major assignment asks students to investigate the meaning of symmetry in disciplines other than art and architecture. Patterns and symmetry in art or architecture are the focus of the second major assignment. Students choose an artist or architectural style to examine; some examples (many taken from Farmer's book [2]) include the art of M. C. Escher, William Morris, or Robert Adam; Islamic art (including the Alhambra); Turkish art or architecture; African art or textiles; American Indian pottery, rugs, or beadwork; Asian carpets or pottery; Amish quilts; and Mayan art and architecture. Students are asked to include a summary of the history of the culture, artist, architect, etc., in question. They must also include and analyze examples of at least six symmetrically different patterns that are appropriate to their topic; any combination of wallpaper patterns, strip patterns, or finite figures is permitted.

In an effort to reinforce the message that symmetry is ubiquitous and expose students to ideas from other cultures, I also require students to read a portion of the chapter "Symmetric Strip Decorations" from Ascher's book *Ethnomathematics* [1]. This chapter compares the strip patterns found on the rafters of marae, the community and spiritual meeting places of the Maori, to the strip patterns found on Inca pottery.

References

[1] Marcia Ascher. *Ethnomathematics: A Multicultural View of Mathematical Ideas*. Brooks/Cole Publishing Company, 1991.

[2] David W. Farmer. *Groups and Symmetry: A Guide to Discovering Mathematics*. The American Mathematical Society, Providence, 1991.

[3] Marjorie Senechal and George Fleck. Patterns of symmetry. In Senechal and Fleck, editors, *Patterns of Symmetry*, pages 3–19. University of Massachusetts Press, Amherst, 1977.

This Equation is Art

Peter James Smith
School of Creative Media
RMIT University
GPO Box 2476V
Melbourne, Victoria, 3001, Australia
E-mail: pjsmith@rmit.edu.au

Abstract

In this paper I advance the notion that the depiction of a mathematical equation becomes a piece of art if its representation carries a *narrative resonance* that allows it to communicate with the viewer. Following Mullins [1] there is greater potential for an equation of importance and depth to carry this resonance well beyond any real world object that it may represent.

Introduction: equations as visual objects

The landmark article *Truth + Beauty*, by Mullins [1], questioned why the beauty of mathematical equations had not been harnessed more widely as a form of contemporary art. He was having a show in London at the time, of photographs of typeset equations from many branches of mathematics and physics. As iconic pairings, Truth and Beauty, Mathematics and Art seem to have a linked duality. Indeed I admit an affinity for the practice of writing equations in, and as, art for more than 30 years. Mullins outlined in his article an intriguing approach: he not only photographed typeset equations, but used an intriguing wall text to spin a narrative around his images, enough to draw the viewer in to take a closer look. I would call this approach, one of bringing a *narrative resonance* to communicate with the viewer, possibly from different standpoints, but all with the endpoint of bringing in an audience.

In compiling his new 2008 book *Formulas for Now*, Hans Ulrich Obrist [2] invited artists, writers, architects, mathematicians and scientists each to contribute an equation for the twenty-first century. The resulting book with an equation per page is a spectacular readable array with a hardcover trapping of pink binding against 1950's-green covers. Respondents took many approaches, from the humorous to the deadpan formulaic. The contributor's name appears at the top of their page, similar in function to named wall texts in museum exhibitions. This work really catalogues how contemporary minds think—'and is testament to the vital role that formulas play in contemporary culture', [2]. The depicted equations are treated as visual 'design' objects. Some of these equation objects surprise: Gerhard Richter provides a page from his *Atlas* containing diagrams reminiscent of graph theory; Tacita Dean's working method text equation is written *chaos / chance = process*, while more mathematically, Benoît Mandelbrot gives his landmark iterative equation $z \rightarrow z^2 + c$ that is used to generate the fractal Mandelbrot Set .

In his quest for mathematical beauty that is art, Mullins [1] noted that 'A piece of mathematics must give some important or original insight to be beautiful'. He quotes the example of Euler's famous formula

$$e^{i\pi} + 1 = 0$$

which links together some of the major symbols of mathematics and complex number theory. Mullins suggests that an equation such as this is visually more powerful than geometric figures and models so

often associated with beauty and mathematical art by the general public. Thus, it is the equation that is art, rather than a model of it. On a more geometric scale, for example, the mathematical representation of complex numbers in the plane is more artful than an image of the plane itself. But how is the bridge between mathematics and art crossed? I would suggest that the key lies in *how* the equations are represented.

Transcendence

The abstract thinking that configures Euler's equation seems to be given an encouraging push along in Obrist [2] by virtue of the fact that it is handwritten, and, has Mandelbrot's signature appended. Suddenly there is a narrative guiding our thinking, and capturing our interest: did Mandelbrot really write this in this hand? There is an intrigue around viewing the handwritten notes of a mastermind. The final handwritten image, as a piece of art, has transcended its original mathematical role in this context. The white handwriting on the dark 'blackboard' page seems quite resonant of the viewer's own schoolroom histories.

The notion of 'transcendence' seems key to understanding why other types of texts, markings, lines and scribbles have the capacity to intrigue and move people, even though their original function is not based on logical deduction. The potential take-up of images or text by contemporary culture is not based around logical reasoning and deduction (as is exhibited by the pictorial role of equations), but rather by a resonance with a subculture. Transcendent images and text communicate to subcultures. Successful images get in there, are threshed about, and are taken up and used. Perhaps this is why the highly resonant, but entirely illogical and scribbled, residue texts, installations, films and acts by Joseph Beuys have infiltrated twentieth century art history (a subculture), forced their way to the top, and remained there, still highly influential. The related term 'trace', which Ingold [3] describes as 'any enduring mark left in or on a solid surface by a continuous movement' seems to give appropriate visual narrative resonance for the viewer. For example, a standard musical score is simply a text of notes on staves that show the performer which notes to *play*. After a violin score has been annotated by the performing violinist, as illustrated by Ingold [3], it seems to be a transcended document of *performance* carrying 'bowings and markings'. This *equation* is art.

Another contributor to Obrist's book of formulas is the Swiss artist Bernar Venet, who offers *Related to 'The Homology (Co-Homology) Sequence of the Pair (X,A)',* 2000. In this work, Venet carefully paints a museum wall fluorescent yellow, and then overpaints the field with precisely extracted equations from a research paper on Algebraic Topology. McEvilley [4] felt that 'the viewer is left with the experience—delight in colours, amusement at chance resemblances and a confrontation with an essential unknowability'. This is because the audience cannot read research-level mathematics.

We have noted here that interpretation, handwriting and authorship can assist with the process of visually representing equations as art. Indeed, to become art, an equation, like any object in the world, must be transcendent—and refer to our understandings of culture beyond its original mathematical function. Venet, for example, has specifically chosen mathematical texts to block viewer understanding of the depicted image, rather than appealing to the viewer to bring their own histories of similar texts. This narrative remains 'confrontational' rather than resonant, and following McEvilley's advice we are left to delight in the colours.

References

[1] J. Mullins, *Truth + Beauty,* New Scientist, Vol. 189 No. 2536, p. 16. 2006.
[2] H. U. Obrist, *Formulas for Now*, Thames and Hudson: London. 2008.
[3] T. Ingold, *Lines: A Brief History*, Routledge: London. 2007.
[4] T. McEvilley, *Monochrome Math*, Art in America, April 2003, pp. 108-113. 2003

ZenArt: Graphic Geometrical Modules

André Génard
Graphic
Sint Andriesplaats 18
Antwerpen B-2000, Belgium
E-mail: info@genard.be

Abstract

I explain the design of a set of graphic geometrical modules - based on the letters of the (Dutch) alphabet - with which various patterns can be drawn. The matrix used as a basis for the (this) design, also determines the guidelines for composing these patterns. From an artistic point of view, the patterns illustrate a view on interconnectivity.

1. Introduction

Around 1975, inspired by the slogan of Marshall McLuhan: 'The medium is the message'[1], and by a trend known by the name of ' Minimal Art'[2] (in which the fewest and barest essentials or elements in the arts, literature, or design are used in order to relate to the environment), I began to experiment with letters taken from the Dutch alphabet, as a basis for creating a set of graphic geometrical modules. This choice ensures consistency of the various shapes within the set, and it limits their number.

Along with that, I tried to eliminate any reference to optical or subjective components that shape a module, reducing it to its essential geometrical form. With the traces of emotive charge removed, these modules were meant to stand on their own, as meaningless objects. In contrast as for instance in the case of the alphabet 'Azart' by Belgian artists Rombouts & Droste[3], they keep the basic characteristics of the Latin alphabet.

2. Drawing the alphabet.

I drew the alphabet on the bases of four geometrical figures, which can be regarded to as being universal: **square**, **cross**, **diagonal** and **circle** (and/or **dot**) (Figure 1). Placing these figures on top of each other they form a grid like matrix, which is shown here by means of dotted lines (Figure 2).

I use these lines as guides for drawing each letter. Square and cross, turned into guides help to draw horizontal and vertical letter strokes. Diagonal and circle are used to draw diagonal and circular letter strokes. 25 dots, matching the thickness of a letter stroke, help shaping the joints and endings of each letter. Each letter may use one or more elements of the four geometrical figures.

In the example the letter 'R' is being drawn: of the **square**, the left and left half of the upper stroke are used, followed by the curve of the **circle**, followed by the horizontal stroke of the **cross** and finally by the downward stroke of the **diagonal**. (Figure 3).

Figure 1: *Universal, geometrical figures: square, cross, diagonal and circle (and/or dot).*

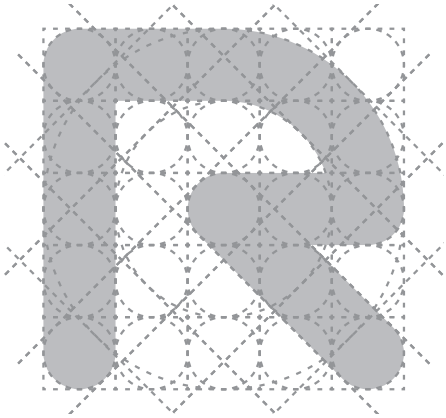

Figure 2: *The letter 'R' drawn onto the matrix.*

Figure 3: *The letter 'R' drawn using parts of the matrix.*

3. Rules for composition, derived from the matrix.

As figures 4 and 5 show, the matrix also determines the way with which the letters are drawn on a sur-

face. Figure 4 indicates directions of possible horizontal, vertical and diagonal moves. Figure 5 shows the possibilities for turning, rotating and mirroring of the letters. In case letters are placed next to one and other, the preferred distance in between equals the thickness of a letter stroke. (Figure 6) In case a letter overlaps another, the overlap should be no less than the thickness of a letter stroke. More precisely, it should at least overlap one of the 25 circular dots as can be found within the matrix. (Figure 7)

4. Composition.

Since the dimensions of the letters match each other, this provides an outline with which compositions can be made. Likewise the rules by which they can be turned, rotated, mirrored, moved and placed separated from each other or overlapping.

Conclusion

It is possible to turn letters of an alphabet into meaningless symbols, but as an ultimate consequence there is no need for them to exist at all. Changing the (minimalist) view on the concept of geometry, in favor of a holistic approach, vast opportunities emerge to produce various works of art.

Given this viewpoint, the challenge is to create patterns within the boundaries of the mentioned composition rules, and yet to make a design that is as powerful and attractive as possible.

This is to be done by the use of color, dimension, and material, and not by choosing words derived from the sources of inspiration as a starting point in creating patterns.

Incidentally, the set was given the name 'ZenArt', a reference to a mystic language 'Zenzar' and to Zen philosophy. Also it refers to the mentioned alphabet 'Azart' of the artists Rombouts & Droste.

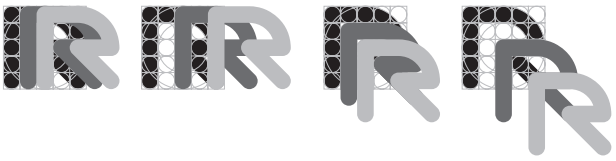

Figure 4: *The letter 'R' moved in different ways according to the restrictions of the matrix.*

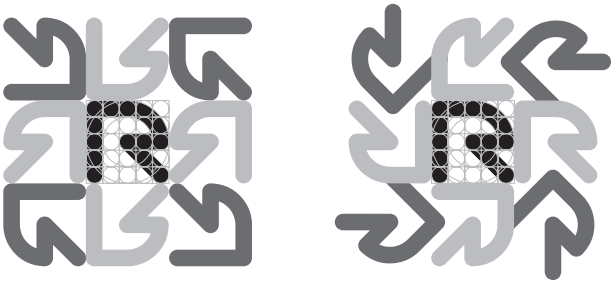

Figure 5: *The letter 'R' turned, rotated and mirrored according to the restrictions of the matrix.*

Figure 6: *The alphabet (lower case only), placed with a space in between that equals the thickness of a letterstroke.*

Figure 7: *A composition with letters that form the word 'BRIDGES' showing overlapping letters.*

References

[1] Marshall McLuhan, 'Understanding Media', Routledge, London. Originally published in 1964 by Mentor, New York; reissued 1994, MIT Press, Cambridge, Massachusetts with an introduction by Lewis Lapham
[2] Gregory Battcock, Anne Middleton Wagner 'Minimal art: a critical anthology'. Published by University of California Press, 1995
[3] Guy Rombouts, Antwerp, Belgium, 2004-2008, www.azart.be/azhelp.htm (accessed April 22, 2009).

Acknowledgement

Helena, Lucas, Bea, Sam and Chris.

Amazing Labyrinths, Further Developments

Samuel Verbiese
Artist
Terholstdreef 46
B-3090 Overijse, Belgium
E-mail: verbiese@alum.mit.edu

Abstract

This short paper elaborates on findings presented at the 2007 Donostia Bridges Conference [1], first bringing some classifying logic in the family of labyrinths of which the 'Classic' and 'Chartres' are the best known examples, with the interesting inclusion of spirals. Second, another 3-dimensional morphing is offered on the surface of a sphere, which underscores the inherent antisymmetric nature of the 'Classic' and Chartres' designs. Third, appealing 3-D forms can result from projections onto polyhedra, here the octahedron/cube duals. Fourth, a recent arrangement of the 'Classic' into a rose-shape is proposed for possible mathematical analysis. The figures of this paper, including an important erratum correcting a wrong figure that didn't make it in the printed Donostia Proceedings, are provided as an appendix in the CD-Rom of the Proceedings of the Conference, but not on the printed Proceedings. They are further expanded by entries at the accompanying Bridges 2009 Mathematical Art Exhibit [2].

Introduction

The title "**Amazing Labyrinths**" [1] goes beyond a mere easy play of words. In the class of *unicursal* '**labyrinths**', we consider from a geometrical viewpoint the subclass 'centered' around the characteristics (see [1]) of the 'Chartres' design amplifying the old 'Classical/Cretan/Knossos' design. Its members share the interesting property that their 'walls', i.e. the space delimiting the 'Ariadne' journey that meanders to the center, actually constitute 'walkable' *multicursal* '**mazes**', complete with 'choices' and 'dead-ends' (refer to those mystifying paths enjoyed by children and adults alike in labyrinthine theme parks and which in fact are mazes). The essential point that makes so special those mazes stemming from this subclass of labyrinths is that their 'dead-ends' are opposite pairs that can be joined by tunnels, bridges or Japanese steps for these mazes to be turned into '**closed circuits**', when in addition the 'transversal choices' are denied access! This was fully expressed in several 'trompe-l'oeil' works and in the sculpture project presented at Bridges Donostia [1] and at the accompanying Mathematical Art Exhibition [3].

1. From Spirals to the 'Classic', 'Chartres' and Beyond

As suggested by Raket [4] the meandering plowed track packing the agriculture field might prefigure the labyrinth, and Kern [5] as well as Raket again see in the spiral a precursor of the 'Classical' labyrinth. So, spirals and 'Chartres'-like labyrinth layouts can be brought in a comprehensive system based (a) on their 'seeds' as in earlier remarks by Tony Phillips found on-line in [6], where some necessary corrections have been introduced, and (b) on further developments of the typical Chartres' 'opposite returns' mentioned in the Introduction. This has led to combining 'seeds' and 'opposite returns' in large complex labyrinths that, with a leap into still further developments as hinted to in the next section, could go 3-D! In the same vein of strange/magic labyrinth generation, we need referring to another spiral-to-'Classic' transform by Slavik Jablan as cited and shown in [7], and, in a ludical context, placing half as many children as there are 'perimetric dots' around a given labyrinth 'seed', seashore or chalk labyrinths can readily be generated in choregraphic pleasing dynamics as displayed in the Math Art Exhibition [2].

2. From Disk to Cylinder to Sphere and Beyond

The Donostia paper [1] illustrated a disk-cylinder morphing transform. Here, pushing this 3-dimensional interpretation to the end, by swelling the mid-part of the cylinder, brings about the spherical labyrinth (see [8,9]) that magnificently stresses the inherent antisymmetric nature of the 'Classic' and 'Chartres' designs related themselves, as described in previous paper and elsewhere, to a Greek freeze meander. 'Chartres' typical turnabouts and trough passages giving rise to the 'pilgrim steps' [1] remain as apparent as on the cylinder and on the rectangle (that by could be curled into a cylinder in the other direction as well, I found out) and suggested the idea this class of labyrinths can be generated from infinite lattices of such steps [10]. No doubt Dick Termes could develop this brilliantly further in his trademarked craft [11]!

3. Projection of Labyrinths onto Polyhedra

This alternate kind of 3-dimensional interpretation to the above-mentioned stems here from the square and hexagon as projections of the octahedron (and of the pyramids it's composed of) and the cube, where the *squared* and *hexagonized* micro-Chartres labyrinths have been used. Such exercises could be further tempted with other polyhedra, which recalls some maze work by Xu and Kaplan [12].

4. A Labyrinth/Knot Rose Submitted to Mathematical Scrutiny

'Roses' are this year's theme of the 'Jardins d'Aywiers' garden fair, so my eighth ephemeral veggie labyrinth there had to feature some rose-like shape, beyond what could have been more simply suggested by the central rose of the Chartres design reflecting the huge stained glass rose above the front porch of the famous cathedral. Pairs of 'walls' of the classic labyrinth have been twisted, which reminds architectural work by Glaeser and Gruber [13].

Acknowledgments, Copyrights and References

Thanks are due to **Mrs. Patricia Limauge** again for gracefully opening 'Les Jardins d'Aywiers' to my eighth veggie labyrinth there (www.aywiers.be), and to Françoise Dierkens for kindly informing us that the personal library of garden books of the famous Belgian garden and landscaping architect René Pechère, a labyrinth lover himself, has been donated and is publicly available, see www.bvrp.net .

[1] Samuel Verbiese, *Amazing Labyrinths*, Proceedings of the Bridges Conference in Sonostia, 2007.
[2] Samuel Verbiese, http://www.bridgesmathart.org/art-exhibits/bridges2009/verbiese.html.
[3] Samuel Verbiese, http://www.bridgesmathart.org/art-exhibits/bridges2007/verbiese.html.
[4] Jacques Raket, *Dernières nouvelles du labyrinthe*, Editions la mesure du possible, 2006.
[5] Hermann Kern, *Through the Labyrinth : Design and Meanings over 5,000 years,* English Edition by editors Robert Ferré & Jeff Saward, Prestel, 2000.
[6] Tony Phillips, http://www.math.sunysb.edu/~tony/mazes/classify.html, many links, a.o. /index.html.
[7] Reza Sarhangi, *Making Patterns on the Surfaces of Swing-Hinged Dissections,* Proceedings of the Bridges Conference in Leeuwarden 2008, p.252.
[8] Jim Buchanan, *Labyrinths for the spirit – how to create your own labyrinths for meditation and enlightenment*, Octopus Publishing Group Ltd, 2007, pp.36-37.
[9] Marianne Ewalt, http://www.marianne-ewaldt.at/kugeln99.htm.
[10] Interesting 'last-minute' discussions with John Sharp and Martin Demaine are here acknowledged.
[11] Dick A. Termes, http://www.bridgesmathart.org/art-exhibits/bridges2008/termes.html.
[12] Jie Xu and Craig S. Kaplan, *Vortex maze construction,* Journal of Mathematics and the Arts, Vol. 1, No. 1, March 2007, p. 18.
[13] Georg Glaeser and Franz Gruber, *Developable surfaces in contemporary architecture,* Journal of Mathematics and the Arts, Vol. 1, No. 1, March 2007, pp.59-71.

Finding a New Route to the Moon using Paintings

Edward Belbruno
Department of Astrophysical Sciences
Princeton University
Princeton, NJ, 08540, USA
E-mail: belbruno@princeton.edu

Abstract

A new theory of space travel using low energy chaotic trajectories was dramatically demonstrated in 1991 with the rescue of a Japanese lunar mission, getting its spacecraft, Hiten, to the Moon on a different type of route. The design of this route and the theory behind it is based on finding regions of instability about the Moon. This approach to space travel was inspired by a painting of the Earth-Moon system which revealed these regions and the new chaotic trajectories. The brush strokes in the painting revealed the dynamics of motion which are verified by the computer. The painting itself can be used as a way to uncover dynamics in the field of celestial mechanics that cannot be easily found my standard mathematical methods.

A New Approach to Space Travel

The classical route from the Earth to the Moon uses the Hohmann transfer, named after the German engineer Walter Hohmann [1]. Let's assume a spacecraft is to go from a circular orbit about the Earth to a circular orbit about the Moon. The Hohmann transfer is a nearly straight path, actually half of a highly eccentric ellipse, from the circular orbit about the Earth to the circular orbit about the Moon. To leave the orbit about the Earth, the spacecraft briefly fires its engines to gain the necessary velocity, then coasts to the Moon in three days. At the Moon, it needs to be captured into the lunar circular orbit. To do that it needs to slow down by about one kilometer per second by firing its engines again. This is called a capture maneuver. It is risky to do and also uses a lot of fuel, which is expensive. Is there a better way to do this?

It would be desirable to go into orbit about the Moon, automatically, without needing to slow down and firing the engines. This is called ballistic capture. Prior to 1986 it was thought to be impossible to do. If it could be done, however, then a spacecraft could go to the Moon and then into orbit with much less fuel and more safely. I got interested in this problem at that time when I was working at NASA's Jet Propulsion Laboratory. I knew that ballistic capture may be possible due to my training as a mathematician, from New York University's Courant Institute. My specialty was celestial mechanics and chaotic dynamics. I figured that there may be a way to utilize the gravitational forces between the Earth and Moon to achieve ballistic capture, but with a longer flight time. In early 1986, I was given three months to try and find a way to achieve ballistic capture for a robotic lunar mission study, called LGAS (Lunar Get Away Special). The ability of achieving ballistic capture would provide a new approach for how spacecraft could go orbit about the Moon with many exciting possibilities. Due to the time allotted, and the complexity of the problem, with nothing in the literature, I felt it was not going to be possible to figure out.

Dynamic Channels, Chaos, and Paintings

To gain an insight into the problem, I sought out help from my other profession as an artist doing paintings. The hunch I followed was something that is evident from looking at a Van Gogh painting, for example,

Figure 1 : *Orbit to the Moon,* 56" $\times$ 72"*, oil on canvas, 1991*

Starry Night. The brush strokes he used are applied very quickly, in a spontaneous manner, being guided by intuition. His paintings reveal a deeper aspect to reality. I felt that if I used his painting style, and painted the Earth-Moon system, the brush strokes may reveal patterns that would give insight into ballistic capture trajectories. The painting I did revealed a region about the Moon that seemed to lie at the boundary of the gravitational field of the Earth and Moon, allowing a trajectory to delicately be captured about the Moon ballistically, which appeared to be a chaotic, that is, sensitive, process, see [1, Figure 6.2]. When I went to the computer and simulated this, I found the ballistic capture transfer and the regions supporting it about the Moon, called weak stability boundaries [1,2]. From a mathematical perspective, these boundaries are associated to a complex network of surfaces called invariant manifolds which define dynamic channels where these chaotic trajectories can move [2,3].

However, a more useful and important ballistic capture transfer was found a few years later in 1990. It was found in order to resurrect a failed Japanese lunar mission and get its spacecraft, Hiten, to the Moon in 1991 [1]. This transfer utilizes the more complex four-body problem in celestial mechanics, where one has to take into account the gravitational interactions of four bodies: Earth, Moon, spacecraft and the Sun. The flight time is only four months making it far more useful. A painting of this transfer is shown in Figure 1. The trajectory starts near the Earth, travels out about 1.5 million kilometers from the Earth where it encounters the boundary of the gravitational fields between the Earth and Sun. In this region, the spacecraft is essentially balancing on the gravitational fields of these two bodies, like a surfer would balance on a wave. It then arcs back to go to ballistic capture about the Moon at an analogous boundary, due to the balancing of the Earth and Moon gravitational fields. As it falls towards the Moon, one can see the brush strokes defining the gravity fields.

These pathways and the underlying theory were inspired by brush strokes in a painting.

References

[1] E. Belbruno. *Fly Me to the Moon: An Insiders Guide to the New Science of Space Travel*. Princeton University Press, 2007.

[2] E. Belbruno. *Capture Dynamics and Chaotic Motions in Celestial Mechanics*. Princeton University Press, 2004.

[3] R. Casselman. Chaos in the Weak Stability Boundary. Cover of the Notices of the American Mathematical Society, Vol. 55, No. 4, April 2008.

Text from Truchet Tiles

David A. Reimann
Department of Mathematics and Computer Science
Albion College
Albion, Michigan, 49224, USA
E-mail: dreimann@albion.edu

Abstract

A way to create text with Truchet tiles is presented where each letter is represented by a particular grouping of Truchet tiles. The resulting text is rendered in a surprisingly and visually appealing manner within a tiled region.

1 Introduction

In 1704, Truchet investigated the patterns obtainable from a single square tile that was bisected along a diagonal into two uniquely colored isosceles right triangles [5]. In 1987, Smith [4] published an article containing a translation of Truchet's original paper with some commentary and new ideas including the use of a random tiling rather than a structured pattern. Smith also included a variant of the Truchet tile that replaced the triangular segmentation with two quarter-circle arcs, resulting in a tiling that is comprised of an aesthetically pleasing, meandering set of mostly closed curves. These tiles are illustrated in Figure 1. Pickover [3] proposed using randomly placed Truchet tiles as a way to visually detect patterns in binary data, noting "the eye perceives no particular trends in the design." However, he does note small features such as circles and dumbbells. Esperet and Girou [2] discuss a variant where the plane is randomly tiled using two tile types, each bicolored as shown in Figure 1. They note the tile's type can be selected using a parity process (row + column mod 2) to create filled regions, regardless of the tile orientation. Browne [1] describes how to generate a closed path (a Truchet contour) using a spanning tree. Browne also gives the simple formula for computing the perimeter and enclosed area of a contour.

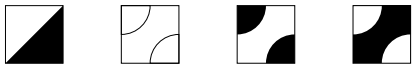

Figure 1: *Truchet tile examples. From left to right: Truchet's original tile, tile with arcs, and the two bicolored versions of tiles with arcs.*

2 Creating Text from Truchet Tiles

One interesting application of Truchet tiling is to intersperse structured sections among a generally random field. More specifically, one can represent each symbol in a font with a simple Truchet contour. An example tiling containing the text "Bridges 2009" is shown in Figure 2. Because of the nature of the connections in the tiling, the baseline of each letter is oriented 45 degrees from the horizontal. While the tiling can be performed relatively easily, one must be careful of a few details. When using colored tiles, parity should

be preserved by selecting an appropriate spacing between letters, words, and baselines. Also, the tile size should be large enough for the curvature of the Truchet contours to be visible, yet small enough to allow rendering of all of the letters required for the text.

As Browne notes, the perimeters and enclosed areas of each Truchet contour are easy to compute. This suggests an interesting exercise for children in which they create their initials or a word and then compute its perimeter and enclosed area. Other applications include quilt making and architecture, where the designer might choose to include a name or other text as a subtle message in an otherwise random field.

The subtle nature of the text's appearance enhances the pleasure in discovering a message in the tiling. While not shown here, visibility of the text can be greatly enhanced by using a contrasting color for the contours or the interior regions of the letters.

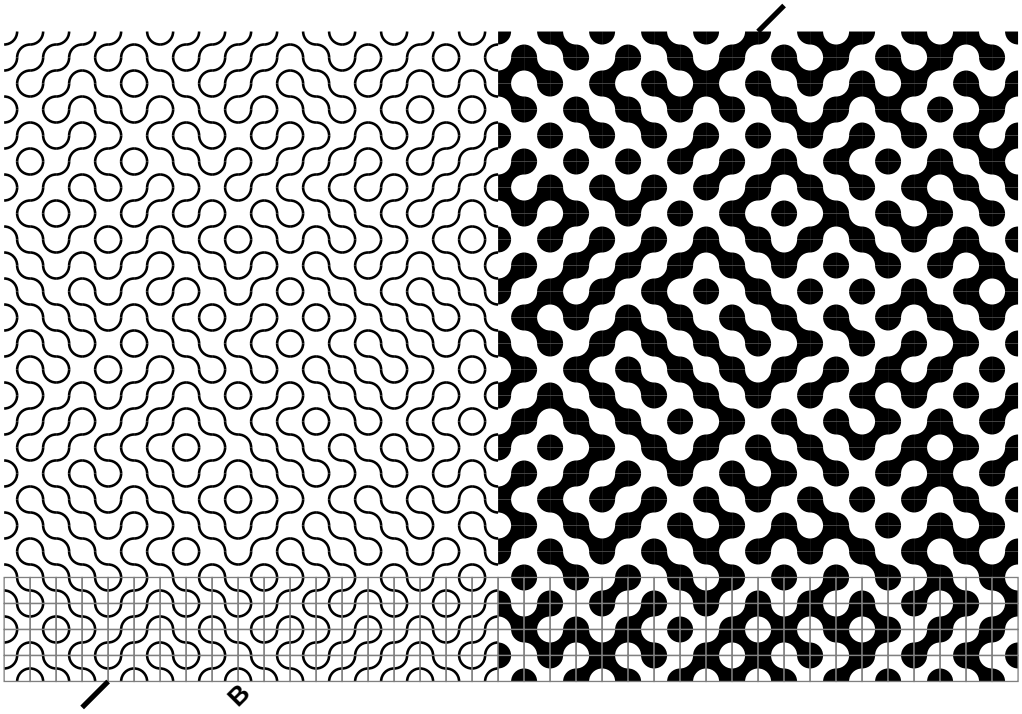

Figure 2: *Examples of a Truchet tiling containing the words "Bridges" and "2009" using uncolored arcs (on left) and colored tiles (on right). The tiling grid is shown in the last four rows. The baseline of the word "Bridges" is along the line defined by the two line segments outside the grid. The start of the word along the baseline is indicated by the "B" at the bottom of the grid.*

References

[1] C. Browne. Truchet curves and surfaces. *Computers & Graphics*, 32:268–281, 2008.

[2] P. Esperet and D. Girou. Coloriage du pavage dit de Truchet. *Cahiers GUTenberg*, 31:5–18, Dec 1998.

[3] C. A. Pickover. Picturing randomness with Truchet tiles. *J. Rec. Math.*, 21(4):256–259, 1989.

[4] C. S. Smith. The tiling patterns of Sebastien Truchet and the topology of structural hierarchy. *Leonardo*, 20(4):373–385, 1987.

[5] S. Truchet. Memoire sur les combinaisons. *Memoires de l'Academie Royale des Sciences*, pages 363–372, 1704.

Geometry and Geodesy: Estimating the Earth's Circumference with Prospective Elementary Teachers

Sandy Spitzer
Mathematics Department
Towson University
8000 York Road
Towson, MD, 21252, USA
E-mail: sspitzer@towson.edu

Abstract

In order to stimulate interest in geometry, model the use of complex, real-world applications of mathematics for prospective teachers, and draw a connection between mathematics, history, and culture, a lesson was designed in which students replicate the experiment of Eratosthenes of Cyrene (c. 275-194 B.C.) to estimate the circumference of the earth. During the lesson, students measure the angle of inclination of the sun on a date near the spring equinox and build models of the situation using dynamic geometry software. This process helps prospective teachers develop knowledge about modeling situations, measurement, similar figures, and other geometric topics.

Introduction and Context

A central concern for those professors teaching mathematics content courses for prospective elementary school teachers is how to maintain a high level of mathematical inquiry while stimulating students' interest and confidence in doing mathematics. Recent recommendations by policy groups and literature analyses [1, 2] suggest that in these courses, a high priority should be put on developing prospective teachers' conceptual understanding of mathematics and modeling effective methods of mathematics instruction. In particular, the Conference Board of the Mathematics Sciences [1] emphasizes the importance of building visualization and modeling skills and encouraging mathematical communication in geometry courses for prospective teachers.

I designed the "Geometry and Geodesy" lesson in an attempt to fulfill these recommendations in a geometry class for prospective elementary teachers. Prior to the lesson, students had completed a three-week unit on basic geometric constructions and attributes as well as a one-day lesson on similar figures. Throughout the course, students are encouraged to describe geometric situations using increasingly precise language and investigate conjectures beginning with empirical methods (such as by using dynamic geometry software to test a conjecture for many examples) and moving toward deductive proof.

The problem under consideration is one that has interested humans since ancient times: how big is our planet? The study of geodesy (the science of measuring the size and shape of the earth) originated with Aristotle, who gave a value for the size of the earth but did not describe his procedure for obtaining this value [3]. The first scientific approach to finding the circumference of the earth was used by Eratosthenes of Cyrene (c. 275-194 B.C.), whose other cultural contributions include a prime number sieve and the invention of the leap day. According to legend, Eratosthenes knew (perhaps by looking into a well and seeing no shadow) that on the day of the summer equinox, the sun was directly overhead in Syene (present-day Aswan, Egypt). By measuring the angle of elevation of the sun on the same day in Alexandria (roughly on the same longitude as Syene) and calculating the over-land distance between the

two cities, Eratosthenes was able to calculate the circumference of the earth using proportional logic (see Figure 1) [3]. Note the elementary geometrical concepts involved, including the ability to identify corresponding angles on parallel lines, the use of proportional reasoning with similar figures, and the ability to model a real-world situation with a condensed and abstract geometric diagram. These are all goals of conducting the activity with prospective teachers.

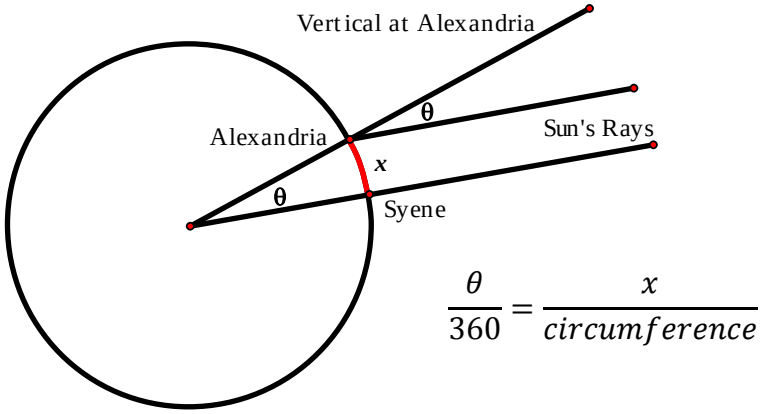

Figure 1: *Eratosthenes' method for calculating Earth's circumference*

Steps of the Activity

In order to carry out the estimation, students are divided into groups, with 3-4 students per group. Each group is given a yardstick and string to measure the length of a shadow. Because these students are unfamiliar with trigonometry, they cannot compute the angle of elevation directly from the measurements. Instead, they use dynamic geometry software to construct a triangle similar to the one formed by the vertical stake and its shadow. They can then use this similar triangle to determine the angle formed. Through an activity sheet, students are then directed to design a model of the earth and sun's rays using dynamic geometry software, determine which angles are congruent, and set up a proportion to solve for the circumference. In order to solve the proportion, students must then use the internet to research the north-south distance between Towson, MD (their location) and the equator. Once the distance is determined, students can solve the proportion. The different groups' estimates are compared and differences explored. This discussion can lead to a rich exploration of the sources of error in a measurement. In this way, students are able to participate in an interactive, engaging lesson which explores an accessible application of geometry to a serious and realistic problem from history.

References

[1] Conference Board of the Mathematical Sciences. *The Mathematical Education of Teachers.* Washington DC: American Mathematical Society and Mathematical Association of America, 2001.

[2] Wilson, Suzanne, Robert Floden, and Joan Ferrini-Mundy. *Teacher preparation research: Current knowledge, gaps, and recommendations.* Seattle: University of Washington, 2001.

[3] Smith, James. *Introduction to Geodesy: The History and Concepts of Modern Geodesy.* Hoboken: Wiley, 1997.

A myriad shades of green

Liselott Flodén, Anders Holmbom, Marianne Olsson, Jens Persson
Department of engineering and sustainable development
Mid Sweden University
Campus Östersund
83125 Östersund, Sweden
E-mail: anders.holmbom@miun.se

Abstract

We discuss the possible application of techniques inspired by the theories of G-convergence and homogenization to understand mixtures of colors and how they appear as observed by the human eye. The ideas are illustrated by pictures describing the equivalent of a convergence process for different kinds of mixtures of colors.

The mathematical theory of homogenization and G-convergence (see [1]) deals with the convergence of balances

$$A^h u^h = f$$

between a source *f*, material properties A^h and a response u^h. When *h* passes to infinity we may reach a limit state described by a similar equation

$$Bu = f$$

where *B* is the effective property of the limit material. This could deal with elasticity or heat conduction in heterogeneous media or flow in porous media so why not colors? Here *f* could be the light illuminating an object, A^h distributions of colors, *B* the "effective color" in the limit and u^h and *u* the way the objects are judged by the human eye, see Figure 1.

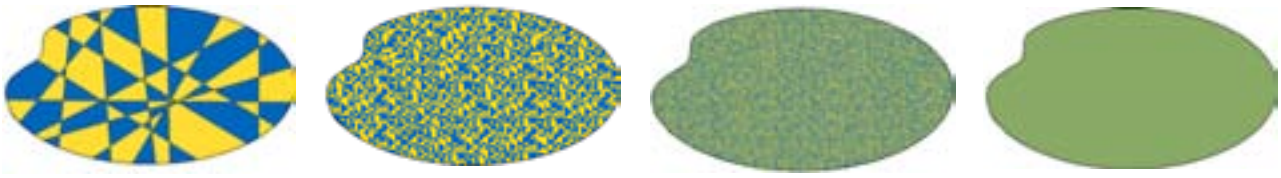

Figure 1: *A sequence of mixtures of colors.*

For periodically arranged materials there are methods to find *B* and hence to compute *u* for any given *f*. Different distributions of materials in the representative unit will result in different limit materials when the size of the repetitive units containing this mixture of materials shrinks to zero and their number hence goes to infinity. The stabilization during this process can be described by the result *u* for the limit equation and a corrector u_1^h as

$$u^h = u + u_1^h$$

Translation to colors *u* is again the limit color as it is observed by the human eye and u_1^h the disturbance of this impression by the heterogeneous pattern of colors that is still possible to view, see Figure 2.
The patterns below have about the same proportions between blue, yellow and white, but the colors are arranged in different ways. We can see that both cases approach a homogeneous green color but is maybe this process faster and passes through other nuances for one of the arrangements than for the other?

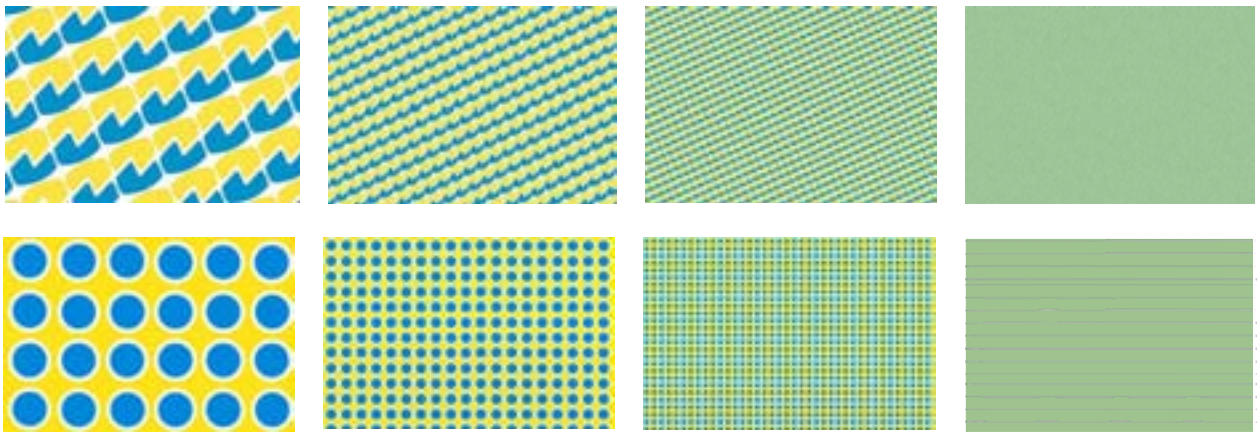

Figure 2: *Two sequences* of *periodically arranged colors.*

We raise the question whether techniques similar to mathematical homogenization can be applied to understand what mixtures of colors in different patterns look like when they appear in front of the human eye. This means that we would like find out if it is possible to find a relationship between this impression and the microstructure of the arrangement of colors that can be subject to computations based on equations formulated on one representative unit in a similar manner as in periodic homogenization. If this is successful the next challenge would be to study the corresponding issues for non-periodic structures.

References

[1] D. Cioranescu and P. Donato, An introduction to homogenization, Oxford Lecture Series in Mathematics and its Applications, 17. The Clarendon Press, Oxford University Press, New York, 1999.

Geometric Transformations in Design Generation

Fatma Mete
Department of Fiber Science & Apparel Design
College of Human Ecology, Cornell University
Ithaca, NY, 14853, USA
E-mail: fm95@cornell.edu

Abstract

We present a method for transforming a simple plane figure or motif into another, which is related to it in a definite way, by applying a group of systematic geometric transformations. The method creates certain classes of star motifs from a basic plane figure. We demonstrate that surface design is an 'atomic' and a 'self-assembly' process, and expansion, figure and motion are the only properties in design which can be directly represented geometrically. By applying a group of fundamental point transformations of the plane, and rearranging the axis of the reflection, we transform a simple figure into a series of complex star motifs. Our ultimate aim is to develop the invariants of design and creative process, and to bring the formal side of art within the purview of mathematics.

Self-Organized Motifs

In order to gain a quantitative and mechanistic understanding of creative design, it is important to understand the recurrence relations and sequential moves in the transformation process. Although the use of symmetry and geometric transformations to make patterns is well-understood and applied to practical applications at a certain extend [2,4], however, there is no established mechanism for creating a range of aesthetic designs and highly extended structures from first 'building blocks'.

Any figure, drawn, painted, printed, embossed, woven, or otherwise executed on a surface, is termed a 'motif', provided there is at least one possible motion which moves the figure, as a whole but not point for point or part for part, back to its initial position [2]. If A and B are two (not necessarily distinct) sets, then a mapping of set A onto set B in which distinct elements of A have distinct images in B will be a transformation (or one-to-one mapping) of A onto B [3]. In three consequent stages, Figures 1, 2 and 3 shows how this method can be applied to construct chains of two dimensional surface designs in which successive designs are derived from the initial figure and earlier ones in the chain. These designs are all composed entirely of one single very basic rectilinear geometric figure and nothing else. A given figure or the first 'atom' is transformed into a new figure by applying certain transformation or symmetry rules. In Figure 1, if O be a fixed point of the plane figure and θ the angle of rotation, we first apply rotation R(O, θ), the figure is rotated in the plane through a certain angle, 180º in this case, about a point, and it turns as a whole to its initial position if we apply an inverse transformation. In this case, the individual points are rotated through this angle about the point. In the second step, we apply mirror superimposed transformation, thus a type of reflection symmetry R(O) about the same point. In order to achieve expansion, in final two steps, we rearrange the point of transformation into another point (O') and apply rotational mirror symmetry R(O', θ), to achieve the final design.

Figure 2 shows the next step and application of first, superimposed mirror transformation R(O') of the final motif of the Stage I, and then rotational transformations R(P, θ), to the resulting motif, where P is another fixed point outside of the final motif. An arrowhead star and cross design is reproduced and rearranged from the building blocks in its whole expanse. Figure 3 shows the application of additional superimposed mirror symmetry R(O') to the final motif of Stage II and then the application of rotational mirror symmetry R(P', θ) to the resulting surface design, where P' is the new fixed point on the plane.

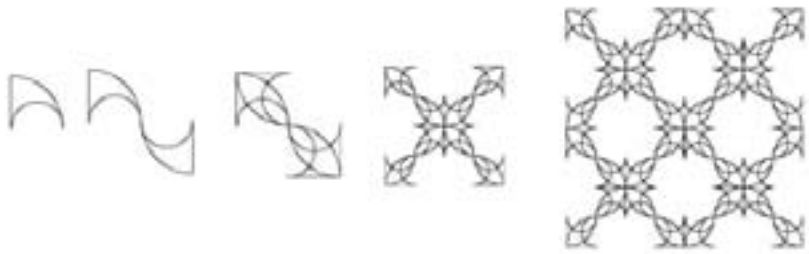

Figure 1: *Geometric transformations in self-organized four-armed arrowhead motif (Stage I)*

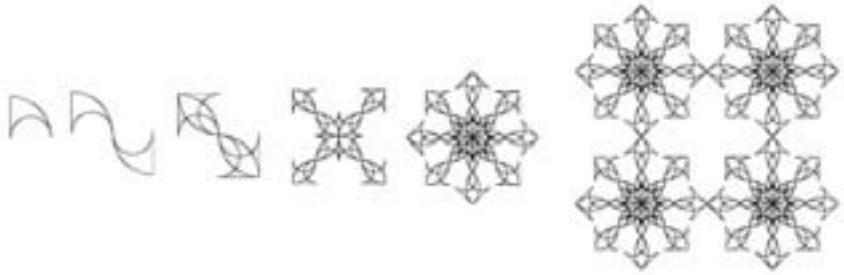

Figure 2: *Geometric transformations in self- organized arrowhead star and cross motif (Stage II)*

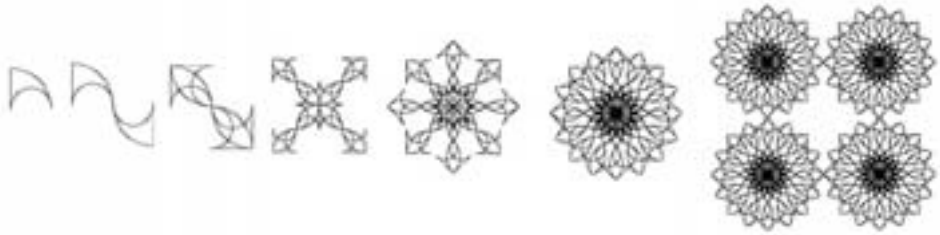

Figure 3: *Geometric transformations in self- organized star motif (Stage III)*

Geometric transformations, as indeed groups and symmetry in mathematics [4], are useful not only for solving problems and discovering new facts, but also in creating new designs [6,8]. This paper shows that the concept of symmetry as understood in light of transformation theory has several advantages in its applicability to many design problems. The process which resembles very closely the self-reproduction of biological molecules also sheds light on uncovering the mathematical mystery in different cultural practices and artifacts[5], such as the geometric decorative motifs in Islamic arts and early Turkish tile and carpet design motifs [1,7].

References

[1] C. Alexander, A Foreshadowing of 21st Century Art: The color and geometry of very early Turkish carpets, Oxford University Press, New York-Oxford, 1993.
[2] G. D. Birkhoff, Aesthetic Measure, Harvard University Press, Cambridge, MA, 1933.
[3] H. W. Eves, A Survey of Geometry, Revised Edition, Allyn and Bacon Inc., Boston, 1972.
[4] D.W. Farmer, Groups and Symmetry: A Guide to Discovering Mathematics, Universities Press, 1998.
[5] P. Gerdes, Geometry from Africa: Mathematical and educational Explorations, The Mathematical Association of America, 1999.
[6] M. Hallett and U. Majer(Eds), D. Hilbert's Lectures on the Foundations of Geometry 1891-1902, Springer, 2003.
[7] C.S. Kaplan and D.H. Salesin, *Islamic Star Patterns in Absolute Geometry,* ACM Transactions on Graphics, Vol. 23 , No.2 , pp: 97 – 119, 2004.
[8] R. Penrose, *The role of aesthetics in pure and applied mathematical research,* 10, pp.266-272, 1974.

The Quinary—Permuting Meaning with Generative Poetry

Brian Evans
Department of Art and Art History
University of Alabama
103 Garland Hall, Box 870270
Tuscaloosa, AL, 35487 USA
E-mail: brian.evans@ua.edu

Abstract

This work is a simple exercise in algorithmic poetry. A generative poetry structure, **the quinary**, is devised and implemented**.** Simple lines and images are ordered randomly within a fixed structure of five groups of five lines (four lines and an image, actually). There's a boy, a girl, aspects of weather and living nature, and random images. Each time the poem is read the lines and images reorder in a random permutation. Meaning slips ever so slightly as haiku meets Hollywood in an Oulipian playground.

Oulipo

This work follows from the ideas of the French group Oulipo, Ouvoir de Littérature Potentielle (Workshop of Potential Literature), an interdisciplinary group started in 1960 and interested in experimental literature and algorithmic process. Raymond Queneau, a founding member, stated their purpose clearly, "What is the objective of our work? To propose new 'structures' to writers, mathematical in nature, or to invent new artificial or mechanical procedures that will contribute to literary activity: props for inspiration as it were, or rather, in a way, aids for creativity [1]."

Queneau himself is known as the author of one of Oulipo's seminal works, *Cent mille milliards de poèmes*, a set of ten sonnets each with the same rhyming scheme and grammatical structure [2]. The poems were printed on cards, with lines cut in strips. This permitted any and all of the 14 sonnet lines from the 10 poems to be freely combined with each other, while each line keeps its place in the overall structure of the sonnet. This allows for 10^{14} different poems! It is estimated that, reading 24 hours a day, it would take 200,000,000 years to read them all.

Generative Poetry

Queneau's poem is an example of generative poetry, where poetic text is data that is organized by some algorithmic process. This process lends itself well to computing, and plenty of examples have appeared over the Internet. One example of note, an inspiration for this project, is *Snaps* by Dirk Hine [3]. *Snaps* combines several short lines of poetry with a large collection of photographs. The user clicks a word and it leads to a new photo and lines. This unfolds as long as the "reader" chooses to participate in the work. The words and images are selected at random and will repeat.

The work *Snaps* exists online as a Javascript program, and it is possible to read and explore the code as freely as one can explore the work itself. This raises questions in regards to digital poetry. Can the code be read as a literary work too? Can an algorithm itself have an aesthetic or artistic/poetic value [4]?

The Quinary

The quinary was created as an experiment in poetry and programming. It is an invented structure (as are all poetic structures). In contrast to the model of *Snaps*, it was decided to fix and close the form, and to focus on permutation rather than combination as the controlling process. Rules were specified as follows:

1) The quinary is defined as a structure of five short poems, each of five lines (or perhaps a combination of text and image, where the image might be substituted for a line).

2) Each line has a general focus, subject or action (in the example the lines include: action of a male, action of a female, an index of organic nature, an index of weather, and a photograph with aspects of nature and man-made objects, but no people).

3) Random permutations of the lines occur, while keeping one of each focus in each poem. (Once a line or image is selected it may not be repeated.)

In this first instance of a quinary, two literary formulas are followed, freely varied, and mixed.[5] First is the cliché Hollywood narrative—boy gets girl, boy loses girl, boy gets girl. The second is the Japanese haiku—two objective descriptions of moments in nature combine to create a Zen-like gestalt. The photographic image provides a link to "new media" and post-modern visual culture. In the spirit of Oulipo, cultural content and mathematical process combine to engage, to experiment, and to play.

```
4.

he wiped the tear secretly

cloudless thunder rumbles

she pretended not to hear

mud dauber buzzsaw
```

Figure 1: *sample page from* quinary #1.

References

[1] Queneau, Raymond, "Potential Literature," *Oulipo, A Primer of Potential Literature*, ed. Marren F. Motte, Jr. 1986, University of Nebraska Press: Lincoln.
[2] Queneau, Raymond, *Cent mille milliards de poèmes,* 1961, Gallimard: Paris.
[3] Hines, Dirk, *Snaps,* Cauldron & Net, Vol. 3, 2001. March 15, 2009 < http://www.studiocleo.com/cauldron/volume3/confluence/dirk_hine/snaps/snaps.html>
[4] Kendall, Robert, "The E-ssence of Literature," presented at *Visionary Landscapes*, Electronic Literature Conference, 2008, Vancouver, WA.
[5] Evans, Brian, *quinary #1,* 2008, March 15, 2009 <http://www.brianevans.net/quinary1>

Spelunking Adventure II: Combining Cyclons

Curtis Palmer
Synergetic Design Inc.
Edmonton, Alberta, Canada
E-mail: clpalmer@telus.net

Abstract

The set of 2D spline curves named 'cyclons' by Palmer [1] that are derived from polyhedra are used in combination to produce more strangely attractive curves for use in print and graphic animation.

Introduction: As reported at Bridges 2005, I used Rhinoceros software to construct a database of polyhedra within unit radius circumspheres. These are projected to the plane and exported to Corel Draw. Here the hard edged linear maps are 'converted' to a set of spline curves, '**cyclons**' that are useful in design applications. Some additive properties of these cyclons are explored here.

Four methods for combining cyclons:

1) **Spins**: Copies of a cyclon are circularly arrayed with rotation angle equal to S/n, where S is the cyclic group angle (e.g. 120 degrees or 2/3 pi) and n is prime so as to avoid duplication.

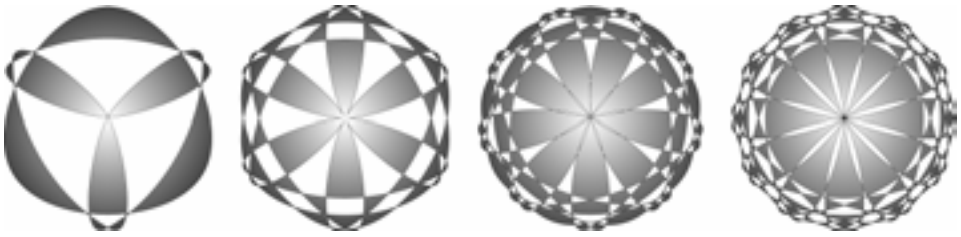

Figure 1: *Tetrahedral cyclon with Spins (n= 2, 3, 5)*

2) **Like with Similar**: Cyclons are combined with other members of their symmetry groups.

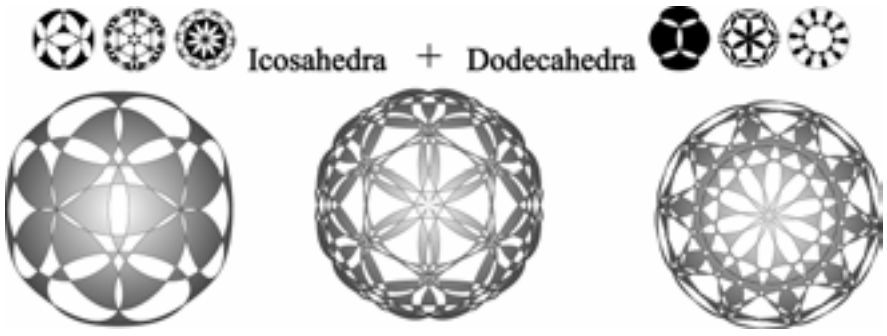

Figure 2: *Pas de Dual.*

3) **Scale**: Cyclons derived from polyhedra modeled with variable circumsphere radii are combined. In the example, radii for five related polyhedra were chosen such that their relative volumes are proportioned (1, 3, 4, 6, and 20).

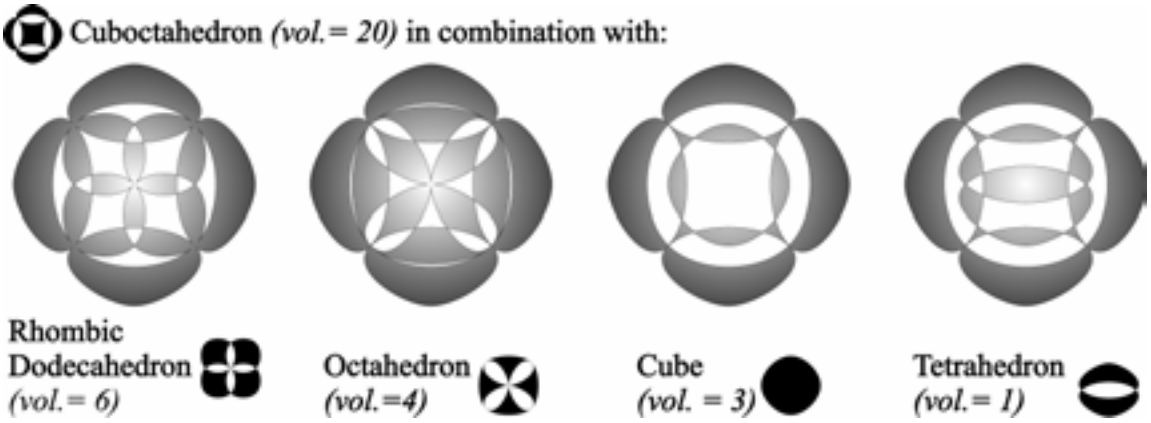

Figure 3: *Cyclons from pairs of polyhedra scaled to rational tetrahedral volumes [2].*

4) **Close Pack**: Space frame arrays of polyhedra are modeled in Rhinoceros and their cyclons are produced.

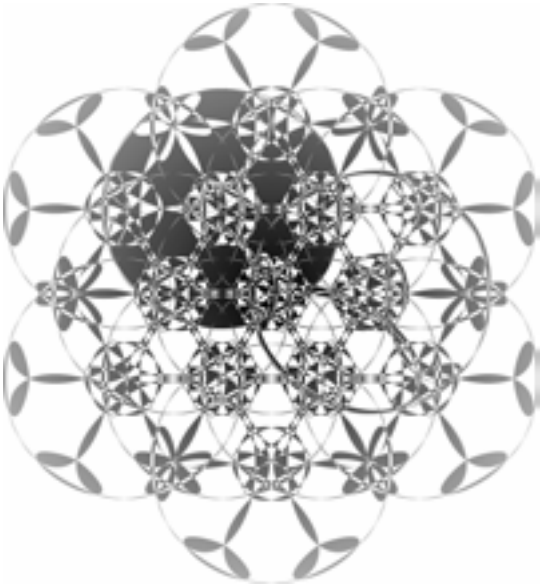

Figure 4: *Close Packed Truncated Cubes.*

Conclusion: These methods of cyclon combinatorics have provided an endless variety of pattern to pique the author's artistic and pedagogic curiosity and drive further spelunking of the 'spline mine'. "What would that look like?"

References

[1] C. L. Palmer, *Digitally Spelunking the Spline Mine,* Renaissance Banff, pp. 309-312. 2005.
[2] R. B. Fuller *Synergetics*, sec. 454.01, Macmillan Publishing 1975.

Binary Based Fresco Restoration*

Wolfgang Baatz
Academy of Fine Arts Vienna,
Institute for Conservation and Restauration,
Schillerplatz 3,
A-1010 Vienna.
Email: w.Baatz@akbild.ac.at

Massimo Fornasier†
RICAM,
Austrian Academy of Sciences,
Altenbergerstrasse 69,
A-4040 Linz.
Email: massimo.fornasier@oeaw.ac.at

Peter A. Markowich‡
DAMTP, Centre for Mathematical Sciences,
Wilberforce Road,
Cambridge CB3 0WA, UK.
Email: P.A.Markowich@damtp.cam.ac.uk

Carola-Bibiane Schönlieb§
DAMTP, Centre for Mathematical Sciences,
Wilberforce Road,
Cambridge CB3 0WA, UK.
Email: c.b.s.schonlieb@damtp.cam.ac.uk

The Neidhart frescoes (located in Tuchlauben 19, 1010 Vienna) from the 14th century are depicting a cycle of songs of the 13th century minnesinger Neidhart von Reuental. The picture on the left shows a part of the Neidhart frescoes. The white holes in the fresco are due to the wall which covered the fresco until a few years ago. They arised when the wall was removed.

In the following we want to apply digital restoration (inpainting) methods to these frescoes. Thereby the main challenge is to capture the structures in the preserved parts of the fresco and transport them into the damaged parts continuously. Due to their great age and almost 600 years of living by owners and tenants in the apartment, saturation, hue and contrast quality of the colors in the frescoes suffered. Digital grayvalue, i.e., color interpolation, in the damaged parts of the fresco therefore demands sophisticated algorithms taking these lacks into account.

In our previous Bridges paper [1] we presented two inpainting methods based on partial differential equations (PDEs) and their application to the reconstruction of the Neidhart frescoes. Because of the lack of space in this paper we refer to Burger et al. [2] for a motivation of the PDE approach and relevant references. The first method in [1] constitutes in a modified Cahn-Hilliard equation for the restoration of the binary structures of the frescoes [2, 3, 4], see Figure 1 for a specific example. The second method is a generalization of this binary inpainting approach for grayvalue images and is called TV-H^{-1} inpainting [2]. The grayvalue approach produced fairly good results for the inpainting of homogeneous areas in the frescoes, but not very satisfying results for the continuation of edges into the holes [1].

*This publication is based on work supported by Award No. KUK-I1-007-43, made by King Abdullah University of Science and Technology (KAUST).

†M. Fornasier acknowledges the financial support provided by the European Union's Human Potential Programme under contract MOIF-CT-2006-039438.

‡P. A. Markowich also acknowledges support from the Royal Society as Wolfson Research Merit Award Holder.

§is partially supported by the project WWTF Five senses-Call 2006, *Mathematical Methods for Image Analysis and Processing in the Visual Arts* project nr. CI06 003, by the FFG project *Erarbeitung neuer Algorithmen zum Image Inpainting* project nr. 813610 and by KAUST (King Abdullah University of Science and Technology).

Figure 1: from left to right: Part of the fresco; binary selection; binarized selection of the fresco; initial condition for the inpainting algorithm where the inpainting region is marked with a gray rectangle; Cahn-Hilliard inpainting result after 200 timesteps with a large diffusion coefficient; Cahn-Hilliard inpainting result after additional 800 timesteps with less diffusion for sharpening the edges

In this work we propose a combined strategy for the restoration of the frescoes, which we call *binary based restoration* method. This method is motivated by the previous work of Fornasier [5], and Fornasier and March [6]. More precisely we propose an inpainting model for grayvalue images which uses a given (or previously obtained) binary structure inside the missing domain D. Thereby the binary structure of the image is usually obtained by a preprocessing step with Cahn-Hilliard inpainting [3, 4] and Figure 1. This new approach is described in the following paragraph and in Figure 2.

Let $f \in L^2(\Omega)$ be a given image which is a grayvalue image in $\Omega \setminus D$ and binary in D. We want to recover the grayvalue information in D based on the binary structure given by f by means of the following minimization problem:

$$u^* = \operatorname{argmin}\{ \quad \tfrac{\mu}{2}\int_{\Omega\setminus D} |u(x)-f(x)|^2\,dx + \tfrac{\lambda}{2}\int_D |\mathscr{L}_{bin}(u(x))-f(x)|^2\,dx + |Du|(\Omega),\ u\in L^2(\Omega,\mathbb{R}_+)\}\,.$$

In our case $\mathscr{L}_{bin}$ is a transformation which projects the grayvalue range of u, e.g., $[0,1]$, on the binary range $\{0,1\}$. For our purpose $\mathscr{L}_{bin}$ is modeled by a relaxed version of the Heaviside function depending on a (presumably) given threshold τ.

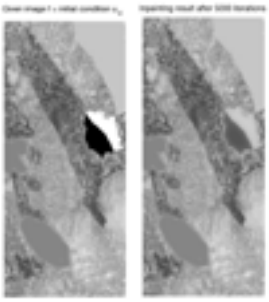

Figure 2: Binary based grayvalue inpainting: (l.) initial condition; (r.) inpainting result with $\mu = \lambda = 10^2$ and 5000 iterations.

References

[1] W. Baatz, M. Fornasier, P. Markowich, and C.-B. Schönlieb, *Inpainting of ancient austrian frescoes*, Conference Proceedings of Bridges 2008, Leeuwarden 2008, pp. 150-156.

[2] M. Burger, L. He, C. Schönlieb, *Cahn-Hilliard inpainting and a generalization for grayvalue images*, UCLA CAM Report 08-41, June 2008.

[3] A. Bertozzi, S. Esedoglu, and A. Gillette, *Inpainting of Binary Images Using the Cahn-Hilliard Equation*, IEEE Trans. Image Proc. 16(1) pp. 285-291, 2007.

[4] A. Bertozzi, S. Esedoglu, and A. Gillette, *Analysis of a two-scale Cahn-Hilliard model for image inpainting*, Multiscale Modeling and Simulation, vol. 6, no. 3, pages 913-936, 2007.

[5] M. Fornasier, *Nonlinear projection recovery in digital inpainting for color image restoration*, J. Math. Imaging Vis. Vol. 24, No. 3, pp. 359-373, 2006.

[6] M. Fornasier, and R. March, *Restoration of color images by vector valued BV functions and variational calculus*, SIAM J. Appl. Math., Vol. 68 No. 2, pp. 437-460, 2007.

[7] G. Gilboa, S. Osher, *Nonlocal operators with applications to image processing*, UCLA-CAM Report 07-23, July 2007.

Plane, Space, Cubism and Perceptual Displacement in 3D Design

Joel Varland
Foundations and Sculpture Departments
Savannah College of Art and Design
342 Bull St
Savannah GA 31404, USA
Email: jnvarlan@scad.edu

Planar construction in design integrates aesthetics, spatial choreography, structural integrity, folded proportions and relational geometry. As such, I have developed a five-tiered exploration of planes and space to explore these relationships. Specifically examined is the work of one multi-tiered studio project in which students approach, synthesize and construct a variety of complex planar and spatial exercises and fold them into one final sculpture/construction.

Planar construction is the process by which any form is expressed through planes. The number, shape, character and spatial relationships of the planes are the focus of this project. The formation of this project reflects research the I have conducted in Japan on the nature of folded space in everything from the folding of the Kimono around a body to the folding of Shoji screens to confine and define a space. It also reflects the work of Picasso, Braque, Tatlin and how their explorations grew into modernism and the international style. As such, planes can be engaged as a structural system, proportioning system, measuring system, folding system, visual rhythm system, polyglot rhythmic system, boundary/border/barrier, tool of analysis, pathway for the eye and choreographer of space.

Before addressing the five stages of the planar analysis, students engage in three preliminary exercises. The first, based on the golden section, addresses creating a freestanding structure which both contains and defines space. For this exercises the design operations are limited to folds, tabs and cuts in which no material may be removed. The second exercise is based on the Japanese proportioning system exemplified by the Tatami mat. The guidelines of this exercise are similar to the previous one except all cuts and folds are placed within the formalist grid. The two classical systems are discussed, contrasted and explored in relationship to the exercise. The third exercise consists of constructing five platonic volumes/forms. Once the exercises are constructed, students deconstruct and reconstruct them using deconstructivist techniques to create a sculpture. A discussion of Plato and Derrida follows to highlight their ideas and their relationship to design. Once students have completed the initial exercises and have been exposed to several disparate aesthetics and notions of form, they are ready to proceed to the project. The objective of these preparatory exercises and ideas is to introduce creating a volume through folding a 2D plane. It is also about initiating the play between volume and void and the continuum of inside and outside spaces. Finally, it is about introducing some rudimentary philosophical structures of which this project engages.

Upon completing the exploratory exercises, students enter into a five-stage process by which they consider the progressively complex interaction of planes and space within a form. The stages and concepts that I have organized to guide students through the process engage an innovative use of planes and spatial expression. The first stage, Encapsulation, is the shielding of a volume with a skin of planes. This is conceptually the most concrete stage and only discussed in preparation for the next stage. Secondly, Rational Ribbed Construction, utilizes an internal rib structure in which the edges of the planes define the external contours of the form. The geometry is perpendicular, hence the label rational. The third stage, Organic Ribbed Construction, utilizes an internal ribbed armature but the planes are assembled and organized in a non-cartesian, fluid and

dynamic mode. The fourth stage, Cubism, utilizes planes as spatial containers and defines a form through the interplay of confined and defined space. The final stage is a hybrid of the previous stages in which multiple creative operations are utilized to engage planes thoughtfully. The visual and spatial complexity of the stages is both additive and increasingly difficult. After students have prepared maquettes of the last four stages, they select one mode for a final project that will challenge their design growth.

Demonstrated through one studio project are a variety of applications of planes, use of proportioning systems and utilization of design operations as an innovative and rigorous approach to design. Also examined is the perception of space in relationship to math, design, art and science. Illustrated is how planes and space can be seen, understood, developed and integrated in a comprehensive studio.

Rational Rib Construction

Organic Rib Construction

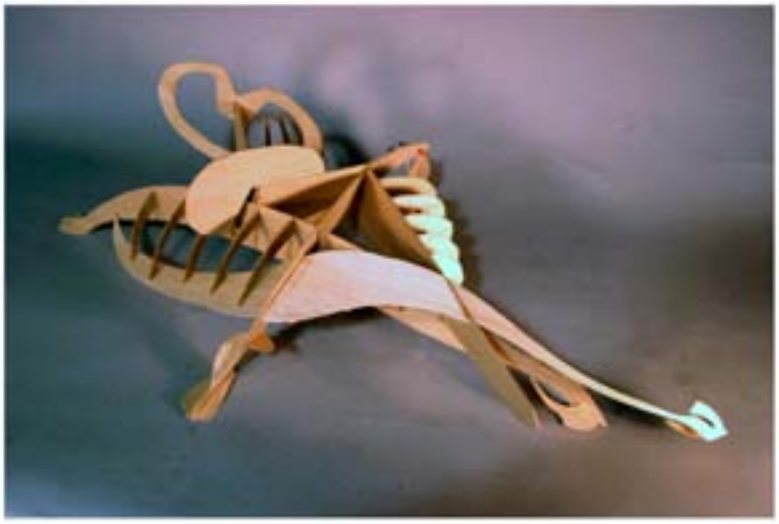

Hybrid Rib Construction

Cubism

Mathematical Classroom Quilts

Elaine Krajenke Ellison
Retired Mathematics Teacher
5739 Wilena Place
Sarasota, Florida 34238
E-mail: eellisonelaine@yahoo.com

Abstract

In an effort to create a visual and historical basis to my classroom instruction, I began quilting high school mathematics topics in the early 1980's. The visual approach to teaching a lesson was successful in that the quilts engaged the students immediately. Students' motivation and enjoyment of mathematics were evident in their enthusiasm for the topic being studied. Cultural and historical connections evolved with the story of each quilt.

Introduction

During the early years of generating classroom quilts, two authors inspired me: Dan Pedoe [13] and Thomas Banchoff [1]. I began to think that a whole new way of teaching mathematics would be possible. Could I use color, form, composition, perspective and formulas to interest students in mathematics? Banchoff and Pedoe inspired me to show the beauty in mathematics.

As the number of quilts grew and lesson plans to go with the quilts were written, I found that other teachers were interested in learning about my unique classroom. Cloth quilts inspired paper quilts and mathematical placemats. My classroom was evolving creatively!

Most recently, I have taken the 39 mathematical quilts and organized them into a PowerPoint presentation that many groups have enjoyed over the last few years. The quilts are organized historically. Each quilt has been used in the high school classroom or could be used in the high school classroom. There is no need to limit the use of these quilts to the high school level.

Topics in the PowerPoint of the Mathematical Quilts

1. Golden Rectangle—around 500 B.C.E.
2. Golden Rectangle at Givemy
3. Fiddle Dee Dee Golden Rectangle #3
4. Labyrinth at Chartres Cathedral—Golden Rectangle
5. Blue-Breasted Hummingbird—Golden Rectangle
6. The Sacred Cut-around 500 B.C.E.
7. The Lutes of Pythagoras—582–502 B.C.E.
8. Spiraling Pythagorean Triples
9. My Spiraling Pythagorean Triples
10. Mathematical Harmony—500 B.C.E.
11. The Wheel of Theodorus—400 B.C.E.
12. The Six Trigonometric Functions—400 B.C.E.
13. The Parabola—375–325 B.C.E.

14. The Hyperbola and Ellipse—375–325 B.C.E.
15. Spiraling Squares—300 B.C.E.
16. Fibonacci x 3—1175–1250
17. Leonardo's Dessert no Pi—1452–1519
18. Leonardo's Claw
19. Lucy's Quilt of Leonardo
20. San Gaku—1603–1867
21. Pascal's Surprise—1623–1662
22. Pascal's Pumpkin
23. Mascheroni Cardioid—1797
24. Poincaré Plane—1854–1912
25. Koch Curve—1870–1924
26. Sierpinski's Gasket—1882–1969
27. Sierpinski's Carpet
28. Indiana Puzzle—Snail's Trail
29. Clifford Torus—1845–1879
30. Tessellation
31. Tessellation
32. Worlds of Geometry—1990—The Geometry Center
33. Orthic Triangles—talk by Douglas Hofstadter at Indiana University
34. Graeco-Latin Squares and Sudoku
35. Fabulous Fibonacci Flowers
36. The Music of the Genes—2007
37. Spiraling Spidrons—2007
38. Buckyballs and Bubbles—2008

References

[1] Banchoff, Thomas F. *Beyond the third Dimension-Geometry, Computer Graphics, and Higher Dimensions*. New York: W. H. Freeman and Co., 1990.

[2] Boles, Martha, and Rochelle Newman. *Universal Patterns*, Books 1 and 2. Bradford, MA: Pythagorean Press, 1990, 1992.

[3] Boulger, William. "Pythagoras Meets Fibonacci." Pp. 277–82 in *The Mathematics Teacher*. Reston, VA: NCTM Publications, 1989.

[4] Cook, Theodore A. *The Curves of Life*. New York: Dover, 1979.

[5] Emmer, Michele, ed. *The Visual Mind: Art and Mathematics*. Cambridge, Mass.: The MIT Press, 1993.

[6] Eves, Howard. *An Introduction to the History of Mathematics*, 4th ed. New York: Holt, Rinehart & Winston, 1976.

[7] Frederickson, Greg N. *Dissections Plane and Fancy*. Cambridge, U.K.: Cambridge University Press, 1997.

[8] Gleick, James. *Chaos: Making a New Science*. New York: Penguin, 1987.

[9] Huntley, H. E. *The Divine Proportion*. New York: Dover, 1970.

[10] Kappraff, Jay. *Connections: The Geometric Bridges between Art and Science*. McGraw-Hill, Inc., 1991.

[11] Mathematical Association of America. *Mathematics Magazine*, Vol 62, No.3, June 1989.

[12] Pappas, Theoni. *Mathematics Appreciation*. San Carlos, CA.: WideWorld Publishing/Tetra, 1986.

[13] Pedoe, Dan. *Geometry and the Visual Arts*. New York: Dover, 1976.

[14] Posamentier, Alfred. S., and William Wernick. *Advanced Geometric Constructions*. Palo Alto, Ca.: Dale Seymour Publications, 1973.

[15] Seymour, Dale. *Visual Patterns in Pascal's Triangle*. Palo alto, Ca. : Dale Seymour Publications, 1986.

[16] Stevens, Peter S. *Patterns in Nature*. Boston: Little, Brown, 1974.

[17] Wills, Herbert III. *Leonardo's Dessert—No Pi*. Reston, Va.: NCTM Publications, 1985.

Mathematical Iconography in Gaudi's Cosmos

Stephen Luecking
College of Computing and Digital Media
DePaul University
243 South Wabash
Chicago, Il 60604
E-mail: sluecking@cdm.depaul.edu

Abstract

The architect Antonio Gaudi created visionary imagery from often profoundly mathematical forms. A sculpture in the garden of his home in Parc Guell ,Barcelona, embeds the Platonic solids and uses these to represent the heavens in the same cosmographic spirit as that of Johannes Kepler in his Harmonices Mundi.

In the garden of Antonio Gaudi's home in Barcelona's Parc Guell stands a sculpture by the famed architect entitled "Cosmos". Actually a copy of an ornament cresting a spire on his unfinished temple, the grand Sangrada Familia, it nevertheless carries all the spatial integrity and thematic clarity of an exceptional stand-alone sculpture. A key ingredient is Gaudi's masterful inclusion of significant mathematical forms, especially those introduced by Johannes Kepler in his 1619 text Harmonices Mundi.

Figure 1: *Antonio Gaudi, Cosmos, ferro-concrete, ca.1907.* **Figure 2:** *detail of Cosmos.*

The sculpture (Figures 1 and 2) presents as a concrete nebula embedded with stars out of which a hawk-like bird streaks earthward. The stars radiate three-dimensionally with various numbers of points spiking outward. About half of the spikes remain embedded in the cloud with the others bristling outward. A closer inspection reveals that these stars possess 4, 6, 8, 12, and 20 points respectively and that they are actually stellated versions of the five Platonic solids.

The star-studded nebula clearly supports the title "Cosmos", but the integration of the Platonic solids greatly extends the sculpture's cosmographic complexity. Historically, the solids have served as insignia

of four classical elements of earth, air, fire and water, plus the fifth element – the quintessence – that to the ancients formed the crystalline substrate of the celestial spheres (Figure 3, lower right.) In this symbolic scheme the hexahedron, octahedron, tetrahedron and icosahedron reference the first four elements respectively, while the dodecahedron signifies the quintessence. A second cosmographic allusion is Kepler's "discovery" that the spheres of the planetary orbits have their proportions determined by these same five polyhedrons (Figure 4.) Gaudi's forms also reference the stellations described in Kepler's Harmonices Mundi of 1619.

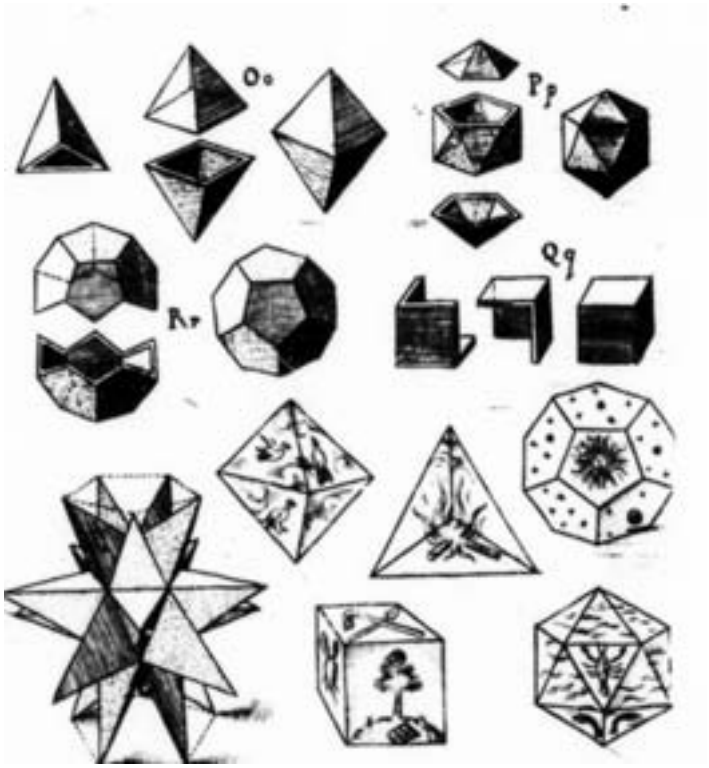

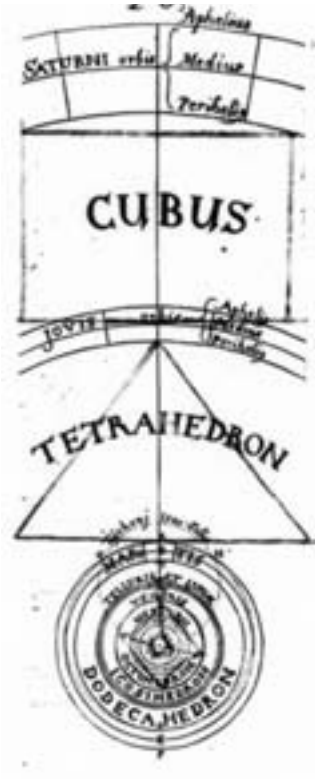

Figure 3: *Johannes Kepler*, *Harmonices Mundi , 1618, detail from page 54.* **Figure 4:** *detail of page 186*

In keeping with the hierarchy implicit in this scheme a single dodecahedral star bobs at the top of the cloud (Figure 2.) Distributed over the cloud below the dodecahedron are two copies each of the hexahedron, the octahedron and the icosahedron, as well as three tetrahedrons. Gaudi's starry polyhedrons are structured so that the point of each ray of the stars corresponds to a vertex of a polyhedron. Given that a dodecahedron has 20 vertices, for example, his dodecahedral star has 20 rays. Technically, the dodecahedron is then the stellated version of its dual, the icosahedron. However, since the star is half submerged in the cloud and its treatment is somewhat loose and organic, it reads primarily as a dodecahedron with each grouping of five points demarcating a pentagon (see stellation in figure 3, lower left.) Similarly, his hexahedral star boasts 8 rays, one for each vertex of the hexahedron. In effect the geometry of each solid is defined by stellations of their duals.

In "Cosmos" Gaudi has orchestrated organic, physical, astronomic, religious and mathematical emblems of the heavens into a churning, multi-layered of faith and nature. In order to do so he needed to understand both the geometry and symbolic history of the Platonic solids, especially as put forth by Kepler.

Chaos – The Movie

Susan Happersett
Jersey City, NJ, USA
E-mail: fibonaccisusan@yahoo.com
Web site: www.happersett.com

It is my personal mission as an artist to illuminate the intrinsic beauty of mathematics in a purely aesthetic realm. Translating mathematical subject matter to the picture plane of my drawings, I strive to enable viewers to appreciate this aesthetic, regardless of their mathematical background. I express the grace and beauty I find in mathematics through symmetries, patterns and proportions in my art. Many of my drawings are related to growth patterns such as the Fibonacci sequence and binary growth. I begin my work process by creating a plan or an algorithm. I make all of the decisions for the work beforehand and make a detailed plan in a large spiral drawing tablet that I refer to as my plan book. After I write out all of the specifications, I generate the actual drawing by hand using the rules from the plan. Through my drawings I hope to express both the aesthetics of my mathematical subject matter, as well as the aesthetics of the process of algorithmic generation.

In the past few years I have become interested in generating drawings using fractal forms based on the repetition of similar shapes. I begin with a largest instance of a shape and incorporate copies scaled by powers of ½. I developed a drawing based on the four quadrants of the Cartesian coordinate system. Each drawing begins with 8 spokes. The line segments fall on the coordinate axes and the lines y=x and y=-x. Once I have drawn the initial shape, each spoke becomes the starting point for a new 8-spoke shape in which the line segments are ½ as long as the original spokes. Then those 64 spokes become the starting point for 8-spoke figures with line segments ¼ the length of the first line segments. Next, the 512 spokes each become the bases for an 8-spoke shape with line segments 1/8 the length of the original spokes. This process creates a circular fractal network of lines. While producing these drawings, I have developed a type of mantra to remember where I am in the drawing. I need to keep count and this becomes quite complicated and rhythmic especially when I reach the third iteration.

Mathematics and art both enable humans to better understand the world around them by uncovering patterns and structures. Chaos Theory is one of the topics in mathematics that, I feel, particularly throws light on the intricacies of the human condition. Chaos Theory shows that even within apparent disorder there can often be found both order and structure. My investigation took me to the earliest ideas on Chaos Theory. In 1961 Edward Lorenz inadvertently discovered the phenomenon of sensitive dependence on initial conditions by noticing the effect of rounding off decimals had in a computer-generated sequence of calculations for weather prediction. This event marked the (re-) discovery of what is now commonly known as Chaos Theory. I decided to visually interpret this phenomenon in my drawings, by using my basic 8-spoke pattern and continuing with multiple iterations using stencils with a small margin of error. The errors accumulate to create these cloud-like, chaos-derived drawings. If the viewer spends a few moments gazing into what at first appears to be a chaotic cloud they will begin to see the pattern of the fractals develop. There is a hidden structure to these drawings, as well as a sense of growth through time. This process of layering iteration

on top of iteration takes weeks of work and through the process the drawings go through interesting changes and developments. I wanted a way to incorporate this sense of time and change into my art. It was time to make a movie.

I started with a fresh large black sheet of paper. Then I installed a digital camera over my drawing table. I began my drawing process, but after each line I took a still shot of the drawing. I continued this process over months. I wanted the movie to have an organic handmade feeling to it so I made a number of changes throughout the process. The frequency with which I photographed the drawing fluctuated. Sometimes I would take a picture after each line, sometimes I would complete a small cycle of lines before taking a picture. This change produced skips and jumps in the rhythm. Occasionally, I moved the camera closer to or farther away from the drawing. I also included myself in the photos as the generating mechanism: there are a few shots where you can see my hands. At a point where the drawing was getting quite complicated, I adjusted the camera so you could see my feet coming and going from view: the drawing was becoming a dance. Leaning over to draw and then pulling away to take a picture created a very physical element to this work and I wanted to express that physicality. Thousands of still digital photographs were taken during the drawing process. These photographs were put into consecutive order and then repeated in reverse to create the sense of both growth and decay. The edited product is a 6 minute video titled “Chaos Night”.

I knew from the beginning of the process that I would add music into the final production. I contacted composer Max Schreier, and discussed the structure and mathematics I wanted incorporated into the music. I wanted to make sure the number 8 played a major role in the structure of the music to mirror the 8 spokes of the drawing. Max agreed to write and perform a 6 minute composition based on these specifications. Influenced by Arnold Schoenberg, he based the music on a series of 8 sequential notes. While the bottom voice of the organ plays a drawn out rhythm associated with the first iteration of the drawing, the violin accelerates with the increased speed of the smaller iterations. The right hand of the organ creates small disturbances, each catalyzed by the random insertions of hands, feet and rulers in the video.

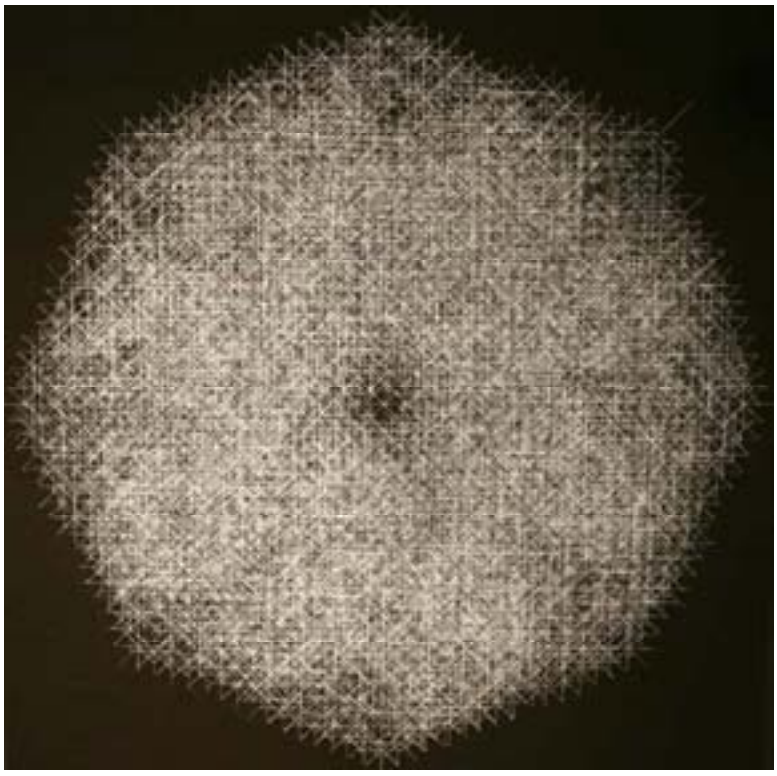

Figure 1: *Drawing for Chaos Night video*

The Frustrated Mathematician: A Call to Artists

Michael Frantz
Department of Mathematics, Physics, and Computer Science
University of La Verne
1950 3rd Street
La Verne, CA 91750, USA
E-mail: frantzm@ulv.edu

Abstract

One source of frustration for some mathematicians is their inability to express sophisticated and beautiful ideas in a language more accessible to the broader community. Five examples of mathematical concepts are provided which lend themselves to artistic interpretation and inspiration, in areas ranging from precalculus to real analysis and differential equations, along with capsule descriptions of the mathematical processes and thumbnail graphics to help illustrate ideas difficult to capture in equations alone. The hope is that these ideas could serve to inspire artists and musicians who are more capable than most mathematicians in alternative forms of expression.

Five Favorite Frustrations

Introduction. Over the past eight years, an artist colleague (Keith Lord) has team-taught an advanced interdisciplinary general education course with me, entitled "The Mysterious Dance of Art, Mathematics, and Music", which we collaborated on developing. We have eight times now experienced anew the joy, wonder, and fascination of learning about the content, methods, and ways of knowing in our disciplines. As wonderful as this experience has been, one source of frustration has been my attendance at Bridges conferences where I have realized that my utter and complete lack of competence in all things artistic prevents me from realizing in any artistic medium ideas inspired by mathematical concepts or problems encountered in the course of earning my livelihood as a mathematician. One possible solution to quelling this frustration might be to share some of those ideas with artists who have an interest in communicating and giving expressive form to mathematical ideas, and what better way to accomplish that than by sharing these thoughts with the mathematically inclined artists and musicians at a Bridges conference? Very few artists and musicians have formal advanced training in mathematics (think Helaman Ferguson as the canonical counterexample), but there is a large set of artists living in the complement of my space, those people who are thoroughly versed in some mode of artistic expression but who search for nuggets of mathematical inspiration and understanding to push their creativity toward new boundaries. It is to these folks that I address this paper.

To Infinity and Beyond. I first encountered the system of nonlinear ordinary differential equations $\frac{dx}{dt} = y - x\sqrt{x^2+y^2}\sin\frac{1}{\sqrt{x^2+y^2}}$, $\frac{dy}{dt} = -x - y\sqrt{x^2+y^2}\sin\frac{1}{\sqrt{x^2+y^2}}$, as a graduate student over three decades ago, but I still recall the wonder with which I regarded the solution curves and limit cycles as described on the chalkboard by my professor (since it was not at all an easy task back then to actually produce a high-resolution graphic plot of such a solution). The solution consists of an infinite number of limit cycle circles of radius $1/(n\pi)$, where the space between any two limit cycles is completely filled by an infinite number of non-intersecting spirals which both spiral inward toward the next smallest limit cycle and outward toward the next largest limit cycle (see Fig. 1). This is one of the most amazing visual expressions of infinity that I have ever encountered, and certainly deserves a more creative form of expression than simple output from a computer plotter.

Bridge to Infinity. A standard problem in many calculus books illustrates the extremely slow yet inexorable growth of the harmonic series $1+\frac{1}{2}+\frac{1}{3}+\cdots$ toward infinity. The problem is to stack as many blocks on top of each other so as to produce the largest overhang possible without the stack of blocks tumbling down. The maximum overhang is achieved when for n stacked blocks, the k[th] block extends past the block below it by $\frac{1}{2k}$ blocks for a total overhang of $\frac{1}{2}+\frac{1}{4}+\frac{1}{6}+\cdots+\frac{1}{2(n-1)}$ blocks, which of course approaches infinity in the limit, thus permitting extensions of any length desired (see Fig. 2). This appears to be a prime candidate for some type of creative sculpture or painting.

Lunar Origami. This example was born in a general education mathematics course, when to illustrate the rapid growth of the exponential function $f(x)=2^x$, I offered a $20 bill to any student who could fold a sheet of notebook paper in half, then in half again perpendicular to the original fold, and so on, for a total of eight folds. To illustrate just how quickly that function grows, on the spur of the moment I gave them a problem for extra credit to determine the exact number of folds in a piece of notebook paper, which if they could be carried out, would produce a thickness of paper which would reach from the earth to the moon. Assuming a ream of 500 sheets of paper has thickness two inches, the answer is just 42 folds, and a "Folding to the Moon" painting or sculpture conceptualizing these 42 folds in some way seems natural.

Noncommutative Sums. The lecture at my very first job interview provided a demonstration that the equality $\sum_{m=1}^{M}\sum_{n=1}^{N} f(m,n)=\sum_{n=1}^{N}\sum_{m=1}^{M} f(m,n)$ does not necessarily hold when $M=N=\infty$, a rather counterintuitive and surprising result. Divide the surface area of a cylinder into m bands of equal width, with each band broken down into n congruent isosceles triangles, then sum the area of the triangles and let the number of bands (m) and the number of triangles per band (n) approach infinity in different orders. The result will be two very different answers for the surface area (see Fig. 3).

Fubini Vindicated. The final example illustrates that exchanging the order of integration in a double integral may resulting in different answers if conditions necessary for applying Fubini's Theorem are not satisfied. If we define a function $f(x,y)=a_{ij}$ on the rectangle $b_{ij}=\left(\frac{1}{i+1},\frac{1}{i}\right)\times\left(\frac{1}{j+1},\frac{1}{j}\right)$ where $a_{ij}=\frac{1}{2^{i-j}}$ if $i>j, a_{ij}=-1$ if $i=j$, and $a_{ij}=0$ if $i<j$, then interchanging the order of integration yields $\int_0^1\int_0^1 f(x,y)\,dxdy=0\neq -2=\int_0^1\int_0^1 f(x,y)\,dydx$. (See Fig. 4 for a rough illustration of the function $f(x,y)$.) The notion that summing the heights of columns in two different directions produces different results is an idea begging for an artist to approach it with more finely tuned visual aesthetics.

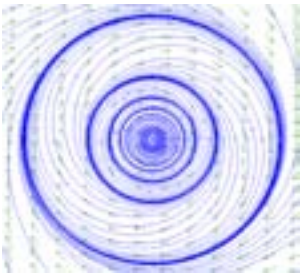

Figure 1: *Circles and spirals*

Figure 2: Bridge to infinity

Figure 3: S*ums*

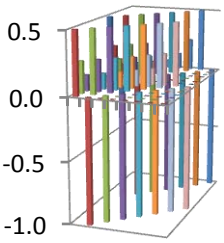

Figure 4: *Fubini*

Conclusion. It is the hope of this author that these examples will serve to pollinate the minds of artists and musicians with mathematical notions which in some way may spawn creative reflections on significant mathematical concepts, and ultimately lead to artistic works which might otherwise not receive the benefit of the perspectives and expressionist forms of painters, sculptors, weavers, musicians, and other artists.

An Optical Demonstration of Fractal Geometry

B C Scannell[†], B Van Dusen and R P Taylor
Department of Physics
University of Oregon
1274 University of Oregon
Eugene, Or 97403-1274
[†]E-mail: billy@physics.uoregon.edu

Abstract

We have built a Sinai cube to illustrate and investigate the scaling properties that result by iterating chaotic trajectories into a well ordered system. We allow red, green and blue light to reflect off a mirrored sphere, which is contained in an otherwise, closed mirrored cube. The resulting images are modeled by ray tracing procedures and both sets of images undergo fractal analysis. We offer this as a novel demonstration of fractal geometry, utilizing the aesthetic appeal of these images to motivate an intuitive understanding of the resulting scaling plots and associated fractal dimensions.

It is rather simple to create a fractal object such as the Sierpinski triangle by using a mathematical prescription or an iterated function. Since fractal geometry offers a useful description of a wide range of physical phenomena, It is not surprising that a physical process such as light rays scattering off of curved surfaces would produce similarly complex images. Intrigued by the apparatus described by Sweet *et al.,*[1] and others [2], we first built a light scattering system consisting of four reflective spheres stacked in a pyramid formation. Expanding on this we built a "Sinai Cube" [3]which offers an analog of an infinite set of stacked spheres. Using front surface mirrors we construct a cube with openings at the upper corners. We suspend a reflective sphere from the top mirror creating the Sinai cube. Three of the top corners are illuminated with colored light, and in the fourth corner we place a camera to capture the image created by the lights repeated reflection off of the center sphere. Figure 1 shows both systems.

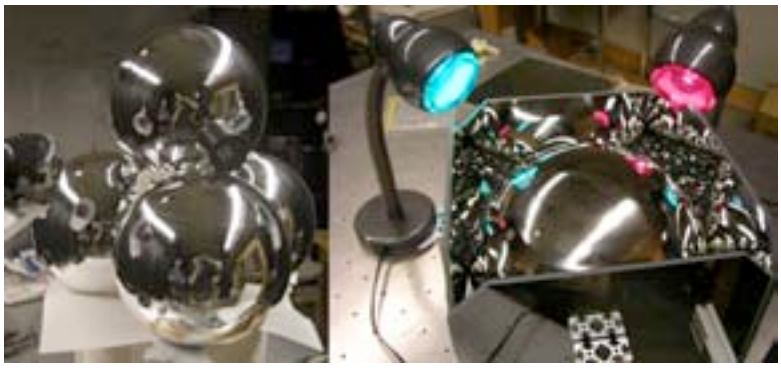

Figure 1: *The two experimental apparatuses are pictured above. On the left is a recreation of the laboratory model presented by Sweet et al. On the right is our Sinai cube shown here without the top mirror in place and with a Sinai diffuser whose diameter is approximately equal to the wall width.*

We use ray tracing techniques [4] to model both the stacked sphere and Sinai cube images with. Figure 2 shows the image obtained from the bottom opening of the stacked sphere configuration (top middle) as well as the ray tracing model (directly below). We also show the experimental (top right) and

modeled (directly below) Sinai cube in which the diffuser diameter is roughly 1/3 the width between the walls. A box counting analysis was performed on both systems and in each case there was good agreement between the simulated and actual images. For the stacked spheres we found D=1.6 in agreement with Sweet *et.al*., similar to the analytic value of the Sierpinski triangle D =1.58. In contrast the Sinai cube has significantly higher value of D = 1.8. The bottom left corner of Figure 2 we show the resulting scaling plots. Since D is the gradient of the scaling plot it is essentially quantifying the ratios of coarse to fine structure, such that fine structure plays a more dominant role in the high D pattern than the corresponding low D pattern. Consequently the high D pattern appears more visually complex as can be seen by visual comparison of the fractal images generated by the Sinai cube and the stacked spheres.

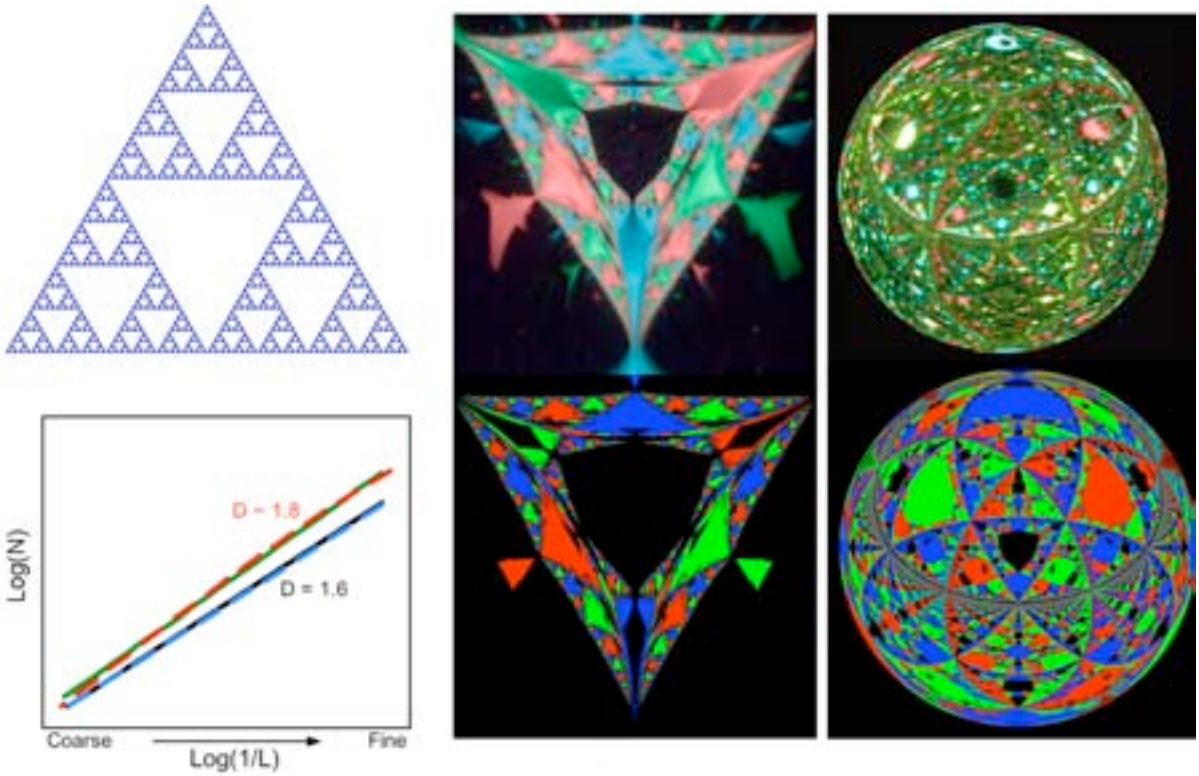

Figure 2: *Clockwise from top left: Sierpinski Triangle, image of the stacked sphere configuration, image of the Sinai cube, ray tracing of the Sinai cube, ray tracing of the stacked spheres, scaling plots of the box counting analysis of the Sierpinski triangle (lower dashed blue) the stacked spheres (lower solid black), and the Sinai cube image (upper dashed red) and ray tracing (upper solid green)*

Acknowledgements

R.P. Taylor is a Cottrell Scholar of the Research Corporation. B. Van Dusen was funded for this project by the M.J. Murdock Foundation, Partners in Science program. We thank M.S. Fairbanks for many fruitful discussions.

References

[1] D. Sweet, E. Ott, J.A. Yorke, *Topology in chaotic scattering*, Nature, Vol. 399, pp315, 1999
[2] K. Amano *et al*., *Fractal dimension of chaotic light scattering in regular polyhedral mirror ball structures*, Phys Rev E, **76** 046213 (2007)
[3] Y.G. Sinai, Dynamical systems with elastic reflections, *Russian Mathematical Surveys* **25**, 137 (1970)
[4] Ray tracing was performed using a 3d modeling program called Cinema4D.

Using Geometer's Sketchpad to Construct Pop-up Polyhedra as a Tool for Classroom Study of Geometry

S. Louise Gould
Department of Mathematical Sciences
Central Connecticut State University
1615 Stanley Street
New Britain, CT, 06050, USA
E-mail: goulds@ccsu.edu.edu

Abstract

This paper demonstrates the use of Geometer's Sketchpad to construct 3-dimensional pop-up polyhedra for students to handle in the study of Platonic and Archimedean solids. It explores some history of the use of pop-up polyhedra to illustrate mathematical shapes, as well as survey strategies for construction. A cloth book for a new granddaughter Eleanor inspired this project. Its pop-ups were an early favorite of Eleanor and her parents.

Historical Context

Visualizing three-dimensional objects has challenged generations of geometry students. Pop-up models take up little space yet provide rigid figures to study.

Examples prior to 1950. Tufte [1] includes a model of a regular tetrahedron fastened to a page that replicates one from John Dee's preface to Henry Billingsley's *Elements of Geometrie.* Published in London in 1570 this is the first English translation of Euclid's *Elements*. The University of Toronto Library has an original copy of this text and provides pictures on the Internet [2]. Cameo Wood posted a movie on You Tube that demonstrates the operation of these pop-ups [3]. John Lodge Cowley's *Geometry Made Easy* first published in 1752 also used pop-up models to illustrate solid geometry. The University of Michigan's rare books library has a copy believed to date from the 1760's [4]. Steinhaus [5] included a dodecahedron that consisted of two six pentagon "flowers" placed back to back with an elastic band threaded alternately above and below the pentagons on opposite sides (see also Ball [6]). Struyk [7] based three models on basic nets of polyhedra with pyramids glued to each of the faces to illustrate a cube with an inscribed regular tetrahedron, a rhombic dodecahedron with an inscribed cube and a rhombic dodecahedron with inscribed regular octahedron. These are interesting folding models, but they do not fold flat for easy transport.

More recent examples. In 1972 Trigg [8] cut a regular octahedron along some edges to achieve a collapsible polyhedron net augmented with regular triangles in strategic places. He described similar constructions for a collapsible tetrahedron from earlier papers. By 1982 Johnny Ball included some basic pop-up models of Platonic solids [6]. In 1992 Baranowski [9, 10] explored properties of some collapsible models of the tetrahedron, cube, octahedron, rhombic dodecahedron and cubo-octahedron. He formulated conditions that these constructions should obey: "Each vertex of the folded model must belong to parts of at least two faces, each paper fold is along an edge, … [and] the surface of the model should have 'no ends'." His models are assembled like a ring. Hans Walser and Scott Johnson have written extensively about folding polyhedra [11, 12]. In 1996 Walser shared an office with Jean Pederson who was working on a

project involving extensions to the Pascal Triangle. Pederson wanted a model that would fold flat in a brief case to travel to lectures [11]. Walser developed a model that interested many of Pederson's students. One, Scott Johnson, was eager to help in the development of a number of pop-up polyhedra. Johnson and Walser described their models and the techniques they developed to build them in [11]. Most of the models they describe are models of the Platonic solids although Walser built a cuboctahedron [13] as the original motivation for their project.

A Catalog of Techniques

Definition of Terms. Ball [6] used rubber bands for automated opening of his polyhedra. Johnson and Walser use rubber bands, pull strings, and paper fastener rotation centers [11]. Dee [2] and Cowley [4] simply used flaps attached to a page and fingers to lift and erect the models. Johnson and Walser [11] describe "edge-jumping" models that open as the result of two edges being caused to move towards each other. The cube, octahedron, icosahedron and dodecahedron all have parallel edges that make this possible. Since the tetrahedron has opposite edges that are not parallel (but are perpendicular when collapsed) they had to design "webbed hinges" that incorporate folding triangles at vertices of adjacent faces to include triangles that touch only at a vertex. They built a "face-jumping" icosahedron and a "vertex-jumping" cube that use brass paper fasteners as pivots. They also introduce "spiral models" where the top and bottom layers turn relative to each other as the models collapse.

Using Geometer's Sketchpad to Construct the Models

Tools from Sketchpad. Geometer's Sketchpad [13] (similar to Cabri) is a tool that can provide precise constructions of the polygons and fold lines. In the process students learn to identify centers and angles of rotation, length and directions of translations and placement of lines of reflection. Ball, and Johnson and Walser [11] provided the examples for classroom use.

A simple place to start. Although Ball [6] used the end of an envelope for his construction of a regular tetrahedron, we will use the tools of Geometer's Sketchpad [13]. A regular tetrahedron has 4 equilateral triangles as faces. We need to fold two of these triangles along their altitudes to enable the model to collapse. Use a unit segment that is not part of the model (see AB in Figure 1 left) to begin construction. This permits us to adjust the size of the model without distortion at some time in the future. First construct an equilateral triangle using this unit. Construct a line through two points C and D. Use C as center and AB as radius to construct a circle. Locate one of its intersections with CD. Label it E. Now construct a circle with radius AB and center E. Locate both intersections of our two circles (F and G). Note CF=FE=CE and CE=EG=CG (Figure 1 left). Connect pairs of these points with segments to construct two equilateral triangles with side lengths equal to AB. Hide any construction objects we no longer need. We need two more faces that will be folded. Construct four more triangles on the sides of our original triangles. Half of each of these triangles will be parts of the faces and half will be tabs to glue together to facilitate the pop-up. Mark segment FE as a mirror and reflect triangle CEF over EF using the reflection transformation. Similarly reflect triangle CEF over CF, and triangle CFG over CG and GE (Figure 1 center). Re-label the images of C and E as shown (C_1 and C_2 and E_1 and E_2). Select point C and segment E_1F to construct a line perpendicular to E_1F through C. This line is also perpendicular to C_2G. Why?Complete the model by making all edges of the final model thick and coloring the tabs. Cut around the perimeter of the figure and fold all interior

segments away from you (Figure 1 right). With glue on the yellow tabs, place triangle C_1JE on top of C_2KE and E_1HC on top of E_2IC. Push gently on the sides and a tetrahedron will pop-up.

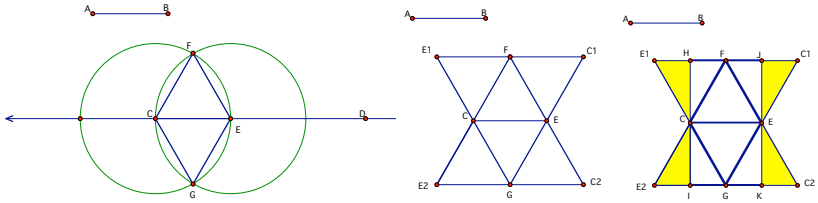

Figure 1: *Geometer's Sketchpad construction of the tetrahedron.*

The cube (Figure 2 left) and octahedron (Figure 2 right) use Johnny Ball's model from [6] page 134 in a similar way.

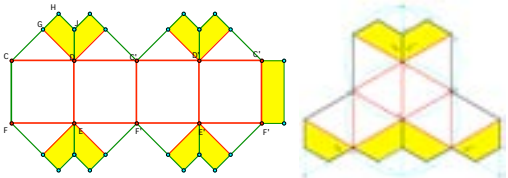

Figure 2: *Sketchpad construction of a cube (left) and an octahedron (right).*

An icosahedron with pivots. This model uses Johnson and Walser's face jumping icosahedron to illustrate the use of pivots. Central (purple shaded) equilateral triangles are connected with trapezoids made of equilateral triangles attached to triangular tabs that pivot. See Figure 3. Cut and fold as before. With the tabs folded to the back, arrange two copies with the central triangles back to back and oriented so that a base of one is opposite the base of the other. Matching one holed tab from the back with a neighboring holed tab from the front insert a brass paper fastener out of sight at 6 different places. Gentle pressure on the "star points" produces an icosahedron. See Figure 3. This pivot method also produces an interesting cube that shows the intersection of the plane intersecting the perpendicular bisector of the diagonal of a cube with the cube. When assembled the folds in the faces of the cube create a regular hexagon.

Figure 3: *An icosahedron with pivots constructed, assembled, and activated.*

Original Pop-up Figures

A Truncated Octahedron and Rhombicuboctahedron. A natural extension of the Platonic models is to see what Archimedean solids might be modeled this way.

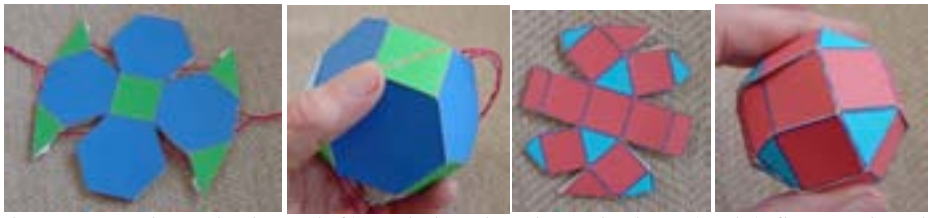

Figure 4: *The truncated octahedron (left) and rhombicuboctahedron (right) flattened and popped up.*

The truncated octahedron and rhombicuboctahedron are two of the simple Archimedean solids. Decide which polygon to use as you start the Geometer's Sketchpad construction. For both models use the parallel square faces as the starting place. Any folded polygons will be folded symmetrically along altitudes or diagonals. See Figure 4.

Conclusion

Ideas for further study. Magnus J. Wenninger [14,15] describes the remaining 11 Archimedean solids and stellated and compound polyhedra.

References

[1] Edward Rolf Tufte*, Envisioning Information*, Graphics Press: Cheshire CT, p. 16. 1990.

[2] http://www.math.ubc.ca/people/faculty/cass/Euclid/dee/dee.html (retrieved January 11, 2008)

[3] Cameo Wood, http://www.youtube.com/watch?v=fT1B_4XEQMU added April 6, 2007 retrieved January 11, 2008.

[4] John Lodge Cowley, appendix to the *Elements of Euclid*, University of Michigan rare books library Special Collections QA31.E88S76 C87 176-.

[5] Steinhaus, H. (1969). *Mathmatical Snapshots.* NY: Oxford University Press.

[6] Johnny Ball, *Johnny Ball's Think Box*, Puffin Books, Penguin Books Ltd. Middlesex, England. Chapter 10. 1982.

[7] Struyk, A. (1956). Three folding models of polyhedra. *Mathematics Teacher , 49*, 286-288.

[8] Trigg, C. (1972). Collapsible models of the regular ocatahedron. *Mathematics Teacher* , 531-533.

[9] Baranowski, J. (1992, September). Pocket Polyhedra. *Mathematic Teaching* , 8-9.

[10] Baranowski, J. (1992). Journal of Polish ATM (NiM Vol. 2). Published in Polish. Personal email April 15 and 16th 2009.

[11] Scott Johnson and Hans Walser, "Pop-up Polyhedra," *The Mathematical Gazette*, Vol. 81, No. 492. (Nov., 1997), pp. 384-380.

[12] Hans Walser, "The Pop-up Cuboctahedron", *The College Mathematics Journal*, Vol. 31, No. 2 (Mar., 2000), pp. 89-92.

[13] Geometer's Sketchpad, software from Key Curriculum Press, Emeryville CA.

[14] Magnus J. Wenninger, *Polyhedron Models for the Classroom*, National Council of Teachers of Mathematics Washington DC. 1966.

[15] Magnus J. Wenninger, *Polyhedron Models*, Cambridge University Press, Cambridge, United Kingdom. 1996 reprint of 1971 edition.

Chaos, Complexity, and Creativity

Krystyna Laycraft
Center for Chaos Studies
P.O. Box 373, Nanton, Alberta T0L 1R0, Canada
E-mail: krystyna@platinum.ca

Abstract

During the workshop, we introduce the main concepts and principles of chaos theory (positive and negative feedback, bifurcation points, attractors, complexity, self-organization, dissipative structures) through brief introductions, discussions, and a variety of stimulating and interactive activities like improvisation, active imagination, exercises of self-reflection, and techniques of disappearing. To illustrate some concepts we use the author's paintings. Then we analyze the process of creativity by applying these concepts. Creativity could be referred to as "self-organizing dissipative structures," originating spontaneously in far-from-equilibrium conditions. They emerge only through a constant exchange of energy/information with their environment, continuously create bifurcation points of instabilities and fluctuations, and transform themselves into new organization of increased order and complexity.

Introduction

In this workshop I will introduce the basic concepts of chaos theory and analyze the process of creativity by applying these concepts. I will guide the participants through a variety of stimulating and interactive activities like improvisation, active imagination, exercises of self-reflection, and disappearing techniques designed to assist in understanding and increasing their creativity.

During the early eighties chaos theory, nonlinear dynamics, fractals, and self-organization were widely discussed and employed in a variety of physical, chemical and mathematical problems.

Now, chaos theory is actively applied to almost everything from psychology to neuroscience, from economics to social dynamics.

A number of researchers have accumulated experimental evidence that the brain is a nonlinear feedback device and some studies show that diverging thinking, considered the general process underlying creative production, can be distinguished from convergent, analytical thought based on the dimensional complexity of ongoing electroencephalographic (EEG) activity [1]. This shows that irregularities (chaos) lead to complexity. Chaos is what makes life and intelligence possible.

Chaos Theory

"We believe that chaos represents the true nature of most psychological phenomena. It provides the alphabet of thought, because it represents the complexity of mind, brain, and behavior. We believe that chaos is the archetype that drives the universe, is its deep structure."

Frederick Abraham [2, p. xxvi]

In the last thirty years, new ways of study and understanding of complex systems have emerged – called chaos theory. Chaos theory acts as a conceptual umbrella for various approaches and explorations of complex systems, like dynamical system theory [3], self-organization [4-5], fractal geometry [6], catastrophe theory [7], theory of dissipative structures [8-11], and complexity theory [12].

Chaos theory studies open, nonlinear, and dynamic systems that constantly interact with and adjust to their environment, changing, growing, learning, and evolving. Chaotic systems exhibit an *extreme sensitivity to their initial conditions,* called popularly the *"butterfly effect."* Slight differences in their starting points make a very large difference in their outcomes. Such systems are highly sensitive because they are always changing through the loops of *positive and negative feedback*, and never precisely recycling to their initial states. Systems that change radically through their feedback are said to be *nonlinear*. In some conditions nonlinear systems behave in a regular, cyclical manner until something sets them off; a critical point is passed and suddenly they go chaotic. This critical point where a system changes character of the motion is a *bifurcation point,* and the states of chaotic motion are *attractors*.

Negative and Positive Feedback

In chaotic systems, everything is connected to everything else through *negative* and *positive feedback* [13]. Negative feedback keeps things in check and regulates the stability of a system. Positive feedback pushes a system for change, where more leads to more and less to less. Sometimes positive feedback drives a system to explode or spiral out of control. One of the most important discoveries of chaos theory has been that positive feedback can cause complex, even chaotic behavior to unfold inside orderly systems. Also that negative feedback can grow inside an otherwise chaotic system, suddenly organizing it and making it stable. Theory of chaos and complexity encourages us to understand how change unfolds through circular patterns of interactions.

Activity I: Improvisation is the root of creativity and can lead to the discovery of new ways to act and new patterns of thought. Improvisation excites self-expression areas and suppresses self-control regions in the brain.

- *"Make a scene using the concepts of positive and negative feedback"*

In this exercise between two people, one person is given the role as the leader. That individual is given an opening sentence, which is spoken aloud. The second person uses that sentence (paying attention to the tone and words) to "create" a scene that makes sense.

- *"Become the psychologist"*

This exercise involves you becoming a psychologist and by using your imagination, you have to talk about a subject chosen by the leader. The purpose of this exercise is to introduce the concept of an attractor.

Attractors

Attractors [13-17] characterize the behavior of a system; the same system can evolve into different types of attractors during its development.

There are three types of attractors: (a) point attractor, (b) periodic attractor, and (c) strange or chaotic attractor.

The most predictable one is *the point attractor,* when the system moves toward it in a condition of asymptotic stability. An example of the point attractor from life dynamics is a fixation on one desire or addiction to drugs, to alcohol, to success, to sex, or to some idea. It leads to monotony, to misery, to depression and very often to death. It is a single-minded attractor: black or white, good or bad, hate or love.

To the group of *periodic attractors* belong a cycle attractor and a torus attractor. *The cycle attractor* has the ability to resist change. Both the point and the cycle attractors describe systems that are highly regular, and thus, predictable. Routine is the perfect life example for the cycle attractor: when we are attracted to two activities, we tend to oscillate between them (e.g., work and family). Another example is our egocentric desires to acquire wealth, power, fame, and to have pleasure of one sort or another. This state of life, when we are moving from one situation to another, fluctuating from one mood to another, and repeating the very same process again and again, brings only dissatisfaction and suffering.

The three-dimensional periodic attractor is *the torus attractor*. It has a higher degree of regularity and complexity than the cycle attractor, but the pattern is again fixed and finite. The torus attractor expresses, for example, a complex set of attracting events that occur to a person on many levels over the course of a year. Then these events repeat again, year in and year out.

The *strange* or *chaotic attractor* describes systems that are in a state of turbulence, such as weather, violent river, brain activity, or our life dynamics. In general, the chaotic attractors can take an infinite number of different forms. Their patterns are fantastic, complex maps that capture the interplay between stability and change in a system. For example, a chaotic attractor portrays our state of consciousness, as a combination of moods, thoughts, memories, and images. They are constantly changing, memories come and go, thoughts pass through the mind only to disappear and return again later and so on. Consciousness exhibits periods of calm, periods of more or less regular oscillations, and periods of chaotic activity. The ability of a system to move in and out of chaos gives it a creative advantage.

Essentially, a chaotic attractor is a process that unfolds through the complex interactions between elements in a system. It is through a pattern of folding and stretching that the structure of the chaotic attractor emerges. Chaotic attractors are the foundation for hidden order in natural systems.

Activity II: Analyze your state; which attractors best describe your actual life dynamics. How do you express your state in the form of art (painting, poems, and music)?

Bifurcations

Bifurcation is a source of innovation and diversification.
Nicolis &Prigogine [8, p.74]

In nonlinear dynamic systems, through the process of positive feedback, abrupt changes of behavior can be observed. These changes called *bifurcation points* [4], [8 -11] occur when system orderliness breaks down, sensitivity to perturbations increases, and new patterns of organization rapidly self-amplify. Far away from a bifurcation point, a system can be well behaved; but as a bifurcation is approached, the system's trajectory becomes random and unpredictable (large fluctuations occur). At this point, the system "hesitates" among various different possible directions of change. Even little fluctuations in the subsystems can combine through positive feedback loops, becoming strong enough to shatter any pre-existing organization. At this point, the disorganized system either disintegrates into chaos, or leaps to a new higher level of order of organization.

When we think of ourselves as nonlinear, dynamic systems, bifurcation points can be viewed as special events along the flow of our lives during which choices can be made to influence future possibilities.

Psychological bifurcations are the rapid transformations of sensory, perceptual, cognitive, and affective experiences that may radically alter our lifestyle. They appear in the process of learning, in motivational states, in brain activity, in developmental stages and in their associated increasing complexity, in personality and family organization [18]. Here are some examples of psychological bifurcation points: a)."Aha!" moments or insight experiences: when rapid perceptual or cognitive restructuring takes place in the context of working on a difficult problem; b) moments when we

experience overwhelming emotional transformations (e.g. falling in love); and c) the moment when "of body" information rises to attention (e.g. feeling of hunger) [19].

Activity III: Reflect upon your life using concepts of attractors, bifurcation, and positive and negative feedback. How do you apply this self-reflection to your art?

Complexity

Complexity theory, which has been developed in the last twenty years, appears to be applicable to an enormous range of phenomena in physics, chemistry, social sciences, economy, psychology, neuroscience, and many more. Complex systems are everywhere; they are our bodies, our brains, our society, our culture. These systems contain many elements interacting reciprocally and nonlinearly by positive feedback mechanism. Two dimensions of *differentiation* and *integration* characterize complex systems. Differentiation means variety, it means that the different parts of the system behave in different ways. Integration, on the other hand, means to link the component parts to one another. Complexity arises when both of these aspects are present [20].

The science of complexity shows how a spontaneous process of *self-organization* can take place when a dynamical system finds itself in a state that is far from equilibrium, without any external force acting on the system.

Self-organization and Dissipative Structure

> *"At equilibrium molecules behave as essentially independent entities; they ignore one another. However, non-equilibrium wakes them up and introduces coherence quite foreign to equilibrium. This is the concept of "order through fluctuations."*
>
> *Prigogine and Stengers [10, p.180]*

All living [5] and psychological [21-22] systems evolve through the process of self-organization. An open, nonlinear and complex system acquires a new state without specific interference from the outside. With a continuous change in one or more control parameters, new states emerge spontaneously purely as a function of the dynamics of non-linear interactions between the system's components. The control parameter creates the necessary conditions for far from equilibrium states and critical fluctuations. Near equilibrium fluctuations are harmless, but far from equilibrium, they play a central role. Fluctuations are continuously probing the system and providing an opportunity to discover new patterns. The emerging patterns are created by the coordination between the parts of the system, but in turn influence the behavior of the parts. This is called a circular causality [23].

Prigogine introduced the concept of *dissipative structures* [8-11]. Such structures, to maintain their existence, must interact with their environment continually, maintaining the flow of energy into and out of the system. Self-organizing system becomes more ordered and more complex over time. Through this process, the system generates something new, unexpected structures, patterns, properties known as *emergence* [20].

The human brain is an example of a complex adaptive system in which single neurons interact in simple ways yet their collective neural network produces highly complex properties such as creativity and consciousness. Creativity and consciousness are examples of emergence**.** The interaction of the processes that form a complex system such as the mind - thoughts, images, memories, and so on - give rise to new processes. These new processes now interact with the original ones to create yet other novel processes, second order emergent events, and these are in principle entirely free and unpredictable.

Activity IV: Techniques of disappearing invented by Keith Johnstone [24]

All participants are asked to open eyes as widely as possible and on a signal start to walk around the room, point at any and every object, and shout as loudly as possible the wrong name.

.

Purpose: To look by fresh eyes on our surroundings. All our habitual overlays of interpretation and conceptualization are removed from the objects and people in front of us. This chaotic state can be described by a pure awareness of things-in-themselves. As adults, we can often give our best performances when we are not aware of ourselves and able to suppress our egos.

The Process of Creativity

"Creativity is a very paradoxical state of consciousness and being.
It is action through inaction.
It is allowing something to happen through you.
It is not a doing, it is an allowing.
It is becoming a passage so the whole can flow through you.
It is becoming a hollow bamboo, just a hallow bamboo."

Osho [25, p.31]

Creativity as an extremely complex process is generally defined very broadly as the capacity to bring something new into existence. Rogers' definition [26, p. 139] that "the creative process is an emergence in action of a novel relational product, growing out of the uniqueness of the individual and materials, events, people, or circumstance of his life" is the closest to our understanding of creativity.

We show that creativity could be described as "self-organizing dissipative structures" originating spontaneously in chaotic (far-from-equilibrium) conditions.

Chaos – The Differentiation Phase

When we approach some challenging, open-ended problems, we plunge into the process of questioning, researching, collecting, and exchanging of information. We work under conditions of emotional fluctuations, tensions, internal conflicts, doubt, and uncertainties.

Our mental state could be described by a variety of chaotic attractors like passion, love, knowledge, freedom, etc. They are constantly changing, interacting, bifurcating from one to another through the loops of positive and negative feedback. Since an enormous amount of information is created, this is the *differentiation* phase.

During this time we have to be "open" to the external and internal environment. Rogers [26] writes that in the person who is open to experience each stimulus flows freely through the nervous system. Whether the stimulus originates in the external or internal environment, it is available to our awareness. This means that we are aware of this existential moment as *it* is. We are able to accept ambiguity and to receive a considerable amount of conflicting information.

Sometimes we reach a point at which we become overwhelmed or blocked by contradictions, difficulties, and inconsistencies. In this situation we should willingly bifurcate to a different state. We should relax, go for walk, meditate, take a nap or start other project, and rely on our unconscious.

Activity V: "Dream and its Images" - Exercise based on Jung's "Active Imagination"

Participants choose a partner. They sit quietly and one tells the other about his/her dream. The partner listens with attention and then asks a participant to choose an image from his/her dream. Then they act

out on the image. They associate to the image. What does the image remind them of? What associations do they have with it? They switch roles. Now the second participant tells a dream to the first, and so on.

Purpose: An active imagination is a state of readiness, and through this process, the images from the unconscious are clarified and brought closer to consciousness. Sometimes active imagination takes place mainly inside our minds. Other time, the imagination is given form through painting, drawing, writing, and so on. As an example we will discuss a painting "Persona", which I painted after having a dream.

Complexity – The Integration Phase

The second phase refers to "the process of removing a problem from conscious awareness temporarily as means of gaining new perspectives on how to solve it" [27, p.389]. Free from rational direction; ideas, thoughts, images, and memories can combine and pursue each other every which way. Because of the freedom, original and new connections have a chance to be established. These new connections now interact with the original ones to create yet other novel processes, second order emergent events, and these are in principle entirely free and unpredictable.

Both increasing order and increasing complexity rely on a basic mechanism of self-organization, the coupling of reciprocally interacting system elements. Through this process, the system generates something new, unexpected structures, patterns, properties known as emergence. The emergent phenomena can be understood on a higher level than the lower level components they emerged from. This is generally the *integrative* process. Complexity arises when differentiation and integration are present. It increases when the number and/ or variety of the elements (thoughts, images, memories) that constitute our mind increase and when the number of relations that link them, i.e. the degree of integration between the elements, increases.

Contrary to the conscious brain, the unconscious brain appears to be a parallel processor, so that novel combinations of information are constantly generated, regardless of the state of attentional control [28].

Neuroscientists [1] show that divergent thinking, considered the general process underlying creative production, can be distinguished from convergent, analytic thought based on the dimensional complexity of ongoing electroencephalographic (EEG) activity. EEG complexity was comparable during divergent thinking and mental relaxation, but reduced during convergent thinking. Results indicate that the basic process underlying the generation of novel ideas expresses itself in a strong increase in the EEG's complexity, reflecting higher degree of freedom in the competitive interactions among cortical neuron assembles. Frontocortical EEG complexity being comparable with that during mental relaxation, speaks for a loosened attentional control during creative thinking.

Creativity – The Dissipative Structures

"One evening, contrary to my custom, I drank black coffee and could not sleep.
Ideas rose in crowds;
I felt them collide until pairs interlocked, so to speak, making a stable combination…"
Poincare [29, p.81]

The spontaneous insights, the "Aha!" moments, and the new ideas usually become conscious by appearing in a working memory during periods of mental relaxation after hard work and mental and emotional struggle.

They are a result of a successful self-organization of the chaotic activities in the unconscious. They are unexpected and unpredictable. They emerge at the "edge of chaos" as an expression of a new order that originates spontaneously from inside the system itself and creates completely new "emergent

property": a new picture, a new mathematical function, or a new song and so on. They are dissipative structures [8-11]. Usually the moment of insight is itself a dense, wordless, and sensory experience. Mihaly Csikszentmihalyi [30] mentions that most people recall with great intensity and precision a particular moment when some major problem crystallized in their mind in such way that a solution become all but inevitable, requiring only a matter of time and hard work.

Activity VI: Close your eyes and think about moments when and how you experienced an insight (your mental and external conditions) and what happened next.

After an insight occurs, one must check it out to see if the connections genuinely make sense. When we are being immersing in chaos, bifurcation happen and moments of flow appears. The flow introduced by Mihaly Csikszentmihalyi, is the period in the creative process when self-consciousness disappears, and is total absorption in the activity. It is the most enjoyable process any human can be involved in. The main elements of flow experience are: (a) immediate feedback to one's action; (b) balance between challenges and skills; (c) action and awareness are merged; (d) no worry of failure; (e) sense of time becomes distorted [31].

Summary

We demonstrate here how chaos theory describes the complex process of creativity. Chaos stimulates creative thinking and creates a necessary condition to initiate the process of self-organization. In the first phase of the process of creativity, the diversity of elements of knowledge appears to be essential. Then through the process of self-organization, these elements; thoughts, ideas, images, and memories interconnect freely and spontaneously and create a completely new organization of an increased order and complexity.

References

[1] M. Molle, L. Marshall, W. Lutzenberger, R. Pietrowsky, H.L. Fehm, & J. Born, Enhanced dynamic complexity in the human EEG during create thinking, *Neuroscience Letters 208*, 61-64. 1996.
[2] F. D. Abraham, The Leibniz-Abraham correspondence. In F.D. Abraham & A.R. Gilden (Eds.), *Chaos theory in psychology*. Westport, Connecticut, London: Praeger. 1995.
[3] E. Thelen & L.B. Smith, *A dynamic systems approach to the development of cognition and action,* Cambridge, MA: Bradford/MIT Press. (1994).
[4] H. Haken, *Synergetics,* Springer. 1983.
[5] H.R. Maturana & F.J. Varela, *The tree of knowledge: The biological roots of human understanding,* Boston, London: Shambhala. 1992.
[6] B.B. Mandelbrot, *The fractal geometry of nature,* New York: W.H. Freeman. 1982.
[7] R. Thom, *Structural stability and morphogenesis,* Reading: Benjamin. 1972/1975.
[8] G. Nicolis & I. Prigogine, *Exploring complexity*, New York: W.H. Freeman and Company. 1989.
[9] I. Prigogine, *From being to becoming, time and complexity in the physical science,* San Francisco: W.H. Freeman and Company. 1980.
[10] I. Prigogine & I. Stengers, *Order out of chaos,* Toronto, New York, London, Sydney: Bantam Books. 1984.
[11] I. Prigogine, *The end of certainty,* New York, London, Toronto, Sydney, Singapore: The Free Press. 1997.
[12] R. Lewin, *Complexity: Life at the edge of chaos,* New York: Macmillan. 1992.
[13] J. Briggs & F.D. Peat, *Turbulent mirror,* Perennial Library. 1990.
[14] R.H. Abraham. & C.D. Shaw, *Dynamics – The geometry of behavior,* Santa Cruz: Aerial Press, Inc.

1984.
[15] J. Gleick*, Chaos, Making a New Science*, Penguin Books. 1988.
[16] J. A. S. Kelso, J. A. S. *Dynamic Patterns, the Self-organization of brain and behavior,* Cambridge, London: A Bradford Book, the MIT press. 1995.
[17] E.N. Lorenz, *The essence of chaos,* Seattle: University of Washington Press. 1993.
[18] F.D. Abraham, Introduction to dynamics: a basic language; a basic metamodeling strategy. In F.D. Abraham & A.R. Gilden (Eds.), *Chaos theory in psychology,* pp. 31- 49. Westport, Connecticut, London: Praeger. 1995.
[19] A.R. Gilgen, A search for bifurcations in the psychological domain, In F.D. Abraham & A.R. Gilden (Eds.), *Chaos theory in psychology,* pp. 139-144. Westport, Connecticut, London: Praeger.1995.
[20] C.S. Bertuglia & F. Vaio, *Nonlinearity, Chaos & Complexity,* Oxford University Press. 2005.
[21] M.D. Lewis, Emotional self-organization at three time scales. In M.D.Lewis and I. Granic (Eds.). *Emotion, development, and self-organization*, pp.37-69. Cambridge University Press. 2000.
[22] M.D. Lewis, *Self-organizing individual differences in brain development.* Developmental Reviews, 25, 252-277. 2005.
[23] H. Haken, Synergetics: An approach to self-organization. In F.E. Yates (Ed.), *Self-organizing systems: The emergence of order*, pp. 417-434. New York: Plenum. 1987.
[24] S. Nachmanovitch, *Free play. Improvisation in life and art,* A Jeremy P. Tarcher/Putnam Book published by G. P.1990.
[25] Osho, *Creativity, Unleashing the forces within*, St. Martin's Griffin; New York. 1999.
[26] C. R. Rogers, Towards a Theory of Creativity. In P.E. Vernon (Ed.), *Creativity*, pp.137-151. Penguin Education. 1970.
[27] R. A. Finke, Imagery, creativity, and emergent structure. *Consciousness and Cognition*, 5, 381-393.1996.
[28] S.M. Gazzaniga, R.B. Ivry, & G.R. Mangun, *Cognitive neuroscience*. New York: Norton. 1998.
[29] H. Poincare, Mathematical Creation. In P.E. Vernon (Ed.), *Creativity*, pp.77-88. Penguin Education. 1970.
[30] M. Csikszentmihalyi, *Creativity. Flow and the psychology of discovery and invention,* Harper Perennial. 1996.
[31] M. Csikszentmihalyi, *Flow. The psychology of optimal experience*, Harper Perennial. 1990.

Stories Count: Narrative Approaches to Quantitative Learning

Suzie Garfield
Storyteller Telling Tales of Modern Life
KMZ Consulting Group, Inc.
P.O. Box 303
Wilmette, IL, 60091, USA
E-mail: Stories_Count@ameritech.net

Abstract

Stories Count: Narrative Approaches to Quantitative Learning is an interdisciplinary approach to education, communication, personal development, and creativity that uses the essential kinship of verbal and mathematical/logical/quantitative systems of coding and decoding to help people think, reason, understand, communicate, and create. *Stories Count* workshops are anchored by original narratives (stories) having significant math and logic embedded in their structure and in their content. The result is that listeners enter into the stories, engage with the narrative form, and simultaneously "do the math." They realize that they can master new and unfamiliar codes as readily as they manage codes in their comfort zones. This workshop program includes storytelling performance by the workshop leader, an interpretive and analytic discussion of the narrative by all the workshop participants, and an opportunity for the participants to explore how they use codes, symbolic structures, and patterns in their own work. In addition, participating in the workshop may lead them to bring *Stories Count* into their own classrooms, programs, and creative projects.

Learning/Discovery Objectives

- To explore the operational kinship of verbal and mathematical/logical/quantitative codes, structures, and patterns
- To enable people to transfer comfort and competence in one domain to the other
- To identify and analyze those codes, structures, and patterns we already use in our work and those that challenge us to new explorations and achievements
- To recognize and develop new ideas, new patterns of meaning, and new connections among established ideas and knowledge
- To demonstrate how narrative can align with other forms of expression and conceptualization and can facilitate learning, communication, personal development, and creativity

Background

Stories Count: Narrative Approaches to Quantitative Learning is an interdisciplinary approach to education, communication, personal development, and creativity that leverages the essential kinship among verbal and mathematical/logical/quantitative systems of coding and decoding to help people think, reason, understand, communicate, and create. *Stories Count* are original narratives that I develop to be told, analyzed, and discussed in participatory learning/discovery workshops, which the stories anchor.

The narratives at the heart of *Stories Count* are simultaneously verbal and mathematical/logical/quantitative compositions. They have memorable characters, inviting settings,

intriguing plots, and all the other traditional features of narrative. They also have math and logic embedded in their structure and in their content: huge numbers that can become large without limit; binary decision-making; chance, probability, and certainty; classical paradoxes and more. The result is that listeners enter into the stories, engage with the narrative form, and also exercise quantitative capabilities beyond computational skills as they "do the math." For people who think they are either verbal or quantitative but not both, the stories help transform strength in one domain into competence in the other. In addition, the stories always invite analysis, critical interpretation, and creative thinking and so they engagingly, comfortably, and immediately lead to a participatory experience that complements the performance/listening, which begins and ends each workshop. Workshop participants can expect to develop new insights, new perspectives, and new connections among concepts they already understand.

Many concerns, experiences, and ideas provide the basis for *Stories Count*. As a math major, a math teacher, and a veteran of the corporate workforce with over 30 years of experience in developing, supporting, and managing corporate computer projects, I know from my experience the value of the mathematical/logical way of thinking, which is convincingly documented in materials published by the National Numeracy Network on its website; see [4]. As a math teacher, and even as a successful learner of mathematical and logical material, I also know first-hand the great resistance people can have to math and logic, whether due to math anxiety (see [7]), matters of style and preference (see [2]), or other causes. Finally, as a student of literature and a performing storyteller, I know that a good story, well-told, can reach the human ability to make sense while attention is focused externally, on the story, not on the encoding medium, or on the psychological process of constructing meaning; see [6]. Having communicated ideas about quantity, equality/equivalence, and logic in the course of telling a story, I recognize the phenomenon that Roland Barthes examined in *S/Z: An Essay* (see [1]), namely how the mind moves among codes; and I know the thrill of eliciting that movement in my listeners.

To see me perform a *Stories Count* narrative based on a binary logical scheme, as suggested by John Allen Paulos (see [5]), please visit YouTube: http://www.youtube.com/watch?v=lJ0qjCCm-kY ; see [3].

A *Stories Count* workshop typically begins with introductions and formulating/stating goals for the workshop. Then I tell/perform a story. Next the group discusses the story. The discussion always addresses the embedded mathematical and logical content—my agenda—as well as any literary, philosophical, cultural or other observations, issues, or topics the other participants introduce. Either combined with the discussion or following it, a more focused discussion, a question-and-answer session, a worksheet, a brainstorming activity, a storytelling game, another exercise, or a combination of these activities addresses the theme of the workshop (example: specific math topics for an Overcoming Math Anxiety workshop). We debrief by articulating takeaways. Finally, I tell/perform a concluding story to end the program. At the Bridges Conference, we will address how we use codes, structures, and patterns in our own classrooms, programs, and creative work, and we will look for connections, insights, and challenges that can help us improve and move forward. Suggestions and requests for topics and for content to develop into new *Stories Count*, and any other questions/issues the stories and discussion might raise will also be encouraged and welcomed.

The workshop will also demonstrate application of the *Stories Count* concept and program. The large and ever-growing *Stories Count* repertoire includes stories and invites discussions to engage learners at different age levels and with a range of interests and concerns. *Stories Count* can subvert math anxiety, encourage insight and creativity, and reinforce connections and convergences that align different symbolic systems. *Stories Count* can be a powerful addition to any teacher's, educator's, or explorer's toolkit of approaches and techniques.

Workshop Experience

Workshop Title: *Stories Count: Narrative Approaches to Quantitative Learning*

Workshop Components:

- Live telling by presenter of original stories with embedded mathematical/logical content.
- Discussions of the introductory story, to include review and explanation of the math/logic.
- Exploration of the codes, structures, and patterns that workshop participants use in their own work. Identification of related and/or contrasting approaches to explore. This activity will begin with worksheets and will move to debriefing in pairs or small groups, question-and-answer, or other activities as permitted by time and by the size, interests, and learning/interactive styles of the participants.

Sample workshop agenda (60-75 minute program):

Topic	**Description**	**Time**
Introduction	We'll introduce ourselves to the entire group or in pairs/small groups and state why we're attending and our goals/what we hope to get from the program. I'll briefly describe the program and review the agenda.	5- 10 minutes
Narrative Opening (Live Storytelling)	I'll tell an original math-and-logic-laden story.	10 minutes
Group Discussion	We'll discuss the story. I'll moderate. We'll discuss any aspects the group wants to explore. I'll make sure we address any awareness of the math/logic that the participants recognized during the telling and how the math/logic patterns work within the narrative.	10-15 minutes
Personal Applications	Participants will receive and be asked to complete a worksheet/questionnaire designed to help them identify and analyze the codes, structures, and patterns they use in their work and to explore new possibilities. If time permits, and depending on participant preferences, we might discuss insights and possibilities in pairs or small groups or explore them in another interactive way.	20-30 minutes
Summary	I'll ask for each participant (including me) to note a learning takeaway. We'll tell the takeaways to the entire group or in pairs/small groups as appropriate.	5-10 minutes
Narrative Closure—I'll tell another story, to close.	Also with embedded math/logic. There won't be follow-up discussion of the story in this session, although there can be discussion later or "off-line."	10 minutes

Presenter Biography

I'm an experienced computer programmer and system designer, a Project Management Professional (PMP), an interpreter of narrative and texts, a veteran teacher of mathematics and of literature, and a storyteller. I'm grounded in technology, the sciences, and the humanities and equally at home in the worlds of business, academe, and performance. I bring this diversity of interests and perspectives to new experiences, environments, and associates wherever I go.

As a designer, developer, and manager of software systems, I've worked with diverse stakeholders—clients and customers, frontline staff, managers, executives, and technology professionals—throughout the retail, financial, manufacturing/distribution, and healthcare industries. I've developed and presented corporate training programs. I've designed and taught academic classes in mathematics, humanities, and critical thinking to students at all levels from middle school through post-graduate, both on-line and at bricks-and-mortar institutions including inner city community colleges, 4-year colleges, and elite universities. I also perform traditional, literary, historical/biographical, and original stories at folklore and storytelling festivals, public concerts, and private events.

I was educated at the University of Illinois, Mills College, and The Johns Hopkins University, and I hold a doctorate in Humanities/Comparative Literature as well as an MBA. I've also studied mathematics at the post-graduate level. I'm certified by the Project Management Institute (PMI) as a Project Management Professional (PMP), and I'm an active member of many professional and cultural organizations including the PMI, the International Institute for Business Analysis (IIBA), the National Numeracy Network, the National Storytelling Network and its Storytelling in Organizations special interest group, Illinois Storytelling, the Northlands Storytelling Network, the North Shore/Nature Center Storytelling Guild and the Fox Valley Storytelling Guild.

References

[1] Roland Barthes. *S/Z: An Essay*. Trans. Richard Miller. New York: Hill and Wang, 1974.

[2] Howard Gardner. *Multiple Intelligences: The Theory in Practice.* New York: Basic Books, 1993.

[3] Suzie Garfield. *How to Govern a Kingdom, Part 1*. http://www.youtube.com/watch?v=lJ0qjCCm-kY.

[4] National Numeracy Network. See http://serc.carleton.edu/nnn/resources/index.html.

[5] John Allen Paulos. *Innumeracy: Mathematical Illiteracy and Its Consequences*. New York: Vintage Books, 1990.

[6] Ferdinand de Saussure. *Course in General Linguistics.* Ed. Charles Bally and Albert Sechehaye with Albert Riedlinger. Trans. Wade Baskin. New York: McGraw-Hill, 1959.

[7] Sheila Tobias. *Overcoming Math Anxiety*. New York: Norton, 1993.

Creating Islamic Patterns from Folded Shapes

E.B. Meenan* and B.G. Thomas
School of Education* and School of Design
University of Leeds
Leeds, LS2 9JT
e.b.meenan@leeds.ac.uk

Abstract

In this practical workshop participants will learn how to fold shapes including squares, equilateral triangles and hexagons from colored paper circles and A-size paper. The participants will then have the opportunity to make Islamic patterns for themselves using the folded shapes. This work can be extended to include participants designing and making their own patterns. There will also be opportunities to discuss implications for classroom practice, and ways in which the ideas can be used for students of varying interests and abilities.

Introduction

Geometry is at the heart of Islamic art. The designs and patterns use a finite number of geometric shapes that combine in many different ways. Traditionally, Islamic patterns are created through compass and ruler constructions but this method is often time consuming and can be complicated to oversee in the classroom. Students frequently do not exercise the precision required to achieve accurate results. An alternative method of creating Islamic patterns in the classroom is through manipulation of folded paper shapes cut from circles or A-size paper. Metric (A-sized) paper is mathematical paper system based on root 2 rectangles and is commonly used throughout the Europe, see [1, 2]. Squares, equilateral triangles, hexagons and rhombi can be quickly and easily folded from colored circles or A-size paper. Fixing these folded shapes onto large sheets of backing paper or card enables the quick assembly of eye-catching and colorful patterns. A photograph of pupils exploring how to create a tiling pattern from folded paper kites is shown in Figure 1.

Figure 1: Pupils exploring Islamic patterns using folded paper kites

The aim of this workshop is to ensure that participants become familiar with the methods for making a variety of folded shapes and using these to create Islamic patterns. This will act as a creative stimulus for designing other patterns, exploring the properties of the folded shapes and investigating how to fold other shapes. Participants will be encouraged to reflect on their own teaching which, in turn, will allow them to introduce new teaching strategies that help to:

- make cross-curricular connections between art and mathematics
- develop two-dimensional spatial awareness
- broaden students' creative outlook and develop practical skills
- increase students' motivation and enjoyment of mathematics

These activities assist in increasing pupils' understanding of two-dimensional shapes, symmetry and pattern. The material in this workshop can also be combined into the teaching of a larger cross-curricular project across the art, religious education and mathematics departments, which could include topics such as symmetry, two-dimensional shapes, tessellations, paper folding and a study of Islam and Islamic geometric patterns. Further examples of patterns that can be created using folded paper shapes are available from [3].

A series of successful workshops have been delivered by Meenan and Thomas to school groups alongside an exhibition of tilings and polyhedra, presented at the University of Leeds [4]. Photographs from one such workshop are shown in Figure 2. A report on a workshop by the accompanying teacher and her class is available from [5].

Figure 2: *Students in a practical paper-folding workshop*

Geometry and Symbolism in Islamic Design

Patterns are symbolic in Islamic culture [6]. It is within the circle, the symbol of unity, that polygons, the building blocks of tiling patterns, are constructed. The circle has also been regarded as a symbol of eternity, without a beginning and without an end. The compass and ruler constructions of the three

fundamental shapes used in Islamic art – the equilateral triangle, the square and the hexagon – are shown in Figure 3.

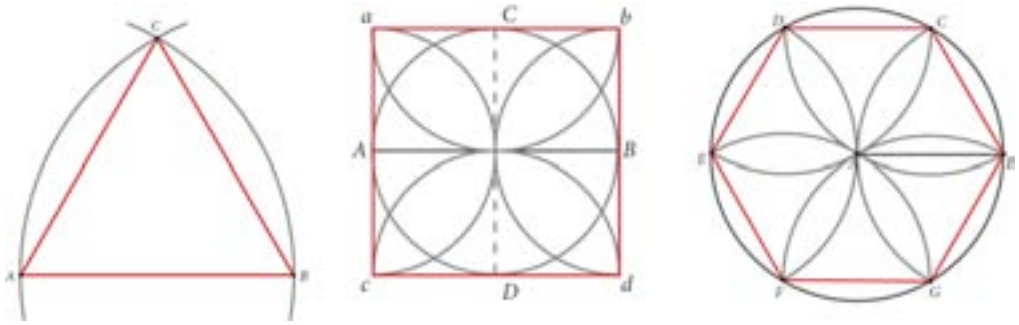

Figure 3: *Constructions of a) a triangle, b) a square and c) a hexagon*

The equilateral triangle, the simplest regular polygon, consists of only three equal lines connected at three vertices. Two lines cannot enclose a plane – three are needed – and so three is the beginning. By tradition the triangle is a symbol of harmony and human consciousness. The square is often taken as the symbol to represent the earth and its four corners symbolically represent the four directions – north, south, east and west or the four states of matter – water/liquid, earth/solid, air/gas and fire/ether. The hexagon represents heaven [6]. Another symbol commonly found in Islamic decoration is the star. The star symbolizes equal distance in all directions from a central point. All stars, whether they have 6, 8, 10 or more points, can be created through division of a circle into equal parts. The center of the star is the center of the circle from which it was created, and its points touch the circumference of the circle. The rays of the star spread out in all directions making the star an appropriate symbol for the spread of Islam.

Repetition and variation are important aspects of Islamic design. A series of tiles may consist of only one or two shapes, although the patterns on the tiles themselves may be different. In other designs, a number of different shapes are combined to create a complex interlocking pattern, as shown in Figure 4.

Figure 4: *A tiling pattern found at the Alcazar, Seville, Spain*

In many Islamic patterns, different elements seem to dominate, depending on how the pattern is viewed. A simple example is shown in Figure 5. It can be considered to be a six-pointed star surrounded by six rhombi or as three rhombi surrounded by three six-pointed stars. For further examples and discussion of Islamic geometrical patterns and their constructions see [6, 7, 8].

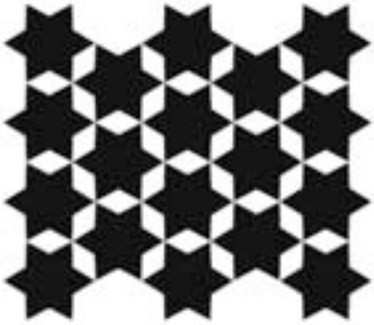

Figure 5: *Six-pointed star tiling*

Creating Shapes and Tiling Patterns

Workshop participants will have the opportunity to fold two-dimensional shapes from colored paper circles or A-size paper. All the shapes are straightforward to accurately fold following the instructions and diagrams shown in Figures 6 – 9. Short video clips demonstrating the folding are available online at [9]. No previous experience is required and pleasing results can be achieved in a relatively short time.

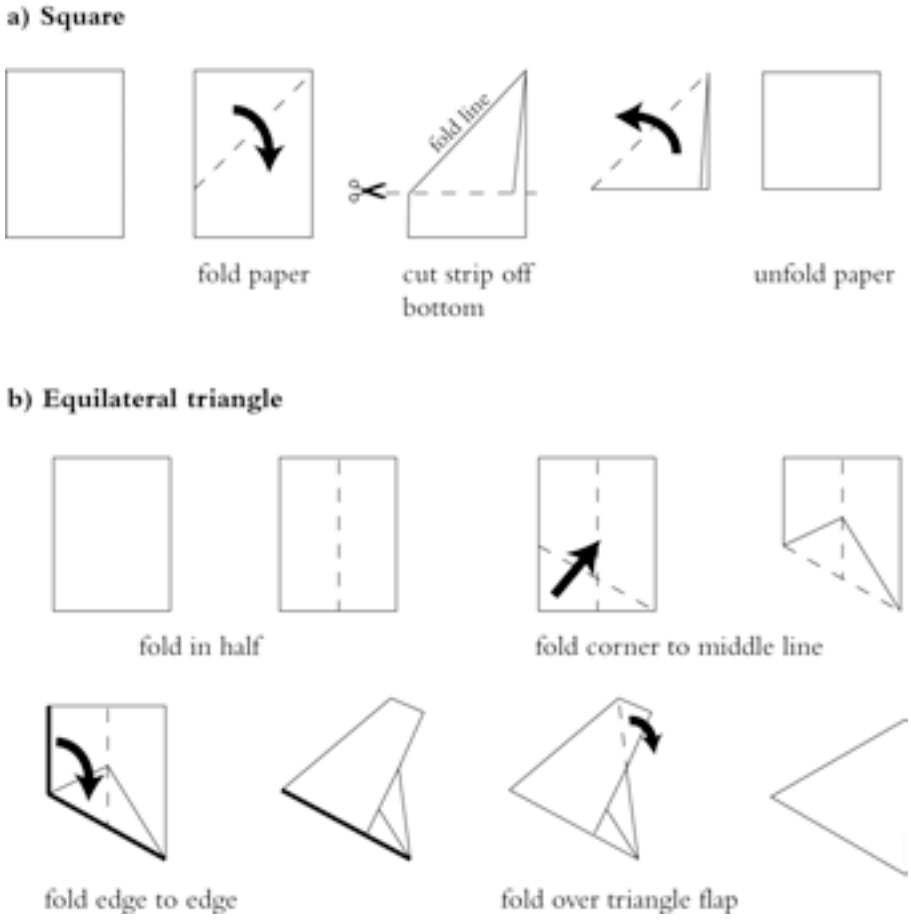

Figure 6: *Folding instructions for a) a square an b) an equilateral triangle from 'A' size paper*

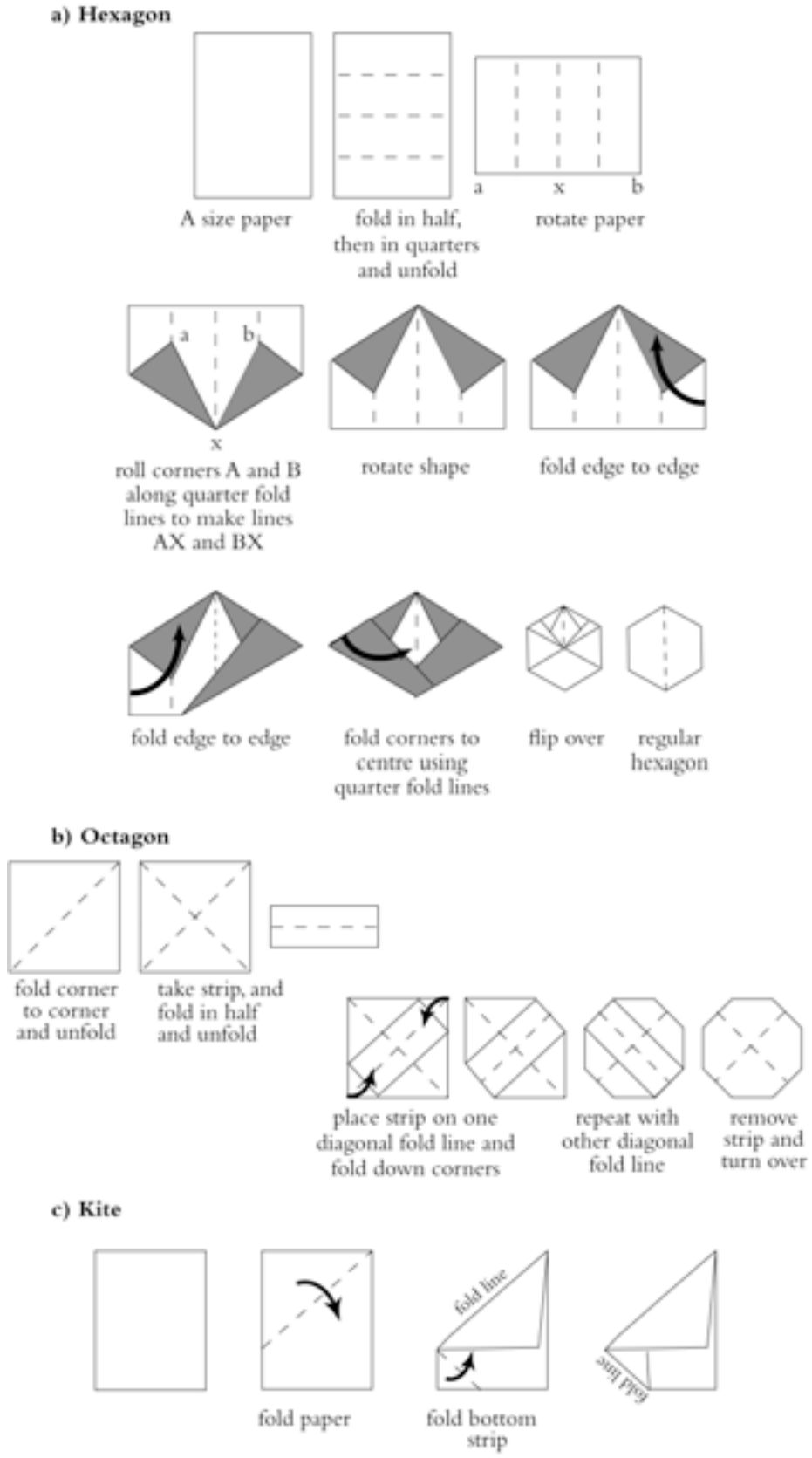

Figure 7: *Folding instructions for a) a hexagon and b) an octagon and c) a kite from 'A' size paper*

a) Square

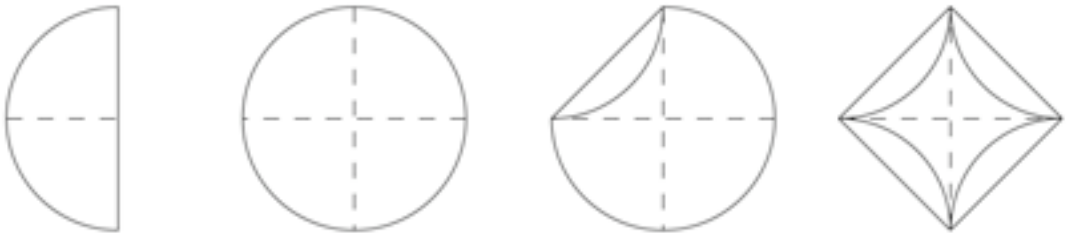

Fold the circle in half. Open and fold the diameter back on itself to create two diameters at right angles.

Then fold in the four flaps as shown to a square.

b) Equilateral triangle

Mark the centre. (The centre can be found by folding the circle in half, then in half again.)

Fold in the edge to the centre.

Fold in the edge the centre again so that the new fold joins previous fold.

Fold in once again to the centre to create an equilateral triangle.

The flaps can be interleaved to give a triangle like this.

c) Rhombus

First fold two arcs to the centre.

Then fold up the end of the chord to the centre of the circle.

Do the same with the end of the other chord.

Tuck in the flaps. You now have a neat rhombus.

Figure 8: *Folding instructions for a) a square, b) an equilateral triangle and c) a rhombus from circles*

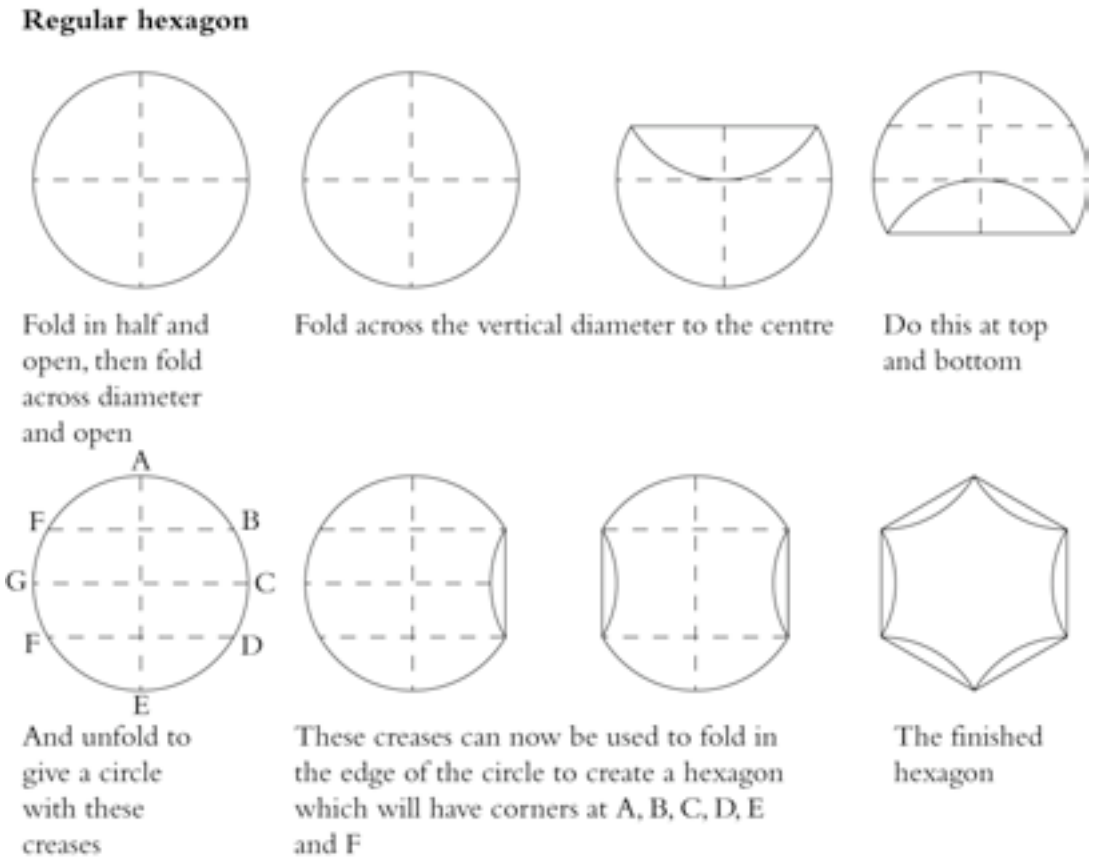

Figure 9: *Folding instructions for a hexagon from a circle*

A selection of Islamic tiling patterns that can be made using folded shapes is illustrated in Figure 10. Decorative designs can be drawn onto the plain tiling patterns once constructed.

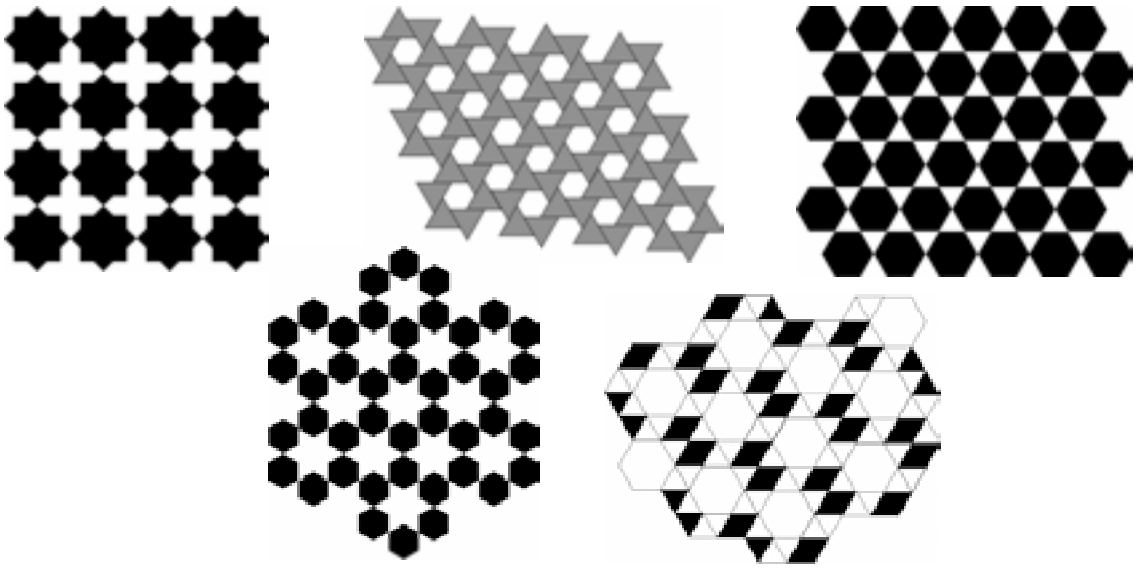

Figure 10: *Islamic tiling patterns*

Summary

This paper presents a novel approach to the teaching of two-dimensional shape and pattern. Setting these subjects in the cross-curricular context of Islamic art makes the topics more relevant to students. It has been observed by the authors that the students involved in the paper folding workshops have shown a deeper engagement with the subject. The material presented in this paper forms a component of a larger seminar, which was designed to promote the teaching of two and three-dimensional geometry in both a visual and practical way. This workshop was successfully targeted at 10 – 16 year old students of a wide range of abilities and was associated with the exhibition *'Form, Shape and Space'* [1]. A freely available teacher's booklet was developed to support this larger seminar and contains activity sheets on making polygons and polyhedra using compass and ruler constructions, as well as paper folding and pull-up net methods [10].

References

[1] K. Elam, *Geometry of Design: Studies in Proportion and Composition*, New York, Princeton Architectural Press. 2001.

[2] W. Gibbs and E.B. Meenan, "Metric Paper Magic", from *TES Magazine* [online]. Accessed 23/04/2009.] Available on the World Wide Web: <http://www.tes.co.uk/article.aspx?storycode=346654>

[3] W. Gibbs, "A collection of activities to help enrich mathematical learning", from *William's Homepage* [online]. Accessed 23/04/2009.] Available on the World Wide Web: <http://www.cyffredin.co.uk>

[4] B.G. Thomas. *Form, Shape and Space: An Exhibition of Tilings and Polyhedra,* The University of Leeds International Textiles Archive, UK. 10 October 2007 – 16 May 2008.

[5] C. Burland. "Aim in Leeds - Engaging Gifted & Talented Pupils in Mathematics Outside the Classroom", from *National Centre for Excellence in the Teaching of Mathematics* [online]. [Accessed 25/02/2009.] Available on the World Wide Web: <http://www.ncetm.org.uk/Default.aspx?page=13&module=res&mode=100&resid=10069>

[6] K. Critchlow, *Islamic Patterns: An Analytical and Cosmological Approach*, New York, Thames and Hudson. 1984.

[7] J. Bourgoin, *Arabic Geometrical Pattern Design*, New York, Dover Publications. 1974.

[8] D. Wade, *Pattern in Islamic Art*, Woodstock, New York, The Overlook Press. 1976.

[9] E.B. Meenan. "MoreMathsGrads Videos", from *YouTube* [online]. [Accessed 25/02/2009.] Available from the World Wide Web: <http://www.youtube.com/user/morematsgrads>

[10] E.B. Meenan and B.G. Thomas. "Form, Shape and Space: Teacher Booklet". from *National Centre for Excellence in the Teaching of Mathematics* [online]. [Accessed 25/02/2009.] Available on the World Wide Web: <http://www.ncetm.org.uk/files/271019/ULITA+Teachers+booklet.pdf>

Acknowledgments

The authors wish to thank the NCETM, particularly Tony Shepherd, for all their support and encouragement throughout this cross-curricular project. Thanks are also due to Margaret Chalmers at the University of Leeds International Textiles Archive and Anna Clapham at South Leeds City Learning Centre, for their support with the workshops and associated activities.

Workshop: Working With Patterns To Introduce Mathematics Concepts To Young Children

Patricia Bentley
Education Curator
Textile Museum of Canada
55 Centre Avenue
Toronto, ON, Canada, M5G 2H5
E-mail:bentley.pbentley@gmail.com; pbentley@textilemuseum.ca

Abstract

In a hands-on activity with crow beads, participants will learn about introducing very young children to patterns by means of number bracelets, and will extend this activity into creating growing and reflecting patterns for older children. Clock (modular) arithmetic will be introduced as a basis for other ways to create patterns for bead bracelets or necklaces. A discussion of modular arithmetic in loom weaving will conclude the workshop.

Introduction

I propose that an ability to recognize, manipulate and construct patterns is a key factor in young children's learning about the world generally and about conceptually-based disciplines like mathematics and science in particular. Following the research of Constance Kamii [1], Ian Stewart [2] and Elizabeth Warren [3], I define patterns as conceptual ordering principles about the ways things repeat. These principles may be represented in the natural and the human-created world by concrete objects or may remain abstract, e.g. as number or shape concepts.

A patterning activity at its most basic sets up the opportunity to group objects according to certain criteria. At the Textile Museum of Canada we use patterning activities with textile materials and techniques as tools for developing skills in both mathematics and textile art. For example, children up to 6 years of age select 8 millimetre plastic beads in different colours, create a simple four to six colour pattern by arranging the beads on a simple printed grid like the one in figure 1, glued to a Styrofoam plate, and then string the beads on an elastic cord, repeating the pattern to make a bracelet. Older children extend this activity by creating growing patterns and/or mirror patterns with the beads.

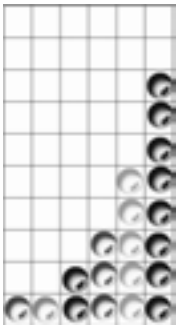

Figure 1: *Bead grid*

Figure 2 is an illustration of beads strung in the Fibonacci number sequence that begins as 0,1,1,2,3,5,8, with the beads starting at 1. The pattern rule is to add each of the last two numbers together to get the next number in the sequence. This sequence has some beautiful qualities that are revealed as the numbers progress from the first steps, easily understood by budding mathematicians, to larger numbers whose ratios, beginning with the ratio of 8 to 13, begin to approach 1.618034 (to six decimal places). This number, represented by the Greek letter phi (Φ) is known variously as the Golden Ratio, Angle, Section or Proportion [[2], 139]. Its principles are found in the growth patterns of many plants, for example the tightly packed arrangement of seeds in the head of a sunflower, and also in art and architecture as a principle of composition or structure.

Figure 2: *Number bracelet*

Make a Number Bracelet

Grade level: K-3

Summary: This activity investigates how numbers can be used to create visual patterns by organizing them on a grid, through the creative work of making jewelry.

Math Expectations: (Numeration) Classify whole numbers; compare and order whole numbers; (Patterning and algebra) explore patterns and pattern rules; (Data and probability) sort and classify concrete materials [[4], 31].

Visual Art Expectations: (Knowledge of elements) Recognize and name the primary colours; (Creative work) make colour choices in artistic work [5], 30]; (Critical thinking) describe how artists use the elements of design to communicate information [5], 31].

Materials: 1 x 1 cm grid printed on paper, with either 4 or 6 columns x 10 rows; a paper plate, 8 mm plastic crow beads, 41 cm piece of round elastic cord.

Description: 1) Tie a bead on one end of the elastic cord so the beads don't slip off as you string them. 2) Cut out a copy of the grid and glue it onto a paper plate. 3) Select a sequence of 4 or 6 numbers from 1 to 10. Numbers can be repeated if you wish. Our example uses the numbers 1,1,2,3,5,8. 4) Pick different colours of beads to correspond to the numbers in your pattern and put them on the grid so you can see the pattern as a chart. 5) Starting at the left of the grid, string the beads in order on the cord. When you have strung all the beads, repeat the pattern until the cord is almost full (about 50 beads). 6) Leave about 7 cm free for tying. Tie the ends of the cord together. Put on your bracelet. It will go twice around your wrist.

Extensions: Once you have strung all the beads on the grid, reverse the pattern when you repeat it.
(Grades 3-5) String all the beads in the sequence then grow it by doubling each number, then tripling them, and so on. Experiment with patterns that grow in different ways.

For older students the grid can also be expanded to numbers from 1-20 and the cord can be lengthened to make a necklace. The number sequence used in the bracelet can be graphed, using the grid and coloured pencils.

Number Bracelets and Clock Arithmetic

Grade level: 4-6

Summary: This activity explores computation, units of measure and creating patterns through the creative work of making jewelry.

Math Expectations: (Numeration) Solve number problems using addition; (Patterning and algebra) create and explore number patterns [[4], 64].

Visual Art Expectations: (Knowledge of elements) Recognize and name the primary colours; (Creative work) make colour choices in artistic work [5], 30].

Materials: 8 mm coloured plastic crow beads in 10 colours, 41 cm piece of round elastic cord.

Description: 1) Choose any two numbers from 1 to 10. 2) Follow this rule: add the two numbers on the right and record just the digit in the ones place in the sum. Add the numbers with the help of the 10-hour clock to see why this works.

2+6=8
6+8=4
8+4=2
4+2=6
2+6=8

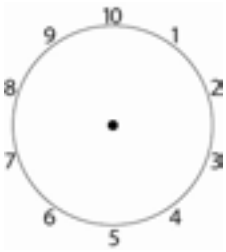

Figure 3: *10-hour clock*

This number pattern repeats after line 4 so you have a pattern of 4 numbers, 8-4-2-6. 3) Select four colours of beads; for example, 8 yellow, 4 blue, 2 orange and 6 green. This is where the artistic creativity comes in. 4) When you are happy with your colour choices for the four numbers in your sequence, string them in repeat to make a bracelet. You may also try mirror or growing patterns with your sequence.

If you think of the numbers as being on a 10-hour analogue clock, which repeats just as a 12-hour clock repeats, you can imagine another kind of clock, for instance a 4-hour clock, and choose a pair of numbers. Here is an example using a 4-hour clock. For any sums over 4, subtract 4. Add the numbers with the help of the 4-hour clock to see why this works.

1+2=3
2+3=1
3+1=4
4+1=1
1+1=2
1+2=3

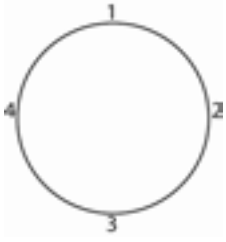

Figure 4: *4-hour clock*

This number pattern repeats after line 5 so you have a pattern of 5 numbers, 3-1-4-1-2. Select five colours of beads as before and use this pattern to make a necklace.

Weaving and Clock Arithmetic

How does clock arithmetic relate to the technology of weaving? A loom is a device for keeping tension on one set of threads, called the warp, so a second set of threads, called the weft, can be inserted in an over – under interlacement, for example the over one – under one pattern called tabby. A foot powered floor loom usually has 4 shafts. Each warp thread is passed through the eye of a needle, or heddle, in a repeated sequence, so the warp thread can be raised to make a space, or shed, for the weft to pass through. The patterns created are usually based on the twill weaves of the familiar blue jeans.

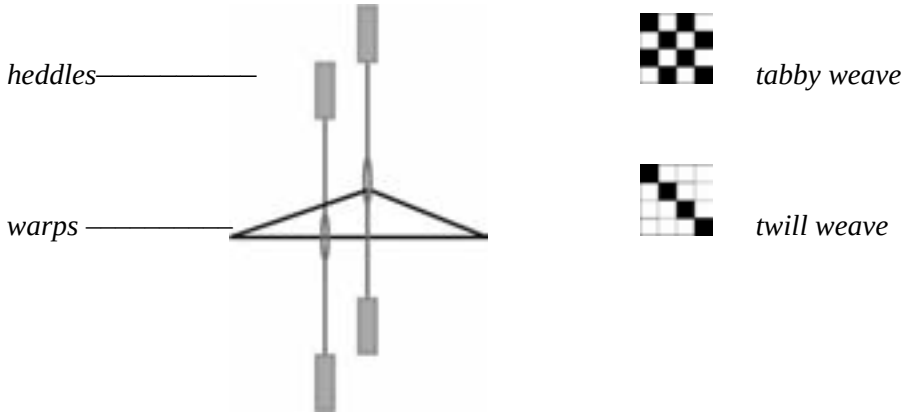

Figure 5: *How a loom works*

On a grid with 4 columns x 24 rows, try filling in cells to discover some of the patterns you can make on a 4 shaft loom. (Any combination of cells will work on a loom except for all blank or all filled - why?) Every 4 columns change the pattern and see what happens. Then cut strips of paper in two colours and interlace them to see how your pattern works.

References

[1] Kamii, Constance. "The Development of Logico-Mathematical Knowledge in a Block-Building Activity at Ages 1-4." *Journal of Research in Childhood Education* 19.1 (2004): 44.

[2] Stewart, Ian. *Nature's Numbers: The Unreal Reality of Mathematics*. New York: Basic Books, 1995.

[3] Warren, Elizabeth. "Generalizing the Pattern Rule for Visual Growth Patterns: Actions that Support 8 Year Olds' Thinking." *Educational Studies in Mathematics* 67.2 (2008): 171.

[4] *Ontario Ministry of Education Mathematics Curriculum, Grades 1-8.* Queen's Printer for Ontario, 2005. Also available online at http://www.edu.gov.on.ca.

[5] *Ontario Ministry of Education Arts Curriculum, Grades 1-8.* Queen's Printer for Ontario, 1998. Also available online at http://www.edu.gov.on.ca.

Exploring Some of the Mathematical Properties of Chains

Eva Knoll
Faculty of Education
Mount Saint Vincent University
Halifax, Nova Scotia, B3M 2J6, Canada
E-mail: Eva.Knoll@msvu.ca

Tara Taylor
Department of Mathematics, Statistics and Computer Science
St. Francis Xavier University
Antigonish, Nova Scotia, B2G 2W5, Canada
E-mail: ttaylor@stfx.ca

Abstract

This workshop aims to explore various mathematical topics that emerge from examining classes of chains and their properties. Basic concepts are taken from topology, an area of mathematics that is concerned with notions like connectedness, how many holes there are, and orientability; geometry, including symmetries; and collapsibility and degrees of freedom. These topics are explored through an examination of a small number of chain designs including examples that are not topologically linked at all, examples in which the relative position of the links determine the symmetries, degrees of freedom, and the way in which their structure is analogous to that of a Moebius band, and finally a model of a chain design with a fractal structure. The workshop will include building human models to explore various properties and other activities where the participants will be able to play with necklace models to better understand the theory and to come up with their own questions to investigate.

Introduction

According to a popular online dictionary [1], a chain is 'a series of connected links', and a link is defined as 'one element of a chain' [2]. A more useful way to define a chain is as follows: a series of interconnected, rigid elements called links which, together, constitute a linear, flexible (non-rigid) object that can be used to connect, wind, hang or wrap. Generally, chains are made of a limited number of different link types that combine in repeating patterns, thereby displaying predictable properties such as symmetries.

Some of the mathematical properties of chains, which are explored in the workshop, include the topological nature of specific designs, the symmetries that are present or absent, degrees of freedom, collapsibility and the significance of the ratio of the sizes of the elements, including the eccentricity, gauge (thickness of the wire) and inner radius of the links. These properties are explored through various examples including the not-link chain, the Byzantine chain design, the 'Rope' chain design and Antoine's Necklace [3].

The Not-Link Chain

In knot theory, a 'link' refers to a 'set of knotted loops' or circles [4]. We call the first example under consideration the 'not-link chain' because although it functions as a chain according to the general definition given above, in knot theory terms it is not linked as the elements are not looped through each other.

Figure 1: *The Not-Link Chain*

In Figure 1 on the left, a section of the chain shows how it alternatively connects two different types of elements: the first is a rod at either end of which is attached a slightly larger metal 'ball', forming an elongated dumbbell; the second element is a small flat figure eight whose holes are of a smaller diameter than the 'ball' of the dumbbell but larger than that of the rod. These size ratios allow some movement in the chain, and prevent it from disconnecting. The right side of Figure 1 shows a connection between the two types in more detail.

The Byzantine Chain

The second example under consideration is known as a Byzantine Chain, King's Chain or Bali Chain [5]. It is related to a design called Idiot's Delight [6], and is made using only one type of element: a simple round ring. Figure 2, below, shows a section of Byzantine Chain made using shower curtain rings. The distinguishing feature of this design is the interlocked 4-ring combination in the circle. This grouping is made rigid by the addition of the rings connecting it to the next interlocked 4-ring grouping.

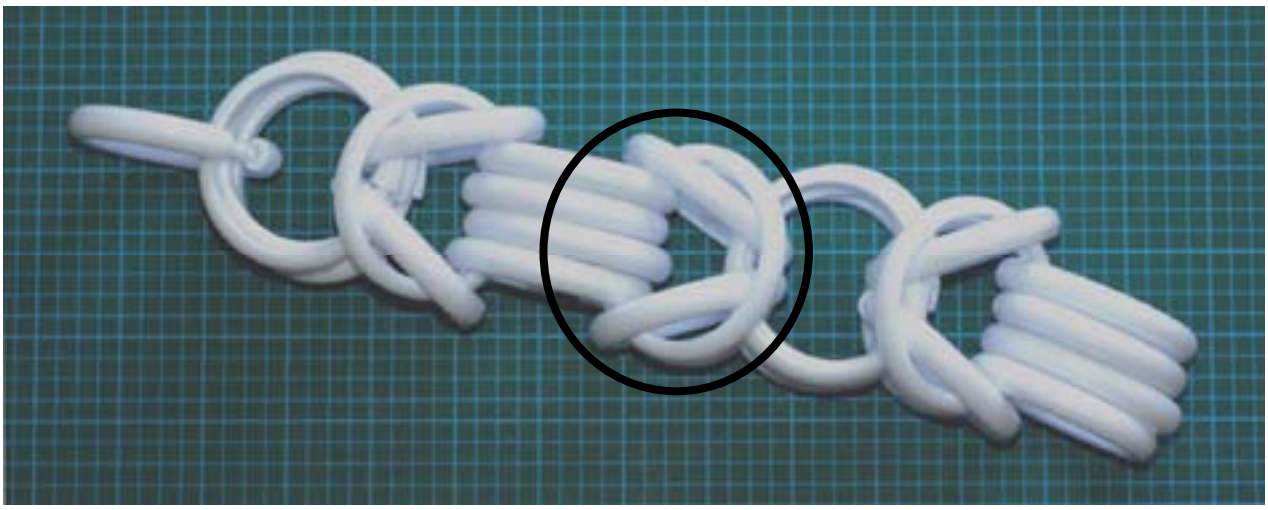

Figure 2: *Three Sections of Byzantine Chain*

The design of the Byzantine Chain is interesting from a topological point of view in terms of the interlocking of the elements. It is also a good example for examining three-dimensional symmetries. In addition to longitudinal translation symmetry, the chain also has reflection symmetry across two perpendicular, longitudinal planes (one parallel to the picture plan, one perpendicular to it) and one type of transversal plane (through each set of four aligned elements). It also has two kinds of 'glide rotation' symmetries. Firstly, locally, the interlocked grouping can be rotated 90^o around the chain's longitudinal axis, then reflected through the transversal plane through its center, and the global positions of the chain are preserved. Secondly, the grouping can be rotated through 90^o again, then translated to the position of the next grouping and globally, the positions are all preserved.

This design is often executed in silver, in a much more compact version than in the figure above. In this case, the links that form the interlocked groupings are oval, only two links are used between the interlocking groupings instead of four, and the chain acquires a more pronounced rigidity [5]. The degrees of freedom are then reduced to rotations around axes located in the centre of the connecting pairs of links. Each alternate joint can only move in one rotational direction, perpendicularly to its neighbours, and the chain is much less fluid.

The 'Rope' Chain

The third example under consideration is a simpler design in that every element is in the same position relative to the others. In tiling terms it is 'monohedral' [7]. In the Rope Chain design, a standard chain design is modified in such a way that every element is connected, not only to its immediate neighbours on either side, but to two or even three. In Figure 3, the elements connect four others each time.

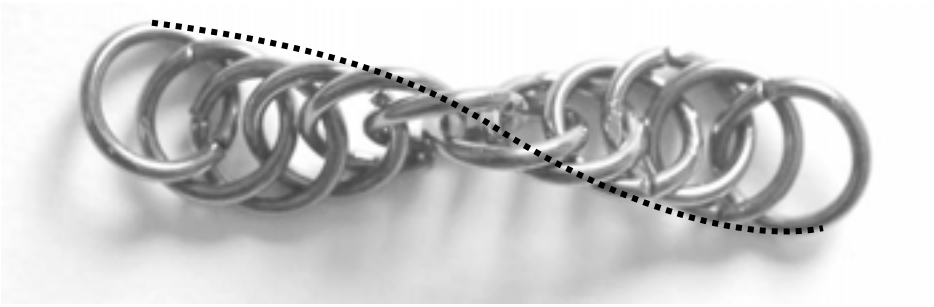

Figure 3: *The Twisted Rope Chain Design*

This design also has several symmetries, including rotation, longitudinal translation and 'glide rotation' through which each element is related to all the others. It has no global reflection symmetry. In the case of the design as executed in Figure 3, the elements are still loose and the chain can be untwisted somewhat so that the staggered positions are not as visible. This flexibility depends on the relationship between the gauge and the inner radius of the rings. As the gauge is increased relative to the inner radius, the chain becomes more rigid and the 'twist' more stable. At the extreme, the flexibility comes solely from the freedom of movement afforded by the rotational symmetry of the individual elements that can slide around each other.

The most interesting feature of this design, from a topological perspective, is the twist built up in the chain. If a line is traced that connects the outermost point of each element, on either side, as shown in Figure 3, then the design can be seen as a band or ribbon that twists around itself and whose ends can be joined, *just like a Moebius band*. The gauge, the inner radius and the number of links that are interconnected together within the length of the chain will determine how many times the 'band' twists around itself and therefore whether the resulting object has one or two edges and one or two faces.

Antoine's Necklace

Antoine's necklace is an interesting topological space that is defined recursively [3]. Start with a torus V. C_1 is a chain of tori linked together as in Figure 1. In each component of C_1, construct a smaller chain of tori (generally with the same number of links as in C_1). Let C_2 denote the union of the smaller tori at this level. Continue this process *ad infinitum*, and Antoine's necklace is the intersection of the C_i. This set is a non-empty, compact subset of $\mathbf{R}^3$. In $\mathbf{R}^3$, being compact is equivalent to being closed (contains its boundary) and bounded. Each C_i is a subset of C_{i-1} (for i greater than or equal to 2), so the intersection of the nested sets is non-empty.

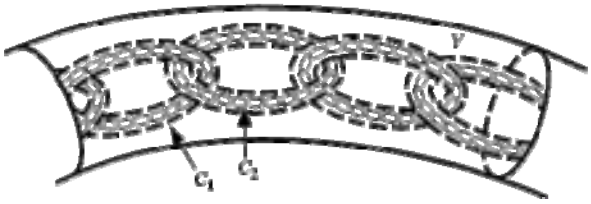

Figure 1: *Antoine's Necklace (http://mathworld.wolfram.com/AntoinesNecklace.html)*

Antoine's necklace is a fractal that is homeomorphic (or topologicially equivalent) to the middle thirds Cantor set [3]. The middle thirds Cantor set can be obtained as follows [8]. Start with a closed interval of unit length, remove the middle third open line segment leaving two closed line segments each of length one third. Then remove the middle thirds of the remaining closed line segments. Continue this process *ad infinitum*. The resulting set possesses many interesting properties. It is compact, uncountable (infinite but cannot be put in one-to-one correspondence with the natural numbers), and disconnected (given any two distinct points x and y in the set, there exist two disjoint open sets U and V such that x is in U and y is in V). The set is also self-similar, and one can find the corresponding similarity dimension D. An example of a more familiar self-similar object is the square. The similarity dimension D of the square is 2 because scaling down by a factor of 2 gives 4 similar squares, thus $2^D=4$. In the Cantor set, the original line segment is scaled down by a factor of 3 to obtain 2 similar line segments, so D is given by $3^D=2$, or $D = \log2/\log3 \approx 0.6309$.

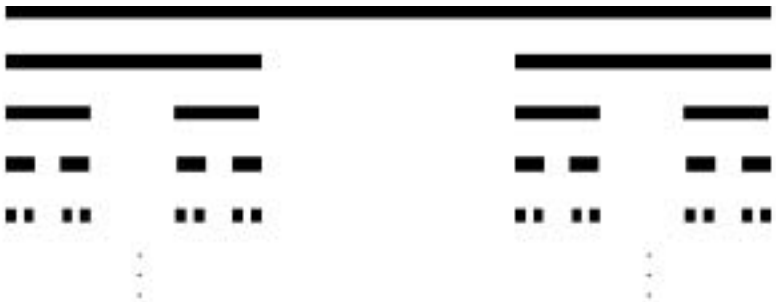

Figure 2: *Middle Thirds Cantor Set*

Conclusion

In summary, the workshop will introduce participants to different mathematical concepts that arise from studying various classes of chains. The hands-on activities will allow participants the opportunity to see and feel the abstract concepts and to come up with their own mathematical discoveries and queries about the chains.

References

[1] http://en.wikipedia.org/wiki/Link_chain, retrieved February 2009.
[2] http://en.wiktionary.org/wiki/link, retrieved February, 2009.
[3] D. Rolfsen, Knots and Links, AMS Chelsea Publishing, 1990.
[4] Adams, C.C. The Knot Book: An Elementary Introduction to the Mathematical Theory of Knots. W.H. Freeman and Co. 1994, p. 17.
[5] Taylor, T. and Whyte, D. Chain Mail Jewelry. Lark Books, 2006.
[6] Waszek, G.F. Making silver Chains: Simple Techniques, Beautiful Designs. Lark Books, 2001.
[7] Grünbaum, B, and Shephard, G.C. Tilings and Patterns. W.H Freeman and Co. 1987.
[8] L. A. Steen and J. A. Seebach, Counterexamples in Topology, Springer-Verlag, 1978.

Bridges 09 Interactive Workshop: The Geometry of Longsword and Rapper Sword Locks

Susan Gerofsky, University of British Columbia, Vancouver, Canada. susan.gerofsky@ubc.ca
Tiddley Cove Morris & Sword Dancers and Steel Phoenix Rapper, Vancouver, Canada.

Abstract

This interactive 75-minute workshop is suitable for teachers, students, geometry enthusiasts, dancers, and parents and children participating in the conference. Working with two traditional English sword dancing teams from Vancouver (Tiddley Cove Morris & Sword Dancers and Steel Phoenix Rapper), we will explore the geometric constraints of longsword and rapper sword "locks" (friction-locked symmetric configurations of wooden and metal "swords"). The workshop will offer demonstrations of these traditional dances and locks, led by the two dance teams; then workshop participants will be encouraged to try building the locks by dancing them (with help from the professional dancers) and by building them with coffee stir sticks. The geometry of locks will be explored in terms of some knot theoretic principles (crossings, sticks), and in terms of star polygons, minimum/ maximum angles, number of sticks, and "physical algorithms" for their production.

Structure of the workshop

Members of the Vancouver longsword and rapper sword teams, Tiddley Cove Morris & Sword and Steel Phoenix Rapper, will collaborate with Susan Gerofsky (herself a member of both teams) in leading an interactive workshop on aspects of mathematics and traditional dance for teachers, students, geometry enthusiasts, dancers, parents and children attending the conference. Demonstrations by the professional dancers will be followed by opportunities for participants to learn parts of the dances, creating longsword and rapper locks with swords through choreographed movements and building miniature versions of the locks with wooden coffee stir sticks, while exploring aspects of geometry and multiple representations and algorithms embodied by these forms.

What are longsword and rapper sword locks?

Longsword and rapper sword dancing are two styles of traditional sword dances recorded and practiced in the north of England [1, 2]. Longsword is performed by a team of dancers, traditionally based in one particular Yorkshire village. The dance uses blunt rigid wooden or metal "swords", held hilt and point by the dancers so that the members of the team are connected to one another by their swords through much of the dance. Longsword dances consist of movment figures danced by the team, punctuated with "locks" – regular geometric shapes, often star polygons – formed through dance moves. Locks weave all the dancers' swords together into an aesthetically pleasing geometric figure, which is held together by friction. Once the lock has been displayed, to the cheers and appreciation of the audience, dancers grasp their own sword and break the lock to continue the dance (often carrying out a mock "beheading" of the team captain or musician in the process!)

Traditional rapper sword dance has been recorded mostly in Northumbria, in the area around Newcastle-upon-Tyne, England. Like longsword, it is performed with blunt metal "swords" held hilt and point by the dancers, but rapper swords are flexible and springy rather than rigid, which affords a different range of shapes and configurations. Rapper sword dance moves are somewhat different from longsword stepping and figures, but like longsword, rapper is also structured as dance figures interspersed with "locks" created through collective movements of the dancers. The flexibility of rapper swords offers more options in the presentation of topologically isomorphic locks.

Exploring the geometry of longsword and wrapper sword locks

These regular figures are formed quickly in the course of a vigourous set dance, and then raised up, usually by one dancer, for watchers to admire. The nature of the production and display of the locks raises the following two interesting issues from a geometric point of view:

1) The locks must be capable of being produced smoothly and quickly through the choreographed movements of the team of dancers – that is, there must be a "physical algorithm" developed through the dance to produce these stellated and other shapes. When the same shapes are created by one person working alone with long wooden coffee stir sticks, it takes much greater time and effort to arrive at the figure. In this participatory workshop we will:
   • explore the nature of the physical algorithm that produces locks with a team of dancers,
   • work on developing small-scale physical algorithms that work with the stir sticks, and
   • compare these stick-based algorithms with other pencil-and-paper algorithms to produce similar figures.

   Throughout these explorations, we will be working on developing the idea of multiple algorithms and multiple representations of mathematical objects, and talking about the kinds of insight gained by noticing equivalencies and differences between these.
2) The locks are held together by friction and tension of materials, in a form that involves weaving of sticks/ swords. This fact, and the physical construction of the two kinds of sword impose geometric constraints on the locks. These constraints can be explored through addressing questions like:
   • what is the minimum/ maximum number of swords that can be used in a lock?
   • what is the minimum/maximum/optimum number of crossings needed for a lock to hold?
   • what constraints are there on the size of the angles in the locks?
   • given these constraints, can we design new locks (other than the traditional ones) that would hold and be constructable using a physical algorithm in the course of the dance?

There is the possibility as well of making lock shapes from string or cord, and exploring isomorphisms of knots and sticks, an area that has been developed in knot theory.

References

[1] Allsop, I. (1996). *Longsword Dances from Traditional and Manuscript Sources*. (A. G. Barrand, Ed.) Brattleboro, VT: Northern Harmony.

[2] Cawte, E.C. (1981). A History of the Rapper Dance. *Folk Music Journal.* 4(2), 79-116.

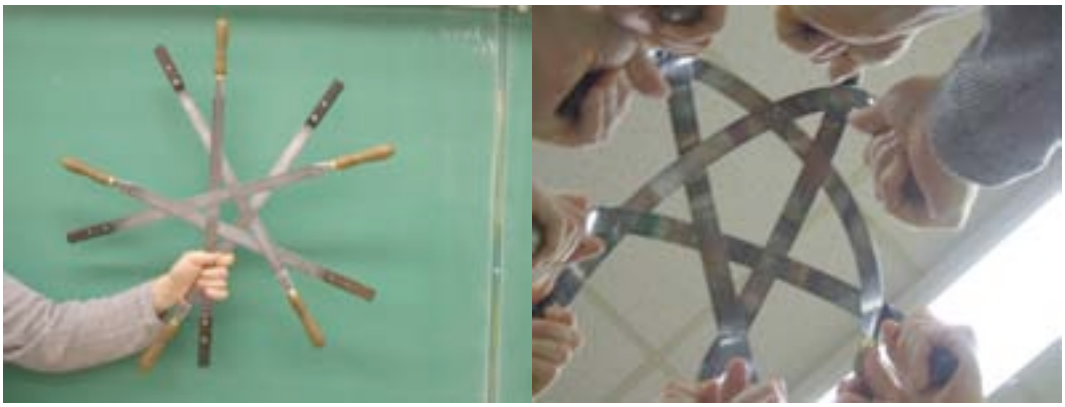

Photos of rapper sword locks with Steel Phoenix Rapper team at a practice (S. Gerofsky)

The Beautiful Triangle

Greg Beiles
The Lola Stein Institute for Leadership in Education
Daphne Rosenwald
The Toronto Heschel School
819 Sheppard Avenue West
North York, ON M3H 2T3
E-mail: greg@lolastein.ca; drosenwald@torontoheschel.org

The Beautiful Triangle workshop introduces to educators a multi-disciplinary study that integrates geometry, spatial sense, aesthetics, language, the history of ideas, and visual arts. The guiding concept of the study is that geometric figures represent and communicate concepts, feelings, and experiences. The workshop, which is rooted in a constructivist pedagogical model, combines both explanatory and experiential learning. By engaging in the same learning activities as the students would, educators gain insight into the analytical and creative processes involved in the study. The learning activities include: making choices based on aesthetic preferences; analyzing these choices through reference to geometric properties; naming triangles based on Greek and Latin roots; experimenting with triangles as analytical tools based on the model of Thales; appreciating and analyzing the work of Wassily Kandinsky as a model of conceptual geometric art; and designing a piece of conceptual geometric art with accompanying Artist Statement. The Beautiful Triangles workshop is based on a unit of study that has been piloted with students at The Toronto Heschel School. The workshop will be of interest to educators who are looking for ways to integrate mathematics and arts in ways that enhance critical and creative thinking.

Introduction

The Beautiful Triangle is a workshop based on a multi-disciplinary study of triangles that integrates geometry, spatial sense, aesthetics, language, the history of ideas, and visual arts. The guiding concept of the study is that geometric figures represent and communicate concepts, feelings, and experiences. The Beautiful Triangle was conceived and developed by educators at the Lola Stein Institute for Leadership in Education and has been piloted for the past four years at the Toronto Heschel School with classes of grade seven students. Through this unit, students appreciate how the properties of triangles can be used to express their own thoughts and ideas. This motivates students to produce innovative conceptual art, and to write insightful Artist Statements that evince a deep understanding of the geometry curriculum. The workshop - which combines presentation with hands-on activities- enables participants to experience the key elements of the unit, and provides them with tools for replicating it with students.

Aesthetics

The Beautiful Triangle workshop begins with an exercise in which participants are asked to look at a collection of triangles arranged on a white page. Participants are asked to consider which triangle is the "most beautiful" or "most appealing", and to rank the triangles in order from most to least beautiful. Participants scribe and then discuss their thoughts and feelings about each triangle. This first stage of aesthetic impression is followed by an analytic stage, in which participants use tools such as a ruler and a protractor to discover the properties of the triangle which they have selected. For instance, a person who

preferred a particular triangle because it appeared to be “balanced” will discover, using a protractor and ruler, that the triangle has three equal angles and three equal sides.

Constructivist Approach to Naming

The next stage involves naming the triangles. A list is provided of root words, suffixes, and prefixes with Greek and Latin etymologies such as *poly-*, *-gon, -skelos*. Using these roots, suffixes, and prefixes, participants construct a name for each triangle. The purpose of this exercise is two-fold, when done with students. Firstly, the activity provides a pretext for a lesson in the history of ideas: it is an opportunity for teachers to expose students to the development of geometry in ancient Greco-Roman civilization. Secondly, the activity constitutes a form of constructivist pedagogy: by allowing students to construct their own terms for the shapes, students recognize how the construction of language has both logical and contingent elements. For example, one might reasonably name the “balanced” triangle with equal angles an *equigon* (*equi-* meaning *equal*, and *-gon* meaning *angle*), or an equilateral (*-lateral* meaning *sides*). Of course, once students have assigned a personal name to their triangle, they are then introduced to the standard accepted nomenclature. This activity is replicated with workshop participants, as a hands-on example of constructivist pedagogy.

History of Geometry in Abstract Thinking

The workshop continues with examples of lessons that demonstrate for students how the ancient Greeks used geometry as an analytical tool. In particular, Thales' use of similar triangles to measure the heights of pyramids is discussed, and a practical way for students to replicate his experiment is provided. The purpose of these lessons is to further enhance students' understanding of how geometric figures can be used to represent and communicate abstract concepts.

Models of Abstract Art

The next stage of the workshop, which reflects the progress of the unit of study, is for participants to examine the abstract art of Wassily Kandinksy. Slides of Kandisky's work which feature the use of geometric figures are shown. Participants respond to the art using the same set of guiding questions that are provided to students. These include questions such as, what emotions does this art evoke? What is the story or message conveyed by this work? What title would you give this work of art? After participants view a few of Kandinsky's works, they have an opportunity to share and discuss responses. The workshop leader provides some examples of additional lessons which can be done with students to enhance their understanding and appreciation of Kandinsky's background, artwork, and aesthetic philosophy.

Student Conceptual Art

The final stage of the Beautiful Triangle unit is for students to create their own abstract geometric art that expresses a concept, emotion, or narrative. Over the years, students have selected topics as diverse as “Trust & Friendship”, “Jewish History”, “Gymnastics”, “Rock and Roll”, “The Cosmos”, “Chaos”, “Creation”, “Acceptance”, and “A Picnic in the Park”. Because of the precision required in forming the geometric images, the first stage of the work is done using a pencil, protractor and ruler. The work is then finished using pencil crayons, or water colour. In longer versions of the workshop (2-2.5 hours) participants have an opportunity to begin creating samples of geometric conceptual art. In shorter versions

(1.5 hours) the workshop leader describes the process through which students develop their artwork, and provides examples of student work that can be used as models.

Artist Statement

Each work of art is accompanied by an Artist Statement, which describes the concept of the work. This statement outlines how the choice of composition, the selection of particular shapes, and the properties of these shapes support and communicate the concept. The Artist Statement iincludes technical information about the shapes used, including their standard nomenclature, various angles and properties such as congruency, similarity, and ratio.

Teaching Tools

Each workshop participant receives a full colour booklet that provides an outline of the unit of study, examples of the key activities, and samples of student art and Artist Statements.

Samples of Student Work

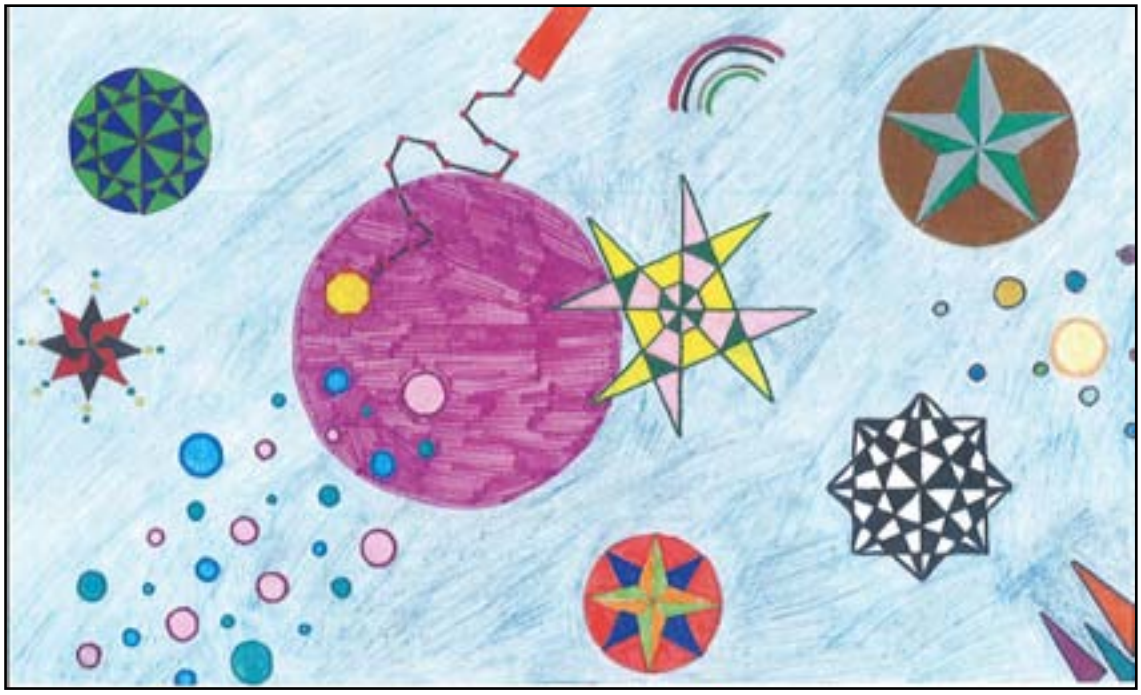

Figure 1: *The Cosmos*

Figure 2: *Everything Revolves Around Art*

Figure 3: *Happiness*

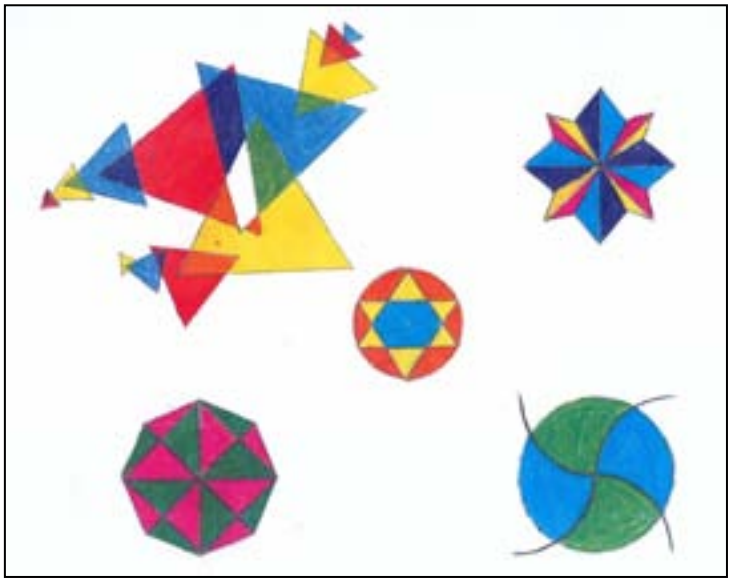

Figure 4: Diversity

Perspectives on Perspective

Sarah C. Melville*
Department of Humanities and Social Sciences
Clarkson University
Potsdam, NY 13699
E-mail: melville@clarkson.edu

Duncan J. Melville
Department of Mathematics
St. Lawrence University
Canton, NY 13617
E-mail: dmelville@stlawu.edu

Abstract

A picture plane is a two-dimensional space that can be approached in many different ways. Different cultures have evolved various conventions for depicting images in space and a study of these representational conventions can, therefore, illuminate important cultural conceptions. In this workshop, we explore the use of artistic conventions as a cultural lens. As illustrative exercises, participants will create and critique pictures using two of the most mathematical representational systems, the ancient Egyptian grid system, and Renaissance perspective as first described by Leon Battista Alberti.

Flattening the World

Since the earliest cave and rock art, people have sought to record their experiences of the world on two-dimensional surfaces. What they choose to record reflects what is important to them, but so too do the techniques used. In this workshop, we will look at a number of ways cultures have chosen to encode representations of space on a two-dimensional surface and use them to frame the cultural issues and questions of meaning embedded in the artifacts.

We will focus on two case studies where important artistic concerns demanded the use of mathematics. The first is how the functional requirements of Egyptian art were served by the development of the grid system, and the second is how the rise of humanism and the privileging of a particular point of space and time led to the introduction of true perspective. We will explain the cultural background and participants will have the opportunity to deconstruct, and to construct, pictures using these two techniques. This type of hands-on classroom activity helps students recognize why and how cultures choose to represent objects in space in a certain way, and how mathematics allows them to fulfill their purpose.

The canon of proportions in Ancient Egypt

Probably the most striking feature of ancient Egyptian art is its remarkable uniformity; only slight changes in emphasis, costume or accoutrements allow viewers to distinguish between objects from different eras. But this fact does not betray a lack of creativity or ability on the part of Egyptian artists, nor does it suggest that Egyptian culture was so stagnant or mired in tradition that it entirely rejected innovation. For over three thousand years composition and style were governed by specific conventions in order to ensure that viewers could instantly decode the meaning of any image and that the image itself could fulfill its intended function, whether as a message to the public, as a representative of the living in the afterlife, or as a connection between the mundane world and the spiritual plane. To the Egyptians, the image was eternal; it was imbued with power and the very essence of life itself. Accordingly, the artist's

goal was to depict the essential and timeless characteristics of an object rather than how it looked at a specific moment or from a particular point in space [1]. A flat, two-dimensional picture plane was perfectly well suited to the task.

Since it was necessary to portray the essential nature of a given object, artists showed as much of it as possible and to that end, they often combined different views to create a composite image. For example, Figure 1 shows a garden pond from a bird's eye view, but the trees, water plants and fauna from a frontal perspective. This was done to include as much of the whole scene as possible.

Figure 1: *Painting of a pond in a garden from the tomb of Nebamun. 18th dynasty.*

The human form was also subject to the essentialist principle described above: the head was shown in profile with a frontal eye and eyebrow; the chest, shoulders and hips were frontal, but one nipple/breast, the small of the back, the legs and feet were all shown in profile. In order to ensure that artists could consistently meet the ideal standards when depicting the human form, Egyptian artists developed a mathematical grid system to govern proportion. The grid system, which was implemented during the Old Kingdom (3rd millennium BCE) and endured with occasional adjustments into the Ptolemaic period (c. 323 to 27 BCE), did not stifle artists' creativity nor was it intended to allow unskilled laborers to produce art mechanically. Rather, the grid system guaranteed that the human figure would consistently be portrayed in its appropriately perfect form. A typical figure drawn according to the canon looks like this:

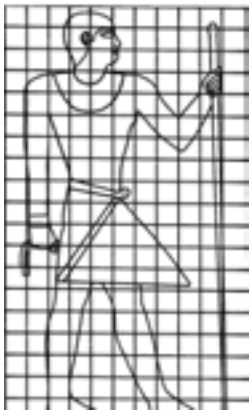

Figure 2: *After Robins [1] and Iverson [2].*

The Egyptian canon of proportions: an exercise for students

In the following exercise students take a modern photograph of a human figure and transform it into an essential composite using the standard Egyptian canon of proportions given below. Any clear photographic image will suffice, but students respond well to familiar figures such as celebrities. Using digital or Polaroid photos of the students is another option. Remember that the picture must conform to both ideal representation in terms of pose and proportionality of body.

For pose, you need

- Head in profile
- Full eye and eyebrow
- Frontal chest and shoulders
- Profile nipple/breast
- Profile small of back
- Full view navel
- Profile legs and feet
- Both feet from inside

For canon of proportions and the grid, you want: 18 squares from hairline to soles of feet.

- H0: Soles of feet
- H3: Middle of calf
- H6: Top of knee
- H9: Lower edge of buttocks
- H11: Small of back (for men)
- H12: Elbow
- H14: Nipple
- H16: Junction of neck and shoulders
- H18: Hairline

Also

- Vertical line through ear bisects figure
- Shoulders 6 squares wide for men, 4 or 5 squares for women
- Armpits 4 squares wide for men, a bit narrower for women
- Feet 3 squares long.

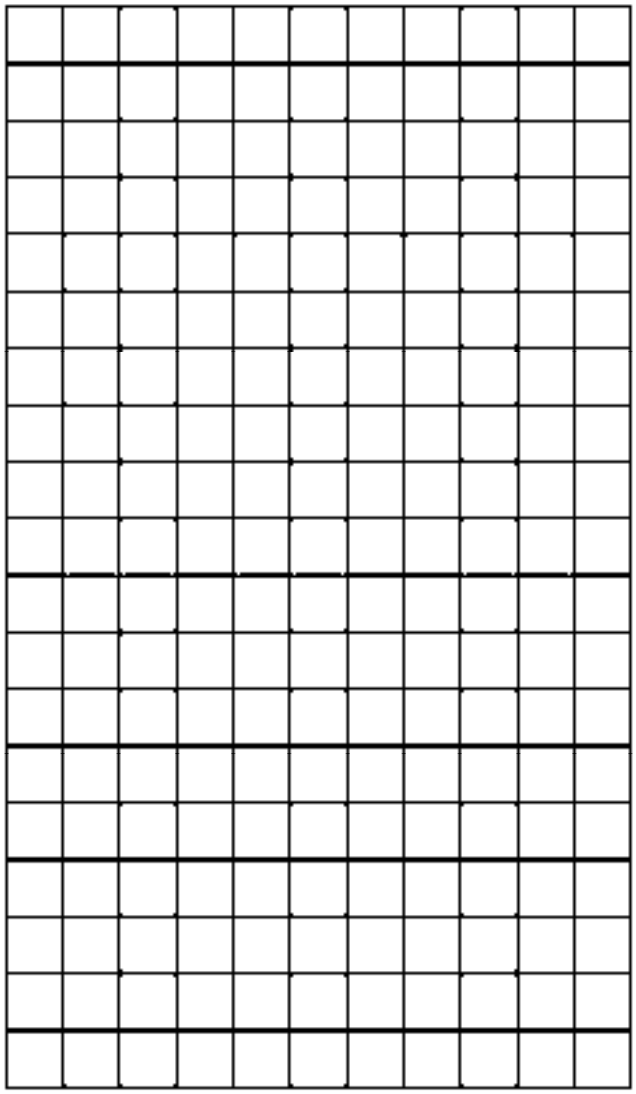

Figure 3: ***A grid for a standing figure.***

Alberti on Perspective

An entire humanistic approach to art is summed up in Alberti's description of preparing to draw, "I inscribe a quadrangle of right lines, as large as I wish, which is to be considered to be an open window through which I see what I want to paint. Here I determine as it pleases me the size of the men in my picture…" [3]

In early fifteenth-century Italy, the rise of humanistic philosophy led to a complex restructuring of the roles of viewer, artist, and representation centered in Florence. A philosophic focus on the individual, and individual experience, thoughts, actions and creativity was bound to have an impact on art. Study of the natural world implied an observer, and this, too, carried over to representation. Painting was to be about people, about specific individuals engaged in specific acts, frozen at a moment in time, and observed by the artist from a specific location. That is, a scene is represented as if through an 'open window' by someone standing at a particular distance from the window.

While these ideas were first articulated and demonstrated by Brunelleschi around 1415, they were first written down some twenty years later by Leon Battista Alberti. Alberti came from a wealthy Florentine family that had been exiled from Florence in one of its periodic political upheavals. Alberti became a Papal Secretary in 1431 at the age of 27 and was sent in the Pope's service to Florence in 1434. Arriving in his hometown, he encountered the artistic ferment there and wrote the first account of the perspective style, *On Painting*, in two versions, Italian for artists, and Latin for patrons.

The basic technical problem in perspective painting is that a distance vertically up the picture represents a distance back horizontally in the scene represented. How far up should represent how far back? Alberti roundly criticizes some of the techniques then in use and lays out his own scheme for creating a projective grid. Once the grid has been constructed, the artist knows the appropriate scale for the people and buildings that filled Alberti's vision of art. Alberti also shows how to use the grid to draw other simple shapes in correct perspective while conceding that after locating a few key points, the artist can fill in the details freehand.

As inheritors of the western Renaissance and having spent our whole lives watching naturalistic perspective representations on a glass window, it can be hard to step back, and realize that what seems obvious to us was originally radical and came from a particular philosophy. Choosing to represent a scene meant forgoing all the cultural markers that earlier painting had used so that it could be read by viewers. If size no longer denoted importance, how was one to know who was important in a painting? Looking through a window limits the use of well-known symbols and reduces a painting to a single frame from the narrative sequences that were often embedded in earlier forms of art. Fixing a point to look at the scene from fixes a point for the viewer to observe the scene. The artist dictates where the viewer should stand and thus re-arranges the relationship between the artist-craftsman and viewer-patron. Returning to the first text on perspective, when the theory was new and being laid out for the first time can help us to reflect on these issues and look at the art, and our own cultural assumptions in a new way.

Albertian Perspective: an exercise for students

In the following exercise, students create a simple scene of buildings and people using Alberti's directions from 1435.

The first step is to fix the scale of the painting by deciding 'the size of the men in my picture'. Dividing the height of a figure in three gives Alberti a scale he can use across the base of his picture. He conveniently bases his scale on a Florentine unit of measurement, the *braccio*, of about 23 inches.

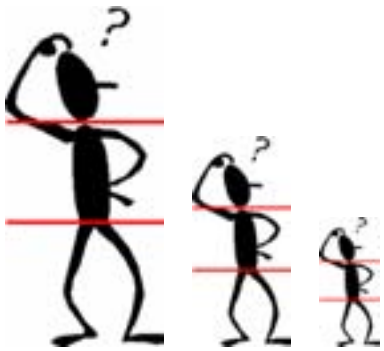

Figure 4: ***Choosing 'the size of the men'***

The next step is to choose a 'centric point' (the point at infinity) equal to the height of a man and join it to the points marked on his base (these are the orthogonals). Now Alberti chooses a position for the observer, for 'a painted thing can never appear truthful where there is not a definite distance for seeing it'. Given the height of the centric point and distance of observer to painting, Alberti shows how to create the horizontals for the projection of a square grid. He makes a copy of the marks across the base of his picture, locates the observer and joins the dots. Where the lines cross the picture plane marks the heights of the horizontals.

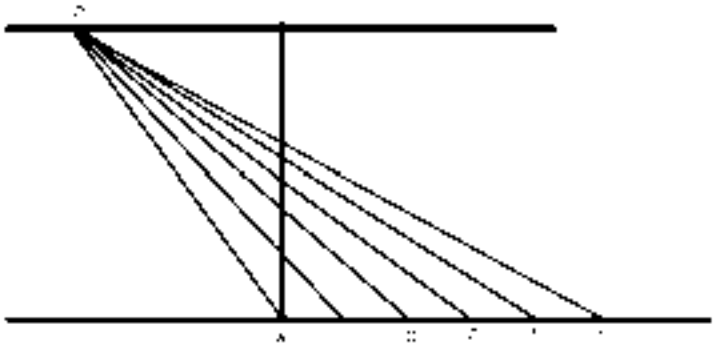

Figure 5: *Constructing the horizontal heights.*

Transferring the heights to his original rectangle, Alberti marks the horizontals for his square grid. The resulting grid is the classic 'pavimento'.

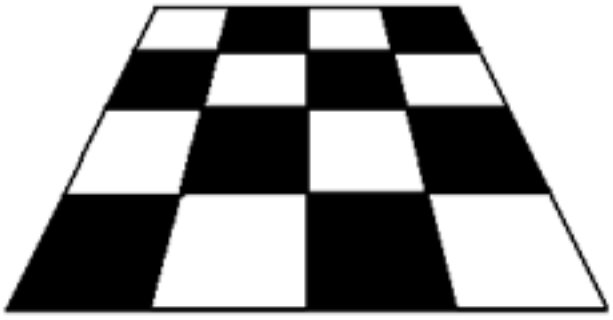

Figure 6: *An Albertian perspective square grid.*

As the horizon at infinity is chosen as the height of the people, all figures in the grid will be as tall as the horizon, and a building that is, say, three times the height of a person, will appear three times that height in the picture. Hence, Alberti has keyed all three axes to his scale.

References

[1] Gay Robins, *Proportion and Style in Ancient Egyptian Art* (Austin, University of Texas Press, 1994).

[2] E. Iversen, *Canon and Proportions in Egyptian Art* (London, Humanities Press, 1975).

[3] Leon Battista Alberti, *On Painting*, trans. J.R. Spencer, (New Haven, Yale University Press, 1966).

Workshop on The Fusion Project: Bridging Art Museums and Middle School Math Teachers

Benjamin Wells
Departments of Mathematics and Computer Science
University of San Francisco, 2130 Fulton Street, San Francisco CA 94117 USA
E-mail: wells@usfca.edu

Philip Wagner *
The Fusion Project, 736 Clipper Street, San Francisco CA 94114 USA

Abstract

The Fusion Project is a research program under development at the University of San Francisco, envisioned by Philip Wagner and directed by Benjamin Wells. With the collaboration of the Fine Arts Museums of San Francisco (and their de Young Museum), it seeks to bring art to the math classroom and math students to the art museum. In this Bridges Workshop, we shall explore the art of the de Young Museum and the mathematics it stimulates. Participants will also learn how to align test problems, outcomes, and works of art. Members of the workshop will have the opportunity to extend and improve Fusion Project instructional materials (and the program itself). The workshop is especially geared to middle school math teachers and to those who are interested in replicating or adapting this program.

1. The Fusion Project Workshop: Introduction and Purpose

Philip Wagner created The Fusion Project [1] (FP) as a collaboration between art museums and middle school mathematics classrooms. The main idea of FP is to engage middle school students in learning some critical math concepts by discovering them displayed in artwork and architectural components of a major art museum. In 2006 Phil approached the Fine Arts Museums of San Francisco (FAMSF) with the idea, and Sheila Pressley, FAMSF Director of Education, saw the value to students and to the museum. She immediately wrote a letter of support for FP. FAMSF defined the initial step of the project as an analysis of their permanent collections' potential for supporting mathematics instruction. They contracted with Benjamin (Pete) Wells to perform alignments of works of art with targeted California 7th grade math standards; these arose from aligning the standards with math test results. Thus began a unique program of using the art museum to enhance standard mathematics curricula in middle schools. The claim of uniqueness is based on surveying teachers, districts, and museums in many states, four countries, and numerous web pages. It is not an exceptionalist claim: we would love to find others doing this work. Indeed, spreading the ideas is the main purpose of this workshop. For more background on FP, see [2–5].

2. The Fusion Project at FAMSF: The Rest of the Stories

Pete's FP report to FAMSF [4] comprises seven *Stories*, later expanded into *Encounters* [5]. These are described in [2], which includes material from three of the seven topic clusters. The remaining four Stories are given below, abbreviated and slightly reorganized from the original form. The reader should keep in mind that these are outlines, like screen treatments, not finished instructional materials. Two of the Stories/Encounters in [2] are much closer to that. All art is from the de Young Museum; works not pictured here may be seen in [2], and there are many additional works listed in [4].

Story 2. Fractions, percent, and breakdown. You enter the gallery that is the new home of the *Piazzoni Murals* (Fig. 1), set into identical alcoves. The *Land* side shows inland scenes, the *Sea* side gives coastal views. It is hard to grasp all of them, and small groups from your math class gather before different scenes. The teacher notices that 1/6 of the class is looking at 1/4 of the murals and these two numbers are the same. Luckily the number of mural wall alcoves is 6 + 6 = 12, and that makes for easy fractions. Harder fractions come from breaking down a mural into sky, water, and land portions.

Figure 1. *Piazzoni Murals Gallery*

Figure 2. Dinner for Threshers[1] *(Wood),* Burning of LA *(Petlin*)

Math questions related to artworks: Problems, skills, and techniques exercised by answering the questions: arithmetic (and maybe some algebra) with fractions, percent, conversion of fractions to percent, easy addition of fractions with unlike denominators.

Piazzoni Murals Gallery by Gottardo Piazzoni (Fig. 1)

A. If 1/6 of the class equals 1/4 of the mural niches, then how many students are in the class?
B. One-sixth of your class would be how many niches? what fraction of niches? what percent?
C. If we add on the niches next to the doors, what percent increase in the number of niches is this? Fractions with denominators 7 and 14 now arise too.
D. Show different ways to pick 1/3 of the murals, 1/4 of them, 1/6 of them.
E. Fraction problems based on the ceiling slots, lights, and the window panels can also work.

Dinner for Threshers by Grant Wood (Fig. 2)

F. Fractions based on 12 again, or 6, 7, 14 by using one side of the table or the head and foot. Then 16 or 17 using the wait-staff, with more people in the wings.

The Burning of Los Angeles, 1965-1967 by Irving Petlin (Fig. 2)

G. Fractions based on 13 strips in each of four panels. Provides parallel to weeks in a year. Also the figures are worth counting. There is only one white figure (or at most a few), so percent could be interesting. How about the fraction of strips with or without smoke?

Story 5. Lines and planes in space, ruled surfaces, and belts. There are only a few ways two lines can be placed in space: on top of each other, parallel, intersecting, or skew. Two or three planes also have limited ways to run along or into each other. With more lines, everything gets more complicated, but there are some neat curved surfaces (called *ruled surfaces*) that are built from lines. The skin of the Hamon Tower (see [2, Figs. 9, 10]) is such a surface. Another kind of ruled surface is a belt, where the lines run across the belt. These too turn up at the de Young Museum.

Math questions related to artworks: Problems, skills, and techniques exercised by answering the questions: how lines and planes interact in 3-dimensional space, recognition and qualitative analysis of ruled surfaces, different ways belts can be connected and run.

Raceme by Daniel Clayman (Fig. 3)

H. A raceme is a flower shape, but this shape is clearly something more familiar. Cones are ruled surfaces, as are cylinders. Planes are ruled, so prisms and pyramids are too. Spheres?

Figure 3. Raceme *(Clayman),* UW84DC#2 *(Deacon), Wuvulu ritual oil dish*

UW84DC #2 by Richard Deacon (Fig. 3)

I. Multiple belts form this sculpture. If a belt is given a half-twist before it is joined in a loop, then it is a Moebius surface or band. This is used in industry for even belt wear, because a Moebius band has only one side. Does this sculpture have any one-sided belts in it?

Wuvulu ritual oil dish (Fig. 3)

J. This shape is simple but it escapes simple description. The surfaces are not only ruled, they are also types of cylinders (the ruling lines are all parallel). Locate the three ruled surfaces.

Hovor II by El Anatsui (Fig. 4)

K. This work is ruled in small areas, but is distorted overall by hanging and by variation in seal sizes. Find some ruled areas and some that are not.

Terrace overhangs/Mondrianic shadows (Fig. 4)

L. Seen from the second floor, the huge Terrace overhangs cast shadows on the courtyards below. The shadows fall from bars arranged in space; how does that affect the lines in the shadows? How will the shadows change as the sun moves?

Figure 4. Hovor II [2] *(Anatsui), Mondrianic shadows*

Figure 5. 3 Gems *(Turrell)—interior*

Story 6. Parallels, perspective, other projections, and the shining sun. Parallel lines and planes abound in normal buildings. There are plenty in the de Young Museum too, but there are some surprising departures built right into the architecture, for example the *Hamon Tower* (see [2, Figs. 9, 10]). In making drawings look realistic, parallel lines (like horizontal ledges on buildings and road edges) are drawn so that, if extended, they meet at a point, called the vanishing point. This is the heart of creating *linear perspective*. Perspective drawing is a type of projection (think of the bulb in a film projector casting rays out in a cone through the film and onto the screen). There is plenty of perspective in paintings at the de Young Museum but there are several other interesting cases of projection too. One is the bright disk cast on the floor in *3 Gems* (Fig. 5); it is not an image of the sun, but an image of the oculus, the hole in the ceiling.

Math questions related to artworks: Problems, skills, and techniques exercised by answering the questions: Geometric and algebraic conditions for parallels; finding vanishing points in perspective drawings; visualizing objects in space; seeing projections and how projections can help us visualize the original objects.



Figure 6. From the Garden of the Chateau *(DeMuth),* Rainy Season in the Tropics[3] *(Church), Igbo door*

3 Gems by James Turrell (Fig. 5)

M. The rings around the central blue/green disk are parallel. Why?

N. At certain times of day, the oculus (the hole in the roof) is projected by the sun on the floor. Because the sun is so far away, its rays are nearly parallel. So the image of the hole on the floor is really the same size as the hole seen along the sunbeams (why? because the oculus is parallel to the floor). What does this say about the size of the hole from below?

From the Garden of Chateau by Charles DeMuth (Fig. 6)

O. This painting purposely distorts perspective. It harks back to the days just before the Renaissance when artists knew something about parallels appearing to meet in the distance but made it more complicated than it needed to be. See if you can find three violations of the rules of perspective here.

Rainy Season in the Tropics by Frederic Edwin Church (Fig. 6)

P. Circles can be parallel too. When does that happen?

Q. The space between the two rainbows is called Alexander's dark band. Describe it.

Igbo door (Fig. 6)

R. There are numerous lines and line segments in this carving. But there seem to be only three different slopes plus vertical segments. How can you figure out the slopes?

Story 7. Uniformity, symmetry, chaos, confusion, and the feeling of being lost. Sometimes art is all about uniformity, but more often it breaks up order and introduces some element of diversity, even chaos or confusion. The de Young Museum features art lying across this entire range. But now we focus on the extremes: great sameness and great differences. The mathematics of sameness is called symmetry, the geometry of chaos is called fractal geometry, and the logic of confusion is called paradox. Any of these extremes can give the sense of being lost. If everything is the same (say, you are in the middle of *Strontium*, [2, Fig. 3]), every place looks alike (but not every direction). If you are on the crack in *Drawn Stone* (Fig. 7), it looks rough, but pretty much like any other place on the crack. If you are looking at *Hovor II* (Fig. 4), you might be looking up, or down, or sideways. People talk about losing themselves in art; in these cases, the loss feels very real.

Math questions related to artworks: Problems, skills, and techniques exercised by answering the questions: finding symmetry and uniformity; finding variety and scaling roughness; finding impossibility and perplexity.

Strontium by Gerhard Richter (see [2, Fig. 3])

S. This work has symmetry: one place is much the same as many nearby places. In particular, there is no difference between one ball and its neighbors of the same size. The picture can shift left or right a column, or up or down a row, and still look the same, but it "resists" being turned sideways because the rows of large balls are different than the columns of large balls (same idea for the small balls, too). This type of symmetry is called *translation symmetry*. Can you see some other translation symmetries in this work of art?

Eucalyptus benches by architects Jacques Herzog and Pierre de Meuron (see [2, Fig. 7])

T. The benches have rotation symmetry. How much do you have to turn a set of 6 benches until it looks like the original (ignore the woodgrain)? How about in the other direction?

3 Gems (Fig. 5)

U. There is rotation symmetry on the floor, and chaos in the mixture of colors in the central disk. If the benches continued all the way around, and the archways were closed, can you describe other rotation symmetries?

Figure 7. Drawn Stone *(Goldsworthy),* Shadow Frieze *(Cook)*

Drawn Stone by Andy Goldsworthy (Fig. 7)

V. This crack is like a coastline, a scaling fractal, a kind of roughness that has the same wiggliness from the second floor window, standing above it, or getting your face close to it. But it is not completely random, for it runs fairly straight across the tiles then turns in order to pass through the benches. Is it a loop? What percent of the tiles does it break? What percent of the benches? How could the artist crack stone in such a controlled way? Did he?

Shadow Frieze by Lia Cook (Fig. 7)

W. There are symmetries that slide the shapes (ignoring the colors) up to the right and up to the left, plus others we can explore. Up close, there is a lot of confused color. At a distance, both this symmetry and this chaos disappear into a coherent picture of draped cloth, which is paradoxical. Can you find a place to stand where all these extremes balance?

3. Outline of Workshop Activities

Several activities will be offered. It is likely that there will be some parallelism, but participants will determine their own preferences for progressing through the topics. We believe this introduction to FP can benefit participants' own classrooms as well as the Fusion Project.

I. Math from art. Examples of art from the FAMSF collection will be shown on slides and posters, and participants will be invited to identify interesting math principles, concepts, and topics that could be supported by or discovered in the artwork. The outcome may be something like the stories outlined above. Our personal experience from taking tours of the de Young Museum with middle school and college math students (more than 50), math teachers, college professors, and interested nonmathematical friends has shown us three things: (1) there is always more to find in the art, (2) students are remarkably insightful, with teachers next, and (3) FP benefits immensely from the visitors' observations.

II. Alignments. Workshop participants will be invited to make their own alignments between math test problems and typical standards, and then between the top standards and works of art. This will be good practice if members are interested in replicating FP in other localities. It can also give one confidence when colleagues make judgments that correlate highly with each other's (and with one's own).

Please see Figs. 8–10 for examples extracted from the FP-FAMSF alignments. These charts are fragments of the full worksheets. In Fig. 8, the problems from a standardized test are associated with the math standards [6] for which they have affinity. The affinity rating depends on the number of incorrect answers to a problem; the pink standards have emerged as targets. Fig. 9 shows an alignment between works of art at the de Young Museum and standards. Fig. 10 shows how the artwork and math topics cluster into stories. These figures are extractions from the full alignments, and the exercises in the workshop will be similarly limited.

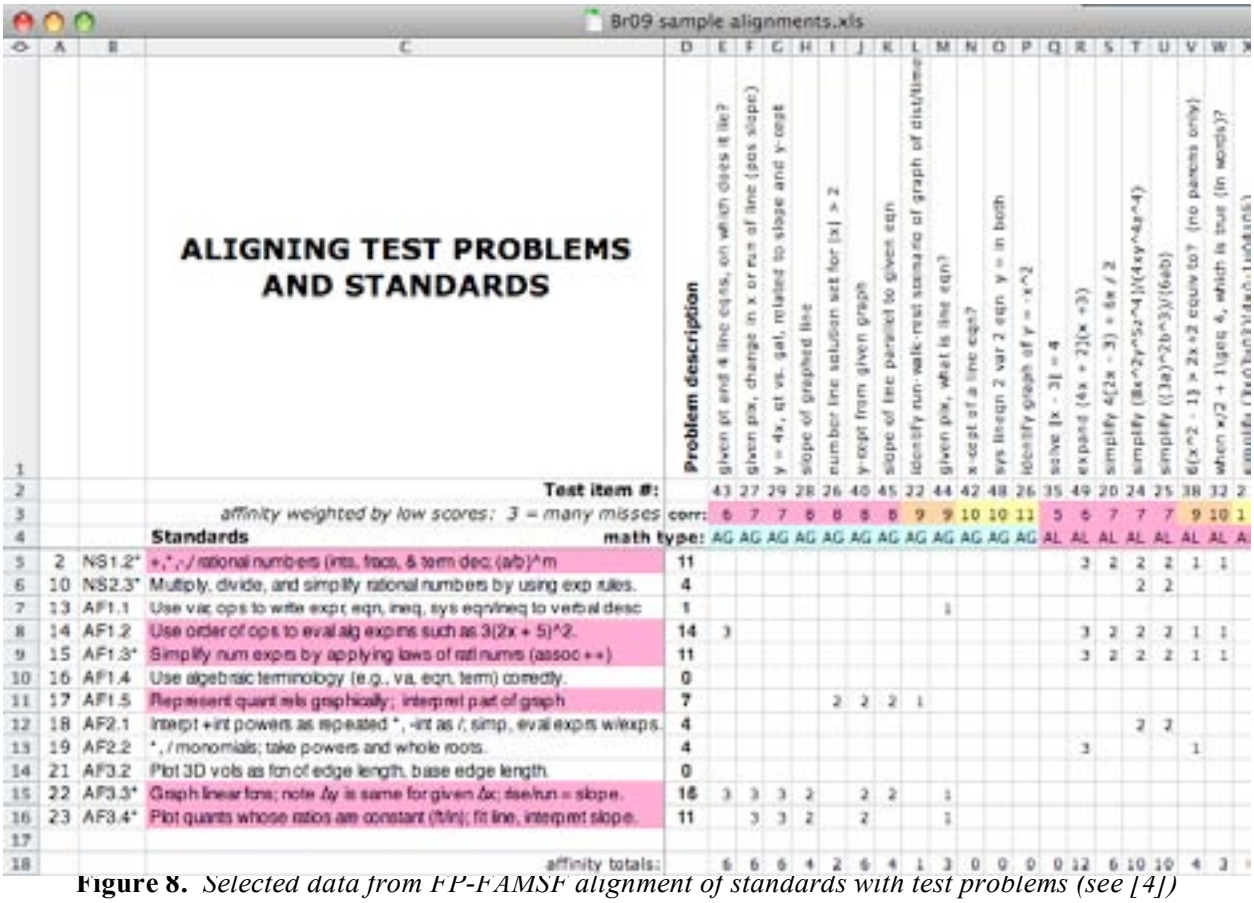

Figure 8. *Selected data from FP-FAMSF alignment of standards with test problems (see [4])*

III. Sharing FP techniques. Workshop facilitators will demonstrate FP enhancements (see [2, pp. 5–7] and invite participants to try them out in the workshop. Some of this is classroom-tested material used in

previous teachers' workshops, including the training of our FP Teachers Advisory Group (TAG). The TAG has been largely responsible for the detailed material we'll share. It is still under active development, so participants' reactions will be most valuable.

Based on FAMSF experience with their program *Get Smart with Art @ the de Young* [7], it is anticipated that several iterations of refinement will be required for a working set of encounter and enhancement materials. Even before that, we are organizing summer workshops for teachers. Then we can evaluate the materials in classroom settings, obtain feedback from the users, and move to distributable printed products, with implementation already underway.

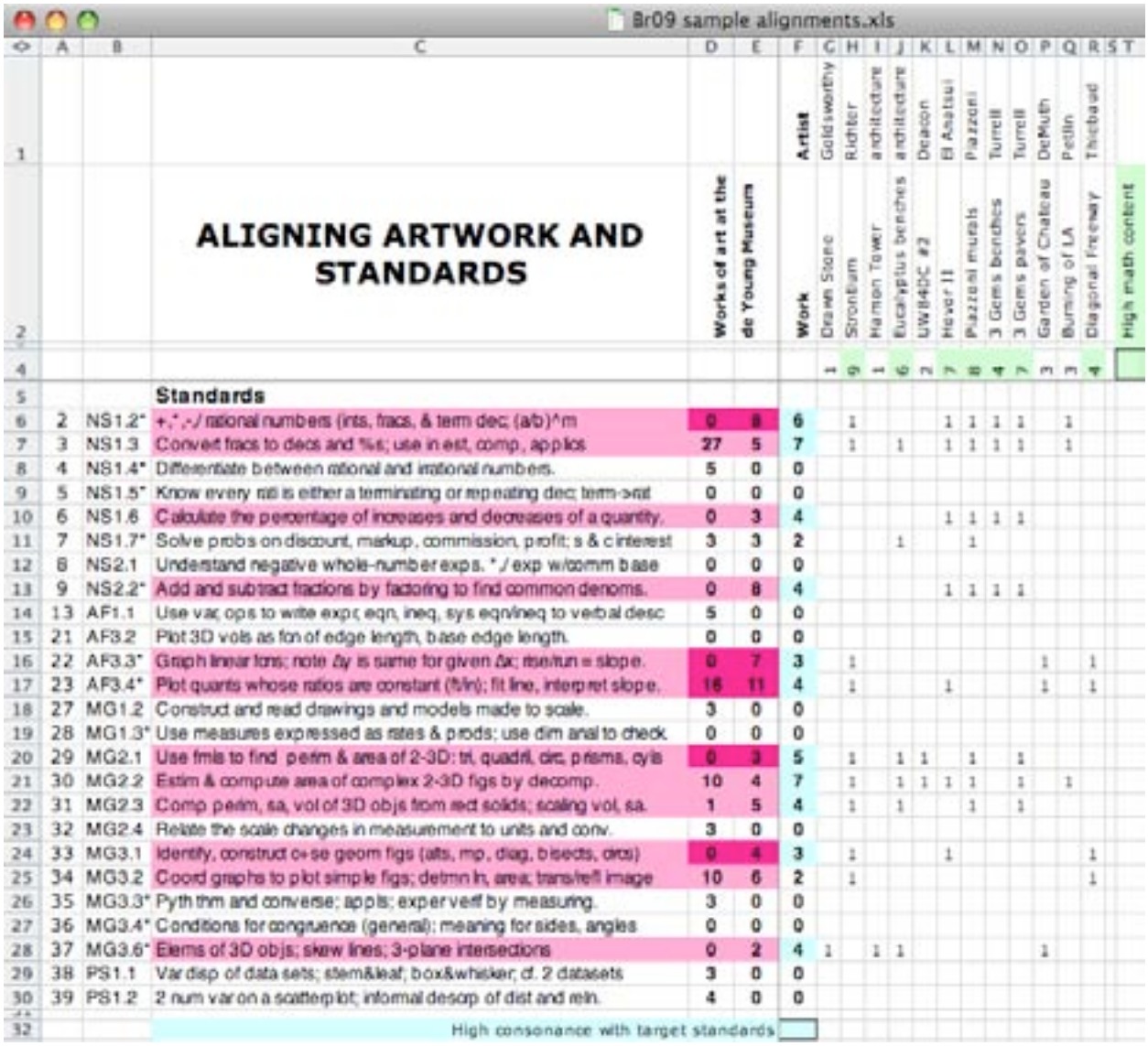

Br09 sample alignments.xls

	A	B	C	D	E	F	G	H	I	J	K	L	M	N	O	P	Q	R	S	T
1						Artist	Goldsworthy	Richter	architecture	architecture	Deacon	El Anatsui	Pazzani	Turrell	Turrell	DeMuth	Petlin	Thiebaud		
2			ALIGNING ARTWORK AND STANDARDS	Works of art at the de Young Museum		Work	Drawn Stone	Strontium	Hamon Tower	Eucalyptus benches	UW840C #2	Hevea II	Piazzoni murals	3 Gems benches	3 Gems pavers	Garden of Chateau	Burning of LA	Diagonal Freeway	High math content	
4							1	9	1	6	2	7	8	4	7	3	3	4		
5			Standards																	
6	2	NS1.2*	+,*,-,/ rational numbers (ints, fracs, & term dec; (a/b)^m	0	8	6		1				1	1	1	1		1			
7	3	NS1.3	Convert fracs to decs and %s; use in est, comp, applics	27	5	7		1		1		1	1	1	1		1			
8	4	NS1.4*	Differentiate between rational and irrational numbers.	5	0	0														
9	5	NS1.5*	Know every rati is either a terminating or repeating dec; term->rat	0	0	0														
10	6	NS1.6	Calculate the percentage of increases and decreases of a quantity.	0	3	4						1	1	1	1					
11	7	NS1.7*	Solve probs on discount, markup, commission, profit; s & c interest	3	3	2				1			1							
12	8	NS2.1	Understand negative whole-number exps. * / exp w/comm base	0	0	0														
13	9	NS2.2*	Add and subtract fractions by factoring to find common denoms.	0	8	4						1	1	1	1					
14	13	AF1.1	Use var; ops to write expr; eqn, ineq, sys eqn/ineq to verbal desc	5	0	0														
15	21	AF3.2	Plot 3D vols as fcn of edge length, base edge length.	0	0	0														
16	22	AF3.3*	Graph linear fcns; note Δy is same for given Δx; rise/run = slope.	0	7	3		1								1		1		
17	23	AF3.4*	Plot quants whose ratios are constant (%/in); fit line, interpret slope.	16	11	4		1				1				1		1		
18	27	MG1.2	Construct and read drawings and models made to scale.	3	0	0														
19	28	MG1.3*	Use measures expressed as rates & prods; use dim anal to check	0	0	0														
20	29	MG2.1	Use fmls to find perim & area of 2-3D: tri, quadril, circ, prisms, cyls	0	3	5		1		1	1		1		1					
21	30	MG2.2	Estim & compute area of complex 2-3D figs by decomp.	10	4	7		1		1	1	1	1		1		1			
22	31	MG2.3	Comp perim, sa, vol of 3D objs from rect solids; scaling vol, sa.	1	5	4		1		1			1		1					
23	32	MG2.4	Relate the scale changes in measurement to units and conv.	3	0	0														
24	33	MG3.1	Identify, construct c-s-e geom figs (alts, mp, diag, bisects, circs)	0	4	3		1				1						1		
25	34	MG3.2	Coord graphs to plot simple figs; detmn ln, area; trans/refl image	10	6	2		1										1		
26	35	MG3.3*	Pyth thm and converse; appls; exper verif by measuring.	3	0	0														
27	36	MG3.4*	Conditions for congruence (general); meaning for sides, angles	0	0	0														
28	37	MG3.6*	Elems of 3D objs; skew lines; 3-plane intersections	0	2	4	1		1	1						1				
29	38	PS1.1	Var disp of data sets; stem&leaf; box&whisker; cf. 2 datasets	3	0	0														
30	39	PS1.2	2 num var on a scatterplot; informal descrp of dist and reln.	4	0	0														
32			High consonance with target standards																	

Figure 9. *Selected data from FP-FAMSF alignment of standards with artwork (see [4])*

IV. Building and truing FP. Workshop members will be invited to contribute now and later to the growing body of FP materials. All those participating in the workshop will be urged to comment on FP and offer suggestions for improving it.

Our model proposed at the University of San Francisco is to pay teachers to take workshops at the de Young Museum in order to implement FP in their classrooms, with the assistance of FP-trained USF students and local peer teachers. We have a list of schools and teachers interested in such workshops, and by the time of Bridges 2009, we may already have held the first round of summer workshops. We hope

our Bridges workshop results in collaborations that can improve our USF program and lead to similar alliances with museums and educational institutions elsewhere.

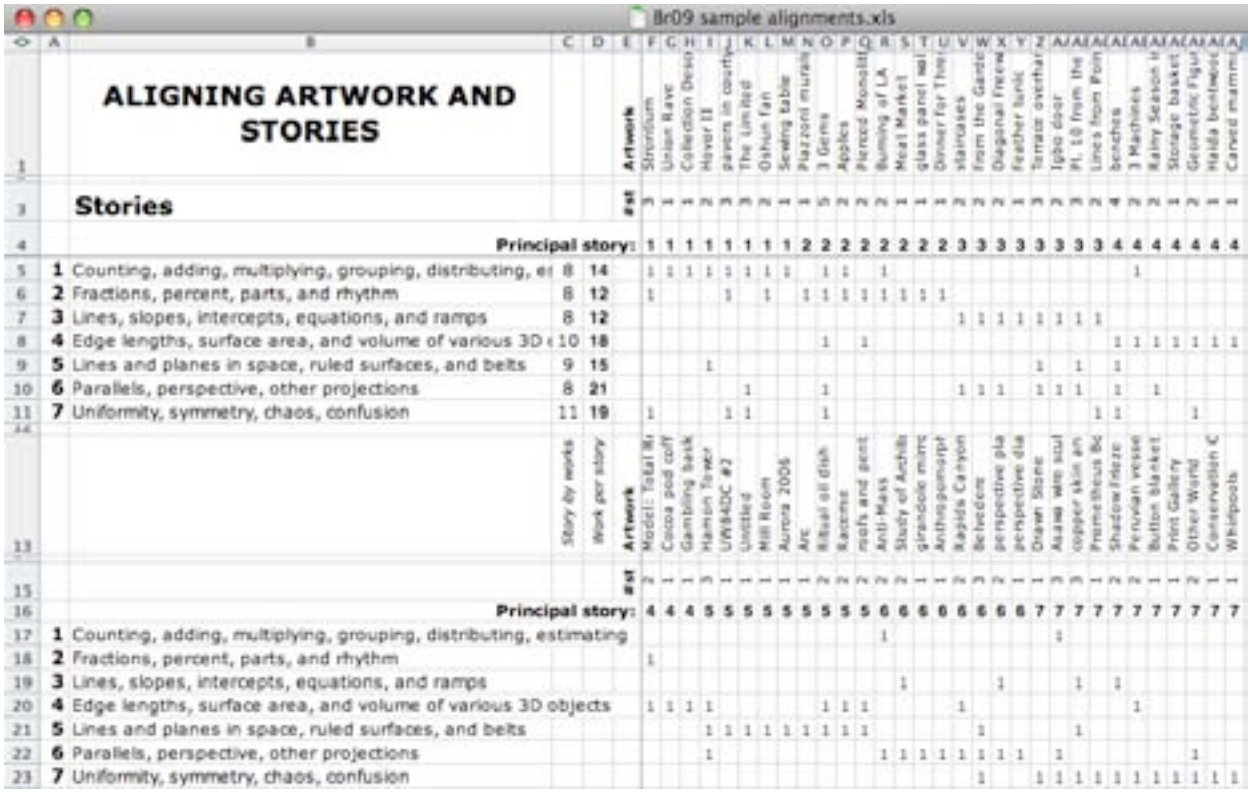

Figure 10. *Selected data from FP-FAMSF alignment of stories with artwork (see [4])*

References

[1] The Fusion Project, http://fusionprojectinfo.com/ —constructed by Cyndi Lott (Align PR Agency)

[2] B. Wells and P. Wagner, *Bridging Art Museums and Middle School Math Classrooms*, submitted to Bridges 2009.

[3] B. Wells and P. Wagner, *The Fusion Project: Bridging the Art Museum and the Middle School Math Classroom*, submitted to the Journal of Mathematics and the Arts.

[4] B. Wells, *Math Stories at the de Young Museum*, private report to FAMSF, 2007, rev. 2009. Contact author for a copy. Some materials used are not yet circulating.

[5] B. Wells, C. Potter, and D. Schattschneider, *Math Encounters at the de Young Museum*, private report to USF College of Arts and Sciences, 2008. Contact author for a copy.

[6] California Department of Education, *Grade Seven Mathematics Content Standards*, in Mathematics Content Standards for CA Public Schools, Sacramento CA, 1997, pp. 31–35.

[7] Get Smart with Art @ the de Young: http://www.famsf.org/fam/education/subpage.asp?subpagekey=19

[1] Photo credit: Janet Haven, http://xroads.virginia.edu/~ma98/haven/wood/threshers.html

[2] Inset photo credit: CRASH-candy, http://flickr.com/photos/crash-candy/2363892635/

[3] Photo credit: Sillieee Bunnieee, flickr.com/photos/sillieeebunnieee/2758468099/

A Workshop to Build Three Simple Tensegrity Models for K-12 Mathematics Classrooms

Robert McDermott
Center for High Performance Computing
University of Utah
Salt Lake City, Utah, 84112, USA
E-mail: mcdermott@chpc.utah.edu

Abstract

In this workshop, participants will build two styles of models. One style of model is built from sticks, and vinyl tubing. This first model will determine lengths of struts and lines, and will also be extensively labeled to help in building finished tensegrity models. A second style of model will be built from PVC pipe, PVC sleeves, and bungee cord. Additional printed information will be provided to help build the finished tensegrity models.

Building physical models [1], [2], [3], and writing about the building process, continues to be my focus. Most recently, I have chosen to build tensegrity models, and to provide clear instructions to help build them from PVC pipes, PVC sleeves, and bungee cords. I have constructed preliminary models from sticks and vinyl tubing, and labeled them extensively in order to assist in the building of the final PVC models. The final models take a considerable amount of time and resources to build. It has been important that the models be durable so they can be handled by students through a number of years, and be of a reasonable size so that they can be seen by 20-30 students in a classroom. Each tensegrity model has an interesting set of spatial properties and is engaging as a physical object.

1. Introduction

Physical models for use in K-12 classrooms can be built from paper [1], from sticks and vinyl tubing [2] or from PVC pipe, PVC sleeves and bungee cord [3]. These models are simple and use inexpensive materials, yet convey meaningful spatial concepts to students who manipulate them in their hands. The models described in this paper are tensegrities which combine both compression members and tension members. The compression members are struts realized with PVC pipe, and the tension members are realized with bungee cords. PVC sleeves interconnect compression members and tension members, **Figure 1**. Tensegrity models are stable, in that their compression members do not move relative to each other. In addition, compression members do not touch each other, giving the viewer the impression that the compression members are floating in space.

In my research of tensegrity models I encountered the work of Kenneth Snelson [4] with his initial discovery of tensegrity structures in 1948. Snelson was an art student at Black Mountain College in North Carolina. Snelson's work of 60 years ago continues to be inspirational for me and is the motivation for this paper. He is an artist with his work being exhibited in many prestigious art galleries.

I have produced two sets of physical models for this paper. The first set of models is built with sticks and vinyl tubing. These models are based on simple geometric shapes such as a cube, **Figure 3a,** a truncated tetrahedron, **Figure 4a,** and a twisted triangular anti-prism, **Figure 5a**. These models contain all the struts of the finished tensegrity models, and are extensively labeled in order to better understand and assist the building of the final tensegrity models. The stick models serve to support all the compression struts of the final tensegrity models.

A cube, **Figure 3a,** provides support for the struts in the building of a 1st tensegrity model which is entitled an extended octahedron, **Figure 6a**. A truncated tetrahedron, **Figure 4a,** serves to support the struts of a 2nd tensegrity model. A twisted triangular prism, **Figure 5a,** serves to support and build a 3rd tower tensegrity model. The stick models provide both the lengths for compressions members of PVC pipe and the length of bungee cord for the tension members.

All struts in a single tensegrity models are the same length. Once there is an understanding of using PVC sleeves and line to connect two struts, all connections in a single tensegrity model are the same. The stick models have their struts labeled and their sleeves labeled and provide a map to follow in assembling them into a complete tensegrity structure. All individual tensegrity models are assembled in an identical manner.

Appendix I itemizes supplies for the individual tensegrity models. This table of supplies has both the length of struts, the length of lines, and the number of sleeves to interconnect compression members and tension members. Labeled figures in the paper provided a plan for assembling the tensegrity models. The labeled figures will hopefully make it easier to be convinced that building these models is a reasonable and manageable task to accomplish.

2. Supplies and Tools

Supplies for these models consist of PVC sleeves cut into short lengths for individual struts, (**Figure 2a**), ½" PVC pipe, (**Figure 2b),** and a roll of 7/16" bungee cord, (**Figure 2c**). A PVC pipe cutter is the principal tool (**Figure 2 d**) for producing the parts for the tensegrity models.

The ½" PVC pipe was chosen to balance with the 16" length of the struts, producing reasonably sized models for teachers and students to use in a classroom. The PVC connectors were used to secure the bungee cord to the PVC struts, as seen in **Figure 1.**

A tape measure was used to measure the length of each strut and each piece of bungee cord. The PVC pipe cutter was used to cut each strut with a straight 90° cut. It was also used to cut sleeves, **Figure 2a,** into pieces; 2 sleeves and a scrap piece. Cuts for stuts were made straight across the pipes in order to form 90° right angles when a piece of PVC pipe was joined together with the PVC connector sleeves. Small slots were cut lengthwise along pipes near the end of the pipes with a finish saw that was wide enough to tightly hold the bungee cord in place.

A solvent was used to clean printing from pipes & sleeves. A power drill with a 1/8" bit was used to drill holes in sleeves and pipes through which the bungee cord was threaded. A sleeve with 4 bungee cord ends was slipped over an end of a piece of PVC pipe to secure each strut to a sleeve as in **Figure 1.**

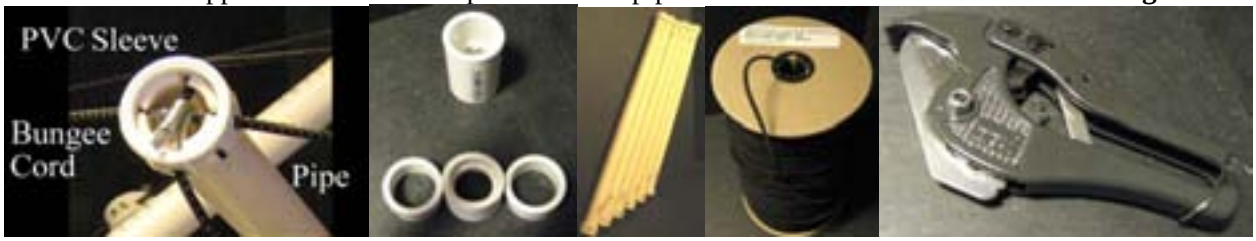

(a) **(b)** **(c)** **(d)** **(e)**

Figure 1: Pipe, sleeve, cord (a), Sleeves (a), Struts & Sleeves (b), Bungee Cord (c), and pipe cutter (d)

3. Tensegrities from a Cube, a Truncated Tetrahedron, and a Twisted Triangular Prism

3.1. A Tensegrity Model based on a Cube. A first tensegrity model can be built using a cube as a supporting structure as in **Figure 3a**. Struts of this tensegrity model can be seen tilted at a 45°angle to the horizon, **Figure 3a**, parallel to the horizon, **Figure 3b,** and perpendicular to the horizon, **Figure 3c.**

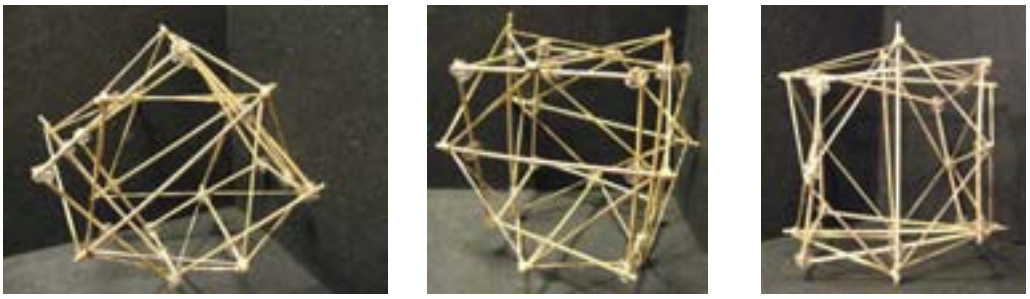

(a) **(b)** **(c)**

Figure 3: A cube with a 45° strut **(a)**, a more horizontal strut **(b),** a more vertical strut **(c).**

The cube was built from 12 sticks and 8 rings of vinyl tubing for its vertices. This tensegrity structure uses 6 struts that have additional vinyl tubing that are located at the middle of edges on each side of the cube. The 24 lines for the tensegrity are positioned in groups of 4 at the ends of the 6 struts. Views of more horizontal struts are seen in **Figure 3b,** and more vertical struts are in **Figure 3c.**

3.2. A Tensegrity Model based on a Truncated Tetrahedron. A second tensegrity model can be built using a truncated tetrahedron as a supporting structure as in **Figure 4a.** This tensegrity model has 6 struts and 24 lines. Initially, a tetrahedron can be built with 6 sticks and 4 rings of vinyl tubing for the vertices. This tetrahedron has 2 additional vinyl tubing rings added on each edge of the tetrahedron for the edges of the truncated tetrahedron, **Figure 4b.** Each strut has 4 lines connected to each end.

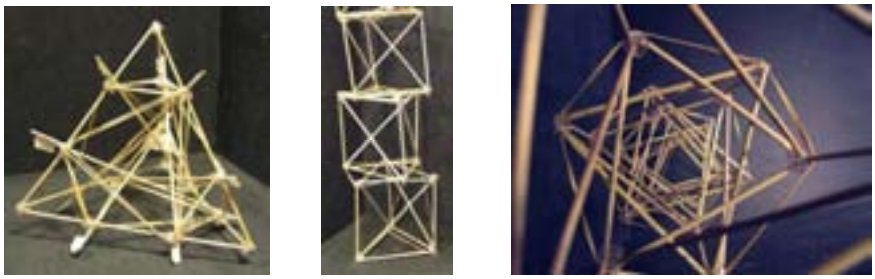

(a) **(b)** **(c)**

Figure 4: A truncated tetrahedron with tensegrity **(a)** **Figure 5**: Three triangular anti-prisms for a tensegrity tower **(b)**, Axial view of tower tensegrity with triangles alternating their direction **(c).**

3.3 A Tensegrity Model based on a Twisted Triangular Anti-Prism. A third tensegrity model can be built using three twisted triangular anti-prisms as supporting structures as in **Figure 5a.** Each twisted triangular anti-prism is rotated in either a clockwise or a counterclockwise direction, one above or below the other **Figure 5a.** Viewing the tower along its long axis, **Figure 5b**, yields a view of triangles that are

pointing either mostly up or mostly down. Many of the sticks appearing in **Figure 5a** will be replaced by lines in the final tensegrity model.

4. Tensegrity Models of PVC pipes, PVC sleeves and Bungee Cord

4.1 A Tensegrity Model Based on a Cube. Six struts with 3 pairs of parallel struts **Figure 6,** 12 sleeves on the 6 struts and 24 bungee cords form an extended octahedron tensegrity model.

4.2 A Tensegrity Model Based on a Truncated Tetrahedron. Six struts where exterior of struts have a truncated tetrahedron with a small triangle and a larger triangle. The model has 12 shorter bungee cords and 12 longer bungee cord lines along edges of the truncated tetrahedron, **Figure 7.**

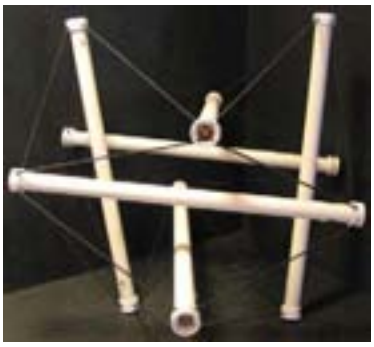

Figure 6: Tensegrity on extended octahedron.

Figure 7: Tensegrity on truncated tetrahedron.

4.3 Tensegrity Model Based on 3 Anti-Prisms. A tower tensegrity model built from 9 struts with 3 sets of 3 parallel edges, with short and long lines for bungee cords, **Figure 8**. An axial view of the tower model yields a view of a central hexagon **Figure 9.**

Figure 8: Tower tensegrity model

Figure 9: Axial view of tower tensegrity model

5. Handling PVC Pipes, PVC Sleeves and Bungee Cord Tensegrity Models

I particularly like the 3 tensegrity models presented in this paper, because each stable model provides a very different spatial experience for the student. The experience gained by building each model helps a great deal toward building a second and third model. These three models allow students to observe structures which have struts that appear to float in space without touching each other.

6. Conclusion

During the past year I learned a very valuable lesson about the size of the physical models for the classroom and the size of the average student in that classroom. There is a relationship between the size of the model where the students are comfortably assembling and manipulating the models in their hands. A somewhat smaller model has emerged where the comfort for the students to manipulate the models has improved. It may be because I usually present the models to adult teachers, that my models have been somewhat larger. However, this year I used smaller models for 6^{th}, 7^{th}, and 8^{th} grade students and the presentations have improved for the students.

These PVC based models were built during the past year for the first time. Preliminary stick models provided me detailed building information and confidence to go ahead and build the tensegrity models, for subsequently presenting them in the classroom and at the conference.

I have given presentations with this paper and these models at the McGillis School in Salt Lake City for 3^{rd} through 8^{th} grades. These presentations have been invaluable for the students, who both listen well and anticipate the opportunity to handle the models. Models that can be thrown somewhat gently around the classroom help to entertain as well as inform the students.

In addition, the presentations with the physical models also help me to learn more about the effectiveness of a particular set of models and their associated building instructions in the classroom. The tactile experience of handling the models provides the students with a more engaging experience than merely viewing three-dimensional images on paper or on a computer monitor.

I have been presenting models in classrooms for over 20 years and they have proven to be well received, in addition to being valuable experiences for me. When I am building models I am imagining them being handled by students and presenting the associated concepts in a classroom for students and teachers. It takes time and effort to build models and I always hope that they will be effective in helping to clearly convey underlying geometric concepts. However, with each new set of models, the testing ground remains in the classroom. The models are only considered a success if the presentations and models are both thought provoking and engaging for students and teachers.

Acknowledgements

I would like to thank, my spouse, Deborah, for proof reading drafts of this paper and I would also like to thank my son, Colin, for lending his two hands to build the PVC models that appear in this paper.

References

[1] McDermott, R. J., "A Physical Proof for 5 &and Only 5 Regular Solids", Bridges Conference, 2005.
[2] McDermott, R.J., "Building Simple and Not So Simple Stick Models", Bridges Conference, 2006.
[3] McDermott, R.J., "Building Models to Transition Between Dimension", Bridges Conference 2007.
[4] Snelson, K., www.**kennethsnelson**.net
[5] Pugh, Anthony, An Introduction to Tensegrity, Univ. of California Press, Berkeley, 1976.
[6] Kenner, Hugh, Geodesic Math & How To Use It, Univ. of California Press, Berkeley, 1976.

Appendix I – 3 Tensegrity Modls

	struts		sleeves		lines	
polyhedron	number	length	#		length	#
Cube	6	16"	12		10"	24
Trunc Tetra	6	16"	12	Short Long	5" 12"	12 12
Tri TwAnti Prism	9	10"	18	Long Short	6" 4"	12 16

Transferring Patterns: From Twill to Peyote Stitch

Eva Knoll
Faculty of Education
Mount Saint Vincent University
Halifax, Nova Scotia, Canada
E-mail: eva.knoll@msvu.ca

Abstract

Crafts are generally known for pieces whose structure and geometry are derived from the constraints of the techniques used. In particular, the look of specific patterns and textures are the natural product of the structure of the specific medium and technique applied to their production. The transfer of a pattern from its natural medium to another whose constraints may differ can sometimes present interesting mathematical challenges. In this workshop, this is exemplified through the transfer of a classic pattern resulting from Twill weaving, the Hound's-Tooth Check as it is transferred to a different medium, known as Peyote, Gourd or Twill Stitch, whereby beads are strung in a traditional bricklaying pattern using an off-loom beading technique. This transfer presents the challenge of adapting a structure so that the transferred pattern still resembles the original, in as simple a way as possible. In the workshop, several possible result of this transfer are compared and materials are made available to both design and create Peyote-stitched hound's tooth surfaces, thereby introducing the participants to some of the mathematical constraints of this type of transfer.

Introduction

The patterns displayed on a handcrafted object are often a natural result of the constraints of the specific technique applied to its creation. In particular, the use of Twill as a weaving technique can produce a variety of patterns including Tartans as well as the Hound's-Tooth Check [1]. Although from a purist perspective a pattern belongs to the technique that produces it, a mathematically interesting problem emerges from the exploration of how it could be produced in a different medium, whose constraints are different. The appearance of the texture produced by Twill weaving is determined mainly by the colour and quality of the threads used, the thread count or sett and the way the loom's harnesses are threaded [2, 3]. The appearance and disappearance of each thread is then predetermined and the finished weave makes the path of the threads intermittently visible.

There is an off-loom beading technique, which produces surface coverings, that is also known as 'Twill' as well as 'Peyote' or 'Gourd Stitch' [4, 5, 6]. This beading technique is more versatile than Twill weaving in that the colour of each bead is completely independent from that of any other bead on the finished surface, unless specified in the design. In addition, the relative position of the beads presents a different basic pattern. Under these conditions, transferring a Twill pattern from weaving to beading necessitates some mathematical reasoning, the process and results of which are presented here and in the workshop, focusing specifically on the application of the Hound's-Tooth Check to Peyote Stitch beading.

Twill Weaving

The Twill weaving method results in a Herringbone pattern, as shown in Figure 1, below, similar to one that is sometimes used in bricklaying. The resulting surface shows diagonal bands of translated, parallel and adjacent 'tiles' and emphasises a single diagonal direction, as determined by the direction of the translation of these parallel 'tiles'. In the case of figure 1, this emphasised diagonal runs from top-left to bottom-right. In addition to translations in two distinct directions, the pattern has 2-fold rotational symmetry and glide reflection symmetry but no reflective symmetry. Unlike in masonry, however, in weaving some of the 'tiles' are connected and their relative colour is determined by the threading: all collinear 'tiles' will have the same colour, and the sett determines the order of the colours along the 'bands'. Visually, therefore, the pattern emphasises three 'axes': that determined by the warp (the

collinear vertical ‘tiles’ are all of the same colour), that determined by the weft (the collinear horizontal ‘tiles’ are all of the same colour), and the diagonal determined by the translation of a tile from row to row.

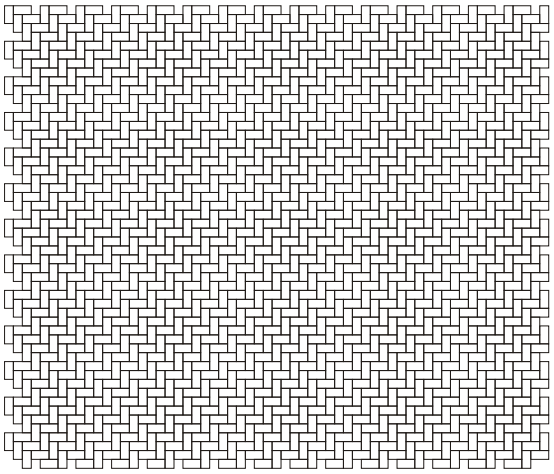

Figure 1: *Herringbone pattern with one-by-two tiles*

In the case of the Hound’s-Tooth Check, the sett for both the warp (the threads that are mounted onto the loom), and the weft (the threads that are passed through with the shuttle) are of the same colour and order and generally the same frequency, namely: x black threads + x white threads. Where the black threads cross each other, the result is a completely black square, and the same is true of the white threads. Where the two colours cross, a square containing a diagonal pattern is produced, with the vertical ‘tiles’ in one colour and the horizontal ‘tiles’ in the other. Overall, this results in a checkerboard pattern in which the solid-coloured squares alternate with the striped squares. However, because each striped square is adjacent to both white and black squares, visually, the diagonal bands are read as being attached to the appropriately coloured adjacent square, giving the Hound’s-Tooth Check its distinctive character, as shown below.

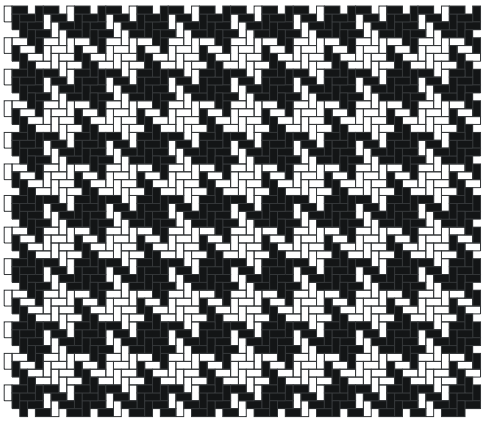

Figure 2: *Applying the Hound’s-tooth sett to the herringbone pattern*

The Hound’s-Tooth Check is one of the simplest that can be applied to the Twill weaving short of making it completely flat by only using one colour, or using one colour for the warp and one for the weft. It uses two contrasting colours, resulting in homeomorphic spaces[1]. It shows with great contrast how the areas of colour combine to emphasise the structure of the weaving method and the way the areas of colour play off each other.

[1] This means that the white areas are of the same shape and size as the black areas, and that one can be transformed into the other by simple symmetry transformations, in this case a translation.

The Peyote Stitch

The Peyote Stitch is an off-loom beading technique that produces flexible surfaces of interconnected beads in the basic form of rectangles, discs or tubes. These forms can be combined to create craft objects such as tubular ropes, pouches, banner-like talismans and to cover most shapes, including bottles, buttons, etc. Its name derives from the fact that many objects used in the Peyote ceremonies of the Native American Church are decorated using this technique [4]. It is also known as the Gourd Stitch and, curiously, the Twill Stitch [5]. It can be found in artefacts from many civilisations, including Ancient Egypt and Native North America [4]. The type of Peyote Stitch of interest here is the flat, rectangular design. Its structure resembles a traditional brick pattern, laid on its side, in that parallel rows of beads are shifted by a half bead width, as shown below:

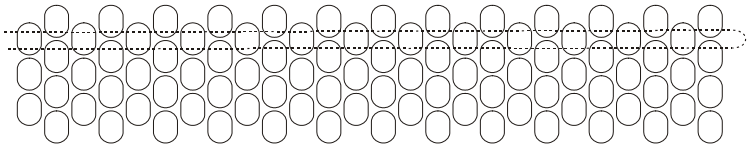

Figure 3: *Bead placement in a rectangular Peyote Stitch sample*

To create the rectangular Peyote Stitch, a craftsperson begins by stringing all the beads at the top of each column in the design, including both the 'up' beads and the 'down' beads. Then, on the way back, the thread is pulled through each existing 'down' bead from the first row, and a new bead is introduced below each 'up' bead, generating the second row. The pattern is continued in the same manner to create a rectangular surface with straight side edges and top and bottom edges showing a wavy finish. Structurally, this is similar to chain link fencing, except that the adjacent 'wires' or thread are not twisted around each other as in fencing, but share a bead instead. In addition to translation in two distinct directions, this pattern has 2-fold rotation symmetry, glide-reflection symmetry along a vertical axis between columns of beads and two perpendicular reflection symmetries corresponding to the reflection symmetries of a single bead.

Visually, the pattern also allows for the emphasis of three main axes: along a column (corresponding to a row of bricks), and, because of the adjacency created by the shifted rows, two diagonal axes, as shown in Figure 4, below. Note that the two diagonal axes are emphasised in a way similar to that in the Twill weaving pattern, by colouring tiles with common edges using the same colour.

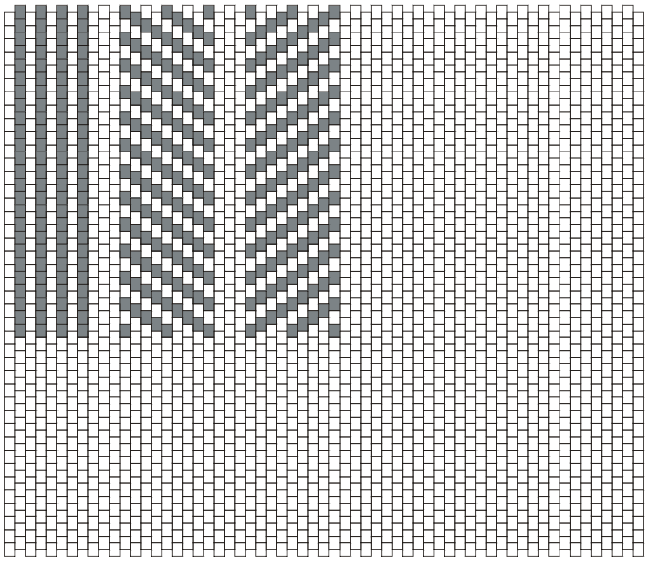

Figure 4: *Rectangular Peyote Stitch sample with emphasised axes*

Transferring the Effect

In both the Twill weave and the Peyote Stitch patterns, there are three main axes that can be emphasised by the basic structure combined with the colour selection, and these are grouped into two similar and one different axis. In Twill weaving, the warp and weft axes have a similar impact on the design, and the diagonal axis stands alone. In the Peyote Stitch, the vertical axis stands alone and the two diagonal axes are equivalent under symmetry. To preserve this relationship, the warp and weft axes of Twill weaving are transferred to the two diagonal axes in the Peyote Stitch pattern and the diagonal of the Twill weaving becomes the vertical on the Peyote Stitch pattern, resulting in the beading pattern of Figure 5, below.

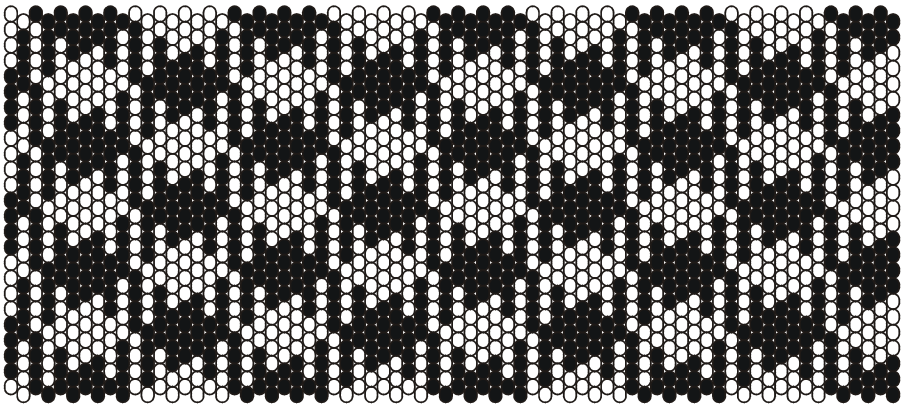

Figure 5. *The Hound's-Tooth Check transferred from Twill weaving onto the Peyote Stitch*

The workshop consists of three parts: a short explanation of the two craft techniques and the way designs can be transferred from one to the other, an activity focusing on the design of a Peyote Stitch rectangle, and a period of time devoted to creating a piece of Peyote Stitching using Pony Beads. For example, the above pattern produces the result of Figure 6, below.

Figure 6. *A sample of the Peyote Stitch version of the Hound's-Tooth Check, using 'Pony' beads*

References

[1] *Online Textile Dictionary*, retrieved January 2009 from www.resil.com/h.htm, n.d.
[2] Black, M.E, *New Key to Weaving*. New York: The Bruce Publishing Company, 1957.
[3] Margeson, F, Personal conversation, January 2009.
[4] Wikipedia, *Peyote Stitch*, retrieved January 2009 from en.wikipedia.org/wiki/Peyote_stitch, n.d.
[5] Vinson, G., *Guide to Beadwork: a Beaded Jewelry Primer*, retrieved January 2009 from www.guidetobeadwork.com/book/twill/TS7.html, n.d.
[6] Dean, D., *Beading in the Native American Tradition*. Loveland CO: Interweave Press, 2002.

Author Index

Akridge, James Luke 215
Baatz, Wolfgang 337
Beiles, Greg 385
Belbruno, Edward 323
Bentley, Patricia 375
Bodner, B. Lynn 147
Bosch, Robert 139
Bowman, Rachel 215
Bracken, Carl 265
Brosz, John 105
Bulatov, Vladimir 193
Bumgardner, Jim 21, 303
Burns, Anne 231
Carpendale, Sheelagh 105, 293
Chavey, Darrah 305
De las Peñas, Ma. Louise Antonette N. 131
Demaine, Erik 1
Demaine, Martin 1
Dunham, Douglas 163
Dunning, Alan 105
Ellison, Elaine F. 341
Erdély, Dániel 271
Etemad, Katayoon 293
Evans, Brian 333
Fathauer, Robert 251
Felix, René 131
Fitzpatrick, Gary 265
Flodén, Liselott 329
Fornasier, Massimo 337
Frantz, Michael 347
Génard, André 319
Gailiunas, Paul 243, 271
Garfield, Suzie 363
Garousi, Mehrdad 313
Gerofsky, Susan 279, 383
Gomez, Francisco 279
Gould, S. Louise 351
Greenfield, Gary 155
Grossman, Bathsheba 301
Höft, Hartmut F.W. 79
Hamburger, Peter 215
Happersett, Susan 345
Hart, George 207
Hart, Vi 169
Hendel, Russell 115
Hizume, Akio 239
Holmbom, Anders 329
Kaplan, Gail 309
Kessler, Bruce 97, 215
Knoll, Eva 379, 409
Konjevod, Goran 47
Kuprešanin, Ana Maria 47
Laigo, Glenn 131
Lakins, Tamara 315
Lang, Robert J. 11
Laycraft, Krystyna 355
Luecking, Stephen 343
Markin, Nadya 265
Markowich, Peter A. 337
McBurney, Susan 287
McDermott, Robert 403
Meenan, E.B. 367
Melville, Duncan 389
Melville, Sarah 389
Mete, Fatma 331
Olsson, Marianne 329
Palmer, Curtis 335
Persson, Jens 329

Pike, Andrew 139
Rappaport, David 279
Reimann, David 325
Roelofs, Rinus 183
Rollings, Robert 199
Rosenwald, Daphne 385
Séquin, Carlo H. 87
Samavati, Faramarz 105
Scannell, Billy C. 349
Schönlieb, Carola-Bibiane 337
Schaffer, Karl 63
Smith, Peter 317
Spitzer, Sandy 327
Swart, David 39
Taleslami, Khalil 313
Taylor, R.P. 349
Taylor, Tara 379
Thomas, B.G. 177, 367
Toussaint, Godfried 279
Tymoczko, Dmitri 29
van Ballegooijen, Walt 271
Van Dusen, Ben 349
Van Loocke, Philip 55
Varland, Joel 339
Verbiese, Samuel 321
Verhoeff, Koos 223
Verhoeff, Tom 223
Wagner, Philip 69, 395
Wang, Hao 105
Wells, Benjamin 69, 395
Yackel, Carolyn 123
Yamagishi, Yoshikazu 239
Zimmerman, Jay 259